Role of pannexin in excitation-contraction coupling of skeletal muscle

Francisco Jaque Fernandez

N°d'ordre NNT : 2021LYSE1082

THESE de DOCTORAT DE L'UNIVERSITE DE LYON
opérée au sein de
l'Université Claude Bernard Lyon 1

Ecole Doctorale 205
(Ecole Doctorale Interdisciplinaire Sciences-Santé)

Spécialité de doctorat : Biologie
Discipline : Physiologie

Soutenue publiquement le 03/05/2021, par :
Francisco Jaque Fernandez

Rôle de la pannexine dans le couplage excitation-contraction du muscle squelettique

Devant le jury composé de :

Kretz-Remy, Carole	Professeure des Universités, Lyon 1	Présidente
Gomez, Ana-Maria	Directrice de Recherche INSERM	Rapporteure
Charnet, Pierre	Directeur de Recherche CNRS	Rapporteur
Csernoch, Laszlo	Professeur des Universités	Rapporteur
Kretz-Remy, Carole	Professeure des Universités	Examinatrice
Rieusset, Jennifer	Directrice de Recherche INSERM	Examinatrice
Casas, Mariana	Professeure assistante	Co-Directrice de thèse
Jacquemond, Vincent	Directeur de Recherche CNRS	Co-Directeur de thèse

UNIVERSITE CLAUDE BERNARD - LYON 1

Président de l'Université	**M. le Professeur Frédéric FLEURY**
Président du Conseil Académique	M. le Professeur Hamda BEN HADID
Vice-président du Conseil d'Administration	M. le Professeur Didier REVEL
Vice-président du Conseil Formation et Vie	M. le Professeur Philippe CHEVALIER
Universitaire	M. Fabrice VALLÉE
Vice-président de la Commission Recherche	M. Damien VERHAEGHE
Directeur Général des Services	

COMPOSANTES SANTE

Faculté de Médecine Lyon Est – Claude Bernard	Département de formation et Centre de Recherche en Biologie
Faculté de Médecine et de Maïeutique Lyon Sud – Charles	Humaine
Mérieux	Directeur : M. le Professeur G.RODE
Faculté d'Odontologie	Directeur : Mme la Professeure C. BURILLON
Institut des Sciences Pharmaceutiques et Biologiques	Directeur : M. le Professeur D. BOURGEOIS
Institut des Sciences et Techniques de la Réadaptation	Directeur : Mme la Professeure C. VINCIGUERRA
	Directeur : M. X. PERROT
	Directeur : Mme la Professeure A-M. SCHOTT

COMPOSANTES ET DEPARTEMENTS DE SCIENCES ET TECHNOLOGIE

Faculté des Sciences et Technologies	Directeur : M. F. DE MARCHI
Département Biologie	Directeur : M. le Professeur F. THEVENARD
Département Chimie Biochimie	Directeur : Mme C. FELIX
Département GEP	Directeur : M. Hassan HAMMOURI
Département Informatique	Directeur : M. le Professeur S. AKKOUCHE
Département Mathématiques	Directeur : M. le Professeur G. TOMANOV
Département Mécanique	Directeur : M. le Professeur H. BEN HADID
Département Physique	Directeur : M. le Professeur J-C PLENET
UFR Sciences et Techniques des Activités Physiques et Sportives	Directeur : M. Y.VANPOULLE
Observatoire des Sciences de l'Univers de Lyon	Directeur : M. B. GUIDERDONI
Polytech Lyon	Directeur : M. le Professeur E.PERRIN
Ecole Supérieure de Chimie Physique Electronique	Directeur : M. G. PIGNAULT
Institut Universitaire de Technologie de Lyon 1	Directeur : M. le Professeur C. VITON
Ecole Supérieure du Professorat et de l'Education	Directeur : M. le Professeur A. MOUGNIOTTE
Institut de Science Financière et d'Assurances	Directeur : M. N. LEBOISNE

Résumé

Rôle de la pannexine dans le couplage excitation-contraction du muscle squelettique

La protéine membranaire $Ca_V1.1$ détecte l'activité électrique de la membrane plasmique pour le couplage excitation-contraction (CEC) et excitation-transcription (CET) des cellules musculaires. Pour le CEC, $Ca_V1.1$ contrôle le canal calcique RyR1 dans la membrane du réticulum. Pour le CET, $Ca_V1.1$ contrôle la pannexine 1 (Panx1), un canal à ATP de la membrane plasmique, responsable de la sortie d'ATP et l'activation d'une cascade de signalisation qui régule la plasticité musculaire. Ce projet visait à -déterminer si Panx1 est un partenaire du CEC, -préciser ses propriétés fonctionnelles sur fibre musculaire isolée, -étudier les altérations du CEC dans un modèle pathologique suspecté associé à une dysfonction de Panx1.

Nous révélons que la sous-expression de Panx1 est associée à des altérations de l'activité de $Ca_V1.1$ et de RyR1 pendant le CEC. De plus, l'inhibition pharmacologique de Panx1 est aussi associée à des altérations délétères de la signalisation calcique musculaire. L'ensemble établit le rôle de Panx1 dans la régulation de l'homéostasie calcique et du CEC.

Par ailleurs, la détection de la libération d'ATP par Panx1 à l'échelle de la fibre musculaire isolée, a été tentée à l'aide de capteurs biologiques : soit des canaux K^+ ATP-dépendants, soit des récepteurs purinergiques. Les deux méthodes fonctionnent mais n'ont pas permis d'identifier de manière reproductible la sortie d'ATP liée à l'activation de Panx1.

Une altération de la fonction de Panx1 dans le muscle est suspectée en situation de diabète de type 2. Nous avons testé si une altération du CEC dans ce modèle. A l'aide d'un modèle murin d'obésité par régime nous avons démontré la préservation remarquable du CEC dans cette situation.

MOTS-CLES= Muscle squelettique; Couplage excitation-Contraction ; Pannexines ; Liberation d'ATP ; Probenecide ; Calcium ; Fonction musculaire ; Obesité

Role of pannexin in excitation-contraction coupling of skeletal muscle

The $Ca_V1.1$ protein senses the electrical activity of the plasma membrane for the processes of excitation-contraction coupling (ECC) and excitation-transcription coupling (ETC) of skeletal muscle cells. For ECC, $Ca_V1.1$ controls the activity of the type 1 ryanodine receptor (RyR1) Ca^{2+} release channel in the reticulum membrane. For ETC, $Ca_V1.1$ controls the activity of pannexin 1 (Panx1), a plasma membrane ATP channel responsible for ATP exit and consequent activation of a signaling pathway involved in muscle plasticity. The present project aimed at -determining the potential role of Panx1 as a partner in ECC, -characterizing Panx1 functional properties in single isolated muscle fibers, investigating the function of ECC in a disease model suspected to be associated with Panx1 dysfunction.

We found that down-expression of Panx1 in muscle fibers is associated with altered functions of $Ca_V1.1$ and RyR1 during ECC. Furthermore, Panx1 pharmacological blockers also alter Ca^{2+} signaling in muscle fibers. Overall results establish a role for Panx1 in the control of muscle Ca^{2+} homeostasis and ECC.

We attempted to detect Panx1-mediated ATP release at the single muscle fiber level using biological sensors: either ATP-dependent K^+ channels or ionotropic purinergic receptors. Both methods work but did not allow detection of Panx1-induced ATP release in a reliable manner.

Altered Panx1 function is suspected in muscles under type 2 diabetes conditions. We tested whether ECC is altered in that situation and contributes to the associated muscle weakness. We found that it is not the case. ECC is remarkably preserved in muscle fibers from a diet-induced mouse model of diabetes and obesity.

KEYWORDS= Skeletal muscle; Excitation-Contraction Coupling; Pannexins; ATP release; Probenecid; Calcium; muscle function; Obesity

Résumé substantiel

Rôle de la pannexine dans le couplage excitation-contraction du muscle squelettique

La fonction première du tissu musculaire squelettique est la contraction et la génération de force et de mouvement, sous le contrôle de la commande par les motoneurones. Dans une fibre musculaire différenciée, la dépolarisation membranaire, portée par les potentiels d'action générés à la plaque motrice, se propage dans l'ensemble du sarcolemme incluant ses invaginations transversales qui constituent les tubules transverses (tubules-T). Les tubules-T interagissent avec la membrane des citernes terminales du réticulum sarcoplasmique (RS) à des sites particuliers appelés triades, au niveau desquels se trouvent les complexes protéiques de libération de Ca^{2+} (CLC). Chaque CLC est constitué de 4 canaux Ca^{2+} voltage-dépendants ($Ca_V1.1$) dans la membrane du tubule-T, associés avec un canal de libération de Ca^{2+}, le récepteur de la ryanodine de type 1 (RyR1), dans la membrane adjacente du RS. Les canaux $Ca_V1.1$ jouent le rôle de détecteurs de potentiel pour le complexe. En réponse à la dépolarisation des tubules-T, ils changent de conformation et induisent l'ouverture du canal RyR1 et ainsi l'efflux de Ca^{2+} de la lumière du RS vers le cytosol. L'augmentation de Ca^{2+} cytosolique qui en résulte active la machinerie contractile. L'ensemble du processus est référencé sous la terminologie de couplage excitation-contraction (CEC).

Au-delà du CEC, les canaux $Ca_V1.1$ participent à un autre processus appelé couplage excitation-transcription (CET), à travers leur association fonctionnelle avec une autre protéine présente dans la membrane des tubules-T, la pannexine 1 (Panx1), qui sous sa forme heptamérique, joue le rôle de canal à ATP. Le processus de CET est déclenché par des fréquences basses de trains de potentiels d'action (10-20 Hz), détectées et transduites par $Ca_V1.1$ en l'ouverture de Panx1. En résulte l'extrusion d'ATP dans le milieu extracellulaire qui active des récepteurs purinergiques métabotropiques (P2Y) dans la membrane plasmique et déclenche ainsi une cascade de signalisation conduisant à la régulation d'expression de gènes favorisant une plasticité musculaire du type rapide vers le type lent. Par ailleurs, Panx1 joue également un rôle dans d'autres processus de la physiologie musculaire tels que la différenciation et la potentialisation contractile. Si $Ca_V1.1$ et RyR1 sont les protéines majeures impliquées dans le CEC, leur fonction est ajustée ou régulée par d'autres protéines qualifiées d'accessoires ou partenaires au CEC.

Mon projet de Thèse s'est basé sur l'hypothèse selon laquelle Panx1 fait partie de ces protéines partenaires, étayée par les faits suivants : -Panx1 est co-localisée avec $Ca_V1.1$ et les deux donnent un signal positif au test de proximité de ligand, -Panx1 co-immuno-précipite avec $Ca_V1.1$, -l'activité de Panx1 est dépendante de $Ca_V1.1$ au-cours du CET.

Dans ce contexte, le premier objectif de mon projet fût d'étudier le rôle de Panx1 dans le CEC des fibres musculaires différenciées. Pour cela, j'ai poursuivi un travail débuté au-cours de mon Master, consistant à caractériser les conséquences de la sous-expression de Panx1 sur le CEC de fibres musculaires isolées des muscles *flexor digitorum brevis* (FDB) de souris, à l'aide d'une combinaison d'électrophysiologie et d'imagerie confocale. J'ai par ailleurs utilisé cette combinaison dans l'ensemble de mon travail de Thèse. La sous-expression de Panx1 dans les muscles FDB fût réalisée par électroporation d'un plasmide codant pour un ARN court en épingle à cheveux, interférant avec la production de Panx1 (shRNAPanx1). Nous avons découvert que la sous-expression de Panx1 est associée à des modifications de l'activité de canal Ca^{2+} de $Ca_V1.1$ et à une réduction considérable de l'efflux de Ca^{2+} du RS par les canaux RyR1, en réponse à la dépolarisation des tubules-T, révélant ainsi pour la première fois un rôle de Panx1 dans le CEC. Ce travail fût complété par une analyse de l'effet d'agents pharmacologiques inhibiteurs de l'activité de Panx1 sur le CEC. Les deux agents testés, la carbénoxolone et le probénécide, furent prouvés affecter l'homéostasie calcique de repos et la libération de Ca^{2+} par le RS. Ces résultats furent complétés par une analyse de l'effet du probénécide sur la contraction de muscles intacts isolés, réalisée en collaboration avec la Plateforme Therassay de l'Université de Nantes : le probénécide induit une réduction d'amplitude de la contraction tétanique de l'ordre de 60 % après 45 minutes d'incubation. Ces résultats confirment les relations étroites entre la fonction de Panx1 et l'homéostasie calcique et le CEC et suggèrent des effets potentiellement adverses des bloqueurs de Panx1 utilisés en clinique, sur la fonction musculaire. Une dernière étape de cet objectif s'est attachée à déterminer si la sur-expression de Panx1 est susceptible d'affecter la signalisation calcique et le fonctionnement du CEC. Les résultats partiels obtenus jusqu'à présent à l'aide de trois constructions plasmidiques suggèrent que ce n'est pas le cas.

La détection de la libération d'ATP à l'échelle d'une fibre musculaire isolée n'a encore jamais été réalisée et reste une étape indispensable à la caractérisation fonctionnelle détaillée de Panx1. Le deuxième objectif de ma Thèse a consisté à relever le défi, à travers deux approches utilisant des capteurs biologiques. La première a consisté à utiliser un patch de membrane plasmique, excisé d'une fibre musculaire, en configuration face interne-dehors, et contenant des canaux K^+ ATP-dépendants (K_{ATP}). La propriété de l'ATP intracellulaire à bloquer l'activité de ces canaux fût utilisé comme sonde de détection des changements d'ATP extracellulaire. L'activité des canaux K^+ dans le patch a pu être détectée en continu alors que ce patch était disposé à proximité immédiate d'une fibre musculaire intacte, par ailleurs soumise à des trains de dépolarisations en potentiel imposé à la fréquence permissive en regard de l'activation de Panx1. Cette méthode, élégante mais délicate a pu être mise en œuvre avec succès sur un nombre substantiel de fibres musculaires. La deuxième approche a consisté à transfecter in vivo des fibres

musculaires de souris avec un plasmide codant pour un récepteur ionotropique purinergique (P2X). Les P2X sont des canaux cationiques absents de la membrane des fibres musculaires différenciées, dont l'ouverture est déclenchée par la présence d'ATP à la face extracellulaire du canal. La stimulation des fibres exprimant le P2X, par des trains de dépolarisations imposées à la fréquence permissive (basse, 20Hz) en regard de l'activation de Panx1, se devait de générer un courant de membrane à travers les canaux P2X en raison de l'augmentation d'ATP extracellulaire. Pour ces deux méthodes, la capacité à détecter un changement d'ATP extracellulaire imposé par une perfusion externe fût testée lors de chaque expérience. Cependant, nous n'avons pas pu observer de réponse convaincante et reproductible qui témoigne de la libération d'ATP en réponse à l'activation d'une fibre musculaire à la fréquence permissive, et ceci avec chacune des deux méthodes. Soit les conditions expérimentales sur fibres musculaires isolées empêchent le fonctionnement correct de Panx1 et la sortie d'ATP en réponse aux trains de stimulations, soit la sensibilité de ces deux méthodes reste encore trop faible pour détecter les changements d'ATP extracellulaire induits.

Nos résultats montrant que Panx1 est un partenaire du CEC du muscle ouvrent la perspective suivant laquelle des anomalies d'expression ou de fonction de Panx1 puissent être associées à des déficiences musculaires. Ceci pourrait être le cas de la situation de diabète de type 2, dont on sait qu'elle est associée à une faiblesse musculaire et dont certaines données suggèrent qu'elle pourrait également être associée à une dysfonction de Panx1. Dans ce contexte, le troisième objectif de ma Thèse fût de caractériser les propriétés de l'homéostasie calcique et du CEC dans un modèle murin d'obésité et de diabète déclenché par un régime riche en sucres et lipides. Indépendamment de la question liée à Panx1, l'étude se devait d'établir la contribution, jusqu'à présent controversée, d'altérations du CEC à la faiblesse musculaire diabétique. En collaboration avec Jennifer Rieusset (CarMEN laboratoire, Université Lyon 1) nous avons réalisé une étude exhaustive des propriétés du CEC dans ce modèle à l'aide d'une combinaison d'électrophysiologie et de microscopie confocale sur fibres musculaires isolées. Cette étude a permis la caractérisation quantitative du réseau de tubules-T, des fonctions de détecteur de potentiel et de canal calcique de $Ca_V1.1$, de la libération de Ca^{2+} par les canaux RyR1, de la vitesse d'extrusion du Ca^{2+} du compartiment cytosolique, de l'homéostasie calcique de repos en termes d'évènements de libération de Ca^{2+} spontanés, de la réponse à un protocole de fatigue. Les résultats ont montré une stupéfiante préservation du contrôle de l'homéostasie calcique et du CEC dans ce modèle. L'altération des capacités intrinsèques du CEC de fibres musculaires issues d'un organisme diabétique ne contribue pas à la faiblesse musculaire associée.

Preamble

My Ph.D. project has been funded by the Chilean National Agency for Research and Development (ANID) under the direction and supervision of Dr. Vincent Jacquemond at the NeuroMyoGène institute (INMG) and the co-direction of Dr. Mariana Casas (Instituto de Ciencias Biomédicas (ICBM), University of Chile). The INMG laboratory is supported by the CNRS, the INSERM, and the University Claude Bernard-Lyon1, and is presided by Dr. Laurent Schaeffer. I was part of Jacquemond team "Excitability and Calcium signaling in normal and diseased skeletal muscle" focused on the physiology and pathophysiology of skeletal muscle function. During my Ph.D. thesis, the team has been composed by Clarisse Fuster (Post-Doc), Candice Kutchukian (Ph.D. student), Colline Sanchez (Ph.D. student), Laloe Monteiro (Assistant Engineering), Thomas Andraud (Master 1 student), Laura Ejarque (Master 2 student), and is currently composed by Vincent Jacquemond (CNRS Director), Bruno Allard (Professor), Christine Berthier (academic-researcher), Romane Idoux (Ph.D. student), Ludivine Rotard (Assistant Engineering), and Youssef Issa (Master 1 student). During my Ph.D. project, I taught in classes of Cellular Biology at the Physical-therapy Institute for students with visual disabilities (IFMKDV-University Claude Bernard-Lyon1). I also taught practical work for Cellular Biology (Skeletal muscle- Digestive System –Skin) in L1 for Biology students. During my last semester, I taught in the Physiology Teaching Department of University Claude Bernard-Lyon1 with an academic-researcher half-time temporary contract (A.T.E.R.) teaching practical and theoretical work about urinary system and hematopoiesis, and practical work about thyroid function, glycolysis and lipolysis, and action potential generation.

The work made during my Ph.D. project produced several manuscripts that have been or are in the process of publication or submission.

Scientific articles:

Jaque-Fernandez F., Beaulant A., Berthier C., Monteiro L., Allard B., Casas M., Rieusset J., Jacquemond V. (2020) "Calcium handling and excitation-contraction coupling in muscle fibers from obese mice" (Diabetologia, 2020 Nov; 63 (11): 2471-2481 https://doi.org/10.1007/s00125-020-05256-8).

Jaque-Fernandez F., Jorquera G., Troc-Gajardo J., Pietri-Rouxel F., Gentil C., Buvinic S., Allard B., Jaimovich E., Jacquemond V. and Casas M. (2020) "Excitation-contraction and excitation-transcription coupling in skeletal muscle: cross talk between dihydropyridine receptor and pannexin-1" (in preparation for resubmission to Journal of General Physiology).

Francisco Jaque-Fernandez, Bruno Allard, Aude Lafoux, Corinne Huchet, Enrique Jaimovich, Mariana Casas, Christine Berthier, and Vincent Jacquemond « Probenecid affects ryanodine-receptor function and force production in skeletal muscle » (Manuscript in preparation).

Nattarayan V., Silva-Rojas R., **Jaque-Fernandez F**., Menuet A., Gomez-Oca R., Goret M., Messaddeq N., Lionello V.M., Reiss D., Kretz C., Cowling B.S., Jacquemond V., Laporte J. "Acute downregulation of dynamin 2 rescues amphiphysin 2 (*BIN1*) centronuclear myopathy in mice" (sent to Brain).

Ghasemizadeh A., Christin E., Guiraud A., Couturier N., Risson V., Laddada L., Sanchez C, **Jaque F.**, Garcia A., Lanfranchi M., Jacquemond V., Gondin J., Courchet J., Schaeffer L., Gache V. (2019) « Skeletal muscle MACF1 maintains myonuclei and mitochondria localization through microtubules to control muscle functionalities » (sent to eLife).

Congress communication:

Jaque-Fernandez F., Beaulant A., Berthier C., Monteiro L., Allard B., Casas M., Rieusset J., Jacquemond V. (2019) « Calcium handling and excitation-contraction coupling in muscle fibers from obese mice » *Journées de la Société Française de Myologie*. Poster. Marseille, France.

Jaque-Fernandez F., Beaulant A., Berthier C., Monteiro L., Allard B., Casas M., Rieusset J., Jacquemond V. (2019) « Calcium handling and excitation-contraction coupling in muscle fibers from obese mice » *24ème Journées Scientifique de l'EDISS*. Poster. Lyon, France.

Jaque-Fernández F., Jorquera G., Troc-Gajardo J., Pietri-Rouxel F., Gentil C., Buvinic S., Allard B., Jaimovich E., Jacquemond V. and Casas M. (2018) "Cross talk between DHPR and Pannexin-1 in Excitation-Contraction and Excitation-Transcription Coupling in Skeletal muscle", *Séminaire interne de l'Institut NeuroMyoGène*. Oral communication. Lyon, France.

Jaque-Fernández F., Gonzalo Jorquera, Jennifer Troc, Bruno Allard, Sonja Buvinic, Enrique Jaimovich, Vincent Jacquemond, Mariana Casas. (2018) Functional cross talk between the dihydropyridine receptor and Pannexin-1 in skeletal muscle, *Journées de la Société Française de Myologie*, Oral communication. Brest, France.

Jaque-Fernández F., Jorquera G., Troc-Gajardo J., Pietri-Rouxel F., Gentil C., Buvinic S., Allard B., Jaimovich E., Jacquemond V. and Casas M. (2017) « Functional cross talk between the dihydropyridine receptor and Pannexin-1 in skeletal muscle ». *XXXI Chilean Society for Cell Biology Annual Meeting*. Oral communication. Puerto Varas, Chile.

Acknowledgments

First, I would like to extend my sincere thanks to the members of my committee: Ana Maria Gomez, Laszlo Csernoch, Pierre Charnet, Carole Kretz-Remy, and Jennifer Rieusset for accepting to examine this Ph.D. manuscript. I would like also to thanks Paul Salin and Rémi Mounier for their advices during all the thesis monitoring committee (CST) of Ph.D. thesis.

I would like to express my deepest gratitude to my Supervisor Vincent Jacquemond. Vincent, I am very grateful for the opportunity that you give me to learn about the world of science, electrophysiology, confocal imaging, muscle physiology, and for your generosity as a mentor and as a person. This project was possible because of your support and guidance. The world of science needs more mentors like you.

I would like to thanks my co-supervisor Mariana Casas and Professor Enrique Jaimovich. Muchas gracias a ambos por abrirme las puertas de su laboratorio en Chile. Mariana muchas gracias por la confianza, el cariño y por permitirme participar de este proyecto de colaboración. Gracias a los integrantes del antiguo team Casas: Carlos, Jennifer, Verónica, David por los momentos compartidos.

I would like to thanks two particular friends and mentors that encourage me to follow this pathway and that until now have always believed in me. Allan y Marcelo: Muchas gracias por su amistad.

I would like also to thanks to the members of my team starting with Christine Berthier and Bruno Allard: merci beaucoup pour avoir eu la générosité de partager vos connaissances avec moi. Je vous remercie également pour les moments partagés ensemble, les conversations et votre bonne humeur. I would like to thanks specially the young researchers and friends that I made during this long process: Candice, thanks a lot for all your help when I arrived into France and for your friendship. Colline, merci beaucoup pour ton amitié, pour m'avoir transmis un peu de tes connaissances et les moments partagés. Clarisse, merci pour ta bonne humeur et pour m'avoir présenté le monde de l'escalade. Romane et Laloé, merci beaucoup pour votre soutien pendant la période de ma thèse. Romane, merci de m'avoir rassuré pendant cette période et pour tes petits rappels. Je te souhaite tout le succès pour la fin de ta thèse. Laloé, todo tu cariño me recargó de energía cada vez que lo necesitaba, y tu ayuda en el proyecto fue fundamental, mis mejores deseos para ti. I would like also to thanks Tamara for all her efforts in this project. J'aimerais remercier aussi Laura, Thomas et Youssef pour les mots de soutien et les moments partagés. The time in France with all of you have been a great adventure that I will never forget!

Thanks to "les copains du labo": Laura, Yoann, Delia, Romane, Laloé, Kassandre. Merci à tous pour tous les moments partagés et pour votre soutien et amitié. Merci également à Mélisse et Sergio pour les conversations et moments partagés. Merci à l'ensemble de l'INMG pour m'accueillir dans ce projet, à l'association YRIN et aux étudiants de l'Institut pour les moments partagés et les encouragements. Gracias a mis amigos en Chile que a pesar de la distancia siempre se hicieron presentes.

Merci à ma Bella, Audrey. Merci beaucoup pour ton soutien et ton amour durant ces années en France et de Thèse. La réussite de ma Thèse et cette expérience de vie est aussi en partie grâce à toi. J'aimerais avoir la chance de continuer à partager avec toi en France, au Chili ou ailleurs.

I would like to thanks to my family. Para mis tíos en Francia: Víctor y Vilma. Muchas gracias por todo su apoyo y cariño. Gracias a mis abuelos: Ricardo y Sylvia, por la confianza que me transmitieron, y al resto de mi familia por su apoyo. Gracias a mis Padres: Sylvia y Francisco, por sus estímulos desde niño, por transmitirme el gusto por aprender y la importancia de la educación, su idealismo y su perseverancia. Gracias a mis hermanos: Sebastián, Constanza y Maximiliano por su apoyo incondicional, aunque estemos a miles de kilómetros. Les dedico este trabajo a ustedes. Con motivación y trabajo duro nada es imposible.

List of abbreviations

α1-AR = **a**dreno**r**eceptors type **α1**

AAV = **a**deno-**a**ssociated **v**irus

ACh = **a**cetyl**ch**oline

AChR = **a**cetyl**ch**oline **r**eceptor

AP = **a**ction **p**otential

ATP/ADP = **a**denosine **t**ri/**d**i **p**hosphate

BRET = **b**ioluminescence **r**esonance **e**nergy **t**ransfer

Ca^{2+} = calcium ion

$Ca_V1.1$ = L-type voltage-dependent Ca^{2+} channel type 1

Cav3 = **cav**eolin type **3**

CaM = **ca**l**m**odulin

CaMKII = Ca^{2+}/**CaM**-dependent protein **k**inase **II**

CALHM = **cal**cium **h**omeostasis **m**odulators

CBX = **c**ar**b**eno**x**olone

CCD = **c**entral **c**ore **d**isease

CCB = **C**a^{2+} **c**hannels **b**locker

Cryo-EM = **cryo**-**e**lectron **m**icroscopy

CNM = **c**entro**n**uclear **m**yopathy

cpFP = **c**ircularly **p**ermutated **f**luorescent **p**rotein

CRU = **C**a^{2+} **r**elease **u**nit

CRC = **c**alcium **r**elease **c**omplex

CSQ = **c**al**seq**uestrin

CTD = **C**-**t**erminal **d**omain

DHPR = 1,4-**d**i**h**ydro**p**yridine **r**eceptors

DMPK = **d**ystrophia **m**yotonica **p**rotein **k**inase

DMD = **d**uchene **m**uscular **d**ystrophy

DWORF = **d**warf **o**pen **r**eading **f**rame

ECC = **e**xcitation-**c**ontraction **c**oupling

ECCE = **e**xcitation-**c**oupled **C**a^{2+} **e**ntry

EDL = **e**xtensor **d**igitorum **l**ongus

EPP = **e**nd**p**late **p**otential

ES = **e**lectrical field **s**timulation

ETC = **e**xcitation-**t**ranscription **c**oupling

FDB = **F**lexor **D**igitorum **B**revis muscle

FF = **f**ast **f**atigable units

FR = **f**atigue-**r**esistance units

FRET = **f**luorescent **r**esonance **e**nergy **t**ransfer

GCTC = **g**ating **c**harge **t**ransfer **c**enter

HypoPP = **hypo**kalemic **p**eriodic **p**aralysis

IO = **i**nter**o**sseus muscle

IP3 = **i**nositol (1,4,5)-tri**p**hosphate

IP3R = **IP3 r**eceptor

JPH1 = **j**uncto**ph**ilin type 1

LGMD1C = **l**imb-**g**irdle **m**uscular **d**ystrophies type **1C**

LRRC8A = **l**eucine-**r**ich **r**epeat-**c**ontaining protein **8** type **A**

MAPK = **m**itogen-**a**ctivated **p**rotein **k**inase

Mg^{2+} = magnesium ion

MHS = **m**alignant **h**yperthermia **s**usceptibility

MmD = **m**ulti-**m**inicore **d**isease

MLN = **m**yoregu**l**i**n**

MyHC = **my**osin **h**eavy **c**hain

lncRNA = **l**ong **n**on**c**oding **RNA**

Na^{+} = Sodium ion

$Na_V1.4$ = voltage dependent Na^{+} channels type 1.4

NFAT = **n**uclear **f**actor of **a**ctivated **T**-cell

NOS = **n**itric **o**xide **s**ynthase

NMDAR = ***N***-**m**ethyl-**D**-**a**spartate **r**eceptor

NMJ = **n**euro**m**uscular **j**unction

NO = **n**itric **o**xide

NST = **n**on**s**hivering **t**hermogenesis

NTH = **N**-**t**erminal **h**elix

Panx1 = pannexin 1

P2YR = purinergic metabotropic receptor

P2XR = purinergic ionotropic receptor

PI3K = **p**hosphatidyl**i**nositide **3**-**k**inase

PLA = **p**rotein **l**igation **a**ssay

PLN = **p**hospho**l**amba**n**

PLC = **p**hospho**l**ipase **C**

PMCA = **p**lasma **m**embrane **C**a^{2+}-**A**TPase

PROB = **Prob**enecid

PKA = **p**rotein **k**inase **A**

P_0 = open probability

RyR1 = **ry**anodine **r**eceptor type **1**

SDH = **s**uccinate **d**e**h**ydrogenase

SERCA = **s**arco**e**ndoplasmic **r**eticulum **Ca**$^{2+}$ pump

SFK = **S**rc **f**amily **k**inases

SOL = **sol**eus

SLN = **s**arco**l**ipi**n**

SR = **s**arcoplasmic **r**eticulum

STAC3 = SH3 and cysteine-rich protein 3

SOCE = **s**tore-**o**perated **C**a^{2+} **e**ntry

TA = **t**ibialis **a**nterior

TnIs = **slow t**ropo**n**in **I**

TnIf = **f**ast **t**ropo**n**in **I**

VGCC = **v**oltage **g**ated **C**a^{2+} **c**hannel

V_m = resting voltage

VSD = **v**oltage-**s**ensing **d**omains

VRAC = **v**olume-**r**egulated **a**nion **c**hannel

VSMC = **v**ascular **s**mooth **m**uscle **c**ells

List of figures

INDEX

INTRODUCTION

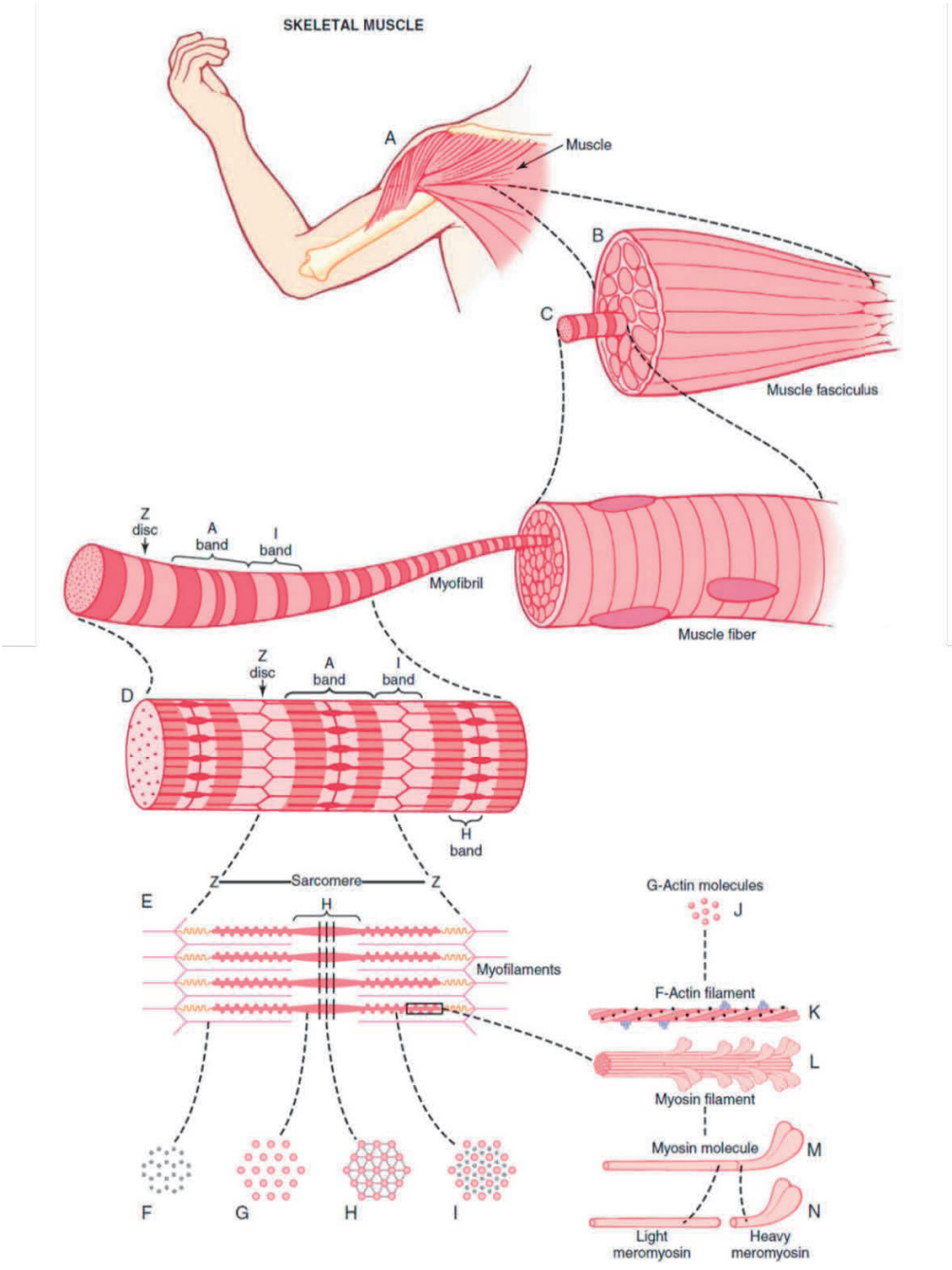

Figure 1. Organization of skeletal muscle, from gross to the molecular level. *A) whole muscle, B) fascicule, C) muscle fiber, D) myofibril, E) sarcomere, and transversal sections at different places (F, G, H, and I). J) G-actin molecules, K) F-actin filament, L) myosin filament, M) myosin molecule, and composition (N). From Guyton and Hall: Textbook of Medical Physiology 12th edition.*

I. CHAPTER 1: Skeletal muscle and contractile function

1.1. Macro and microstructure skeletal muscle

1.1.1. Muscle, fascicule, myofiber, and sarcomere

Approximately 40% of the bodyweight is produced by skeletal muscle which in normal conditions allows movement, force production, and heat generation. There are two types of muscles: the striated muscles, a highly organized tissue, and the smooth muscle, a non-organized one. The skeletal muscle, together with the cardiac muscle, belong to the striated muscle type.

A whole skeletal muscle (organ level) is composed of hundreds of fascicles (tissue level), each made of hundreds of fibers (cellular level). The fibers are big multinucleated cells formed by thousands of myofibrils that contain thousands of *myosin* filaments and *actin* filaments (molecular level) (Fig. 1A, 1B, 1C, and 1D). Each myosin filament or thick filament is made up of 200 individuals myosin molecules (Fig. 1L). One end of myosin molecule is made up of two heavy chains that wrap spirally around each other to form the *tail* or light meromyosin. On the other end, the two heavy chains fold bilaterally, associated with 4 light chains to form twice, a globular structure called *myosin's head* (or heavy meromyosin) (Fig. 1M-N). A myosin filament has a tridimensional relationship with actin filaments; the myosin's head interacts with 6 actin filaments around it (Fig. 1I). On one side of a myosin filament, tails stick together to form the body, while at the other side they hang out providing an arm that extends the heads. These protruding arms associated with the heads constitute the *cross-bridges* when they interact with the active site in the actin filament. Each actin filament or thin filament (Fig. 1K) is a large polymerized protein composed of two *F-actins* (filamentous actin) which form a helix. Each F-actin is composed of *G-actin* (globular actin) molecules. The F-actin double-stranded structure works as the backbone and its wrapped spirally by tropomyosin molecules which are intermittently associated with troponin molecules, a three subunits complex (troponin I, T, and C) (Fig. 2B). At rest, the tropomyosin-troponin complex covers the active site of the actin filament, preventing the interaction with the myosin's heads (Gordon et al., 2000; Mukund & Subramaniam, 2020).

These two types of filaments, thin and thick partially overlap (Fig. 1E) and generate a pattern of light and dark bands, that at the myofiber scale (Fig. 2), give the striated pattern. The light bands or *I bands* (isotropic to polarized light) represent the portions that only content actin filaments while the dark bands or *A bands* (anisotropic to polarized light) represent the overlap of myosin filaments with the end portion of actin filaments. As we can observe in Fig. 1E and Fig. 2, the other end of the actin filaments reaches an

antiparallel protein structure called the *Z disc*, which is perpendicular to the longitudinal axis in a muscle fiber. We can also observe a small elastic protein called *titin* (Fig. 1E and 2B) that connects the myosin filaments with the Z-disc at each side and helps to maintain the filament in place during and after a contraction. From one Z-disc to another, in a single myofiber is represented the contractile basic unit, called *sarcomere*. During muscle contraction, the cross-bridges interaction produces the *power stroke* to slide the actin filament with the reduction of the I band length, associated with the reduction of the sarcomere length (Gordon et al., 2000; Divet et al., 2007; Luther, 2009).

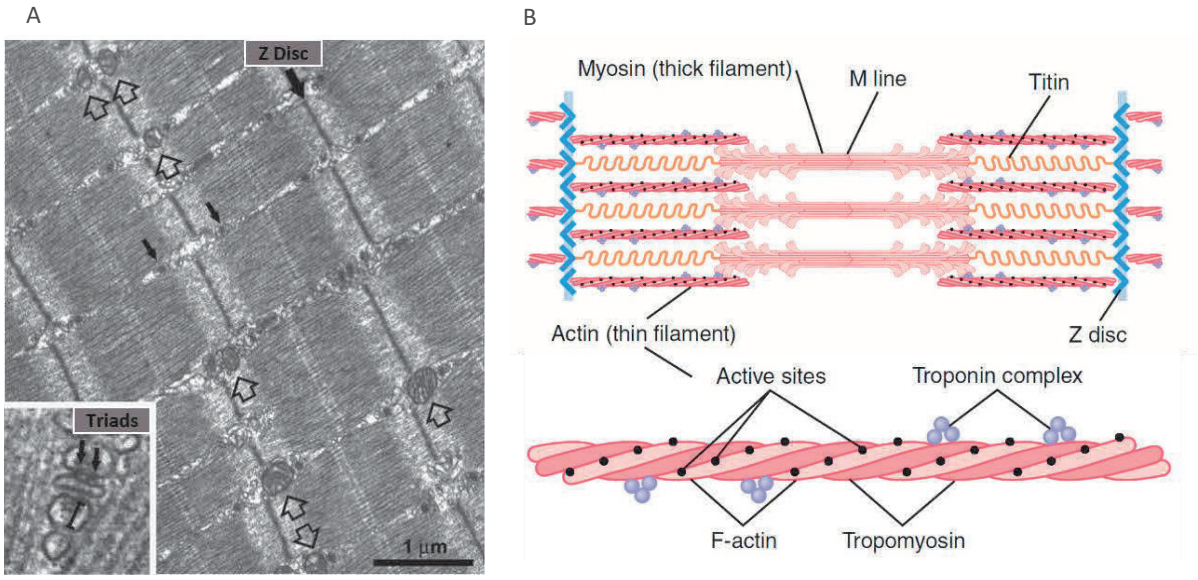

Figure 2. Skeletal muscle cellular organization: Sarcomere, T-tubule membrane and triads. *A) The architecture of Extensor Digital Longus (EDL) from Wild Type (WT) mice. Analysis by Electron Microscopy (EM). Image modified from Divet et al., 2007. Longitudinal section with several myofibril segments and sarcomeres well -aligned. At the bottom, a magnified picture of a triad (small arrows): the association of one T-tubule membrane (middle structure) with 2 terminal cisternae of the Sarcoplasmic Reticulum (at each side). B) Organization of proteins in a sarcomere and actin filament structure. Image is taken from Guyton and Hall: Textbook of Medical Physiology 12th edition.*

1.1.2. Sarcoplasmic reticulum, T-tubules and triads

A single adult skeletal muscle fiber, in normal conditions, has between 50-1000 nuclei (depending on its length) located at the periphery of the cell. These nuclei regulate and maintain the protein composition of the *sarcoplasm*; the fluid between the myofibers (Bruusgaard et al., 2003). The plasma

membrane, called "*sarcolemma"*, wraps the muscle fibers and produces membrane invaginations, called *T-tubules*, which are transversal organizations going deep into the fiber. From a sagittal perspective, one sarcomere is crossed by two T-tubules, which are located at the Z-disc level in the amphibians (Fig. 3), and at the A-I bands junctions in mammals. There is also a specialized endoplasmic reticulum surrounding the myofibers called the *sarcoplasmic reticulum (SR).* The SR spreads throughout the myofiber and creates a big network that extends inside along the fiber (Ogata & Yamasaki, 1997). Two main SR compartments are distinguished, the longitudinal SR and the junctional SR also referred to as SR terminal cisternae. The physical apposition of one T-tubule with two SR terminal cisternae at the level of the A-I bands intersection (in mammals) shapes a very important functional structure called the *Triad* (Fig. 3). The SR has an important role in skeletal muscle as a *calcium ion (Ca^{+2})* store and, in association with the T-tubules at the triad, allows an important step in the *Excitation Contraction Coupling (ECC)* process (Sandow, 1952), and the beginning of the *contractile cycle* (Franzini-Armstrong & Jorgensen, 1994; Gordon et al., 2000; Mukund & Subramaniam, 2020).

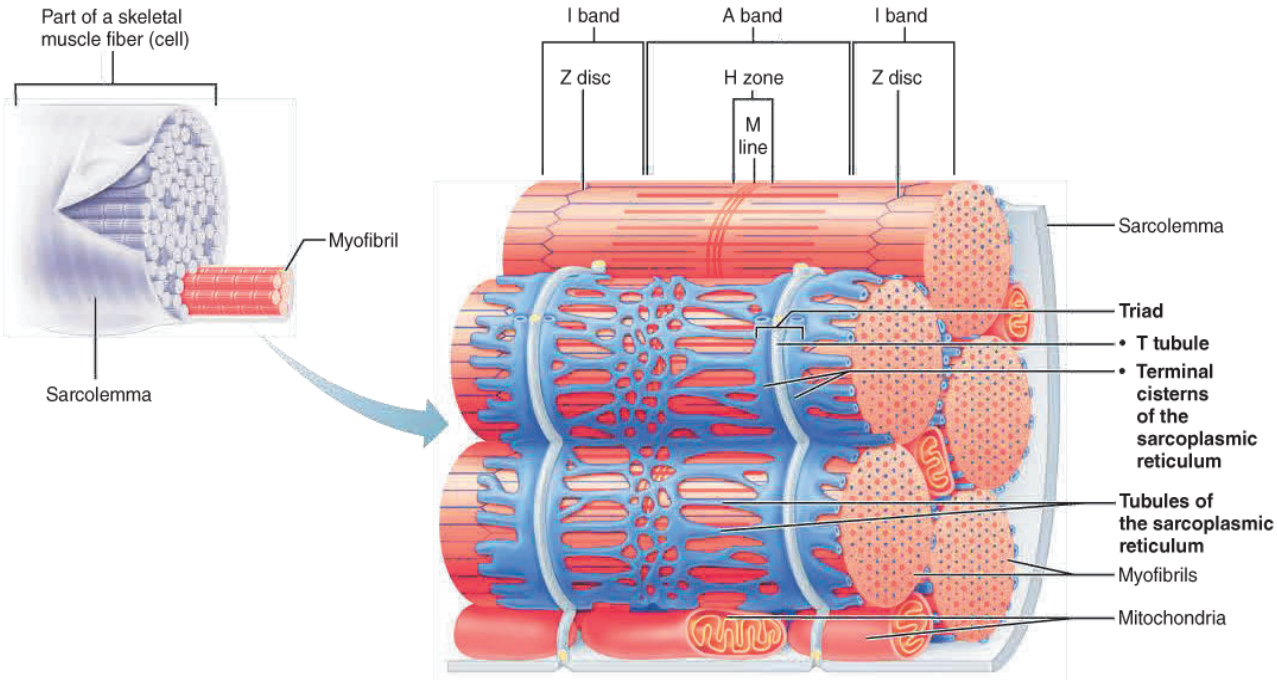

Figure 3. Organization of the muscle fiber membrane compartments in relationship with the Triads and myofibrils: *T-tubules and adjacent terminal cisterns of sarcoplasmic reticulum are lined up at the level of the A-I bands junctions. The contractile unit "sarcomere" is crossed by two T-tubules in white. In blue, the organization of the longitudinal, and junctional SR interaction with the T-tubules forming the Triads. It is also shown the mitochondria position within the fibers and its relationship with respect to the myofibrils. The image was taken from Guyton and Hall: Textbook of Medical Physiology 12th edition.*

1.2. Skeletal muscle function

1.2.1. Action potential and Excitation-contraction coupling

Muscle contraction begins with the generation of an *action potential (AP)* in the muscle fiber. An action potential is an all-or-nothing transient and regenerative electrical response, in which the *membrane potential (V_m)* rapidly rises from a *negative resting voltage (V_{rest})* to a peak approaching +50 mV, the equilibrium potential for *sodium ions (Na^+)*. The generation of an action potential starts with a small depolarization from V_{rest} to a threshold level (≈ -40 mV) that activates voltage-dependent Na^+ channels.

The initial small depolarization of the muscle fiber is generated by the *α-motoneuron*, at the *synapse* with the sarcolemma, called *Neuromuscular Junction (NMJ).* The NMJ is normally located near the center of the fiber and is composed of 1) the axon terminal of the α-motoneuron, 2) the sarcolemma of the fiber with junctional folds and 3) the space between them, called *synaptic space*.

The axon terminal depolarization produces Ca^{2+} entry into the cytosol of the α-motoneuron which triggers the exocytosis of vesicles into the synaptic space (Katz & Miledi, 1967). These vesicles are filled with an excitatory transmitter called *acetylcholine (ACh)* (Hubbard, 1973; Katz, 1996). In this region, ACh diffuses into the junctional folds of the sarcolemma, which have a high expression of nicotinic acetylcholine-gated channels, called *acetylcholine receptors (AChR)*. Once two ACh molecules bind to one AChR, there is a conformational change that opens the channel, producing an inward (positives charges from the extracellular space into the cytosol) Na^+/Ca^{2+} small current. This generates a small depolarization or *endplate potential (EPP)*, which shifts V_{rest} towards more positive values reaching the AP threshold. This causes the opening of *voltage-dependent Na^+ channels ($Na_V1.4$)* concentrated at the bottom of the junctional folds, generating the firing of the action potential that propagates through the sarcolemma (Adrian et al., 1970; Bezanilla et al., 1972; Adrian & Marshall, 1977).

Subsequently, the AP propagates axially along the myofiber, and radially deep into the fiber (Huxley & Taylor, 1958; Adrian et al., 1969) through the T-tubules, activating the *L-type Ca^{2+} channel ($Ca_V1.1$)* that is highly expressed in this region initiating the process called *excitation-contraction coupling (ECC)*. During the membrane depolarization in ECC, $Ca_V1.1$ suffers a conformational change that opens the *type 1 ryanodine receptor* (*RyR1)* through a physical interaction. The opening of RyR1, a Ca^{2+} channel located in the SR generates Ca^{2+} release from the sarcoplasmic reticulum into the cytosol. Ca^{2+} interacts with the actin-myosin machinery starting the contractile cycle (Rebbeck et al., 2014; Hernandez-Ochoa & Schneider, 2018).

Repolarization of the sarcolemma is due to the inactivation of $Na_V1.4$ and the opening of voltage-dependent and voltage-independent K^+ channels ($K_V1.4$, $K_V3.4$, $K_V7.5$, Kir2.1, Kir6.1, KCa1.1) and voltage-dependent Cl^- channels (ClC1 and ClC2) (Jurkat-Rott et al., 2006).

1.2.2. Contractile cycle

The contractile cycle is a chain of biochemical reactions that produce the conformational change of the myosin's motor domain and the formation of the cross-bridges with the actin filament. From a microscopic perspective, this generates the sliding of actin filaments along the myosin filaments. From a

macroscopic perspective, the muscle contraction. This series of reactions need Ca^{2+} and energy from the high-energy bonds in the *adenosine triphosphate (ATP)* molecule. In the absence of Ca^{2+}, the interaction of the myosin's heavy chain with the actin filaments is inhibited by the troponin-tropomyosin complex wrapped around the actin filaments active sites (Fig. 2B). At rest, the troponin complex (T, I, and C subunits) maintain tropomyosin bound to the actin filament, which inhibits the actin active site that interacts with the myosin's heavy chains. As a consequence of ECC, cytosolic Ca^{2+} concentration increases and interacts with the troponin C subunit, which changes troponin complex affinity for actin. This rotates tropomyosin, setting the actin filament's active sites free, and allowing its interaction with the myosin's head. All cross-bridge cycling can be resumed in four main steps (Goody, 2003):

1. The myosin head binds ATP. ATPase activity cleaves ATP, producing ADP and phosphate ion which stay bound to the head. This process produces a conformational change of the myosin's head which stores energy like a "spring".
2. The troponin-tropomyosin complex binds Ca^{2+} and uncovers the actin filament's active sites allowing myosin heads interaction.
3. The interaction between the myosin's head and the actin filament's active site produces a conformational change in the head and the arm which tilts around the myosin's hinge. This change uses the phosphate energy stored in the myosin's head and power stroke to pull the actin filament.
4. After myosin's head tilts, it releases the ADP and phosphate ion stored before, allowing binding of a new ATP molecule and the detachment of the myosin's head from the actin. After the head detaches, a new ATP molecule is cleaved to start a new cycle.

A

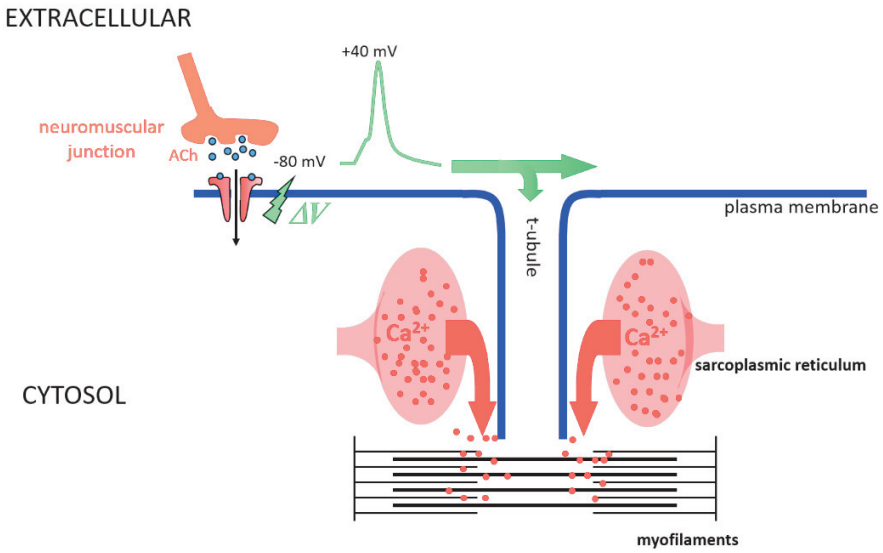

B

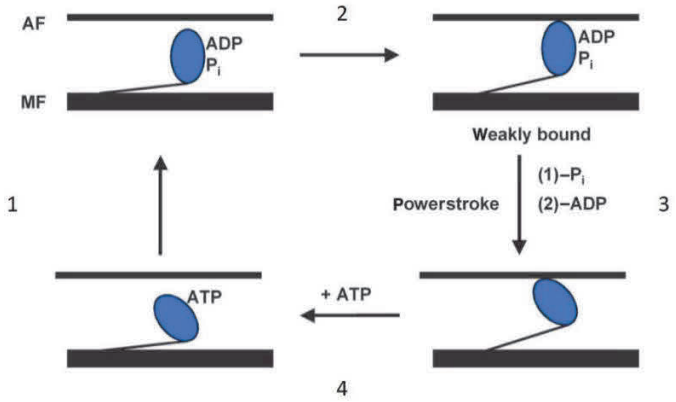

Figure 4. Action potential and contractil cycle*. A) Scheme of Action Potential generation and propagation through the sarcolemma, T-tubules and Ca^{2+} release into cytosol upon a membrane depolarization (ΔV) that produce and action potential. Modified from Goody et al 2003. B) Cross-bridges cycling. Actin filament (AF) and myosin filament (MF).*

II. CHAPTER 2: Excitation-contraction coupling: molecular mechanism and regulators

2.1. T-tubule organization, triads and $Ca_V1.1$ in ECC

2.1.1. Role of T-tubule organization and triads

The action potential propagates deep into the fiber through the T-tubules. The T-tubules are membrane invaginations that penetrate through the muscle fiber, from one side to the other, interlacing between the myofibrils. Because they are an extension of the sarcolemma, they are in contact with the extracellular space on one side and with the cytosol on the other, and thus, they transmit the action potential (see Rall, 2020).

As introduced in the first chapter, upon T-tubules depolarization, an important interaction between $Ca_V1.1$ and RyR1 occurs at specific junctions called triads. Each triad consists of two sarcoplasmic reticulum terminal cisternae flanking one T-tubule (Flucher, 1992). At these specific sites, both membranes, T-tubule and SR interact through a multi-molecular calcium release complex (CRC). The organization and disposition of the triad are critical for the normal cross-talk between $Ca_V1.1$ and RyR1 (Franzini-Armstrong & Jorgensen, 1994). This organization allows the direct and physical transduction of the $Ca_V1.1$ conformational change into RyR1 opening, playing a critical role in ECC (Flucher & Franzini-Armstrong, 1996). The CRC at the triads also contains several regulatory proteins like calsequestrin, junctin, and triadin which can regulate the RyR1 function or the organization of the molecular complex (Flucher, 1992). At the triad, RyR1 feet interact with an arrangement of four $Ca_V1.1$ assembled together, called tetrads (Block et al., 1988). The close relationship between the RyR1 feet and the tetrads is needed for the correct ECC, but surprisingly, in a row of RyR1 there is an alternated presence of $Ca_V1.1$ tetrads and empty spaces. This generates two populations of RyR1; the first one, is in close apposition with a $Ca_V1.1$ tetrad, while the second one, is not (Franzini-Armstrong & Kish, 1995).

2.1.2. $Ca_V1.1$ family

In mammals, $Ca_V1.1$ belongs to a large family of voltage-gated Ca^{2+} channels (VGCCs) which are present in different tissues. This large family of VGCCs has been classified by the different types of Ca^{2+} currents based on physiological and pharmacological criteria. The L-type group is present in skeletal, smooth, and cardiac muscle. It is characterized by high-voltage activation, high single-channel conductance, and a slow voltage-dependent inactivating Ca^{2+} current. The T-type group is present in

Note: For simplicity, we will use the standard symbols ($Ca_V1.1$, RyR…) when referring to the protein and the same terminology with upper case and italicized fonts (*CAV1.1*, *RYR1*) when referring to the corresponding gene and mutations.

various tissues including dorsal root ganglion neurons. It is characterized by low-voltage activation, small single-channel conductance, and a rapidly-inactivating Ca^{2+} current. The last group is present principally in neurons. It is characterized by a Ca^{2+} current faster than L-type, but slower than T-type. It was initially called N-type, but was finally divided into three groups: N-type, P/Q, and R-type because of differences in toxin sensitivity. Thus, VGCCs family can be classified into Ca_V1 (L-type), Ca_V2 (N, P/Q, R), and Ca_V3 (T-type) Ca^{2+} channel types (see Table 1) (Catterall, 2011).

Among these, Ca_V1 channels are subdivided into $Ca_V1.1$, $Ca_V1.2$, $Ca_V1.3$, and $Ca_V1.4$ whose principal subunit α1 is encoded by the *CACNA1S*, *CACNA1C*, *CACNA1D*, and *CACNA1F* genes to produce α1S ($Ca_V1.1$), α1C ($Ca_V1.2$), α1D ($Ca_V1.3$), and α1F ($Ca_V1.4$) subunits, respectively (Ertel et al., 2000). They are part of L-type high-voltage-activated Ca^{2+} channels, exhibiting a similar structure but different tissue distribution (skeletal, smooth, and cardiac muscle). They present an L-type Ca^{2+} current which can be inhibited using Ca^{2+} antagonist drugs like dihydropyridines, phenylalkylamines, and benzothiazepines. $Ca_V1.1$ is the only isoform present in the T-tubule of the skeletal muscle fibers, while $Ca_V1.2$ is present in heart muscle and $Ca_V1.4$ in neurons (see table 1) (Catterall, 2011; Bannister & Beam, 2013). The L-type voltage-dependent Ca^{2+} channels (Ca_V1) are also known as 1,4-dihydropyridine receptors (DHPR) because of the L-type Ca^{2+} current sensitivity to dihydropyridine drugs (Tanabe et al., 1987).

2.1.3. $Ca_V1.1$ structure and subunits

At the structural level, Ca_V1 are protein complexes (440 kDa) composed of 4 subunits: 1) the principal transmembrane subunit *α1* which supports the channel ion conductance, 2) an extracellular subunit *α2*, 3) an intracellular subunit *β1* and 4) a transmembrane subunit *γ1* (Fig. 5A). In skeletal muscle, the isoforms that form $Ca_V1.1$ are *α1S, α2-δ*, *β1a*, and *γ1*. The subunits α2-δ, β1a, and γ1 have auxiliary functions (see below for further details) modulating the activation and inactivation kinetics, gating properties, and membrane trafficking of the α1S subunit, which is responsible for pore permeability and sensitivity to the changes in the membrane potential. $Ca_V1.1$ has unique characteristics that differentiate it from the rest of VGCCs, principally because of its α1S subunit (α1C is expressed in the heart), with the slowest current activation and inactivation kinetics (Bannister & Beam, 2013; Hernandez-Ochoa & Schneider, 2018).

2.1.4. α1S subunit of $Ca_V1.1$

The α1S subunit of $Ca_V1.1$ is coded by the *CACNA1S* gene located in the q32 position, chromosome 1 (Schartner et al., 2017). It is a protein of 2000 amino acid residues (190 kDa), organized into 4

homologous, voltage-sensing domains (I-IV) (VSDs), each with 6 transmembrane segments (S1-S6), connected by intracellular and extracellular loops, and it has a three-dimensional structure close to α-subunits of Na^+ and K^+ voltage-dependent channels, with the segments S1 to S4 providing the voltage sensitivity (Catterall, 2000). More specifically the S4 segment has 4-5 positively charged amino-acid residues, which confer the voltage-sensing properties to the channel (Fig. 5B) (Bezanilla, 2008). These amino-acids move in response to the change in the electrical field, produced by the change in the membrane potential, and generate the $Ca_V1.1$ conformational changes needed for activating its functions (Bannister & Beam, 2013; Hernandez-Ochoa & Schneider, 2018). The selectivity of voltage-dependent L-type Ca^{2+}channels for Ca^{2+} involves four conserved glutamate residues distributed in equivalent position on the pore region of each VSD (I-IV). All of them have a contribution in Ca^{2+} binding with the one in repeat III having the strongest effect (Yang et al., 1993).

The α1S subunit of $Ca_V1.1$ is critical for muscle function, and therefore for life. Genetic ablation produces a lethal mouse model, called dysgenic mouse, where ECC and L-type Ca^{2+} current are lost, causing postnatal death due to respiratory failure (Tanabe et al., 1988).

The carboxyl-terminus of α1S and the cytoplasmic II-III, and III-IV loops are believed to interact directly or indirectly with the amino-terminal (N-terminus) region of RyR1, which bridge the 12 nm of myoplasm (cytosolic space) between the sarcolemma and the SR (Bannister, 2007). An electron microscopy study has shown that administration of 500 μM of ryanodine, (a RyR1 blocker at that concentration), produces a change in the distance between two $Ca_V1.1$ within a tetrad, from 19.5 nm to 17.5 nm, providing evidence for the physical interaction between both proteins (Paolini et al., 2004b). In the nineties, two groups showed the relevance of the α1S II-III loop for this interaction and for the ECC. The first group generated several chimeras including one made of α1S (skeletal isoform) II-III loop in α1C (cardiac isoform), and expressed them in dysgenic myotubes (myotubes not expressing $Ca_V1.1$): this allowed identifying the II-III loop as the principal contributor in the ECC (Tanabe et al., 1990). The second group synthesized the II-III loop peptide, and applied it to RyR1 channel reconstituted in a lipid bilayer to measure RyR1 single-channel activity (experiment explained in 2.6 B). They observed an increased RyR1 open probability in the presence of the peptide, providing further evidence for the interaction and regulation of RyR1 activity by the α1S II-III loop (Lu et al., 1994).

The α1S carboxyl-terminus (C-terminus) in skeletal muscle contains a PDZ domain (residues 1543-1647) that is critical for targeting α1S to the triad, as expression of a α1S chimeras together with a C-

terminus from α1A (neuron isoform without this PDZ domain) prevents $Ca_V1.1$ surface expression in dysgenic myotubes (Flucher et al., 2000).

The α1S III-IV loop is not directly involved in ECC but can control Ca^{2+} release from the SR by regulating $Ca_V1.1$ gating (Bannister et al., 2008), and mutations affecting this domain have been associated with the pharmacogenetic disorder malignant hyperthermia (Jurkat-Rott et al., 2000).

Finally, it has been shown that the α1S amino-terminus (residues 2-37) is not essential for ECC, but that its integrity is necessary for $Ca_V1.1$ sarcolemmal expression (Bannister & Beam, 2005) (for more detail see Bannister et al. 2007).

2.1.5. β1a, α2δ-1 and γ1 subunits of $Ca_V1.1$

The β1a subunit of $Ca_V1.1$ is coded by the *CACNB1* gene present in chromosome 17 in human. It has a modular structure consisting of five distinct regions and interacts directly with the α1S I-II loop. It is essential for $Ca_V1.1$ function, localization, and ECC. It has been shown that the genetic ablation of *CACNB1* is lethal in mouse: it severely compromises α1S proper localization and prevents ECC in myotubes (Gregg et al., 1996). Schredelseker et al. in 2005 studied the β1a-null zebrafish myotubes and observed a significant reduction of the amount of intramembrane charge movement, which is a measure of $Ca_V1.1$ density at the sarcolemma (see 2.2.B for details). They observed a normal $Ca_V1.1$ triad organization (SR-T-tubules junctions), but a loss of ECC, even though the fibers were still responsive to caffeine, a RyR1 agonist, generating SR Ca^{2+} release. More importantly, using freeze-fracture analysis of $Ca_V1.1$ clusters, they observed that the lack of β1a prevents the skeletal muscle characteristic arrangement of $Ca_V1.1$ in tetrads. Normally the tetrads are organized into orthogonal arrays, and in opposition to the RyR1 subunits, which is essential for ECC in differentiated skeletal muscle. They probed that the lack of β1a produces the loss of tetrads organization, the disruption of $Ca_V1.1$-RyR1 interactions, and the loss of ECC (Schredelseker et al., 2005), while the expression of β1a restores tetrads organization and ECC (Schredelseker et al., 2009). It has been proposed that β1a acts as a glue that holds together $Ca_V1.1$ and RyR1, and that β1a interacts with RyR1 too. Several studies have proposed that the β1a C-terminus could have an important role in $Ca_V1.1$-RyR1 interaction (see Bannister et al., 2013). The α2δ-1 deletion results in a viable mouse with no significant alteration in muscle function but with slower L-type Ca^{2+} current kinetics (Obermair et al., 2005). No apparent adverse mouse phenotype was reported upon deletion of γ1 either and the subunit was concluded to be unessential for SR Ca^{2+} release and force production (Ursu et al., 2001). However, muscle fibers from the $\gamma^{-/-}$ mice were found to exhibit a right-shifted voltage-dependence of

both Ca^{2+} current and SR Ca^{2+} release inactivation (Ursu et al., 2004). Further work by the same team then led to the conclusion that the subunit acts as a Ca^{2+} antagonist, and could limit Ca^{2+} entry and Ca^{2+} release under stress conditions (Andronache et al., 2007).

Ca^{2+} current type	**α1 Subunits**	**Specific blocker**	**Principal physiological functions**	**Inherited diseases**
L	$Ca_V1.1$	DHPs	Excitation-contraction coupling in skeletal muscle, regulation of transcription.	Hypokalemic periodic paralysis.
	$Ca_V1.2$	DHPs	Excitation-contraction coupling in cardiac and smooth muscle, endocrine secretion, neuronal Ca^{2+} transients in cell bodies and dendrites, regulation of enzyme activity, regulation of transcription.	Timothy syndrome: cardiac arrhythmia with developmental abnormalities and autism spectrum disorders.
	$Ca_V1.3$	DHPs	Endocrine secretion, cardiac peacemaking, neuronal Ca^{2+} transients in cell bodies and dendrites, auditory transduction.	
	$Ca_V1.4$	DHPs	Visual transduction.	Stationary night blindness.
N	$Ca_V2.1$	ω-CTx-GVIA	Neurotransmitter release, Dendritic Ca^{2+} transients	
P/Q	$Ca_V2.2$	ω-Agatoxin	Neurotransmitter release, Dendritic Ca^{2+} transients	Familial hemiplegic migraine, cerebellar ataxia.
R	$Ca_V2.3$	SNX-482	Neurotransmitter release, Dendritic Ca^{2+} transients	
T	$Ca_V3.1$ $Ca_V3.2$ $Ca_V3.3$	None	Pacemaking and repetitive firing Pacemaking and repetitive firing	Absence seizures

Table 1: From Catterall et al, 2011. Subunit composition and function of Ca^{2+} channel types

Abbreviations: DHP, dihydropyridine; ω-CTx-GVIA, ω-conotoxin GVIA from the cone snail conus geographus, SNX-482, a synthetic version of a peptide toxin from the tarantula Hysterocrates gigas.

2.2. $Ca_V1.1$ functions

2.2.1. $Ca_V1.1$: A voltage-sensor for excitation-contraction coupling

In skeletal muscle, $Ca_V1.1$ works as a voltage-sensor activating the ECC (Schneider & Chandler, 1973; Beam et al., 1986; Rios & Brum, 1987; Tanabe et al., 1987; Adams et al., 1990; Tanabe et al., 1990). It is important to highlight that in skeletal muscle, ECC operates distinctively from that in heart muscle. In skeletal muscle, there is a direct and physical interaction between $Ca_V1.1$ and RyR1 to produce RyR1 opening (Block et al., 1988; Paolini et al., 2004b), while in the cardiac muscle, Ca^{2+} entry through the $Ca_V1.2$ channel activates RyR2 channel by a process called calcium-induced calcium release (CICR) (for more details see next chapter) (Cannell et al., 1995; Dirksen & Beam, 1999).

2.2.2. $Ca_V1.1$: Non-linear capacitive current and charge movement

Associated with $Ca_V1.1$ conformational change there is an important event called the *"Intramembrane Charge Movement" (charge movement)* that was predicted by Hodgkin and Huxley in 1952 and revealed in the early years of ECC investigations (Schneider & Chandler, 1973). In skeletal muscle, the charge movement is produced during the conformational change of the $Ca_V1.1$ channel as a consequence of the movement of amino-acids with positive charge present in the S4 segment of each homologous *voltage-sensitive domain (VSD)* of the α1S subunit. This movement of positively charged residues (4-6 amino acids; lysine or arginine) generates a nonlinear intramembrane small capacitive current, that can be measured in the absence of all ionic currents, following subtraction of the linear capacitive current. This current can be used to calculate the total quantity of displaced charge or charge movement (Schneider & Chandler, 1973; Hernandez-Ochoa & Schneider, 2018). All transmembrane proteins with charged residues can generate charge movements, like Na^+ or K^+ voltage-dependent channels (Bezanilla, 2000), but because of the very high density of $Ca_V1.1$ in the skeletal muscle T-tubule membrane, it is generally accepted to be the main contributor to the charge movement induced by T-tubules depolarization in skeletal muscle (Tanabe et al., 1988; Adams et al., 1990). The non-linear capacitive current (charge movement) represents α1S kinetics. Upon membrane depolarization, the VSDs (S4 segment from each homologous domain in α1S) move from a resting state, with the positive charges toward the cytosol, to an activated state, with the positive charges toward the extracellular space. In the process of activation, this chronologically generates: 1) A non-linear capacitive positive current called Q_{on}, 2) the conformational change of $Ca_V1.1$, which activates RyR1-dependent SR Ca^{2+} release, and 3) the opening of the α1S pore allowing the L-type Ca^{2+} current. At the end of the membrane depolarization, the

positive charges of the voltage-sensing domains return to their original position, the resting state, and generate in the process an equal (to Q_{on}) and negative non-linear capacitive current called Q_{off} (Rios et al., 1992). Q_{on} and Q_{off} are a measurement of charge movement and allow the study of activation and inactivation kinetics of α1S, respectively. The amount of Q_{on} and Q_{off} are employed to study the voltage dependence of activation and inactivation, using the Boltzmann equation to fit the relationships (Hernández-Ochoa & Schneider, 2012) (see Fig. 5). In this process, there is an almost simultaneous coordination between the activation of all α1S in the membrane (Q_{on}), and the beginning of RyR1-dependent SR Ca^{2+} release. However, the generation of the Ca^{2+} current is an extremely slow (100-10 ms time constant of activation) process. It has remained unclear how the same VSDs control these two processes at completely different speeds. Recent studies from Olcese's group presented at the Biophysical Congress in 2019 proposed the first possible explanation to this subject. They used voltage-clamp fluorometry to study each VSDs (I-IV) individually and recorded the ionic current and individual fluorescence studying their kinetics and voltage dependence. They found that VSD-I is the domain that is most sensitive to membrane potential changes but also exhibits similar time-dependent properties to Ca^{2+} current activation, while VSD II-IV displayed faster activation, compatible with RyR1-dependent SR Ca^{2+} release. They confirm their result using; 1) a structurally-relevant allosteric model of $Ca_V1.1$ activation, which shows that $Ca_V1.1$ opening is mostly driven by VSD-I activation, and 2) using a charge neutralizing mutation (R174W, replacing an arginine for tryptophan in position 174) in VSD-I, which impaired $Ca_V1.1$ activation by stabilizing VSD-I in a resting state. In a second study, they observed that VSD-I and VSD-IV are activated at more hyperpolarized potentials than VSD-II and VSD-III, and that the VSD-I and VSD-II displayed a slow activation kinetics, while VSD-III and VSD-IV activated rapidly. Finally, they studied the movement of the VSDs under physiologically-relevant action potential clamp (skeletal muscle AP) and observed no clear structural rearrangement of the slowest VSDs but a readily activated response of VSD-III and VSD-IV. Using all of these results they conclude that VSD-III is the best candidate as a sensor conferring voltage-dependent properties related with RyR1-dependent SR Ca^{2+} release (Savalli et al., and Angelini et al., unpublished data from Biophysical Congress, Volume 118, 105a and 498a, 2019).

2.2.3. $Ca_V1.1$: A voltage-dependent L-type Ca^{2+} channel

The macroscopic Ca^{2+} current through $Ca_V1.1$ has been used to study its functional state over the years (Bannister et al., 2009). Despite $Ca_V1.1$ channel properties, the Ca^{2+} current has been proved not to play a relevant role in the ECC process in adult skeletal muscle fibers, where the skeletal ECC has been defined as Ca^{2+} current-independent (Chiarandini et al., 1980; Gonzalez-Serratos et al., 1982;

Schredelseker et al., 2010). As mentioned before, the $Ca_V1.1$ channel exhibits slow opening kinetics (Catterall, 2000) and needs longer depolarization time (at least 80 ms) than normally produced by an action potential (≈2 ms), to generate a substantial macroscopic Ca^{2+} current. Still, even if the Ca^{2+} current role in ECC has been discarded, its physiological relevance in skeletal muscle Ca^{2+} homeostasis remains controversial. At some point it was postulated to be independent of a "supposedly" new process called excitation-coupled Ca^{2+} entry (ECCE) before ECCE was admitted by the same groups to be essentially carried by $Ca_V1.1$ (Cherednichenko et al., 2004; Bannister et al., 2009). More recently, $Ca_V1.1$-mediated Ca^{2+} entry was suggested to have an important role in SR loading under intense solicitation of the ECC machinery (Robin & Allard, 2015).

Another function for $Ca_V1.1$ Ca^{2+} current was proposed by Lee et al. in 2015. This group generated a mouse with a mutation in *CAV1.1* (E1014K, substitution of a glutamate for a lysine in position 1014), which produces a defect in binding/permeation sites for Ca^{2+} in the pore. They showed a relationship between the loss of Ca^{2+} permeation and CAMKII activation and refilling of sarcoplasmic reticulum Ca^{2+} stores, leading to downstream alterations of the signaling pathway-related to protein synthesis (Ras/Erk/mTORC1). Overall consequences were increased fatigue, decreased fiber size, and increased IIb fibers type expression (Lee et al., 2015).

During development, a "developmental isoform of $Ca_V1.1$" ($Ca_V1.1_e$) is expressed in embryonic skeletal muscle. This $Ca_V1.1_e$ generated by skipping exon 29, which produces a smaller (19 amino acids less) extracellular loop S3-S4 in the fourth homologous VSD of α1S (Tuluc et al., 2009). This isoform can still activate ECC coupling independently of Ca^{2+} current, but presents a Ca^{2+} current conductance 6-8 times larger than the full adult $Ca_V1.1$ (see Fig. 7B), and has been associated with muscle weakness in myotonic dystrophy (Tang et al., 2012). In a recent study by Sultana et al. in 2016, the deletion of exon 29 from the α1S in adult $Ca_V1.1$ as achieved to generate a mouse model expressing an embryonic-$Ca_V1.1$-like isoform. The mice did not show motor performance alterations, but they presented a decrease in grip force and voluntary running. Authors also studied the Ca^{2+} current, Ca^{2+} handling, isolated muscle force, and myosin isoforms expression from this model and observed an increase in $Ca_V1.1$ Ca^{2+} influx, the presence of $Ca_V1.1_e$-dependent Ca^{2+} sparks, a decrease in contractile force (single twitch and tetanus), an increase in endurance, and an increase of expression of a slower myosin isoform. Hence, they concluded that Ca^{2+} influx has an important role in the regulation of fiber type composition (Sultana et al., 2016).

Nevertheless, Dayal et al. in 2017 derived strikingly different conclusions using a homozygous mutant mouse model expressing a non-conducting $Ca_V1.1$, elaborated with the N617D (substitution of

Asparagine for aspartate in position 617 in the α1S subunit) mutation that imitates the normal zebrafish $Ca_V1.1$ isoform which does not carry Ca^{2+} current. Using this model, they showed no difference in SR Ca^{2+} release, locomotor activity, motor coordination, muscle strength, and susceptibility to fatigue. They concluded that $Ca_V1.1$-mediated Ca^{2+} influx in mammalian skeletal muscle is an evolutionary remnant with no physiological role (Dayal et al., 2017).

The different conclusions reached by these groups about the physiological role of $Ca_V1.1$-mediated Ca^{2+} influx were obtained with the use of distinct models and α1S mutations sites. More

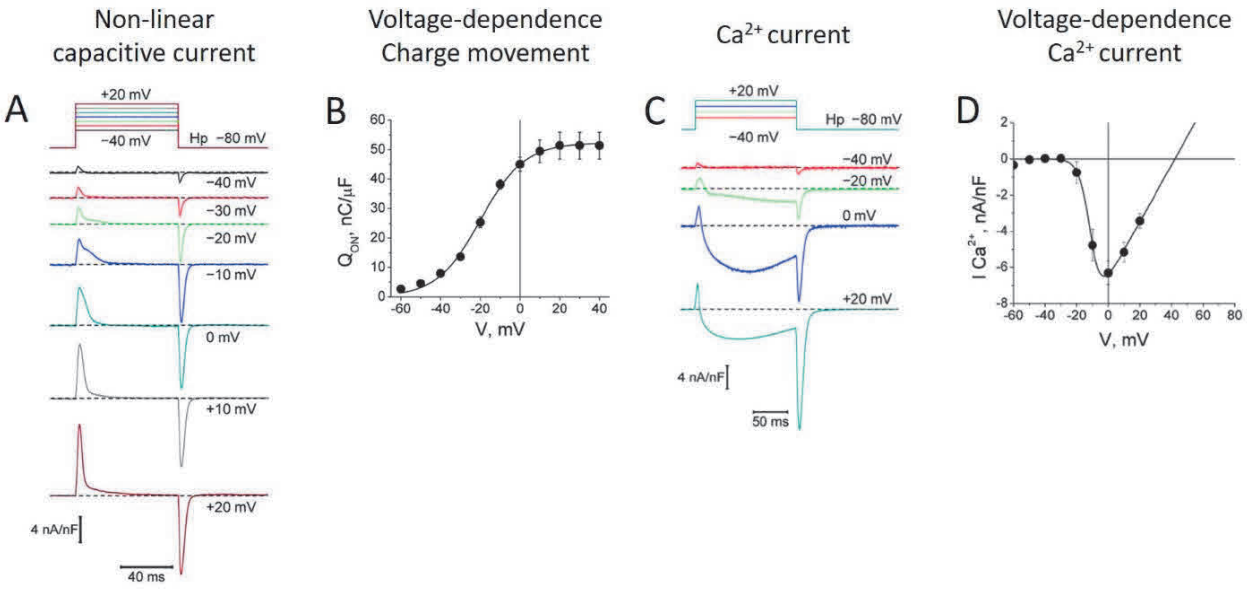

Figure 5. Classical experiments to study $Ca_V1.1$ function in differentiated skeletal muscle fibers. *A) Non-linear capacitive currents generated by several voltage-clamp depolarizing pulses of increasing amplitude (from -40mV to +20 mV) from a resting voltage or holding potential (Hp) of -80mV. B) Estimation of the quantity of charge moved at the beginning of the pulse (Q_{ON}) and its voltage-dependence. The values are shown as the total charge normalized by the capacitance (nC/µF) at each voltage. C) Ca^{2+}current generated by voltage-clamp depolarizing pulses of increasing amplitude from a Hp= -80mV. D) Voltage-dependence of peak Ca^{2+}current. Values are normalized by the capacitance (nA/nF). Data taken from Hernandez-Ochoa & Schneider, 2012.*

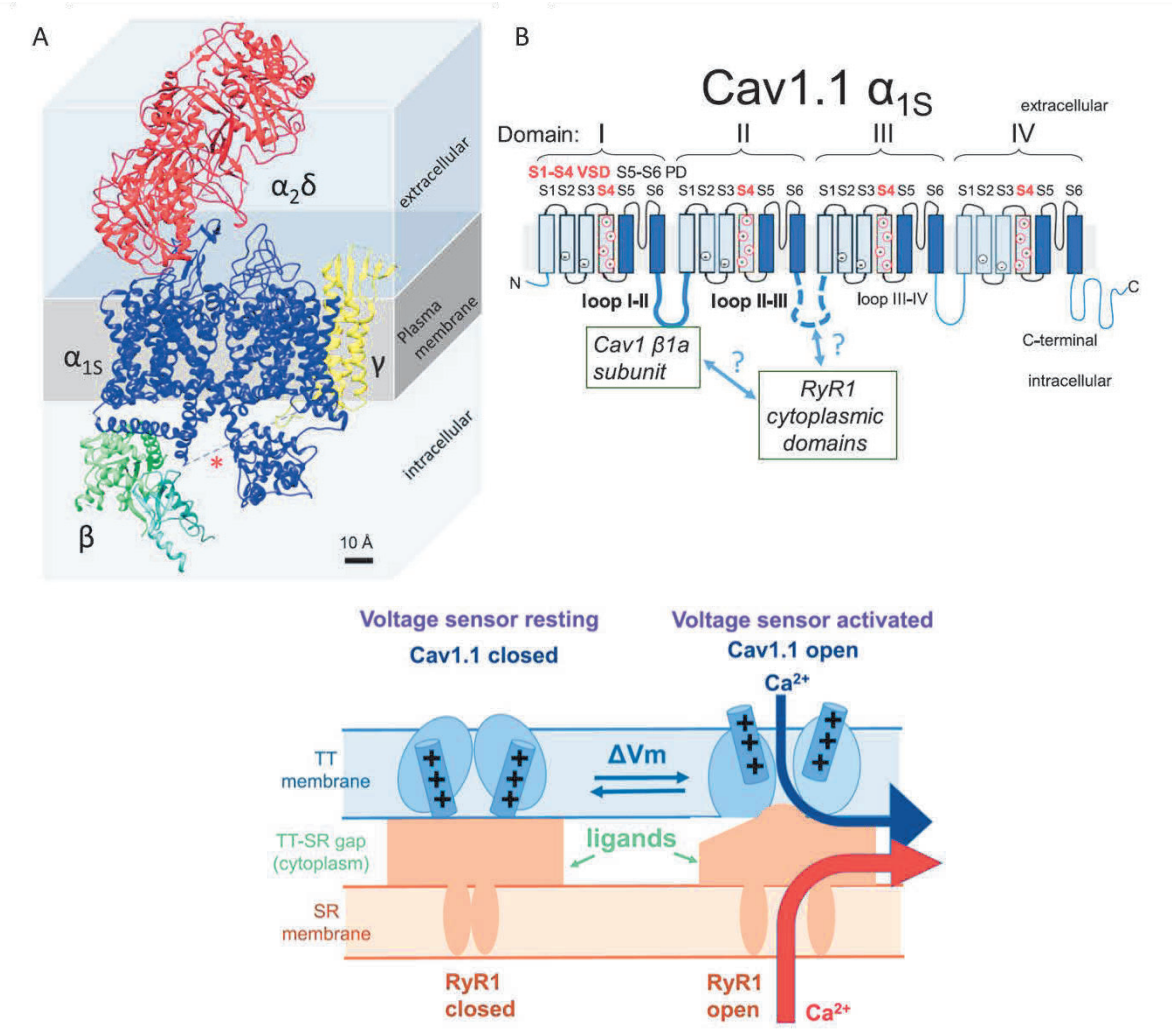

Figure 6. L-type voltage-dependent Ca^{2+} channel ($Ca_V1.1$): Structure and function. *A) Side view of a cryo-EM reconstruction of the DHPR or $Ca_V1.1$; B) Molecular structure of $Ca_V1.1$ α1S subunit. C) Representation of positive charges and their displacement during L-type Ca^{2+} current and ECC in a triad. Images taken from Hernandez-Ochoa & Schneider, 2018.*

importantly, these mutation sites generate different changes in the $Ca_V1.1$ channel properties, making it difficult to conclude on the physiological role for Ca^{2+} influx/current.

2.2.4. $Ca_V1.1$: A frequency-dependent voltage-sensor for excitation-transcription coupling

In the last decade, a new function has been revealed for $Ca_V1.1$ in skeletal muscle, that relates his voltage sensor activity to transcriptional changes in skeletal muscle fibers. For this, $Ca_V1.1$ works as an action-potential's frequency sensor in the process called excitation-transcription coupling (ETC) (Jorquera et al., 2013).

In ETC, as in ECC, one major protagonist is $Ca_V1.1$ which participates in activating a series of signaling transduction steps that result in a gene expression change dependent on the frequency of stimulation. In adult muscle fibers these transcriptional changes are associated with plasticity in muscle fibers. In particular, Jorquera et al. (2013) reported a pathway that is activated at a low frequency of electrical stimulation (less than 50 Hz), and that relies on the activation of ATP release, the production of Inositol triphosphate (IP3), and is associated with the change from fast-twitch to slow-twitch muscle fiber phenotype (Jorquera et al., 2013). This pathway is dependent on the frequency of electrical stimulation according to a gaussian shaped intensity of response that produces maximum values within 10-20 Hz (Casas et al., 2010). In this process, $Ca_V1.1$ interacts with a membrane protein called *Pannexin 1 (Panx1)*, that has an important role in ETC in both myotubes and adult skeletal muscle fibers (Buvinic et al., 2009; Jorquera et al., 2013), and that I will discuss in details in the 4th chapter of this Introduction because of its relevance to my project.

2.3. $Ca_V1.1$ in skeletal muscle pathologies

$Ca_V1.1$ is exclusively expressed in skeletal muscle and has a critical role in ECC. As previously shown its principal subunit is the α1S confers the voltage sensitivity, forms the pore, and is responsible for orthograde regulation of ECC. Consequently, α1S mutations will potentially produce muscle diseases. Up to this date, 4 different types of $Ca_V1.1$-related diseases have been shown to be produced by mutations or splicing defects in the α1S gene (*CACNA1S*).

First, the Hypo- and normokalemic periodic paralysis; second, malignant hyperthermia susceptibility; third, $Ca_V1.1$-related myopathy and fourth, myotonic dystrophy type 1 (Flucher, 2020).

2.3.1. Hypokalemic periodic paralysis (HypoPP)

Hypokalemic periodic paralysis (HypoPP) is an inherited dominant autosomal disease, which presents episodes of flaccid generalized muscle weakness associated with low serum potassium levels (<3.5 mM) (Cannon, 2015). In most of the patients, the weakness is associated with progressive muscle degeneration. The episodes are most usually triggered at rest following exercise, carbohydrates consumption, insulin administration, or cold stress. During an attack, the voltage-gated sodium channels become inactivated because of membrane depolarization (from -90 mV to ~-60 mV) (Jurkat-Rott et al., 1998).

Behind the development of this disease there are mutations in two different voltage-gated cation channels genes, *CAV1.1* (60% of cases) and *NAV1.4* (20 % cases). In both cases, the mutations neutralize the gating charges of the S4 segment in the VSDs of the α1S subunit. As described in the previous section, these positive gating charges (4-6 arginines and lysines in each S4 segment) have multiple important functions in the $Ca_V1.1$ function. The changes of these amino-acids could generate defects in the channel gating and provoke HypoPP. For $Ca_V1.1$-related HypoPP, they are several well-known mutations. We can mention first, the replacement of arginine by glycine at position 528 (R528G) of α1S, which affects the outermost arginine (R1) in the VSD of the second homologous repeat (VSDII). Second, replacement of arginine by serine at position 897 (R897S), and at position 900 (R900S), which correspond to R1 and second outermost arginine (R2) in VSD III, respectively. Third, the replacement of arginine by glycine/histidine at position 1239 (R1239G/H), which corresponds to R2 in VSD IV. Several characterizations of calcium current properties of $Ca_V1.1$ mutations R528G and R1239G/H in myotubes indicated a loss of channel function. Indeed, it was shown that current through the mutant channels exhibits a slow activation and a reduced amplitude. Also, it was observed a left-shift in the voltage dependence for Ca^{2+} current inactivation and a wider and smaller action potential (Lapie et al., 1996; Morrill et al., 1998; Jurkat-Rott et al., 1998; Morrill & Cannon, 1999). However, these changes do not explain the long-lasting depolarization observed in HypoPP muscles. This is explained by a new transmembrane current component called "*gating pore current*" (or "Omega current"). Gating pore currents are leak currents through the channels genetically altered at the positions of the gating charges (Starace & Bezanilla, 2004). These gating pore currents are not related to the channel's pore domain (S5-S6 segment in α1S subunit), and they are significantly smaller (<1%) than the ionic Ca^{2+} current through the channel pore. The mutations in R1 and R2 in α1S disrupt the interaction between the S4 segment and the *gating charge transfer center (GCTC),* which normally separates the intracellular and extracellular crevices. Thus, the disruption of S4-GCTC interaction abolishes the seal between the outer hydrophilic vestibule and the cytoplasmic compartment and generates a fast activating, non-inactivating alternative cation-selective permeation pathway of low conductance, or *gating pore* (Chanda & Bezanilla, 2008; Moreau et al., 2014; Flucher, 2020). The gating pore current is state-dependent because it depends on the position of the mutated charge in the S4 helix, and it can flow at hyperpolarized (resting) or depolarized (activated) conditions. In 2017, a study published by Fuster et al. using the expression of the α1S mutation (R1239H) in adult mouse muscle fibers reported a decrease in the Ca^{2+} current and a larger resting leak inward current that was increased by external acidification. Their results suggested that the $Ca_V1.1$ mutation induces an elevated H^+ leak current at rest flowing through a gating pore, which could

explain why the episodes of flaccid generalized muscle weakness occur principally during the recovery period following muscle exercise (Fuster et al., 2017). The gating pore currents (leak currents) are generally accepted to be responsible for the long-lasting membrane depolarization in HypoPP fibers. The proposed mechanism behind is that both, lowering the extracellular K^+ concentration or increasing the inward leak current, contribute to shift the membrane potential towards a less polarized stable state near -50 mV, which causes the inactivation of the $Na_V1.4$ channels (needed for the onset of the AP) and provokes a temporary loss of excitability of the muscle cells. Currently, as a consequence of this knowledge, the use of repolarizing drugs, like carbonic anhydrase inhibitors, which shifts the muscle membrane potential back to the normal resting level or targeting serum potassium levels by aldosterone antagonists, appear as promising treatments (Flucher, 2020).

2.3.2. Normokalemic periodic paralysis

In normokalemic periodic paralysis, *CAV1.1* is associated with a mutation that affects the third outermost arginine (R3) of the fourth VSD, with the substitution of an arginine for glycine in position 1242 (R1242G) of the α1S subunit. In this condition, channels conduct leak current in the activated state and generate muscle weakness with normal potassium levels. The expression of mutated $Ca_V1.1$ (R1242G) in dysgenic myotubes showed a 20% reduced $Ca_V1.1$ current amplitude and a 20 mV left-shifted voltage-dependence of inactivation. Both changes were related to an outward omega current at positive potentials, which may cause slower AP onset rate by 36%, and are associated with muscle hypoexcitability, permanent weakness, and myopathy in the patients (Fan et al., 2013).

2.3.3. Malignant hyperthermia susceptibility

The malignant hyperthermia susceptibility (MHS) is an autosomal dominant predisposition that, in normal condition, is reported to be clinically asymptomatic. However, upon interaction with volatile anesthetics and/or certain muscle relaxants, the predisposition produces uncontrollable Ca^{2+} release and massive muscle contracture, muscle rigidity, acidosis, increase in body temperature, and untreated patient death (Dowling et al., 2014). This condition, in most of the cases (>70%), is related to *RYR1* mutations (further details are given later in this document), but in some rare cases (1%) has been associated with mutations in the $Ca_V1.1$ α1S (*CACNA1S* gene) subunit. The *CACNA1S* mutations corresponding to the substitution of an arginine for a histidine/cysteine/serine in position 1086 (R1086H/C/S), and the substitution of a threonine for serine in position 1354 (T1354S), affect the arginine located in the α1S III-IV cytosolic loop, and the α1S outer pore region, respectively, and alter calcium

release. Both mutations, when expressed in dysgenic myotubes, altered L-type Ca^{2+} current and increased the sensitivity of RyR1-dependent SR Ca^{2+} release to low concentrations of Caffeine (< 2 mM). These results show that R1086H/C/S and T1354S mutations disrupt the normal inhibition that $Ca_V1.1$ exerts on RyR1, causing RyR1 hypersensitivity to physiological activation (voltage stimulation) but also to pharmacological effectors (e.g. caffeine), which is responsible for the MHS crisis (Weiss et al., 2004; Pirone et al., 2010).

2.3.4. $Ca_V1.1$-related congenital myopathies

The fourth type of pathology is $Ca_V1.1$-related myopathies. They are part of the congenital myopathy classification, a genetically heterogeneous group of early-onset, non-dystrophic muscle diseases with muscle weakness and particular histopathological features including central cores, multi-minicores, central nuclei, and nemaline rods (strand-like abnormal proteins structures). They include disorders in ECC and calcium handling, related to RyR1 mutations. Recent studies have also shown mutations in *CACNA1S* in patients with perinatal hypotonia, severe axial and generalized weakness, and ophthalmoplegia. The consequences of these specific *CACNA1S* mutations on ECC and Ca^{2+} handling remain to be studied (Jungbluth et al., 2018; Flucher, 2020).

2.3.5. Myotonic dystrophy type 1 (DM1)

The last type of *CAV1.1*-related muscle disease is *myotonic dystrophy type 1 (DM1)*. Myotonic dystrophies (DM1 and DM2) are autosomal dominant disorders characterized by symptoms in multiples organs including skeletal muscle, with muscle weakness and slow muscle relaxation (myotonia). DM1 is produced by cytosine-thymine-guanine (CTG) triplet repeats in the 3' untranslated region of the dystrophia myotonica protein kinase (DMPK gene), which binds to the muscleblind-like 1 (MBNL1) protein with high affinity, resulting in the sequestration of MBNL1 in nuclear foci and the loss of its activity as a splicing regulator. This causes the unregulated splicing of several genes including chloride channels (muscle-specific isoform, *CLCN1* gene), insulin receptor gene, and *CAV1.1* (Miller et al., 2000). The myotonia-related muscle function alteration can be explained by mutations in chloride and calcium channels. The chloride channel provides 80% of the skeletal muscle fibers resting conductance, making it crucial in the control of muscle excitability (Jentsch & Pusch, 2018). Thus, *CLCN1* mutation can produce impairment of the channel function and/or altered membrane localization (Lueck et al., 2007) which triggers involuntary muscle action potentials (Mankodi et al., 2002). A DM *CAV1.1*-related mouse model has been produced as mentioned before (in section 2.2.5) by a splicing defect in α1S with the exon 29

inclusion, which is normally absent in $Ca_V1.1$ from adult fibers. In this $Ca_V1.1_e$-expressing mouse model, the right-shift of the voltage dependence and the increased conductance of the $Ca_V1.1$-dependent Ca^{2+} current are associated with a pathologically enhanced calcium influx, with the production of muscle weakness and an increased frequency of centrally located myonuclei (Tang et al., 2012). But compared with more representative models of DM disease like the MBLN1 knockout mouse model, the DM *CAV1.1*-related mouse model in which the only feature is the expression of $Ca_V1.1_e$, initially does not show DM-like muscle weakness, but progressively appears mitochondrial damage and loss, producing a reduction in the endurance capabilities of the mouse. This supports the hypothesis that the increase in calcium influx due to $Ca_V1.1_e$ expression induces myopathy and therefore contributes to the pathology of DM1 (Sultana et al., 2016).

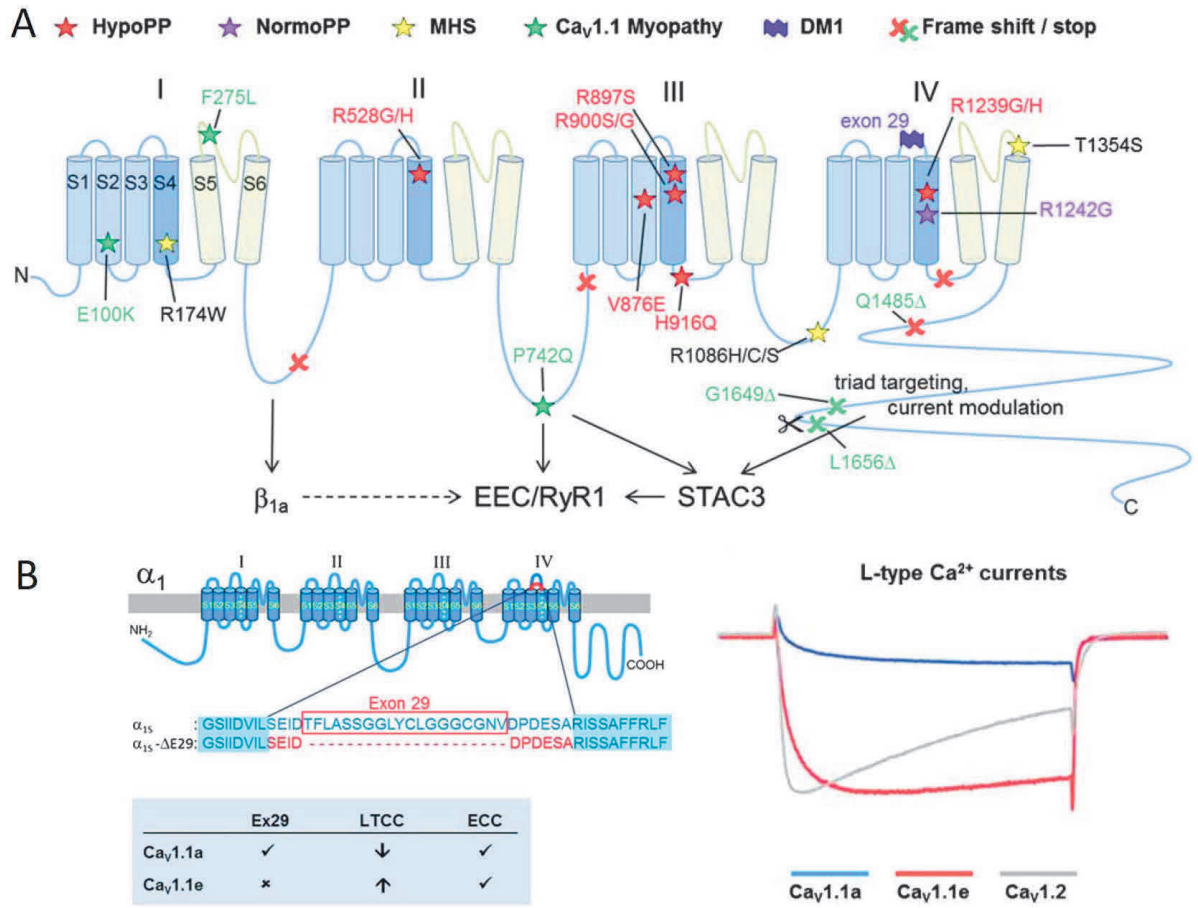

Figure 7. $Ca_V1.1$ channelopathies and their mutations sites. *A) Positions of disease mutations in the topology model of $Ca_V1.1$ α1S. CACNA1S variants and splicing defects related with muscle diseases concern principally the VSDs and the P-loop involved in ion conduction and selectivity as well as alterations in different intracellular loops that affect the interaction with associated proteins. Some mutations produce the disease by affecting directly $Ca_V1.1$ (Ca^{2+}currents, gating pore currents), while others alter the interaction with RyR1 (ECC, Ca^{2+} leak). The mutation sites for HypoPP, NormoPP, MHS, $Ca_V1.1$-related myopathy and DM1 are indicated. Red-X and green-X represent truncation producing non-functional and functional channels, respectively. B) left; domain structure of $Ca_V1.1$ α1S highlighting the alternatively spliced exon 29, and right; comparison of calcium currents of $Ca_V1.1a$ with exon 29 (blue) and $Ca_V1.1e$ without exon 29 (red). Adapted from Flucher et al. 2020.*

2.4. $Ca_V1.1$ Pharmacology

There is a big list of compounds described to regulate the voltage-dependent Ca^{2+} channels. They are several different chemical classes of voltage dependent Ca^{2+} channels blockers (CCBs) (Zamponi et al., 2015). We can classify them into three different organic classes: 1) The L-type Ca^{2+} channels blockers or the 1,4-dihydropyridine series (DHPs), like nifedipine, which are widely used in the treatment of hypertension. 2) The phenylalkylamines, like verapamil, and 3) benzothiazepines like (+)-cis-diltiazem. Despite their structural differences, they all interact in a reversibly manner with dissociation constants in the nanomolar range (Striessnig et al., 1998), modulating the channel' resting, open and inactivated states. The DHPs principally stabilize and induce the channel inactivated state. The phenylalkylamines and benzothiazepines bind to open and inactivated states with high affinity and stabilize inactivated channel states, slowing recovery from inactivation, and producing in all cases a decrease of inward Ca^{2+} current through L-type Ca^{2+} channels. Instead, the DHPs have two groups: 1) inhibitory DHPS: the clinically used amlodipine, felodipine or isradipine, which always produce an inhibitory effect on the current, and 2) potentiating DHPs: (-)-BayK8644 and (+)-SDZ202-791 which are examples of molecules that increase the current amplitude, tail currents and single channel open probability (Striessnig et al., 2015).

Different ions are capable of blocking the voltage-dependent calcium channels by binding to domains in the pore with more affinity that Ca^{2+} (Lansman et al., 1986). If the high-affinity site is within the membrane electrical field, the block will depend on the voltage. For example, Cd^{2+} will efficiently block the voltage-dependent Ca^{2+} channels near 0 mV, but at strong negative or positive values it will be forced through the channels. The same happens when using Ca^{2+} to block monovalent current (Jones, 1998).

Current understanding of the voltage sensor domains structure is making progress including how the alteration of the interaction between the S4 segment and the gating charge transfer (S4-GCTC) produces gating pore current and its possible regulation with specifically designed molecules. Some toxins are able to interact with specific VSD of the voltage-dependent Na^{+}-channels (Moreau et al., 2014). Because of the increased structural knowledge of Ca^{2+} and Na^{+}-voltage dependent channels, the development of drugs related to their structure specificities opens news perspectives for the treatments of several neurological, neuromuscular, and cardiovascular diseases (Catterall et al., 2020).

2.5. Type 1 Ryanodine receptor or RyR1

2.5.1. RyR1 family

The ryanodine receptors (RyRs) are intracellular Ca^{2+} channels located in the endoplasmic reticulum (Takeshima et al., 1989). RyRs are named based on their ability to bind ryanodine molecules (extracted from the plant alkaloid ryanodine), which lock RyR channels into a subconductance state at micromolar concentrations, and block RyR at higher concentrations (> 100 μM) (Fleischer et al., 1985), at least in vitro. The ability of ryanodine to lock RyR channels in an open state results in an uncontrolled Ca^{2+} release and muscle tetany (Kushnir & Marks, 2012). In mammals, the RyR family is composed of three isoforms (RyR1, RyR2, and RyR3) from three different genes (*RYR1*, *RYR2*, and *RYR3*). *RYR1* is located in chromosome 19q13.1, comprises 106 exons, and is principally expressed in skeletal muscle (MacKenzie et al., 1990). The *RYR2* is located on chromosome 1q43, is composed of 102 exons, and is expressed principally in cardiac muscle and neurons. The *RYR3* is located in the chromosome 15q13.3-14, is composed of 103 exons, and is expressed in the brain, smooth muscle, during skeletal muscle development, and in slow-twitch skeletal muscle (Lanner et al., 2010). *RYR1* and *RYR2* share approximately 70% sequence identity, with the strongest similarities in the C-terminal region that form the transmembrane, ion-conducting pore domain of the channel (Nakai et al., 1990). Their opening can be triggered by a rise in Ca^{2+} near the cytosolic channel face. This is why often they are referred to as Ca^{2+}-induced Ca^{2+}-release channels allowing Ca^{2+} release from the intracellular stores in response to an initial cytosolic Ca^{2+} elevation (Endo, 2009).

2.5.2. RyR1 structure

RyR1s are organized in regular checkered arrays in the terminal cisternae of the SR (Franzini-Armstrong et al., 1998). Half of RyR1s are associated with $Ca_V1.1$, while the other half are not associated or uncoupled (Franzini-Armstrong & Kish, 1995). The RyR1-$Ca_V1.1$ arrangement is critical for ECC in skeletal muscle, and is also called Ca^{2+} release unit (CRU) or couplon when referred to a set of RyR1s-$Ca_V1.1$s on one side of a triad junction (Franzini-Armstrong et al., 1999).

In striated skeletal muscle, RyR1 is a homotetramer (≈2.2 MDa) of formed of four identical 565 kDa subunits channel-forming polypeptides of 5000 amino acids each. Each identical subunit from a RyR1 binds to the immunophilin, a 12-kDa binding protein for the immunosuppressant drug FK506, called "*FKBP12*", and interacts in the cytosol with $Ca_V1.1$ (α1S and β1a subunits) and with various accessory proteins like calmodulin, homer, S100A1, protein kinases, and protein phosphatases. Together with

regulatory subunits, enzymes, and their respective targeting/anchoring proteins, it makes a complex exceeding the three millions of Daltons (Meissner, 2017; Kushnir et al., 2018).

Several recent single-particle cryo-electron microscopy (cryo-EM) studies at a high resolution (3-6 Å) confirmed that RyR1 has a fourfold symmetric mushroom-like superstructure with 80% of the mass in the cytosol (the cap of the mushroom or the "feet", early identified with electron microscopy) and the stalk embedded in the SR membrane. In the mushroom-like structure of RyR1, the cytosolic portion is formed by 10 different domains per subunit and forms the regulatory portion, spanning the gap of 12 nm between the T-tubules and the SR membrane in cardiac and skeletal muscle. The cytoplasmic domain of RyR1 interacts with Ca^{2+} and Mg^{2+} ions and with ligands such as ATP, caffeine, ryanodine, and accessory proteins such as calmodulin (CaM) (in details in 2.5.3.). The three-dimensional reconstruction of frozen-hydrated RyR1 specimen reveals a 28-x 28-x 12-nm large cytoplasmic assembly with a 12-x 12-x 6-nm transmembrane domain. The SR transmembrane region forms the Ca^{2+} release channel (pore of the protein), and the functional states in RyR1 (close and open) involve conformational changes in the cytoplasmic and transmembrane domains producing either dilation, or constriction around the pore. The pore of the protein (approximately 10 Å) is produced by six transmembrane helices surrounding a central pathway. Sequence comparisons and mutagenesis studies have shown that the central ion-conduction pathway is formed by the S6 segment and the selectivity filter from each subunit, like in K^+ channels. Because of elongated S6 segments and the luminal loops above the selectivity filter, the conducting pathway RyR1 is extraordinarily long, with 90 Å (9 nm) from the SR lumen to the cytoplasm. In the SR lumen, RyR1 interacts indirectly with calsequestrin (CSQ) through the membrane-anchored proteins triadin and junctin, which have a transmembrane helix and an intra-SR domain (Zalk et al., 2015; Efremov et al., 2015; Yan et al., 2015; Bai et al., 2016; des Georges et al., 2016; Wei et al., 2016) (See Fig.7).

Each RyR1 subunit is formed by the following domains: 1) the N-terminal domain forms the cytoplasmic vestibule, participates in the interaction with $Ca_V1.1$, and is the target of different disease mutations; 2) the 3 SPRY domains, SPRY1 is the binding site for FKPB12, SPRY2 interacts with II-III loop of the α1S subunit of $Ca_V1.1$ for ECC in skeletal muscle, SPRY3 does not have a clear role; 3) the P1 domain is a small L-shaped appendage in the outer corner of the clamp domain; 4) the Handle domain is like a flat paving stone and forms the side of the square, it is part of the binding sites for FKB12, apoCaM, and Ca^{2+}-CaM; 5) the P2 domain is a phosphorylation site, it is not completely resolved; 6) the junctional solenoid (Jsol) and the bridging solenoid (Bsol) contain PKA, and Ca^{2+}/CaM-dependent protein kinase II (CaMKII) phosphorylation sites; 7) the central solenoid (Csol) domain contains 2 EF-hand Ca^{2+} binding motifs; 8) the

transmembrane domain which forms the conductance pathway for Ca^{2+}; 9) the C-terminal domain (CTD), which forms part of the Ca^{2+}, ATP, and caffeine activation sites (Samsó, 2017) (see Fig. 6).

2.6. RyR1 function: In vitro and in vivo experiments

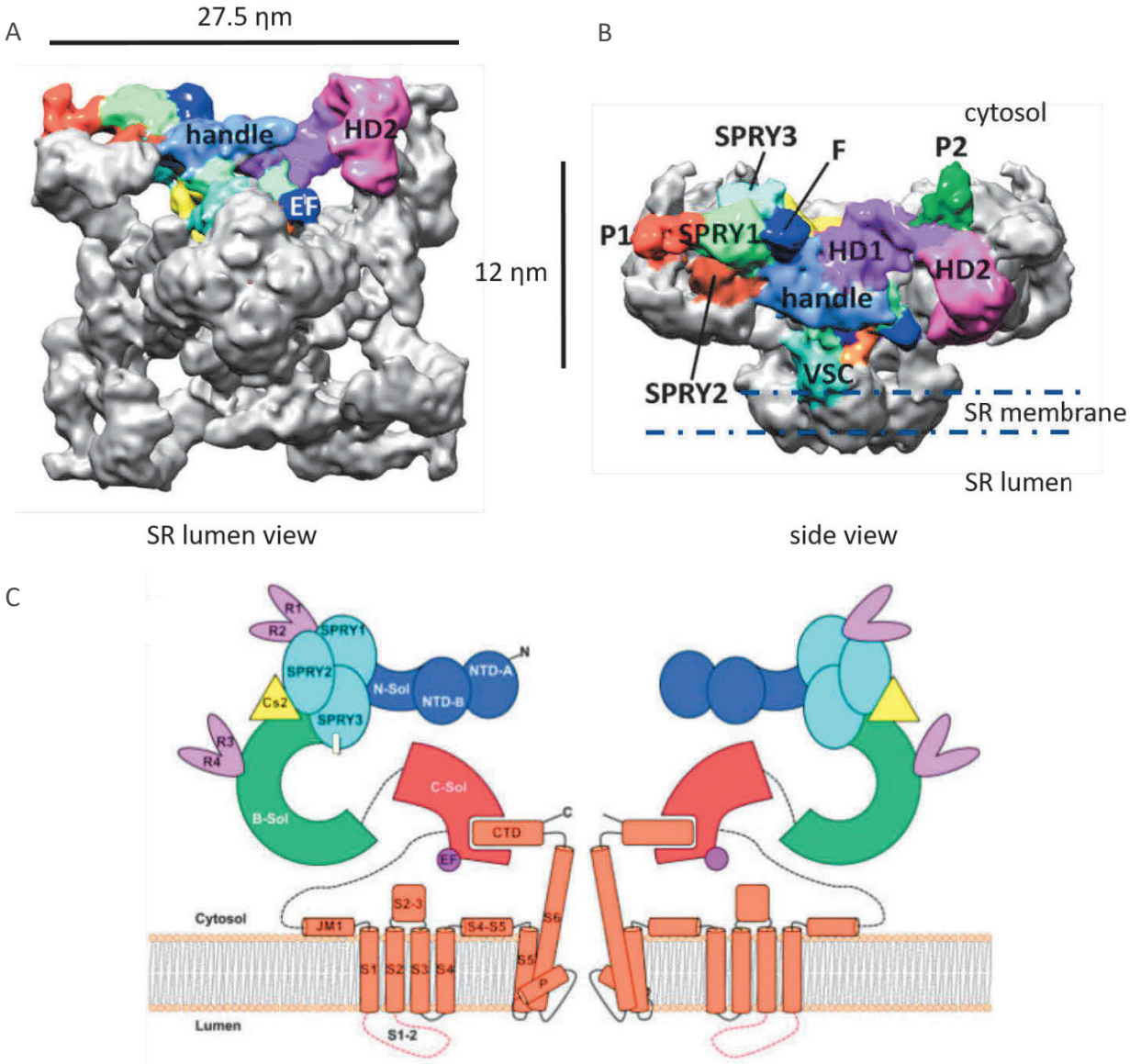

Figure 8. RyR1 tridimensional structure and subunits. *A) SR lumen view of a cryo-EM reconstruction of the RYR1; B) Side view of a cryo-EM reconstruction of the RYR1. Colors represent the different domains that compose each RYR1 subunit. Images modified from Samsó et al. 2017. C) Sagittal sight of the different domains for two RyR1 monomers showing domains in the cytoplasmic region (N-terminal) and the transmembrane segments of the pore region (C-terminal). Scheme took from Zalk et al. 2015.*

2.6.1. Non-physiological conditions: In vitro experiments

In skeletal muscle, the principal function of RyR1 is Ca^{2+} release from the SR into the cytosol, the activation of which depends on $Ca_V1.1$ in the process called excitation-contraction coupling (Franzini-Armstrong & Protasi, 1997). Thus, to study RyR1-dependent SR Ca^{2+} release in physiological conditions it is necessary to maintain this $Ca_V1.1$-RyR1 relationship, the structurally developed T-tubules, triads, and tetrads organization, which are critical in ECC, and are normally present in differentiated muscle fibers (Collet et al., 2004; Jacquemond, 2012). As mentioned before, RyR1 knockout (dyspedic mice) results in a lethal phenotype because of respiratory failure. Muscles from the mutant mice display also skeletal abnormalities and similarities with those from dysgenic mice ($Ca_V1.1$ knockout) (Takeshima et al., 1994). In both model, the study of differentiated muscle fibers is unavailable and the studies have been performed in myotubes (further described).

In non-physiological fragmented preparations, some of the following: $Ca_V1.1$-RyR1 relationship, T-tubule integrity, triads and tetrads organization are lost, therefore normal ECC cannot be produced. However, experiments in such non-physiological conditions have been an important way to study RyR1 properties from the beginning of the ECC studies and gave us a huge amount of structural and functional information about RyR1 function, improving our understanding. Different techniques have been developed, like the insertion of either isolated RyR1 channels or SR membrane fragments in lipid bilayers for single-channel records, or the isolation of SR membrane vesicles for measurements of SR Ca^{2+} fluxes. We can mention also RyR1 expression in different cell lines (like HEK293) for studying the impact of mutations at different sites on the RyR1 function (see Meissner, 2017). As presented before, there has been a recent breakthrough gain of information from RyR1 cryo-EM studies, in which RyR1 is frozen under solutions containing inhibitor or activator molecules to observe the closed, and the open molecular configuration, respectively (see Samsó, 2017).

2.6.2. RyR1 single-channel/SR records in lipid bilayer membranes

Under physiological and non-physiological conditions, RyR1 is capable of allowing the passage of several ion species, and to interact with several molecules and proteins, as has been shown by an extensive list of scientific works over the last four decades. In single-channel records using RyR1 purified protein, and SR membrane insertion in lipid bilayers, RyR1 channels have shown a high and non-selective conductance (110-125 pS for Ca^{2+} in the presence of 50 mM luminal Ca^{2+}, > 700 pS for K^+ in the presence of symmetrical 250 mM KCl), and they readily allow the passage of both monovalent and divalent cations

(K^+ > Rb^+> Na^+ ≈ Cs^{2+} and Ba^{2+} > Ca^{2+} > Mg^{2+}) (Meissner, 2017). RyR1 has several regulatory sites at the cytosolic and SR luminal regions, allowing a fine regulation with multiple mechanisms (des Georges et al., 2016). Using the planar lipid bilayer method, it has been shown that Ca^{2+} and Mg^{2+} strongly affect RyR1 activation by ATP. In the absence of both ions, millimolar concentration of ATP weakly activate RyR1 (Tripathy & Meissner, 1996). In the cytosol, most of cellular ATP is present as Mg-ATP complex. An increase in Mg^{2+} with increase Mg-ATP complex, decreased free ATP, and RyR1 activity (Meissner et al., 1986). Using SR membranes incorporated into planar lipid bilayers and single channels recordings it was shown that both cytosolic and luminal Ca^{2+} can regulate RyR activity, according to three different Ca^{2+} binding-sites: high-affinity (activating) and low-affinity (inactivating) sites at the cytosolic region, and low-affinity sites at the luminal side. ATP-dependent RyR1 activation is inefficient in the absence of millimolar luminal Ca^{2+} (Sitsapesan & Williams, 1995).

The cytosolic ion Mg^{2+} also plays an important role in RyRs inhibition through three possible different mechanisms: 1) Mg^{2+} competes with Ca^{2+} for high-affinity cytosolic sites, 2) Mg^{2+} binds with similar affinity as Ca^{2+} to low-affinity cytosolic sites, and 3) Mg^{2+} reduces the Ca^{2+} flux through the channel (Meissner et al., 1997). In single-channel records using planar lipid bilayers, RyR1 was shown to be also regulated by other divalent cations like Zn^{2+} (Xia et al., 2000), present in physiological conditions (pM-nM range), which increases RyR1 open probability, or cations that are not present in physiological conditions like Sr^{2+}, which acts as RyR1 activator at 1mM, or Ba^{2+}, as an inhibitor at high molar concentrations (Olivares et al., 1993).

2.6.3. Cryo-electron microscopy of RyR1 in open/closed state

In recent structure-function experiments Des Georges et al. (2016), used cryo-EM reconstruction of isolated rabbit RyR1 and single-channel recordings from SR vesicles. They proposed a structural description of the RyR1 activation sequence in their experimental conditions. They characterized: 1st, RyR1 closed state in the absence of Ca^{2+}; 2nd, a priming state for opening, either in the presence of 30 µM Ca^{2+} or 2 mM ATP that stabilizes the channel in a permissive pre-opening state; 3rd, the fully open state with the combination of three ligands Ca^{2+}, ATP, and caffeine (5 mM); and finally 4th, an open-locked subconducting state in the presence of 10 µM of ryanodine (des Georges et al., 2016). Such molecular dissection of the several configurations of the channel throughout the processes of opening and closening is a definite breakthrough in the field. Accordingly, there is a great amount of ongoing work using molecular simulations on the basis of the new structure knowledge, aiming at understanding the details of the channel structure-function relationships in the normal and disease conditions (Samsó, 2017; Iyer et

al., 2020). Still, these approaches are achieved with channels under steady-states of their functional capabilities, and, up to now, the details of how RyR1 is gated by $Ca_V1.1$ in physiological conditions are not resolved.

2.6.4. Myotubes and skinned fibers experiments

The study of the different factors that can regulate $Ca_V1.1$-RyR1 relationship and ECC in skeletal muscle was also made under more physiological approaches over the decades, that is RyR1-expression in cell lines, developing myotubes, cut fibers, or mechanically skinned fibers (or "peeled") technique.

The cultured myotubes model has generated major progress for our understanding of the relevance of the critical partners of ECC which, if knocked-out, generate lethal animal models that never get fully developed skeletal muscle fibers. First breakthrough was the discovery of the $Ca_V1.1$ knockout mouse model as the dysgenic mouse (Klaus et al., 1983) with associated critical impairment of ECC in cultured myotubes and its restoration with the microinjection of a plasmid encoding $Ca_V1.1$ α1S subunit cDNA (Tanabe et al., 1988). Second, was the characterization of the RyR1 knockout model as the dyspedic mice also exhibiting a lethal phenotype, from which the myotubes also lack ECC (Takeshima et al., 1994). Both dysgenic and dyspedic myotubes models have been used over the last decades to generate a very important amount of the current ECC knowledge, through expression of different mutant constructions and chimeras of $Ca_V1.1$ and associated subunits, mutant forms of RyR1, and the studying of their interactions through ECC measurements (Hernandez-Ochoa & Schneider, 2018). The myotubes model is still generally used, and important for the field, but lacks fully developed and ultimately organized T-tubules and triads which is needed to understand ECC in fully differentiated physiological conditions (Schneider, 1994; Collet et al., 2004).

In the skinned technique, the sarcolemma is removed by microdissection, of a single muscle fiber or of a portion of single muscle fiber (Costantin & Podolsky, 1967). This preparation has the advantage over the above-mentioned methods that the structure and the normal relationships between the proteins that are important for RyR1-dependent SR Ca^{2+} release remain unaltered including the triads and $Ca_V1.1$ tetrads organization (Murphy et al., 2009). Because it allows the full control of the intracellular medium composition, the skinned fiber preparation has been specifically important to understand the effects of the changes in cytosolic components over the physiological relationship and the function of the important ECC protein partners, this through measurements of RyR1-dependent SR Ca^{2+} release, or of single muscle fiber force (see Lamb et al., 2018). In this preparation, however, there is some limit to the physiological

conclusions. First, the T-tubule is sealed at the fiber surface and generates an electrically and chemically isolated compartment. In addition, the complete wash-out of the intracellular medium may remove some precious soluble modulators of ECC. Finally, although action-potentials can be produced by electrical field stimulation, the system lacks the conditions to do electrophysiological measurements such as charge movements, and also lacks the conditions to quickly modify T-tubules voltage in a controlled manner (by voltage-clamp) to carefully study the voltage dependence SR Ca^{2+} release (Schneider, 1994).

2.6.5. Physiological conditions: In vivo assessment of RyR1 and excitation-contraction coupling function

For more integrative and physiological assessments of ECC function, as we mentioned before, there is need for differentiated muscle fibers with the ECC partners intermolecular and structural interactions preserved, and this associated with the possibility to directly or indirectly measure ECC and RyR1 activity, and ultimately to do this under conditions allowing control or detection of membrane voltage. In this document, we will refer to these conditions as in vivo measurements. With this goal, several muscle fibers preparation and electrophysiological techniques have been developed over the years. We can mention 1) the use of intact fibers isolated by dissection or investigated within a muscle bundle, 2) the single isolated fibers cut at one or both ends (Schneider, 1994), or 3) the intact enzymatically isolated skeletal muscle fibers (Jacquemond, 1997) which is a method I have largely used in my project. Electrophysiological tools include microelectrodes and various “gap” (vaseline-, sucrose-) techniques. RyR1-dependent SR Ca^{2+} release can be indirectly detected by the measurement of the fiber contraction, or directly by using Ca^{2+} indicator dyes introduced in the cytosol and associated with optical techniques as has been widely done since the 80s (Baylor et al., 1982; Palade & Vergara, 1982; Kovács et al., 1983; Brum et al., 1988). In many of these studies, the variation in cytosolic [Ca^{2+}] was used to derive the change in total Ca^{2+} (Ca^{2+}_T) occurring in the cytosol and from this, the rate of RyR1-dependent SR Ca^{2+} release which can be calculated as dCa^{2+}_T/dT.

Using differentiated fibers, the different steps of ECC can be approached: either action potential generation or voltage-clamped sarcolemma and transverse tubule, voltage sensor activation ($Ca_V1.1$ activation), SR Ca^{2+} release (RyR1 function), Ca^{2+} reuptake (SERCA function), and force development. ECC was first studied using microelectrodes and force transducers to measure APs and muscle tension (Kahn & Sandow, 1950), then from the seventies until today there has been widespread development of different electrophysiological techniques to measure or control the membrane voltage (Adrian et al.,

1970; Schneider & Chandler, 1973; Hernández-Ochoa & Schneider, 2012; Hernandez-Ochoa & Schneider, 2018).

2.6.6. Voltage-clamp in differentiated skeletal muscle

As previously mentioned, voltage-clamp has been widely used for the study of $Ca_V1.1$ function and ECC in skeletal muscle (Rios et al., 1992). However, in order to use this system for the study of a fast process, within millisecond time scale like ECC, the voltage must be spatially uniform over the membrane area of interest, a condition that is hard to fulfill in differentiated muscle fibers. This problem was solved by the development of different techniques like the two- or three- microelectrodes voltage-clamp, the single- and double- vaseline gap techniques used with fibers either cut at one end (single-) or both ends (double), the double sucrose-gap technique used with intact fibers (see for review Hernández-Ochoa & Schneider, 2012). Another technique, the whole-cell silicon voltage-clamp technique was developed in our laboratory (Jacquemond, 1997; Collet et al., 2004), and is the one used in this project.

This method is most commonly used on enzymatically dissociated adult muscle fibers of the "*Flexor Digitorum Brevis" (FDB*) and "*Interosseus" (IO)* from mice (or rat), which have a diameter of 20-50 µm and are 500 µm to 1 mm long. Silicone grease is used to electrically insulate most of the fiber length, leaving a 50-100 µm fiber portion outside the silicone, on one end of the fiber. In this condition, the fibers are clamped using a single-microelectrode impaled in the silicone-insulated portion of the fiber (more details in methods). Over the years, this method has proved its reliability and efficiency to investigate the properties of ECC in normal and diseased conditions (Jacquemond, 1997; Collet et al., 2004).

2.6.7. Ca^{2+} sensitive fluorescent dyes to study excitation-contraction coupling

The use of Ca^{2+} sensitive indicator dyes to detect the changes in global cytosolic Ca^{2+} associated with contractile activation in skeletal muscle started in the seventies (Miledi et al., 1977). With the progress in the techniques, charge movement and SR Ca^{2+} release were measured simultaneously or in parallel, which revealed, the close relationship between the two (Hernández-Ochoa & Schneider, 2012). Measurements of Ca^{2+} current and of non-linear capacitive currents (charge movement) have been used to characterize $Ca_V1.1$ function, while the SR Ca^{2+} release flux could be derived from the optical signal from a Ca^{2+} indicator to assess RyR1 function (more details in methods).

In the 1990s the advent of laser-scanning confocal imaging has made it possible to visualize localized intracellular Ca^{2+} release events, called SPARKS, which underlie ECC in cardiac muscle (H. Cheng, Lederer, & Cannell, 1993) and in frog skeletal muscle (Tsugorka et al., 1995; Klein et al., 1996). In contrast, SPARKS

scarcely occur in mammalian skeletal muscle in physiological and healthy condition (Csernoch, 2007). Nevertheless, SPARKS were shown to be present in mammalian muscle at rest under disease or distress conditions as during aging (Weisleder & Ma, 2008) or in myotubular myopathy (Kutchukian et al., 2019). Conversely, it has been proposed that voltage-activated SPARKS are exclusively related to the expression of the RYR3 isoform (Pouvreau et al., 2007), which is presented at a negligible level in mammalian muscle.

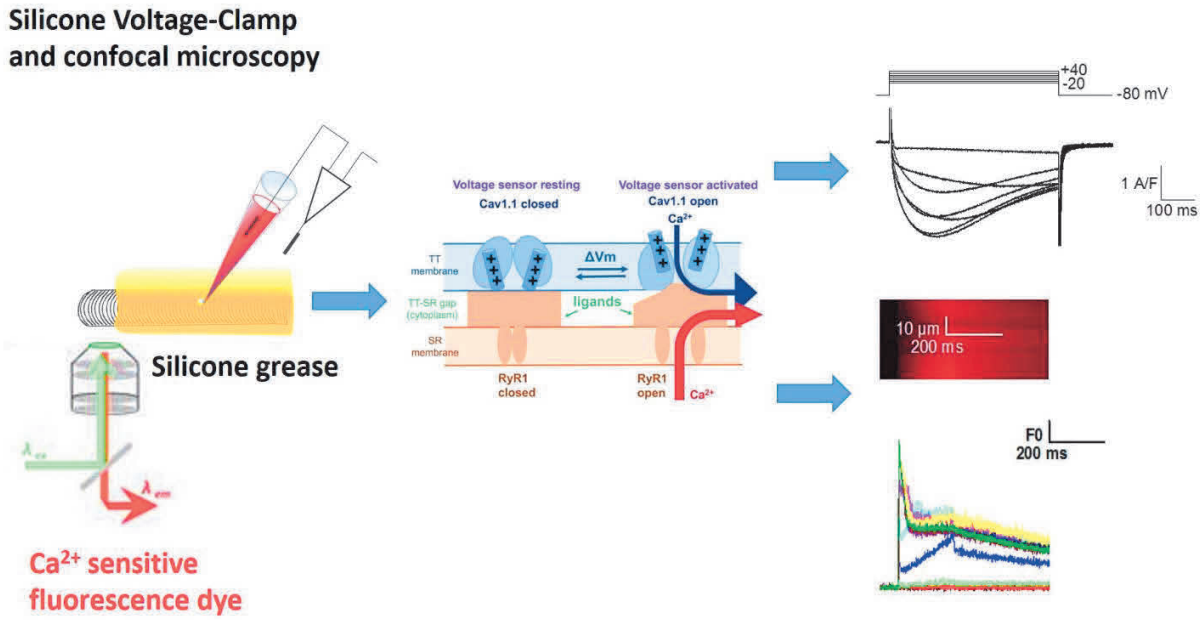

Figure 9. Schematic representation of ECC investigation using intracellular Ca^{2+} measurements and the silicone voltage-clamp technique. *The silicone grease used to electrically isolate most of the adult muscle fiber is represented in yellow. The system is associated with simultaneous laser stimulation and confocal fluorescence detection in the free portion of the fiber. This allows measurement of $Ca_V1.1$ activity as Ca^{2+} current, and RyR1 function (and ECC) from the increase in fluorescence in response to voltage pulses of increasing amplitude.*

2.7. RyR1 regulatory partners

2.7.1. RyR1 cytosolic regulation by $Ca_V1.1$ α1S and β1a subunits, and by Ca^{2+}

In opposition to CICR in cardiac muscle fibers, during the ECC of differentiated skeletal muscle fibers, RyR1 is under the strict control of $Ca_V1.1$ through the α1S and β1a subunits. Indeed, it has been shown that both dysgenic mice (α1S-null mice), and mice devoid of β1a ($Ca_V1.1_\beta$ null mice) lack Ca^{2+} release and exhibit a lethal phenotype, suggesting that both subunits are important for the control of RyR1 function and ECC (Beam et al., 1986; Gregg et al., 1996).

The influence of $Ca_V1.1$ in RyR1 activation in ECC is now well documented and accepted. It should be further stressed however that, even though recent progress from the cryo-EM techniques has provided an unprecedented resolution of the structure of the two partners, their exact molecular interactions taking place during ECC are still elusive (Samsó, 2015, 2017).

In differentiated skeletal muscle, only half of the RyR1 channels interact with $Ca_V1.1$. The other half, that does not interact with $Ca_V1.1$, was earlier thought to be activated by CICR (Stern et al., 1997). However, voltage-activated Ca^{2+} sparks, which represent the clearest manifestation of CICR in skeletal muscle (frog) require RyR3 (Pouvreau et al., 2007).

RYR3 is negligible in mammalian muscle and it has been recently proposed that, in fact, CICR may not contribute at all to ECC (see Rios, 2018; and Rios et al., 2019; for a comprehensive review). Thus Ca^{2+} as an activating signal may not play an important role in the modulation of ECC coupling in mammalian skeletal muscle. In contrast, there has been substantial evidence given for the fact that Ca^{2+}-dependent inactivation of RyR1 channels contributes to the early decline of Ca^{2+} release during a membrane depolarization (Simon & Hill, 1992; Szentesi et al., 2000).

2.7.2. Other RyR1 partners at the cytosolic face: Calstabin1 or FKBP12, calmodulin or CaM, and S100A1

In physiological conditions, it has been suggested that RyR1 can be also regulated by multiple mechanisms at different cytosolic and/or SR intraluminal sites; this includes intracellular ions, adenine nucleotides (ATP), cytosolic regulatory proteins (FKBP12, calmodulin, S100A1), SR intraluminal regulatory proteins (calsequestrin, junctin, triadin), and post-translational modification (oxidation, S-nitrosylation, phosphorylation) (Capes et al., 2011). FKBP12, calmodulin and S100A1 are major accessory protein regulators of RyR1 on the cytosolic side (see Fig. 10).

FKBP12 or ***Calstabin1*** (named for **Cal**cium channel **stab**ilizing binding prote**in**) and Calstabin2 (FKBP12.6), are cytosolic 12-kDa immunophilin proteins, present in skeletal and cardiac muscle. In cardiac muscle, it has been shown that phosphorylation of FKBP12.6 by PKA dissociates FKBP12.6 from RyR2 producing an increase in the sensitivity for calcium of CICR and an associated defective channel function, a process related with failing heart (Marx et al., 2000). The overexpression of cardiac FKBP12.6 in the heart prevents the development of ventricular tachycardia, by reducing diastolic sarcoplasmic reticulum Ca^{2+} leak. The RyR2-FKBP12.6 interaction could then be a pharmacological target to prevent ventricular tachycardia (Gellen et al., 2008). In skeletal muscle FKBP12 binds to RyR1 (Collins, 1991; Samsó et al., 2006), interacting with the N-terminal and central domains of the channel (Girgenrath et al., 2013), stabilizing it in the close state (Brillantes et al., 1994) and reducing the subconductance states (Mayrleitner et al., 1994). In cultured skeletal myotubes, it was shown that *RYR1* mutations that disrupt FKBP12 interaction affect voltage-activated RyR1-dependent Ca^{2+} release (Avila et al., 2003; Eltit et al., 2010; Eltit et al., 2011). In differentiated muscle fibers, there is an overwhelming concept according to which FKPB12 dissociation from RyR1 increases the channel open probability so as to make it leaky (Ahern et al., 1997). This would occur under several stress conditions including RyR1 hyperphosphorylation (Marx et al., 2000; Aydin et al., 2008) and excess of reactive oxygen/nitrogen species (Bellinger et al., 2008). FKBP12 dissociation would then be involved in several muscle distress conditions as Duchenne dystrophy (Bellinger et al., 2009), cancer-induced cachexia (Waning et al., 2015), artificial ventilation-induced diaphragm dysfunction (Waning et al., 2015). In contrast, a mild RyR1 Ca^{2+} leak due to FKBP12-RyR1 dissociation would be a key trigger of signaling pathways involved in fatigue resistance (Ivarsson et al., 2019).

Calmodulin (CaM) is a 17 kDa protein that regulates RyR1 activity directly and indirectly as a cofactor for *calmodulin kinase II (CaMKII)*. CaM has four high-affinity Ca^{2+}-binding motifs and has two different functional states: A Ca^{2+}-free CaM called *apocalmodulin*, and a Ca^{2+}-bound CaM or *Ca^{2+}-CaM*. The apocalmodulin form is a RyR1 agonist, while Ca^{2+}-CaM is a RyR1 antagonist. Thus, the CaM direct regulation over RyR1 channel is biphasic (Tang et al., 2002). CaM increase RyR1 channel activity at low [Ca^{2+}] while decreasing its activity at high [Ca^{2+}] during in vitro experiments (Tripathy et al., 1995), but the physiological relevance for ECC regulation is limited in cultured myotubes (O'Connell et al., 2002). In skeletal muscle, CaM is proposed to play a role in protecting RyR1 from oxidative stress (Eu et al., 2000). It has been shown that the influence of CaM in the RyR1 function can be modulated by S100A1, which competes with CaM for RyR1 binding sites (Wright et al., 2008). CaM has also an indirect modulation role on RyR1. In its activated version (Ca^{2+}-CaM) CaM activates CaMKII which phosphorylates RyR1, producing

the dissociation of FKBP12 and increasing RyR1 open probability in in-vitro experiments (Capes et al., 2011).

S100A1 is a homodimer part of the S100 family of proteins, which are thus named because of their solubility in 100% of ammonium sulfate. There are 25 different S100 proteins in human (Gonzalez et al., 2020), and S100A1 is highly expressed in cardiac and skeletal muscle. S100A1 is a 21-kDa Ca^{2+} binding protein without enzymatic activity. It has been shown that S100A1 regulates Ca^{2+} signaling and contractility in cardiac muscle through interactions with RyRs and phospholamban/SERCA (Duarte-Costa et al., 2014). More specifically, an S100A1 knockout mouse model was shown to exhibit an increase in cardiomyopathy incidence (Most et al., 2006) while expression of the S100A1 gene improved cardiac contractility markers and Ca^{2+} cycling (Most et al., 2004), highlighting S100A1 cardioprotective role and Ca^{2+} handling regulation properties. Using the same S100A1 knockout mice model and studying differentiated skeletal muscle fibers ECC, Prosser et al. observed a decrease in RyR1-dependent SR Ca^{2+} release triggered by electrical field stimulation, which was rescued when infecting S100A1 KO fibers with an adenovirus containing S100A1. They demonstrated the physiological relevance of S1001A for ECC in skeletal muscle fibers and proposed a model according to which S100A1 and Calmodulin share an overlapping RyR1 binding domain: under resting conditions the domain would be essentially regulated by S100A1 which would potentiate SR Ca^{2+} release upon voltage activation. Then, upon maintained

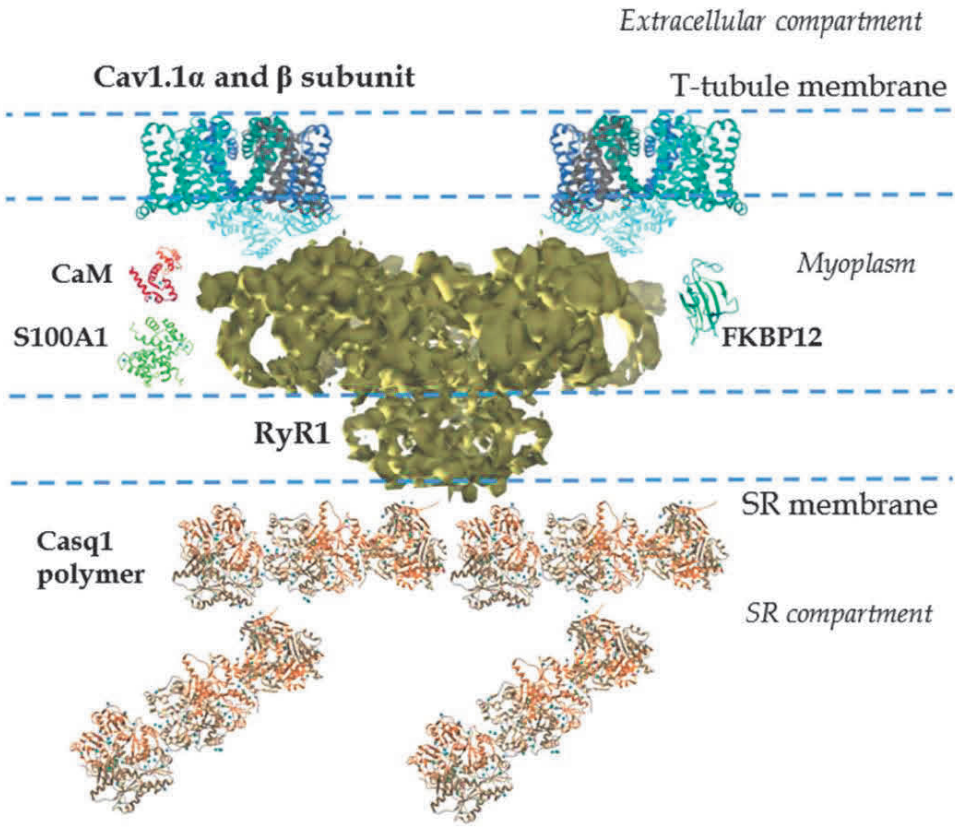

Figure 10. Cryo-EM reconstruction of the mammalian RyR1 and its relevant regulators. *The Cryo-EM presents a 4.8 Å resolution showing different regions; cytosolic region, cavities and processes, the SR transmembrane region, which forms the Ca^{2+} conduction pathway. Several 3-D structures of proteins that interact with RyR1 are also presented like calsequestrin-1 (Casq1) polymer, FKBP-12, S100A1, α1S and β1a subunits of $Ca_V1.1$. The interaction of one RyR1 with two α1S and β1a is shown. Remember that in differentiated skeletal muscle fibers $Ca_V1.1$ are clustered in tetrads (group of four) facing a single RyR1. One $Ca_V1.1$ interacts with each RyR1 homologous subunit. Images taken from Hernandez-Ochoa et al., 2016.*

stimulation conditions with elevated cytosolic Ca^{2+} levels, Ca-CaM would displace S100A1 from the binding domain, promoting channel closure (Prosser et al., 2008).

2.7.3. RyR1 luminal regulatory partners: triadin, junctin, and calsequestrin (CSQ)

In the SR lumen, the major Ca^{2+} buffering protein is calsequestrin type 1 (CSQ1), and interacts with RyR1 indirectly through the triadin and junctin proteins: CSQ1 polymerizes in a Ca^{2+}-dependent manner

and regulates RyR1 activity (Beard et al., 2009). The complex triadin-junctin-calsequestrin senses cytosolic Ca^{2+} content and modulates RyR1 activity (Capes et al., 2011) (se Fig. 11).

The skeletal muscle **triadin** is a small integral SR protein of 95 kDa. It is the product of alternative splicing of a single gene with several isoforms in skeletal muscle (Peng et al., 1994), which share the N-terminal region, but with specific features in the C-terminal domain related to their functions (Marty, 2004). There are two isoforms, Trisk95 and Trisk51, that are present in the SR terminal cisternae, but it seems that only Trisk95 can modulate ECC in myotubes (Rezgui et al., 2005). Also in cultured myotubes, mutations in RyR1 that disrupt RyR1-Trisk95 interaction generate a reduced rate of SR Ca^{2+} release (Goonasekera et al., 2007). Furthermore, the study of triadin-null myotubes showed a significant decrease in the FKBP12/RyR1 interaction generating an elevated resting Ca^{2+} level (Eltit et al., 2010). However, the issue remains controversial as others studies using triadin knock-down strategies have shown no essential influence on ECC (Shen et al., 2007; Fodor et al., 2008; Wang et al., 2009). Furthermore, Eltit et al. suggested that the small decrease of ECC in triadin-null myotubes is a consequence of the alteration of the FKBP12/RyR1 relationship and not of the absence of triadin (Eltit et al., 2011). However, it is widely accepted that triadin (Trisk95) has a role in anchoring CSQ1 at the triad and in the formation of triadin-juntin-calsequestrin complex. Two mouse models of triadin-null mice were generated (Shen et al., 2007; Oddoux et al., 2009): both were viable and suffered from subtle muscle ultrastructure alterations and from modest muscle weakness, suggesting no direct critical role of triadin in skeletal muscle ECC. In contrast, these mice have a clear cardiac phenotype that makes them affected by catecholaminergic polymorphic ventricular tachycardia (CPVT) (Chopra & Knollmann, 2009), and triadin mutations have now be identified in CPVT patients (Roux-Buisson et al., 2011). In a recent review, triadin (Trisk95) has been proposed as a scaffolding protein through -its capability as a polymer to alter the SR membrane shape and thus improve $Ca_V1.1$-RyR1 contacts and -its interaction with the microtubule network necessary for the stability and maintenance of the triadic ECC molecular complex (Marty, 2015).

Junctin together with triadin, are part of the triadin-junctin-calsequestrin complex that regulates, through CSQ, the RyR1 activity. Using mouse models lacking either triadin, or junctin or both, and comparing the effects on triad structure and Ca^{2+} handling it has been proposed that triadin plays a more relevant role in both features as compared to junctin (Boncompagni et al., 2012). A detailed model arrangement of Trisk95, junctin and CSQ has been proposed by Dulhunty et al. (2017) (Dulhunty et al., 2017).

Calsequestrin (CSQ) is the most abundant Ca^{2+} buffering protein in the SR of skeletal muscle with values between 11-36 µmol/L of fiber volume that vary depending on the fiber type. CSQ1 is the only isoform present in fast-twitch muscle fibers while both CSQ1 and the cardiac isoform CSQ2 are present in slow-twitch muscle fibers (Murphy et al., 2009). The two isoforms buffer SR luminal Ca^{2+} at 1-2 mM during the contraction/relaxation cycle. The impact of CSQ deficiency on intra-SR Ca^{2+} handling was elegantly demonstrated by Canato et al. 2010 (Canato et al., 2010). On the other hand, the functional role of CSQ1 in mouse muscle ECC has been carefully examined by E. Rios group: they reported that CSQ is essential for the process of closure of RyR1 channels, and thus termination of SR Ca^{2+} release, likely through the luminal Ca^{2+}-sensing capability of the protein, transmitted to RyR1 by a conformational change (Sztretye et al., 2011; Manno et al., 2017). This is in line with the general view that CSQ1 works as a Ca^{2+} sensor that communicates the calcium store load to the RyR1 channel.

Also worth mentioning is that CSQ1 has a role in Ca^{2+} signaling in a process called store-operated Ca^{2+} entry (SOCE) in skeletal muscle (Shin et al., 2003).

Finally, it is important to stress that CSQ1 knockout leads to malignant hyperthermia (Dainese et al., 2009) and environmental heat stroke (Michelucci et al., 2017) phenotypes, with some data pointing to a role of SOCE in the muscle contractures associated to these syndromes (Canato et al., 2010).

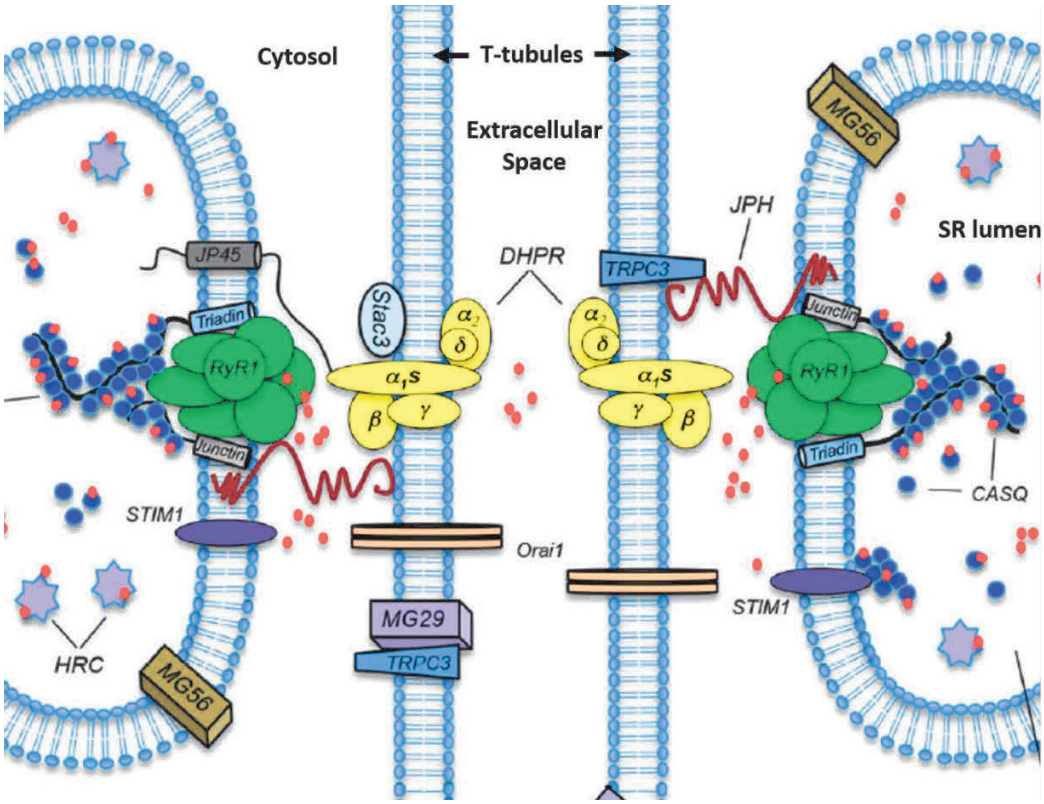

Figure 11. Schematic model of the triad in skeletal muscle and the protein complex relationship. *Two sarcoplasmic reticulum (SR) terminal cisternae are present on the opposite sides of a central t-tubule. We observe some of the different subunits and proteins that regulates ECC, T-Tubules and triad organization: $Ca_V1.1$ and its subunits, RyR1 and its homologous subunits, Stac3, JP45, Junctin, triadin and CASQ. Intraluminal interaction of RyR1, junctin, triadin, and Ca^{2+}-dependent polymerization of CASQ. Image modified from Barone et al. 2015.*

2.7.4. RyR1 phosphorylation, oxidation, and nitrosylation

RyRs phosphorylation has a role in RyR2 function and ECC in cardiac muscle as reported in a mouse model of atrial fibrillation where RyR2 hyperphosphorylation by CaMKII was associated with the induction of RyR2 into a leaky state (Li et al., 2014). RyR1 has several phosphorylation sites and can be phosphorylated by different enzymes like protein kinases A, G, C (PKA, PKG, PKC) or CaMKII which affects RyR1 open probability during in vitro experiments (Meissner, 2017). It has been proposed that RyR1 phosphorylation could be partially responsible for the fight-or-flight response not only in the heart (Shan et al., 2010) but also in the skeletal muscle, in which the contractile force is enhanced under acute

adrenergic stress. The enhancement of contractile force (inotropy) in skeletal muscle following the neuro-endocrine release of catecholamine and activation of β-adrenergic receptors has been widely studied. Andersson et al. in 2012 suggested that the phosphorylation of the residue serine in position 2844 (S2844) of RyR1 by protein kinase A (PKA) is critical for skeletal muscle inotropy. They treated fast-twitch skeletal muscles from wild type mice, with isoproterenol (a β-adrenergic agonist) and observed increased PKA-dependent RyR1 phosphorylation, RyR1-dependent Ca^{2+} release, and force generation. Then, they used mutated RyR1 replacing the serine for an alanine (S2844A) and observed no changes in all parameters when muscles were treated with isoproterenol, suggesting that the enhances in inotropy requires at least in part PKA-dependent RyR1-phosphorylation in serine 2844 (Andersson et al., 2012). Still, the extent of the β-adrenergic-induced gain in peak Ca^{2+} transient and force reported in this study were quite modest (~10%) raising doubt regarding the physiological relevance of this process.

Oxidative stress can regulate RyR1 activity through **RyR1-oxidation**. The oxidative modification of thiol residues in free cysteines, producing S-nitrosylation, S-glutathionylation, and disulfide oxidation can modulate RyR1 (Aracena et al., 2003; Aracena-Parks et al., 2006; Durham et al., 2008). The oxidative modifications can also affect the binding of accessory proteins. Some studies suggest that nitric oxide (NO) increases RyR1 channel activity through S-nitrosylation (Aracena-Parks et al., 2006), and produce CaM detachment and the reversion of CaM inhibitory effect over RyR1 (Moore et al., 1999). The role of oxidation in RyR1 and skeletal muscle function was postulated to participates in the pathogenesis of *Duchene muscular dystrophy (DMD)*, and this has been a matter of discussion over the years. The role of RyR1 hypernitrosylation in the pathogenesis of DMD was suggested using the mdx mouse model (Bellinger et al., 2009). DMD is a congenital and genetically X-linked disorder, produced by dystrophin deficiency, and is characterized by muscle weakness and early death. One hypothesis suggests that the lack of dystrophin leads to pathologic Ca^{2+} signaling which damages the fibers. Bellinger et al. reported an age-dependent increase in RyR1 S-nitrosylation correlated with the dystrophic changes in the disease muscles. They observed that S-nitrosylation depleted the FKBP12 protein, which produces unstable leaky RyR1 channels. After treating mdx mice with S107, a compound that enhances the FKBP12 binding to the RyR1 channel, there was an inhibition of the SR Ca^{2+} leak, improvement of histologic markers, of muscle function, and of exercise performance. Authors concluded that FKBP12 depletion and SR Ca^{2+} leak through S-nitrosylated RyR1 contribute to muscle weakness in the mdx mouse model of muscular dystrophy. These authors may have been inspired by a previous study by Pouvreau et al. (2004) who used isolated adult mouse muscle fibers to study the effect of nitric oxide (NO) as a modulator of RyR1 activity. They used sodium nitroprusside, which breaks into NO, and studied the resting Ca^{2+} and RyR1-depending Ca^{2+} release

under silicone- voltage-clamp conditions using the fluorescence dye indo-1. They found that NO produced an increase in resting Ca^{2+} that was triggered by depolarization-induced SR Ca^{2+} release. Their results suggest that large concentrations of NO capable of produce RyR1-oxidation generate a Ca^{2+} leak, observed as an increase in resting Ca^{2+}. They proposed that this alteration could have a role in the regulation of voltage-activated calcium release. Still, although several studies reported a reduction in voltage-activated SR Ca^{2+} release in muscle fibers from mdx mice (Woods et al., 2004; DiFranco et al., 2008), other did not (Head, 1993; Collet et al., 1999). However, the concept according to which RyR1-oxidation associated with nitric oxide and nitric oxide synthase (NOS) activity modulates ECC and RyR1 function in skeletal muscle and has an important role in the pathogenesis of DMD tends to be generally accepted (Allen et al., 2016).

A relationship between RyR1-oxidation and SR Ca^{2+} leak has also been raised in the condition of aging muscle: using 24-month-old mice, Andersson et al. observed an increased RyR1-oxidation as a RyR1-cysteine-nitrosylation, which produced "leaky" channels, a decrease in FKBP12 binding, an increase in RyR1 open probability, an intracellular Ca^{2+} leak, and muscle force impairment (Andersson et al., 2011).

2.8. RyR1 in skeletal muscle pathologies

Close to 300 human RyR1 mutations have been identified and associated with a wide array of skeletal muscle diseases (Lawal et al., 2020b). Because the corresponding literature is enormous it will not be our purpose to provide here a comprehensive view of all related aspects which have been covered by recent reviews (Lawal et al., 2018; Bauerová-Hlinková, et al., 2020; Lawal et al. , 2020a; Lawal et al., 2020b; Ogawa et al. 2020).

For simplicity, we will group them into two big categories depending upon their major effects on the RyR1 function. The first category generates a higher probability of RyR1 activation by muscle fiber electrical depolarization or by RyR1 activators, producing malignant hyperthermia susceptibility (MHS) features. In the second category, mutated RyR1 is leaky leading to Ca^{2+} handling dysregulation and SR Ca^{2+} depletion, which produce central core diseases (CCD) and multi-minicore disease (MmD) (Meissner, 2017).

2.8.1. Malignant hyperthermia Susceptibility (MHS)

The first group, as we introduced before, the Malignant Hyperthermia Susceptibility (MHS) is in most cases associated with RyR1 mutations as a subclinical, autosomal dominant, pharmacogenetic

disease, which causes a sudden intracellular Ca^{2+} dysregulation, triggered by the inhalation of volatile anesthetics (isoflurane, sevoflurane, halothane) or depolarizing muscle relaxants (succinylcholine). The MHS episodes are rare, but in their most complicated presentation, the patients develop muscle rigidity, hyperkalemia, arrhythmias, respiratory and metabolic acidosis, and an alarming increase in body temperature. Untreated MHS crisis is lethal in 90% of the cases, and sequels include brain, kidney, and muscle tissue damages (Rosenberg et al., 2007). A way to study MHS has been a close model of the disease in pigs, called porcine stress syndrome (PSS), which results from a RyR1 mutation (R615C, the substitution of arginine for cysteine in position 615) that is triggered by several events like exercise, parturition, and overcrowding. Muscles from animals suffering PSS and from human patients with MHS are hypersensitive to caffeine, which constitutes the basis for a clinical test of susceptibility in humans. RyR1 channels isolated from MHS human patients exhibit a greater Ca^{2+} sensitivity for Ca^{2+}-dependent activation and resistance to Ca^{2+}-dependent inactivation, with longer RyR1 opening time and higher Ca^{2+} requirement for inactivation during single-channel records in lipid bilayers (Valdivia et al., 1991). Today, it is generally accepted that the mechanism underlying MHS is SR Ca^{2+} leak due to RyR1 hyperactivity and approximately 100 different RyR1 mutations related to MHS have been characterized in different cellular models, like cultured myotubes (Bannister et al., 2010; Chelu et al., 2006), matures muscle fibers from animal models (Chelu et al., 2006; Andronache et al., 2009), and from human patients (Melzer & Dietze, 2001). This disease condition alters Ca^{2+} homeostasis, increases cytosolic Ca^{2+} and promotes ATP hydrolysis by the *SarcoEndoplasmic Reticulum Ca^{2+} pump (SERCA)*, which is on high demand to reestablish the Ca^{2+} homeostasis, generating the characteristic heat in MHS. Thus, it is generally accepted that MHS mutations are characterized by a gain of function, hyperactivity, and hypersensitivity to pharmacological activators which lead to current treatments focuses on the suspension of the triggering agents, cooling measures, 100% oxygen administration, and the administration of RyR1-dependent SR Ca^{2+} release inhibitors like dantrolene sodium (Szentesi et al., 2001; Kobayashi et al., 2005; Oo et al., 2015).

2.8.2. RyR1-related congenital myopathies: Central core disease, Multiminicore myopathy and Centronuclear myopathy

The RyR1-related congenital myopathies are a group of disorders that present either autosomal dominant or recessive inheritance pattern, characterized by generalized muscle weakness or low muscle tone, from birth or starting during childhood. They are many forms of congenital myopathy, with specific patterns of histological abnormalities and clinical prognosis (Nance et al., 2012). The common clinical presentation includes ophthalmoparesis (eye muscle weakness), myasthenia (muscle weakness),

abnormal movement, associated less frequently with respiratory muscle dysfunction, scoliosis, or swallowing impairments (Jungbluth et al., 2018). *Central core disease (CCD)* and *Multiminicore myopathy (MmD)* are the most common subgroup in RyR1 related congenital myopathies. CCD is an autosomal-dominant myopathy associated with mutations in RyR1. CCD presents non-progressive muscle weakness, hypotonia, and motor deficiencies. It affects predominantly type 1 skeletal muscle fibers, generating Ca^{2+} leaks associated with the lack of mitochondria in the central areas of the muscle fibers. At the cellular level, core myopathies shown region in the muscle fibers lacking mitochondria and appear as large "cores" longitudinally extended on oxidative stains. The MmD has shown shorter cores that vary in size and location (Capes et al., 2011).

Different mutations in RyR1 are been related with malignant hyperthermia susceptibility (MHS) and central core disease (CCD) simultaneously. In a mixed MHS/CCD model associated with Y522S-RyR1 mutation (the substitution of tyrosine for serine at position 522) it was shown an increased Ca^{2+} leak, the activation of reactive nitrogen species, the induction of RyR1 S-nitrosylation, which increase its sensitivity to temperature, and produce a mitochondria alteration (Durham et al., 2008). Conversely, the pure CCD mutation related phenotypes are characterized by a reduction on SR Ca^{2+} release independent of change in RyR1 sensitivity or SR Ca^{2+} content. Avila et al. (2001) expressed different CCD mutation NHT-related and expressed in myotubes from RyR1-knockout (dyspedic) mice. They observed an elevation in resting Ca^{2+} associated with smaller and more negative activated RyR1-dependent SR Ca^{2+} release. They conclude that NHT-related CCD mutants enhance release channel sensitivity to voltage-dependent activation leading to SR Ca^{2+}, store depletion, and a reduction voltage-gated in Ca^{2+} release (Avila & Dirksen, 2001).

In 2011, Lefebvre et al. studied the CCD-related I4897T-RyR1 mutant (the replacement of an isoleucine for a threonine in position 4897 of RyR1). They expressed transitory the I4897T-RyR1 mutant in adult skeletal muscle fibers and observed no relevant changes in the RyR1-dependent Ca^{2+} release and conclude that RyR1 density is tightly regulated even under conditions of forced exogenous expression (Lefebvre et al., 2011). In another work the same group evaluated the function of R4892W and G4896V RyR1 mutants associated with CCD in humans. They expressed the mutant first in RyR1-null (dyspedic) myotubes and observed the absence of voltage-gated Ca^{2+} release, and only a partial restoration when coexpressing RyR1 mutant together with wild-type RyR1. Second, they expressed the RyR1 mutants in fibers from adult WT mice and observed the location in restricted regions with a pattern representative of triadic localization. In the G4896V-RyR1 mutant expressing regions of the differentiated muscle fibers, they observed a 30% decrease in the peak rate of voltage-gated RyR1-dependent SR Ca^{2+} release, with no

changes SR Ca^{2+} contents or $Ca_V1.1$ and SERCA expression evaluated by immunostaining. Conversely, they didn't observe any change in the R4892W-RyR1 mutation, even with good level of junctional expression, and concluded that this particular RyR1 mutation present a low functional penetrance in CCD disease (Lefebvre et al., 2013).

It has been proposed that the mechanism behind the RyR1-related CCD phenotype is a dominant-negative suppression of RyR1 channel Ca^{2+} permeation which produce a reduction in the magnitude and rate of RyR1-dependent SR Ca^{2+} release during ECC (Loy et al., 2011).

In others models, the decrease in electrically evoked Ca^{2+} release and force production in a CCD-related RyR1-mutation, it has been associated to an 80% decrease in RyR1 channel expression, with a reduced body/muscle mass and myofiber hypotrophy (Brennan et al., 2019). In a related study, Pelletier et al. (2020) generate a mouse model with inducible muscle specific RyR1 deletion. They observed that tamoxifen-induced recombination in the *RYR1* gene in adult mice result in a progressive reduction of RyR1 protein content reaching the 50 % of the initial values, and was associated with a progressive muscle weakness and atrophy. In collaboration with our laboratory, they studied isolated muscle fibers and observed a reduction in the amplitude of RyR1-dependent SR Ca^{2+} release, fibers atrophy, abnormal mitochondria distribution and membrane remodeling. In this model they demonstrated that RyR1 reduction is sufficient to reproduce most features of CCD (Pelletier et al., 2020).

RyR1 mutations have also been suspected to be associated with certain forms of *centronuclear myopathy* (CNM) (Wilmshurst et al., 2010). CNMs represents a heterogeneous group of muscle diseases (see Jungbluth et al. 2018) which, besides being all characterized by muscle weakness (of various extent and age of onset), essentially only share the presence of nuclei in central position in the patient's myofibers with no associated degeneration/regeneration processes. It is associated with mutations in the myotubularin gene *MTM1* (X-linked, most severe form), autosomal dominant mutations in dynamin 2 (*DNM2*), autosomal dominant and recessive mutations in amphiphysin II (*BIN1*), and autosomal recessive mutations in Titin (TTN), and *RYR1* (Jungbluth et al., 2018). In 2009 Al-Qusairi et al. used an MTM1 deficient mouse model of CNM, and observed an abnormal longitudinally oriented T-tubule network, associated with a strongly depressed RyR1-dependent SR Ca^{2+} release under voltage-clamp conditions, which strongly suggest that defective RyR1-mediated SR Ca^{2+} release function is responsible for the muscle function failure in this type of CNM (Al-Qusairi et al., 2009). SR Ca^{2+} release defects have also been revealed in other types of CNMs (Kutchukian et al., 2017; Huntoon et al., 2018). How these CNMs are associated with SR Ca^{2+} release deficiency still remains obscure. Conversely, no model of RyR1 mutation-

induced CNM has been investigated yet. This may provide in the future interesting clues into the diseases mechanisms.

2.9. RyR1 Pharmacology

The **ryanodine** receptors (RyRs) have their names from the strong affinity and binding to the alkaloid ryanodine, found naturally in the stem and roots of the plant Ryania speciosa. This strong affinity has allowed the isolation and characterization of RyRs (Fill & Copello, 2002). Three concentration-dependent types of effects on single RyR1 channel function are observed in the presence of ryanodine. At low nanomolar concentrations, ryanodine produces an increase in channel opening at a full conductance state. At submicromolar (0.01-1μM) the RyR is locked in a slow-gating subconductance state, producing long-lived small unit currents (≈1/3 or ≈1/2 of control amplitude) (Hymel et al., 1988; Lai et al., 1988; Smith et al., 1988). The application of ryanodine at this concentration in cardiac muscle produces a Ca^{2+} leak current from intracellular stores into the cytosol, but elevated cytosolic Ca^{2+} is removed rapidly from the cell by strong Ca^{2+} extraction mechanisms generating a flaccid cardiac paralysis. Skeletal muscle does not have strong Ca^{2+} extraction mechanisms, thereby ryanodine-RyR1 binding produces a chronic increase of cytosolic Ca^{2+}, a sustained contraction associated with a rigid skeletal muscle paralysis (Fill & Copello, 2002). The application of ryanodine at a higher concentration (>10μM) increases the open probability (P_0) while decreasing single-channel ion conductance (ion translocation through a single channel). The marked increase in P_0 far outweighs the reduced conductance, and it is expected to increase the rate of Ca^{2+} release. However, ryanodine at high concentration, with time, promotes closure of the channels. Related to these experimental data, it was shown that RyRs have high (K_D 1-10nM) and low (K_D 1-10μM) affinity binding sites (Sutko et al., 1997). It is proposed that the concentration dependence is explained because ryanodine should reach an intracellular concentration sufficient to allow the interaction with low-affinity sites to produce the RyRs inhibition. It was also shown that RyRs are more sensitive to ryanodine in their open state. A study made in our laboratory, by Collet et al. using enzymatically digested mouse skeletal muscle fibers under silicone voltage-clamp condition, confirm the use-dependence and open-locked theory in physiological conditions. These authors also showed that both: the amplitude and the duration of plasma membrane depolarization enhance the quantity of RyR1 channels accessible to ryanodine (Collet & Jacquemond, 2002). Therefore, ryanodine is a highly specific modulator of RyR-dependent SR Ca^{2+} release and has been extensively used for the study of this process (Thomas & Williams, 2012).

The local anesthetic **tetracaine** inhibits SR Ca^{2+} release in muscle (Zucchi & Ronca-Testoni, 1997). At millimolar concentration tetracaine produces a decrease in RyR-dependent Ca^{2+}-release and a decrease in contraction, and both with time, return to control values (Thomas & Williams, 2012). In experiments with isolated rat skeletal muscle fibers under vaseline gap voltage-clamp, Csernoch et al, showed that 50μM tetracaine in the cytosol decreases RyR1-dependent SR Ca^{2+} release, and suggested that it was the consequence of a decrease in the open probability of RyR1s when interacting with the drug (Csernoch et al., 1999).

The clinically used RyR1-inhibitor is **dantrolene**, which has a presumably identified binding site of action in the primary sequence of the RyR protein (Paul-Pletzer et al., 2002) is used for clinical treatment of MH (Zucchi & Ronca-Testoni, 1997). However, the treatment is not 100% effective, and the action mechanism behind the RyR1-inhibition by dantrolene is unclear. Several groups are shown contradictory results related to the inhibitory effects of dantrolene under different conditions (Szentesi et al., 2001; Diaz-Sylvester et al., 2008; Wagner et al., 2014). Szentesi et al. observed that dantrolene was able to inhibit Ca^{2+} release from intact fibers and SR vesicles, but failed to inhibit RyR1 single channel currents. They concluded that there is an important cofactor for dantrolene action that is lost during the purification procedure of RyR. In a recent work, the same group used RyR1 single-channel recording in lipid bilayer, and observed that dantrolene-dependent RyR1 inhibition needs the presence of millimolar levels of ATP and Mg^{2+} to properly work (Diszházi et al., 2019).

For the pharmacological stimulation of RyR1, several compounds have been described like **caffeine** and ruthenium red, which increase the open probability of the channel in single-channel records in lipid bilayers (Zucchi & Ronca-Testoni, 1997). In this context, the golden standard for the diagnosis of MHS, is the halothane/caffeine contracture test which makes use of muscle fibers bundles from a biopsy. However, there is variability in the responses that overlap that of normal fibers (von Breunig et al., 2004). Furthermore, some patients test positive to halothane only and may represent a separate diagnostic group (Figueroa et al., 2019).

2.10. The sarco-Endoplasmic Reticulum Ca^{2+} ATPase or SERCA pump

2.10.1. SERCA family

The sarcoEndoplasmic Reticulum Ca^{2+} ATPase (SERCA) pump is a versatile, evolutionary conserved transmembrane protein present in prokaryotes and eukaryotes. As a calcium transporter, SERCA keeps a

low cytosolic Ca^{2+} level, allowing regulation of a large array of signaling pathways and physiological processes like synaptic transmission or muscle contraction and plays a role in several cell functions like growth and differentiation.

In vertebrates, SERCA protein is coded by three different genes; *SERCA1* (or *ATP2A1*), *SERCA2* (or *ATP2A2*), and *SERCA3* (or *ATP2A3*); which produce ten isoforms through alternative splicing. *SERCA1* is expressed in fast-twitch skeletal muscle and suffer alternative splicing to produce SERCA1a and SERCA1b isoforms. *SERCA2* encodes SERCA2a isoform which is expressed in cardiac muscle and slow-twitch skeletal muscle fibers, SERCA2b is weakly expressed in all tissues and SERCA2c only in cardiac muscle. Finally, *SERCA3* is expressed in non-muscle tissue but also in skeletal muscle, and codes for 6 isoforms (Periasamy & Kalyanasundaram, 2007).

2.10.2. The SERCA structure

SERCA belongs to a family of P-type ATPases, as plasma membrane Ca^{2+}-ATPase (PMCA), Na^{+}/K^{+}-ATPase, and H^{+}, K^{+}-ATPase. SERCA is a single polypeptide of molecular mass 110 kDa and is located in the SR membrane of the muscle fibers (Sweadner & Donnet, 2001). The primary structure of SERCA is highly conserved between all the isoforms. SERCA2a isoform is about 84% identical to SERCA1a, and SERCA3 isoform is 75% identical to SERCA1 or SERCA2, so the proteins are predicted to have essentially identical transmembrane topologies and tertiary structures. The SERCA1a pump is composed of 994 amino acids and his crystal structure confirm the presence of 10 transmembrane helices (M1-M10), three cytoplasmic domains; an anchor domain (A domain), a phosphorylation domain (P domain), and a Nucleotide (N domain) (see Fig. 12) (Periasamy & Kalyanasundaram, 2007). Each cytoplasmic domain has a unique role in regulating the SERCA function. The A domain provides the pivot for the translocation of Ca^{2+} while the ATP hydrolysis takes place at the interface between the N and P domains. Using mutagenesis of several sites in the protein, it has been shown that Ca^{2+} binding sites are near the center of the transmembrane domain, near the cytoplasmic surface of the lipid layer, with 1 binding site on each side (Clarke et al., 1989; Toyoshima, 2009).

2.11. SERCA function and related skeletal muscle pathologies

2.11.1. SERCA function

The SERCA pumps are capable of transferring a phosphate from ATP, producing a conformational change coupled to the movement of ions through a biological membrane against their concentration gradient. Once the calcium sites are occupied, the SERCA uses the energy from the hydrolysis of one molecule of ATP to produce its conformational change and transport two Ca^{2+} across the SR membrane into the SR lumen, while at the same time two-to-three protons are counter-transported into the cytoplasm. This active transport is achieved, by changing the affinity of Ca^{2+} binding sites from high (E1) to low (E2) affinity. This process takes place during the transition from phosphorylated E1 (E1P) to a phosphorylated E2 (E2P) (by using ATP, the SERCA pump generates autophosphorylation on an aspartyl residue, position 351 in P domain) (Fig. 12).

Because the SERCA pump is highly expressed in the SR, Ca^{2+} reuptake takes only a few milliseconds, allowing a fast rate of relaxation in mice (Periasamy & Kalyanasundaram, 2007).

Besides the SERCA pump activity related to the cytosolic Ca^{2+} regulation, there is another important function for SERCA related to the *"nonshivering thermogenesis" (NST).* In this process, it has been shown that sarcolipin (SLN) is necessary for the NST because, in the presence of a SR Ca^{2+} leak, its interaction with SERCA activation promotes heat generation. In a study made by Bal et al., in 2012, using $SLN^{-/-}$ null mice vs wild type, when they surgically ablated interscapular brown adipose tissue of both groups and expose them to 4°C, the $SLN^{-/-}$ null mice were not capable to keep their core body temperature at 37° and develop hypothermia with death after 10 hours of exposure, while overexpressing SLN in the null mice completely restored muscle-based thermogenesis. They also showed that SLN can interact with SERCA at high Ca^{2+} concentration and they concluded that SLN promotes the uncoupling of the SERCA pump, leading to increased ATP hydrolysis and heat production. This process is responsible for 40-50% of the skeletal muscle basal metabolism which, as observed in Bal et al. study transferred into a bigger increase in the body weight and fat accumulation in $SLN^{-/-}$ mice under high fat diet (HFD) as compared with HFD wild type mice (Bal et al., 2012; Smith et al., 2013).

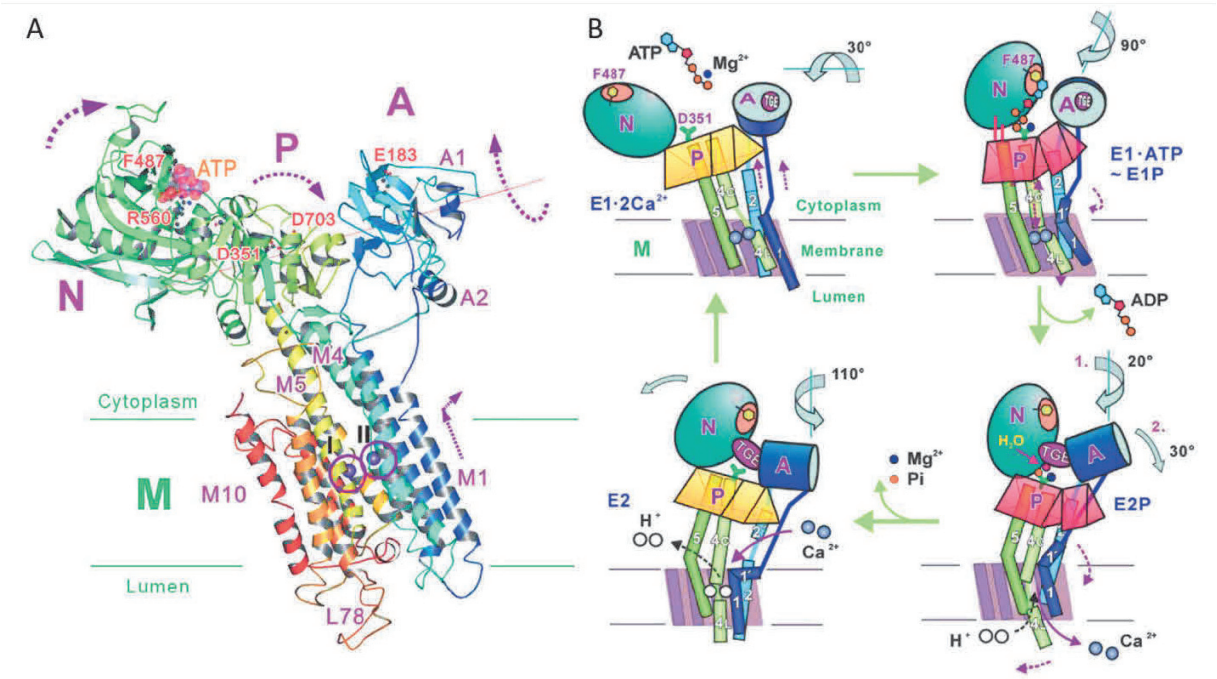

Figure 12. Architecture of sarcoendoplasmic reticulum Ca^{2+} pump (SERCA) and its ion pumping mechanism. *A) secondary and tertiary representation of SERCA subunits in the E1 ·2Ca^{2+} state. We observe the 10 transmembrane domains from the amino terminus (blue) to the carboxyl terminus (red), and the cytosolic N, P and A domain. Purple spheres represent Ca^{2+} bound. Axis of rotation (or tilt) is indicated with the orange line. B) A cartoon illustrating the structural changes of SERCA during its reaction cycle, based on the crystal structure analysis in different states. Image taken from Toyoshima et al. 2009.*

2.11.2. SERCA regulatory partners

SERCA pump activity can be regulated by Ca^{2+} ion concentration, ATP level, pH, ADP, and inorganic phosphate levels, affecting one or more of its functional steps: Ca^{2+} affinity, phosphorylation rate, E-P formation (ATP binding and hydrolysis), and decomposition of E-P (see Fig.10). Using adenoviral gene transfer and heterologous expression in COS-1 cells lines, Sumbilla et al. compared the exponential decay of the phosphorylated enzyme intermediate state and showed that Ca^{2+} transport in SERCA1a was two times higher than in SERCA2a suggesting a functional advantage of SERCA1 present in muscle fibers which require a faster rate of Ca^{2+} uptake (Sumbilla et al., 1999). The SERCA pump activity is also regulated by small proteins located in the SR; phospholamban, sarcolipin, and myoregulin in a tissue-specific manner.

Phospholamban (PLN) is a small protein (52 aa) expressed in the SR of cardiac muscle fibers (principally, fibers from the ventricles) and slow-twitch muscle fibers. At low cytosolic Ca^{2+} concentrations, PLN works as an active inhibitor of SERCA2a, decreasing its apparent affinity for Ca^{2+}. At high cytosolic Ca^{2+} concentration, PLN is inhibited by Ca^{2+}/calmodulin kinase (CaMKII) (a serine/threonine-specific kinase) which phosphorylates PLN at threonine position 17, increasing SERCA2a activity 2-3 times (see Fig. 11). Under β-adrenergic stimulation, SERCA2a activity is increased as a consequence of the inhibition of PLB by protein kinase A (PKA). β-adrenergic stimulation activates PKA, which phosphorylate PNL at the serine position 16, and blocks the inhibition of SERCA2a, increasing its activity 2-3 fold and enhancing the rates of contraction and relaxation in cardiac muscle (Simmerman & Jones, 1998; Toyoshima et al., 2003; Periasamy et al., 2008). Thus, the regulation in the PLN content or phosphorylation state is critical for the activity of SERCA2a in the heart. Phospholamban is expressed in slow-twitch skeletal muscle fibers, but it doesn't have an important role in the regulation of calcium uptake suggesting that is not tightly coupled to the SERCA pump activity and that it maybe plays another role in the slow-twitch skeletal muscle fibers (Briggs et al., 1992). In more recent works it has been shown using PLB-null mice that PLN deficit does not alter SERCA2a function in the soleus, a slow-twitch fibers type muscle (Gamu et al., 2019).

Sarcolipin (SLN) , already mentioned in the previous section, is an homolog of PLN with a well-conserved transmembrane domain although smaller (31 aa) (see Fig. 13), expressed at high levels in the heart (principally the atria) and in fast-twitch type muscle fibers, with lower expression in slow-twitch type fibers (Babu et al., 2007). As PLN, SLN physically interacts with the SERCA pump, decreasing the apparent Ca^{2+} affinity of the pump.

Babu et al. used a sarcolipin-null mice model and did not found developmental abnormalities or cardiac pathologies, neither changes of expression in other Ca^{2+} handling proteins, in particular PLN. They observed, in cardiac muscle fibers from the atria, that the ablation of sarcolipin produces an increase in the affinity of the SERCA pump for Ca^{2+}, an increase of the maximum values of Ca^{2+} uptake rates, and an increase in Ca^{2+} transients enhancing atrial contractility (Asahi et al., 2003; Gramolini et al., 2006; Babu, et al., 2007). Similar to PLN, SLN phosphorylation at the threonine position 5 by serine/threonine kinase 16 (STK16), produces the dissociation of SLN from SERCA and is believed to mediate the relaxation under β-adrenergic stimulation (Bhupathy et al., 2009). Further, it has been found that SLN expression is dysregulated in patients with cardiovascular disease (Zheng et al., 2014). SLN has also been implicated in the regulation of SERCA1a isoform in fast-twitch skeletal muscle (Asahi et al., 2003). There is also another role proposed for SLN as a regulator of thermogenesis and whole-body metabolism: as mentioned before

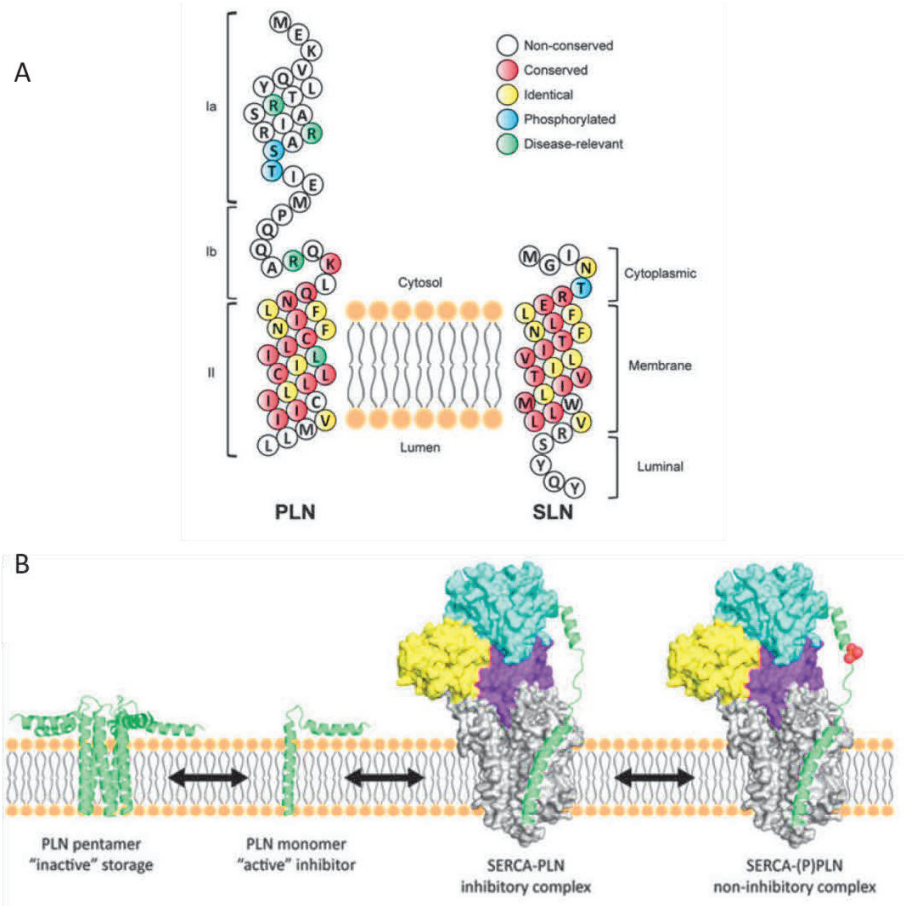

Figure 13. Interaction of SERCA with the regulatory proteins PLN and SLN. *A) Topology model of PLN and SLN. Domain structure is shown on the left and right for PLN and SLN, respectively. Non-conserved, conserved, identical and phosphorylated residues colors are explained in the legend. B) SERCA representation with P-domain in magenta, N-domain in cyan and A-domain in yellow. The transmembrane domain is in grey and PLB is in green. Phosphorylated PLN is shown with orange spheres in the cytoplasmic domain. We observe that PLN exists in dynamic equilibrium between pentameric and monomeric states. Monomeric PLN works as a SERCA inhibitor. Phosphorylation of PLN relieves the inhibition of SERCA. Image taken from Gorski et al. 2017.*

it is suggested that SLN participates in the regulation of skeletal muscle thermogenesis through SERCA regulation promoting uncoupling of the pump and increasing total energy expenditure (Bal et al., 2012; Bombardier et al., 2013; Gamu et al., 2014).

SLN has also a role in the pathogenesis of *Duchenne Muscular Dystrophy (DMD)*. Three important works highlighted this new role. First, Schneider et al. showed that in DMD mouse models, SLN is abnormally high and that this correlates with a decrease in maximum velocity of SR Ca^{2+} uptake in fibers from soleus, diaphragm, and quadriceps of mild (mdx) and severe (mdx:$utr^{-/-}$) DMD mouse models (J. S. Schneider et al., 2013). Then, Voit et al. showed in 2017, that a decrease in SLN expression improves DMD in the most representative mouse model of the human DMD clinical presentation. They used the dystrophin/utrophin double mutant (mdx:$utr^{-/-}$) mouse model, and observed an upregulation of SLN in cardiac and in skeletal muscle. When they inactivated one allele, there was normalized SLN expression and restoration in SERCA function associated with an improvement in muscle regeneration and lifespan (Voit et al., 2017). Finally, Niranjan et al. suggested that SLN has a role in the impaired myogenic differentiation in DMD, using cultured muscle cells from a dystrophin-deficient dog model. They found an SLN upregulation in myoblasts and myotubes from this model, associated with Ca^{2+} mishandling, and this phenotype was partially reversed by inhibition of the overexpressed SLN (Niranjan et al., 2019).

In 2015, two micropeptides were identified and found to interact with SERCA in muscle: myoregulin and dwarf open reading frame (Anderson et al., 2015; Nelson et al., 2016).

Myoregulin (MLN) is a 46 amino acid transmembrane peptide expressed in fast-twitch skeletal muscle that inhibits SERCA according to a similar mechanism (also exhibiting a similar structure) as PLN and SLN (Anderson et al., 2015).

Recently Nelson et al. have shown a new regulator for SERCA activity in muscle, named ***"dwarf open reading frame" (DWORF)***. DWORF is a peptide of 34 amino acids produced by a muscle-specific long noncoding RNA (lncRNA). DWORF enhances SERCA activity by counteracting the SERCA inhibitors: phospholamban, sarcolipin, and myoregulin. These authors generated a DWORF KO mouse model, a DWORF overexpression model, and studied DWORF expression in different tissues, muscle force, and Ca^{2+} handling. First, they observed that DWORF is present only in the heart and in the soleus, a muscle enriched in slow-twitch fibers. They showed that DWORF KO generates a decrease in the Ca^{2+} affinity and an increase in the relaxation time for the heart muscle, and they also observed a decrease in the apparent Ca^{2+} affinity of SERCA, and increased fatigability of soleus muscle under tetanic stimulation (Nelson et al., 2016).

There is also a **hormonal regulation** of SERCA pump expression. It has been shown that deficits in the Thyroid hormone (T4) levels, decrease SERCA2a, and increase phospholamban expression in the heart

(Kiss et al., 1994). It was also found a protective effect or T4 in the development of hypertrophic cardiomyopathy. The treatment with T4 improved cardiac fibers contractility with faster relaxation and cytosolic Ca^{2+} decline (Chang et al., 1997). In skeletal muscle, the response to alteration in T4 is fiber-type dependent with a decrease of both isoforms (SERCA1 and SERCA2) in slow muscle type (soleus), and an increase of SERCA2a in fast muscle type (EDL) (Sayen et al., 1992).

Physical exercise has a role in SERCA2a regulation. It is generally accepted that aerobic exercise enhances SERCA2a mediated Ca^{2+} uptake and cardiomyocytes contractility (Wisløff et l., 2002). It has been proposed that this occurs through phosphorylation of CaMKII and phospholamban (Kemi et al., 2007). Accordingly, several works highlighted the SERCA2a regulation in the heart with different endurance training (Stammers et al., 2015).

The different SERCA isoform relies on the **innervation** and frequency of stimulation. It has been shown that the denervation generates a change in the expression of SERCA1a or SERCA2a depending on the muscle studied (Periasamy & Kalyanasundaram, 2007). Pette et al. have shown that after 30 days of chronic low-frequency electrical stimulation in tibialis anterior from a rabbit, there was an upregulation in SERCA2a (slow isoform) and a downregulation of SERCA1a showing that innervation and frequency of stimulation regulate excitation-contraction properties and the expression of different SERCA isoforms (Pette & Vrbová, 1999).

2.11.3. SERCA in skeletal muscle pathologies

SERCA genes mutations generate human diseases. The most well-known is Brody's disease, a rare inherited disorder in which the SERCA1a gene is mutated, affecting skeletal muscle function. The patients suffer from severe cramps and manifest exercise-induced impairment of skeletal muscle relaxation because of an ineffective transport of Ca^{2+} into the SR after muscular contraction (Odermatt et al., 1996).

The deletion of both copies of the *SERCA2* is lethal in most species including nematode, Drosophila, and mouse. Deletion of just one copy of *SERCA2* causes and autosomal-dominant skin disease in human, Darier's disease, producing keratinized squamous epithelial cells without any heart disease, showing that a single SERCA2 allele is sufficient to maintain normal cardiac function (Shull et al., 2003; Periasamy & Kalyanasundaram, 2007;).

2.12. Bidirectional relationship $Ca_V1.1$-RyR1: Orthograde and retrograde coupling

The control of RyR1 by $Ca_V1.1$ has also been called "orthograde" coupling because during ECC, the RyR1 activation takes place downstream of $Ca_V1.1$ activation. An upstream-like regulation, called "retrograde" coupling, has also been demonstrated, through which RyR1 is capable of regulating $Ca_V1.1$ function. The bidirectional coupling, orthograde and retrograde between $Ca_V1.1$ and RyR1 has been largely described over the past two decades (Nakai et al., 1996; Bannister & Beam, 2009; Bannister et al., 2016;). The initial observation was reported in 1996 by Nakai et al.: studying the role of RyR1 using RyR1-deficient myotubes (myotubes from dyspedic mice) these authors observed that together with the suppression of sarcoplasmic reticulum Ca^{2+} release, the L-type Ca^{2+} current was strongly reduced. However, the charge movement was preserved, assessing the conservation of $Ca_V1.1$ density and voltage-sensing function. When then, expressing RyR1 in the dyspedic myotubes, not only Ca^{2+} release was recovered but also the L-type Ca^{2+} current through $Ca_V1.1$. This was the first demonstration for a retrograde signal and authors proposed that the presence of RyR1 stabilizes higher-conductance states and/or affects the open probability of $Ca_V1.1$ (Nakai et al., 1996). These results implied that the presence of RyR1 somehow increases $Ca_V1.1$ P_0 (open probability). Other studies have shown that RyR1 has also an impact on $Ca_V1.1$ activation kinetics, with dyspedic L-type Ca^{2+} currents showing accelerated activation compared with normal myotubes or dyspedic myotubes transfected with wild-type RyR1 (Avila & Dirksen, 2000; Sheridan et al., 2006). In 2009, Bannister and Beam investigated the myotubes response to high concentrations of ryanodine (200 µM, 1 hour at 37°C) which, supposedly, locks RyR1 in a non-conducting and inactivated conformational state. In this condition, they observed a potentiation of the L-type Ca^{2+} current and a small but consistent hyperpolarizing shift in the voltage dependence of its activation associated also with a hyperpolarizing shift in the voltage dependence of charge movement for $Ca_V1.1$. To clarify the possible direct interaction between the ryanodine drug and $Ca_V1.1$, they realized the same series of experiments in a group of dyspedic myotubes and they did not observe any change in the L-type Ca^{2+} current or charge movement. Thus, they concluded that ryanodine-mediated potentiation of skeletal muscle L-type Ca^{2+} current requires the presence of RyR1 (Bannister & Beam, 2009). It has also been shown that the α1S II-III loop of $Ca_V1.1$, and the carboxyl-terminus of the β1a auxiliary subunit of $Ca_V1.1$ are the important structures that interact with RyR1 in this bidirectional relationship (Sheridan et al., 2004; Cheng et al., 2005; Sheridan et al., 2006). Finally, a more recent study made in 2016 by Bannister, Sheridan, and Beam, used myotubes from homozygous lethal RyR1 mutant mice (RyR1-E4242G, the substitution of Glycine for Glutamate at position 4242 of RyR1) which are incapable of Ca^{2+} release and

electrically evoked contractions, because of a consequent ablation of orthograde $Ca_V1.1$-RyR1 coupling. They observed in this model an important reduction of L-type Ca^{2+} current density, $Ca_V1.1$ $P_{0,}$ and $Ca_V1.1$ expression. They also studied charge movement and ionic tail currents and concluded that the reduction in current amplitude was a consequence of both a decrease in $Ca_V1.1$ membrane expression (50%) and a reduced channel P_0 (55%). In opposition, kinetics activation of L-type Ca^{2+} current in RyR1-E4242G fibers were similar to normal myotubes, contrary to dyspedic myotubes (RyR1 null), in which L-type Ca^{2+} current exhibits an important acceleration on its activation kinetics. According to these observations, they concluded that RyR1-E4242G affects the retrograde coupling in two functionally independent components; increasing $Ca_V1.1$ P_0 and slowing down L-type Ca^{2+} current activation, which should be related to different structural elements of RyR1 (Bannister et al., 2016). In any case, it is now clear that another function for RyR1 is the retrograde regulation of open probability (P_0) and activation kinetics of $Ca_V1.1$ L-type Ca^{2+} channels and that $Ca_V1.1$ and RyR1 have a bidirectional relationship (Andronache et al., 2009; Bannister et al., 2016). These results have critical relevance for our project because they open the possibility for other bidirectional relationships, for example between $Ca_V1.1$ and Panx1, which already have a unidirectional relationship described in more detail in the next chapter.

2.13. Other important proteins that regulate $Ca_V1.1$, $Ca_V1.1$-RyR1 interaction, and ECC

As we mentioned in the previous section, they are several proteins that can regulate RyR1 and ECC. We can mention cytoplasmic proteins that classically have been related to RyR1 like CaM, S100A1, FKBP12, and luminal regulation through the triadin-junctin-CSQ complex.

Several proteins have the ability to regulate $Ca_V1.1$ α1S subunit, as the auxiliary subunits, β1a (Schredelseker et al., 2009), α2δ (Obermair et al., 2005), and γ1 (Freise et al., 2000) as well as Caveolins (Couchoux et al. 2011). The $Ca_V1.1$ regulatory proteins present in the SR include JP45 (A. A. Anderson et al., 2006), Junctophilins (Golini et al., 2011), and RyR1 with the retrograde regulation. Other cytosolic regulators of $Ca_V1.1$ include CaM (Ohrtman et al., 2008; Stroffekova, 2008) and STAC3 (Horstick et al., 2013; Linsley et al., 2017).

Because of our interest in the potential regulation of $Ca_V1.1$ and ECC by the plasma membrane protein pannexin 1, we are going to further focus in the present section on other proteins that can influence $Ca_V1.1$ and muscle function in a relevant way, like STAC3, caveolin-3 and junctophilins.

In 2013, two independent laboratories found a new triadic protein called ***"SH3 and cysteine-rich protein 3" (STAC3)*** that plays a critical role in the regulation of $Ca_V1.1$, the $Ca_V1.1$-RyR1 interaction, and ECC function (Horstick et al., 2013; Nelson et al., 2013). STAC3 is a skeletal muscle-specific adaptor protein essential for ECC. Human mutations in STAC3 have been related with Native American myopathy (Horstick et al., 2013) and recently, three different case-report studies found non-Native American families, with myopathy-like muscle impairments (Grzybowski et al., 2017; Telegrafi et al., 2017; Zaharieva et al., 2018). To understand the role of STAC3, Horstick et al. in 2013 used a zebrafish model with an autosomal recessive *STAC3* mutation and severe motor defects. The embryos in this model were immotile and the muscle failed to generates SR Ca^{2+} release and to contract under electrical stimulation. They observed that in normal skeletal muscle STAC3 co-localizes and co-immunoprecipitates with $Ca_V1.1$ and with RyR1. However, the *STAC3* zebrafish mutants does not exhibit changes in triads ultrastructure despite the important decrease of SR Ca^{2+} release, highlighting its direct relevance for ECC. Horstick et al. also found that a point mutation in the human *STAC3* locus (W284S, replacement of tryptophan for serine in position 284 of STAC3) was associated with the congenital Native American myopathy and could explain at least partially its characteristic muscle weakness. In another study, Nelson et al. characterized *STAC3* knock-out mice. They observed that the homozygous deletion of *STAC3* in a mouse model leads to complete lack of ECC, paralysis, and perinatal lethal asphyxia. In myotubes from this mouse model, the ECC defect was not related to a RyR1 dysfunction or to an SR content defect. These results further highlighted the direct interaction of STAC3 with the ECC machinery (Nelson et al., 2013). In 2017, Linsley et all. expressed the STAC3 mutation responsible for the native American disease in zebrafish muscle fibers and investigated its consequences using electron microscopy, electrophysiology, and dynamic Ca^{2+} imaging. They found that the mutated STAC3 is associated with a decrease in $Ca_V1.1$ level, functionality and stability. Mutated STAC3 also was associated with an increase in the caffeine-induced RyR1-dependent SR Ca^{2+} release, without changes in caffeine sensitivity but an increased SR luminal Ca^{2+} concentration (Linsley et al., 2017). In heterologous systems of expression, Niu et al. observed an important role for STAC3 and CaM in $Ca_V1.1$ trafficking and gating through interaction with it C-carboxyl terminus. They also observed that mutated STAC3 shows weak channel binding and decreased trafficking (Niu et al., 2018). Therefore, STAC3 is now considered as a part of the selected and small group of proteins essential for ECC together with $Ca_V1.1$ α1S and β1a subunits, and RyR1. STAC3 expression allows the expression of $Ca_V1.1$ in heterologous systems and It has been proposed as an important adaptor protein in the molecular interaction between $Ca_V1.1$-RyR1 for the ECC (Flucher & Campiglio, 2019).

$Ca_V1.1$ interacts also with proteins present in the sarcolemma, in particular ***caveolin-3 (Cav3)***. Caveolins are scaffolding membrane proteins (which means that they contribute to assembling protein complexes) that are important in diverse signaling pathways. Caveolins participate in the formation of the organelles and membrane invaginations called caveolae. The family is composed of 3 genes *CAV1*, *CAV2,* and *CAV3* which produce caveolin-1, caveolin-2, and caveolin-3 (Cav3), respectively. Caveolin-1 and caveolin-2 are distributed in different tissues while caveolin-3 is expressed exclusively in skeletal muscle (Way & Parton, 1995). It has been shown that different mutations in *CAV3*, the encoding gene for muscle-specific isoform Cav3, produce several skeletal muscle disorders, like limb-girdle muscular dystrophies type 1C (LGMD1C), rippling muscle disease, familial hypertrophic cardiomyopathy, distal myopathy, and isolated hyperCKemia (Cohen et al., 2004; Gazzerro et al., 2010). Several studies have proposed caveolae and caveolin-3 to participate in T-tubules development during myogenesis (Parton et al., 1997; Nixon et al., 2005). In 2007, Couchoux et al. observed that in mice myotubes lacking endogenic Cav3 there was a 50% reduction of the conductance of $Ca_V1.1$ Ca^{2+} current, suggesting that Cav3 is involved in the regulation of $Ca_V1.1$ function (Couchoux et al., 2007). In another study realized by Weiss et al (2008), authors expressed in adult mouse muscle fibers a pathologic mutant form of Cav3, $Cav3^{P104L}$ (substitution of Proline by Leucine in position 104 of Cav3) responsible for LGMD1C. The consequences of the $Cav3^{P104L}$ expression in the adult skeletal muscle were the decrease in Cav3 expression, reproducing an endogenic Cav3 knock-down model. In terms of function, expression of the mutated $Cav3^{P104L}$ resulted in an important decrease in the $Ca_V1.1$ Ca^{2+} current while charge movement and Ca^{2+} release was not affected. Therefore, it showed that the endogenous Cav3 does not play a role in ECC, but does interfere with $Ca_V1.1$ channel function (Weiss et al., 2008). In another study, Couchoux et al. demonstrated that Cav3 is not only expressed in the caveolae. They observed that Cav3 immunolocalized within T-tubules and that it interacts with the I-II loop of $Ca_V1.1$, explaining the molecular basis behind the $Ca_V1.1$-dependent Ca^{2+} current alteration in the endogenous Cav3 knock-down of adult muscle fibers (Couchoux et al., 2011). In the last years, several studies provided further insights into the Cav3 role in skeletal muscle. The Cav3 mRNA overexpression in skeletal muscle cells was related to muscle impairment in myasthenia gravis patients (Iwasa et al., 2016). Recently, it has been found that two dystrophy-associated Cav3 mutations; the $Cav3^{P28L}$ (substitution of Proline by leucine in position 28 of Cav3) and the $Cav3^{R26Q}$ (substitution of arginine by glutamine in position 26 of Cav3), importantly decreased the presence of caveolae in myotubes, produced an alteration of the normal response to mechanical stress, and the activation of IL6/STAT3 signaling pathway. The presence of the mutated Cav3 in the myotubes leads to a constitutive hyperactivation of the pathway and an increase in the associated muscle genes expression, while the

expression of normal Cav3 fully reversed the alteration in caveolae formation and the mechanical stress response defects (Dewulf et al., 2019). More recently, it was observed that Cav3 has also a role in mitochondria formation and function. Indeed, it was reported that the expression of $Cav3^{P104L}$ in myoblasts produces major disturbances in mitochondrial respiration and that this could contribute to the physiopathology of LGMD1C (Shah et al., 2020). Altogether Cav3 has been highlighted as a sarcolemma protein capable of playing a relevant role in $Ca_V1.1$ function and to simultaneously play a role in several relevant signaling pathways of skeletal muscle normal function.

Additionally, in the last two decades another protein, ***Junctophilin-1 (JPH1)*** was attributed a role in the regulation of $Ca_V1.1$ function. This protein is highly conserved in a family with 4 isoforms (JPH1, JPH2, JPH3, and JPH4). They are involved in the anchorage of the sarcoplasmic reticulum to the plasma membrane (T-tubule in skeletal muscle) and they are differentially expressed in excitable cells. JPH3 and JPH4 are expressed in neurons. JPH1 and JPH2 are expressed in striated muscles. JPH2 is the only isoform expressed in heart muscle and smooth muscle, while JPH1 and JPH2 are both expressed in skeletal muscle, involved in the formation and stabilization of the triads (Takeshima et al., 2000; Ito et al., 2001). JPH1 knock-out produces neonatal mortality with muscle cells presenting disorganization in internal membrane structures and impaired contraction (Takeshima et al., 2000; Kakizawa et al., 2002). Also, it has been shown that patients with a mutation in the gene encoding JPH2 suffer from hypertrophic cardiomyopathy, whereas in related animal models, the decrease in JPH2 expression level induces hypertrophic and dilated cardiomyopathy (Landstrom et al., 2011). Overall, these studies have proved that JPH1 and JPH2 play an important role in the formation of a union complex between the sarcoplasmic reticulum and the T-tubule membranes, which is needed for cardiac and skeletal muscle ECC. At the structure level, the C-terminal transmembrane domain anchors the protein to the membrane of the SR while the *N-terminal lipid-binding membrane occupation and recognition nexus (MORN)* cytosolic region binds to the T-tubule membrane (Takeshima et al., 2000). In 2011, Golini et al. evaluated $Ca_V1.1$ function in C2C12 myotubes knocked-down for JPHs. They determined by co-immunoprecipitation that both JPHs are associated with $Ca_V1.1$, RyR1, and Cav3, forming a protein complex that could regulate $Ca_V1.1$ function. Moreover, using immunofluorescence against JPHs they observed a loss of the normal punctuated pattern observed for these proteins and a more diffuse and less organized signal for $Ca_V1.1$ and RyR1 in the JPHs-deficient myotubes. Interestingly, JPHs knock-down was associated with a decrease in $Ca_V1.1$ expression, while RyR1 expression did not change. Authors also reported a decrease in the L-type Ca^{2+} current and charge movement in JPHs-deficient myotubes, while Ca^{2+} transients were preserved. Although the absence of effect on the Ca^{2+} transients was unexpected, results provided evidence that JPHs are needed for correct

coupling in the ECC $Ca_V1.1$–RyR1 machinery (Golini et al., 2011). In a more recent scientific work, Nakada et al. confirmed these results. Using co-immunoprecipitation and GST pull-down they demonstrated that JPH1 and JPH2 physically interact with the C-terminal of $Ca_V1.1$ α1S subunit and that the disruption of this interaction locates $Ca_V1.1$ channels out the triads. Then, using adeno-associated virus (AAV) injection they expressed a mutant JPH1 lacking its C-terminus including transmembrane domain (JPH1ΔCT) in adult mouse tibialis anterior (TA) and flexor digitorum brevis (FDB) muscles. The expression of JPH1ΔCT produced the localization of $Ca_V1.1$ over the entire sarcolemma, disturbed $Ca_V1.1$-RyR1 coupling in the triads, significantly reduced SR Ca^{2+} release, and the contractile force in the evaluated fibers and muscles. There was no associated change in SR Ca^{2+} content or in triad structure, conclude for a specific role of JPHs in the recruitment of $Ca_V1.1$ into the triads through physical interaction, ensuring normal ECC in adult skeletal muscle (Nakada et al., 2018a).

III. CHAPTER 3: Skeletal muscle plasticity and excitation-transcription coupling

3.1. Different types of muscle fibers

3.1.1. Muscle fiber classification: A brief history

Skeletal muscles in mammals are a heterogeneous mix of different motor unit types (from ten to hundreds in a same muscle) which have a specific and distinct contributions to the whole muscle function. The motor units heterogeneity allows the great muscle functional flexibility, from continuous low-intensity activity (posture), repeated submaximal contractions (locomotion) to fast and strong maximal contractions (jumping). The different motor units are associated with specific characteristics in the structural and functional properties of the skeletal muscle fibers, normally referred to as ***fiber phenotype***. The adult skeletal muscle fiber phenotype can be regulated by hormonal and neuronal influence but is principally determined by the nerve-activity of the α-motoneurons (Hughes, 1998; Spangenburg & Booth, 2003; Schiaffino & Reggiani, 2011).

The first classification of muscle fiber composition in the skeletal muscles dates from the 19th century and associated the *"red"* or *"white"* colors in the whole muscle to their slow or fast contractile properties, respectively. This vision did not change much until 1930, when the model was implemented with the "white" fast-twitch having muscle fibers characterized by glycolytic metabolism and phasic activity and the "red" slow-twitch having muscle fibers rich in myoglobin and oxidative enzymes, with a more continuous activity (Needham, 1926). The links between the biochemical and mechanical properties

started with the association of actin-activated ATPase activity of myosin and the speed of muscle shortening (Bárány, 1967).

Since then, this vision has largely evolved starting with four independent lines of evidence: 1) histochemical and physiological studies of individual motor units, 2) electron microscopy of fast and slow skeletal muscles, 3) new histochemistry techniques for ATPase study, and 4) biochemical studies on oxidative and glycolytic enzymes in different muscles (Schiaffino & Reggiani, 2011).

In the sixties, the study of single motor units from the tibialis anterior (TA) muscle from albino rats classified the muscle fibers into three types based on their levels of succinate dehydrogenase (SDH) activity, which is an enzyme of the respiratory chain complex in the mitochondria, and their contractile properties. According to these results, it was first proposed the A, B, and C classification: The A-type fibers were characterized as white and large-diameter muscle fibers with low SDH activity and fast-twitch contractile properties. The B- and C-types were both red fibers with high enzymatic activity. C-type were the smallest-diameter fibers with the highest SDH activity and slow-twitch contractile properties. B-type was a more heterogeneous group with large diameter, intermediate SDH activity, and fast-twitch contractile properties but resistant to fatigue (Edström & Kugelberg, 1968). Using SDH and myoglobin staining, Close et al. found similar results in the fast-twitch muscle *extensor digitorum longus* (EDL) (Close, 1967), in which all fibers present a richly developed SR, in contrast with the poorly developed SR of slow-twitch soleus muscle fibers. It was also observed that the mitochondria-rich muscle fibers from fast- and slow muscles present a thicker Z line. Overall, this leads to structure-function relationships according to which the speed of contraction is correlated with SR development, and fatigue-resistance to mitochondrial content and Z line thickness (Schiaffino et al., 1970). Using physiological-histochemical correlations between myosin ATPase and SDH staining in cat muscle, the existence of two types of fast-twitch motor units was confirmed: fast fatigable (FF) units composed of fibers weakly stained for SDH (2B) and fatigue-resistant (FR) units composed of fibers staining strongly for SDH (2A) (Burke et al., 1971). Additional experiments showed high levels of glycolytic enzymes in 2A and 2B fibers from fast-twitch muscle, producing the current classification of slow-twitch oxidative (type 1), fast-twitch oxidative glycolytic (2A), and fast-twitch glycolytic fibers (2B) (Peter et al., 1972). The use of monoclonal antibodies and electrophoretic analysis of myosin heavy chain (MyHC) led to the identification of a third fast fiber type (2X) based on the characterization of three fast-twitch MyHC isoforms (2A, 2B and 2X) (Bär & Pette, 1988; Schiaffino et al., 1989). Type 2X fibers have a rich mitochondrial content (Gorza, 1990) and have a resistance to fatigue that is intermediate between fibers of the type 2A and 2B motor units (Larsson et al.,

1991). The maximal velocity of shortening for muscle containing principally MyHC-2X is intermediate between that of muscles with MyHC-2B and MyHC-slow isoforms (Bottinelli et al., 1994).

3.1.2. Myosin heavy chain isoform (MyHC) and fiber type classification (I, IIA, IIX, and IIB)

Several studies of the MyHC isoforms confirmed the existence of a spectrum of fiber types with pure or hybrid MyHC composition, following the next order: 1 ↔ 1/2A ↔ 2A ↔ 2A/2X ↔ 2X ↔ 2X/2B ↔ 2B (Schiaffino & Reggiani, 2011). However, this pattern has exceptions and some fibers co-express 1/2X in normal muscle (Caiozzo et al., 2003). A similar fiber type profile has been observed in different mammalian species like mice, rats, rabbits, and guinea pigs. Interesting, in human muscle, MyHC-2B is not detectable, despite the fact that the corresponding *MYH4* gene is present in the genome (Fig. 14). It is generally accepted that in humans, MyHC-2B is represented by MyHC-2X (Smerdu et al., 1994). In contrast with rat data, human 2X fibers have the lowest level of SDH activity compared with all other fiber types. The four fiber types discussed above are distributed in different proportions depending on the specific

muscle and anatomic site. In general, in the posterior leg or hind limb muscles, there is a more abundant presence of slow-twitch fibers, while in the arms or forelimbs the fast-twitch fibers are more numerous. The exact proportion of each fiber type also depends on the species, making not straight forward interspecies extrapolations. The central role of myosin as a molecular motor in muscle cells and the

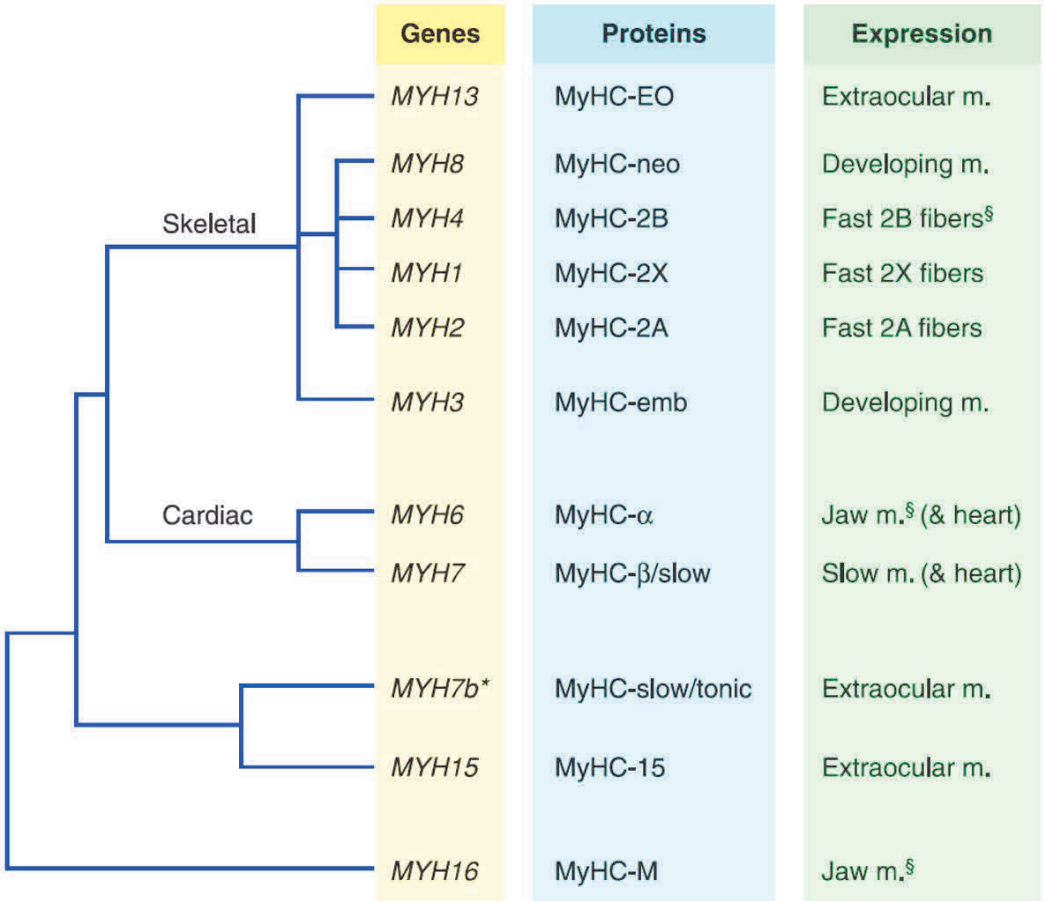

Figure 14. Myosin heavy chain (MyHC) isoforms: Genes, proteins and expression distribution. *1) The MYC genes in mammals with the corresponding MyHC protein products and their expression pattern. 2) The evolutionary relationship is showed in the phylogenetic tree on the left. Scheme taken from Schiaffino et* diversities of isoforms differentially distributed in the different described fiber types makes MyHC the best-known marker for fiber typing (see Fig. 14) (Schiaffino & Reggiani, 2011).

The classification of fiber types based only on 1 protein has been discussed and the use of microarrays with a more complex profile and classification considering different proteins of the skeletal muscle fiber has been developed without clarifying results (Campbell et al., 2001). The model based on the four major fiber types, one slow-twitch, and three fast-twitch types, has remained the reference to

study the fiber heterogeneity and muscle plasticity in mammalian muscle. Nevertheless, we can mention some atypical fibers present in specifically developed muscles like head and neck muscles, extraocular muscles (EOMs), jaw muscles, middle ear muscles, laryngeal muscles, and muscle spindles (Schiaffino & Reggiani, 2011).

3.1.3. Fibers type, Ca^{2+} handling, and ECC

The fast and slow fibers, from soleus and EDL muscles respectively, present different Ca^{2+} handling properties and kinetics. Slow fibers (type I) present a larger cytosolic Ca^{2+} concentration in resting conditions than fast fibers (type IIA, IIX, and IIB) (Sreter et al., 1987; Fraysse et al., 2003). These two main groups are different also with regard to the dynamic Ca^{2+} handling when stimulated by a single PA. Regarding the peak amplitude of the Ca^{2+} transient, controversial results were reported with either no (or a very limited) difference (Carroll et al., 1997; Calderón et al., 2010) or a twice reduced peak amplitude in the slow-twitch fibers (Baylor & Hollingworth, 2003, 2012; Hollingworth et al., 2012). Conversely, there is a general agreement for a slower decay of the Ca^{2+} transient in slow muscle fibers as compared with fast muscle fibers (Carroll et al., 1997; Carroll et al., 1999; Baylor & Hollingworth, 2003; Calderón et al., 2010). At the expression level, a significant reduction in the content of relevant proteins involved in ECC was reported in slow fibers, including $Ca_V1.1$ (Lamb, 1992), RyR1 (Reggiani & Kronnie, 2006), and SERCA (Delbono & Meissner, 1996). The expression/content level of cytosolic Ca^{2+} binding proteins, like parvalbumin (Huber & Pette, 1996; Chin et al., 2003), which is expressed in fast fibers at concentrations of ≈1mM, is negligible in slow fibers (Campbell et al., 2001). Parvalbumin has a critical role in the speed of relaxation and fast-twitch muscles from parvalbumin-KO mice exhibit slow relaxation (Schwaller et al., 1999).

3.1.4. Role of the innervation, firing pattern, and muscle plasticity

Force and movement generation are controlled by the nervous system and depend on the motor task. We can classify them into three categories: 1) postural function like joint stabilization, 2) long-term and repetitive activities, like locomotion, and 3) fast and powerful actions like jumping. Associated with each task, the force generation is controlled by the frequency of stimulation (firing pattern of stimulation) and recruitment of specifics motor units groups. The *motor unit* is made by several hundreds of homogenous muscle fibers that are innervated by a specific α-motoneuron which generates specific firing patterns of activity. This, not only allows the correct use of the fibers and the execution of the specific task, but also plays a major role in the regulation of adult fibers **muscle plasticity**, which is the change in

muscle fiber phenotype related to the environmental requirements. The *motor units* can be classified into three different types: 1) low firing pattern (≈20 Hz), with a high amount of activity per day (300000-500000 impulses), and long-lasting trains (300-500s), associated with slow-twitch fiber type, 2) high-firing pattern (70-90 Hz), with a modest amount of activity per day (3000-10000 impulses) and short trains duration (< 3 s), associated with 2B fibers type, and 3) high-firing pattern (50-80 Hz) with bigger activity per day (90000-250000 impulses) and long trains duration (60-140 s) associated with 2A/2X fibers. The muscle fibers in each motor unit are not all grouped together but overlap with fibers in other motor units in micro arrangements of 3-15 fibers, which allows the different motor units to work asynchronously and to alternate their contractile activity in support of one another. The heterogeneity of skeletal muscle fibers reflects the adaptation to the different patterns of activity, which determines specialization in membrane properties, calcium handling mechanisms, contractile machinery, cytoskeleton structure, and energy metabolism (Schiaffino & Reggiani, 2011). The fiber-type distribution can be also a consequence of whole-body metabolism, because of the role that the muscles plays to maintain plasma glucose concentration via gluconeogenesis, increasing glycemia, or via the insulin-dependent translocation of GLUT4, decreasing glycemia. The type 2B glycolytic muscle fibers are more sensitive to fasting exposure, showing greater atrophy, while the type 1 oxidative muscle fibers showed a more active glucose removal from de blood, which could be explained by the mitochondria content (Lowell & Shulman, 2005).

Skeletal muscle has a great capacity of adaptation to the environmental requirements (use or disuse) through muscle plasticity, producing a change in fiber size (muscle hypertrophy vs atrophy) associated with the improvement or loss of force, and fiber type change (fast-to-slow fiber type switch) associated with the improvement of fatigue resistance. The role of physical exercise is typically important in these processes and has been highlighted and studied over the last decades, including its biological relationship with the improvement of metabolic disease and diabetes condition. Several biological factors are related to different skeletal muscle adaptations during muscle plasticity. We can mention motor-unit firing patterns, mechanical load, and circulating factors (hormones) (see Schiaffino et al. 2011).

In this section, we are going to focus on how the **firing patterns of stimulation** (α-motoneuron) influences skeletal muscle plasticity.

The role of the nerve pattern of activity was first studied by Buller et al. (1960) using a cat model by the transposition of - a slow nerve from the soleus, into the *flexor digitorum longus* (FDL), a fast-type muscle, and - a fast nerve from the FDL transposed into the soleus, a slow-twitch muscle. They observed that the slow-type muscles under the fast nerve influence acquired fast properties, and vice-versa (Buller

et al., 1960). Similar experiments were made in a rat model using the extensor digitorum longus (EDL), a fast-twitch muscle and the soleus (Hoh, 1975). According to these results, several studies have used external electrical stimulation of innervated or denervated muscles to reproduce the different firing patterns of stimulation of the fast (≈ 100 Hz) and slow (≈ 20 Hz) α-motoneurons and observed a relationship between the pattern of stimulation and the muscle fiber type (Hennig & Lømo, 1985). Phasic high-frequency external electrical stimulation, as in fast-type α-motoneurons (≈ 100 Hz), produces a slow-to-fast change in the fiber type following 1 → 2A → 2X → 2B, while a tonic low-frequency (≈ 20 Hz) of external electrical stimulation produces a fast-to-slow change in fiber type. It has been shown that muscle plasticity depends on the initial fiber type composition and on muscle intrinsic factors, limiting the range of adaptation. Fast muscle can adapt mostly in the range 2B ↔ 2X ↔ 2A and slow muscle in the range 1 ↔ 2A ↔ 2X (Schiaffino & Reggiani, 2011). The thyroid function has also an important role in determining muscle fiber type composition. Hyperthyroidism combined with mechanical unloading leads to the expression of MyHC-2B in slow muscles (Caiozzo et al., 1998), while hypothyroidism combined with mechanical overload or chronic low-frequency external electrical stimulation can induce the expression of MyHC-slow in fast muscles (Kirschbaum et al., 1990; Caiozzo et al., 2000). Muscle plasticity depends on the specific muscle identity (localization/function in the body), fibers type distribution, the embryonic individual fiber phenotype (primary generation) and the postnatal developmental plasticity (secondary generation), the specie, the stimulus- type and duration. In humans, it has been shown that 7 years of spinal cord injury produces an almost complete disappearance of slow-twitch muscle fibers (Grimby et al., 1976). In another study, using biopsies from 3 different groups, it was observed that endurance-trained subjects present increased levels of MyHC-slow and MyHC-2A containing fibers, while sedentary subjects have increased type 2A and MyHC-2X fibers (Klitgaard et al., 1990).

During postnatal development and regeneration, a pathway nerve-activity-independent controlled by thyroid hormone regulates muscle fiber differentiation, activating the *fast gene program*, while the *slow gene program* is regulated by the slow motor neuron activity (Butler-Browne & Whalen, 1984; Esser et al., 1993). The slow gene program and the slow fiber phenotype are difficult to reverse and require an extremely long period of inactivity or denervation (like in a spinal cord injury) to produce an increase in MyHC-2X/2A.

The fast-to-slow switch can be induced by chronic electrical stimulation (Ausoni et al., 1990) or different endurance exercises like running or swimming, which produce incomplete changes in the MyHC spectrum (2X → 2A in humans, 2B → 2X → 2A in rats and mice) that do not reach type 1 slow profile (Allen

et al., 2001). The muscle fiber plasticity involves changes in all muscle compartments, including components of ECC, cell metabolism, and contractile machinery (Pette & Staron, 1997). Initially it was suggested that during the course of these changes, the metabolic properties adaptations precede the contractile properties adaptation. However, the opposite was observed in response to activity/inactivity. Currently, the idea of two separate signaling pathways for each kind of adaptation is gaining popularity, because moderate endurance training shows adaptation in the metabolic machinery but not in the contractile machinery (see Schiaffino et al. 2011).

3.1.5. Signaling pathways of muscle plasticity

Muscle fiber plasticity involves the coordinated and opposed regulation of fast and slow gene programs. When the fast gene pathway is activated, the slow gene pathway is simultaneously repressed. There are three specifics mechanism which allow both processes to coordinate the up-and down-regulation of different fast and slow muscle genes: 1) transcription factors acting as activators and repressors, 2) bidirectional promoters, and 3) miRNAs hosted in MyHC genes (see Fig. 15) (see Schiaffino et al. 2011).

The first mechanism includes the calcineurin-dependent nuclear factor of activated T-cell (NFAT), described in the next section. It acts as activator or repressor of distinct MyHC genes (Fig. 15A). NFAT activity is decreased by denervation and increased by electrostimulation of denervated muscles with a low-frequency firing pattern. The transfection of a plasmid coding for VIVIT, a specific peptide inhibitor of calcineurin (Cn)-mediated NFAT activation blocks the expression of MyHC-slow, which is normally induced by slow motor neuron activity in a regenerating soleus muscle model. VIVIT also inhibits the expression of MyHC-slow transcripts and the activity of the MyHC-slow promoter in adult soleus. The expression of a constitutively active NFATc1 mutant stimulated the MyHC-slow, inhibited the MyHC-2B promoter in adult fast muscles, and induced MyHC-slow expression in regenerating muscle fibers. The Cn-NFAT signaling act as a nerve activity sensor in skeletal muscle in vivo and controls nerve activity-dependent fast-to-slow MyHC plasticity (McCullagh et al., 2004).

The second mechanism involves the role of bidirectional promoters located between two MyHC genes. The sarcomeric MyHC genes are organized in two clusters: cardiac MyHC-α and MyHC-β/slow (skeletal muscle isoform), and 2A-2X-2B genes (Fig. 15B). The antisense transcription is a common regulator of mammalian gene expression, linked especially to the regulation of its neighboring genes (Katayama et al., 2005). An association was shown between the triiodothyronine (T3)- dependent

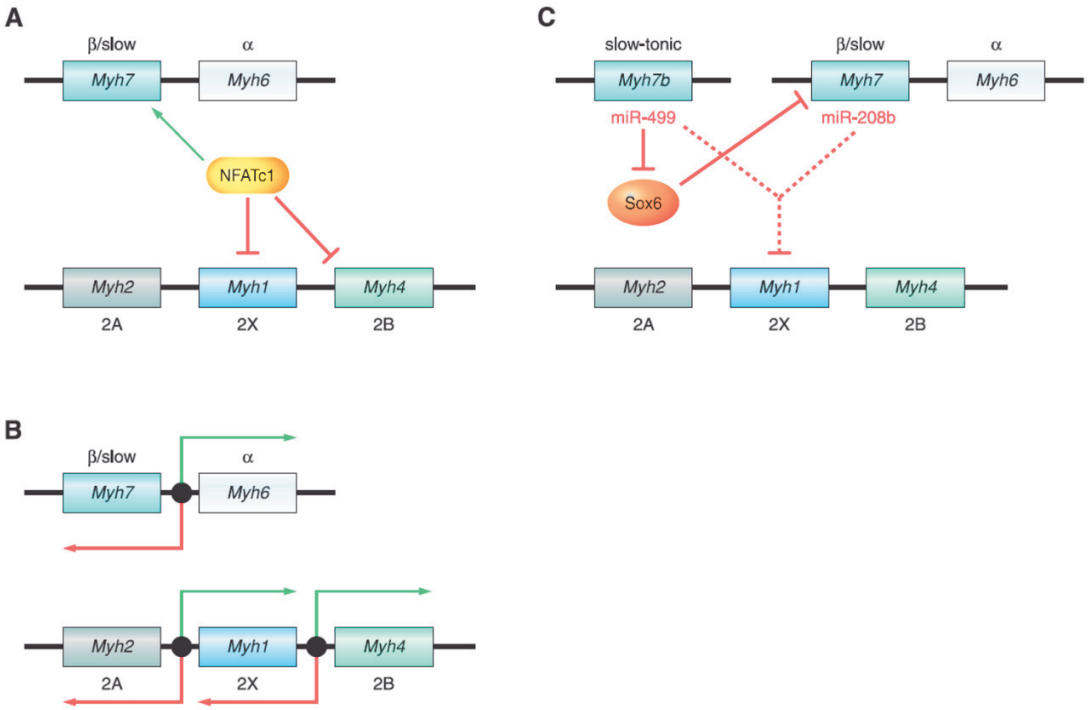

Figure 15. Different mechanisms of control of MyHC genes expression during muscle fibers types transitions. *A) transcription factors acting as activators (green) and repressors (red) of MyHC genes (Myh), like NFATc1 B) Bidirectional promoters generating sense (green) and antisense (red) transcription C) microRNAs hosted in MyHC genes. Dotted lines show the undefined and indirect mechanisms. Scheme taken from Schiaffino et al. 2011.*

regulation of the MyHC expression in the heart, and the antisense transcription factor. Between the cardiac myosin genes, *MYH6* (MyHC-α) and *MYH7* (MyHC-β), there is an intergenic region with bidirectional transcriptional activity. The antisense RNA product seems to exert an inhibitory effect on the MyHC-β gene transcription, but without a clear mechanism (Haddad et al., 2008). In the skeletal muscle isoforms genes, similar bidirectional promoters exist with antisense RNA products that regulate the expression of MyHC-2A and MyHC-2X genes (MYH2 and MYH1 respectively) (Pandorf et al., 2006), and the expression of MyHC-2X and MyHC-2B genes (Rinaldi et al., 2008).

The third mechanism of fast and slow gene program regulation includes the muscle-specific intronic microRNAs (miRNAs) located and co-expressed with MyHC genes (Fig. 15C). We can mention miR-208a and miR-208b, encoded by introns of *MYH6* and *MYH7* respectively, and miR-499, coded by *MYH7b*. Both, miR-208b and miR-499, activate the slow gene program and repress the fast gene program. The double knockout mice (for miR-208b and miR-499) showed a marked slow-to-fast switch in MyHC

expression, while miR-499 muscle-specific overexpression produces a complete fast-to-slow switch in the MyHC profile of the soleus, and a switch from MyHC-2B to -2X in fast muscles (van Rooij et al., 2008; van Rooij et al., 2009). Different targets mediated the effects of the miRNA, like the transcriptional repressor Sox6, which controls the slow gene program. In a model of Sox6 overexpression there is a reduction of MyHC-β/slow in mouse muscle, while in a non-functional Sox6 gene mutant, there was a marked fast-to-slow switch in the MyHC gene expression (Hagiwara et al., 2005; Hagiwara et al., 2007). These mechanisms have been highlighted during development, but their relevance in adult skeletal muscle plasticity remains an open question.

Within the scope of my project, we are specifically interested in the first mechanism because it is related to the firing pattern of stimulation by the α-motoneuron, the cytosolic Ca^{2+} changes, and it was proposed as the mechanism behind Pannexin 1-dependent excitation-transcription coupling.

3.1.6. Cytosolic calcium signaling

The free calcium ion (Ca^{2+}) level in resting fast-twitch fibers is approximately 50 nM (Westerblad & Allen, 1991) and prolongated chronic stimulation of skeletal muscle results in sustained elevation of cytosolic free Ca^{2+} to a range of 100-300 nM (Chin & Allen, 1996), enough to activate a subset of calcium-regulated enzymes (Chin et al., 1998; Wu et al., 2001), resulting in fast-to-slow fiber transformation, implicating Ca^{2+} as a critical regulator in this process (Kubis et al., 1997; Carroll et al., 1999). One of the relevant mediators for Ca^{2+} signaling is Calcineurin-NFAT, which is only activated under chronic elevation in Ca^{2+} levels (Dolmetsch et al., 1997). The increase of cytosolic Ca^{2+} resting value produces a change in the activity of the adult fast MyHC promoters in the direction of fast-to-slow adaptation. This Ca^{2+} signal generates the increase of MyHC IIa promoter in a calcineurin-NFAT-dependent manner, and it is also related to members of the mitogen-activated protein kinase (MAPK) family (Allen & Leinwand, 2002).

3.1.7. Calcineurin-NFAT signaling

Calcineurin is a Ca^{2+}/calmodulin-regulated phosphatase that interacts with the NFAT family and induces their translocation into the nucleus. Calcineurin is a heterodimer with a 59-62 kDa catalytic A subunit (CnA) and a 15 kDa regulatory B subunit (CnB). Three catalytic genes (encoding A subunits) have been identified in vertebrate species (Crabtree, 1999). In skeletal muscle, the calcineurin isoforms present are CnB1 and CnAβ. The sustained elevation of cytosolic Ca^{2+} leads to activation of calcineurin and consequent alteration of gene expression through transcriptional effectors protein (Chin et al., 1998). One mechanism is the association with the **nuclear factor of activated T cells (NFAT)** family, with 4 isoforms

(NFATc1-c4) being regulated by calcineurin-mediated dephosphorylation (Rao et al., 1997). In skeletal muscle, the dephosphorylation of the NFATc1, normally hyperphosphorylated and sequestered into the cytosol, produces its translocation into the nucleus and the regulation of gene expression (see Fig. 16). NFATc1 translocation into the cytosol depends on the firing pattern of electrical stimulation. Slow firing patterns produce NFATc1 translocation while fast firing patterns do not (Liu et al., 2001). In denervated slow muscle, NFATc1 activity is decreased and increased under continuous low firing pattern of stimulation, but not with phasic high-firing pattern (see Schiaffino et al. 2011).

Transgenic mice overexpressing activated calcineurin allowed to show calcineurin role as an activator of the slow gene program in skeletal muscle fibers. Indeed, this model is associated with an increase in MyHC-slow-expressing fibers, an increase in myoglobin expression (Naya et al., 2000) and in mitochondrial oxidative phosphorylation (Ryder et al., 2003), the increase of MyHC-2A fibers and the parallel decrease of MyHC-2B fibers (Chakkalakal et al., 2004). Using the same transgenic mice allowed to also demonstrate the role of calcineurin in the regulation of the peroxisome proliferator-activated receptors (PPARα and PPARδ), and PPARγ coactivator 1α (PGC1α), which are both transcription regulators of the expression of metabolic and mitochondrial genes (Long et al., 2007). The inhibition of calcineurin using cyclosporine A (Chin et al., 1998) and the knockout for CnAα and CnAβ isoforms produce a dramatic down-regulation in the oxidative/slow fiber type gene expression program in skeletal muscle fiber (Parsons et al., 2003).

The direct relationship between nerve-activity and the calcineurin-NFAT pathway was assessed using specific calcineurin inhibitors (cyclosporine A, FK506 and cabin-1) and stimulation at a low frequency of slow motor neuron in regenerating rat soleus muscle: this proved the critical role of calcineurin in the maintenance of the slow muscle fiber gene program in adult skeletal muscle and its regulation by the firing pattern of stimulation from the nerve (Serrano et al., 2001).

Some other studies used transgenic mice overexpressing an inhibitory protein of calcineurin and reported that the calcineurin-NFAT pathway does not play a critical role in the initial diversification of fast and slow fibers during development, but is necessary for the nerve-dependent maintenance of MyHC-slow type fibers in postnatal adult life (Rothermel et al., 2000; Oh et al., 2005), with no associated change in the oxidative capacity, myoglobin content and mitochondrial abundance. Overall, the details of how calcineurin-NFAT influences hypertrophy or metabolic adaptation remain controversial (see Schiaffino et al. 2011).

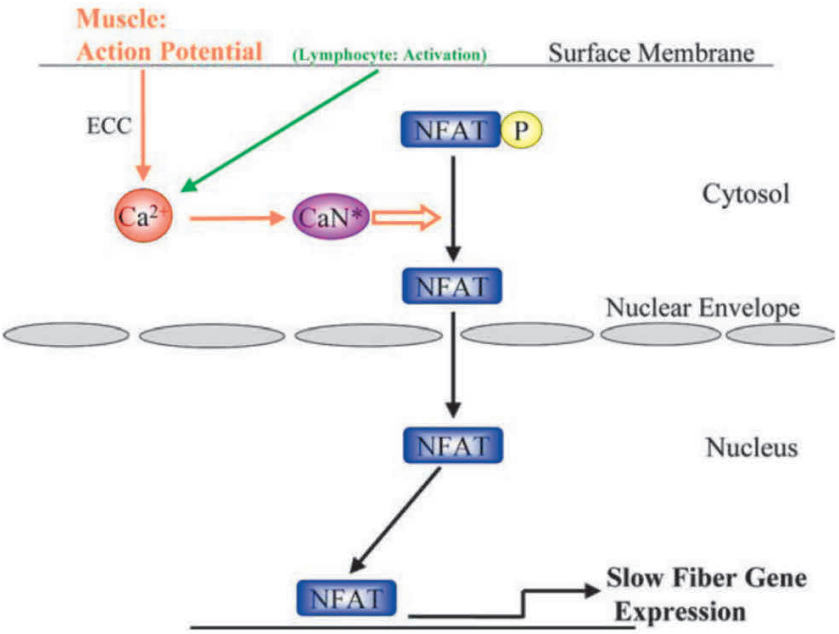

Figure 16. A diagram of the Ca^{2+}-calcineurin-NFAT pathway for activation of slow skeletal muscle fiber gene expression. *Elevated cytosolic Ca^{2+} in response to an action potential activates Calcineurin, which dephosphorylates cytosolic NFAT-P. This allows a nuclear localization signal to promote NFAT translocation into the nucleus and the slow fiber genes activation. The boxes denote transcriptional regulatory proteins, the elipses denote kinases or phosphatases. Open arrows denote phosphatase or kinase enzymatic activity and circles denote phosphorylated serine groups (yellow) or elevated [Ca^{2+}] (orange). Scheme taken from Liu et al. 2005b.*

3.1.8. MEF2, HDAC, and CaMK

The **myocyte enhancer factors-2 (MEF2)** are transcription factors that regulate muscle differentiation and have been involved in muscle fiber type remodeling. MEF2 are part of a family with 4 isoforms (MEF2a, -2b, -2c and -2d) (Black & Olson, 1998). MEF2 transcription factors have a higher expression in slow type muscle fibers compared with fast type. MEF2 are stimulated by endurance exercise or motor nerve stimulation at a slow-firing pattern, are associated with the transformation of myofiber subtype from fast to slow, and are blocked by calcineurin inhibitors (Wu et al., 2001). Calcineurin removes phosphate groups from MEF2, increasing the transcriptional activity of MEF2 and interaction

with DNA binding domains. Thus, Calcineurin-MEF2 is proposed as another pathway of regulation mediated by cytosolic Ca^{2+} signaling (Fig. 17) (Wu et al., 2000).

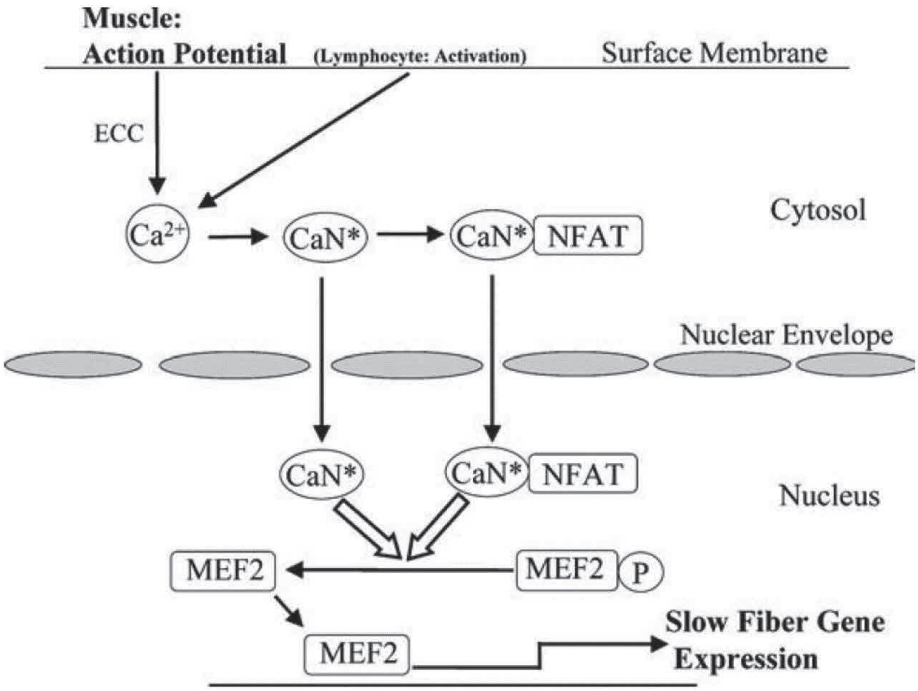

Figure 17. A diagram of the Ca^{2+}-calcineurin-MEF2 pathway for activation of slow skeletal muscle fiber gene expression. *Elevated cytosolic Ca^{2+} in response to an action potential activates Calcineurin, which enters the nucleus alone or as a complex with activated (dephosphorylated) NFAT. Within the nucleus, activated calcineurin catalyzes the dephosphorylation of MEF2, which increases transcriptional activation of slow fiber genes. The boxes denote transcriptional regulatory proteins, the ellipses denote kinases or phosphatases, open arrows denote phosphatase or kinase enzymatic activity and circles denote phosphorylated serine groups or elevated [Ca^{2+}]. Scheme taken from Liu et al. 2005b.*

The **class II histone deacetylase (HDACII)** proteins are transcription factors that work as transcriptional repressors of MEF2. HDACII is part of a histone deacetylases (HDACs) protein family with an important role in homeostasis and development (Haberland et al., 2009). In humans, there are 18 types of HDACs, classified into 4 categories or classes (I, II, III, and IV) (Seto & Yoshida, 2014). *HDACII* transcriptional levels are higher in slow-twitch than in fast-twitch muscle fibers, but protein levels are higher in fast-twitch muscle fibers. This is, at least in part, because slow-twitch muscle fibers fail to

accumulate HDACII as they are selectively ubiquitinated and degraded by the proteasome. HDAC suppresses the expression of slow-twitch, oxidative fibers through the repression of MEF2 activity, while the expression of a hyperactive MEF2 promotes the slow fibers and enhances running endurance compared with wild type littermates (Potthoff et al., 2007).

In cultured muscle cells, MEF2 is controlled by HDACIIs, HDAC4, and HDAC5 which bind to MEF2 and repress MEF2-dependent genes, while MEF2 activity is induced by HDAC kinases like CaMK (McKinsey et al., 2000). In cultured adult skeletal muscle, the slow firing pattern of electrical stimulation produces HDAC4-GFP translocation from the nucleus into the cytosol and is blocked by KN-62, a non-specific CaMK inhibitor. It was then postulated that Ca^{2+} signals from slow- but not fast-stimulation firing patterns generate enough CaMKII activation to produce a net nuclear efflux of HDAC4 (Fig. 18) (Liu et al., 2005).

The **Ca^{2+}-CaM-dependent protein kinase (CaMK)** is a group of proteins that are regulated by the Ca^{2+}-CaM complex with several isoforms (CaMKI, CaMKII, CaMKIV, and CaMKK) (Hook & Means, 2001). The covalent regulation of proteins through a Ser/Thr phosphorylation by CaMK is another mechanism by which Ca^{2+} signals modulate skeletal muscle function and signaling. CaMKII is the predominant isoform expressed in human skeletal muscle and is stimulated by muscle activity (Rose et al., 2007) and shows a possible role in the translocation of HDAC4 from the nucleus into the cytosol upon a slow-firing pattern of electrical stimulation (Liu et al., 2005) (Fig. 18).

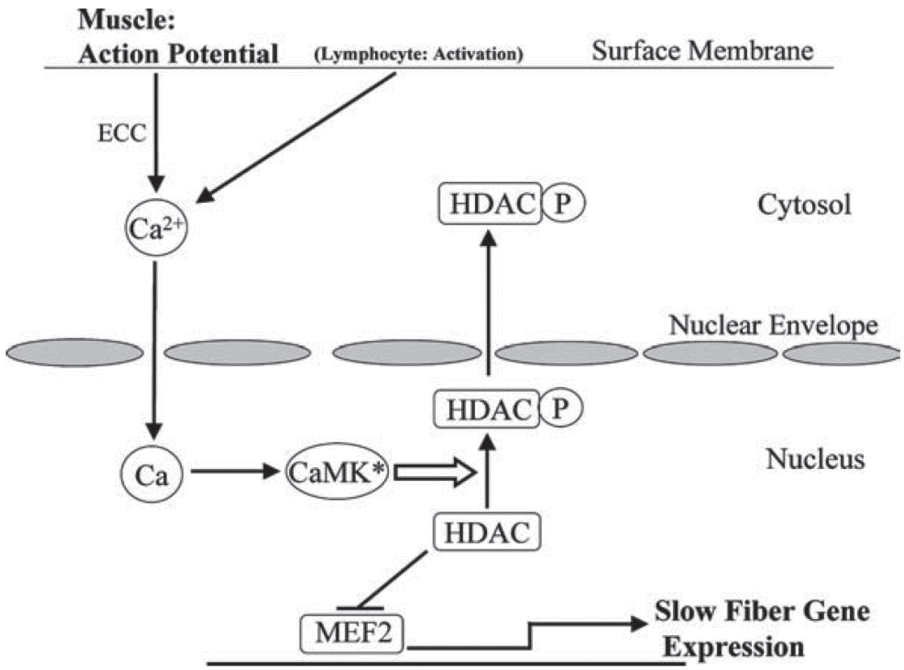

Figure 18. A diagram of the Ca^{2+}-CaMK-HDAC pathway for activation of slow skeletal muscle fiber gene expression. *Elevated cytosolic Ca^{2+} in response to an action potential causes Ca^{2+} entry into the nucleus through nuclear pores and activates intranuclear CaM kinase, which phosphorylates HDAC in the nucleus producing HDAC exit from the nucleus into the cytosol. HDAC removal from the nucleus prevents HDAC repression of MEF2 activating slow fiber type gene expression. The boxes denote transcriptional regulatory proteins, the elipses denote kinases or phosphatases, open arrows denote phosphatase or kinase enzymatic activity and circles denote phosphorylated serine groups or elevated [Ca^{2+}]. Scheme taken from Liu et al. 2005b.*

In neurons, the role of the *cAMP-responsive element-binding protein (CREB)*, has been highlighted as a key regulator of gene expression, being activated by phosphorylation on Ser-133. The

phosphorylation process can be mediated by different intracellular signaling cascades. It was proposed that the fast, CaMK-dependent pathway can be followed by a slower pathway that includes Ras/mitogen-activated protein kinase (MAPK) which may inform the nucleus about stimulus amplitude, while the calcineurin-NFAT pathway may carry the information about the stimulus duration (Wu et al., 2001).

We need to mention the existence of others important players in skeletal muscle plasticity like **AMK, PPARβ/δ,** and **PGC-1,** which are relevant in the fast-to-slow adaptation, specifically in the mitochondrial and metabolic machinery changes in response to AMP and ATP consumption, not directly related to Ca^{2+} cytosolic levels or firing pattern of stimulation. Given the amount of literature regarding the related mechanisms they will not be reported here as this would bring us well beyond the scope of my project (see Schiaffino et al. 2011).

3.2. Excitation-transcription coupling and the role of Panx1

3.2.1. Excitation-transcription coupling

The process behind cellular plasticity, which allows the translation of the different firing patterns of stimulation by the nerve into specific gene regulation is called *excitation-transcription coupling (ETC)* and is the other important process of this project. ETC includes several mechanisms depending on the cellular type (neurons, cardiac or skeletal muscle), and Ca^{2+}-dependent signaling is the ultimate step to activate specific transcription programs (Kim & Kim, 2018; Tyssowski et al., 2018). In skeletal muscle, as mentioned before, the action potential and the firing pattern of stimulation generate different Ca^{2+} signals which regulate gene expression associated with different types of muscle plasticity. In the example of fast-to-slow muscle plasticity, it has been well described that the Ca^{2+}-CaM-calcineurin-NFAT pathway, which is produced by a slow-firing pattern of stimulation, is associated with the chronic increase of cytosolic Ca^{2+} (see Fig. 19) (Hughes, 1998; Schiaffino et al., 1999; Bassel-Duby & Olson, 2006). But how the different patterns of stimulation can activate different Ca^{2+} signaling pathways capable of orienting fiber typing in a new direction remains poorly understood?

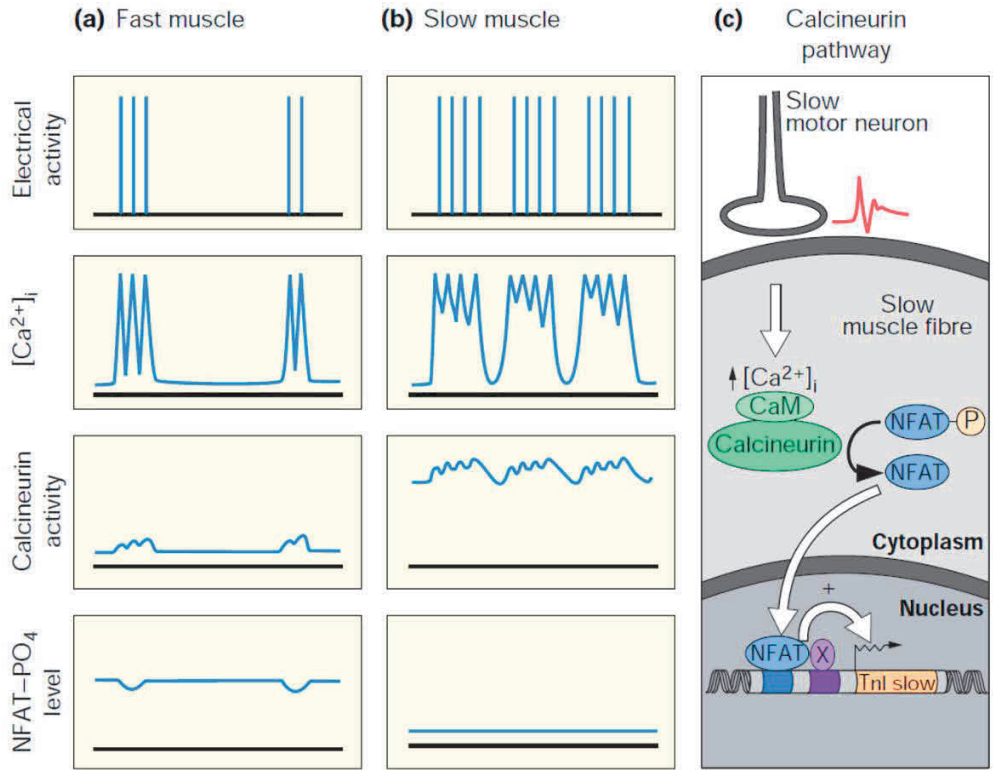

Figure 19. A diagram of the NFAT pathway and of excitation-transcription coupling in skeletal muscle. *Specific firing patterns and some components of the associated pathways are shown. (a) Bursts of fast firing pattern in fast muscle produce transient elevation of cytosolic free Ca^{2+} which neither activate calcineurin nor produce NFAT dephosphorylation. (b) Slow firing patterns produce a chronic cytosolic calcium rise, activate calcineurin and produce NFAT dephosphorylation, allowing NFAT to enter the nucleus, activating slow-fiber types -specific genes. (c) The proposed calcineurin signal transduction pathway in slow fibers. Scheme taken from Hughes et al. 1998.*

In the excitation-transcription coupling of skeletal muscle fibers, during membrane depolarization and associated with the firing pattern of stimulation, $Ca_V1.1$ works as the frequency-decoder and activates signaling pathways related to gene expression regulation. $Ca_V1.1$ activation is the first step of a fully described excitation-transcription coupling pathway that regulates muscle plasticity from fast-to-slow muscle fiber phenotype (Jorquera et al., 2013). In this pathway, 1) a slow frequency of external electrical stimulation (20 Hz) "activates" $Ca_V1.1$, 2) activated-$Ca_V1.1$ stimulates Panx1, an ATP channel located in the T-tubule membrane, 3) Panx1 activation generates ATP release from the cytosol out to the extracellular space, 4) extracellular ATP interacts with purinergic metabotropic (P2Y) and ionotropic (P2X) receptors located in the sarcolemma in an autocrine/paracrine regulation, 5) G-protein coupled P2Y

receptors stimulate of phosphoinositide 3-kinase (PI3K) and phospholipase C (PLC) activities, 6) PI3K and PLC stimulate the production of inositol (1,4,5)-triphosphate (IP3) in the cytosol, 7) cytosolic IP3 interacts with the IP3 receptors (IP3R) present in the SR and in the nucleus membranes, generating Ca^{2+} release into the cytosol (and Ca^{2+} increase in nuclei), and activation of the calcineurin-NFAT pathways with the consequence regulation of gene expression (Jaimovich et al., 2000; Powell et al., 2001; Araya et al., 2003; Buvinic et al., 2009; Casas et al., 2010; Jorquera et al., 2013; Casas et al., 2014) (Fig. 20).

The present project has been focused on the relationship between the two first proteins that participate in this pathway, both located in the sarcolemma of adult skeletal muscle fibers: $Ca_V1.1$ and Panx1, and on the associated consequences for ECC function.

3.2.2. $Ca_V1.1$-Pannexin-1 relationship in muscle fiber excitation-transcription coupling

Studying the regulation of ETC, Jorquera et al. used adult skeletal muscle fibers and showed first that following electric field stimulation, there is an increase of cytosolic IP3 and ATP release into the extracellular space. They observed that this response was frequency-dependent with the production of two peaks of cytosolic IP3, at 15 s and 5 min following fiber's stimulation at 20 Hz. When using 90 Hz

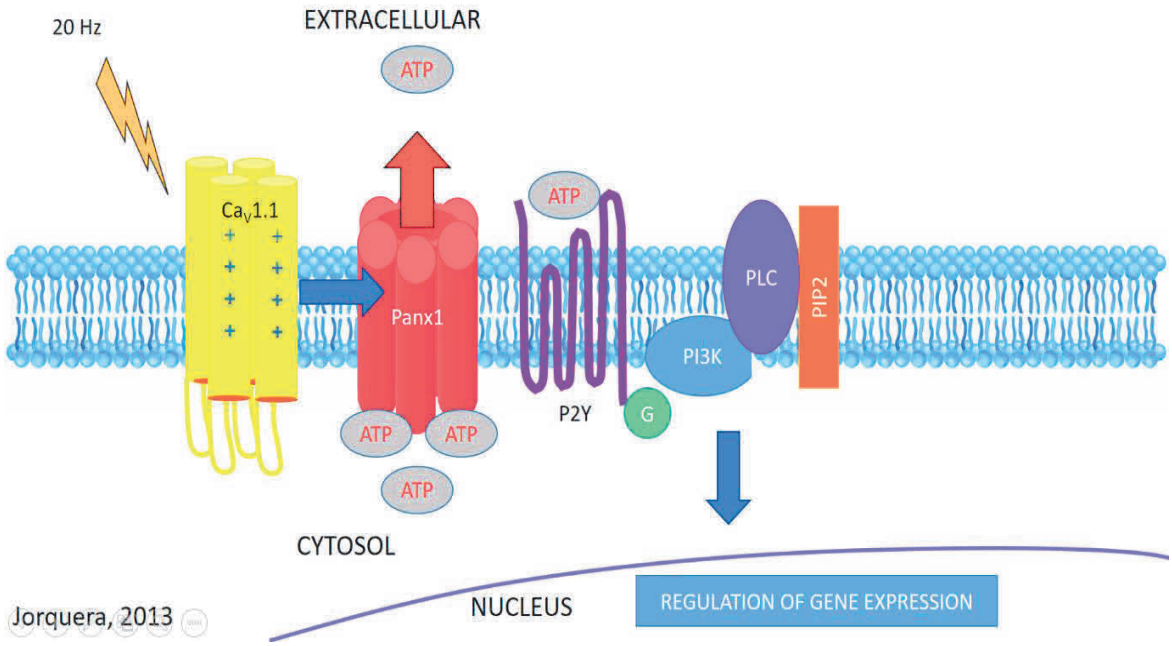

Figure 20. A diagram of excitation-transcription coupling (ETC) in skeletal muscle. *A slow frequency of electrical stimulation activates $Ca_V1.1$ (yellow), which activates Panx1 (red) allowing ATP release and autocrine purinergic signaling. G-coupled protein P2Y receptors activate a series of intracellular signals that end with the regulation in gene expression. Image modified from Jorquera et al. 2013.*

stimulations there were no changes in cytosolic IP3 levels. The relationship between ATP release and the stimulation frequency showed a bell-shaped curve with a maximum at 20 Hz, and almost no ATP release when fibers were stimulated at frequencies higher than 60 Hz. As in the case of IP3 changes, ATP release showed two peaks. The first peak took place between 15-30 s and the second peak 3-5 min post-stimulation. Carbenoxolone (CBX), a Panx1 blocker, prevented ATP release post-20Hz-stimulation.

In order to address gene regulation associated with muscle plasticity under their experimental conditions, Jorquera et al. measured troponin I protein mRNA. Troponin I is a protein of the contractile machinery with two isoforms that are differentially expressed in fast and slow muscle fibers, with a regulation under the control of motor neuron activity (Chin et al., 1998; Rana et al., 2009). Jorquera et al. (2013) observed in fast-type adult muscle fibers that 4 hours after a 20 Hz-stimulation, there was an increase in the slow troponin I (TnIs) and a decrease in the fast troponin (TnIf) mRNA levels, as was also reported previously by Casas et al. in 2010 (Casas et al., 2010). When fibers were stimulated at 90 Hz there was a decrease of TnIs and an increase of TnIf mRNA levels, contrary to what happened following 20 Hz stimulation. At 90 Hz the gene expression regulation was independent of the IP3 and ATP signaling, while after 20 Hz-stimulation the inhibition of ATP release or of cytosolic IP3 increase, prevented the changes in mRNA levels. They also observed that the application of 30 µM extracellular ATP reproduces the transcriptional change of 20 Hz-stimulation in TnIs and TnIf mRNA levels (Jorquera et al., 2013).

These results were in agreement with a previous study using rat cultured myotubes, through which the same group showed that after electrical stimulation, there is ATP release accompanied by an increase in cytosolic Ca^{2+} (Buvinic et al., 2009) that was independent of Ca^{2+} entry (Casas et al., 2010). Jorquera et al. (2013) performed the same experiment using dysgenic myotubes, and observed almost no change in extracellular ATP compared with wild types myotubes after 20 Hz-stimulation. Considering these results, they evaluated the $Ca_V1.1$ role in adult muscle fibers using 20 µM of nifedipine, a $Ca_V1.1$ channel blocker, and 10 µM of (-)S-BayK 8644 (BayK), a $Ca_V1.1$ channel activator. Both drugs produced a marked decrease in ATP release and the inhibition of gene expression normally observed at 20 Hz electrical stimulation. This result, together with data from the dysgenic myotubes, supports the idea of a relationship between $Ca_V1.1$ and Panx1 in which $Ca_V1.1$ would regulate the functional state of Panx1 and, as a consequence, the excitation-transcription coupling (ETC) associated with the slow-firing pattern of stimulation and fast-to-slow muscle plasticity.

Further proof for $Ca_V1.1$-Panx1 interaction was provided by in situ protein ligation assay (PLA) showing a positive response for $Ca_V1.1$ and Panx1 demonstrating a close relationship between the two in

the sarcolemma. Immunofluorescence staining of both proteins also showed that Panx1 co-localizes with $Ca_V1.1$ according to a T-tubule pattern. Finally, using triad's enriched fractions of skeletal muscle, they also observed that both proteins co-immunoprecipitated. Overall, they proposed that the influence from $Ca_V1.1$ to Panx1 could be related to a conformational change of the first one, somehow transmitted to the second one (Jorquera et al., 2013).

IV. CHAPTER 4: Pannexin 1

4.1. Pannexin channels

4.1.1. Panx1 family

Pannexin 1 (Panx1) is an integral-membrane glycoprotein that belongs to a family of three genes in vertebrates (*PANX1*, *PANX2*, and *PANX3*) first discovered in 2000 by Panchin and colleagues (Panchin et al., 2000). It was originally proposed as the homologous of the invertebrate's gap-junction proteins, innexines, and to share several functional characteristics with the vertebrate gap junction proteins, the connexins (Cxs). Panx1 have a widespread distribution in mammalian tissues, being expressed in the brain, heart, skeletal muscle, skin, testis ovary, placenta, thymus, prostate, lung, liver, small intestine, pancreas, spleen, colon, blood endothelium, and erythrocytes (Baranova et al., 2004). Panx2 is expressed in the brain (Bruzzone et al., 2003), spinal cord, and eyes (Dvoriantchikova et al., 2006), and Panx3 is principally expressed in the human hippocampus, osteoblast, synovial fibroblast, whole joints of mouse paws, the cartilage from the inner ear (Bruzzone et al., 2003), and skeletal muscle during differentiation (Pham et al., 2018). The pannexin proteins form large-pore channels that we will call "Pannexin channels" (also called Pannexons) that play important roles in cell-to-cell communication by responding to several stimuli and releasing signaling molecules like ATP (Giaume et al., 2013; Dahl, 2015). To form a functional channel, the interaction between seven Panx1 proteins is required (Deng et al., 2020; Jin et al., 2020; Michalski et al., 2020; Qu et al., 2020; Ruan et al., 2020) (See Fig 21 and 22).

4.1.2. Panx1 structure and subunits: Pore and regulatory subunits

Pannexin channels are nonselective large-pored, ATP-permeable channels that share structure features not only with connexins and innexines but also with volume-regulated anion channels (VRACs), and calcium homeostasis modulators (CALHMs). Pannexin protein tridimensional structure includes four α-helical transmembrane (TM) domains, two extracellular loops (EL), and 1 intracellular loop (IL) and with

the amino (NT) and carboxyl (CT) termini region in contact with the cytosol (Fig. 21A). Between the three pannexin protein isoforms, the NT region is the most conserved domain, while the CT presents a high variability. Panx2 and Panx3 have a closer structure with each other than with Panx1 (Yen & Saier, 2007). Panx1 presents a C-terminal tail (CTT) with an auto-inhibitory role over its function as an ATP channel. The Panx1 channel is a heptamer, composed of seven identical Panx1 proteins (Michalski et al., 2020; Ruan et al., 2020) and contains from top to bottom: 1) an extracellular domain (ECD), 2) a transmembrane domain (TMD) and 3) an intracellular domain (ICD).

Recently, Ruan et al. (2020) identified two conducting pathways associated with the structure and the function of Panx1: the classically described main pore along the axis, formed by the seven Panx1 proteins that could allow ATP conduction, and seven new, previously undescribed side tunnels in the ICD which allow only ion conduction (Ruan et al., 2020).

4.1.3. Panx1 main pore and ion selectivity

The CTT blocks the ICD entrance to the main pore in normal conditions and an access to the pore is granted when caspase 7 releases blockage by cleaving the CTT, which activates Panx1-dependent ATP release. The main pore narrows along the axis toward the extracellular side, with the smallest opening at the ECD entrance restricted by seven tryptophan residues at position 74 (W74) (one from each Panx1 protein). These residues form a ring proposed to discriminate the molecules based on their charge and size (Michalski et al., 2020; Ruan et al., 2020). However, mutations in W74 affect but do not abolish the anion selectivity, partially explained by the participation of another positively charged amino acid, Arginine at position 75 (R75). It was proposed that the cation interaction between W74-R75 plays an important role in the anion selectivity of Panx1 (Michalski et al., 2020). In the TMD, four transmembrane helices (S1-S4) frame the exterior wall, and the N-terminal helix (NTH) lines the interior wall. The NTH interacts with the TMD of the adjacent subunits and it was proposed to maintain a rigid TMD with a large pore. The removal of the NTH produces a TMD in a truncated elliptical-cone shape (Fig. 21A and 22B). The main pore has the shape of a truncated cone with the extracellular and intracellular entrances positively charged, allowing the passage of negatively charged molecules like chloride and ATP (Fig. 21A and Fig. 22B) (Ruan et al., 2020).

4.1.4. Panx1 domains interaction and seven side tunnels

The ECD and the lower part of the ICD of the seven subunits present a close relationship. In opposition, the TMD and the upper part of the ICD present some gaps. In the TMD these gaps are filled

with lipid-like densities similar to the leucine-rich repeat-containing protein 8 type A (LRRC8A) (Fig. 21A) (Deneka et al., 2018). In contrast, the gaps in ICD are free exposed to the solvent and connected to the main pore, implying the existence of an ion pathway, forming one side tunnel at each ICD from each Panx1 protein. All together produce seven side tunnels that allow only the passage for anions, and are an alternative pathway to the main pore, which are believed to be open permanently. It was also observed strong lipid-like densities surrounding the upper part of the TMD (like a lipid belt) (Fig. 21A). Each Panx1 protein consists of a TMD connecting the ECD and ICD. The ECD is composed of two extracellular linkers, EL1 and EL2, and presents an asparagine at position 255 (N255), located at the top of the ECD in helix EH3, which is the target of glycosylation. It has been shown that glycosylation at N255 prevents two Panx1 hemichannels from forming a gap junction (Ruan et al., 2020).

The TMD consists of the short NTH and of a tight helix bundle formed by four transmembrane segments (S1-S4). The NTH is extended to the cytosolic half of TMD and connected to S1 through a long and flexible linker (NTH-S1 linker), lining the main pore (Ruan et al., 2020). It has been proposed that NTH may also play a role in ion permeation or ion selectivity (Michalski et al., 2020) as W74 ring's in the ECD.

The ICD is a helix-rich structure formed by the linker connecting S2, S3, and S4 and presents the seven side tunnels located between the TMD and ICD for each subunit. The CTT is located at the end of the last intracellular helix (IH7) after the caspase cleavage site (Fig. 21A and 21B) (Ruan et al., 2020) and presents a putative leucine-rich repeat (LRR) needed for Panx1 cell surface localization and for oligomerization of Panx1 proteins to form Panx1 channels (Epp et al., 2019).

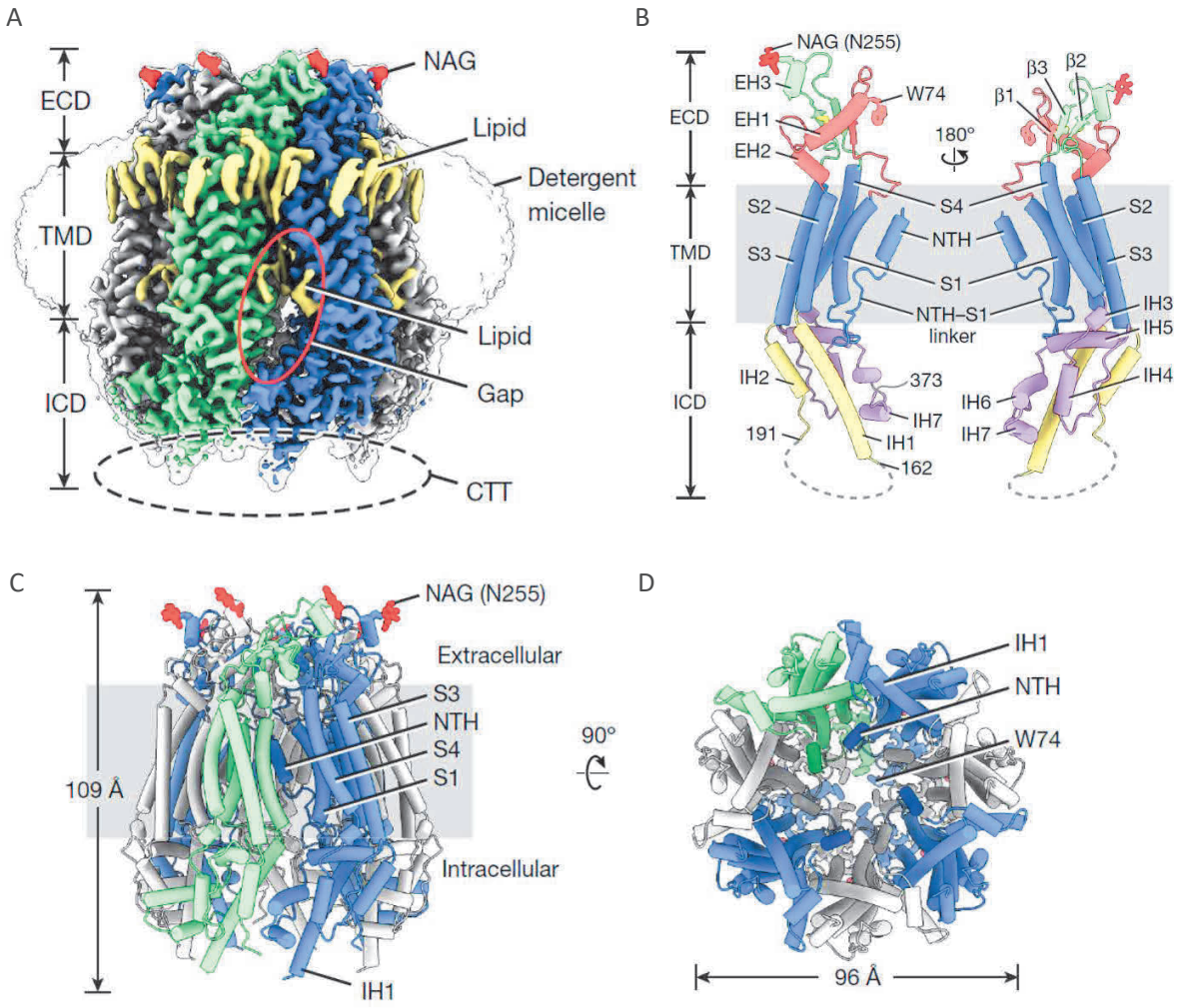

Figure 21. Pannexin 1 (Panx1) protein and Panx1 channel cryo-EM tridimensional reconstruction. *A) cryo-EM reconstruction of human Panx1 channel. It is an heptamer formed by seven Panx1 proteins with their ECD, TMD and ICD. The dashed ellipse highlights the CTT in the cytosol and the red ellipse highlights the gap between two adjacent subunits (proposed as an alternative ion passage). Lipid-like densities are shown in yellow. B) two Panx1 proteins with their structural organization in ECD, TMD and ICD domains and their relationship with the main pore within a Panx1 channel. We observe the Helix EH1 that makes an angle of 45° with the membrane and forms the extracellular entrance with its residue W74. At the top in red for A), B) and C) we observe the glycosylation target (N255A) which prevents two hemichannels from forming a gap junction. C) Side view of a Panx1 channel with the scale and the position of the different TMD (S1-S4) and NTH in the internal wall of the pore. D) Bottom or cytosolic view of the Panx1 channel and its ICD. Image modified from Ruan et al. 2020.*

4.2. Panx1 functions

The main function of pannexin 1 (Panx1) channels is ATP release. ATP release through pannexin was shown first by Dahl et al. in 2004 by expressing Panx1 in oocytes, and using path-clamp and luminometry luciferin/luciferase assays. They observed a mechanical sensitivity of the channel associated with its opening and ATP release (Bao et al., 2004; Dahl, 2015).

ATP release through Panx1 channels participates in several cell types and processes and it has been proposed to be regulated by several stimuli including voltage, membrane stretch and increased intracellular calcium levels. Panx1 has also been proposed to be regulated by signaling effectors like proteases and kinases, which can permanently or temporarily stimulate the channel activity (Chiu et al., 2018). The stimuli that activate or block the Panx1 channel have been proposed in several cases on the basis of studies that did not systematically measure ATP release, which now becomes a problem when interpreting results. Indeed, the cryo-EM reconstruction of Panx1 with a resolution of 2.8 Å by Ruan et al. 2020 (Fig. 21 and Fig. 22) led to the completely new proposal according to which the CTT has the critical role of blocking the ATP conductance (which is physiologically only open under caspase cleavage or by phosphorylation) next to which alternative ion-conducting tunnels that reach the main pore reveal the possibility of chloride currents without opening of the cytosolic entrance of the main ATP-permeant pore. Both pathways are affected by the classical Pannexin blocker carbenoxolone (CBX), which either blocks the main pore at the ECD (Ruan et al., 2020) without changing Panx1 conformational state (Jin et al., 2020) or generates an allosteric inhibition by interacting with the two extracellular loops, producing a conformational change (Michalski & Kawate, 2016; Michalski et al., 2020). Overall, this discovery promotes that conclusions from many previously published experiments and results need either to be considered carefully or to be revisited.

4.2.1. Pressure/stretch-induced activation of Panx1 channels

The first direct experimental evidence for Panx1 channel function was obtained by Bao et al in 2004 (Bao et al., 2004), using a heterologous expression system. Following the injection of a plasmid coding for mRNA of human Panx1 in oocytes and using the path-clamp technique, they observed a channel activity with increased open probability (P_o) when negative pressure was applied in the pipette. At voltages more negative than −20 mV, channels were closed whereas voltage steps to values ≥ +20 mV resulted in rapid inactivation of the currents. Using a luminometry assay, the channel was proved to conduct ATP because oocytes expressing pannexin 1 exhibited an elevated ATP efflux only under

conditions favoring channel opening. ATP permeability was also proved from measurements of current reversal potentials carried out as potassium-ATP gradients were applied to excised patches containing single pannexin 1 channels (Bao et al., 2004). In another study, Locovei et al. used a luciferase assay and showed increased ATP release from erythrocytes when using hypotonic solutions that produce a mechanosensitive activation of Panx1, which was blocked by the application of CBX (Locovei et al., 2006). When using Panx1 knockout ($Panx1^{-/-}$) erythrocytes, ATP release decreased importantly and was insensitive to 1mM of probenecid (PROB), another classical Panx1 blocker (Qiu et al., 2011). In a more recent study, Panx1 was proposed to play a role in the stretch-sensitivity of the bladder. Using a luciferin-luciferase assay and Panx1 blockers (CBX and Brilliant Blue FCF) Panx1-dependent ATP release was shown to be associated with stretch-activation in urothelial cells for the regulation of bladder activity (Beckel et al., 2015). As for the underlying mechanism, it has been shown that the Panx1 CTT interacts with actin providing a potential physical transduction mechanism for channel activation in response to membrane stretch (Bhalla-Gehi et al., 2010). Nevertheless, despite this piece of evidence, the exact transduction mechanism from membrane stretch to Panx1 activation still remains unclear. One additional difficulty is that there are other channel protein candidate that could be responsible for the ATP release as for instance the leucine-rich repeat-containing protein 8 (LRRC8/SWELL) that is sensitive to carbenoxolone and to hypotonicity (Chiu et al., 2018).

4.2.2. Elevated extracellular potassium induces activation of Panx1 channels

Several studies have shown that Panx1 can be activated by high concentrations of extracellular K^+. Silverman et al. in 2009 studied Panx1 in neurons and astrocytes and showed that 20 mM of extracellular K^+ (threshold concentration) produces an increase in Panx1-dependent current independent of the membrane potential in a dose-dependent manner, and that is inhibited by CBX (Silverman et al., 2009).

Wang et al. in 2014 proposed that Panx1 has two open-channel conformations depending on the mode of activation. They studied a Xenopus oocytes Panx1-expressing system using electron microscopy and patch-clamp measurements. They observed that the stimulation with K^+ produces a Panx1 conformational state with a high conductance (≈500 pS) that allows ATP passage, while in the absence of K^+, the channel has a low conductance (≈50 pS) with no detectable ATP permeability (Wang et al., 2014). These results may be, to some extent, correlated with the 2 independent pathways described by Ruan et al. in 2020. However, the mechanism to explain how high extracellular K^+ activates Panx1 channels remains unclear (Chiu et al., 2018). Jackson et al. in 2014, observed that the K^+-dependent Panx1

activation, measured as whole cell inward currents in single oocytes, was dose-dependent, starting at 10 mM with saturation at ≈75 mM. They also measured YoPro dye uptake and observed dose-dependence with the highest values at 50 mM K^+. These effect was inhibited by the addition of 1 mM of PROB and by 500 µM CBX. They also proposed that K^+ compete with extracellular ATP, which acts as a Panx1 inhibitor, on similar extracellular binding sites of Panx1. Extracellular ATP is capable of decreasing K^+-dependent Panx1 activation at concentrations lower than 75 mM of extracellular K^+, above which ATP is no longer effective (Jackson et al., 2014). However, in another study, Chiu et al. used HEK293T cells and measured Panx1 current or dye uptake under high K^+-stimulation and did not corroborate Jackson's results (Chiu et al., 2017). Either the model or the experimental conditions, particularly the way to study Panx1 function, could influence the response to the different stimuli. The physiological relevance of K^+-dependent activation has been proposed in relation with central neurons pathophysiology as high concentrations of extracellular K^+ (7∼80 mM) have been observed in conditions such as epileptiform convulsions or ischemic injury (see Chiu et al. 2018).

4.2.3. An increase in intracellular Ca^{2+} induces Panx1 activation

It has been well described the activation of the Panx1 channels by G-protein coupled receptors like P2Y purinergic receptors or protease-activated receptors (PARs). This regulation has been associated with an increase in cytosolic Ca^{2+}. This was first postulated from experiments in oocytes expressing-Panx1 showing an increase in whole-cell current following application of A23187, a calcium ionophore, and confirmed under inside-out patch-clamp conditions where an increase in Panx1 channel activity was triggered upon exposure to elevated Ca^{2+} on the cytosolic side of the path, in a dose-dependent manner (Locovei et al., 2006). Another study reported that the cell-permeable Ca^{2+} chelator, BAPTA-AM, reduced thrombin-induced ATP release measured simultaneously by luciferin/luciferase assay and propidium iodide uptake from A549 cultured cells, also suggesting the Ca^{2+}-dependence of Panx1 activation (Seminario-Vidal et al., 2009). However, in other studies, the change in cytosolic Ca^{2+} was unable of activating Panx1. It seems that there is a co-dependence of cytosolic Ca^{2+} and receptor-associated mechanisms of activation. It is also important to consider that Panx1 channels do not have conventional calcium-binding domains and it has remained unclear whether cytosolic Ca^{2+} can activate directly or indirectly Panx1 (Chiu et al., 2018). In any case, a Ca^{2+} elevation is definitely not compulsory for Panx1 activation as shown in a recent study where α1-adrenergic receptor-mediated Panx1-dependent ATP release in vascular smooth muscle occurred independently of intracellular calcium, but was sensitive to Panx1 tyrosine phosphorylation (DeLalio et al., 2019).

4.2.4. Phosphorylation induces activation of Panx1

There is evidence that Panx1 channels can be activated through posttranslational modification like phosphorylation by the Src kinases family (SFK). Lohman et al. in 2015 used endothelial cells to study ATP release through Panx1 channels. They used the stimulation of endothelial cells with pro-inflammatory cytokine TNF-α and measured ATP release through luciferin/luciferase assay associated with the pharmacological inhibition of Panx1 channels (50 μM of CBX) and of type-1 TNF receptors (10 μM of WP9QY). They showed that ATP release through Panx1 channels from the endothelial cells was produced in response to Panx1-phosphorylation at tyrosine 198 (Y198) by a signaling cascade starting with the pro-inflammatory cytokine TNF-α, which interacts with type-1 TNF receptors, producing SFK activation and finally Panx1-phosphorylation. ATP release was decreased when using type-1 TNF receptor blockers or when using a siRNA-mediated Panx1 knockdown (Lohman et al., 2015). In a more recent study, Delalio et al. (2019) demonstrated that Panx1-mediated ATP release depends on the phosphorylation at tyrosine 198 in the intracellular loop, by the Src kinase (part of the SFK family). The inhibition of Src kinase blocks Panx1 opening, ATP release, and ATP release-dependent vasoconstriction (DeLalio et al., 2019).

Panx1 phosphorylation has also been associated with anoxia and neuronal death. During anoxia/ischemia, the activation of NMDA receptors (NMDARs) by excessive glutamate produces SFK activation, and Panx1 phosphorylation at tyrosine 308, activating Panx1 (Weilinger et al., 2012). This cascade has been proposed as a new signaling pathway for excitotoxicity and neuronal death. In agreement, it was observed that the disruption of NMDAR-Src-Panx1 interaction in vitro or in vivo by the administration of an interfering peptide was neuroprotective during ischemia or after stroke (Weilinger et al., 2016). However, in both studies, ATP release through Panx1 was not measured, so these results should be considered with caution before concluding that phosphorylation of tyrosine 308 opens the main pore of the channel and allows ATP release and that this promotes neuronal death. In addition to SFK Panx1 has been proposed to be regulated by other kinases, like c-Jun NH_2-terminal kinase (JNK) and protein kinase G (PKG) in hepatoma cells and hepatocytes respectively (Chiu et al., 2018).

4.2.5. Caspase-mediated C-tail cleavage activates Panx1 in an irreversible manner

In contrast to the above-described mechanisms that are reversible, Panx1 can be activated irreversibly by cytosolic caspases. In T lymphocytes, during apoptosis, caspases 3 and 7 are capable of cleaving Panx1 channels at the C-terminal site, producing Panx1 opening, ATP release, and generating a “find-me” signal, which recruits phagocytes. Using a luciferin/luciferase assay to measure ATP release,

Chekeni et al. (2010) observed that either pharmacological inhibition (500 µM CBX or 2 mM PROB) or Panx1 knockdown (by siRNA), decreases ATP release and monocytes recruitment by apoptotic cells, while Panx1 overexpression enhances nucleotide release from apoptotic cells and phagocytes recruitment. Using patch-clamp current recording, these authors observed an increase in Panx1 activity produced only under apoptotic conditions. Accordingly, when expressing a truncated version of Panx1 at the site of caspases cleavage, they observed a constitutively open state of Panx1 (Chekeni et al., 2010). Their results were confirmed by other two studies: 1) Qu et al. observed in thymocytes lacking Panx1, the defective uptake of the dye YO-PRO-1 during early apoptosis, and failure to recruit wild-type peritoneal macrophages, normally dependent on the ATP "find-me" signal (Qu et al., 2011), 2) Sandilos et al. used patch-clamp recording in an immortalized T-lymphocytes cell line (Jurkat) expressing human Panx1 (hPanx1): they showed that application of caspase-3 produced a fast increase of the current, that was completely blocked by CBX, but without apoptotic events. These authors also used a hPanx1 mutant with a tobacco etch virus protease (TEVp) site at the C-terminal, and expressed it in HEK293T cells. When applying TEVp, they observed an increase in whole-cell currents and uptake of the To-Pro-3 dye, witnessing Panx1 channel opening. Their results showed that the C-terminal cleavage is sufficient for hPanx1 activation. Also quite convincing was the demonstration that the constitutively active Panx1 channel is inhibited by application of the hPanx1 C-terminus as a purified peptide, in inside-out and whole-cell patch-clamp recordings (Sandilos et al., 2012). A more recent study made by Chiu et al. (2017) proposed that the Pannexin 1 channel presents a quantized and progressive activation during both the irreversible (C-terminal cleavage) and the reversible (adrenoreceptors-mediated) activation process. For this, authors expressed, in HEK293T cells, hexameric Panx1 channels composed of different proportions of monomers carrying a TEVp site in the CT. Using patch-clamp current records with this system they show that progressive removal of C-terminal regions leads to stepwise channel activation, with graded effects on unitary properties. Indeed, they were able to detect a wide range of Panx1 channel activity, from Panx1 without any TEVp site (called 6(6CT)) to Panx1 with all subunits expressing the TEVp site in each CT (called 6 (0CT)). Following application of TEVp, Panx1 channels present a current directly related to the number of modified CTs. Furthermore, using single-particle EM analysis, they could show that the 6 (0CT) version presents an annular configuration with a clear pore domain. These results proved the direct modulation of Panx1 activity and conformation by the CT termini and suggest a quantized and fine-tuning of Panx1 channel activity. Concurring results were obtained when using luciferin/luciferase assay to measured ATP release from the HEK293T cells expressing the same constructs: ATP release increased as the number of intact C termini was decreased, reaching maximal levels in cells expressing 6(1CT) or 6(0CT) (Chiu et al.,

2017). As described before in the present document, their conclusion was clarified by five cryo-EM studies that recently reported the Panx1 heptameric channel tridimensional structure (Deng et al., 2020; Jin et al., 2020; Michalski et al., 2020; Mou et al., 2020; Ruan et al., 2020) (see Fig. 21 and 22).

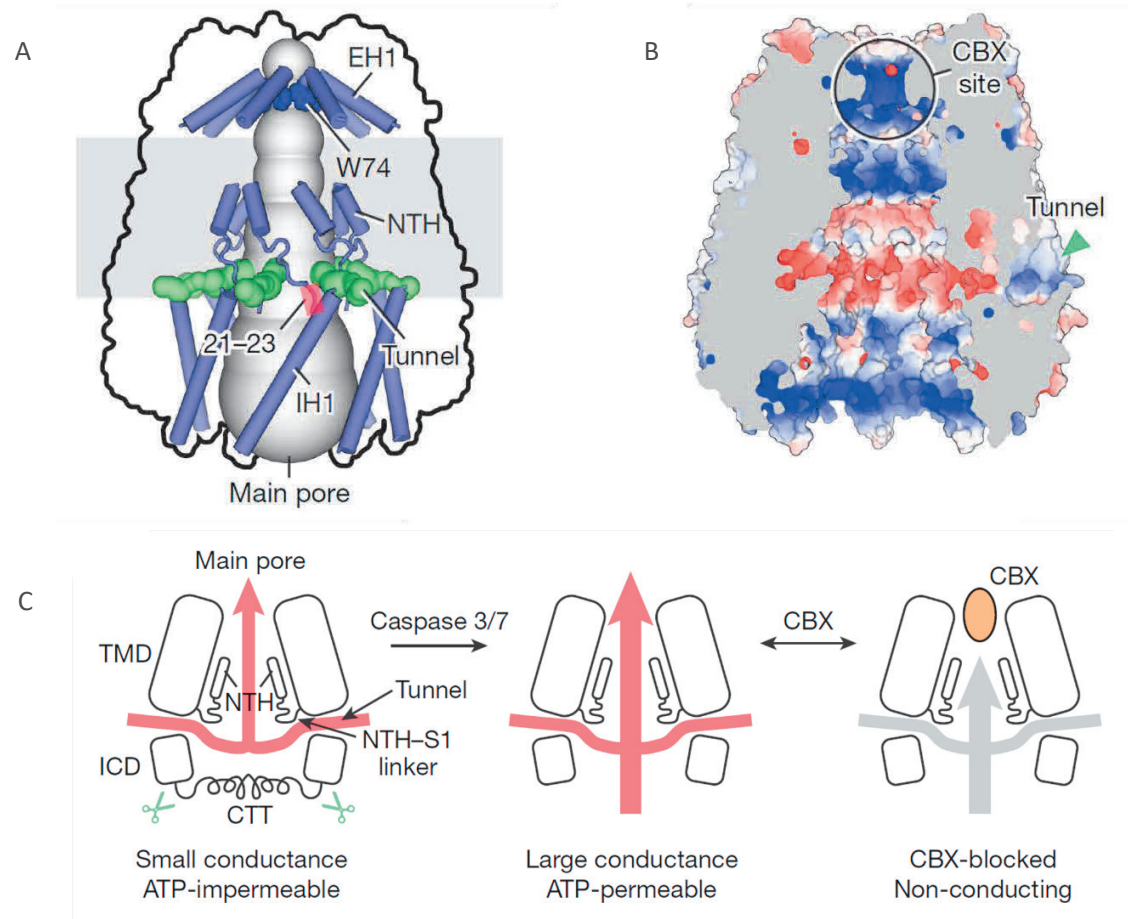

Figure 22. Scheme of Panx1 ion conducting pathways and channel gating. *A) Overview of the main pore (grey) and side tunnels (green) in a Panx1 channel. The position of the disease-causing gain of function mutation in the NTH-S1 linker is highlighted in red. B) The interior surface of Panx1 is shown colored according to the electrostatic surface potential, from negative to positive (red to blue). We observed the side tunnels entry and the position of interaction with CBX in the extracellular entry of the main pore. C) Cartoon showing the two internal pathways, the relationship between the conductance and CTT, and the mechanism of CBX blocking proposed by Ruan et al. 2020. Images modified from Ruan et al. 2020.*

4.2.6. Pannexin 1, ATP release and ligand-gated receptor signaling

Extracellular ATP can activate either metabotropic (Locovei et al., 2006) or ionotropic purinergic receptors (Locovei et al., 2007), potentially capable of producing a process called ATP-induced ATP release to amplify ATP release signaling.

ATP release through pannexins channels and its consequent activation of several membrane receptors has been shown to play a role in biological processes like apoptosis (Chekeni et al., 2010), blood pressure regulation (Billaud et al., 2011; Billaud et al., 2015), and neuropathic pain generation (Bravo et al., 2014; Weaver et al., 2017).

4.2.7. Panx1 and ionotropic receptors signaling

The ***N*-methyl-D-aspartate receptor (NMDAR)** is a ligand-gated ionotropic receptor important in neuronal death. Its activation occurs during synaptic activity and requires binding of glutamate and glycine/d-serine, associated with a membrane depolarization to relieve Mg^{2+} block in the pore. These simultaneous stimuli activate NMDAR, which is a non-selective cation channel, therefore producing Ca^{2+} influx. It has been shown that NMDARs activate Panx1 channels to improve their influence on membrane potential participating in a process called “interictal bursting”, a rhythmic and synchronized neuronal discharge observed in seizure susceptible brains. During this process, Panx1 potentiates the response of NMDRs under pathological conditions (Thompson et al., 2008; Weilinger et al., 2012). Thompson et al. studied NMDAR activation-induced Panx1-associated secondary current. They used isolated hippocampal neurons and measured whole-cell patch-clamp currents during the application of either continuous or repeated applications of 100 µM NMDA and simultaneously applied voltage pulses from -80 mV to +80 mV. They also measured the cytosolic Ca^{2+} changes using Ca^{2+}-sensitive fluorescence dyes to monitor the activation of NMDAR, and the efflux of calcein red/orange dye to monitor the activation of Panx1 under NMDA exposure. They observed in all their experiments that 50 µM CBX or 100 µM ^{10}panx (a Panx1 inhibitor peptide) decreased the secondary current and the efflux of the dye during NMDA stimulation, highlighting the role of Panx1 in this process (Thompson et al., 2008). In another study, Weilinger et al. showed that pharmacological Panx1 inhibition or conditional genetic Panx1 deletion attenuates the anoxia-dependent depolarization of pyramidal neurons in acute brain slice from rats and mice and that Panx1 activation was mediated by SFK as described previously. They concluded that NMDARs activation during anoxia/ischemia produces Panx1 opening through SFK recruitment (Weilinger et al., 2012).

The **purinergic ionotropic receptors (P2XRs)** are ion channels activated by purine triphosphate nucleotides like ATP. They are part of a family with seven isoforms (P2X1-7Rs) (Burnstock, 2017). Panx1 channels functionally interact with purinergic ionotropic receptors by releasing ATP, and this regulation has been particularly highlighted with P2X7R. As extracellular ATP activates P2X7Rs, this enhances the cellular inflammasome leading to caspase-1 activation and releasing interleukin 1β, opening the possibility that ATP release could be potentiated by the activation of purinergic receptors (Isakson & Thompson, 2014). Gulbransen et al. studied inflammatory bowel diseases and the mechanism underlying the inflammation-induced enteric neuronal death. They studied an in vivo model of enteric neuron death and observed the activation of the signaling complex of P2X7R, Panx1 channels, the adaptator protein Asc (apoptosis-associated speck-like protein containing a CARD), and caspases. The inhibition of P2X7Rs, Asc, caspase, or of Panx1 activity prevented inflammation-induced neuronal death (Gulbransen et al., 2012).

4.2.8. Panx1 and metabotropic receptors signaling

Panx1 has been related principally to the activation of the purinergic metabotropic receptors (P2YR). They are G-protein coupled receptors, part of a family with 8 isoforms (P2Y1, P2Y2, P2Y4, P2Y6, P2Y11, P2Y12, P2Y13, and P2Y14). Panx1-dependent ATP-release and P2Y activation has been studied in different tissues and cell types. Panx1 has been associated with the activation of P2Y receptors in coronary circulation for the regulation of the smooth muscle tone, endothelial cells during sheer stress, response to mechanical deformation or hypoxia in blood cells, regulation of the vascular tone, signaling in leukocytes promoting leukocyte adhesion and emigration, among others (Burnstock, 2017).

In skeletal muscle, we already mentioned Panx1-dependent ATP release and the activation of the metabotropic P2Y receptors during ETC (Buvinic et al., 2009; Gonzalo Jorquera et al., 2013; Valladares et al., 2013). Of importance along this is that Buvinic et al. (2009) showed that Panx1 co-precipitates with $Ca_V1.1$ and the metabotropic P2Y2 receptor, raising the likelihood for the existence a closely interacting macromolecular complex.

In smooth muscle, Panx1-dependent ATP release has been associated with the activation of adrenoreceptors type α1 and the vasoconstriction response to noradrenaline. It has been proposed that one possible explanation for this influence could be a G-protein depending response associated with either ATP release or changes in the ionic flux (Vettel et al., 2012; Isakson & Thompson, 2014). The role of Panx1 in smooth muscle is visited in more details in the next section.

4.2.9. Panx1 role in smooth muscle

Recent studies have revealed that Panx1 has an important role in the regulation of noradrenergic-dependent vasoconstriction and blood pressure regulation (Billaud et al., 2011; Billaud et al., 2015;). The vascular smooth muscle cells (VSMCs) in the arteries control peripheral resistance under the regulation of sympathetic nerves. The local innervation co-releases norepinephrine and ATP (Burnstock, 2010). The activation of adrenoreceptors type α1 (α1-AR) located in the plasma membrane of the smooth muscle cells generates downstream signaling events including Panx1 channels opening which promotes and coordinates vasoconstriction of neighboring cells playing a role in the control of vascular tone and blood pressure (Billaud et al., 2015). Indeed, Billaud et al. showed that α1-AR-dependent vasoconstriction was not straightforward, and requires Panx1 activation. For this, they used mice conditionally lacking Panx1 in smooth muscle cells and Panx1 pharmacological inhibition. They found that noradrenaline indirectly stimulates vasoconstriction by activating Panx1 channels, which release ATP into the extracellular space. Extracellular ATP stimulates vasoconstriction through purinergic receptors in an autocrine manner (Fig. 23) (Billaud et al., 2015). Specifically, authors could show that Panx1 blockers decrease phenylephrine- and noradrenaline-induced vasoconstriction. They used an ATP bioluminescence assay to demonstrate that phenylephrine stimulates ATP release from the arteries, and that this was blocked by Probenecid and ^{10}Panx1. To confirm Panx1 role, they used a tamoxifen-inducible smooth muscle-specific Panx1 knockdown preparation and observed a decrease in the phenylephrine-dependent contractile response.

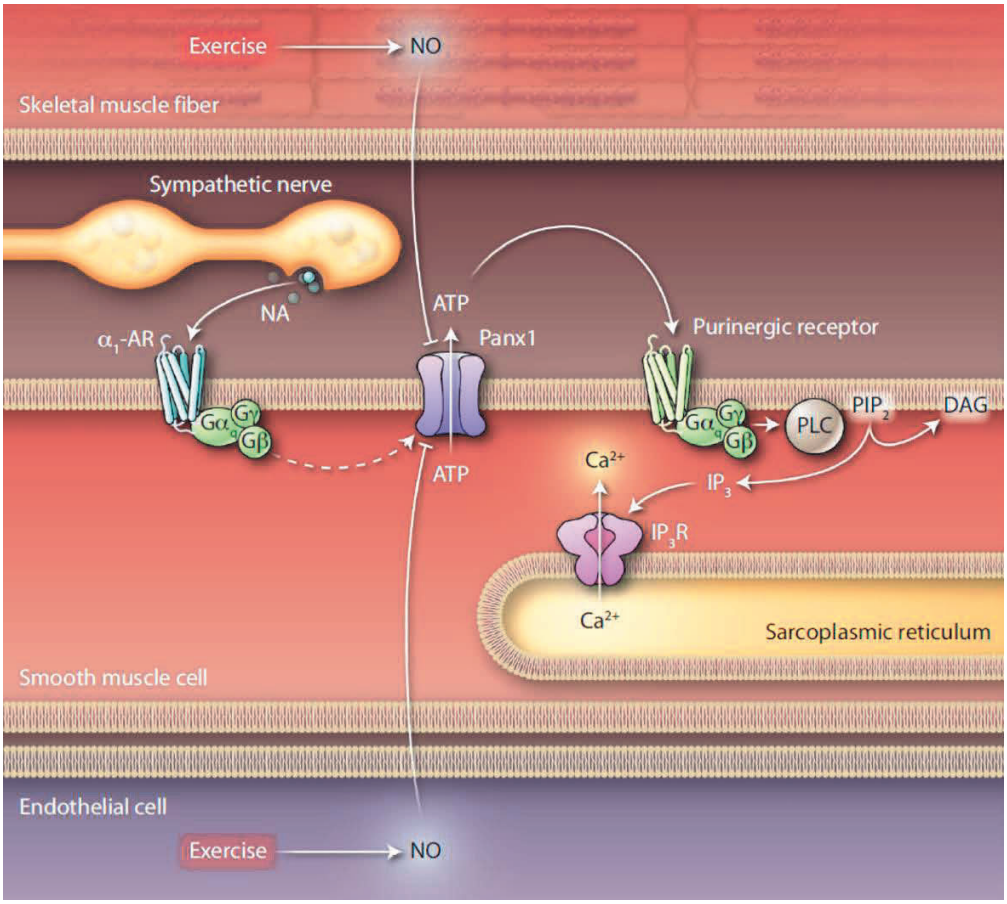

Figure 23. Model of sympathetic vasoconstriction, mechanism of regulation by physical exercise and Panx1 role. *Sympathetic vasoconstriction based on Billaud et al. 2015, in which sympathetic nerve activity releases noradrenaline (NA), which activates Panx1 through α1-AR activation. Panx1 releases ATP which binds to G-coupled purinergic receptors activating phospholipase C (PLC), which cleaves phosphatidylinositol-bisphosphate (PIP_2) into IP_3 and diacylglycerol (DAG). IP_3 bind IP_3-receptors (IP_3Rs) located in the sarcoplasmic reticulum membrane, which release Ca^{2+} into the cytosol to activate contraction. Nielsen et al. proposed that exercise could regulate this process through the production of nitride oxide (NO) in skeletal muscle and endothelial cells. NO would close Panx1 channels by S-nitrosylation. Image taken from Nielsen et al. 2015.*

Then, they investigated the cytosolic α1-AR-Panx1 interactions by producing different peptides that correspond to the Panx1 intracellular loops: two peptides for the first intracellular loop (IL1 and IL2), one for the second intracellular loop (CT1), and a last one for the CTT (CT2): IL1 reduced the phenylephrine-dependent vasoconstriction while the IL1 scramble and the other peptides did not produce any change (Billaud et al., 2015).

In smooth muscle, Panx1 has also been associated with $Ca_V1.2$: Dahl et al. in 2016, studied the effect of Clevidipine, a dihydropyridine analog, on smooth muscle function and blood pressure regulation. Administration of Clevidipine produced a decrease in the blood pressure, classically explained by L-type Ca^{2+} current inhibition, specifically the $Ca_V1.2$ channels (gene *CACNA1C*). However, they observed that Clevidipine has a particularly strong effect on pulmonary vascular resistance compared with systemic vascular resistance, and produces effects that are different from other dihydropyridines, suggesting some particular variation in $Ca_V1.2$. Using human lung tissue mRNA analysis, they found a specific $Ca_V1.2$ splice variant that, when co-expressed with Panx1 in Xenopus oocytes, improves its sensitivity to Clevidipine (Dahl et al., 2016).

4.3. Panx1 in skeletal muscle physiology and pathology

4.3.1. $Ca_V1.1$-dependent Panx1-activation and ATP release in the mdx mouse model of Duchenne muscle dystrophy

We already presented one Panx1 channel function in adult skeletal muscle associated with $Ca_V1.1$ activation, ATP release, and ETC through gene expression regulating fast-to-slow muscle plasticity in muscle fibers stimulated at 20 Hz. Upon tetanic stimulation, ATP is also released from myotubes in culture, a phenomenon blocked by Panx1 inhibitors (Buvinic et al., 2009; Jorquera et al., 2013). Related to these results, Valladares et al. (2013) found that 20 Hz electrical stimulation also has an anti-apoptotic effect in normal adult isolated muscle fibers, repressing the expression of the pro-apoptotic genes Bax, Bim, and PUMA (Ren et al., 2010). Addition of extracellular ATP (10-100 µM) to normal adult muscle fibers showed similar effects. Valladares et al. also studied ATP release from adult fibers isolated from the Duchenne muscular dystrophy (DMD) mouse model, the mdx mouse, using a luciferin/luciferase assay: they observed an elevated ATP release basal level as compare with the control mice, and the absence of ATP release after electrical stimulation, suggesting uncoupling between electrical stimulation and ATP release in this disease condition. Subsequently, they studied $Ca_V1.1$ and Panx1 relationship and observed a decrease in the co-immunoprecipitation, suggesting physical uncoupling of this signaling complex in mdx muscle fibers. Interestingly, they also found that addition of extracellular ATP to mdx fibers, contrary to normal fibers, induces the transcription of Bax, Bim, PUMA, and increases the levels of activated Bax and cytosolic cytochrome C, which are markers of apoptosis at the mitochondria (Valladares et al., 2013). This

provides evidence for a role of the Panx1-ATP pathway in the activation of cell death in muscular dystrophy, opening perspectives for new therapeutic targets.

Altamirano et al. (2013), further investigated the possible role of $Ca_V1.1$-dependent activation of Panx1 channel and ATP-release in skeletal muscle alterations of mdx mice. They confirmed the increased basal ATP release levels, as measured by a Luciferin/Luciferase assay, in mdx myotubes and in mdx adult muscle fibers (FDB), and the association with upregulation of pro-apoptotic genes, as previously shown (Valladares et al., 2013). Altamirano et al. (2013) treated mdx mice with nifedipine, a $Ca_V1.1$ inhibitor that inhibits Panx1-dependent ATP-release in skeletal muscle (Jorquera et al., 2013). Mdx mice treated with nifedipine exhibited a significant reduction in basal ATP release level as measured from cultured myotubes and from differentiated adult muscle fibers. They also found a reduction in mRNA levels of pro-oxidative/nitrosative (iNOS and NOX2 subunits), pro-apoptotic (Bax) genes and an increase in muscle performance as assessed by grip-hanging test and exercise tolerance (swimming). Mdx cultured myotubes exhibit an elevated resting cytosolic [Ca^{2+}] level that was decreased by nifedipine, and similar results were obtained when comparing muscle fibers from mdx mice with and without nifedipine treatment. They proposed that nifedipine through $Ca_V1.1$ blocking reduces Panx1-dependent ATP-release, which decreases purinergic receptor activation, decreasing basal cytosolic [Ca^{2+}] and altering mRNA regulation of the mentioned genes (Fig. 24) (Altamirano et al., 2013). A more recent study, made by Róg et al. (2019), further supports purinergic receptor signaling alteration in mdx mice myoblasts, associated with an increase in basal cytosolic [Ca^{2+}] levels and the modulation of different proteins with a role in Ca^{2+} handling. Specifically, these authors reported a decrease in Gq11 subunit α, plasma membrane calcium ATPase, IP3R, and an increase in phospholipase Cβ, SERCA pump, and Na^{+}-Ca^{2+}-exchanger (Róg et al., 2019).

4.3.2. Panx1-dependent ATP-release and potentiation of skeletal muscle contraction

Another function for Panx1 was proposed in skeletal muscle, in a process called “contractile potentiation”. Contractile potentiation corresponds to the increase in force after repetitive twitches. This response has been related to an increase in cytosolic [Ca^{2+}] and it requires extracellular ATP (Sandonà et al., 2005). Accordingly, application of extracellular ATPases inhibits the potentiation response. It has been suggested that in adult skeletal muscle the potentiation response is mediated by P2Y receptors and that ATP-release through Panx1 channels has an important role in this process. Panx1 channels activated by electrical stimulation would allow ATP release and glucose uptake (as measured by the glucose analog 2-NDBG) which seems to be needed for potentiation of muscular contraction (Sandonà et al., 2005;

Riquelme et al., 2013). Muscles from Panx1 knockout mice ($Panx1^{-/-}$) do not exhibit contractile potentiation but it could be restored by addition of 200 µM extracellular ATP. In summary, these results highlight the role of Panx1 channels in the contractile potentiation response and support the hypothesis that potentiation *in vivo* could be produced by the permeability of Panx1 channels to ATP in activated skeletal muscles (Cea et al., 2014).

In a more recent work, Ziganshin et al. (2019) compared the effect of ATP and adenosine on EDL muscle contractility at normal and low temperatures. They used mouse and rat EDL muscles and two different methods to induce muscle contraction: 1) the application of exogenous carbachol, an enzymatically stable analog of acetylcholine and 2) electrical field stimulation (ES). In the presence of 100 µM extracellular ATP, they reported a decrease in carbachol-induced contraction in rat and mouse EDL at all temperatures, and a decrease in ES-induced contraction in rat EDL. In contrast, exogenous ATP in mouse EDL potentiated the ES-induced contraction (Ziganshin et al., 2019). Their results also support the hypothesis that Panx1-dependent ATP release could have a role in the regulation of force production.

4.3.3. Panx1 and Panx3: role in skeletal muscle differentiation and regeneration

In 2014, it was reported that Panx1 and Panx3 are differentially expressed in human and rodent skeletal muscle, depending on the developmental stage. Panx1 levels are very low in undifferentiated human primary skeletal muscle cells and myoblasts, but increase importantly during differentiation so as to become the main Panx isoform expressed in differentiated muscle cells. Panx3 was also found in skeletal muscle and present two different molecular species, differentially expressed through the development. A lower molecular weight specie (≈ 43 kDa) was prominently expressed in adult skeletal muscle, but very low in fetal tissue, in undifferentiated skeletal muscle cells, and in myoblasts. On the other hand, the higher molecular weight specie (≈ 70 kDa), likely glycosylated, sialylated, and phosphorylated was highly expressed in proliferative myoblasts but decreased during differentiation to levels almost below detection (Langlois et al., 2014; Pham et al., 2018). Langlois et al. results proposed then a new role for Panx1 and Panx3 in myogenic commitment, myoblast proliferation, and differentiation of skeletal muscle cells. They observed that overexpression of the Panx3 43 kDa inhibits myoblast proliferation and stimulates their differentiation, while the reduction of Panx3 70 kDa (using shRNAs) significantly inhibits myoblast proliferation (Langlois et al., 2014). Associated with their results, it was also reported that Panx1-dependent ATP release mediates the acquisition of myogenic commitments of the C2C12 reserve cells through the activation of purinergic receptors, the regulation of cytosolic [Ca^{2+}] and MyoD expression levels (Riquelme et al., 2015).

Recently, Pham et al. (2018) studied adult skeletal muscle from male and female wild type and mdx mice, and their Panx isoforms expression in fast- and slow-twitch muscles. Panx1 and Panx3 were differentially expressed in fast- and slow-twitch muscle and were co-expressed in human and mice satellite cells, playing a role in muscle regeneration. They observed by Western blot that Panx1 has also various molecular weight (MW) species, reflecting different glycosylation status, and observed increased Panx1 mRNA levels in the soleus (SOL), a slow-twitch muscle, compared with the TA and EDL fast-twitch muscles. In contrast, Panx3 transcripts levels were decreased in SOL compared with EDL muscles. These authors also studied the role of Panx1 and Panx3 on regeneration after the injection of cardiotoxin (CTX) in TA muscle in adult mice. They perform Western blots measurements at 2, 4, 7, and 14 days after CTX injection, and they observed an important decrease of Panx1 protein expression 2 days post-injury compared with controls. Panx1 protein levels recovered to normal values after 14 days when fibers were fully regenerated. They also saw the same behavior for the Panx3 43 kDa. In contrast, Panx3 70 kDa drastically increased at day 2 post-injury and decreased at 14 days. Taken together, they demonstrated that Panx1 and Panx3 are regulated during myogenesis. Associated with these results they also demonstrate dysregulation of Panx1 and Panx3 levels in dystrophic skeletal muscles, suggesting that Panx1 could play another important role in healthy and diseased skeletal muscles (Pham et al., 2018) additionally to the role in ETC.

4.3.4. Panx1 knockout and skeletal muscle function

Several independent Panx1 knockout (KO) mouse lines have been developed (Anselmi et al., 2008; Dvoriantchikova et al., 2012; Qu et al., 2011), and Panx1 KO transgenic mouse were generated by different institutions like the knockout mouse project (KOMP) at Davis University (www.komp.org) or the Panx1 KO model produced by Genetech (www.genetech.com). Independent teams also produced single Panx1 KO (Romanov et al., 2012) and double Panx1/Panx2 KO (Bargiotas et al., 2011). The KOMP Panx1 KO was though shown to be incomplete(70 % decrease of Panx1) (Hanstein et al., 2013). In all these studies, there was no report of gross phenotypic alteration.

Panx1 KO mice do not suffer from a deficit in skeletal muscle myogenesis, despite the reported role in myoblast commitment (Riquelme et al., 2015) and Panx1 deficiency seems to produce limited functional changes and loss of contractile potentiation (Riquelme et al., 2013). The absence of important skeletal muscle alteration in Panx1 KO mouse models could be explained by an incomplete knockout as reported in the KOMP model, or by compensation through overexpression of the Panx3 isoform, also

present in skeletal muscle. Because of this, there is increasing interest in developing/investigating double KO models for Panx1/Panx3 (Pham et al., 2018).

Accordingly, It appears also of strong interest to study the consequences of acute Panx1 knock-down in differentiated muscle fibers, to better understanding of the relevance of Panx1 function in muscle physiology, for ETC, for potentiation of skeletal muscle force, and for muscle regeneration/differentiation. To this aim, an acute and transitory Panx1 knockdown model was generated by the “Centro de estudios moléculares de la célula” and Casas’s Team, at the Institute of Biomedical Science (ICBM) at the University of Chile. I have used this model during my Master degree in Chile, within an international collaboration with the team of V. Jacquemond at INMG at Université Claude Bernard-Lyon 1.

4.3.5. Panx1 in non-muscular human diseases

Until recently, there were no reports of germ-line mutation in pannexin-encoding genes linked to human diseases (Penuela et al., 2014). Since then, mutations in *PANX1* were shown associated with female infertility via a phenotype called "oocyte death" in which Panx1 glycosylation pattern is affected, influencing the subcellular localization of the protein, and generating aberrant channel activity and ATP release in oocytes (Sang et al., 2019). Also worth being mentioned is a very recently described *PANX1* variant identified in a patient tumor, which was found to prevent phosphorylation of a particular residue and to affect glycosylation and intracellular localization of the protein (Nouri-Nejad et al., 2021).

Conversely, there are several examples in which Panx1 could be linked to human diseases like melanoma, ischemia/stroke, epilepsy, hypertension, inflammatory bowel diseases, Alzheimer’s, and diabetes (Penuela et al., 2014). This will be briefly presented here with reference to cancer, ischemia and stroke, and to inflammatory bowel disease as examples of roles for Panx1 in human diseases (for more details, see Penuela et al. 2014).

Panx1 has been related to **cancer** onset and progression, but the literature presents some contradictions. Lai et al. showed that ectopic overexpression of Panx1 in C6 gliomal cells reduces their migratory capacity, proliferation, and growth. Authors expressed these Panx1-overexpressing cells in nude mice and observed a significant reduction in the tumor size. Their results implicate that Panx1 is tumor suppressive in gliomagenesis (Lai et al., 2007). It was then proposed that this effect may be a consequence, at least in part, of Panx1 interaction with actin and actomyosin and its effect on the cell cycle progression (Bao et al., 2012). In contrast with these findings, Penuela et al. observed that up-regulation of Panx1 plays a role in melanoma progression. They also found that Panx1 protein expression

was higher in aggressive BL6 melanomas when compared with less aggressive isogenic counterparts (Penuela et al., 2012). Over the recent years, it has been accepted that Panx1 has a role in tumor progression or suppression depending on ATP release, its concentration, the specific ectonucleotidases and receptors expressed by the immune and cancer cells. It has been suggested that the tumor microenvironment levels of ATP have a central role in determining tumor fate and it is a suitable target for cancer therapy (Vultaggio-Poma et al., 2020).

Panx1 has been linked to **ischemia and stroke**. As we mentioned previously, in neurons, the function of Panx1 channels has been associated with cell death. First, Thompson et al showed that Panx1 was responsible for the depolarization of hippocampal neurons in acute brain slices, resulting in neuronal cell death. After, they showed that Panx1 can be activated by *N*-methyl-D-aspartate receptors (NMDARs) and results in an epileptiform seizure-like activity that could be inhibited using a Panx1-blocking peptide (Thompson et al., 2006; Thompson et al., 2008). Finally, they proposed that the mechanism behind the interaction between Panx1 and NMDAR during anoxic depolarization involves activated SFKs (Src family kinases) that directly or indirectly regulate Panx1 channels (Weilinger et al., 2012) as mentioned previously. For another group, it was shown that the use of Probenecid, a Panx1 blocker, reduces the focal ischemic brain injury by inhibiting cerebral inflammation and edema in a mouse model of middle cerebral artery occlusion (Xiong et al., 2014). Interestingly, the constitutive ablation of Panx1 was not enough to produce a protective effect, while Panx1/Panx2-double-knockout mice exhibited a reduction in total infarct size upon stroke (Bargiotas et al., 2012).

Today, it is generally accepted that Panx1 participates in the regulation of ischemia and stroke through ATP release. Upon binding to purinergic receptors expressed in neural cells, ATP triggers cellular responses like proliferation, cell morphology changes, release of cytokines and regulates neuronal excitability via the release of glutamate, GABA, and ATP itself. The excitatory effect of ATP on neuronal activity is principally related to the activation of P2X receptors, while it also presents an inhibitory effect related to the metabolism of ATP into ADP and the activation of inhibitory P1 adenosine receptors. Thus Panx1 plays a dual role in neuronal excitability (Scemes & Velíšková, 2019).

Panx1 has also been associated with **inflammatory bowel diseases**. These inflammatory diseases are caused by enteric nervous system dysfunction and enteric neuronal cell death associated with gastrointestinal inflammation. There are two main types of inflammatory bowel diseases: ulcerative colitis and Crohn's disease. It has been demonstrated that Panx1 participates in bowel diseases through ATP release, P2X7 receptor activation, Asc adaptor protein, and caspases (Gulbransen et al., 2012). The study

of patients suffering bowel disease revealed a decrease of Panx1 mRNA expression in myenteric ganglia of ulcerative colitis patients, and in the muscular layer of Crohn's disease patients indicating a potential role for Panx1 in inflammatory bowel diseases (Diezmos et al., 2013). At present, the pathophysiology of these diseases remains largely unknown, but include the participation of P2X7R, Panx1 channel, and Cx43 (Diezmos et al., 2016).

4.4. Panx1 channel pharmacology

The pharmacology of Panx1 remains complicated as several of the initially described blocker candidates are not specific (Dahl et al., 2013). Panx1 channels, as hemichannels, in resting conditions seem to be mainly closed and to be open by specific physiological or pathological stimuli (Willebrords et al., 2017). Considering the structural knowledge acquired recently, and the increasingly known functional role of ATP release in many physiological and pathological mechanisms, there is strong interest and potential for further pharmacological investigations of Panx1 function and for design and test of new specific agents. The use of Panx1 inhibitors after Panx1 activation by caspases or phosphorylation combined with extracellular ATP measurements is likely to be one most reliable strategy to assess the effect of the molecules. From all currently used molecules, the most used and accepted are the peptide ^{10}panx (Wei et al., 2020), and the drugs carbenoxolone and probenecid. The properties of carbenoxolone and probenecid are more specifically emphasized in the following sections because I used them during this project.

4.4.1. Carbenoxolone (CBX)

Carbenoxolone (CBX) is a derivative of glycyrrhetinic acid found in the root of *Glycyrrhiza glabra* or *Licorice*, and it has been used for peptic and oral ulcers since the sixties. It is a hydrosoluble drug used as a classic blocker of gap junction channels and hemichannels, including Panx1 (Poklis et al., 2019). It was first studied as a Panx1 channel blocker with a low IC_{50} (5 μM) when measuring ionic current through Panx1 expressed in Xenopus laevis oocytes (Bruzzone et al., 2005) or in HEK293T cells (4 μM) (Ma et al., 2009). It has also been used to block ATP release through Panx1 channels in myotubes and adult skeletal muscle fibers at the same concentration (≈ 5 μM) (Buvinic et al., 2009; Jorquera et al., 2013; Valladares et al., 2013). However, most of the functional studies in different tissues reported larger effective concentrations, like in smooth muscle studies (≈ 50 μM) (Billaud et al., 2011; Billaud et al., 2015), neurons (≈ 50 μM) (Thompson et al., 2008) or immune system studies using Jurkat cells at even higher concentration (≈ 500 μM) (Chekeni et al., 2010). There are two possible action mechanisms proposed to

explain CBX action over Panx1. It was first proposed that CBX works as an inhibitor by interacting with the first extracellular loop in an allosteric manner, potentially producing a conformational change on Panx1 tridimensional structure (Michalski & Kawate, 2016). Recently, this idea has been refuted by the cryo-EM studies of two different groups: Jin et al. (2020) showed not conformational change in the presence of CBX (Jin et al., 2020) and Ruan et al. (2020) proposed that CBX works as a channel blocker by interacting with the extracellular selectivity filter in the main pore composed by a ring of the W74 residues from each subunit (Ruan et al., 2020). When considering the last results, it is accepted that CBX blocks the extracellular exit of the main pore and prevents simultaneously ion current and ATP release. However, a CBX-binding associated Panx1 conformational change cannot be completely excluded.

4.4.2. Probenecid (PROB)

Probenecid (PROB) is a lipid-soluble benzoic acid drug widely used in the treatment of gout, acting as a blocker of organic anion transporters. Probenecid-sensitive transporters are widely distributed, even found in plants. Clinically, probenecid has been used to increase the renal absorption of antibiotics, chemotherapeutics, and other drugs (Willebrords et al., 2017). It has also been used as a doping masking agent in high-level sports competitions and has been added to the prohibited list since 1987 (Hemmersbach, 2020). Probenecid has also been associated with the activation of a Ca^{2+} channel, called transient receptor potential vanilloid 2 (TRPV2) present in neurons (Bang et al., 2007) and cardiac muscle. In a recent human study, the daily administration of 2000 mg of Probenecid has been associated with the activation of TRPV2 and an improvement in cardiac function in patients with heart failure and reduced ejection fraction (Robbins et al., 2018). It is important to also mention that Probenecid has been used to prevent fluorescent dyes loss in various cell types during single cell physiological studies (Silverman et al., 2008).

With reference to Panx1 inhibition, probenecid was shown to operate as an ATP-release blocker in several cellular models and was shown to inhibit Panx1-dependent current without affecting connexins (Silverman et al., 2008). Probenecid was proposed to have an interaction on Panx1 similar to that of CBX, originally proposed to be an allosteric interaction with the first extracellular loop of Panx1 (Michalski & Kawate, 2016). Probenecid EC_{50} for Panx1 was reported to be ~150 µM, but Panx1-dependent ATP-release is routinely shown to be completely blocked by concentrations in the mM range (Chekeni et al., 2010; Billaud et al., 2015). In terms of related therapeutic potential, a recent study using a rabbit's sepsis model, showed that probenecid blocks Panx1-dependent ATP-release during inflammation, preventing cellular energy crisis and histopathological damage on skeletal muscle, cardiac muscle, and kidney (He et al.,

2018). In human studies, probenecid has also been used to block ATP-release through Panx1 during adrenergic-dependent smooth muscle vasoconstriction, using oral administration of 3000 mg. This should result in an ~700 µM plasma concentration which produced a significant decrease in the vasoconstrictive response (Nyberg et al., 2018).

During my PhD project, we were interested in the role of Panx1 in adult skeletal muscle function and ECC. We used PROB and CBX to study their effect on skeletal muscle Ca^{2+} handling, ECC, and muscle function. This work is presented in the second manuscript in the Results section.

4.5. Measurements of ATP release from single isolated cells

As described in the third chapter, Panx1 activation by various types of stimuli allows ATP release, which has multiple roles in a wide range of tissues and cell types, through activation of ionotropic and metabotropic purinergic receptors. Thus, the possibility to measure ATP release is anticipated to considerably help to understand Panx1 function and extracellular ATP dynamics associated with ATP release (and for instance the related role of ectonucleotidases), as well as downstream autocrine or paracrine signaling processes (Corriden & Insel, 2010). Still, the methods dedicated to the detection of ATP release have limitations in their specificity, sensitivity, and temporal and spatial resolution. Because one of the aims of the present PhD project was to develop a method to measure ATP release through Panx1 channels in a single cell configuration, with a good sensitivity and temporal resolution, it was of specific interest to make a review of the methods so far developed and used in the field.

Such investigations are particularly relevant for the study of skeletal muscle function with regards to the processes of ETC, contractile potentiation, and differentiation. Electrically stimulated ATP release from skeletal muscle has been described to exhibit a bell-shaped relationship versus stimulation frequency, with largest ATP release at 20 Hz and with two peaks: at 15 seconds and 3-5 minutes following a stimulation train (Jorquera et al., 2013). This was assessed, as in many other studies, used most common and well-accepted Luciferin/Luciferase assay (see Fig. 25).

4.5.1. Luciferin/Luciferase assay

Bioluminescence from luciferases is used for the visualization of cellular activity. The luciferase is an enzyme that reacts with its exogenous substrate luciferin to produce light and this can be used to measure ATP because this chemiluminescence reaction is ATP dependent. Luciferase adenylates luciferin, which consequently can be converted into oxyluciferin, increasing proportionally the luminescence to the ATP concentration (Lundin, 2014).

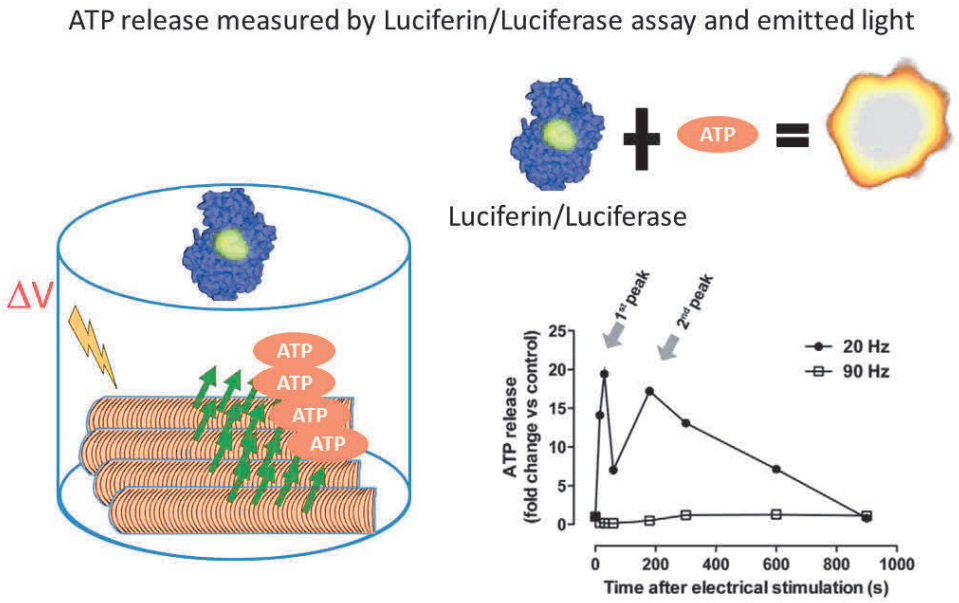

Figure 25. ATP release measurement: Luciferin/Luciferase assay in muscle fibers. *From Buvinic et al. (2009). Rat skeletal myotubes were cultured on 35-mm plates and after 5-7 days, the extracellular medium was replaced by Krebs solution 1 hour before applying a field electrical stimulation protocol at 45 Hz. Extracellular aliquots are collected from 0 to 60 min post-stimulation and the emitted light (Luminescence) from a Luciferin/Luciferase assay is detected with a luminometer. Values are quantified from a calibration of ATP vs luminescence and normalized by the quantity of total protein from each plate. The curve is from Jorquera et al. (2013) who adaptated this protocol to study ATP release from adult mouse skeletal muscle fibers. Results show 2 peaks of ATP release following electrical stimulation at 20 Hz that were not present following 90 Hz electrical stimulation. The 20 Hz stimulation train elicited ATP release (~20-fold change in basal value) but with a poor temporal resolution (1 data point every 30 seconds at the beginning of the experiment). Results taked from Jorquera et al. (2013)*

Luciferin/Luciferase assay has been widely used by several groups in relevant studies showing the ATP release from Panx1 channel as mentioned previously (Chekeni et al., 2010; Billaud et al., 2011; Riquelme et al., 2013; Billaud et al., 2015). In skeletal muscle, this was the method used in the studies of $Ca_V1.1$-Panx1 interactions, ATP-release, and ETC (Buvinic et al., 2009; Gonzalo Jorquera et al., 2013; Valladares et al., 2013; Casas et al., 2014) (see Fig. 25). This method presents a good sensitivity, but requires protein content normalization, a large number of muscle fibers, and has a poor temporal resolution because the samples are taken manually (≈ 30 seconds between two measurements) (Buvinic et al., 2009).

4.5.2. Other methods for measuring ATP

There are many methods that allow ATP measurements, but the study of ATP release in live specimens, especially from single cells has much fewer candidates. ATP release can be classified into two forms: ATP release through membrane channels or ATP release through vesicles during exocytosis. Because our interest is ATP release through Panx1, we focus, in the following paragraph, on the methods that allow direct extracellular ATP detection or that can possibly be adapted to measure it (see Rajendran et al. 2016).

Extracellular ATP detection can be achieved with enzyme coated-platinum electrodes or optical fibers, but these methods lack spatiotemporal resolution or compatibility with live specimens. Here below is a selection of molecular probes specific for free ATP, which allow real-time analysis with a good resolution and compatibility with live specimens. We can classify them into two types: Non-imaging and imaging methods (Rajendran et al., 2016).

The **non-imaging approaches** include for example a spectroscopic technique taking advantage of a sensor-based on malonyl-coenzyme A synthetase, which suffers a conformational change when binding to ATP and produces an increase in fluorescence intensity with high selectivity for ATP at micromolar range (Vancraenenbroeck & Webb, 2015). Electrophysiology is also a source of relevant approaches. For instance, extracellular ATP can be detected using P2X receptors, which are ATP-gated cation channels and thus produce ATP-dependent currents. It has been shown that the expression of P2X receptors in the plasma membrane of PC12 cells (Praetorius & Leipziger, 2009) or HEK293 cells (Hayashi et al., 2004), associated with path-clamp electrophysiology in outside-out or whole-cell mode can be used to detect ATP in the vicinity of the electrode or of the cell of interest. Another never-tried before electrophysiological possibility could be the use of ATP-sensitive potassium (K_{ATP}) channels as ATP biosensors, as their physiological activity is inhibited by intracellular ATP (Gribble et al., 2000). These two approaches have been tested within the present project to try to detect Panx1-dependent ATP release from isolated differentiated skeletal muscle fibers.

For the **imaging approaches**, several methods have been developed. Their aim is to generate a quantitative, non-invasive, and probe-free visualization of ATP in living conditions with high spatial and temporal resolution. However, a method that fulfills all these criteria does not yet exist (Rajendran et al., 2016). We can mention first: magnetic resonance spectroscopy techniques, based on the phosphorous

magnetization transfer. This is an imaging non-invasive method that can quantify ATP in vivo, but needs long acquisition times and presents a limited availability for biologists (Befroy et al., 2012).

Most commonly developed imaging methods rely on optical microscopy paired with molecular probes which produce signals specific for ATP, with a variety of physical formats from small organic indicators to nanoparticles, with direct and indirect assays.

Magnesium green is a magnesium-sensitive small organic fluorophore capable of indirectly detect ATP hydrolysis. Its mechanism of action is based on the fact that cytosolic ATP is normally complexed with divalent magnesium ions (Mg^{2+}), as MgATP. Thus, this method allows the measurement of the free cytosolic Mg^{2+}, as an indirect measurement of ATP hydrolysis (Leyssens et al., 1996), and does not allows extracellular ATP measurements.

For the direct visualization of the ATP pool, several fluorescent analogs were developed that can be used as tracers once loaded into the tissues, cells, or organisms. They are made by conjugated fluorescence groups like methylanthraniloyl (mant) to the nucleobase, ribose, or phosphate group of ATP. Such approached have been used to monitor vesicular ATP release from dopaminergic neurons (Ho et al., 2015).

Other small molecular sensors for ATP, as for example, quinacrine, have been used. This is a fluorescence acridine derivative that stains peptide-bound ATP in high concentration in intracellular granules. It has been used to image vesicular ATP release in endothelial and epithelial cells (Akopova et al., 2012).

The aptamers are also molecules used to detect ATP. They are single-stranded DNA or RNA engineered to detect ATP at micromolar to millimolar ranges (0.01-2 mM range) (Wang et al., 2013). However, they present poor cell permeability and are degraded by DNases and RNases. This problem has attempted to be solved by the use of nanoparticles to deliver, protect, and prevent quenching of aptamers (Qiang et al., 2015). In this condition, ATP depletion releases free aptamers, increasing their fluorescence, which could be used to quantitate ATP in live cells (Torabi & Lu, 2014). These biosensors pose a challenge in sample preparation and require cell penetration or cell loading of the exogenous reagent that needs sustained incubation, electroporation, or microinjection.

In contrast, the genetically encoded indicators are protein-based reagents that are in part or completely encoded by a gene sequence. Thus, they offer the advantage of being compatible with a wide variety of specimens with the administration modes including transfection reagents, viral transduction,

electroporation, and tissue-specific expression in transgenic mice. Recent examples are the expression of luciferases and fluorescent proteins. Luciferases were already introduced in the preceding chapter. There are several types of luciferases and the most commonly used are the firefly and beetle luciferases. Different mutagenesis processes have been used to improve luciferase sensitivity in live cells. For example, comparison of a chimeric luciferase with the commercial Omega Luc2 variant, showing three-fold higher sensitivity (Branchini et al., 2015). In another study, the luciferase was modified by shifting its luminescence towards red. This chimeric luciferase presents a lower intensity of luminescence but also suffers less tissue absorbance making it a good reporter for in vivo imaging (Branchini et al., 2010; Liang et al., 2012). Currently, this method does not provide the condition to make ATP quantification because it depends also on oxygen concentrations and needs the exogenous application of luciferin as a substrate, which could be toxic for some specific cellular types. Nevertheless, it has been already used in several cellular types (HEK293, cardiomyocytes, and neurons) to monitor ATP changes in the cytosol (Rajendran et al., 2016). Luciferase has also been used to study ATP release by tethering the enzyme to the extracellular face of the plasma membrane by the conjugation to primary IgG antibodies that bind surface antigens (Praetorius & Leipziger, 2009). However, this method requires long exposure times that limit spatiotemporal resolution and it also presents with low luminescence, which limits the use for real-time ATP imaging (Rajendran et al., 2016). In one study, Furuya et al. used specialized equipment and measured the ATP release with a temporal resolution of 100-ms by using a cooled electron-multiplying charge-coupled device (EMCCD) camera associated with an image intensifier to overcome the low photon emission levels. They used low-magnification, high numerical aperture, and succeed to monitor ATP release from a single cell with 10 nM detection sensitivity (Furuya et al., 2014).

Another tool for imaging ATP has been the development of fluorescent protein-based ATP sensors. They have the advantage of not requiring the addition of an exogenous substrate like luciferin, and they can be manipulated at the DNA level and expressed in cells in vivo. For example, K_{ATP} channels have been modified by the addition of an ECFP-EYFP cyan and yellow proteins pair, a fluorescent resonance energy transfer (FRET) system, to observe ATP level changes in HEK293 cells (Tsuboi et al., 2004). Imamura et al. developed a family of FRET-based sensors, called ATeam. The original ATeam was composed by the ε subunit of the bacterial F_0F_1-ATP synthase sandwiched by the cyan- and yellow fluorescent proteins. The ε subunit is a 14 kDa protein subunit, composed of an N-terminal β-barrel and 2 C-terminal helices. It suffers a big conformational change when binding ATP. They estimated sensitivity for ATP between 7.4 μM to 3.3 mM with a 10- to 100-fold higher selectivity for ATP over ADP, and a response kinetics on the timescale of seconds (Imamura et al., 2009). The ATeam sensors have been used

to study ATP changes in bacterial cells, neurons, and other cell types in different species (Imamura et al., 2009; Toloe et al., 2014). These sensors operate in the 400 nm to 500 nm spectral range, which could present problems in relation with the autofluorescence background, for example, the autofluorescence produced by flavin adenine dinucleotide (FAD). Nakano et al, to mitigate spectral overlap with FAD, replaced the CFP and YFP in the original ATeam sensors with a different FRET pair: they used GFP and OFP fluorescence proteins to generate a red-shifted ATeam named GO-ATeam (Nakano et al., 2011) and it was used to image ATP changes in the presence and absence of Ca^{2+} upon NMDA exposure in neurons (Rueda et al., 2015).

Another family of sensors called QUEEN, are related to ATeam sensors, but with some architectural differences. They use a circularly permutated fluorescent protein (cpFP) inserted between the 2 α helices of the F_0F_1 ATP synthase ε subunit with linkers. Two variants were designed with apparent affinities of 7 μM and 2 mM, called QUEEN-7mu and QUEEN-2m, respectively. These sensors were used to quantify ATP distribution in isolated E. coli (Yaginuma et al., 2014). Another related sensor was developed by Tantama et al, who used the circular permutation strategy to improve the original ATP-to-ADP ratio sensor, Perceval (Berg et al., 2009). The new sensor, PercevalHR, was used to visualize activity-dependent intracellular changes in ATP:ADP in neurons exposed to diverse stimuli. They could record simultaneously the ATP:ADP ratio, and ATP-sensitive potassium current through K_{ATP} channels in single cells, proving that PercevalHR biosensor could be a versatile tool to monitor changes in cellular energetics within seconds, and a relevant tool for metabolic research (Tantama et al., 2013).

Finally, another method of image ATP changes was recently designed by the fusion of fluorescent protein technologies and luciferase enzyme, producing bioluminescence resonance energy transfer (BRET). These sensors present better brightness and red-shifted, luciferase-based imaging (Chu et al., 2016), but still present limited changes in the signal in the presence of ATP (≈4%) and temporal kinetics within the second's range (for more details see Rajendran et al. 2016).

In summary, there are several available possibilities for measuring ATP, but no optimal method has been designed yet that could be used for measuring ATP release from a single adult muscle fiber. During this project, we developed and tested two methods to measure extracellular ATP and study the ATP release from a differentiated single muscle fiber after electrical stimulation: excised K_{ATP} channels, which are expressed in adult skeletal muscle fibers (Allard & Lazdunski, 1993; Allard et al., 1995; Allard & Rougier, 1997), and expression of a P2X channel.

SYNTHESIS AND RESEARCH PROBLEM

Synthesis and research problem

The Pannexin 1 (Panx1) protein is a member of a family of pannexin proteins with three isoforms (*PANX1*, *PANX2,* and *PANX3*) expressed in different tissues and cells type. Panx1 is expressed in skeletal muscle and is capable to form heptameric channels (Panx1 channel) located in the sarcolemma and T-tubules. They can be activated, either by phosphorylation or by caspases cleavage allowing ATP release and purinergic signaling activation. Panx1 channels have been associated with several physiological processes in undifferentiated and differentiated skeletal muscles, like contractile potentiation (Riquelme et al., 2013), differentiation (Pham et al., 2018), and excitation-transcription coupling (ETC) (Jorquera et al., 2013). ETC is a process behind the regulation of gene expression during fast-to-slow muscle plasticity. In this process $Ca_V1.1$ senses the frequency of membrane depolarization, during trains of action potentials, and activates Panx1 channel in the T-tubule of the sarcolemma, allowing ATP release. These two proteins have a close relationship as shown by co-immunoprecipitation, co-localization, and protein-ligand assay (PLA) (Jorquera et al., 2013; Riquelme et al., 2013). Besides ETC, $Ca_V1.1$ has two main functions as an L-type voltage-dependent Ca^{2+} channel and as a voltage sensor in excitation-contraction coupling (ECC). During ECC, the sarcolemma depolarization induces a $Ca_V1.1$ conformational change which physically activates Ryanodine receptor type 1 (RyR1) in an anterograde control. RyR1 opening allows Ca^{2+} release from the lumen of the sarcoplasmic reticulum (SR) into the cytosol, starting the contractile cycle. There are several proteins capable of regulating either $Ca_V1.1$, RyR1, or their interactions, affecting their function and in some cases ECC. RyR1 can be regulated by the cytosolic proteins CaM, S100A1, FKBP12, and the luminal triadin-junctin-CSQ complex, and $Ca_V1.1$ can be regulated by the RyR1 in a retrograde control, by the cytosolic protein STAC3, and by the proteins Caveolin-3 and Junctophilins. Most of these proteins have a close relationship with $Ca_V1.1$ and a relevant role in skeletal muscle function. Considering this knowledge and the already demonstrated relationship between $Ca_V1.1$ and Panx1 during ETC, the first objective of this project was to: **1) Assess the role of Panx1 channel in ECC in adult skeletal muscle.** This objective presented 3 steps. The first step aimed at "*investigating the role of Panx1 down-expression on $Ca_V1.1$ function and ECC in differentiated skeletal muscle"*. For this, starting during my Master studies and continuing on during my PhD thesis, I joined an international collaboration between two laboratories: the "Centro de Estudios Moleculares de la Celula" in the "Instituto de Ciencias Biomedicas" (ICBM) at the University of Chile under the supervision of M. Casas, and the "Excitabilité et signalisation calcique dans le muscle normal et pathologique" at University Claude Bernard-Lyon 1, under the supervision of V. Jacquemond. We used transitory knockdown of Panx1 channels in differentiated skeletal muscle fibers

from the fast-twitch FDB muscle. To achieve this, we electroporated in vivo a plasmid developed by M. Casas that coded for a shPanx1 coexpressed with a red fluorescence protein mCherry, which after two weeks produced 70% decrease in Panx1 protein content. We used the transfected fibers to study: 1) $Ca_V1.1$ function: by measuring voltage-dependent Ca^{2+} current and charge movement using silicone voltage clamp, and 2) ECC and RyR1-dependent Ca^{2+} release using simultaneously silicone voltage clamp, Ca^{2+}-sensitive fluorescence dyes, and confocal microscopy (Kutchukian et al., 2016; Kutchukian et al., 2017). Furthermore, during my Ph.D. we also studied the effect of Panx1 channel overexpression in differentiated adult skeletal muscle. For this, we used 2 Panx1 plasmids: one tagged with a green fluorescent protein (GFP) at the C-terminal and a second-one tagged with an auto-cleavable GFP. I cloned a third non-tagged Panx1-plasmid. All plasmids were transfected by electroporation in vivo in the FDB muscles from wild type mice. We then studied $Ca_V1.1$ function, and RyR1-dependent Ca^{2+} release in the transfected fibers. The second step aimed at "*to assessing the functional consequences of Panx1 pharmacological inhibition on $Ca_V1.1$ function and ECC in differentiated skeletal muscle"*. For this, I used two common Panx1 pharmacological blockers: Carbenoxolone and Probenecid. I simultaneously measured voltage-dependent Ca^{2+} current through $Ca_V1.1$ and RyR1-dependent Ca^{2+} release using silicone voltage clamp, fluorescence dyes, and confocal microscopy. I used 2 different protocols: 1) an acute protocol that aims at investigating the effect of acute application and of removal of the inhibitors in the same fiber, and 2) A chronic protocol that compared one group of fibers after 30 minutes of exposure to the inhibitors vs a control group. The third step, aimed at "*determining the effect of a Panx1 pharmacological inhibitor on whole adult skeletal muscle contractile function".* For this we made a collaboration with Corinne Huchet and Aude Lafoux from Therassay (preclinical therapeutic assay) at the University of Nantes who assessed the changes in contractile properties of the fast-twitch EDL muscle in vitro using electrical field stimulation after 30-45 minutes of chronic exposure to the Panx1 blocker, probenecid.

Panx1 principal function is presumed to be ATP release and it has been observed after 20 Hz of electrical field stimulation in undifferentiated and differentiated skeletal muscle fibers. The current through Panx1 channel has been used in the past as an indicator of its functional state (open and close). However, this has been essentially achieved in expression systems and is much more challenging in native cells. Furthermore, a recent study has revealed that Panx1 exhibits 2 parallel and independent pathways for ATP release and for ionic current, separate (Ruan et al., 2020), prompting the importance of methods capable of directly detecting ATP release from a single cell. Such measurements are of high interest but the current tools still suffer from limitations (Rajendran et al., 2016). A second objective of this project

was thus: **2) to develop a new method to detect ATP release from a single differentiated skeletal muscle fiber** to characterize Panx1 channel functional state and associated ATP release in response to different frequencies of stimulation. For this we developed 2 different methods: First, we used the ATP-sensitive K^+ channels (K_{ATP}), normally expressed in the sarcolemma of differentiated skeletal muscle fibers (Allard & Lazdunski, 1993; Allard et al., 1995; Allard & Rougier, 1997). For this, we used the inside-out patch-clamp technique after excision of a K_{ATP} channels containing membrane portion of a differentiated adult muscle fiber. These channels have a K^+ current that is blocked by cytosolic ATP. We used the excised patch as a biosensor of ATP release from a single fiber under silicone voltage-clamp, stimulated at various frequencies.

The second approach consisted in transfecting, by electroporation in vivo, mouse muscle fibers with a plasmid coding for an ATP-sensitive purinergic channel (P2X) provided by Francois Rassendren from the "Institut de Genomique Fonctionnelle" at the University of Montpellier. In normal conditions, the differentiated fast-twitch skeletal muscle fibers do not express P2X channels. In the presence of extracellular ATP, P2X channels get activated which can be detected as an inward cationic current. We used the transfected fibers to try to detect changes in whole-cell P2X current following voltage-clamp stimulations at different frequencies.

Panx1 is a protein that plays a role in multiple physiological processes associated with ATP release and purinergic activation. Because of this, Panx1 has been associated with several pathological processes in which ATP release could play a role. In skeletal muscle, this for instance is the case of the mdx mouse model of Duchenne dystrophy (Altamirano et al., 2013). Moreover, our results showing that Panx1 down-expression alters $Ca_V1.1$-dependent Ca^{2+}-current and RyR1-dependent Ca^{2+} release opened the prospect that physiological or pathological reduction of Panx1 expression and/or function could alter muscle function. Preliminary results in M. Casas laboratory at University of Chile suggest that this is the case for muscles experiencing a diabetic environment, and that it could play a role in the reported associated loss of muscle force in patients. Along this, the third objective of my project was to: **3) Study ECC and Panx1 role in a skeletal muscle disease model of obesity and diabetes**, in which the relationship between $Ca_V1.1$-Panx1 and ECC could be altered. Based on -results from M. Casas laboratory in Chile showing an alteration of ATP release in skeletal muscle fibers from mice made obese with a High Fat Diet (HFD), and -the association between obesity and type 2 diabetes with skeletal muscle dysfunction (Eshima et al., 2017; Tallis et al., 2018) we decided to study $Ca_V1.1$ function, ECC, and RyR1-dependent Ca^{2+} release in differentiated skeletal muscle fibers from a similar model. For this, we made a collaboration with Jennifer

Rieusset team in CarMeN Laboratory at University Claude Bernard-Lyon1. We used their obese, insulin resistance, and glucose intolerance mouse model (obtained by a high-fat, high-sucrose diet (HFHSD) for more than 16 weeks) to study 1) $Ca_V1.1$ function: by measuring voltage-dependent Ca^{2+} current and charge movement using silicone voltage clamp, and 2) RyR1-dependent Ca^{2+} release using simultaneously silicone voltage clamp, Ca^{2+}-sensitive fluorescence dyes and confocal microscopy.

METHODS AND MATERIALS

METHODS AND MATERIALS

During this project, all the experiments and procedures with animals were performed according to the guidelines of the local "animal experimentation and ethics committee" of the University Claude Bernard-Lyon 1, the ethical principles of the French Department of Veterinary Services, and the French Ministry for Higher Education and Research, the French Ministry of Agriculture (decree 87/848) and by the revised European Directive 2010/63/EU. They also follow the recommendations published by "The Journal of Physiology and Experimental Physiology" (Grundy, 2015). The experimental protocol of diet-induced obesity was approved by the Animal Experimentation Committee no. C2EA-15 of the Rhône-Alpes Region. All the experiments were made at room temperature (20-22°C).

I. Animal and muscle models.

For the transitory Panx1 knockdown mouse model see the methods in the first manuscript.

For all experiments performed on electroporated and non-electroporated mouse muscles in France, 4-weeks-old Swiss OF1 male mice were purchased (Charles River Laboratory) and housed within cages at the ANIPHY animal house facility at the Rockefeller Medicine Faculty of the University, until they were 8-16 week-old (Charles River Laboratory). Then, they were either electroporated or sacrificed to obtain the muscles: flexor digitorum brevis (FDB) and interosseous (IO).

For the study of Ca^{2+} homeostasis and EC coupling in the mouse model of diabetes, 4-week-old C57BL/6JO1aHsd male mice were purchased by our collaborator (Jennifer Rieusset at CarMeN laboratory) from ENVIGO (Gannat, France) and separated into two groups:

Control group: with free access to the standard chow diet (SCD) (Rod16-A, Genobios: 16.9% protein, 4.3% lipids, 55.5 % carbohydrate).

High-fat high-sucrose diet (HFHSD) group: with free access to the following diet: 260HF U8978 version 19; SAFE; 20% protein, 36% lipids, 37% carbohydrate including 14.5% starch and 17.9% sucrose. After 16-18 weeks, the mice were sacrificed from each group to obtain the FDB and IO muscles (for more details see the article published in Diabetologia in the "Results" section).

II. In vivo transfection

All in vivo transfections were realized either by our Engineer-assistant, Laloe Monteiro, or by myself during the period of this project.

The expression of the shPanx1 and Panx1 genes was achieved by intra-muscular injection of the corresponding plasmids, followed by electroporation, as previously described (Lefebvre et al., 2011). The transfection was made to target FDB and IO muscles of the animals. For this, mice were anesthetized by isoflurane inhalation using a commercial delivery system (Univentor 400 Anesthesia Unit; Uninventor). Then, 20 µl of a solution containing 2mg/ml hyaluronidase dissolved in sterile saline was injected into the footpads of each hind paw. 45 minutes after, the mouse was reanesthetized by isoflurane and injected with 20 µl of a solution containing 30 µg plasmid DNA diluted in NaCl 0.9% in the same place. ≈5-10 minutes after injection, two gold-plated stainless acupuncture needles connected to the electroporation apparatus were inserted under the skin in the two extremes of the ventral side of the foot. The standard protocol was the application of 20 pulses of 120 V/cm amplitude, 20-ms duration at 1 Hz by a BTX ECM 830 square wave pulse generator (Harvard Apparatus). Depending on the plasmids, muscle fiber isolation was performed 3-14 days later.

The pCMV-PANX1 plasmid was co-transfected with the pmEGFP-C1 plasmid that expresses enhanced green fluorescent protein (EGFP) which was rendered monomeric thanks to A206K mutation. mEGFP is cytosolic and served as a reporter. Both pCMV-PANX1 and pmEGFP-C1 plasmids were co-electroporated at a ratio of 70%-30% of each plasmid respectively (21 µg and 9 µg of each plasmid respectively). Control consisted in electroporating 9 µg of pmEGFP-C1. Expression was allowed for either 7 or 14 days post-electroporation.

III. Cell cultures and transfection

COS-7 cells were grown in DMEM (4.5g.L-1 glucose) supplemented with 5% fetal calf serum, glutamine, sodium pyruvate and penicillin-streptomycin at 37°C in a humidified 5% CO_2-containing atmosphere. Cells grown on polymer coverslip in 35-mm large dishes compatible with subsequent imaging using immersion oil (Ibidi) were transfected using FuGENE HD (Promega) and 2 µg of plasmid. Cells were imaged after 2 to 3 days of expression. These experiments were performed by Laloe Monteiro and Christine Berthier, a scientist in our team.

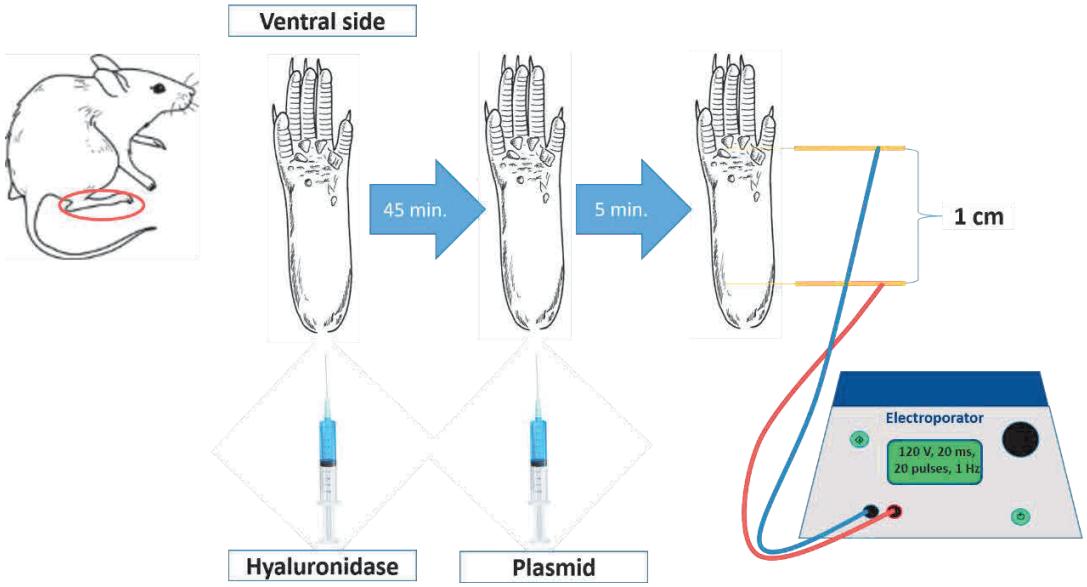

Figure 26. In vivo transfection by electroporation of a plasmid in Flexor digitorum brevis (FDB) and interosseus (IO) muscles. *The critical steps of the in vivo transfection by electroporation are illustrate: first, the injection of 20 µl of hyaluronidase for the enzymatic degradation of the connective tissue. Second, after 45 minutes the injection of 20 µl of the plasmid solution. Finally, the electroporation, which consists in the application of 20 pulses of electrical field stimulation at 120V/cm, 1 Hz with the electrodes at ≈1 cm from each other (anode (red) placed near the heel, and cathode (blue) placed close to the toes).*

IV. Plasmids

Exogenous proteins of interest were systematically expressed in electroporated muscles of the right hind paw whereas control proteins were expressed in the left hind paw of each mouse. Different control plasmids were selected considering the intracellular localization of the fluorescent reporter protein.

4.1. Panx1 knockdown

Knockdown of Panx1 was achieved with the plasmid pshPanx1-mCherry which led to the expression of Panx1-specific short hairpin RNAs, inducing transitory Panx1 knockdown by RNA interference, together with the expression of mCherry, a red fluorescent protein, as a reporter. pmCherry plasmid was used as a control. In vivo expression lasted two weeks before muscle fibers were isolated (see the first manuscript in the “Results” section).

4.2. Panx1 overexpression

4.2.1. pCMV-PANX1-tGFP and pEGFP-Dr-VSP

The pCMV-PANX1-tGFP plasmid is a commercial plasmid (Origene) comprising a CMV-promoter and the human Panx1 mRNA sequence (NM_015368) fused in-frame at its 3'-end with the green fluorescent protein turboGFP sequence. TurboGFP is an improved variant of the green fluorescent protein CopGFP cloned from the marine arthropod *Pontellina plumata* (excitation/ emission max = 482/ 502 nm) (Shagin et al., 2004). The corresponding Panx-1 protein tagged in C-term with tGFP was expressed for 7 days after electroporation of mouse hindlimb muscles and for 1-2 days after transfection of cultured COS-7 cells. The pEGFP-Dr-VSP plasmid was used as a control (referred to as EGFP-DrVSP in manuscript). This plasmid enables the expression of the fusion protein EGFP-Dr-VSP, a green fluorescent EGFP protein addressed to the plasma membrane thanks to the fusion at its N-terminus with the voltage-sensitive protein (VSP) of *Danio rerio* (Dr-VSP) (Hossain et al., 2008). This plasmid was kindly provided by Professor Y. Okamura (Osaka University, Suita, Japon).

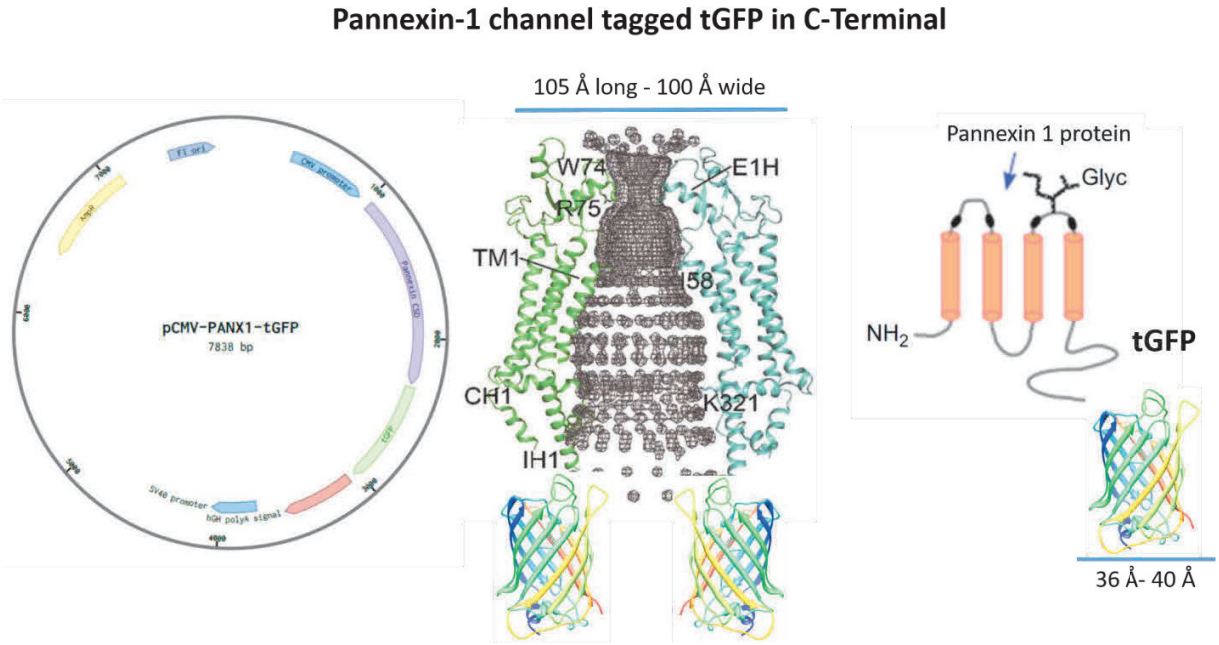

Figure 27. Plasmid map and representative model of PANX1-tGFP. *A. Simplified pCMV-PANX1-tGFP plasmid map given by Origene company with the location of the tGFP and the antibiotics resistance region. B. Representative tridimensional relationship of the tGFP fluorescent protein in a heptameric Panx1 channel (adapted from Guo et al. 2020). C. Scheme of the PANX1-tGFP fusion protein (modified from Penuelas et al. 2013).*

4.2.2. pCMV-PANX1 and pmEGFP-C1

The pCMV-PANX1 plasmid led to the expression of a native, tag-free, version of Panx1. The cloning strategy was designed by Christine Berthier, using the Benchling platform (www.benchling.com) and I did the cloning experiments under supervision of Christine Berthier and Laloe Monteiro. Cloning was performed using the Gibson assembly method, which allow the insertion of an insert into a vector after adding sequences homologous to the vector at each end of the insert by using polymerase chain reaction (PCR) and appropriate primers.

The commercial plasmid pmEGFP-C1 (Clontech) was used as backbone vector, after deleting the EGFP coding sequence by restriction digest. The PANX1 insert was synthetized by PCR using the commercial pPANX1-tGFP (Origene) as template.

Polymerase chain reaction (PCR) and Gibson assembly cloning

The sequence of mEGFP was removed by restriction digest using NheI and BamH1 and digested plasmid was separated from on an agarose gel and gel-purified using QIAExII gel extraction kit (Qiagen). PCR was used to amplify the PANX1 sequence using pPANX1-tGFP as template and using the following primer pair : a 72 nt-long forward primer (ctatataagcagagctggtttagtgaaccgtcagatccggc caccatggccatcgctcacctggccacggag) and 60-nt long reverse primer (cctctacaaatgtg gtatggctaattatgatcagttatgcaagaagaatccagaagtctc). Amplification was performed using Prime STAR GXL DNA high fidelity polymerase (Takara) and the following cycling conditions: 1) Initial denaturation step at 94°C, 5min;2) Cycling= 30 cycles of 10 seconds at 98°C followed by 84 seconds at 68 °C; 3) final polymerization step at 68°C, 10 min. The size of the polymerized DNA fragment was confirmed by electrophoresis on agarose gel and the fragment was purified using Qiaquick PCR purification kit (Qiagen). Assembly of insert and vector was performed for 1h at 50°C in a reaction mix containing Phusion DNA polymerase (Thermofisher), T5 Exonuclease and Taq ligase (both from New England Biolabs, USA). In order to amplified newly generated constructs, competent cells were transformed (NEB 10-beta Competent E. coli, New England BioLabs) and selected by incubation at 37°C overnight on Petri dishes containing liquid broth-agar supplemented with 50µg/ml of kanamycin.

Plasmid purification, restriction analysis and sequencing

Selected bacterial clones were pre-cultured overnight at 37°C in 4 mL of kanamycin-supplemented liquid broth. After centrifugation, plasmid “mini-preparations” were performed by submitting the bacterial pellets to a purification protocol using a Nucleospin Plasmid Prep kit (Macherey-Nagel). In brief, bacterial cells were resuspended and lysed and after a centrifugation step, DNA-containing supernatants were collected and poured onto silica-containing DNA-binding columns. After repeated washing steps, DNA samples were eluted and checked by restriction analysis. Selected DNA samples were sequenced by GATC Eurofins Genomics and sequence analysis was performed by Christine Berthier. The appropriate DNA clone was amplified by bacterial culture in 500 mL of liquid broth and plasmid DNA was purified by the Neuromyogene Institute facility using Plasmid Mega kit (QIAGEN).

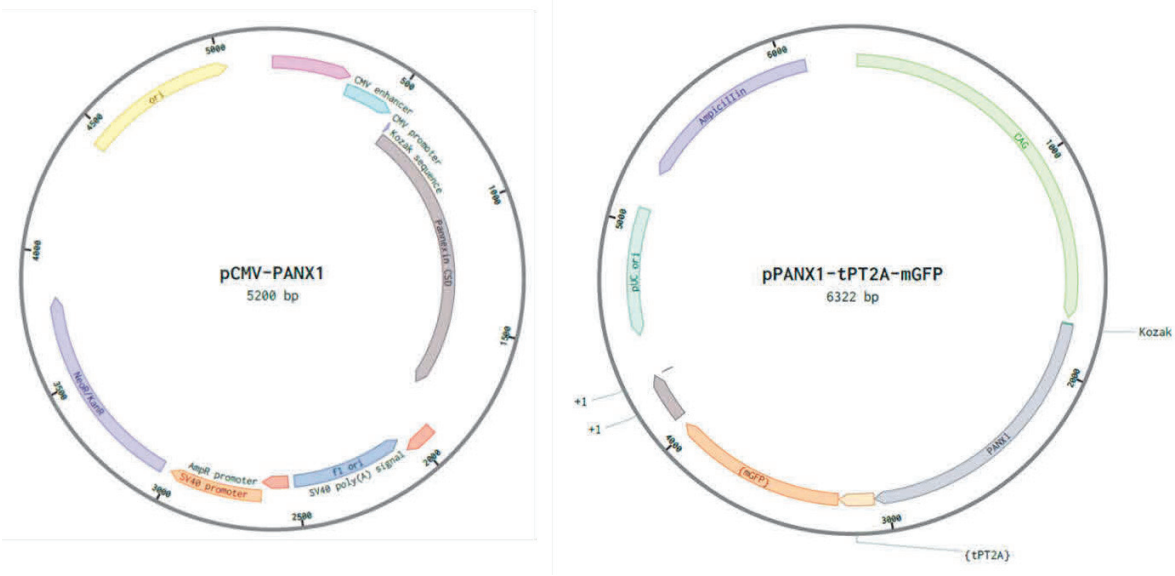

Figure 28. Map of pCMV-PANX1 plasmid and of pPANX1-tPT2A-mGFP. *At the left It is shown the map of the pCMV-PANX1 plasmid cloned in our laboratory and presented a resistance to Kanamycin. At the right the plasmid pPANX1-tPT2A-mGFP that was cloned by VectorBuilder and presented resistance to Ampicillin.*

4.2.3. pPANX1-tPT2A-mEGFP

The pPANX1-tPT2A-mGFP plasmid is a bicistronic plasmid that leads to the expression of (tag-free-) Panx1 and of mEGFP, a variant of enhanced GFP (EGFP) rendered monomeric by a *A206K* mutation (Zacharias et al., 2002). The tPT2A peptide designed to link both protein sequences mediates ribosome-skipping and leads to the distinct translation of both upstream and downstream proteins (Liu et al., 2017). The pPANX1-tPT2A-mGFP construct was designed by Christine Berthier and synthetized by VectorBuilder (see Fig. 28).

4.3. Developing methods for ATP release: P2X-GCaMP wild type and mutant

Two different plasmids were used in order to express the ATP-sensitive Ca^{2+}-channel P2X2 receptor. Both plasmids used pcDNA3 as backbone and were kindly provided by Dr. Francois Rassendren (Institut de Genomique Fonctionnelle, Université de Montpellier). The first plasmid, pP2X-GCaMP6s-P2A-Scarlett is a bicitronic plasmid which leads to the expression of 1/wild type P2XR fused at its C-terminal with GCaMP6s, a green fluorescent calcium-sensing protein (Chen et al., 2013) and 2/the red fluorescent protein Scarlett, a strongly fluorescent protein reporter. In the second plasmid, pP2X2 N333A-GCaMP6s-

P2A-Scarlett, wild type P2X2 was replaced by its N33A-mutant counterpart which presented an enhanced affinity for ATP (Ollivier et al., 2021).

V. Preparation of isolated muscle fibers

Single fibers were isolated from FDB and interosseous (IO) muscles using a previously described procedure (Jacquemond, 1997). Mice were put into sleep using Isoflurane anesthesia and then killed by cervical dislocation.

Step 1: The muscles were dissected and incubated at 37°C in Tyrode solution containing 2mg/ml of collagenase type 1 (Sigma, type 1) for 60 minutes.

Step 2: The muscles were rinsed with collagenase-free Tyrode solution and stored in Tyrode solution at 4°C over the night.

Step 3: We used these muscles over the following 36 hours. For each experiment, isolated fibers were obtained by gentle mechanical trituration of the enzyme-treated muscles through a cut disposable tip of a Pipetman within a culture µ-dish (Ibidi, Planegg/Martinsried, Germany) filled with culture medium containing 10% FBS (MI199; Eurobio, France). The bottom of the culture µ-dish was previously covered with a thin layer of silicone grease (Dow Corning® High vaccum grease). Experiments were performed at room temperature (20-22°C).

Step 4: The fibers selected according their proper shape (appropriate length and width, intact well-defined plasma membrane, peripheral nuclei, appropriate sarcomere length, together with, when appropriate, expression of the fluorescent protein were embedded within additional silicone grease (SILBIONE Paste 70,428; Elkem Silicones, Saint-Fons, France) from their top surface, so that only a portion of the fibers remained in contact with the extracellular medium.

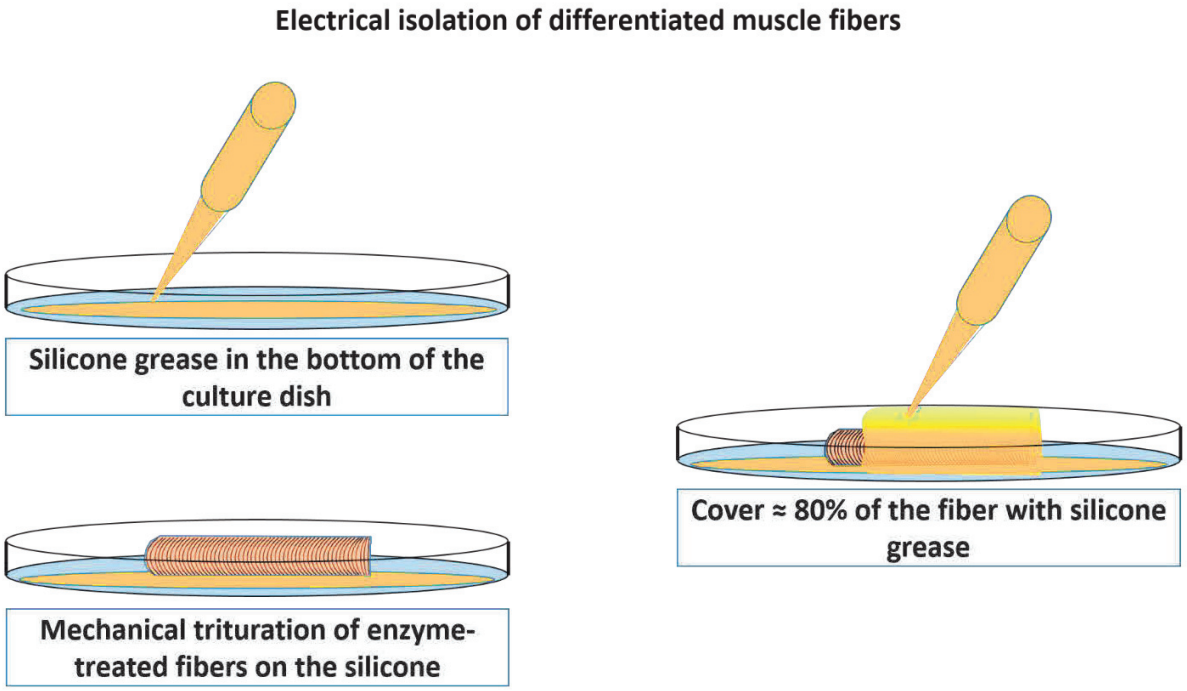

Figure 29. Schematic representation of partial electrical isolation of a differentiated muscle fiber using silicone grease (V. Jacquemond, 1997). *The process is divided in 3 steps: 1) covering the bottom of the culture µ-dish with a thin layer of silicone grease. 2) Gentle mechanical trituration of muscles to obtain isolated muscle fibers over the silicone layer. 3) delicate application of silicone grease on the top of the fiber so that ≈ 80 % of the total surface of fiber is covered.*

VI. Electrophysiology

Over the last 5 years, starting during my master and then throughout my Ph.D. training, under the supervision of Mariana Casas, Jorge Hidalgo, Enrique Jaimovich, Bruno Allard, and my Ph.D. supervisor Vincent Jacquemond I learned, developed, and used different electrophysiological techniques and setups, associated with this project.

6.1. Brief principles for channel current recording in electrophysiology

The function of an ionic channel can include 3 states: closed (C), open (O), and an inactivated (I) state. For the voltage-dependence channels, the transition between the different states is controlled by the voltage and changes with time. It can be reversible at a specific potential and reach a stationary state. The transitions between the different states are produced by different processes: activation (C to O),

deactivation (O to C), inactivation (O to I), and reactivation (I to C, upon return to the resting potential). Several other factors can regulate the transitions like phosphorylation, temperature, pH, pharmacology ligands (intra- o extracellular), or association with regulatory subunits. The biological currents from a muscle fiber, as measured with a voltage-clamp amplifier, present two groups of different magnitudes: at the single ionic channel level, current is expressed in pA and at the whole-cell level in nA. The headstage of the amplifier is connected with an ensemble of electronic circuits and allows the calibration and correction of the acquired signals, including the compensation of junction potential, electrode capacitance, series resistance, and filtering. The critical element in the circuit is an operational amplifier which has a very high input resistance (Ri> 10^{12} ohms), making the other resistances (like pipette resistance) insignificant. This allows recording of transmembrane current with small errors and the injection of a current to impose a specific value of membrane potential (voltage-clamp). When studying channel properties, an important concept is the channel conductance (G), which is the inverse of electrical resistance (R). At the single ionic channel level, the conductance is calculated from the voltage dependence of the current through the single-channel (IV curve), using: *V= I/G,* where V= voltage, I= current, and G= conductance, so the slope of the IV curve represents the channel conductance. It is usually expressed as γ = i/V at the single ionic channel level and Gm= I/V at the whole-cell macroscopic channel population level. In electrophysiology, the use of conductance has been preferred because, when considering the individual conductance of several channels located in parallel in a membrane, the total conductance can be calculated by a simple sum. The conductance is measured in Siemens (S) (pS at the channel level, and nS-µS at the macroscopic current level) and it allows characterization of the permeation properties of the pore of the channel and/or estimation of the number of activated channels under a given condition. At the whole-cell level, the macroscopic conductance is also calculated from the IV curve. The macroscopic conductance represents the conductance of the ensemble of active channels present in the membrane of a cell. Therefore, it depends on the number of active channels and their open probability (P_0).

In the voltage-clamp technique, the membrane potential is controlled at a set value (clamped), while the ionic current flowing through the membrane is measured.

For the normalization of the current recorded from different cells with different sizes, and therefore with different numbers of active channels (assuming the same density all over the membrane), we use the membrane capacitance of the cell. The lipid bilayer that constitutes the plasma membrane (sarcolemma in muscle fibers) act as a capacitor, which means that it has the property of accumulating

electrical charges, during the “charging” step, and to release the electrical charges, during the “discharge” step, the amount of charge depending on the membrane potential change.

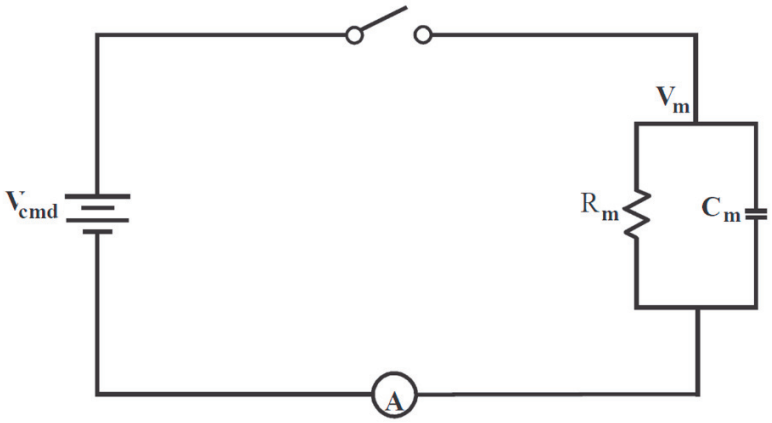

The ideal voltage clamp

Figure 30. The ideal voltage clamp circuit. *The ideal voltage clamp consists in a battery, a switch, a wire, the cell and an ammeter. In this experiment the voltage is the independent variable. Its value is controlled and equal to the battery value. The current is the dependent variable and its value is measured by the ammeter.*

In standard experimental conditions, a cell presents a capacitance of 1 µF/cm^2. The calculation of the membrane capacitance (measured in Farads, F) of a cell allows an estimation of the size of the plasma membrane from which we measure the macroscopic ionic current (measured in Ampere, A), and the normalization of this current by expressing it as a density of current (A/F). In the analysis of results during this project, the integration of the positive capacitive current produced at the end of a -20 mV prepulse (discharge) was systematically used to calculate the amount of accumulated charge (in Coulomb, C), and this value was used to calculate the capacitance of the cell with the following equation (Equation 1):

$$C = Q/V$$

; where Q= charge, C= capacitance, and V=voltage.

6.2. Silicone whole-cell voltage-clamp (Silicone voltage-clamp)

As described in the introduction, several approaches have been developed to study differentiated skeletal muscle fibers, their excitability properties, the properties of ion channels and ECC in physiological conditions (Jacquemond, 1997; Collet et al., 2004). Throughout my PhD work I have used the silicone voltage-clamp technique developed by Jacquemond et al. (1997) for the measurements of $Ca_V1.1$-

dependent Ca^{2+} current and charge movement currents, and also to trigger voltage-activated cytosolic Ca^{2+} transients in differentiated muscle fibers from FDB and IO mouse muscles. These muscle fibers are 0.3-1 mm in length and 20-50 µM in diameter, preventing the control of the membrane potential of a whole muscle fiber in a uniform and fast manner with a single voltage-clamp pipette in whole-cell configuration. With the silicone voltage-clamp technique, we artificially decrease the length of portion of the fiber electrically active by isolating ≈80% of the fiber surface with silicone grease (Fig. 26). Thus, the depolarizing pulses and current records are limited to the electrically conducting uncovered region of the muscle fiber and can be performed with a single-electrode clamp technique.

6.3. Whole-cell Ca^{2+} current measurements

Silicone voltage-clamp was used to measure whole-cell voltage-dependent Ca^{2+} currents in 1) fibers expressing shRNA-Panx1 (Panx1 knockdown) and/or mCherry (Control) plasmids as described in the first manuscript (see Results), 2) for studying the effect of Panx1 inhibitors on Ca^{2+} current, and 3) for the study of HFHSD-induced obese mouse model. The Ca^{2+} current measurements for the Panx1 knockdown project were achieved in Chile during my Master Thesis. For this, an Axopatch 200B patch-clamp amplifier (Molecular Devices, Sunnyvale, CA) was used. For data acquisition and command voltage pulse generation a Digidata 1322A analog-digital, digital-analog converter (Axon Instruments, Foster City, CA) controlled by pClamp software (Axon Instruments) were used. To measure $Ca_V1.1$-dependent Ca^{2+} current, the standard TEA-containing solution (see VII, Solutions) also contained the Ca^{2+} chelator ethylene glycol-bis (β-aminoethyl ether)-N,N,N',N'-tetraacetic acid (EGTA) conjugated with an acetoxymethyl ester (AM) group (5 µM), allowing EGTA go through the plasma membrane and accumulate in the cytosol under the free form because of the action of cytosolic esterases which hydrolyze the AM group. Fibers were loaded with EGTA-AM for 30 minutes before wash and electrical isolation with silicone grease. In France, throughout my PhD, the fibers were bathed with a standard TEA-containing extracellular solution for simultaneous detection of Ca^{2+} currents and SR Ca^{2+} release (see VII, Solutions). For this, voltage-clamp was performed with a micropipette filled with an intracellular solution (see VII, Solutions) which contained 15 mM EGTA and the Ca^{2+} sensitive indicator rhod-2. The intracellular solution was dialyzed for 30 minutes to equilibrates the EGTA and rhod-2 within the fiber cytosolic volume. EGTA prevents contraction and facilitates the estimation of the SR Ca^{2+} release flux (see section 6.3.1). Inside the pipette, a silver/silver chloride wire was connected to the headstage of an RK-400 patch-clamp amplifier (Bio-Logic, Claix, France) in combination with an analog-digital converter (Digidata 1440A, Axon Instruments, Foster City, CA, USA) controlled by pClamp 9 software (Axon Instruments). After analog compensation of the series

resistance, we applied 0.5 s-long depolarizing steps (pulses) of increasing amplitude from a holding potential of -80 mV. The linear leak was subtracted by using the scaled value of the current measured during a -20 mV prepulse applied before each pulse. The voltage-dependence of the peak current normalized by the fiber capacitance was fitted by a Boltzmann equation (in Origin 7) (Equation 2):

$$I(V)=Gmax(V-Vrev)/\{1 + \exp[(V0.5-V)/k]\}$$

Where I (V) is the peak current density at the given command voltage, Gmax represents the maximum conductance, Vrev the apparent reversal potential, V0.5 the half-activation potential, and k the steepness factor.

For the measurements of intramembrane charge movement in the HFHSD-induced obesity model, we used an RK-400 patch-clamp amplifier (Bio-Logic, Claix, France) in combination with an analog-digital converter (Digitada 1440A, Axon Instruments, Foster City, Ca, USA) controlled by a pClamp 9 software (Axon, Instruments). For the records of intramembrane charge movements currents, holding potential was set to -100 mV and 25 ms-long depolarizing steps of increasing level applied in the presence of a specific extracellular solution (see VII, Solutions) containing low [Ca^{2+}] (0.1 mM), and the overall composition of which was designed to block all ionic currents. The removal of the linear leak and capacitive components of the current change elicited by a depolarizing pulse was achieved using previously described procedures (Collet et al., 2003). In briefs, scaled control records elicited by 25-ms-long prepulses of -20 mV were subtracted from the current elicited by the depolarizing pulses of the same duration to each voltage. The amount of charge was calculated by the integration of the on (Q_{on}) and off (Q_{off}) portion of each test pulse. The steady-state distribution of the curve was fitted using the average of Q_{on} and Q_{off} normalized by the capacitance using a two-state Boltzmann function (Equation 3):

$$Q(V)=Qmax/(1+\exp[(V0.5-V)/k])$$

Were Q max representing the maximally available charge, V0.5 the voltage of equal charge distribution, and k the steepness factor.

6.4. Measurement of K_{ATP} channel activity in inside-out patch-clamp measurements

One of the methods developed during this project to measure ATP release from a single isolated fiber was the use of an inside-out membrane patch biosensor obtained by excising a patch of plasma membrane from an adult muscle fiber containing ATP-sensitive K^+ (K_{ATP}) channels.

Potassium conductance in excitable cells are critical in determining the membrane potential and shaping the action potential characteristics. The potassium channels opening hyperpolarizes the membrane potential toward the potassium equilibrium potential and participate in the repolarization of the action potential. There is a big number of families with different electrophysiological properties and a big molecular diversity that are not the focus of this project (Tinker et al., 2018). The K_{ATP} family have as a particular characteristic the opening in response to metabolic changes, especially a decrease in the K^+ current in the presence of ATP or an increase in the K^+ current in the presence of ADP. The K_{ATP} family is part of the inwardly rectifying family of potassium channels, which means that this type of channels passes more inward current at potentials negative to the potassium equilibrium potential, and their driving force is determined by the differences between the membrane potential and the potassium equilibrium potential and not only by the membrane potential like for the voltage-gated potassium channels. The K_{ATP} channels were first described in cardiac myocytes, but also are present in pancreatic β cells, skeletal muscle, neurons, smooth muscle, kidney and epithelial cells (Tinker et al., 2018). In our laboratory, the K_{ATP} channels have been extensively studied in differentiated skeletal muscle fibers in mouse models (Allard et al., 1995; Allard & Rougier, 1997; Allard et al., 2006).

Our methods were conceived and developed with the help and advisory of the Researcher and Professor Bruno Allard and the Ph.D. student Romane Idoux. The method consisted in positioning the inside-out patch in close proximity of a muscle fiber stimulated at 20 Hz using the silicone voltage-clamp technique to release ATP. For the silicone voltage-clamp, the same setup described for charge movements and Ca^{2+} current recordings was used, associated with a second electrophysiological setup used for measuring single channel currents through K_{ATP} channels. This last set-up was composed of an RK-400 patch-clamp amplifier (Bio-Logic, Claix, France) connected to an analogue-digital converter (Digitada 1440A, Axon Instruments, Foster City, Ca, USA) controlled by the Axoscope software (Molecular Devices).

6.5. Brief principles of the inside-out configuration of the patch-clamp technique and the use of K_{ATP} channels as ATP biosensors

The patch-clamp technique is a voltage clamp technique in which the tip of a glass pipette is sealed on the membrane of a cell to electrically isolate a small patch of membrane and to measure in this way the small currents flowing through a limited quantity of channels confined to the membrane area ringed by the pipette rims. This step is the so-called cell-attached configuration and is the compulsory first step for all the other patch-clamp configurations. In the cell-attached configuration, the extracellular medium of the membrane patch under study corresponds to the intrapipette medium while the intracellular

medium corresponds to the cytoplasm of the cell. Starting with the cell-attached configuration, the inside-out configuration was obtained and used during this project. For this, the cell-attached membrane was excised by briefly moving the pipette away from the cell. In this new condition, the intracellular face of the membrane is exposed to the bath solution. This needs to be taken into account when preparing the experiments (see Hille, third edition, 2001). The inside-out patch membrane potential is clamped at a potential opposite to the potential applied in the pipette and a recorded negative current corresponds to an outward cationic current (positive charges going inside the pipette) and reciprocally, the opposite direction to what happens with the same current measured in the whole-cell configuration.

The K_{ATP} channel is a K^+ selective channel whose activity is inhibited by intracellular ATP. It was discovered and first described by Akinori Noma in cardiac cells in 1983 (Noma, 1983). Several reviews are available in which K_{ATP} properties in several tissues are well described and are not the focus in this work (Flagg et al., 2010; Foster & Coetzee, 2016; Tinker et al., 2018). I am going to highlight some important experimental characteristics for the development of K_{ATP} channel as ATP biosensor. Spruce et al. (1985) recorded unitary currents through K^+ selective channels in inside-out membrane patches excised from sarcolemmal vesicles formed from frog skeletal muscles. By showing that the open probability (P_0) of the channels was decreased by ≈70% in the presence of 0.5 mM of ATP at the cytoplasmic face, these channels were identified as K_{ATP} channels expressed at high density in skeletal muscle fibers (~3-4 channels per membrane area of 0.3-0.4 µm diameter) (Spruce et al., 1985). These channels were later found in inside-out membrane patches from adult mouse muscle fibers, displaying high activity in Ca^{2+}-free, Na^+ rich internal solutions. It was observed in that experiments that the presence of 0.1-2mM Ca^{2+} at the cytosolic face induced an irreversible and fast decrease of the activity (within seconds) (Hehl et al., 1994). K_{ATP} channels inactivated by Ca^{2+} (0.1 mM) were also found to be more sensitive to ATP inhibition. This is the reason why in the present study a high concentration of EGTA was used (see solutions) to obtain low levels of free Ca^{2+} in the bath solution, the solution to which the internal face of the inside-out patch membrane is exposed. K_{ATP} channels can also be modulated by intracellular [Mg^{2+}]. Allard et al. (1995) showed in inside-out patches from adult mouse muscle fibers (from FDB) that in the absence of Mg^{2+} at the cytoplasmic face the activity of K_{ATP} channels was higher. When applying 3mM Mg^{2+} the activity of the channel decreased by ≈76%. They also calculated the unitary conductance in the presence of 1 mM Mg^{2+} and in absence of Mg^{2+} at the cytoplasmic face and observed a maximal conductance of 21 and 31 pS, respectively, showing a ≈33% decrease in the presence of Mg^{2+} (Allard et al., 1995). Finally, it was also observed that the inhibitory effect of ATP was reduced in the presence of Mg^{2+}. In another relevant study for us, Allard et al. (1997) observed larger values of K_{ATP} channels density than observed in frog (≈ 50

channels per membrane patch). More important for us, they also described the sensitivity of K_{ATP} channels to ATP in these conditions and observed a reduced activity of 33%, 6%, and 0% in the presence of 30, 100, and 300 µM of ATP, an effect that was partially reversible after washout (Allard & Rougier, 1997). In a proof of concept work for the development of our biosensor, Allard et al. (2006) combined whole-cell silicone voltage-clamp and single channel recording using the cell-attached configuration of the patch clamp technique in the same isolated mouse muscle fiber. They were able to control the voltage of the cell by using one electrophysiological setup and one pipette inserted in the cell covered by the silicone grease, while at the same time they recorded the unitary currents with the use of a second electrophysiological setup and one pipette sealed on the silicone-free portion of the same fiber (Allard et al., 2006).

In our configuration, several bath solutions were tried until finding a composition that allows us to measure the activity of the inside-out membrane patch while stimulating at the same time the fiber using the silicone voltage-clamp technique. The chemical gradient for potassium was reversed from what was used by Allard et al in 1997, adding 140 mM K^+ in the pipette and leaving low [K+] (5 mM K^+) in the bath to avoid muscle fiber depolarization and inactivation of contraction (see solutions). The [Mg^{2+}] concentration in the bath was maintained to 6 mM despite its inhibitory effect on the K_{ATP} channels because a more stable patch activity was observed in its presence. 2 mM Ca^{2+} was added in the bath solution because otherwise the fibers died. As mentioned above, to limit inactivation of K_{ATP} channel by the high concentration of Ca^{2+}, 5 mM EGTA were added, which is a Ca^{2+} chelator, leaving small concentration of free Ca^{2+}. The voltage of the patch membrane was systematically fixed at 0 mV during the experiments or hyperpolarized to -20 or -40 mV by applying, as explained above, the opposite voltage in the pipette. Under these experimental conditions, according to the Nernst equation, the K^+ equilibrium potential (E_K) was +85 mV (58.Log(140/5) mV at 20°C), and the single channel current was inward since the voltage applied to the membrane patch was lower than E_K.

6.6. Chronology of experimental procedures used for combining patch-clamp and silicone voltage-clamp

1. the bath solution of the muscle was changed from Tyrode to an external free Ca^{2+} solution
2. the bottom of a culture µ-dish was covered with a fine layer of silicone grease
3. the enzymatically-treated muscle was triturated in the µ-dish with the external solution to isolate fibers

4. several fibers were electrically isolated in the μ-dish with silicone grease as previously described
5. the patch clamp pipette was filled with a K^+-rich filtrated solution
6. continuous positive pressure was applied in the pipette using a syringe connected to the pipette-holder
7. the pipette was positioned over the fiber without touching it and then was slowly brought closer with the micromanipulator
8. the pipette resistance was continuously monitored until a decrease was observed when the pipette gently makes contact with the cell membrane. The positive pressure was released
9. negative pressure was applied in the pipette until a gigaseal was obtained
10. the inside-out configuration was obtained by moving the pipette away from the fiber, exposing the cytoplasmic face of the patch to a 5 mM K^+-containing solution devoid of ATP
11. voltages pulses of +20 and +40 mV were applied in the pipette to clamp the membrane patch at -20 and -40 mV respectively. Inward currents of increasing amplitude were expected when switching the potential from -20 to -40 mV to provide evidence of activity of a K^+-selective channel
12. the cytoplasmic face was exposed to a solution containing 1 mM ATP to check sensitivity of K+ channel activity to ATP
13. another partially isolated fiber covered by silicone grease was voltage clamped
14. the inside-out patch is approached as close as possible to the uncovered portion of the silicone-clamped fiber
15. the silicone-clamped fiber was stimulated at 20 Hz during 30-45 seconds and after the channel activity in the inside-out patch was recorded for 5 minutes.

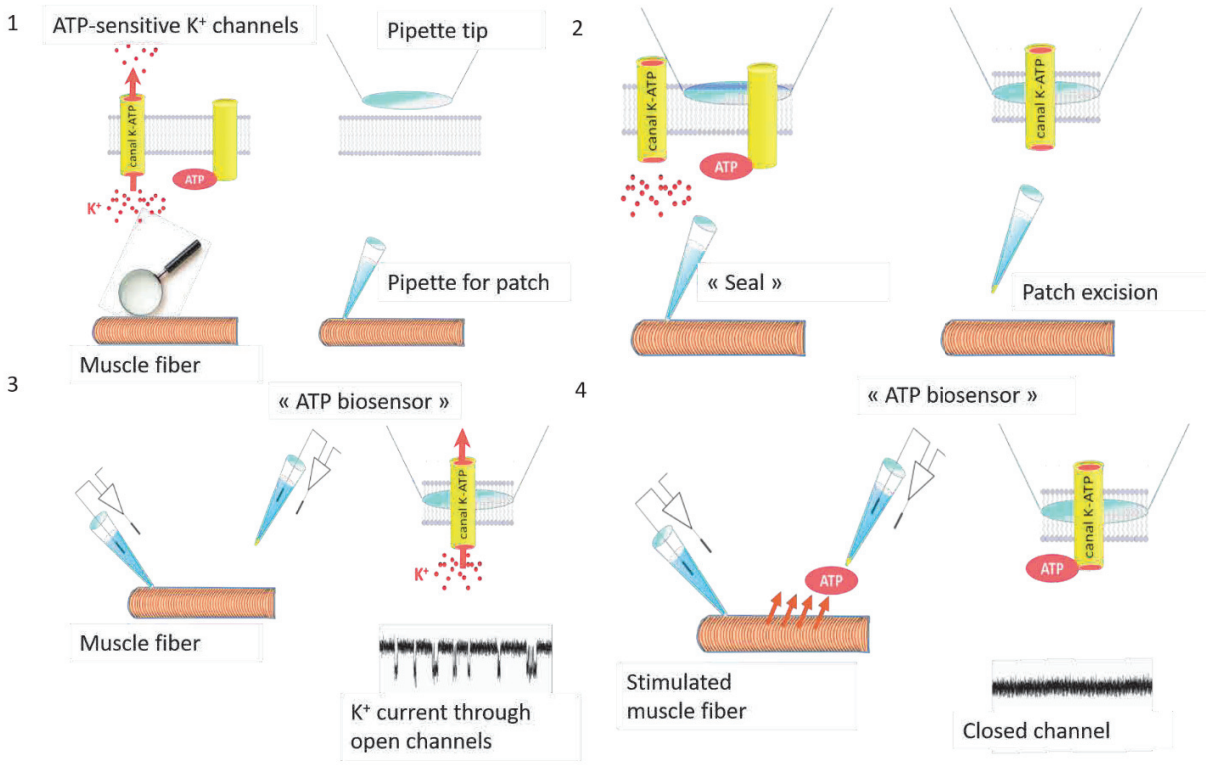

Figure 31. Representation of the 4 steps of ATP release measurement with our ATP biosensor. *1) we sealed a patch-clamp pipette on the surface of a muscle fiber and excised the membrane patch to obtain the inside-out configuration. (2) the presence of KATP channels in the membrane patch was checked by superfusing ATP at the cytoplasmic face. 3) we approached the ATP-sensitive biosensor in the vicinity of a second voltage-clamped muscle fiber. 4) we stimulated the fiber at 20 Hz during 30-45 seconds and recorded simultaneously the change in the activity of the ATP biosensor.*

6.7. P2X receptor channel whole-cell current measurements

These experiments used in vivo transfection of a plasmid encoding an ionotropic purinergic receptor fused to a Ca^{2+}-biosensor, P2X2-GCaMP6s (P2X2 wild type form), in adult mouse skeletal muscle fibers. The plasmid also contained a sequence coding for the self-cleaving peptide domain P2A fused to the red fluorescent protein Scarlet. The plasmid was a generous gift from Dr. F. Rassendren (IGF, Montpellier). Plasma membrane localization of the P2X receptor (P2XR) was checked by expression in COS-7 cells. Plasmid electroporation in mouse FDB and IO muscles was followed by a period of expression of either 1 or 2 weeks. P2X2 ion channel current was measured in whole- cell mode using the silicone voltage-clamp technique. Before the electrical insulation process, fibers were selected based on their

GCaMP-related green fluorescence and we made sure that the portion of fiber outside the silicone was green-fluorescence positive. Expression in the T-tubules was checked by analysis of the transversal profile (using methods described in section 6.2.4). In order to assess the functional presence of the P2X channels, we systematically measured the membrane current response to application of 100 µM of extracellular ATP, using a perfusion system. In one group of fibers, we applied the ATP-sensitivity test at the end of the experiment, while in another group we applied it at the beginning. In fibers identified positive for green fluorescence and for response to extracellular ATP, we analyzed the whole-cell current for 4 minutes following whole-cell stimulation with short depolarizing pulses from -80 to +40 mV delivered at 20 and 90 Hz during 30-45 seconds. The train-induced change in current was measured with reference to the current in the resting condition, before the stimulations (see Results).

VII. Confocal microscopy and intracellular Ca^{2+} imaging

7.1. Confocal microscopy: line-scan and time-series

Confocal microscopy is an optical microscopy technique in which the signal produced by the fluorescent molecules is collected within a limited volume called “focal plane” with, under optimal conditions, a *x*, *y* and *z* resolution of approximately 0.1, 0.1, and 0.5 µm.

In laser-scanning confocal microscopy, the excitation is produced by a laser beam focused as a diffraction-limited spot on the sample, illuminating only one point of the object at a time. The laser light is regulated by a diaphragm called pinhole before being directed towards a crystal AOTF (acoustic-optic tunable filter) which allows modulation of the intensity and wavelength of the beam. Light is then reflected by a beam splitter (dichroic mirror) and focused onto the sample to excite the fluorescent molecules. The fluorescence is collected by the objective and directed onto the detector (photo-multiplier, PMT), passing through the dichroic beam splitter. The wavelength of interest is further selected by an emission filter (see Fig. 32). A pinhole is set in front of the detector, on a plane conjugate with the focal plane of the objective, obstructing the light coming from the sample regions outside the focal plane (above or below), thus excluding them from detection and providing the confocal mode. Control of the pinhole diameter (confocality degree) is allowed, and when the aperture is fully opened, the image is no-longer confocal. Fluorescent photons on the PMT are converted into electrons and amplified according to the selected parameters (detector gain). The sample is excited point by point in the *x*,*y* plane (scanned))

through motorized mirrors in the optical trajectory of the laser beam. The confocal fluorescent image is then reconstituted point by point.

Most experiments were conducted with a Zeiss LM5 Exciter microscope equipped with a 63 × oil-immersion objective (N.A., 1.4). A configuration with the 488 nm line of an argon laser and a 505 nm long-pass filter on the detection channel was used for green fluorescence detection (e.g. when using fluo-4, fluo-4 FF, GCaMP), whereas excitation was from the 543 nm line of a HeNe laser and fluorescence was collected above 560 nm for orange-red fluorescence (e.g. when using rhod-2 or mCherry). Most recent experiments were achieved with an upgraded version of the system (LSM-800) equipped with diode lasers. Initial experiments in Chile during my Master degree were conducted with a Zeiss LSM 710 system, with properties very similar to the Zeiss LM5 Exciter.

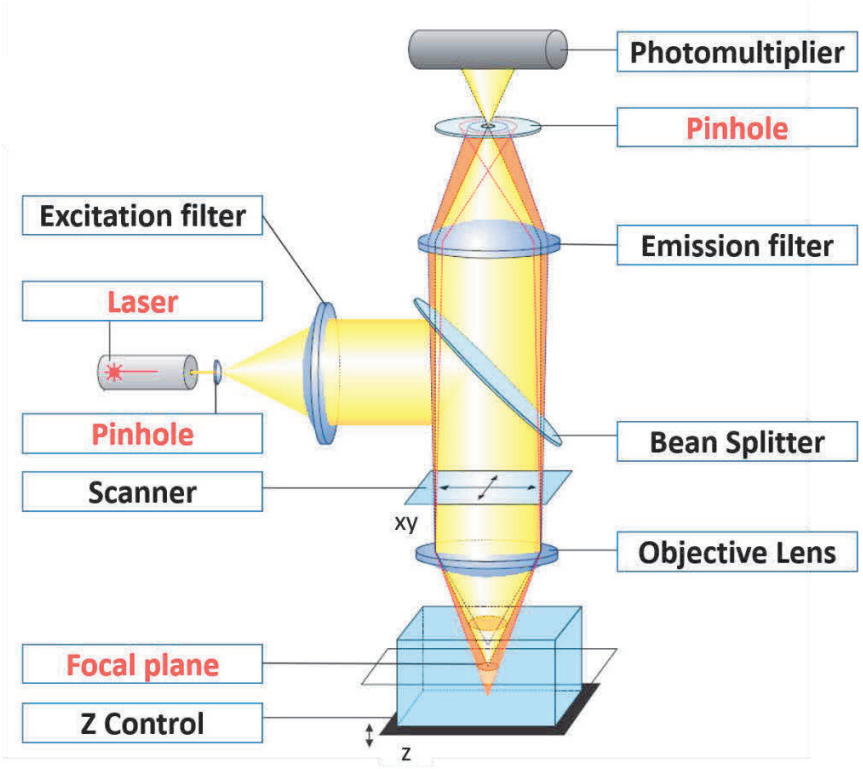

Figure 32. Structural and functional scheme of a laser scanning confocal microscope. *See text for details.*

When using *x*,*y* imaging, frames of 512×512 pixels (routinely 51 × 51 µm) were acquired at a maximal rate of 2-3 frames/s. This mode allowed visualizing and quantifying fluorescence changes within a field of the cell and was typically used for probe localization and for the study of Ca^{2+} sparks. For

measurements of voltage-clamp-activated Ca^{2+} transients, the line-scan mode of the system was used with a sampling rate of 1 line (512 pixels routinely corresponding to 51 µm) every ms or so.

Detection of intracellular Ca^{2+} can be achieved with a wide range of either chemical or genetically encoded fluorescent indicators, with differing affinity, spectral properties and quantum yield. Accordingly, the selection of a specific indicator relies on the properties of the process to be investigated, including the size of the related Ca^{2+} change and their kinetics.

The Ca^{2+} affinity of a fluorescent dye can be expressed by the dissociation constant (Kd). We can define Kd as the concentration of Ca^{2+} for which 50% of the fluorescent dye (indicator) molecules are Ca-bound (Equation 4).

$$Kd = ([Ca^{2+}]x[Indicator])/[Ca\text{-}Indicator] = k_{off}/k_{on}$$

Thus, when a molecule has a high Kd, the Ca^{2+} affinity is poor and when it has a low Kd is affinity is larger. During my Master and my Ph.D. project, I used Rhod-2, Fluo4, Fluo4-FF, and Indo-1.

Rhod-2: rhod-2 is a single wavelength rhodamine-based, orange fluorescent Ca^{2+} indicator. rhod-2 presents a Ca^{2+} Kd= 570 nM, a maximum fluorescence excitation at 552 nm and emission at 581 nm (Minta et al., 1989). The fluorescence intensity increase in the presence of saturating Ca^{2+} levels is >100 fold (in the book). When associated with Ca^{2+} presents Excitation/Emission maxima of 530/576 nm.

Fluo-4: fluo-4 is also a single-wavelength dye, generating green fluorescence upon blue excitation. It is an analog of fluo-3 with two chlorines replaced by fluorines. Fluo-4 exhibits a larger increase in fluorescence upon Ca^{2+} binding than fluo-3. Fluo-4 presents a maximum fluorescent intensity increase on Ca^{2+} binding given >100 fold (Harkins et al., 1993). Fluo-4 has a Kd= 345 nM. When associating with Ca^{2+}, fluo-4 has a maximum excitation/emission at 494/516 nm.

Fluo4-FF: is also a single wavelength green fluorescent dye, analog of fluo-4 but with a lower Ca^{2+}-binding affinity, making it suitable for detecting intracellular calcium levels in the 1-100 µM range that normally saturate the response of rhod-2 and fluo-4. Fluo-4 FF dissociation constant is given as 9.7 µM, and its excitation/emission maximum is 495/516 nm. Maximum fluorescence intensity increase upon binding Ca^{2+} is also given to be > 100 fold.

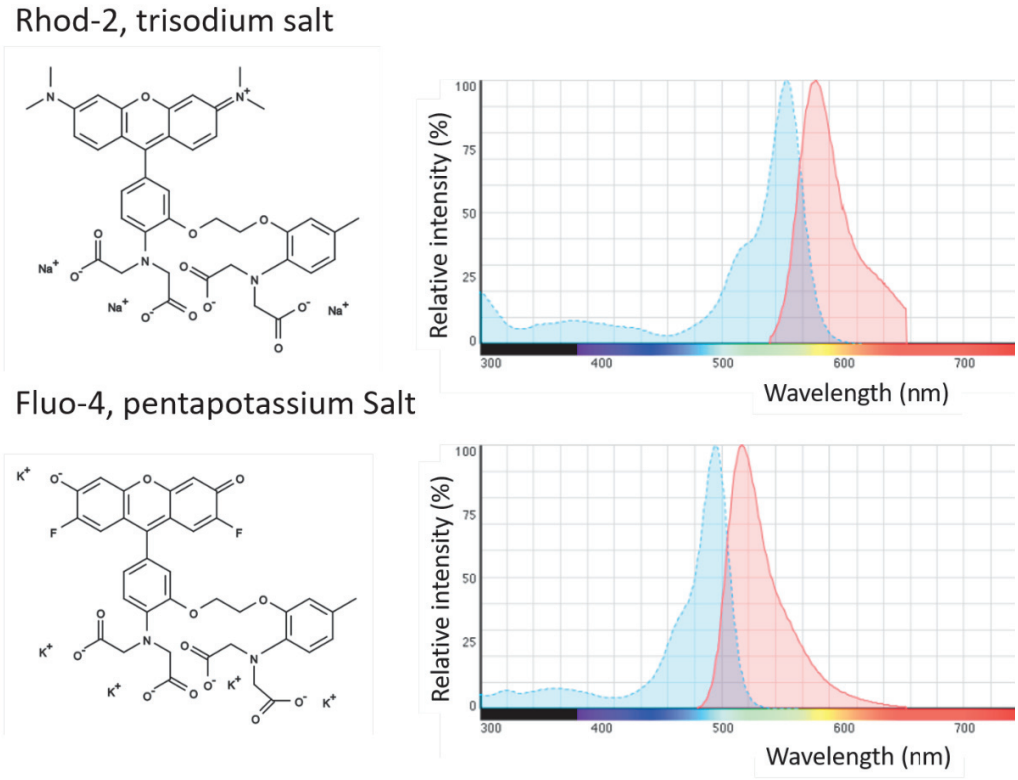

Figure 33. Rhod-2 and fluo-4 fluorescent indicators molecules and their excitation/emission spectra. *Both molecules are represented at the left in their salt version. The excitation and emission spectra of rhod-2 are wider than those of fluo-4. Both molecules do not suffer spectral shifts when binding calcium. Calculation of calcium changes are made from the ratio F/F_0, with F the fluorescence and F_0 the initial baseline fluorescence. Imaged were taken from Thermo-fisher.*

Indo-1: is a high affinity, ratiometric Ca^{2+} indicator with a Kd= 0.23 µM, excitable by UV light, with an excitation maximum at 344 nm, and an emission that shifts from 480 nm in the absence of Ca^{2+} to 400 nm in the presence. The ratio R= F405/F485 allows us to calculate [Ca^{2+}] (see Jacquemond, 1997).

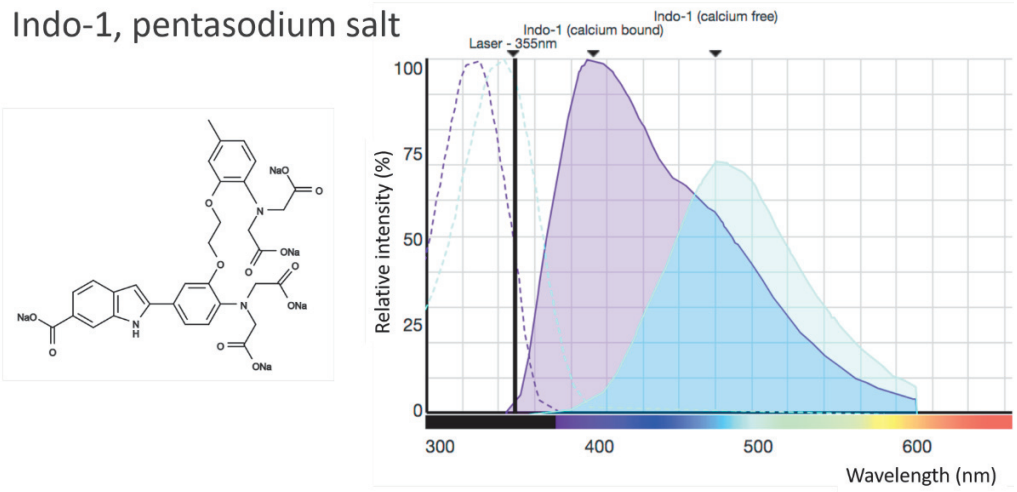

Figure 34. Indo-1 molecule and its ratiometric excitation/emission wavelength. *The Indo-1 molecule in its salt version is shown on the left. Image was taken from Thermo-fisher.*

7.2. General experimental conditions

7.2.1. Ca^{2+} measurements in Panx1-knockdown muscle fibers

For the intracellular Ca^{2+} measurements in fibers expressing shRNA-Panx1, we used the Ca^{2+} sensitive fluorescence dye fluo-4. For this, all fibers dispersed in a µ-dish were loaded for 30 minutes with 10 µM fluo-4 AM, before establishing the silicone voltage-clamp. In this model, fluo-4 was used because it has a wavelength of excitation at 488 nm and maximum emission at 516 nm (in the green zone), which contrasts with the excitation at 584 nm and emission at 610 nm of the red fluorescent protein mCherry, used as a control of expression. Fluo-4 Ca^{2+} transients were measured with the line-scan mode (1.53 ms per line) using a Zeiss LSM 710 confocal microscope. The dye was excited at 488 nm with an argon laser and a 505-530 nm bandpass filter was used for the detection channel. Fluo-4 Ca^{2+} transients were expressed as F/F_0, where F_0 is the baseline fluorescence. For these experiments, contraction was blocked by adding 50 µM of *N*-benzyl-p-toluene sulphonamide (BTS), a myosin ATPase inhibitor, in the TEA-standard solution. We also measured, in this model, the SR Ca^{2+} content using a method described by Al-Qusairi et al. (Al-Qusairi et al., 2009). For this, fibers were equilibrated with the voltage-clamp pipette intracellular-standard solution containing indo-1 and EGTA (see solutions). Indo-1, as presented before, is a ratiometric fluorescent Ca^{2+} indicator that upon excitation at 360 nm, produces a Ca^{2+}-dependent simultaneous change in fluorescence of opposite directions at 405 nm (F405) and 485 nm (F485). We used a standard ratio method for calculating $[Ca^{2+}]$ from R= F405/F485, with in vivo values for the calibration

parameters Rmin, Rmax, KD, and β determined as previously described (Jacquemond, 1997). We applied 50-ms-long depolarizing pulses from -80 to +10 mV, before and after applying 50 µM cyclopiazonic acid (CPA), a SERCA blocker, in the extracellular medium. The maximum change in baseline indo-1 saturation level following pulses in the presence of CPA was taken as an index of the SR Ca^{2+} content.

7.2.2. Standard measurements of voltage-activated Ca^{2+} transients with rhod-2 in the presence of EGTA

This configuration was used routinely to characterize the properties of SR Ca^{2+} release in various models and conditions (mouse model of diabetes, pharmacological effectors, Panx1 over-expression …). For this we used our standard TEA-containing extracellular solution (see VII). The voltage-clamp pipette was filled with the standard intracellular solution also containing rhod-2 and 15 mM EGTA (see VII Solutions). Once the silicone-clamp condition was established, the fiber was left for 30 minutes to allow for equilibration of the intracellular solution within the myoplasm. Rhod-2 fluorescence transients were then detected in response to voltage-clamp depolarizing pulses of various amplitude and duration. Rhod-2 F/F_0 fluorescence transients were then used to calculate the rate of SR Ca^{2+} release ($d[Ca_{Tot}/dt]$) using a previously described procedure (Pouvreau et al., 2006, Lefebvre et al., 2011, see 6.3.1).

7.2.3. Testing the effects of the Panx1 inhibitors probenecid and carbenoxolone on voltage-activated Ca^{2+} transients

To study the effects of chronic application of probenecid and carbenoxolone, muscle fibers established in the silicone-clamp conditions, under the configuration described in the previous section, were left throughout the dialysis period in the presence of one inhibitor. We then applied 0.5 s-long depolarizing steps of increasing amplitude from the -80 mV holding voltage. To study the effect of acute Panx1 pharmacological inhibition with probenecid, we also used the configuration described in the previous section. For this, we challenged the fibers with 200 ms-long depolarizing pulses from -80 mV to -20, 0, and +20 mV. Each pulse was applied twice during each step of the protocol which were: -a control step before applying probenecid DMSO, -a test step after adding 1 mM Probenecid (or only DMSO) to the bath, -a post-wash step, after replacing the extracellular solution with the control solution. The absolute change in resting Ca^{2+} concentration induced by probenecid was estimated in each fiber assuming an initial resting Ca^{2+} concentration of 0.1 µM, and F_{max}/F_{min} and K_D values for Rhod-2 of 30 and 1.63 µM, respectively.

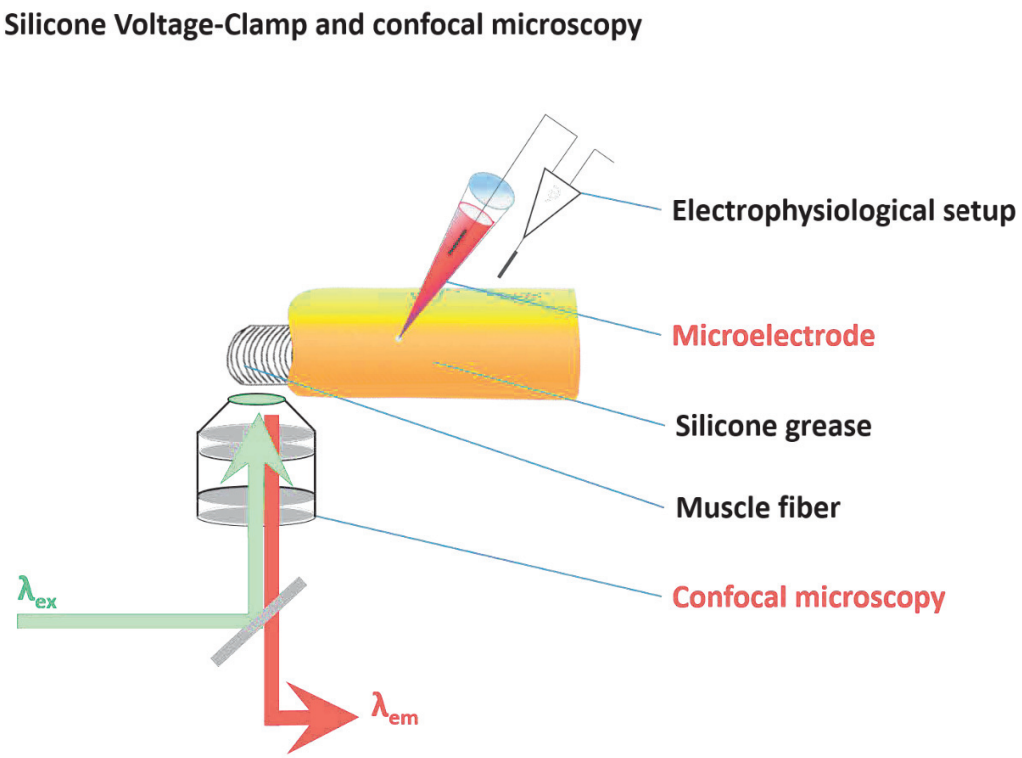

Figure 35. Graphic representation of the conditions allowing simultaneous silicone voltage-clamp and confocal microscopy. *The voltage-clamp electrode is inserted within the fiber through the silicone grease. The intracellular solution containing the Ca^{2+}indicator, and in some cases EGTA to block the contraction, is dialyzed for 30 minutes. Fluorescence is detected with a 63x oil-immersion objective, from the portion of fiber outside the silicone which is under voltage-control from the electrophysiological setup. Different lasers and configurations were used, depending on the fluorescent indicator*

7.2.4. Ca^{2+} measurements in HFHSD-induced obese mice model

Rhod-2 Ca^{2+} transients and corresponding rate of SR Ca^{2+} release were measured and calculated as described in sections 6.2.2, and 6.3.1. Fluo4-FF fluorescence transients were measured in our standard silicone-clamp/confocal configuration (see 6.2.2 and Figure 35) with the intracellular solution devoid of EGTA and with the extracellular soluton containing 50 µM BTS to block contraction.

7.2.5. T-tubules measurement and Ca^{2+} sparks

For studying the T-tubule network in the obese mouse model we used di-8-anepps, which is a dye that presents with fluorescence when interacting with lipids in biological membranes. This characteristic allowed us to estimate the T-tubule density and the T-tubule proper organization with respect to the muscle fibers morphology. Di-8-anepps exhibits an optimal excitation/emission ratio of 470/588 nm in the T-tubule membrane (DiFranco et al., 2005). For imaging the T-tubule network, FDB and IO muscle fibers were incubated for 30 minutes in the presence of 10 µM of di-8-anepps in Tyrode solution. Di-8-anepps fluorescence was detected in *x*,*y* mode above 505 nm upon 488 excitation. Estimation of T-tubule density from di-8-anepps fluorescence was carried from a region of interest excluding the plasma membrane. Two images were systematically taken from two distinct locations in each fiber. The analysis was made in ImageJ (NIH, Bethesda, MD, USA) as described in the manuscript.

For Ca^{2+} sparks detection, muscle fibers were incubated for 30 minutes in the presence of 10 µM fluo-4 AM in Tyrode solution. After fluo-4 AM wash, fluo-4 fluorescence were detected above 505 nm upon 488 nm excitation. Thirty consecutive confocal frames of fluo-4 fluorescence were acquired (for more details see methods in the first manuscript).

7.3. Fluorescence data analysis

7.3.1. Calculation of the RyR1-dependent Ca^{2+} flux

Fluorescence images were processed with ImageJ (National Institute of Health (NIH)) and Origin 7/8 (Originlab, Northampton, MA, USA).

The flux of calcium through RyR1 channels in the SR membrane during ECC was calculated from the voltage-activated F/F_0 rhod-2 transients using a previously described procedure consisting in estimating the total [Ca^{2+}] variation (dCa_T) that would have appeared over time if we consider the contribution of Ca^{2+} bound to the major Ca^{2+} buffers in the cytosol and the SR Ca^{2+} uptake mechanism (Lefebvre et al., 2011). This model takes into consideration the following factors

1. The interaction of Ca^{2+} and Mg^{2+} with the parvalbumin (PV) protein present in the cytosol with a concentration of bonding sites of 2000 µM, the association rate constant for Ca^{2+} ($k_{on,\ CaPV}$) of 0.125 μM^{-1} x ms^{-1}, the dissociation rate constant for Ca^{2+} ($k_{off,\ CaPV}$) of 0.0005 ms^{-1}, the association rate constant for Mg^{2+} ($k_{on,\ MgPV}$) of 3.3 x 10^{-5} μM^{-1} x ms^{-1} and the dissociation rate constant for Mg^{2+} ($k_{off,\ MgPV}$) of 3.003 x 10^{-3} $\mu M^{-1}.ms^{-1}$.

2. The interaction of Ca^{2+} with the troponin C (TnC) with a total binding sites concentration of 250 µM, the association rate constant for Ca^{2+} ($k_{on,\ CaTN}$) of 57.5 x 10^{-3} μM^{-1} x ms^{-1} and the dissociation rate constant for Ca^{2+} ($k_{off,\ CaTN}$) of 0.115 ms^{-1}.
3. The interaction of Ca^{2+} with EGTA, with an estimated concentration of 80% of the free EGTA in the intracellular solution after 30 minutes of dialysis. In this condition EGTA is the Ca^{2+} buffer present in the cytosol. Changes in [Ca-EGTA] were calculated with the association rate constant for Ca^{2+} ($k_{on,\ CaEGTA}$) of 0.056 μM^{-1} x ms^{-1} and the dissociation rate constant for Ca^{2+} ($k_{off,\ CaEGTA}$) of 0.002 ms^{-1}.
4. The reuptake of Ca^{2+} in the SR was included with a rate assumed to be proportional to the fractional occupancy of the SR pump sites using an equilibrium dissociation constant for Ca^{2+} (Kd_{CaPump}) of 2 µM and a maximum uptake rate of 10 $\mu M^{-1}.ms^{-1}$
   The flux was calculated as the time derivative of the change in total myoplasmic Ca^{2+}, that is the change in free Ca^{2+} plus the changes in Ca^{2+}-bound to the intracellular sites plus the change in Ca^{2+} due to uptake by the pump ($d[Ca]_T/dt$).

7.3.2. T-tubule density and distance

For each tested fiber, analysis of T-tubules density has been realized with ImageJ from two di-8-ANEPPS images taken in different regions. For each frame, the largest possible region excluding the sarcolemma was considered. An automatic threshold based on Otsu method was used to produce a binary image of the T-tubule network. The T-tubule density was determined as the ratio of the T-tubule area to the total area selected for the analysis.

7.3.3. Ca^{2+} Sparks

Sparks analysis was restricted to determination of the relative fiber area exhibiting local Ca^{2+} release events. For this, 30 consecutive *x*,*y* confocal frames (512×512, 102×102 µm) of fluo-4 fluorescence were collected. A fiber region excluding the sarcolemma was selected and smoothed throughout the pile of frames. The corresponding standard deviation (SD) for each pixel intensity through the 30 frames was calculated. The 20 % largest values in the SD image were removed to calculate the mean standard deviation of silent areas. Active area was then defined as pixels positions exhibiting at least 1.5 times larger values of standard deviation than the mean standard deviation value from silent areas.

VIII. Solutions

All concentrations values are expressed in mmol/l. The pH was always adjusted at 7.2. In whole-cell voltage-clamp, the intracellular solution corresponds to the solution in the pipette (electrode) that was dialyzed into the intracellular space of the fibers. In the case of the inside-out patch-clamp configuration, the extracellular solution is in the pipette. All extracellular solutions were stored at 4°C and all intracellular solutions were aliquoted and stored at -20 °C, with the exception of the intracellular solution for inside-out patch-clamp which was stored at 4°C and filtered before use.

8.1. Tyrode solution: 140 NaCl, 5 KCl, 2.5 $CaCl_2$, 2 $MgCl_2$, 10 HEPES. This solution was used as an extracellular solution for 1) enzymatic treatment of the muscles with type 1 collagenase (2 mg/ml), 2) muscles storage at 4°C after the enzymatic digestion, 3) Ca^{2+} sparks experiments. For this, fibers were loaded with fluo-4 by a 30 min exposure to 10 µM of fluo-4 acetoxymethyl ester (AM). The Tyrode solution was also used to follow intracellular basal Ca^{2+} changes following application of probenecid to fluo-4-loaded fibers.

8.2. Culture medium: Medium 199 containing 10% Fetal Bovine Serum (SVF) and 10 mM HEPES.

Ca^{2+} current and SR Ca^{2+} release

8.2.1. Extracellular solution: 140 tetraethylammonium (TEA)-methasulfonate ($MeSO_3$), 2.5 $CaCl_2$, 2 $MgCl_2$, 1 4-aminopyridine (AP), 10 HEPES, 0.002 tetrodotoxin (TTX). For the measurements of Fluo-4FF Ca^{2+} transients it also contained 0.05 N-benzyl-p-toluene sulphonamide (BTS) to block contraction. For the experiments with probenecid, the drug was dissolved in DMSO at 300 mM and stored at -20°C. This solution was diluted to 5 mM in the extracellular solution, stored at 4°C no longer than a week, and diluted to 1mM the experimental day. Carbenoxolone was prepared in the extracellular solution at 10 mM, stored at 4°C and diluted to 100 µM before use.

8.2.2. Intracellular solution: 120 K-glutamate, 5 Na_2-ATP, 5 Na_2-phosphocreatine, 5.5 $MgCl_2$, 5 glucose, 5 HEPES. For measurements of rhod-2 (Ca^{2+}-sensitive fluorescent indicator) Ca^{2+} transients it also contained 15 EGTA (a Ca^{2+} chelator to block contraction), 6 $CaCl_2$ and 0.1 rhod-2. The Ca^{2+}-sensitive fluorescent indicator fluo-4FF was used at 0.1 mM (with no EGTA).

8.3. Charge movement

8.3.1. Extracellular solution: 140 TEA-$MeSO_3$, 0.1 $CaCl_2$, 3 $MgCl_2$, 1 $CdCl_2$, 0.5 $MnCl_2$, 1 4-AP, 0.5 9-anthracene-carboxylic (9-AC) acid, 10 HEPES and 0.002 TTX. To prepare this solution the order of the different steps is important to prevent precipitation. We first diluted together TEA-OH, HEPES, 9-AC, and 4-AP. Second, as 9-AC precipitated, the solution was sonicated for 30 minutes. Third, pH was adjusted, and finally, we added $CdCl_2$, $MnCl_2$, $CaCl_2$, and TTX. This order was necessary to end-up with a limpid homogeneous solution.

8.3.2. Intracellular solution: 140 TEA-$MeSO_3$, 5 Na_2-ATP, 5 Na_2-phosphocreatine, 5.5 $MgCl_2$, 5 glucose, 5 HEPES. pH adjusted with MES.

8.4. Simultaneously inside-out patch-clamp and whole-cell voltage-clamp for ATP release

8.4.1. Extracellular solution: 140 NaCl, 5 KCl, 6 $MgCl_2$, 10 Hepes, 5 EGTA, 2 $CaCl_2$.

8.4.2. Intra-pipette solution for the inside out patch-clamp: 140 KCl, 1 $MgCl_2$ and 10 Hepes.

8.4.3. Intra-pipette solution for whole-cell voltage-clamp for ATP release: 120 K-glutamate, 15 Na_2-ATP, 5 Na_2-phosphocreatine, 5.5 $MgCl_2$, 5 glucose, 5 HEPES.

8.5. P2X whole-current measurements

8.5.1. Extracellular solution: 140 Na-$MeS0_3$, 20 TEA-$MeSO_3$, 1 4-AP, 10 HEPES, 1 MgCl2, 2.5 CaCl2, 0.001 TTX. In order to block contraction, 0.05 BTS was added before the experiments.

8.5.2. Intracellular solution: 120 K-glutamate, 5 Na_2-ATP, 5 Na_2-phosphocreatine, 5.5 $MgCl_2$, 5 glucose, 5 HEPES and 15 Na_2-ATP.

IX. Statistical analysis

Data was analyzed using Origin (OriginLab Corp, Northampton, MA, USA). Values are presented as mean ± standard error (SE) for a n number of fibers. We used Shapiro-Wilk to determine the normal distribution of the data for each condition of each group. We evaluated the significance between groups using: 1) two-tailed unpaired t-student tests for comparisons between groups of fibers under different experimental conditions, and 2) two-tailed paired t-student tests for the comparisons between different conditions for the same fibers. We considered that two groups were different when fulfilling $p< 0.05$ * ($p< 0.01$ **, $p< 0.001$ ***).

RESULTS

RESULTS

I. Results - 1st objective

Section 1.1.

EFFECTS OF TRANSITORY PANX1 KNOCKDOWN ON EXCITATION-CONTRACTION COUPLING OF ADULT SKELETAL MUSCLE FIBERS

Article 1: Francisco Jaque-Fernández, Gonzalo Jorquera, Jennifer Troc-Gajardo, France PietriRouxel, Christel Gentil, Sonja Buvinic, Bruno Allard, Enrique Jaimovich, Vincent Jacquemond and Mariana Casas. Excitation-contraction and excitation-transcription coupling in skeletal muscle: functional interaction between dihydropyridine receptor and pannexin-1 (submitted to J. Gen. Physiol. 2021).

This study started with the hypothesis that $Ca_V1.1$ and Panx1 exhibit a bidirectional relationship through which, not only $Ca_V1.1$ is capable of regulating Panx1 during excitation-transcription coupling (ETC), but Panx1 is also capable of regulating $Ca_V1.1$ function and excitation-contraction coupling (ECC). The arguments behind this hypothesis came from a number of previous works from the laboratory of Enrique Jaimovich and Mariana Casas at University of Chile, showing that $Ca_V1.1$ activity determines activation of ATP release through Panx1 channels in muscle cells in a frequency of excitation-dependent manner, according to which trains of action-potentials at a 10-20 Hz frequency are permissive for Panx1 activation and subsequent activation of inositol (1,4,5)-trisphosphate-dependent Ca^{2+} signals that regulates gene expression (Buvinic et al., 2009; Casas et al., 2010; Jorquera et al., 2013; Arias-Calderon et al., 2016). Specifically, it was shown that $Ca_V1.1$ and pannexin-1 colocalize in the transverse tubule membrane and the functional regulation of Panx1 by $Ca_V1.1$ was established using pharmacological effectors acting on $Ca_V1.1$ and Panx1. The working model considers that 20 Hz trains of electrical activity activate $Ca_V1.1$, which activates Panx1 opening and ATP release. Extracellular ATP activates P2YR in the sarcolemma and, as a consequence, a G-protein and inositol-trisphosphate receptor-dependent signaling pathway that regulates gene expression associated with muscle plasticity (Jorquera et al., 2013). The present project aimed at providing further evidence for $Ca_V1.1$-Panx1 interactions by characterizing the consequences of $Ca_V1.1$ down-expression on ATP release and of Panx1 down-expression on ECC.

My contribution to this project was specifically related to the consequences of Panx1-down-expression on ECC.

Transitory knockdown conditions for $Ca_V1.1$ and Panx1 were separately achieved in *Flexor Digitorum Brevis (FDB)* muscles from adult mice.

For Panx1 down-expression, in vivo transfection of an AAV-mCherry-U6-mPANX1-shRNA plasmid (shPanx1) (obtained from Vector Biolabs) was used. Plasmid electroporation was carried out in the FDB muscles of either Swiss OF1 (charge movement and SR Ca^{2+} content measurements) or BalbC (Ca^{2+} currents and Ca^{2+} release measurements) male mice. After two weeks of expression, we obtained a ≈65% decrease in the Panx1 protein content.

For $Ca_V1.1$ down-expression we used a U7-exon-skipping strategy with a previously designed adenovirus-associated viral vector (AAV-U7deIα1s) and corresponding control as described earlier (Pietri-Rouxel et al. 2010). After 4 months of expression, we obtained a ≈60% decrease in the $Ca_V1.1$ protein content.

Down-expression of $Ca_V1.1$ in adult muscle fibers alters the function of Pannexin-1

The functional impact of $Ca_V1.1$ down-expression on $Ca_V1.1$ Ca^{2+} current and on voltage-activated SR Ca^{2+} release was assessed and quantified. Regarding Panx1 function and ETC, $Ca_V1.1$ down-expressing fibers, showed an increase in the basal levels of ATP release, which indicates dysregulation of the normally closed configuration of Panx1 channels. Associated with this, there was an increase in the basal mRNA levels of the slow isoform of Troponin I (TnIs) and a decrease in mRNA levels of the fast isoform (TnIf), as previously reported after 20 Hz electrical stimulation (ES) or addition of external ATP (Jorquera et al., 2013).

Down-expression of Pannexin-1 suppresses low frequency electrical stimulation-induced ATP release in adult muscle fibers

The shPanx1 plasmid induced: 1) a 65% decrease in Panx1 protein level, 2) a significant decrease of the ATP release in basal conditions, 3) suppression of 20 Hz electrical stimulation-induced ATP release and Troponin mRNA levels adaptation (previously described by Jorquera et al., 2013).

Down-expression of Pannexin-1 alters Ca^{2+} current through $Ca_V1.1$

Panx1 down-expressing fibers under silicone voltage-clamp condition were used to measure the $Ca_V1.1$-dependent Ca^{2+} current upon 0.5 s-long depolarizing pulses of increasing amplitude. Panx1 knockdown was associated with a ~30% reduction in the $Ca_V1.1$ channels maximum conductance and with altered kinetic properties of the current. Altogether, the down-expression of Panx1 alters $Ca_V1.1$-

dependent Ca^{2+} current properties, supporting the hypothesis of a reciprocal functional interaction between $Ca_V1.1$ and Panx1.

Down-expression of Pannexin-1 depresses voltage-activated SR Ca^{2+} release

We studied the effect of Panx1 down-expression on ECC of differentiated muscle fibers. Panx1 down-expression was associated with a 60% reduction in the maximum rate of rise of fluo-4 Ca^{2+} transients. The corresponding time course of Ca^{2+} transients decay was unaffected, suggesting that SERCA function was normal. We excluded the possibility that the decrease in Ca^{2+} transients was the consequence of a decrease in the SR Ca^{2+} content by showing that the value of this parameter did not differ between control and Panx1-downexpressing fibers. These results support the hypothesis that the decrease amplitude of Ca^{2+} transients is the consequence of an alteration in RyR1 function.

Intramembrane charge movement is not altered in fibers down-expressing Pannexin-1.

Because of the Panx1 down-expression-induced changes in $Ca_V1.1$-dependent Ca^{2+} current and SR Ca^{2+} release, it was of critical interest to assess the $Ca_V1.1$ voltage sensing properties from intramembrane charge movement in that condition. We found that Panx1 down-expression does not affect intramembrane charge movement. Thus, neither the decrease in $Ca_V1.1$-dependent Ca^{2+} current, nor in SR Ca^{2+} release are a consequence of a decrease in $Ca_V1.1$ expression level and/or of its voltage-sensing properties.

Conclusions

This work provides the first pieces of evidence for a bidirectional interaction between $Ca_V1.1$ and Panx1. We knew that the control of ATP release through Panx1 by $Ca_V1.1$ was crucial for the regulation of ETC and muscle plasticity. We now show that Panx1 is also a critical partner for the proper function of $Ca_V1.1$ and for RyR1-dependent SR Ca^{2+} release. The Panx1-knockdown-induced changes in the $Ca_V1.1$ channel activity were not a consequence of altered $Ca_V1.1$ protein content as proved by the intramembrane charge movement measurements. The severe decrease in voltage-activated Ca^{2+} transients has to be a consequence of either altered $Ca_V1.1$-RyR1 interaction during ECC, or of RyR1 function. Therefore, results support the hypothesis that Panx1 is a critical functional interactor of the ECC machinery. Whether there is direct physical interaction between $Ca_V1.1$/RyR1 and Panx1 or whether another intermediate protein partner is playing a role in this interaction remain open questions and will need further studies.

Excitation-contraction and excitation-transcription coupling in skeletal muscle: functional interaction between dihydropyridine receptor and pannexin-1

Francisco Jaque-Fernández[1,5], Gonzalo Jorquera[1,3], Jennifer Troc-Gajardo[1], France PietriRouxel[4], Christel Gentil[4], Sonja Buvinic[6], Bruno Allard[5], Enrique Jaimovich[1,2], Vincent Jacquemond[5] and Mariana Casas[1]

[1]Programa de Fisiología y Biofísica, ICBM, Facultad de Medicina, Universidad de Chile, Santiago, Chile

[2]Center for Exercise, Metabolism and Cancer, ICBM, Facultad de Medicina, Universidad de Chile, Santiago, Chile.

[3]Centro de Neurobiología y Fisiopatología Integrativa, Instituto de Fisiología, Facultad de Ciencias, Universidad de Valparaíso, Chile.

[4]UPMC Université Paris 06/INSERM/CNRS/Institut de Myologie/Centre de Recherche en Myologie (CRM), GH Pitié Salpêtrière, Paris, France.

[5]Univ Lyon, Université Claude Bernard Lyon 1, CNRS UMR-5310, INSERM U-1217, Institut NeuroMyoGène, Lyon, France.

[6]Institute for Research in Dental Sciences, Faculty of Dentistry, Universidad de Chile, Santiago, Chile.

Running Title: $Ca_V1.1$-Pannexin interdependent-function in skeletal muscle

Corresponding author:

M. Casas, Programa de Fisiología y Biofísica Facultad de Medicina, Universidad de Chile Avda.

Independencia 1027 838-0453, Santiago Chile Email: mcasas@med.uchile.cl

Summary

Down-expression of $Ca_V1.1$ in muscle fibers produces elevated ATP release, consistent with disruption of Panx1 activity. Down-expression of Panx1 depress the $Ca_V1.1$-dependent Ca^{2+} currents and intracellular Ca^{2+} release. We conclude that Panx1 is a reciprocal partner of $Ca_V1.1$ for both E-C and E-T coupling.

Abstract

Electrical activity in the membrane of skeletal muscle fibers triggers contraction and also controls transcriptional activity related to muscle plasticity. Both processes are triggered by the dihydropyridine receptor (DHPR, $Ca_V1.1$) in the transverse tubule membrane. $Ca_V1.1$ is a voltage sensitive calcium channel which simultaneously acts as a voltage sensor for excitation-contraction (EC) and for excitation-transcription (ET) coupling. EC coupling relies on $Ca_V1.1$ interacting with the type 1 ryanodine receptor (RyR1) Ca^{2+} release channel in the sarcoplasmic reticulum membrane. ET coupling operates in part through interaction between $Ca_V1.1$ and the ATP-releasing channel Pannexin-1 (Panx1) in the transverse tubule membrane. We show now that down-expression of $Ca_V1.1$ produces chronically elevated extracellular ATP concentrations at rest, consistent with disruption of the normal control of the Panx1 activity. Conversely, down-expression of Panx1 in adult muscle fibers not only suppresses electrical stimulation-induced ATP release and the consequent changes in mRNA content of TnIs and TnIf in isolated muscle fibers, but it also alters the calcium channel activity of $Ca_V1.1$ and strongly depresses RyR1-mediated Ca^{2+} release. Overall results reveal that Panx1 is a reciprocal functional partner of $Ca_V1.1$ for EC and ET coupling processes, suggesting that the machinery of these two processes are somehow linked at the molecular level. Importantly, our results now show that there is bidirectional signaling between $Ca_V1.1$ and Panx1, with relevance not only over the ET coupling process but also over EC coupling.

Introduction

Besides its role in energy transfer, ATP is known to operate as an extracellular messenger for autocrine and paracrine signaling (Corriden & Insel, 2010). Specifically, in a variety of cell types including muscle cells, ATP can be released across the plasma membrane into the extracellular medium through pannexin channels (D'Hondt et al., 2011). Pannexin-1 is an integral membrane glycoprotein that belongs to a family of proteins encoded by three genes in vertebrates (*Panx1*, *Panx2,* and *Panx3*). A widespread tissue distribution of Panx1 has been established, with highest levels found in skeletal muscle (Baranova et al., 2004).

Roles for Panx1 have been described in a variety of physiological and pathological processes including propagation of intercellular Ca^{2+} (Locovei, Wang, et al., 2006), afferent neurotransmission (Romanov et al., 2007), activation of the inflammasome (W. R. Silverman et al., 2009), recruitment of macrophages to apoptotic cells (Chekeni et al., 2010), pressure overload-induced fibrosis in the heart (Nishida et al., 2008) and ionic dysregulation during stroke-induced ischemic neuronal death (Thompson et al., 2006). Panx1 has also been shown to contribute to epileptic-form seizure activity (Thompson et al., 2008). The opening of Panx1 channel is essential to its function and any deregulation leading to uncontrolled opening may cause cell death (Thompson et al., 2006). Thus, a robust mechanism controlling the opening and closure of Panx1 is of vital importance to the cells. Along this line, Panx1 channels are known to be potentially activated by different stimuli like mechanical stress (L. Bao et al., 2004), elevation of intracellular [Ca^{2+}] (Locovei, Wang, et al., 2006), activation of P2Y purinergic receptors (Locovei, Wang, et al., 2006; Pelegrin & Surprenant, 2006) and ischemic or hypoxic conditions (Sridharan et al., 2010; Thompson et al., 2006). Despite the high level of expression of Panx1 in differentiated muscle, its role in this tissue has remained obscure until Panx1 was found to be involved in an interaction with the membrane protein $Ca_V1.1$ (Arias-Calderon et al., 2016; G. Jorquera et al., 2013).

$Ca_V1.1$ is the voltage sensor for skeletal muscle Excitation Contraction (EC) coupling. Upon membrane depolarization, it undergoes conformational changes that trigger the opening of Ryanodine Receptor 1 (RyR1) channels in the Sarcoplasmic Reticulum (SR) membrane, through protein-protein conformational coupling: this generates a rise in cytosolic [Ca^{2+}] that activates contraction (see(Rios & Pizarro, 1991; M. F. Schneider, 1994)). The coupling of Cav1.1 with RyR1 is a particular case because beyond the orthograde control that $Ca_V1.1$ exerts over RyR1 activity, there is also a retrograde control of $Ca_V1.1$ by RyR1

(Andronache et al., 2009; Bannister & Beam, 2009; Esteve et al., 2010; Nakai et al., 1996). These two proteins interact physically and functionally to make the robust complex that ensures EC coupling (Beam & Bannister, 2010; C. Paolini, J. D. Fessenden, I. N. Pessah, & C. Franzini-Armstrong, 2004a; Rebbeck et al., 2014; Rios & Brum, 1987; Samso, 2015).

$Ca_V1.1$ operates also as a voltage-gated Ca^{2+} channel responsible for a slow Ca^{2+} entry across the t-tubule membrane upon membrane depolarization (Rios & Pizarro, 1991; Tanabe et al., 1990). Although not essential for EC coupling (A. Dayal et al., 2017), there is evidence that this Ca^{2+} entry contributes to refilling of the SR Ca^{2+} store (Lee, Dagnino-Acosta, Yarotskyy, Hanna, Lyfenko, Knoblauch, Georgiou, Poche, et al., 2015; Robin & Allard, 2015) and that it is also coupled to CaMKII activation with consequent impact on downstream signaling pathways affecting muscle metabolism (Georgiou et al., 2015; Lee, Dagnino-Acosta, Yarotskyy, Hanna, Lyfenko, Knoblauch, Georgiou, Poche, et al., 2015).

A third role for $Ca_V1.1$ was demonstrated in recent years, as a trigger for activation of a frequency-dependent signaling cascade related to Excitation Transcription (ET) coupling, where $Ca_V1.1$ voltage-sensing activity is coupled to activation of ATP release out of the muscle cells through Panx1 channels after electrical stimulation, in a frequency-dependent manner (Arias-Calderon et al., 2016; Buvinic et al., 2009; G. Jorquera et al., 2013). Released ATP binds purinergic receptors which activate a signaling cascade responsible for changes in the transcriptional activity of genes involved in muscle plasticity. Moreover, electrical stimulation-dependent ATP release is practically absent in cultured muscle cells lacking $Ca_V1.1$, and the $Ca_V1.1$ blocker nifedipine completely abolishes both ATP release and transcriptional activity produced by a permissive frequency of electrical stimulation (ES) in adult muscle fibers (Casas et al., 2014; G. Jorquera et al., 2013). It has been shown that Panx1 is in close proximity to several proteins related to ET coupling, including $Ca_V1.1$ (Arias-Calderon et al., 2016; G. Jorquera et al., 2013) and P2Y2 (Arias-Calderon et al., 2016).

In the past years, knock-down or expression of mutated forms of other proteins has been shown to affect either $Ca_V1.1$ membrane expression and/or functional features of $Ca_V1.1$, as EC coupling. Notably, it has been stablished that, besides $Ca_V1.1$ and RyR1, β1a, Stac3 and junctophilin-2 are necessary for activation of EC coupling in skeletal muscle (Couchoux et al., 2007; Golini et al., 2011; Mosca et al., 2013; Perni, Lavorato, & Beam, 2017; Polster, Nelson, Olson, & Beam, 2016; N. Weiss et al., 2008). Other protein can also modulate $Ca_V1.1$ activity, like Cav3, JP-45 and junctophilin-1, altering either or both, calcium current

and activation of intracellular Ca^{2+} release (A. A. Anderson et al., 2006; N. Weiss et al., 2008).

In the present work, we propose that Panx1 belongs to the family of proteins that are functional interacting partners of $Ca_V1.1$, affecting its role in ET and EC coupling. Indeed, a reduction of Panx1 alters $Ca_V1.1$ Ca^{2+} channel properties, compromises the EC coupling function and impairs transcriptional activation of target genes after low frequency electrical stimulation of fully differentiated muscle fibers. Moreover, we show that Panx1 and $Ca_V1.1$ may also be reciprocal partners capable of mutually regulating their respective function, because a reduction in $Ca_V1.1$ content alters Panx1 proper control of ATP release and consequently affecting transcriptional activity also.

Materials and methods

Ethical approval

All experiments and procedures were conducted in accordance with the guidelines of the local animal ethics committee of the University of Chile, University Paris 06, University Claude Bernard Lyon 1, the French Ministry of Agriculture (decree 87/848) and the revised European Directive 2010/63/EU, and conform to the principles and regulations as described in the Editorial by Grundy (2015).

Down-expression of Pannexin-1 in muscle fibers

AAV-mCherry-U6-mPANX1-shRNA plasmid was obtained from Vector Biolabs. It targets a specific sequence of mouse Panx1 and has been validated for ~90% knockdown of mRNA in B16-F0 cells.

Exogenous expression by electroporation was performed in the *flexor digitorum brevis* (*fdb*) muscles of 6-7-week-old either Swiss OF1 (charge movement measurements) or BalbC (Ca^{2+} current and Ca^{2+} release measurements) male mice using a general procedure previously described (Legrand et al., 2008). Mice were anaesthetized either by isoflurane inhalation (3% in air, 300 $ml.min^{-1}$) using a commercial delivery system (Univentor 400 Anaesthesia Unit, Uninventor, Zejtun, Malta) or by intraperitoneal injection of a mix of 0.1 g/kg ketamine and 0.01 g/kg xylazine. Twenty-five microliters of a solution containing 2 mg/ml hyaluronidase dissolved in sterile saline were then injected into the footpads of each hind paw. Forty minutes later the mouse was re-anaesthetized using the same procedure as for hyaluronidase injection. A 20 µL volume of Tyrode solution containing 1µg/µL mCherry DNA was injected into the footpad of a

hind paw whereas the same volume of solution containing 1 µg/µL mCherry and 1µg/µL shRNA-Panx1 DNA was injected into the footpad of the contralateral hind paw. Following the injections, two gold-plated stainless-steel acupuncture needles connected to the electroporation apparatus were inserted under the skin, near the proximal and distal portion of the foot, respectively. The standard protocol used consisted in 20 pulses of 100 V/cm amplitude and 20 ms duration delivered at a frequency of 1 Hz by a BTX ECM 830 square wave pulse generator (Harvard Apparatus, Holliston, USA). Experimental observations and measurements were carried out 2 weeks later. Fibers positive for mCherry that were isolated from muscles co-transfected with mCherry and shRNA-Panx1 and from muscles transfected with solely mCherry are referred to as shRNA-Panx1 and corresponding control fibers, respectively.

Down-expression of $Ca_V1.1$ in muscle fibers

Down expression of α1s subunit of DHPR was achieved by a U7-exon skipping strategy using adenovirus-associated viral vectors (AAV-U7delα1s). Previously designed antisense sequence and control non-functional construct were used as described earlier (Pietri-Rouxel et al., 2010). In brief, adult C57/Black6 mice were anaesthetized with a mix of 0.1 g/kg ketamine and 0.01 g/kg xylazine. Two intramuscular injections in 24 h of a mixture containing AAV (U7-SA) and AAV (U7-ESE) were carried out in one footpad and the contra-lateral footpad was injected with the control AAV (U7-Ctrl). Experimental measurements were carried out 4 months later. Fibers isolated from muscles treated with the active AAV and with the non-functional construct are referred to as U7-exon skipped and corresponding control fibers, respectively.

Preparation of isolated muscle fibers for electrophysiology and Ca^{2+} measurements

Single fibers were isolated from the *flexor digitorium brevis* (fdb*)* muscles using a previously described procedure (Jacquemond, 1997). In brief, mice were killed by cervical dislocation before removal of the muscles. Muscles were treated with collagenase (Sigma, type 1) for 60 min at 37°C. Single fibers were then obtained by triturating the muscles within the experimental chamber. Fibers were dispersed on the glass bottom of a 50 mm wide culture µ-dish (Ibidi, München, Germany). Fibers were first partially insulated with silicone grease, as described previously (Jacquemond, 1997) so that only a portion of the fiber extremity was left out of the silicone. All experiments were performed at room temperature (20-22 °C).

Extracellular ATP measurement

50 µL of extracellular media aliquots from electrically stimulated or control fibers were removed at different times post-stimulation. ATP concentrations were measured with the CellTiter-Glo® Luminescent Cell Viability Assay (Promega, Madison, WI, USA), as reported (G. Jorquera et al., 2013). Data were calculated as pmol extracellular ATP/µg total RNA and the ratios between experimental versus control points were reported. Normalization by total RNA instead of total protein was chosen because adult muscle fibers were seeded on a matrigel coated surface (containing a large amount of protein), which may affect the protein determination associated to fibers only. Total RNA was obtained from skeletal muscle fibers employing Trizol reagent (Invitrogen, Corp., Carlsbad, CA, USA) according to manufacturer's protocol

Western Blot Analysis

Muscles were lysed in 60 µL of ice-cold lysis buffer (20 mM Tris-HCl, pH 7.4, 1% Triton X-100, 2 mM EDTA, 10 mM Na_3VO_4, 20 mM NaF, 10 mM sodium pyrophosphate, 150 mM NaCl, 1 mM PMSF and a protease inhibitor mixture). 30 µg of total protein from cell lysates were separated in 10% SDS-polyacrylamide gels and transferred to polyvinylidenedifluoride membranes (Millipore). Membranes were blocked at room temperature for 1 h in Tris-buffered Saline containing 3% fat-free milk, with or without 0.5% Tween 20, and then incubated overnight with the appropriate primary antibody. For $Ca_V1.1$, a mouse monoclonal antibody (1:2.000) from Abcam (ab2862) was used (Hu et al., 2015) (Hu *et al.*, 2015). For Panx-1, a rabbit polyclonal antibody (1:10.000) from Thermo Fisher Scientific (N°Cat: 487900) was used (Melhorn et al., 2013). alpha-actin (1:1000) from Sigma-Aldrich (a2066) (Mormeneo et al., 2012) or D-tubulin from Cell Signalling (11H10) (Gallot et al., 2017) were used as charge control for normalization of different lanes.
Membranes were incubated with the secondary antibody at room temperature for 1.5 h. The immunoreactive proteins were detected using ECL reagents according to the manufacturer's instructions. For loading control, membranes were stripped in buffer containing 0.2 M Glycine (pH 2) and 0.05% Tween 20, at room temperature for 30 min, blocked as previously, and assessed with the corresponding control antibody.

Electrophysiology

Whole-cell voltage-clamp experiments were performed: for measurements of DHPR Ca^{2+} current and intracellular Ca^{2+} transients in fibers expressing shRNA-Pnx1 and/or mCherry, an Axopatch 200B patch-clamp amplifier (Molecular Devices, Sunnyvale, CA) was used and data acquisition and command voltage pulse generation was achieved with a Digidata 1322A analog-digital, digital-analog converter (Axon Instruments, Foster City, CA) controlled by pClamp software (Axon Instruments). For measurements of DHPR Ca^{2+} current in fibers down-expressing $Ca_V1.1$, an RK-400 patch-clamp amplifier (Bio-Logic, Claix, France) was used in combination with a Digidata 1322A converter (Axon Instruments) controlled by pClamp software (Axon Instruments). For measurements of intracellular Ca^{2+} transients in fibers down-expressing $Ca_V1.1$ and for measurements of intramembrane charge movement in fibers expressing shRNA-Pnx1 and/or mCherry, an RK-400 patch-clamp amplifier (Bio-Logic, Claix, France) was used in combination with a BNC-2120 converter (National Instruments, Austin, TX) controlled by WinWCP software (University of Strathclyde, Glasgow, UK). Fibers were bathed in a TEA-containing extracellular solution (see Solutions). Voltage-clamp was performed with a micropipette filled with the intracellular-like solution (see Solutions). The tip of the micropipette was inserted through the silicone within the insulated part of the fiber and it was slightly crushed against the bottom of the chamber in order to decrease the access resistance. Analog compensation was adjusted to further decrease the effective series resistance. Membrane depolarizing steps were applied from a holding command potential of -80 mV. The $Ca_V1.1$ Ca^{2+} current was measured in response to 0.5 s-long depolarizing steps of increasing level. The linear leak component of the current was removed by subtracting the adequately scaled value of the steady current measured during a 20 mV hyperpolarizing step. Peak current values were normalized by the fiber capacitance. The voltage dependence of the peak current was fitted with the following equation:

$$I(V) = Gmax(V-Vrev)/(1+\exp(V0.5-V)/k]) \quad (1)$$

with *I(V)* the peak current density at the command voltage *V*, *Gmax* the maximum conductance, *Vrev* the apparent reversal potential, *V0.5* the half-activation potential and *k* the steepness factor. It should be stressed that Ca^{2+} current measurements designed to test the consequences of Pannexin-1 down expression and of CaV1.1 down-expression, respectively, were performed on muscle fibers from mice of different strains and age and under slightly differing conditions which explain the difference in current density between the two data groups.

Intramembrane charge movement currents were measured and analyzed according to previously described procedures (Collet et al., 2003; S. Pouvreau, Allard, Berthier, & Jacquemond, 2004). In brief,

adequately scaled control current records elicited by 50 ms-long hyperpolarizing pulses of 20 mV were subtracted from the current elicited by test depolarizing pulses of the same duration to various levels. In a few cases, test records were further corrected for a sloping baseline using previously described procedures (Horowicz & Schneider, 1981). The amount of charge moved during a test pulse was measured by integrating the *on* and *off a* portion of the corrected test current records. The calculated charge was normalized to the capacitance of the fiber. The steady-state distribution of the normalized charge was fitted with a two-state Boltzmann function: $Q(V)=Qmax/(1+\exp[(V0.5-V)/k])$ (2)

Qmax corresponding to the maximally available charge, *V0.5* to the voltage of equal charge distribution and *k* to the steepness factor.

Intracellular Ca^{2+} measurements

Voltage-activated Ca^{2+} transients in fibers expressing shRNA-Panx1 and/or mCherry were measured with the dye fluo-4: for this, muscle fibers were equilibrated for 30 minutes in the presence of 10 µM fluo-4 AM prior to establishing the silicone voltage-clamp conditions. Fluo-4 Ca^{2+} transients were measured with the line-scan mode (1.53 ms per line) of a Zeiss LSM 710 confocal microscope. The dye was excited with the 488 nm line of the argon laser and a 505-530 nm band pass filter was used on the detection channel. Fluo-4 Ca^{2+} transients were expressed as F/F0 where F0 is the background corrected baseline fluorescence. Voltage-activated Ca^{2+} transients in fibers down-expressing CaV1.1 and corresponding control fibers were measured with the dye indo-1 following previously described procedures (S. Pouvreau et al., 2004; N. Weiss et al., 2010). In brief, prior to voltage clamp, the Ca^{2+} sensitive dye indo-1 was introduced locally into the fiber by pressure microinjection through a micropipette containing 1 mM indo-1 dissolved in the intracellular-like solution (see Solutions). Fibers were then left for 1 h to allow for intracellular equilibration. Indo-1 fluorescence was measured on an inverted Nikon Diaphot epifluorescence microscope equipped with a commercial optical system allowing simultaneous detection of fluorescence at 405 nm (F405) and 485 nm (F485) by two photomultipliers (IonOptix, Milton, MA, USA), upon excitation at 360 nm. The standard ratio method was used to calculate $[Ca^{2+}]$ from R=F405/F485, with *in vivo* values for the calibration parameters Rmin, Rmax, KD and β determined as previously described (Jacquemond, 1997).

This same set-up and related procedures were also used to estimate the SR Ca^{2+} content in fibers expressing shRNA-Panx1 and/or mCherry using a method described by Al Qusairi et al., (2009). For this, muscle fibers were equilibrated for 30 minutes with the voltage-clamp pipette intracellular-like solution

also containing indo-1 and EGTA (see Solutions). Then, 50-ms-long depolarizing pulses from -80 to +10 mV were applied, before and after applying 50 µM cyclopiazonic acid (CPA) in the extracellular medium, using a thin polyethylene capillary perfusion system operating by gravity. The maximum change in baseline indo-1 saturation level following pulses delivered in the presence of CPA was taken as an index of the SR Ca^{2+} content.

Solutions

The standard intracellular-like solution used in the voltage-clamp pipette contained (in mM) 140 K-glutamate, 5 Na2-ATP, 5 Na2-phosphocreatine, 5.5 MgCl2, 5 glucose, 5 HEPES. For $Ca_V1.1$ Ca^{2+} current measurements in fibers expressing shRNA-Panx1 and/or mCherry, this solution also contained 20 mM EGTA. For the experiments aimed at estimating the SR Ca^{2+} content in fibers expressing shRNA-Panx1 and/or mCherry, the standard intracellular-like solution also contained containing 0.2 mM indo-1, 20 mM EGTA and 8 mM CaCl2. For intramembrane charge movement, the intra-pipette solution contained 140 TEA-methanesulfonate, 5 Na2-ATP, 5 Na2-phosphocreatine, 5.5 MgCl2, 5 glucose, 20 EGTA, 5 HEPES.
The standard extracellular solution contained (in mM) 140 TEA-methanesulfonate, 2.5 CaCl2, 2 MgCl2, 1 4-aminopyridine, 10 TEA-HEPES and 0.002 tetrodotoxin. For $Ca_V1.1$ Ca^{2+} current measurements in fibers down-expressing CaV1.1 and corresponding control fibers, the standard solution also contained EGTA-AM (5 µM). For Ca^{2+} measurements with fluo-4, 50 µM N-benzyl-p-toluene sulphonamide (BTS) was added to the standard solution. For intramembrane charge movement the extracellular solution contained 140 TEA-methanesulfonate, 0.1 CaCl2, 1 MnCl2, 1 CdCl2, 1 4-aminopyridine, 10 TEA-HEPES and 0.002 tetrodotoxin. All solutions were adjusted to pH 7.20.

Statistics

Statistical analysis was performed using Microcal Origin, version 8.0 (OriginLab Corp., Northampton, MA, USA) and GraphPad Prism 7. Least-squares fits were performed using a Marquardt-Levenberg algorithm routine included in Microcal Origin. Data values are presented as means ± S.E.M. for *n* fibers. Statistical differences were determined using a Student's t-test assuming significance for $P < 0.05$ (*$P < 0.05$, ** $P < 0.01$, *** $P < 0.005$, **** $P < 0.001$).

Results

Down-expression of $Ca_V1.1$ in adult muscle fibers alters the function of Pannexin-1

We have described that ATP release through Panx1 is activated by $Ca_V1.1$ at low frequencies of electrical stimulation in adult muscle fibers (Casas et al., 2010; G. Jorquera et al., 2013). In order to study a possible change in Panx1 activity induced by the loss of $Ca_V1.1$ in adult muscle, we used a model of down-expression of $Ca_V1.1$ taking advantage of a U7-exon skipping strategy (Pietri-Rouxel et al., 2010). In these muscles, we observed a reduction of 60% in protein levels of $Ca_V1.1$ (Fig. 1A). Importantly, in these fibers down-expressing $Ca_V1.1$, we observed increased basal levels of ATP release (Fig. 1B), indicating a deregulation of the normally closed configuration of Panx1 channel in resting conditions. Accordingly, the maintained increase in extracellular ATP levels, induced an increase in basal mRNA levels of the slow isoform of Troponin I (TnIs) and a decrease in mRNA levels of the fast isoform of this gene (TnIf) (Fig. 1D), a phenomenon previously seen in fibers stimulated with 20 Hz electrical stimulation (ES) or of fibers exposed to 30 µM external ATP (G. Jorquera et al., 2013). An extreme example of the absence of $Ca_V1.1$ is the mdg muscle cell, originally obtained from dysgenic mice not expressing $Ca_V1.1$. These cells showed to have increased values of basal ATP release compared to wild type myotubes and this release was inhibited by carbenoxolone (Fig 1C), indicating that ATP release occurs via Panx1 channels.

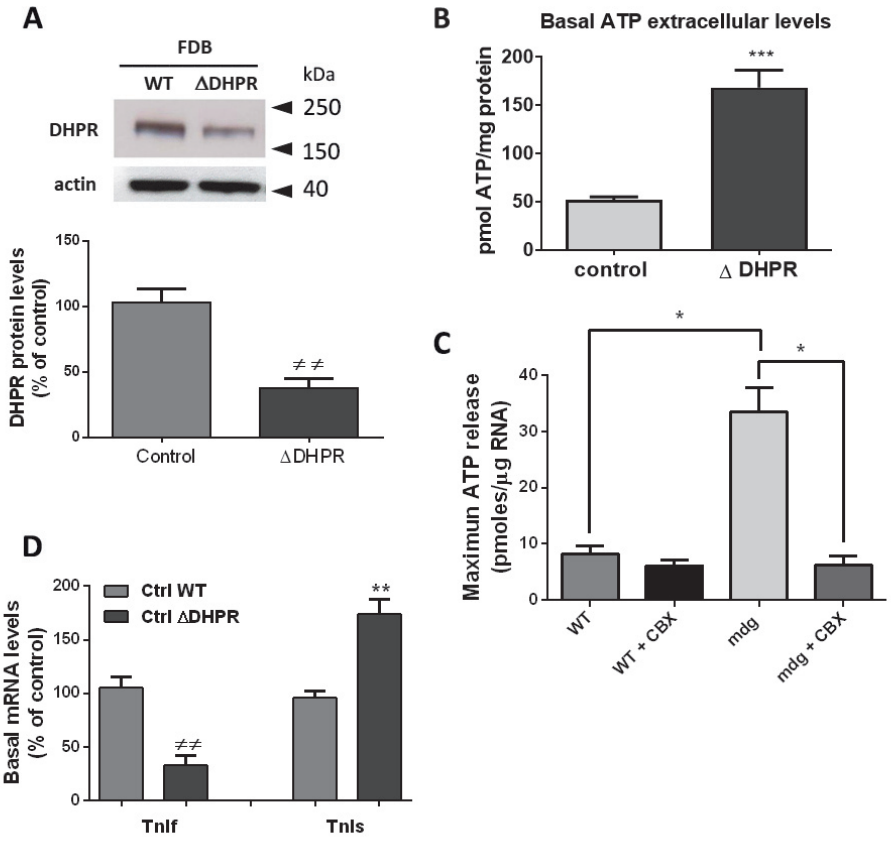

Figure 1. Leaky behavior of Pannexin-1 in adult muscle fibers down-expressing $Ca_V1.1$. *A,* $Ca_V1.1$ down-expression by U7-exon skipping strategy induces a reduction of more than 60% in $Ca_V1.1$ protein level: the top panel shows a representative blot image while quantification is shown at the bottom (n=3 muscles from distinct mice). *B*, increase by more than three times of the basal ATP release level in muscle fibers down-expressing $Ca_V1.1$ as compared to control ones. *C*, increase in extracellular ATP basal levels observed in myotubes lacking $Ca_V1.1$ (mdg) are suppressed by incubation of myotubes with 5µM of the specific Panx1 inhibitor Carbenoxolone (CBX). *D*, increased basal levels of mRNA for the slow isoform of TnI and decreased level for the fast isoform of TnI are observed in CaV1.1 knock-down muscles (n=4 distinct mice).

To check the functional consequences of $Ca_V1.1$ down-expression, voltage-activated Ca^{2+} current and cytosolic Ca^{2+} transients were measured in a separate set of muscle fibers from control and U7-exon treated muscles, 4 months following AAV transfection. Figure 2A shows representative Ca^{2+} current traces from a control fiber and from a U7-exon skipped fiber. Figure 2B shows the mean values for peak Ca^{2+} current density *versus* voltage in the two populations of fibers. Fitting the individual series of data points in each fiber with equation 1 gave mean values for *Gmax*, *Vrev*, *V0.5* and *k* of 234 ± 19 S/F, 68 ± 2 mV, 5 ± 1 mV, 6 ± 0.4 mV, and 166 ± 14 S/F, 69 ± 3 mV, 3 ± 1 mV, 5 ± 0.4 mV, in control (n=20) and U7-exon skipped

fibers (n=20), respectively (Fig. 2B, right panel). There was a significant ~30 % reduction in the maximal conductance in the U7-exon skipped fibers. The left panel in Figure 2C shows indo-1 Ca^{2+} transients from a control fiber and from a U7-exon skipped fiber obtained in response to depolarizing pulses from -80 to +10 mV of 20 ms duration. Resting [Ca^{2+}] level did not differ between the two groups of fibers (Fig. 2C, right). Also, fitting a single exponential function to the decay of the Ca^{2+} transients showed no significant difference in the mean values between control and U7-exon skipped fibers, suggesting that the Ca^{2+} removal capabilities of the fibers were unaffected (mean τ values were 48.2 ± 9 and 49.5 ± 13 ms in control and U7-exon treated fibers, respectively). Conversely, the peak [Ca^{2+}] level reached in response to a depolarizing pulse was significantly depressed in the U7exon skipped fibers, by 34 % (Fig. 2C, right). Altogether, these results establish a significant alteration of the Ca^{2+} channel and EC coupling activity of $Ca_V1.1$ in fibers treated with the active AAV. The fact that the relative depression in Ca^{2+} current density was lower than the decrease in protein level (Fig. 1A) was likely due to the use of different preparations of AAV in the two sets of experiments.

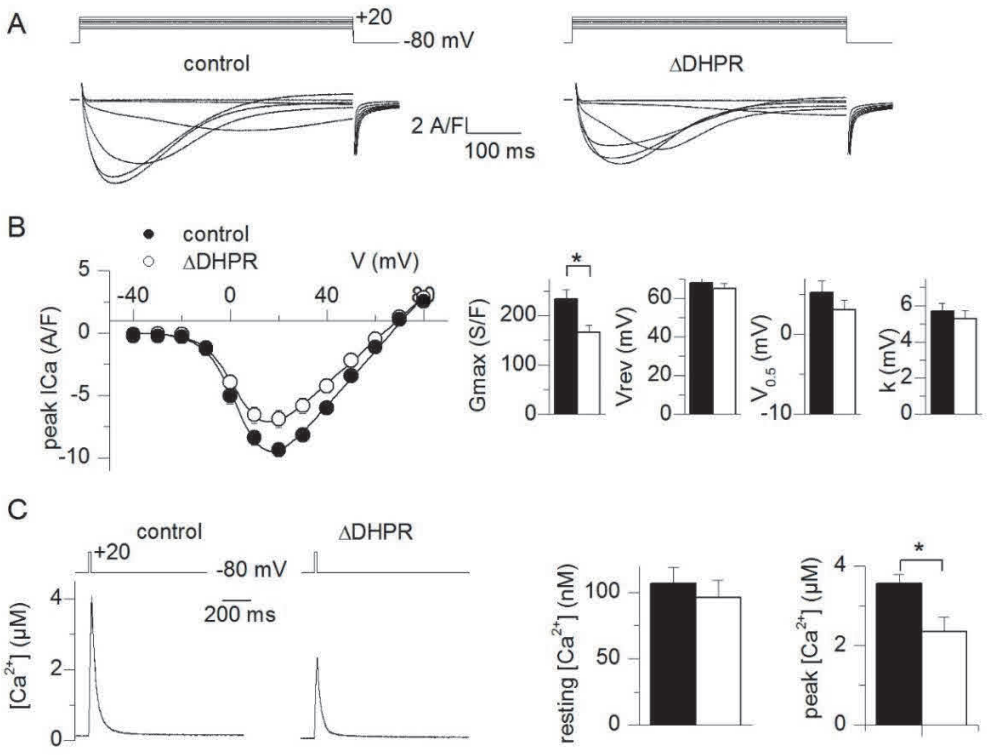

Figure 2. Reduced voltage-activated Ca^{2+} current and intracellular Ca^{2+} release in muscle fibers down-expressing $Ca_V1.1$

A, Ca^{2+} current records from a control fiber (left) and from a fiber down-expressing $Ca_V1.1$ (right). Currents were recorded in response to the voltage pulses shown on top. *B*, mean voltage-dependence of the peak

$Ca_V1.1$ Ca^{2+} current density in control fibers and in fibers down-expressing $Ca_V1.1$. Graphs on the right show corresponding mean values for the current-voltage parameters obtained by fitting individual series of data points with equation 1 (results are from 20 control fibers and 20 fibers down-expressing $Ca_V1.1$ from 3 mice). *C,* indo-1 Ca^{2+} transient elicited by a 20 ms-long depolarizing pulse to +10 mV in a control fiber and in a fiber down-expressing $Ca_V1.1$. Graphs on the right show corresponding mean values for resting and peak [Ca^{2+}] levels (results are from 14 control fibers and 14 fibers down-expressing $Ca_V1.1$ from 4 mice).

Down-expression of Pannexin-1 suppresses low frequency electrical stimulation-induced ATP release in adult muscle fibers

We first performed experiments to validate the Panx1 knock-down model. For this aim, we electroporated the AAV-mCherry-U6-mPANX1-shRNA plasmid (shPanx1) in the *fdb* muscles of mice. In order to distinguish the effects of Panx1 down-expression from possible consequences of electroporation and overexpression of a fluorescent protein, we electroporated a mCherry carrying plasmid in the muscle from the contralateral paw to use the corresponding fibers as controls. We waited for two weeks to evaluate levels of expression of Panx1 and the consequent disturbance of ATP release induced after electrical stimulation (ES) of fibers at 20 Hz (G. Jorquera et al., 2013). In Fig. 3A we show the expression of the mCherry reporter in muscles electroporated with the shPanx1 (carrying mCherry marker) and mCherry (alone) plasmid. We observed a broad level of fluorescence indicating expression of the fluorescent protein. Results in Fig. 3B (representative western blot and quantification of protein levels from 3 different preparations) show that Panx1 protein level had dropped by about 65% in muscles electroporated with the shPanx1 plasmid. This reduction in protein levels correlates with changes in ATP release in those fibers: in basal condition, extracellular ATP levels were significantly lower in shPanx1 expressing fibers compared with control ones (Fig. 3C upper graph). Importantly, the two peaks of ATP release observed after 20 Hz ES (G. Jorquera et al., 2013) were almost completely suppressed in shPanx1 expressing fibers (Fig. 3C lower graph). After 20 Hz electrical stimulation (ES) of control muscle fibers, there is an increase in mRNA levels of slow isoform of Troponin I (TnIs) and a decrease in mRNA levels of the fast isoform (TnIf) (Fig. 3 D) as previously published (G. Jorquera et al., 2013). Nevertheless, in fibers electroporated with the shPanx1 plasmid, the electrical stimuli failed to induce these transcriptional changes.

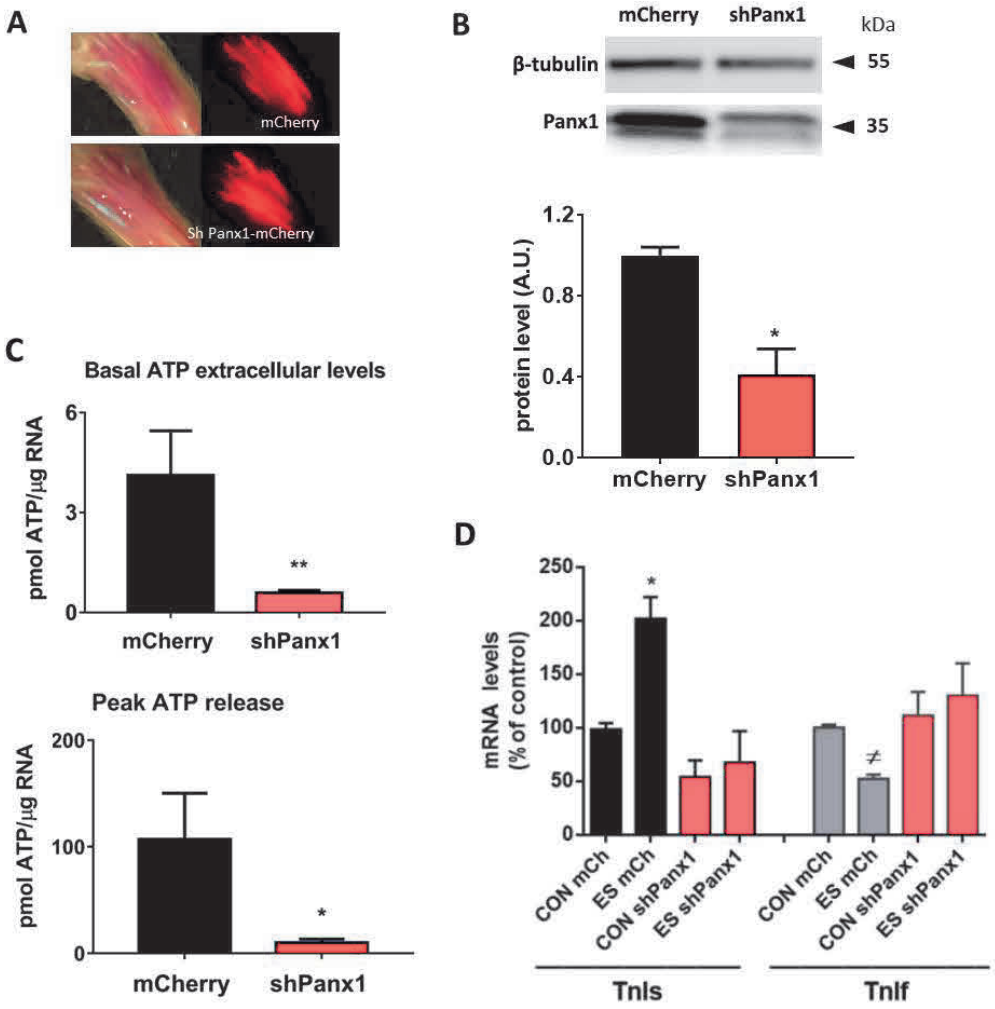

Figure 3. Down expression of Panx1 decreases basal and post-20 Hz electrical stimulation levels of extracellular ATP altering ES-dependent changes in gene expression. *A*, plasmid expression of an mCherry (upper panel) and shPanx1-mCherry (lower panel) as witnessed by the presence of mCherry in *fdb* electroporated muscles. The corresponding transmitted light images demonstrate broad expression of the plasmids. *B*, quantification of western blots against Panx1 shows that the shRNA against Panx1 reduces protein levels by ~65% (n=3 muscles from distinct mice). *C*, the reduction of Panx1 significantly decreases basal levels of extracellular ATP (top) and ES-activated ATP release (bottom) (n=5 plates from 3 distinct mice). *D*, 20 Hz electrical stimulation-related changes in mRNA levels of TnIs and TnIf are suppressed in fiber knock down for Panx1 (n=3).

Down-expression of Pannexin-1 alters Ca^{2+} current trough $Ca_V1.1$

We previously showed that pharmacological alteration of $Ca_V1.1$ activity is associated with an altered Panx1 function (G. Jorquera et al., 2013). In the present work, we looked for a possible involvement of Panx1 over $Ca_V1.1$ function. We first examined the Ca^{2+} channel activity of $Ca_V1.1$ in

voltage clamped fibers down-expressing Panx1, while mCherry expressing fibers were used as control, as described in Methods section. Mean values for the capacitance in the mCherry and in the shPanx1 groups of fibers in these experiments were 1.02 ± 0.14 and 1.22 ± 0.08 nF, respectively, statistically not different. Regarding the assess resistance, as explained in the Methods section, its value is minimized by crushing the tip of the voltage-clamp micropipette once it is inserted in the silicone-embedded portion of muscle fiber. In order to test for a possible difference in voltage-clamp kinetics between the two groups of fibers we fitted the decay of the capacitive transient elicited by a 20 mV hyperpolarizing voltage step with a double-exponential function. Mean values for the fast and slow time constants in the mCherry and in the shPanx1 groups were 0.77 ± 0.14 and 0.57 ± 0.09 ms, and 2.52 ± 0.22 and 3.14 ± 0.55, respectively, also not statistically different. Figure 4A shows Ca^{2+} current records from a control fiber and from a fiber transfected with the shPanx1 plasmid. Records were obtained in response to 0.5 s-long depolarizing pulses from -80 mV to levels ranging between -20 and +40 mV. The peak amplitude of the current was lower in the shPanx1 condition and the kinetics of the Ca^{2+} current also appeared slower. Figure 4B shows the mean peak current *versus* voltage relationship from measurements in 22 control fibers and 21 fibers expressing the shRNA against Panx1. Individual series of data points in each fiber were fitted with equation 1, mean corresponding values for the parameters are reported in Fig. 4C, showing a 27 % reduction in the maximal conductance in fibers expressing the shPanx1 as compared to mCherry expressing fibers, whereas other parameters were unchanged. In addition, the time to peak Ca^{2+} current was significantly increased in the shPanx1 fibers (Fig. 4D), suggesting that not only the Ca^{2+} conducting properties but also the current kinetics were altered by loss of Panx1. The spontaneous Ca^{2+} current decay during the large pulses also appeared slower in shPanx1 as compared to control fibers. As it was too slow to be fitted with a single exponential, we evaluated this parameter by counting the number of fibers yielding at least a half decrease of the peak current during the pulse to +20 mV. This corresponded to 81 % and 33 % of the control and shPanx1 fibers, respectively. Altogether, down-expression of Panx1 thus produced substantial alterations in $Ca_V1.1$ Ca^{2+} current properties, consistent with the possibility of reciprocal functional interactions between the two proteins. The size of both control and shPanx1 fibers Ca^{2+} currents is smaller than that shown in Fig. 2. This is due to the fact that eight-month-old C57/Bl6 mice were used for experiments described in that figure as compared to 6-7 weeks-old BalbC mice in Fig.4.

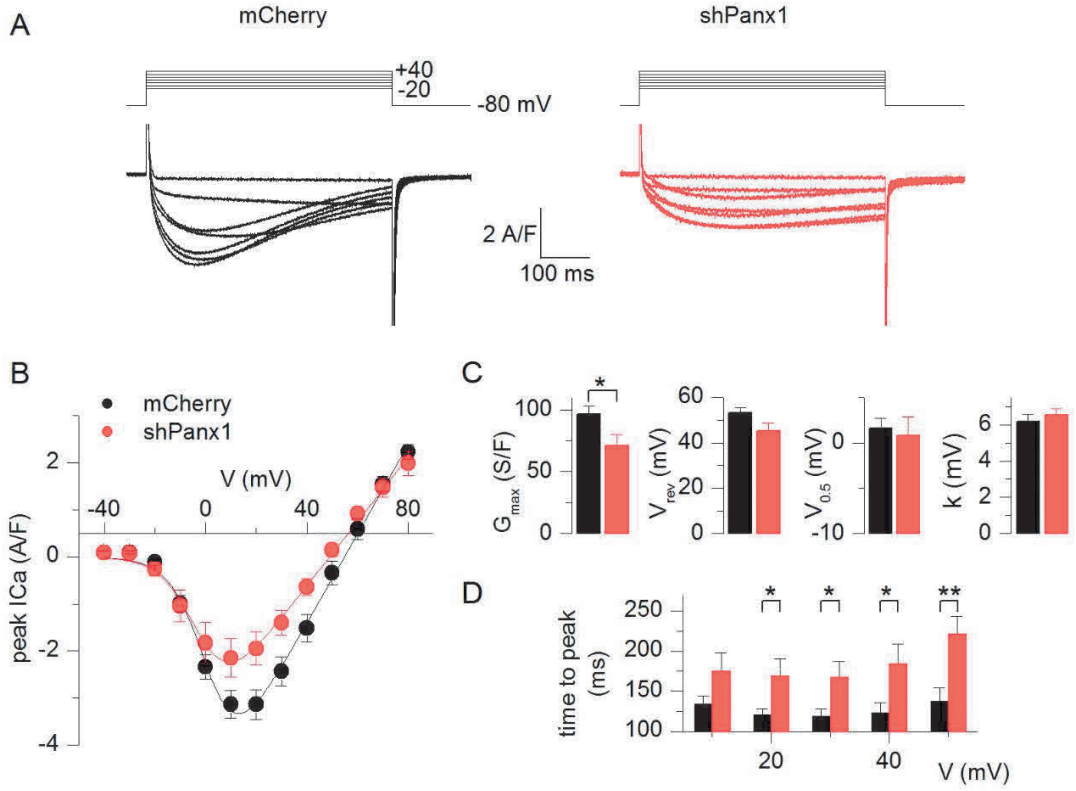

Figure 4. Reduced expression of Pannexin-1 alters Ca^{2+} current through $Ca_V1.1$. *A*, Ca^{2+} current records from a control fiber (left) and from a fiber down-expressing Panx1 (right). Currents were recorded in response to the voltage pulses shown on top. *B*, mean voltage-dependence of the peak $Ca_V1.1$ Ca^{2+} current density in control fibers and in fibers down-expressing Panx1. *C*, the corresponding mean values for the current-voltage parameters obtained by fitting individual series of data points with equation 1. *D*, mean values for the time to peak Ca^{2+} current in the two groups of fibers. Mean values for the capacitance in the mCherry and in the shPanx1 groups of fibers used were 1.02 ± 0.14 and 1.22 ± 0.08 nF (n = 22 control fibers from 3 distinct mice and 21 fibers expressing the shRNA against Panx1 from 4 distinct mice).

Down-expression of Pannexin-1 depresses voltage-activated SR Ca^{2+} release

One critical function of the $Ca_V1.1$ protein is its role in EC coupling. We addressed the issue of whether RyR1-mediated SR Ca^{2+} release would be altered in this condition of Panx1 down-expression. Figure 5A shows representative fluo-4 Ca^{2+} transients elicited by a train of short depolarizing pulses of increasing amplitude in a control (mCherry) and in a shPanx1 muscle fiber. While the overall qualitative time course of change in Ca^{2+} was similar in the two fibers, the peak amplitude of the Ca^{2+} signals was severely depressed at all voltages in the shPanx1 fiber. This was a reproducible feature as shown by the voltage-dependence of the mean values for peak rate of rise of fluo-4 Ca^{2+} transients in the two groups of fibers (Fig. 5B, n=17 and 21 control and shPanx1 fibers, respectively). Fitting a Boltzmann function to

the peak rate values *versus* voltage in each fiber gave the mean parameters shown in the first row of the right panel in Fig. 5B. There was a 60 % reduction in the maximum rate of rise of fluo-4 fluorescence in the shPanx1 fibers whereas the midpoint voltage and steepness factor were unchanged. The apparent time course of Ca^{2+} decay appeared unaffected in the shRNA-Panx1 fibers (Fig. 5A), suggesting that SERCA-mediated Ca^{2+} uptake was properly operating in this condition. To quantitatively appreciate the cytosolic Ca^{2+} removal capabilities of the fibers, we fitted a double exponential function to the decay of the Ca^{2+} transient after the end of the last depolarizing pulse of the protocol. The result from the fit is shown in blue superimposed to the traces in Fig. 5A. Mean values for the time constants did not differ between control and shRNA-Panx1 fibers but the final level was moderately but significantly depressed in the shPanx1 fibers (1.14 ± 0.04, as compared to 1.41 ± 0.07 in mCherry expressing fibers, bottom row in the right panel of Fig. 5B).

As the reduced peak amplitude of voltage activated Ca^{2+} transients in shPanx1 muscle fibers may result from altered RyR1 activity or from the depressed driving force for the Ca^{2+} exit because of reduced SR content, we test whether the SR Ca^{2+} content differ between control and shPanx1 fibers. We used a protocol consisting in measuring the saturation level of the Ca^{2+}-sensitive dye indo-1 in fibers loaded with a high concentration of EGTA and challenged with repeated depolarizing pulses in the presence of cyclopiazonic acid (CPA), so as to release the SR Ca^{2+} content into the cytosol (see Methods). The left panel in Figure 5C shows the time course of resting indo-1 saturation level in a control and in a shPanx1 muscle fiber during that protocol. The right panel shows corresponding mean values obtained from 12 controls and 12 shPanx1 muscle fibers, respectively. There was no significant difference between the two datasets. The SR Ca^{2+} content was estimated in each fiber from the difference between the initial resting indo-1 saturation level before CPA application and the level reached at the end of the protocol, assuming 10 mM free EGTA was present in the intracellular medium and that EGTA and indo-1 have the same affinity for Ca^{2+}. This gave mean SR Ca^{2+} content values of 1.03 ± 0.13 and 1.24 ± 0.13 mM in control and shPanx1 fibers, respectively.

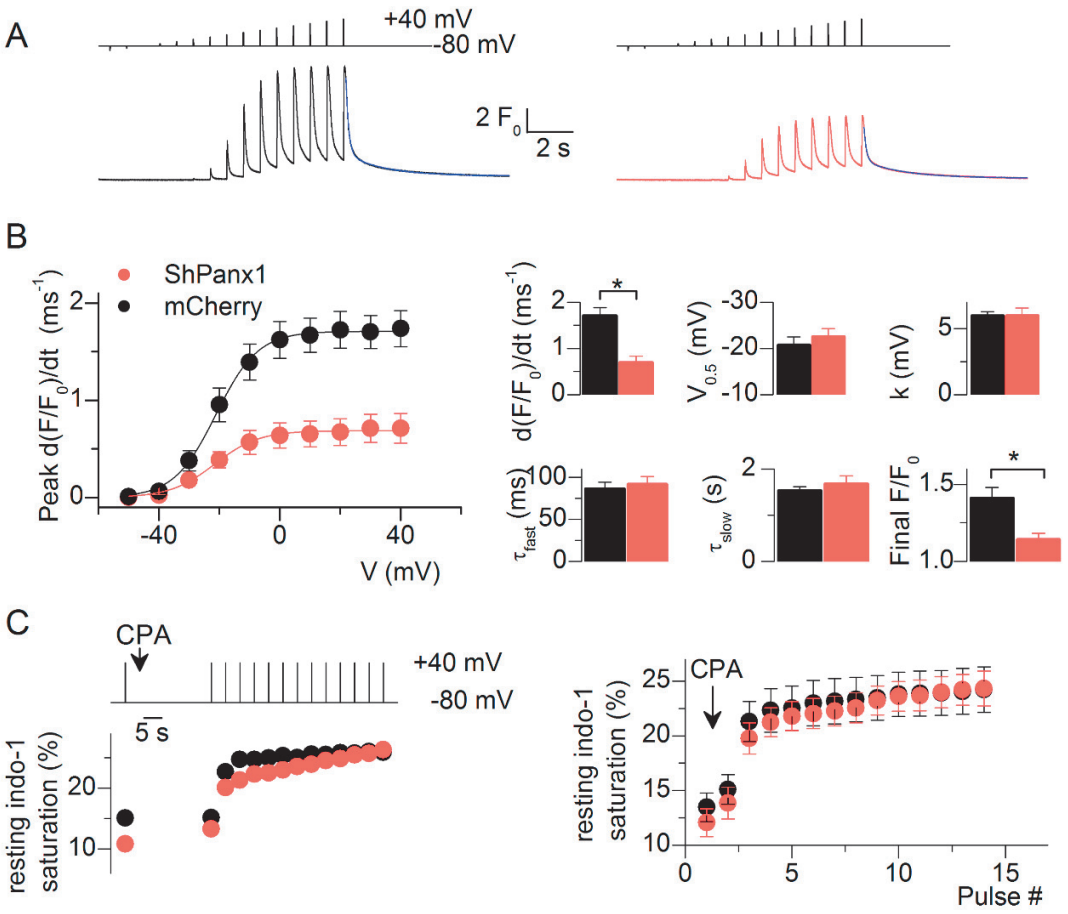

Figure 5. Reduced expression of Pannexin-1 drastically alters voltage-activated SR Ca^{2+} release. *A*, fluo-4 F/F_0 Ca^{2+} transients recorded from a control fiber (left) and from a fiber down-expressing Panx1 (right). Transients were recorded in response to the voltage protocol shown on top. The superimposed blue line at the end of the record corresponds to the result from fitting a double-exponential plus constant function to the decay of the signal. *B*, voltage-dependence of the mean peak rate of rising of fluo-4 fluorescence in control fibers and in fibers down-expressing Panx1. Graphs in the upper row on the right show corresponding values for the Boltzmann parameters obtained from fitting individual series of data points with equation 2. Graphs in the bottom row on the right show mean values obtained from fitting the double exponential plus constant function to the final decay of the Fluo-4 transient. *C*, estimation of the SR Ca^{2+} content: indo-1 resting saturation level was measured in control fibers and in fibers down-expressing Panx1 challenged by repeated depolarizing pulses in the presence of CPA. An example of the corresponding time course of change in indo-1 saturation in a fiber of each group is shown on the left. Mean values are shown on the right (n=12 fibers for both control and shPanx1 muscles from 4 distinct mice).

Intramembrane charge movement is not altered in fibers down-expressing Pannexin-1.

We tested whether the changes in $Ca_V1.1$ function induced by reduced Panx1 expression were paralleled by changes in $Ca_V1.1$ voltage-sensor properties. For this, the intramembrane charge movement

was compared between shPanx1 fibers and control fibers. Figure 6A shows representative traces of charge currents from a fiber of each group while Fig. 6B shows the mean voltage-dependence of the charge density from 11 and 16 control and shPanx1 fibers, respectively. Fitting individual series of data points in each fiber with equation 2 gave mean values presented in Fig. 6C for the Boltzmann parameters. There was no difference in any parameter between control and shRNA-Panx1 fibers demonstrating that down-expression of Panx1 did not affect the $Ca_V1.1$ intramembrane charge movement and also demonstrating that the decreased Ca^{2+} channel conductance reported in Fig. 4 was not the consequence of reduced CaV1.1 expression level.

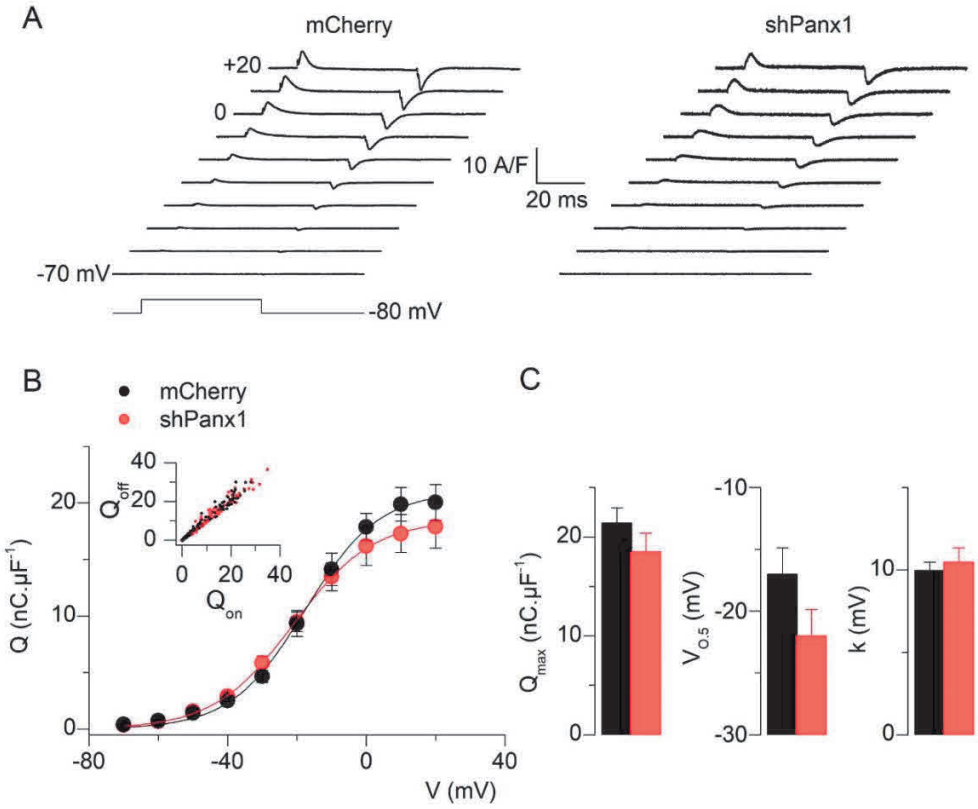

Figure 6. Expression of shRNA against Pannexin-1 does not alter intramembrane charge movements in fibers down-expressing Pannexin-1. *A*, illustrative traces of intramembrane charge current in a control fiber (left) and in a fiber down-expressing Panx1 (right). *B*, the voltage dependence of the mean amount of charge in control fibers and in fibers down-expressing Panx1. The inset shows the good equality between *on* and *off* charge. *C*, mean values for the parameters obtained from fitting a Boltzmann function to the individual series of data points (n=12 fibers for both control and shPanx1 muscles from 4 distinct mice).

Discussion

$Ca_V1.1$ plays an essential role in skeletal muscle and its regulation by interaction with partner proteins or protein complexes has shed light into the very exquisite manner it performs and regulates its functions. In the present work, we provide evidence for bidirectional interaction between $Ca_V1.1$ and Panx1. Control of Panx1 activity by $Ca_V1.1$ is involved in decoding the frequency of electrical activity and transducing it into transcriptional events crucial for muscle plasticity. In return, Panx1 now appears as a compulsory partner for proper function of $Ca_V1.1$ in EC coupling.

We demonstrate here that reduced levels of Panx1 protein alter $Ca_V1.1$ Ca^{2+} channel function and activation of voltage-dependent SR Ca^{2+} release. Altered CaV1.1 activity was not due to a reduced amount of the $Ca_V1.1$ protein in the t-tubule membrane as is the case, for instance, under conditions of down-expression of other proteins interacting with $Ca_V1.1$ and regulating its function (e.g. JP45 and junctophilin, (Golini et al., 2011; Yasuda et al., 2013)). Thus, changes in $Ca_V1.1$ channel activity and Ca^{2+} release must result from disruption of Panx1- $Ca_V1.1$ functional interaction and of proper organization and/or function of the $Ca_V1.1$-RyR1 interaction (EC coupling machinery), respectively. It is interesting to notice here, that there is not a simple correlation between change in $Ca_V1.1$ membrane content, changes in Ca^{2+} current and voltage-dependent SR Ca^{2+} release. By instance, in junctophilin1 deficient muscle cells, there is reduction ~ 60 % of peak amplitude of Ca^{2+} transients, without changes in Ca^{2+} currents or $Ca_V1.1$ membrane content (Nakada et al., 2018b). Also, in muscle fibers from JP45/CASQ1 double KO mice, there is no significant change in $Ca_V1.1$ membrane content, but there is a robust increase of 45% in the Ca^{2+} conductance (Gmax) compared to fibers from WT mice (Mosca et al., 2013). As proposed for other proteins, Panx1 could play a role in proper $Ca_V1.1$ tetrad formation. This is indeed a possibility as the functional phenotype combining reduction in $Ca_V1.1$ Ca^{2+} current and in SR Ca^{2+} release, together with preserved intramembrane charge movement, is reminiscent of what occurs either in the absence of RyR1(Nakai et al., 1996) or in the presence of a truncated form of the β_{1a} subunit of the DHPR (Eltit, Franzini-Armstrong, & Perez, 2014), both condition being associated with disorganization of the standard arrangement of $Ca_V1.1$s in tetrad arrays (Eltit et al., 2014; Protasi, Franzini-Armstrong, & Allen, 1998). Accordingly, it may be that loss of Panx1 also contributes to disentangle the arrays so as to affect both orthograde and retrograde $Ca_V1.1$-RyR1 signaling.

We previously showed that $Ca_V1.1$ activates ATP release upon 20 Hz electrical stimulation in adult muscle fibers, leading to the activation of a signaling cascade related to muscle plasticity (G. Jorquera et

al., 2013). Our present results demonstrate that, in addition to the control of $Ca_V1.1$ over Panx1, there is also a control of $Ca_V1.1$ by Panx1, through which Panx1 deficiency leads to dysfunction of $Ca_V1.1$ Ca^{2+} channel activity and of its effect in EC coupling. We must be cautious in that a direct physical interaction between $Ca_V1.1$ and Panx1, although is suggested by the experimental evidence (co-immuno precipitation, co-localization using proximity ligation assay, co-migration in the same protein complex) described in (Arias-Calderon et al., 2016; G. Jorquera et al., 2013) has not been fully demonstrated or molecularly mapped. The direct interaction may be the simplest explanation for our results, but we cannot exclude that other mechanisms/mutual interactions between $Ca_V1.1$ and Panx1, and/or between Ca^{2+} and ATP signaling also contribute to the effects we describe. Noteworthy, the functional interaction between $Ca_V1.1$ and Panx1 is important not only for activation of Panx1 following electrical activity. Indeed, in resting conditions, the interaction also controls basal levels of ATP release. We previously reported that dysgenic myotubes (lacking $Ca_V1.1$), have increased levels of extracellular ATP release in basal conditions (G. Jorquera et al., 2013).We now show that in these cells the high level of ATP release is due to Panx1 activity. Importantly, we also show that knock-down of $Ca_V1.1$ by a U7-exon skipping strategy in differentiated fibers also results in an increased resting level of ATP release and in altered expression of TnI isoforms. This suggests that, in these conditions, increased resting ATP release is sufficient to activate signaling pathways related to muscle plasticity in control muscle fibers.

Interestingly, in the mdx mouse model of Duchenne Muscular Dystrophy (DMD), increased levels of resting ATP release are also observed and are associated with activation of pro-apoptotic pathways (Valladares et al., 2013). In this model, there is then a loss of negative control of ATP release in resting conditions. Furthermore, mdx fibers also suffer from “uncoupling” between electrical stimulation and ATP release, also consistent with loss of control of $Ca_V1.1$ over Panx1 channels. The fact that the $Ca_V1.1$ blocker nifedipine improves the muscular function of mdx mice (Altamirano et al., 2013) highlights the importance of the above-mentioned interaction in this pathological muscle condition. Also, since there is evidence that Ca^{2+} release is depressed in mdx muscle fibers (Hollingworth, Zeiger, & Baylor, 2008; Woods et al., 2004), it could be speculated that this occurs, at least in part, as a consequence of the reduced interaction between $Ca_V1.1$ and Panx1.

As our experiments show no changes in SR Ca^{2+} content, maybe Panx1 absence disrupts $Ca_V1.1$ relationship with RyR1 by perturbing physical interaction between them. Panx1 may be a good candidate to study in other models of dystrophies because the loss of Panx1 causes a deficient depolarization induced Ca^{2+} release that could contribute to muscle weakness present in several muscle pathologies.

Altogether, $Ca_V1.1$-Panx1 interactions are essential for activation of gene transcription related to muscle plasticity, but they also may play an important role in certain muscle disorders, pointing to $Ca_V1.1$ as a potential target for the development of therapies. This latter point may also have important outcomes beyond the muscle field because of interaction between Panx1 and other Ca_V channels. $Ca_V1.2$ is present and functional in other tissues like lungs where it was found that Clevidipine, used to lower blood pressure, has an increased effect over $Ca_V1.2$ when Panx1 is present (G. P. Dahl et al., 2016). This may have an important clinical consequence because it would support the use of this dihydropyridine to reduce breathing problems and possibly also in the treatment of acute heart failure (G. P. Dahl et al., 2016). Thus, the functional interaction between Ca_V1 and Panx1 appears to be crucial not only for skeletal muscle but also for other tissues. Considering the widespread expression of Panx1 together with the presence of different members of the Ca_V family in heart, brain, and smooth muscle, we speculate that functional interaction between the two may be relevant in several physiological and pathological conditions.

Acknowledgements

We thank Jorge Hidalgo for his help in establishing and maintaining the electrophysiological set-up in Chile, and for helpful discussion and comments throughout the project. We thank Mónica Silva for providing isolated muscle fibers.

This work was supported by the Chilean-French cooperation program ECOS-Conicyt (#C13B01), by Fondecyt (grant #1151293 and postdoc # 3170194 to GJ), by Conicyt (fellowship #21130284 to J.T-G) and by grants from CNRS, INSERM, University Claude Bernard -Lyon 1 and the Association Française contre les Myopathies (AFM-Téléthon) to the Institut NeuroMyoGène.

Author contributions

Measurements of intramembrane charge movement (Fig. 6) and SR Ca^{2+} content (Fig. 5C) and of Ca^{2+} current and Ca^{2+} transients in muscle fibers down-expressing CaV1.1 (Fig. 2) were performed at Institut NeuroMyoGène, University Claude Bernard, Lyon 1. Measurements of DHPR protein level, ATP levels and gene expression in fibers down-expressing CaV1.1 (Fig. 1) were performed at Institut de Myologie, Université Paris 6. All other experiments were performed at the Muscle Physiology Laboratory, ICBM, University of Chile. Francisco Jaque, Gonzalo Jorquera, Mariana Casas (MC) and Vincent Jacquemond (VJ) performed experiments, analyzed results and assembled figures. Jennifer Troc-Gajardo, Sonja Buvinic, and Bruno Allard performed experiments and analyzed results. Christel Gentil performed experiments, France Pietri¬Rouxel contributed to design the experimental strategy, planned experiments and analyzed results. Enrique Jaimovich planned experiments, discussed results and revised the manuscript. MC and VJ designed the project, planned the experiments and wrote the manuscript. All authors approved the final version of the manuscript, agree to be accountable for all aspects of the work in ensuring that questions related to the accuracy or integrity of any part of the work are appropriately investigated and resolved. All persons designated as authors qualify for authorship, and all those who qualify for authorship are listed.

References

Altamirano, F., Valladares, D., Henriquez-Olguin, C., Casas, M., Lopez, J. R., Allen, P. D. and Jaimovich, E. (2013). "Nifedipine treatment reduces resting calcium concentration, oxidative and apoptotic gene expression, and improves muscle function in dystrophic mdx mice." PLoS One **8**(12): e81222.

Anderson, A. A., Altafaj, X., Zheng, Z., Wang, Z. M., Delbono, O., Ronjat, M., Treves, S. and Zorzato, F. (2006). "The junctional SR protein JP-45 affects the functional expression of the voltage-dependent Ca2+ channel Cav1.1." J Cell Sci **119**(Pt 10): 2145-2155.

Andronache, Z., Hamilton, S. L., Dirksen, R. T. and Melzer, W. (2009). "A retrograde signal from RyR1 alters DHP receptor inactivation and limits window Ca2+ release in muscle fibers of Y522S RyR1 knock-in mice." Proc Natl Acad Sci U S A **106**(11): 4531-4536.

Arias-Calderon, M., Almarza, G., Diaz-Vegas, A., Contreras-Ferrat, A., Valladares, D., Casas, M., Toledo, H., Jaimovich, E. and Buvinic, S. (2016). "Characterization of a multiprotein complex involved in excitation-transcription coupling of skeletal muscle." Skelet Muscle **6**: 15.

Bannister, R. A. and Beam, K. G. (2009). "Ryanodine modification of RyR1 retrogradely affects L-type Ca(2+) channel gating in skeletal muscle." J Muscle Res Cell Motil **30**(5-6): 217-223.

Bao, L., Locovei, S. and Dahl, G. (2004). "Pannexin membrane channels are mechanosensitive conduits for ATP." FEBS Lett **572**(1-3): 65-68.

Baranova, A., Ivanov, D., Petrash, N., Pestova, A., Skoblov, M., Kelmanson, I., Shagin, D., Nazarenko, S., Geraymovych, E., Litvin, O., Tiunova, A., Born, T. L., Usman, N., Staroverov, D., Lukyanov, S. and Panchin, Y. (2004). "The mammalian pannexin family is homologous to the invertebrate innexin gap junction proteins." Genomics **83**(4): 706-716.

Beam, K. G. and Bannister, R. A. (2010). "Looking for answers to EC coupling's persistent questions." J Gen Physiol **136**(1): 7-12.

Buvinic, S., Almarza, G., Bustamante, M., Casas, M., Lopez, J., Riquelme, M., Saez, J. C., Huidobro-Toro, J. P. and Jaimovich, E. (2009). "ATP released by electrical stimuli elicits calcium transients and gene expression in skeletal muscle." J Biol Chem **284**(50): 34490-34505.

Casas, M., Buvinic, S. and Jaimovich, E. (2014). "ATP signaling in skeletal muscle: from fiber plasticity to regulation of metabolism." Exerc Sport Sci Rev **42**(3): 110-116.

Casas, M., Figueroa, R., Jorquera, G., Escobar, M., Molgo, J. and Jaimovich, E. (2010). "IP(3)-dependent, post-tetanic calcium transients induced by electrostimulation of adult skeletal muscle fibers." J Gen Physiol **136**(4): 455-467.

Collet, C., Csernoch, L. and Jacquemond, V. (2003). "Intramembrane charge movement and L-type calcium current in skeletal muscle fibers isolated from control and mdx mice." Biophys J **84**(1): 251-265.

Corriden, R. and Insel, P. A. (2010). "Basal release of ATP: an autocrine-paracrine mechanism for cell regulation." Sci Signal **3**(104): re1.

Couchoux, H., Allard, B., Legrand, C., Jacquemond, V. and Berthier, C. (2007). "Loss of caveolin-3 induced by the dystrophy-associated P104L mutation impairs L-type calcium channel function in mouse skeletal muscle cells." J Physiol **580**(Pt.3): 745-754.

Chekeni, F. B., Elliott, M. R., Sandilos, J. K., Walk, S. F., Kinchen, J. M., Lazarowski, E. R., Armstrong, A. J., Penuela, S., Laird, D. W., Salvesen, G. S., Isakson, B. E., Bayliss, D. A. and Ravichandran, K. S. (2010). "Pannexin 1 channels mediate 'find-me' signal release and membrane permeability during apoptosis." Nature **467**(7317): 863-867.

D'Hondt, C., Ponsaerts, R., De Smedt, H., Vinken, M., De Vuyst, E., De Bock, M., Wang, N., Rogiers, V., Leybaert, L., Himpens, B. and Bultynck, G. (2011). "Pannexin channels in ATP release and beyond: an unexpected rendezvous at the endoplasmic reticulum." Cell Signal **23**(2): 305-316.

Dahl, G. P., Conner, G. E., Qiu, F., Wang, J., Spindler, E., Campagna, J. A. and Larsson, H. P. (2016). "High affinity complexes of pannexin channels and L-type calcium channel splice-variants in human lung: Possible role in clevidipine-induced dyspnea relief in acute heart failure." EBioMedicine **10**: 291-297.

Dayal, A., Schrotter, K., Pan, Y., Fohr, K., Melzer, W. and Grabner, M. (2017). "The Ca(2+) influx through the mammalian skeletal muscle dihydropyridine receptor is irrelevant for muscle performance." Nat Commun **8**(1): 475.

Eltit, J. M., Franzini-Armstrong, C. and Perez, C. F. (2014). "Amino acid residues 489-503 of dihydropyridine receptor (DHPR) beta1a subunit are critical for structural communication between the skeletal muscle DHPR complex and type 1 ryanodine receptor." J Biol Chem **289**(52): 36116-36124.

Esteve, E., Eltit, J. M., Bannister, R. A., Liu, K., Pessah, I. N., Beam, K. G., Allen, P. D. and Lopez, J. R. (2010). "A malignant hyperthermia-inducing mutation in RYR1 (R163C): alterations in Ca2+ entry, release, and retrograde signaling to the DHPR." J Gen Physiol **135**(6): 619-628.

Gallot, Y. S., McMillan, J. D., Xiong, G., Bohnert, K. R., Straughn, A. R., Hill, B. G. and Kumar, A. (2017). "Distinct roles of TRAF6 and TAK1 in the regulation of adipocyte survival, thermogenesis program, and high-fat diet-induced obesity." Oncotarget **8**(68): 112565-112583.

Georgiou, D. K., Dagnino-Acosta, A., Lee, C. S., Griffin, D. M., Wang, H., Lagor, W. R., Pautler, R. G., Dirksen, R. T. and Hamilton, S. L. (2015). "Ca2+ Binding/Permeation via Calcium Channel, CaV1.1, Regulates the Intracellular Distribution of the Fatty Acid Transport Protein, CD36, and Fatty Acid Metabolism." J Biol Chem **290**(39): 23751-23765.

Golini, L., Chouabe, C., Berthier, C., Cusimano, V., Fornaro, M., Bonvallet, R., Formoso, L., Giacomello, E., Jacquemond, V. and Sorrentino, V. (2011). "Junctophilin 1 and 2 proteins interact with the L-type Ca2+ channel dihydropyridine receptors (DHPRs) in skeletal muscle." J Biol Chem **286**(51): 43717-43725.

Hollingworth, S., Zeiger, U. and Baylor, S. M. (2008). "Comparison of the myoplasmic calcium transient elicited by an action potential in intact fibres of mdx and normal mice." J Physiol **586**(21): 5063-5075.

Horowicz, P. and Schneider, M. F. (1981). "Membrane charge moved at contraction thresholds in skeletal muscle fibres." J Physiol **314**: 595-633.

Hu, H., Wang, Z., Wei, R., Fan, G., Wang, Q., Zhang, K. and Yin, C. C. (2015). "The molecular architecture of dihydropyrindine receptor/L-type Ca2+ channel complex." Sci Rep **5**: 8370.

Jacquemond, V. (1997). "Indo-1 fluorescence signals elicited by membrane depolarization in enzymatically isolated mouse skeletal muscle fibers." Biophys J **73**(2): 920-928.

Jorquera, G., Altamirano, F., Contreras-Ferrat, A., Almarza, G., Buvinic, S., Jacquemond, V., Jaimovich, E. and Casas, M. (2013). "Cav1.1 controls frequency-dependent events regulating adult skeletal muscle plasticity." J Cell Sci **126**(Pt 5): 1189-1198.

Lee, C. S., Dagnino-Acosta, A., Yarotskyy, V., Hanna, A., Lyfenko, A., Knoblauch, M., Georgiou, D. K., Poche, R. A., Swank, M. W., Long, C., Ismailov, II, Lanner, J., Tran, T., Dong, K., Rodney, G. G., Dickinson, M. E., Beeton, C., Zhang, P., Dirksen, R. T. and Hamilton, S. L. (2015). "Ca(2+) permeation and/or binding to CaV1.1 fine-tunes skeletal muscle Ca(2+) signaling to sustain muscle function." Skelet Muscle **5**: 4.

Legrand, C., Giacomello, E., Berthier, C., Allard, B., Sorrentino, V. and Jacquemond, V. (2008). "Spontaneous and voltage-activated Ca2+ release in adult mouse skeletal muscle fibres expressing the type 3 ryanodine receptor." J Physiol **586**(2): 441-457.

Locovei, S., Wang, J. and Dahl, G. (2006). "Activation of pannexin 1 channels by ATP through P2Y receptors and by cytoplasmic calcium." FEBS Lett **580**(1): 239-244.

Melhorn, M. I., Brodsky, A. S., Estanislau, J., Khoory, J. A., Illigens, B., Hamachi, I., Kurishita, Y., Fraser, A. D., Nicholson-Weller, A., Dolmatova, E., Duffy, H. S. and Ghiran, I. C. (2013). "CR1-mediated ATP release by human red blood cells promotes CR1 clustering and modulates the immune transfer process." J Biol Chem **288**(43): 31139-31153.

Mormeneo, E., Jimenez-Mallebrera, C., Palomer, X., De Nigris, V., Vazquez-Carrera, M., Orozco, A., Nascimento, A., Colomer, J., Lerin, C. and Gomez-Foix, A. M. (2012). "PGC-1alpha induces mitochondrial and myokine transcriptional programs and lipid droplet and glycogen accumulation in cultured human skeletal muscle cells." PLoS One **7**(1): e29985.

Mosca, B., Delbono, O., Laura Messi, M., Bergamelli, L., Wang, Z. M., Vukcevic, M., Lopez, R., Treves, S., Nishi, M., Takeshima, H., Paolini, C., Martini, M., Rispoli, G., Protasi, F. and Zorzato, F. (2013). "Enhanced dihydropyridine receptor calcium channel activity restores muscle strength in JP45/CASQ1 double knockout mice." Nat Commun **4**: 1541.

Nakada, T., Kashihara, T., Komatsu, M., Kojima, K., Takeshita, T. and Yamada, M. (2018). "Physical interaction of junctophilin and the CaV1.1 C terminus is crucial for skeletal muscle contraction." Proc Natl Acad Sci U S A **115**(17): 4507-4512.

Nakai, J., Dirksen, R. T., Nguyen, H. T., Pessah, I. N., Beam, K. G. and Allen, P. D. (1996). "Enhanced dihydropyridine receptor channel activity in the presence of ryanodine receptor." Nature **380**(6569): 72-75.

Nishida, M., Sato, Y., Uemura, A., Narita, Y., Tozaki-Saitoh, H., Nakaya, M., Ide, T., Suzuki, K., Inoue, K., Nagao, T. and Kurose, H. (2008). "P2Y6 receptor-Galpha12/13 signalling in cardiomyocytes triggers pressure overload-induced cardiac fibrosis." EMBO J **27**(23): 3104-3115.
Paolini, C., Fessenden, J. D., Pessah, I. N. and Franzini-Armstrong, C. (2004). "Evidence for conformational coupling between two calcium channels." Proc Natl Acad Sci U S A **101**(34): 12748-12752.
Pelegrin, P. and Surprenant, A. (2006). "Pannexin-1 mediates large pore formation and interleukin-1beta release by the ATP-gated P2X7 receptor." EMBO J **25**(21): 5071-5082.
Perni, S., Lavorato, M. and Beam, K. G. (2017). "De novo reconstitution reveals the proteins required for skeletal muscle voltage-induced Ca(2+) release." Proc Natl Acad Sci U S A **114**(52): 13822-13827.
Pietri-Rouxel, F., Gentil, C., Vassilopoulos, S., Baas, D., Mouisel, E., Ferry, A., Vignaud, A., Hourde, C., Marty, I., Schaeffer, L., Voit, T. and Garcia, L. (2010). "DHPR alpha1S subunit controls skeletal muscle mass and morphogenesis." EMBO J **29**(3): 643-654.
Polster, A., Nelson, B. R., Olson, E. N. and Beam, K. G. (2016). "Stac3 has a direct role in skeletal muscle-type excitation-contraction coupling that is disrupted by a myopathy-causing mutation." Proc Natl Acad Sci U S A **113**(39): 10986-10991.
Pouvreau, S., Allard, B., Berthier, C. and Jacquemond, V. (2004). "Control of intracellular calcium in the presence of nitric oxide donors in isolated skeletal muscle fibres from mouse." J Physiol **560**(Pt 3): 779-794.
Protasi, F., Franzini-Armstrong, C. and Allen, P. D. (1998). "Role of ryanodine receptors in the assembly of calcium release units in skeletal muscle." J Cell Biol **140**(4): 831-842.
Rebbeck, R. T., Karunasekara, Y., Board, P. G., Beard, N. A., Casarotto, M. G. and Dulhunty, A. F. (2014). "Skeletal muscle excitation-contraction coupling: who are the dancing partners?" Int J Biochem Cell Biol **48**: 28-38.
Rios, E. and Brum, G. (1987). "Involvement of dihydropyridine receptors in excitation-contraction coupling in skeletal muscle." Nature **325**(6106): 717-720.
Rios, E. and Pizarro, G. (1991). "Voltage sensor of excitation-contraction coupling in skeletal muscle." Physiol Rev **71**(3): 849-908.
Robin, G. and Allard, B. (2015). "Voltage-gated Ca(2+) influx through L-type channels contributes to sarcoplasmic reticulum Ca(2+) loading in skeletal muscle." J Physiol **593**(21): 4781-4797.
Romanov, R. A., Rogachevskaja, O. A., Bystrova, M. F., Jiang, P., Margolskee, R. F. and Kolesnikov, S. S. (2007). "Afferent neurotransmission mediated by hemichannels in mammalian taste cells." EMBO J **26**(3): 657-667.
Samso, M. (2015). "3D Structure of the Dihydropyridine Receptor of Skeletal Muscle." Eur J Transl Myol **25**(1): 4840.
Schneider, M. F. (1994). "Control of calcium release in functioning skeletal muscle fibers." Annu Rev Physiol **56**: 463-484.
Silverman, W. R., de Rivero Vaccari, J. P., Locovei, S., Qiu, F., Carlsson, S. K., Scemes, E., Keane, R. W. and Dahl, G. (2009). "The pannexin 1 channel activates the inflammasome in neurons and astrocytes." J Biol Chem **284**(27): 18143-18151.
Sridharan, M., Adderley, S. P., Bowles, E. A., Egan, T. M., Stephenson, A. H., Ellsworth, M. L. and Sprague, R. S. (2010). "Pannexin 1 is the conduit for low oxygen tension-induced ATP release from human erythrocytes." Am J Physiol Heart Circ Physiol **299**(4): H1146-1152.
Tanabe, T., Beam, K. G., Adams, B. A., Niidome, T. and Numa, S. (1990). "Regions of the skeletal muscle dihydropyridine receptor critical for excitation-contraction coupling." Nature **346**(6284): 567-569.
Thompson, R. J., Jackson, M. F., Olah, M. E., Rungta, R. L., Hines, D. J., Beazely, M. A., MacDonald, J. F. and MacVicar, B. A. (2008). "Activation of pannexin-1 hemichannels augments aberrant bursting in the hippocampus." Science **322**(5907): 1555-1559.
Thompson, R. J., Zhou, N. and MacVicar, B. A. (2006). "Ischemia opens neuronal gap junction hemichannels." Science **312**(5775): 924-927.
Valladares, D., Almarza, G., Contreras, A., Pavez, M., Buvinic, S., Jaimovich, E. and Casas, M. (2013). "Electrical stimuli are anti-apoptotic in skeletal muscle via extracellular ATP. Alteration of this signal in Mdx mice is a likely cause of dystrophy." PLoS One **8**(11): e75340.
Weiss, N., Couchoux, H., Legrand, C., Berthier, C., Allard, B. and Jacquemond, V. (2008). "Expression of the muscular dystrophy-associated caveolin-3(P104L) mutant in adult mouse skeletal muscle specifically alters the Ca(2+) channel function of the dihydropyridine receptor." Pflugers Arch **457**(2): 361-375.

Weiss, N., Legrand, C., Pouvreau, S., Bichraoui, H., Allard, B., Zamponi, G. W., De Waard, M. and Jacquemond, V. (2010). "In vivo expression of G-protein beta1gamma2 dimer in adult mouse skeletal muscle alters L-type calcium current and excitation-contraction coupling." J Physiol **588**(Pt 15): 2945-2960.

Woods, C. E., Novo, D., DiFranco, M. and Vergara, J. L. (2004). "The action potential-evoked sarcoplasmic reticulum calcium release is impaired in mdx mouse muscle fibres." J Physiol **557**(Pt 1): 59-75.

Yasuda, T., Delbono, O., Wang, Z. M., Messi, M. L., Girard, T., Urwyler, A., Treves, S. and Zorzato, F. (2013). "JP-45/JSRP1 variants affect skeletal muscle excitation-contraction coupling by decreasing the sensitivity of the dihydropyridine receptor." Hum Mutat **34**(1): 184-190.

Section 1.2.

EFFECTS OF THE PANX1 PHARMACOLOGICAL BLOCKERS: CARBENOXOLONE AND PROBENCID ON EXCITATION-CONTRACTION COUPLING IN ADULT SKELETAL MUSCLE FIBERS

Article 2: Francisco Jaque-Fernandez, Bruno Allard, Aude Lafoux, Corinne Huchet, Enrique Jaimovich, Mariana Casas, Christine Berthier, and Vincent Jacquemond « Probenecid affects ryanodine-receptor function and force production in skeletal muscle » (Manuscript in preparation).

This study was prompted by the results described in the first manuscript (Section1.1.) that provided evidence for a bidirectional functional interaction between $Ca_V1.1$ and Panx1 channels. Because we proved that down-expression of Panx1 alters ECC in differentiated muscle fibers, we postulated that pharmacological alteration of Panx1 functional state may also affect ECC.

Of specific additional interest in regard to this issue was that two of the most widely used Panx1 blockers: carbenoxolone (CBX) and probenecid (PROB), have been used in patients for the treatments of different pathological conditions. CBX has been used for the treatment of digestive tract ulcers and PROB has been widely used in the treatment of gout and also for maintaining antibiotics blood levels. The possibility that Panx1 inhibitors would alter ECC could then raise the relevant question of possible effects on whole muscle function in the living organism.

We tested two different conditions for studying the effect of Panx1 inhibitors on ECC: 1) a 30 minutes exposure of isolated muscle fibers to either 100 µM Carbenoxolone or 1mM Probenecid before assessing ECC function; these concentration levels produce a similar inhibitory effect on Panx1-mediated ATP release (Patel et al., 2014; Michalski et al., 2016), 2) continuous assessment of ECC function while transiently exposing muscle fibers to 1 mM of Probenecid.

ECC function was assessed in enzymatically isolated mouse muscle fibers under a combination of silicone voltage-clamp conditions and intracellular Ca^{2+} imaging with the dye rhod-2 (Pouvreau et al., 2006; Lefebvre et al., 2011), allowing characterization of the voltage-dependence of RyR1-dependent SR Ca^{2+} release. For this, we used line-scan confocal microscopy combined with a protocol of stimulation consisting of depolarizing pulses of 0.5 s-long of increasing amplitude from -80 mV.

For the acute effect of probenecid, we used the same conditions with a protocol of stimulation consisting of series of 200 ms-long pulses to -20 mV, 0 mV, and +20 mV delivered first in the control

condition, then in the presence of probenecid, and then after probenecid wash. A group of fibers challenged with the same protocol with no probenecid application was used as control.

Finally, in order to assess the physiological outcome of our results in terms of force production, we tested the efficiency of probenecid on Extensor Digitalis Longus (EDL) in vitro tetanic contraction.

Probenecid and carbenoxolone affect SR Ca^{2+} release

We found that muscle fibers exposed for 30 minutes to probenecid and carbenoxolone exhibit a ≈40% and >70% decrease in maximum SR Ca^{2+} release. These are severe effects, very likely to affect force production and whole muscle function, quite unexpected considering that ECC is a quite secure process, known so far to be affected by a limited number of pharmacological or toxic agents. The protocol of transient application of probenecid confirmed the alteration of peak SR Ca^{2+} release, but also revealed that one immediate effect of the drug was to increase resting Ca^{2+}. This was not associated with a reproducible increase in plasma membrane conductance and the effect persisted in the absence of extracellular calcium, meaning that an intracellular Ca^{2+} source is involved, most likely the SR considering the substantial amplitude of the Ca^{2+} rise. This probenecid-induced SR Ca^{2+} leak likely either contributes to, or is the major determinant of, -the reduced peak amplitude of voltage-activated SR Ca^{2+} release, through SR lumen Ca^{2+} depletion.

Altogether, even though the underlying molecular mechanisms are not identified, results demonstrate that Panx1 blockers alter resting Ca^{2+} homeostasis and voltage-activated SR Ca^{2+} release.

Probenecid reduces whole muscle tetanic force in vitro

As mentioned above, Panx1 blockers have been used as therapeutic agents. Thus, our results showing their potency to affect Ca^{2+} homeostasis prompted us to test whether muscle contraction is affected. This part of the project was made in collaboration with Corinne Huchet and Aude Lafoux at the Therassay core facility of University of Nantes. There, the effect of probenecid was tested on whole mouse EDL muscle tetanic force evaluated in vitro. The protocol consisted in tetanic trains of electrical stimulation at 60 Hz of 500 ms duration delivered every 15 minutes. The peak tetanic force (normalized by the muscle weight) suffered a progressive decrease in maximal amplitude in the presence of probenecid, as compared to the control condition. On average, there was a 60 % decrease in tetanic force after 45 minutes in the muscles challenged with probenecid, whereas the corresponding decrease in the control group was of 10 %.

Interestingly also, after 30 minutes of exposure to probenecid, there was also a substantial increase in resting tension that became more prominent after 45 minutes exposure to the drug. We anticipate that the probenecid-increased resting Ca^{2+} underlies this effect.

Altogether we provide here consistent data demonstrating that probenecid depresses muscle contraction by affecting SR Ca^{2+} homeostasis.

Conclusions

The Panx1 blockers carbenoxolone and probenecid, strongly decrease RyR1-dependent SR Ca^{2+} release in differentiated mouse muscle fibers. Although these drugs (and specifically probenecid) have several molecular targets, we believe that Panx1 is the most likely to be involved in these effects, further supporting the hypothesis of a regulation from Panx1 either to $Ca_V1.1$, or RyR1 or the interaction between the two within the ECC machinery. Even though the precise molecular mechanism remains undefined at this point, an important outcome, further strengthened by our concurrent data on whole muscle contraction, is the potential physiopathological importance of these results. Indeed, because Panx1 blockers have already been used in clinic (and incidentally probenecid was also used as a masking agent for doping in sport) with new therapeutic applications having been recently highlighted, our results should be taken as a warning with respect to possible adverse effects on muscle function.

Probenecid affects sarcoplasmic reticulum Ca^{2+} release and depresses contractile activation in skeletal muscle

Francisco Jaque-Fernandez[1], Bruno Allard[1], Aude Lafoux[2], Corinne Huchet[2] [3], Enrique Jaimovich[4], Mariana Casas[4], Christine Berthier[1], and Vincent Jacquemond[1]

[1] Univ Lyon, Université Claude Bernard Lyon 1, CNRS UMR-5310, INSERM U-1217, Institut NeuroMyoGène, 8 avenue Rockefeller, 69373 Lyon, France.

[2] Therassay Platform, CAPACITES, Université de Nantes, Nantes, France.

[3] Nantes Gene Therapy Laboratory, Université de Nantes, INSERM UMR 1089, Nantes, France.

[4] Centro de Estudios Moleculares de la Célula, Instituto de Ciencias Biomédicas, Facultad de Medicina, Universidad de Chile, Santiago, Chile.

Short title: Probenecid-induced muscle weakness

Corresponding author:

Vincent Jacquemond

Institut NeuroMyoGène

UMR CNRS 5310 - INSERM U1217 - Université Claude Bernard Lyon 1

Faculté de Médecine et de Pharmacie

8, Avenue Rockefeller, 69373 Lyon, France

Tel. (33) 4 26 68 82 69

E-mail : vincent.jacquemond@univ-lyon1.fr

ORCID iD : 0000-0003-4944-270X

Key words: skeletal muscle, excitation-contraction coupling, ryanodine receptor, sarcoplasmic reticulum Ca^{2+} release, pannexin.

Abstract

Tight control of sarcoplasmic reticulum (SR) Ca^{2+} release and resultant contractile activation in skeletal muscle fibers, is secured by the excitation-contraction coupling (ECC) protein complex. This molecular machinery allows the plasma membrane voltage to tune the activity of the type 1 ryanodine receptor (RyR1) Ca^{2+} release channel in the SR membrane. We report here that the prescription drug probenecid affects intracellular Ca^{2+} handling and ECC: acute application of probenecid on isolated mouse muscle fibers generates a rise in resting cytosolic Ca^{2+}, accompanied by a depression of voltage-activated Ca^{2+} release through RyR1. On average, muscle fibers incubated for 30 min in the presence of probenecid exhibited a 40 % reduction in the peak rate of voltage-activated SR Ca^{2+} release. Application of probenecid on electrically-stimulated whole mouse muscle induced a >50 % reduction of peak tetanic force accompanied by a slight rise in resting tension. Carbenoxolone also produced a major reduction of voltage-activated SR Ca^{2+} release, consistent with the effect of the two drugs being mediated by their common target, the membrane channel protein pannexin. Results provide evidence for functional interactions between pannexin and the muscle ECC molecular machinery. Furthermore, because probenecid has been used both in the clinic and as a masking agent for doping in sport, our results raise the issues of -whether potential adverse muscular effects may have been overlooked, and -whether probenecid-induced altered Ca^{2+} homeostasis may be shared by other tissues that are therapeutic targets of the drug.

Introduction

Skeletal muscle contraction and relaxation are determined by RyR1-mediated SR Ca^{2+} release and sarco-endoplasmic reticulum Ca^{2+}-ATPase (SERCA)-mediated SR Ca^{2+} re-uptake, respectively. RyR1 channel activity is under the control of the plasma membrane voltage through interactions with the $Ca_V1.1$ voltage-sensor; this molecular partnership constitutes the core of the ECC machinery (Rebbeck et al., 2014; Hernandez-Ochoa et al., 2018; Rios, 2018). ECC is a very secure process and there is actually a limited number of known pharmacological agents that can modify or disrupt its function so as to alter muscle force production in the intact organism (see Mackrill, 2010). Still, the possibility cannot be excluded that adverse effects of certain therapeutically-approved molecules in the form of weakness and/or fatigue, are related to alteration of Ca^{2+} homeostasis and ECC.

Pannexins correspond to a family of three plasma membrane channel proteins (Panx1, 2, 3), Panx1 is so far the best characterized. It is ubiquitously expressed and exhibits a large, poorly selective pore allowing small molecules, and believed to mediate ATP release from the cytosol (see Dahl, 2015; Whyte-Fagundes and Zoidl, 2018). The recently solved cryo-EM structure of Panx1 heptameric assembly has revealed co-existence of a large conducting pathway together with 7 additional chloride-conducting side tunnels, making the functional channel heptamer capable of passing ion current without necessary releasing ATP (Ruan et al., 2020). Panx1 is involved in a wide range of physiological and pathophysiological functions in different cell types (see Wang et al., 2013; Dahl, 2018). Accordingly, it is a therapeutic target of increasing interest for many pathological conditions, including infectious diseases, cancer, inflammation, several diseases of the central nervous system (e.g. Dahl and Keane, 2012; Eugenin, 2014; Navis et al., 2020; Vultaggio-Poma et al., 2020; Giaume et al., 2021).

Skeletal muscle activity is associated with ATP release in the interstitial space (Li et al., 2003), with potential downstream autocrine and paracrine functions through purinergic receptors (e.g. Nyberg et al., 2013; Ito et al., 2018). Several lines of evidence have promoted a function for Panx1-mediated ATP release and consequent autocrine activation of purinergic signaling, in the control of muscle plasticity (Buvinic et al., 2009; Jorquera et al., 2013; Bustamante et al., 2014). This process operates in an action-potentials frequency-dependent manner, sensed and transduced by $Ca_V1.1$ to Panx1 (Casas et al., 2010; Jorquera et al., 2013). Consistently, a multiprotein complex including $Ca_V1.1$, Panx1, and P2Y2 has been described (Arias-Calderón et al., 2016). The close molecular and functional interactions between the ECC machinery and Panx1 led us to postulate that, altering Panx1 function may affect intracellular Ca^{2+} handling and ECC. To address this issue, we focused on a molecule classically used to block Panx1: probenecid, which has also been used for clinical purposes. We show that probenecid affects resting Ca^{2+} homeostasis, voltage-activated Ca^{2+} release and whole muscle force production.

Methods

Experiments were performed following the ethics principles of the French Department of Veterinary Services and the French Ministry for Higher Education, Research and Innovation, in accordance with the guidelines of the local animal ethics committee of University Claude Bernard Lyon 1 and of University of Nantes, the French Ministry of Agriculture (decree 87/848), and the revised European Directive 2010/63/EU.

Isolation and preparation of muscle fibers for voltage-clamp

Single fibers were isolated from the *flexor digitorum brevis* muscles of 8-12-week-old OF1 male mice (Charles River, L'Arbresle, France). Procedures were as described previously (Jacquemond, 1997; Lefebvre et al., 2011). In brief, mice were anaesthetized by isoflurane inhalation and killed by cervical dislocation. Muscles were removed and incubated for 60 minutes at 37°C in the presence of Tyrode solution containing 2 mg/mL of collagenase (Sigma, type 1). Single intact muscle fibers were then released by gentle mechanical trituration of the enzyme-treated muscles. Trituration was achieved within the experimental chamber: a 50 mm wide culture µ-dish, Ibidi, Planegg / Martinsried, Germany), in the presence of culture medium containing 10% bovine fetal serum (MI199; Eurobio, France). Prior to trituration, the bottom of the chamber had been covered with a thin layer of silicone grease. This enabled single fibers to be covered with additional silicone so that a 50-100 µm-long portion of the fiber extremity was left out, as previously described (Jacquemond, 1997). The culture medium solution was replaced by our standard extracellular solutions (see Solutions). The tip of a glass micropipette filled with an intracellular-like solution containing a Ca^{2+}-sensitive dye (see Solutions) was inserted into the silicone-embedded fiber portion. The silver-silver chloride wire inside the micropipette was connected to an RK-400 patch-clamp amplifier (Bio-Logic, Claix, France) used in whole-cell voltage-clamp configuration. Command voltage pulse generation was achieved with an analog-digital converter (Digidata 1440A, Axon Instruments, Foster City, CA) controlled by pClamp 9 software (Axon Instruments). The tip of the micropipette was gently crushed against the bottom of the chamber to reduce the series resistance. Analog compensation was adjusted to further decrease it. Unless otherwise specified, voltage-clamp steps were applied from a holding command potential of -80 mV. $Ca_V1.1$ Ca^{2+} current traces were corrected for the linear leak component using previously described procedures (Collet et al., 2003). All experiments were performed at room temperature (20–22°C).

Ca^{2+} imaging

Detection of fluorescence from the Ca^{2+}-sensitive dye dialyzed into the fiber's cytosol was achieved with a Zeiss LSM 800 microscope equipped with a 63× oil immersion objective (numerical aperture 1.4). Standard green and red configurations were used for detection of the fluorescence of fluo-4 and rhod-2, respectively. Voltage-activated fluorescence changes were imaged using the line-scan mode (x,t) of the system. They were expressed as F/F_0 with F_0 the baseline fluorescence. In graphs presenting fluorescence

transients, the y scale bar corresponds to the indicated multiple of F_0. Quantification of the Ca^{2+} release flux underlying the rhod-2 Ca^{2+} transients was performed as previously described (Lefebvre et al., 2011; Kutchukian et al. 2016). For results shown in Fig. 5 and in Fig. 6, the change in resting Ca^{2+} concentration induced by probenecid was implemented in the Ca^{2+} release flux calculation: the resting Ca^{2+} level in the presence of probenecid was calculated from the increase in resting fluorescence, assuming an initial resting [Ca^{2+}] level of 0.1 µM, and F_{max}/F_{min} and K_D values for rhod-2 of 30 and 1.63 µM, respectively (Sanchez et al., 2021).

Muscle force measurements

Electrically-stimulated isolated *extensor digitorum longus* (EDL) muscles were used to assess the effect of probenecid on force development. For this, 8-week-old OF1 male mice were anesthetized by isoflurane inhalation and killed by cervical dislocation and EDL muscles were removed. Force measurements were performed using the 1205A Isolated Muscle System from Aurora Scientific (Aurora, ON, Canada). The EDL muscle was mounted in the experimental chamber in the presence of a Ringer solution (see Solutions) maintained at 25°C and continuously bubbled with 95% O_2 / 5% CO_2. The muscle was stretched to the optimum length for production of maximum isometric twitch force triggered by a supra-maximum 0.2-ms-long electrical stimulation. From this time-point, the muscle was repeatedly stimulated by series of 5 such electrical stimulations applied at 0.1 Hz, every 5 minutes, throughout the experiment. Force measurements were performed in response to 60 Hz supra-maximum tetanic trains of stimulations of 0.5 s total duration, applied every 15 minutes. Following the first tetanic response, the Ringer solution was exchanged for the DMSO-containing Ringer with or without probenecid.

Solutions

Tyrode solution contained (in mM): 140 NaCl, 5 KCl, 2.5 $CaCl_2$, 2 $MgCl_2$, 10 HEPES. The standard extracellular solution contained (in mM) 140 TEA-methane-sulfonate, 2.5 $CaCl_2$, 2 $MgCl_2$, 1 4-aminopyridine, 10 HEPES and 0.002 tetrodotoxin. The standard pipette solution contained (in mM) 120 K-glutamate, 5 Na_2-ATP, 5 Na_2-phosphocreatine, 5.5 $MgCl_2$, 5 glucose, 5 HEPES. For measurements of rhod-2 Ca^{2+} transients it also contained 15 EGTA, 6 $CaCl_2$ and 0.1 rhod-2. For measurements with fluo-4, isolated muscle fibers were incubated for 30 min in the presence of Tyrode solution containing 10 µM fluo-4 AM.

Fluorescent indicators were purchased from Thermo Fisher Scientific (Illkirch, France). All solutions were adjusted to pH 7.20. The Ringer solution used for muscle force measurements contained (in mM) 140 NaCl, 6 KCl, 3 $CaCl_2$, 3 $MgCl_2$, 10 HEPES, adjusted to pH 7.40. Probenecid was prepared as a 0.3 M aliquoted stock solution in DMSO and used in the experimental buffer solution at 1 mM. carbenoxolone (CBX) was prepared as a 10 mM stock solution in the experimental buffer solution and used at 0.1 mM.

Statistics

Data values are presented as means ± SEM for either *n* fibers or *n* muscles. For single muscle fiber measurements, statistical significance was determined using a Student's t-test (*P≤0.05). For muscle force measurements in control conditions and in the presence of probenecid, a Mann Whitney Wilcoxon Test was used to compare the amplitude of tetanic force at a given time point of the experiment. A Friedman's nonparametric test for repeated measurements followed by Dunn's post hoc test was used to compare the time-dependent changes in the tetanic force amplitude in the two groups (*P≤0.05).

Results

Depressed SR Ca^{2+} release in muscle fibers incubated in the presence of either probenecid or carbenoxolone

The effect of probenecid (1 mM) and carbenoxolone (0.1 mM) on ECC was first tested in steady state conditions using a pre-incubation protocol. For this, voltage-activated Ca^{2+} transients were measured from fibers bathed in the presence of one of the two drugs from the beginning of the intracellular dialysis with the rhod-2 containing solution (that is, 30 minutes before taking measurements). Results were compared to data collected from fibers bathed in the standard extracellular solution. Following the dialysis, each fiber was challenged by 0.5 s-long depolarizing pulses of increasing amplitude. Figure 1 presents results from muscle fibers isolated from 3 mice, using that protocol. Illustrative rhod-2 F/F_0 traces from one fiber of each group from the same mouse are shown in Fig. 1A while the underneath series of traces show the corresponding calculated SR Ca^{2+} release flux (dCa_{Tot}/dt), using an expanded time scale (time period corresponding to that indicated by a double-arrow below the control F/F_0 traces). The probenecid- and CBX-treated fibers generated F/F_0 transients smaller than those from control fibers. Analysis of data collected from 3 mice is presented in Fig. 1B. The top left panel shows the individual values of the peak

SR Ca^{2+} release flux *versus* voltage in all fibers, with values from fibers from the same mouse being shown with the same symbol. Superimposed curves show the result of fitting each individual dataset with a Boltzmann function. The bottom left panel shows the corresponding mean values from all fibers. From the Boltzmann fits, mean values for the maximum Ca^{2+} release flux were significantly reduced in the probenecib group (38.7 ± 7.3 $\mu M.ms^{-1}$, n=6, P=0.002) and in the CBX group (19.7 ± 4.6 $\mu M.ms^{-1}$, n=7, P<0.001) as compared to the mean value in the control group (77.1 ± 6.1 $\mu M.ms^{-1}$, n=7), whereas mean values for mid-activation voltage and steepness factor did not differ between the control and the two treated groups.

The top right panel in Fig. 1B shows the voltage dependence of individual values in each fiber for the total amount of Ca^{2+} released (Ca_{Tot}) by each depolarizing pulse, calculated from the running integral of the release flux. The bottom right panel shows the corresponding mean values from all fibers. The reduced early peak activity of RyR1 channels in presence of the drugs was not compensated by slower kinetics of the overall release flux. Instead, there was a marked reduction in the total amount of released Ca^{2+} in the presence of both drugs for the largest values of membrane depolarization.

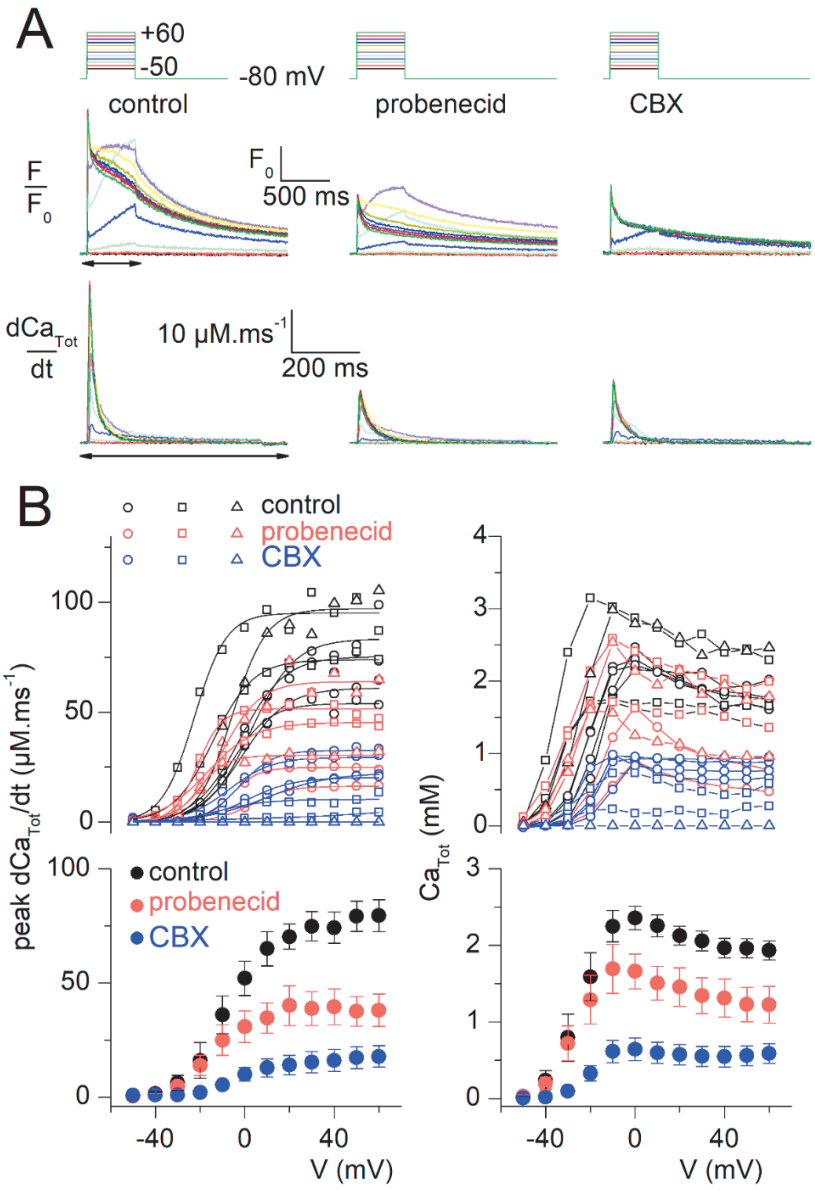

***Figure 1. Probenecid and carbenoxolone (CBX) depress voltage-activated SR Ca^{2+} release. A**, illustrative examples of rhod-2 fluorescence transients (F/F_0 traces) and corresponding calculated SR Ca^{2+} release flux (dCa_{Tot}/dt) elicited by the voltage-clamp pulse protocol shown on top in a control fiber, in a fiber equilibrated in the presence of probenecid and in a fiber equilibrated in the presence of CBX. **B**, Voltage-dependence of the peak amplitude of SR Ca^{2+} release (left panels) and of the corresponding total amount of released Ca^{2+} (right panels) in the three groups of fibers tested as shown in A. The top panels show individual values in each muscle fiber with different symbols corresponding to fibers from the same mouse. For the peak SR Ca^{2+} release flux, each dataset was fitted by a Boltzmann function (superimposed continuous lines). Bottom panels show the voltage-dependence of the corresponding mean values.*

Acute application of probenecid releases stored Ca^{2+}

The depressing effect of a chronic exposure to probenecid or carbenoxolone on SR Ca^{2+} release prompted us to determine whether it was associated with other chronic or transient changes that may be hard to reveal from a comparison of data between a control group and a treated group of fibers at steady state. A protocol of acute transient drug application was thus used which also allowed testing the reversibility of the effects. For this, we first measured rhod-2 Ca^{2+} signals in response to repeated series of voltage-clamp depolarizing pulses delivered to a same fiber in control conditions, after applying probenecid and then after probenecid wash-out. Because the combination of measuring SR Ca^{2+} release in response to

repeated voltage-clamp depolarizing pulses, together with extracellular solution changes, is a challenging experimental situation, we performed an identical series of control experiments through which only DMSO was applied to the fibers (referred to as test-control protocol).

An example of data collected from one fiber that could be challenged first with a test-control protocol, and then with probenecid application, is shown in Fig. 2. It shows, from left to right, raw rhod-2 fluorescence transients elicited by 200 ms-long pulses to -20, 0 and +20 mV -in the initial control condition, -after adding DMSO (test control), -after DMSO wash out (test wash), -after adding probenecid, and finally after probenecid wash-out. Each pulse was repeated twice to check for stability of the response in each given condition. Traces show that the fiber tolerated well the protocol, generating quite reproducible transients under the control, test-control and test-wash conditions. Throughout these first sets of measurements, the resting rhod-2 fluorescence level tended to slightly increase with time, likely due to the non-entirely complete equilibration of the pipette solution with the cell interior. However, then upon probenecid application, there was a reduction in the relative amplitude of the rhod-2 transients, accompanied by an increase in the baseline fluorescence level. Both effects tended to be reversed upon probenecid wash-out. This result provides a compelling indication that probenecid affects intracellular Ca^{2+} homeostasis. Completing an entire set of control and then test measurements on a same fiber as shown in Fig. 2 was complicated to achieve in many fibers. Instead, we relied on the comparison of data between a group of fibers experiencing the control protocol and a group of fibers challenged with probenecid application.

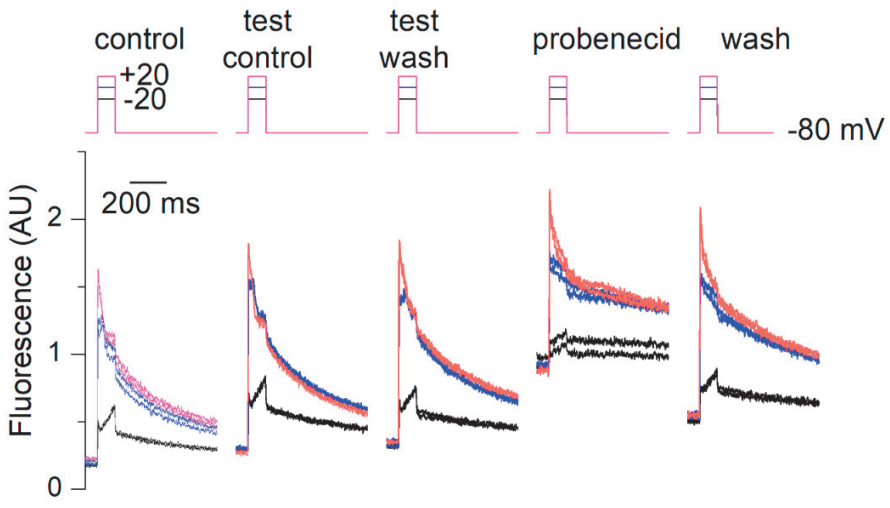

Figure 2. Effect of a transient application of probenecid on voltage-activated Ca^{2+} transients in a muscle fiber. *Rhod-2 Ca^{2+} transients elicited by the pulse protocol shown on top upon successive changes in the extracellular solution. Each membrane depolarization was applied twice. From left to right, DMSO was added to the extracellular solution (test control), then washed (test wash), then probenecid was added, and then washed (wash).*

We first focus here on the effect of probenecid on the resting rhod-2 fluorescence. The evolution of this parameter over the course of the acute probenecid application protocol is shown in Fig. 3A. As the exact timing of pulses delivery and of probenecid application was not identical for all experiments, data points from each and every fiber tested are shown, with each symbol type corresponding to a distinct fiber. Black and red symbols correspond to data from fibers challenged with the control and with the probenecid protocols, respectively. Open symbols correspond to data collected before application of probenecid (or of DMSO) and after wash-out, whereas corresponding filled symbols show data collected in the presence of the drug (or of DMSO for the control cells). For a given fiber, all pre-pulses baseline fluorescence levels were normalized to the baseline value measured before the first pulse was applied (referred to as "initial F_0"). The inset in Fig. 3A shows the raw data while the main panel shows the same data after normalizing each dataset by a liner function fitted to the data points before application of probenecid, and extrapolated to the entire set. This correction was not entirely satisfactory over the full experiment's duration, as most corrected F_0/initial F_0 values tended to decline with time. Nevertheless, results clearly show that, as compared to the control experiments, probenecid application reproducibly and reversibly enhanced resting rhod-2 fluorescence. Using calibration values given in Methods and measurements taken from 9 fibers, the mean resting Ca^{2+} concentration was estimated to rise from a resting level of 0.1 to 0.26 ± 0.02 µM following probenecid application. In two fibers, application of 0.1 mM CBX also generated an increase in resting rhod-2 fluorescence that was reversed upon wash-out, although the time-course of increase appeared slower than with probenecid (not shown). The bar graphs at the bottom of Fig. 3A show the mean values for F_0/initial F_0 during the application of probenecid (or during the corresponding period for the control fibers), and after wash.

Above results suggest that a rise in resting Ca^{2+} is accompanying the depressing effect of probenecid on voltage-activated SR Ca^{2+} release. As a control, in vitro measurements using droplets of rhod-2-containing solution showed that probenecid has no effect on the fluorescence, excluding an interaction of the drug with the dye to explain the effect. We also excluded the possibility that the rise in fluorescence would result from an increased rhod-2 concentration level due to probenecid-induced inhibition of rhod-2 leakage out of the cell. This possibility could be raised because probenecid was shown to block extracellular leakage of calcium-sensitive dyes (e.g. Di Virgilio et al., 1988). In our conditions, baseline rhod-2 fluorescence increased on average by a factor of 1.8 within ~2 min, following probenecid application, as compared to control fibers (see Fig. 3A). If this resulted from a rhod-2 leakage block, it would mean that, in normal conditions, we are losing approximately half the cytosolic dye concentration every 2 min and that this is fully compensated by dye diffusion from the voltage-clamp pipette so that

concentration is maintained constant, or is slightly increasing. This is most unlikely. Furthermore, we have considerable evidence from our experience with isolated muscle fibers that there is no detectable dye loss due to leak in the extracellular space, including a history of experiments performed with dyes pressure-microinjected in isolated fibers, for which dye concentration remained very stable over the course of the experiments (e.g. Collet and Jacquemond, 2002). Overall, the probenecid-induced rise in resting rhod-2 fluorescence is obviously due to a rise in cytosolic Ca^{2+}.

We previously reported several experimental situations associated with an increase in resting Ca^{2+} that was triggered upon ECC activation in a use-dependent manner. This was due to continuous SR Ca^{2+} leak through RyR1 release channels that failed to close, once they had been activated upon membrane depolarization, in the presence of the triggering agent (Collet and Jacquemond, 2002; Pouvreau et al., 2004, 2006). This was not the case here: following the probenecid-induced rise in Ca^{2+}, there was no further incremental change in resting Ca^{2+} upon application of voltage-clamp depolarizing pulses.

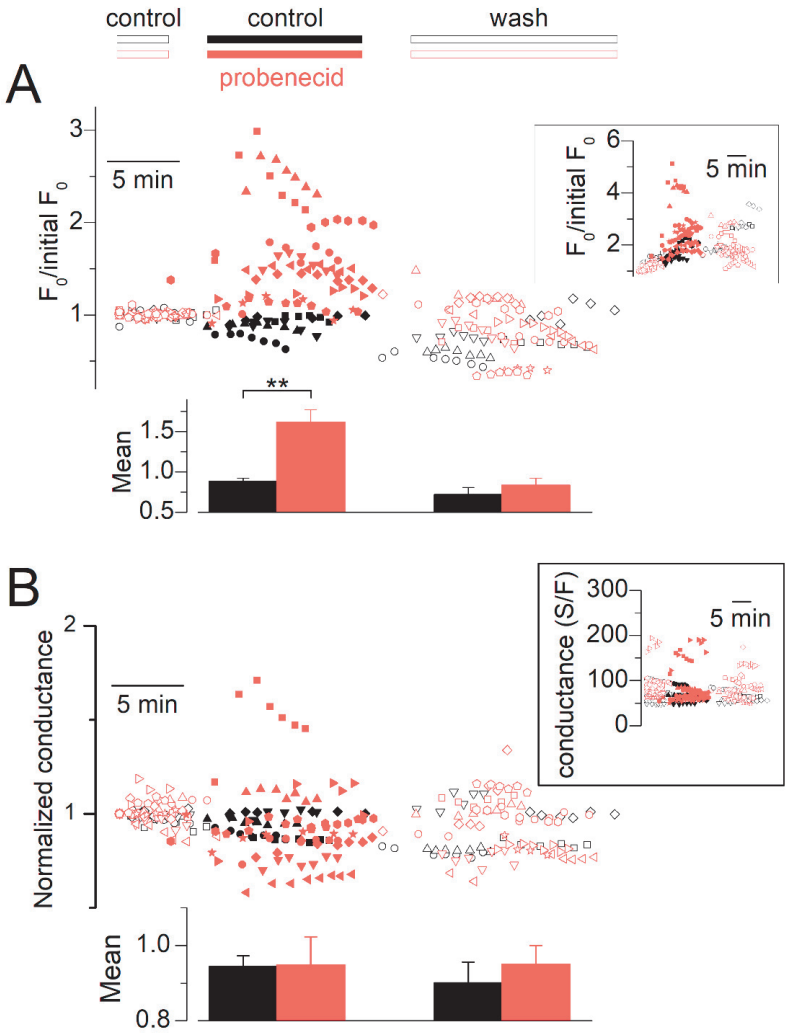

Figure 3. Effect of probenecid on resting Ca^{2+} and resting membrane conductance. ***A****, Resting rhod-2 fluorescence level (normalized to the initial value: initial F_0) along the course of experiments designed to test the effect of acute application of probenecid. Each symbol corresponds to a distinct muscle fiber. Red symbols are from fibers challenged with probenecid. Black symbols are from fibers challenged with the control protocol. Open symbols correspond to values before application of probenecid (or DMSO for the control experiments) and after wash. The inset shows the raw data while the main panel shows the same data after normalization by a linear function fitted to the data points before application of probenecid (see text for details). The bar graphs show the mean values for F_0/initial F_0 calculated from the above datasets, during probenecid (or DMSO for the control experiments) application and after wash. For this, for each fiber, all F_0/initialF_0 values obtained during the test period and then after wash, were averaged.* ***B****, Resting membrane conductance along the course of the same experiments as in A, assessed from the change in membrane current elicited by a 20 mV hyperpolarization from the holding voltage. The inset shows the raw values while the main graph shows the values normalized to the initial conductance level. As in A, the bar graphs at the bottom show the mean values for normalized conductance calculated from the above datasets, during probenecid (or DMSO) application and after wash.*

Throughout this series of measurements, each depolarizing test pulse was preceded by a 20 mV hyperpolarizing pulse to check for possible changes in resting membrane conductance. Corresponding data are shown in Fig. 3B: the inset shows the raw values while the main graph shows the same data after normalization by the initial conductance value at the beginning of the experiment. One fiber (squares) did exhibit an increase in membrane conductance during probenecid application, that was also accompanied by an inward shift of the holding current of ~0.2 A/F. However, other fibers did not show a uniform trend of change in membrane conductance, which we took as an indication that the probenecid-induced rise in resting Ca^{2+} was not associated with an electrogenic Ca^{2+} entry across the plasma/t-tubule membrane. To

further check this point, measurements were carried in two fibers in the nominal absence of extracellular Ca^{2+} in the extracellular solution. To simplify the experimental conditions, this was performed without voltage-clamp, with muscle fibers bathed in the presence of Tyrode solution and loaded with the Ca^{2+}-sensitive dye fluo-4 (see Methods). Probenecid application in this situation still produced an increase in resting fluorescence (Fig. 4A), although in several fibers this could not be reliably followed because it was accompanied by an irreversible contracture. Since RyR1-mediated SR Ca^{2+} release gets inactivated upon prolonged t-tubule membrane depolarization (Hodgkin and Horowicz, 1960), it was also of interest to check whether probenecid would raise resting Ca^{2+} in that situation. For this, rhod-2 fluorescence was measured under the same conditions as in Fig. 3, but in fibers held at a holding voltage of -10 mV, a level from which depolarizing pulses no more elicit any rise Ca^{2+} release. Figure 4B shows corresponding values for F_0/initial F_0 along the course of the experiments. Datasets were corrected, as in Fig. 3, by normalization with a linear function fitted to the data points before application of the drug. Probenecid still elicited a rise in resting Ca^{2+} in the voltage-inactivated fibers.

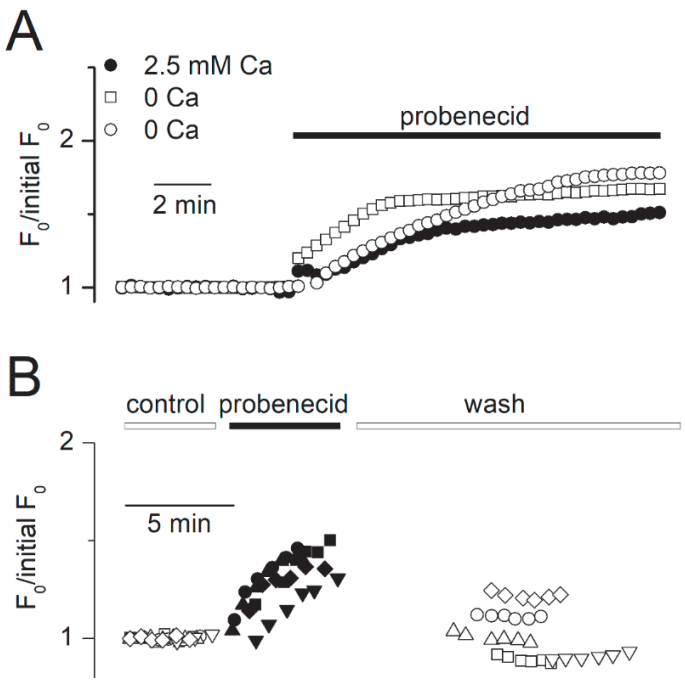

***Figure 4. The probenecid-induced cytosolic Ca^{2+} elevation persists in the absence of extracellular calcium and under voltage-inactivated conditions. A**, Time course of probenecid-induced increase in fluo-4 fluorescence in one fiber bathed in the presence of calcium-containing Tyrode solution (filled circles) and in two fibers bathed in calcium-deprived Tyrode (open symbols). **B**, Probenecid-induced rise in rhod-2 fluorescence in 5 muscle fibers voltage-clamped at a holding voltage of -10 mV.*

Probenecid simultaneously affects resting Ca^{2+} homeostasis, $Ca_V1.1$ Ca^{2+} current and SR Ca^{2+} release

Typical changes in membrane current and SR Ca^{2+} release recorded over the course of the acute probenecid application protocol, and of the corresponding control protocol, are shown in Fig. 5B and Fig. 5A, respectively. The three series of trace in Fig. 5A and Fig. 5B correspond, from top to bottom, to the voltage-activated rhod-2 fluorescence records (F_0 unit), the corresponding calculated SR Ca^{2+} release fluxes ($\mu M.ms^{-1}$ unit) and the simultaneously measured changes in membrane current, corrected for the passive linear components (A/F unit), respectively. Changes were elicited by the voltage-clamp pulses shown on top. The rhod-2 fluorescence records were all normalized to the F_0 level of the first record to follow changes in resting fluorescence. The membrane current during the pulse allowed assessing changes in the properties of the $Ca_V1.1$ Ca^{2+} current, most well detected at 0 and +20 mV. The control experiment (Fig. 5A) shows that there was some run-down in SR Ca^{2+} release, and also to some extent, in $Ca_V1.1$ Ca^{2+} current, over time. Nevertheless, probenecid under the same protocol conditions severely depressed the amplitude of SR Ca^{2+} release, with no sign of reversion upon wash out. This effect was concomitant with the increase in resting rhod-2 fluorescence, that was partially reversible upon probenecid wash out. As compared to the control experiment, there was also a clear reduction in the magnitude of the $Ca_V1.1$ Ca^{2+} current that, in that particular fiber, showed tendency for reversion upon wash out.

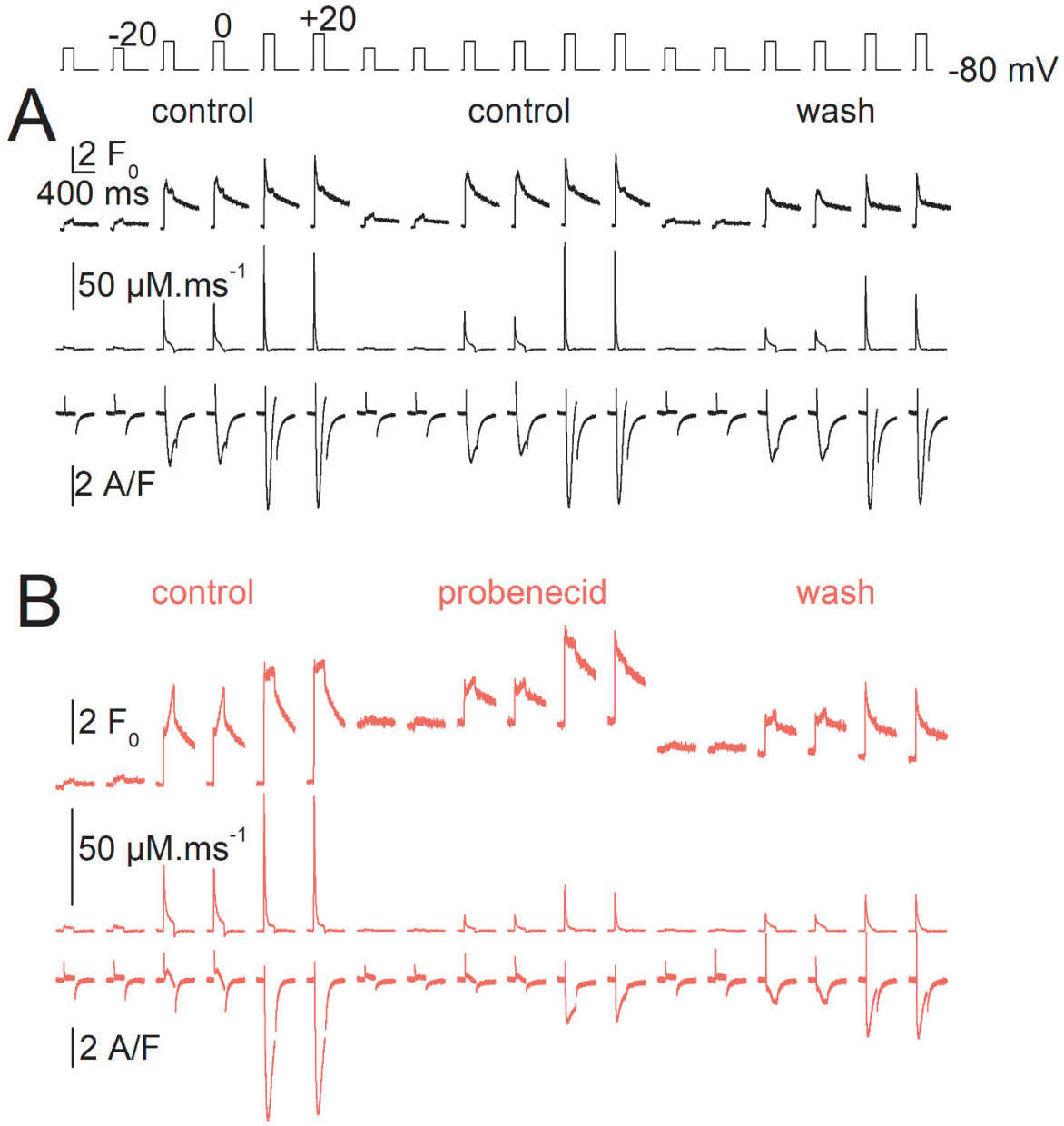

***Figure 5. Changes in voltage-activated SR Ca^{2+} release flux and $Ca_V1.1$ Ca^{2+} current during probenecid application. A**, Control experiment: rhod-2 Ca^{2+} transients (top, F_0 unit), corresponding SR Ca^{2+} release flux (middle, µM.ms^{-1}) and membrane current (bottom, A/F) recorded in response to the voltage pulses shown at the top, in a muscle fiber challenged by the control protocol. **B**, Test experiment, same measurements as in A from a muscle fiber challenged with probenecid, and after wash.*

Figure 6A shows the mean normalized values for the peak rate of SR Ca^{2+} release along the protocol in control fibers (top) and in probenecid-treated fibers (bottom). In each fiber, values for the peak rate of Ca^{2+} release in response to each consecutive pair of pulses of identical amplitude (to -20, 0 and +20 mV) were averaged and normalized to the value measured in response to the first pair of pulses to +20 mV (in the control condition). Although there was run-down in both groups of fibers, values for normalized peak rate of Ca^{2+} release in the presence of probenecid were significantly lower than in the control group for pulses to 0 and +20 mV. In parallel, the mean peak amplitude of $Ca_V1.1$ Ca^{2+} current (normalized to the initial value in control condition) in response to the pulse to +20 mV was also significantly reduced during probenecid application (Fig. 6B). These results demonstrate that probenecid concomitantly alters resting Ca^{2+} homeostasis and voltage-activated $Ca_V1.1$ Ca^{2+} current and SR Ca^{2+} release.

Figure 6. Average changes in the amplitude of peak SR Ca^{2+} release flux and $Ca_V1.1$ Ca^{2+} current following

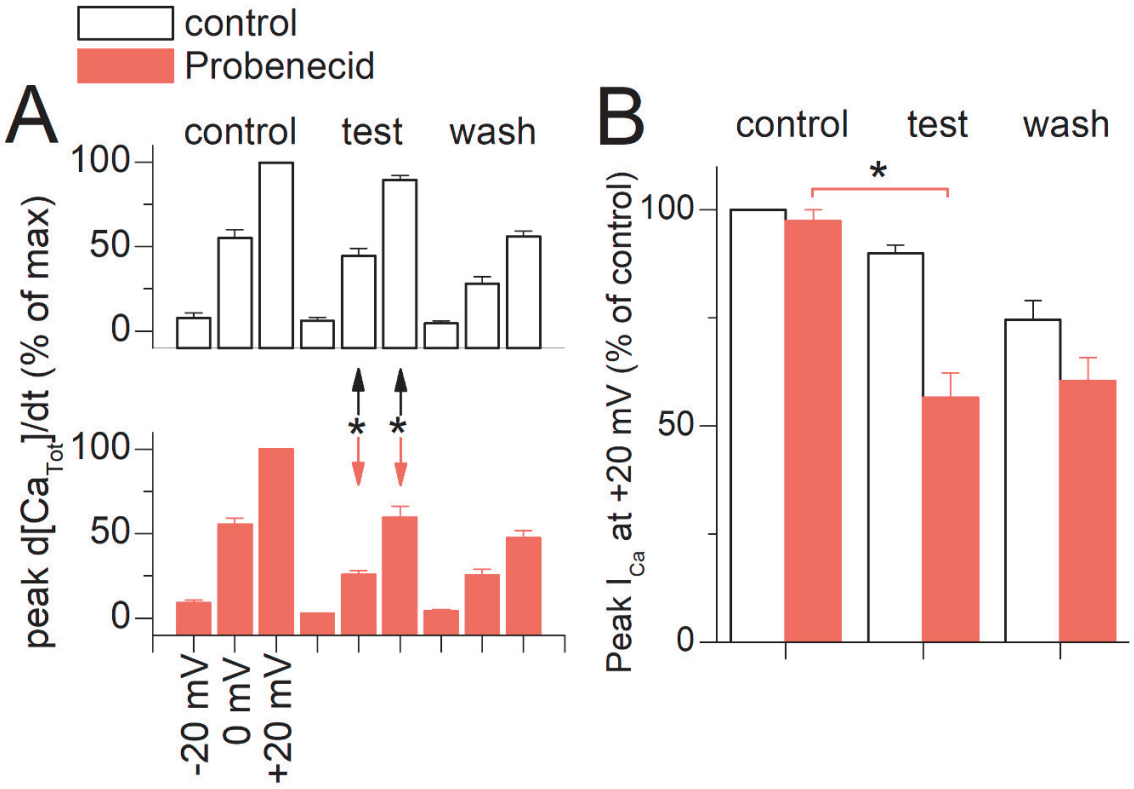

probenecid application and wash. *Data are from the same fibers as in Fig. 3.* ***A****, Mean values for the peak SR Ca^{2+} release flux during control experiments (top) and during probenecid experiments (bottom). For the two groups, all values from each fiber were normalized to the corresponding average value in response to the first pair of pulses to +20 mV (in the control situation).* ***B****, Mean values for the peak $Ca_V1.1$ Ca^{2+} current during control and probenecid experiments. In each fiber, peak current values were normalized to the average value in response to the first pair of pulses to +20 mV (in the control situation).*

Probenecid depresses muscle force

The effects of probenecid on SR Ca^{2+} release prompted us to check whether muscle force production is affected by the drug. For this, resting tension and electrically triggered tetanic contractions were measured in isolated mouse EDL muscles. Tetanic contractions were triggered by trains of stimulations at 60 Hz: a first train was applied in the control solution and then repeated every 15 minutes either in the presence or absence or 1 mM probenecid. Results from 5 EDL muscles tested in the control situation (black symbols) and in probenecid (red symbols) are shown in Fig. 7. Tension values were normalized by the muscle weight. Graphs in Fig. 7A and Fig. 7B show results from the resting and tetanic tension measurements, respectively, with the right-most graphs reporting the corresponding mean values. As compared to the control measurements, application of probenecid generated a substantial drop in peak tetanic tension at times 30- and 45-minutes following drug application, while resting tension was enhanced at 45 minutes.

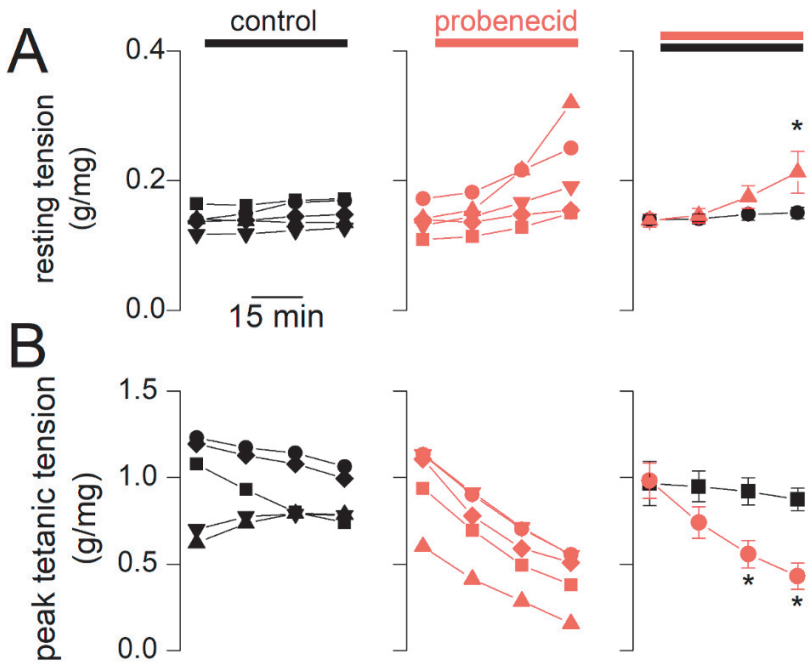

Figure 7. Effect of probenecid on whole muscle resting and tetanic tension. ***A****, Resting tension from 5 isolated EDL muscles electrically stimulated by a 60 Hz train applied every 15 minutes, and challenged either with the control protocol (black) or with probenecid (red). In both groups, the first measurement was taken in the presence of the control Ringer solution. The right-most graph shows the mean values from the two groups.* ***B****, Corresponding values for the peak amplitude of the tetanic tension.*

Discussion

We demonstrate that probenecid affects muscle function through perturbation of Ca^{2+} homeostasis and ECC. Beyond the specific interest in terms of underlying cellular mechanisms and physiological outcome, these results are also relevant to the use of probenecid in clinics as they raise issues regarding potential adverse muscular effects. Furthermore, results are also relevant in terms of general functional impact for cellular homeostasis, as probenecid-induced changes in Ca^{2+} regulation may be shared by other tissues that are therapeutic targets of this drug.

Probenecid has had a history of clinical use for its potency to inhibit organic anion transporters, making it efficient as a uricosuric agent for gout treatment (Gutman and Yu, 1951; Roch-Ramel et al., 1997) and as an adjuvant to increase the concentration of antibiotics and chemotherapeutic agents (e.g. Burnell and Kirby, 1951). There are also repositioning perspectives for its use as an antiviral and anticancer agent (Ahmed et al., 2015) and also because of its potency to block inflammasome activation (Dahl and Keane, 2012). In this context, potential benefit of probenecid as a therapeutic agent has been considered for trauma and stroke in the central nervous system, and also for disease situations such as multiple sclerosis (Hainz et al., 2017).

Of related interest is the fact that probenecid also gained popularity within the sport performance doping field, presumably because of its capacity to reduce excretion of anabolic-androgenic steroids (Hemmersbach, 2020). None less to mention that the exact conditions of dosing for that particular purpose remain poorly documented. In healthy volunteers, a single 2.0-g oral dose (which is a commonly prescribed daily dosage for adult patients) was shown to result in a peak plasma level in the half millimolar range and higher levels may be reached under conditions of repeated dosing (Selen et al., 1982).

Under our conditions, 1 mM probenecid reduces the amplitude of voltage-activated SR Ca^{2+} release in isolated muscle fibers, and this has to make a major contribution to the probenecid-induced reduction of whole-muscle tetanic contraction. Probenecid also induces Ca^{2+} release from an intracellular store at rest, which may be responsible for the observed increase in muscle resting tension. In our experiments with rhod-2, we estimated that probenecid elevated the resting cytosolic free Ca^{2+} level by ~0.1-0.2 µM. Considering that this elevation was achieved in the presence of an intracellular solution containing millimolar levels of EGTA, the total amount of released Ca^{2+} was much more than the change in free Ca^{2+}, likely within the several hundreds of micromolar to the millimolar range. This has two major implications: first, the corresponding intracellular store has to be the SR, as there is no other compartment in muscle

with such Ca^{2+} storage capacity. Second, the SR had to become, to some extent, Ca^{2+}-depleted, upon probenecid application, and this is likely to contribute to, if not to fully underlie, the probenecid-induced depression of voltage-activated SR Ca^{2+} release.

Three major mechanisms of action for probenecid have so far been reported. Probenecid inhibits organic anion transporters, but we hardly see how this could be involved in alterations of Ca^{2+} homeostasis and ECC. Probenecid is an agonist of TRPV2 channels (Bang et al., 2007). In cardiac cells, TRPV2 operates as a mechanosensitive channel involved in Ca^{2+} entry across the sarcolemma (see Entin-Meer and Keren, 2020) with a potentially important role in normal heart function (Rubinstein et al., 2014). Of interest in this context, probenecid-induced TRPV2 activation was shown to improve cardiac function in patients with heart failure (Robbins et al., 2018). In skeletal muscle, TRPV2 in the plasma membrane also operates as a mechanosensitive channel, involved in osmo-sensation, capable of contributing to t-tubule membrane depolarization and consequent SR Ca^{2+} release (Zanou et al., 2015). However, in this configuration, TRPV2 is certainly not involved in the effects we report here on Ca^{2+} homeostasis. This is because -the voltage-clamp conditions preclude any TRPV2 activation-induced membrane depolarization and consequent SR Ca^{2+} release, -we found no reproducible evidence for a probenecid-induced increase in membrane conductance, -the probenecid-induced rise in cytosolic Ca^{2+} persisted in the absence of extracellular calcium.

The third major target of probenecid is the membrane channel protein Panx1 (Silverman et al., 2008), involved in ATP release out to the extracellular space and consequent activation of purinergic receptors. In skeletal muscle, Panx1-mediated ATP release was reported to be closely linked to muscle fiber activation and ECC (Buvinic et al., 2009; Jorquera et al., 2013; Bustamante et al., 2014). Although we cannot exclude that probenecid alters Ca^{2+} homeostasis through another target, this close connection encourages us to favor the implication of Panx1. The fact that CBX, another Panx1 blocker, alters Ca^{2+} homeostasis in a similar way as probenecid, further argues in favor of this possibility. How probenecid and CBX affect the control of Ca^{2+} release through Panx1 cannot yet be fully understood. We believe that it cannot occur through inhibition of ATP exit and consequently altered purinergic signaling. Indeed, this would mean that a chronic feedback of released ATP-induced purinergic signaling operates on RyR1-mediated SR Ca^{2+} release, that would be essential for proper ECC function. This is hardly workable. Alternatively, since Panx1 is part of a complex including $Ca_V1.1$ (Arias-Calderón et al., 2016), we favor the option that probenecid interaction with Panx1 alters protein-protein interactions within this complex, so as to induce Ca^{2+} leak through RyR1. Interestingly, probenecid was still capable of inducing SR Ca^{2+} release

in fibers maintained at a depolarized voltage that inactivates $Ca_V1.1$ (Fig. 4B). This indicates that the mechanism of probenecid-induced RyR1 Ca^{2+} leak bypasses the control of RyR1 by $Ca_V1.1$. Also informative is that there was no use-dependence of the probenecid-induced SR Ca^{2+} leak, which means that RyR1 channel opening does not promote efficiency of the drug.

Irrespective of the details of the mechanism, our results provide strong evidence that probenecid alters muscle Ca^{2+} homeostasis so as to affect muscle force production. There is no straightforward mention in the literature of muscle weakness or muscle fatiguability as side-effects of the drug for patients. This may indeed be the case; for a variety of reasons, as for instance ineffective concentration levels reached in the muscle interstitial tissue, probenecid may never affect force production in the whole organism when used at the commonly used therapeutic dosage. Alternatively, it may also be that the effect on muscle function has remained undetected if corresponding to a minor drawback of this medication. With respect to doping in sport, this may be the case too. Still, our results should tend to discourage probenecid use when looking for improved muscle performance.

REFERENCES

Ahmed MU, Bennett DJ, Hsieh TC, Doonan BB, Ahmed S, Wu JM. 2016. Repositioning of drugs using open-access data portal DTome: A test case with probenecid. Int J Mol Med 37:3-10

Arias-Calderón M, Almarza G, Díaz-Vegas A, Contreras-Ferrat A, Valladares D, Casas M, Toledo H, Jaimovich E, Buvinic S. 2016. Characterization of a multiprotein complex involved in excitation-transcription coupling of skeletal muscle. Skelet Muscle 6:15.

Bang S, Kim KY, Yoo S, Lee SH, Hwang SW. 2007. Transient receptor potential V2 expressed in sensory neurons is activated by probenecid. Neurosci Lett 425:120-125.

Burnell JM, Kirby WM. 1951. Effectiveness of a new compound, benemid, in elevating serum penicillin concentrations. J Clin Invest 30:697-700.

Bustamante M, Fernández-Verdejo R, Jaimovich E, Buvinic S. 2014. Electrical stimulation induces IL-6 in skeletal muscle through extracellular ATP by activating Ca2+ signals and an IL-6 autocrine loop.

Am J Physiol 306:E869-82.

Buvinic S, Almarza G, Bustamante M, Casas M, López J, Riquelme M, Sáez JC, Huidobro-Toro JP, Jaimovich E. 2009. ATP released by electrical stimuli elicits calcium transients and gene expression in skeletal muscle. J Biol Chem 284:34490-34505.

Casas M, Figueroa R, Jorquera G, Escobar M, Molgó J, Jaimovich E. 2010. IP3-dependent, post-tetanic calcium transients induced by electrostimulation of adult skeletal muscle fibers. J Gen Physiol 136:455-467.

Collet C, Jacquemond V. Sustained release of calcium elicited by membrane depolarization in ryanodine-injected mouse skeletal muscle fibers. 2002. Biophys J 82:1509-1523.

Collet C, Csernoch L, Jacquemond V. 2003. Intramembrane charge movement and L-type calcium current in skeletal muscle fibers isolated from control and mdx mice. Biophys J 84:251-265.

Dahl G. 2015. ATP release through pannexon channels. Philos Trans R Soc Lond B Biol Sci 370:20140191.

Dahl G. 2018. The Pannexin1 membrane channel: distinct conformations and functions. FEBS Lett 592:3201-3209.

Dahl G, Keane RW. 2012. Pannexin: from discovery to bedside in 11±4 years? Brain Res 1487:150-159.

Di Virgilio F, Fasolato C, Steinberg TH. 1988. Inhibitors of membrane transport system for organic anions block fura-2 excretion from PC12 and N2A cells. Biochem J 256:959-963.

Entin-Meer M, Keren G. 2020. Potential roles in cardiac physiology and pathology of the cation channel TRPV2 expressed in cardiac cells and cardiac macrophages: a mini-review. Am J Physiol 318:H181-H188.

Eugenin EA. 2014. Role of connexin/pannexin containing channels in infectious diseases. FEBS Lett 588:1389-1395.

Giaume C, Naus CC, Sáez JC, Leybaert L. 2021. Glial Connexins and Pannexins in the Healthy and Diseased Brain. Physiol Rev 101:93-145.

Gutman AB, Yu TF. 1951. Benemid (p-di-n-propylsulfamyl)-benzoic acid) as uricosuric agent in chronic gouty arthritis. Trans Assoc Am Physicians 64:279-288.

Hainz N, Wolf S, Beck A, Wagenpfeil S, Tschernig T, Meier C. 2017. Probenecid arrests the progression of pronounced clinical symptoms in a mouse model of multiple sclerosis. Sci Rep 7:17214.

Hemmersbach P. The Probenecid-story - A success in the fight against doping through out-of-competition testing. 2020. Drug Test Anal 12:589-594.

Hernández-Ochoa EO, Schneider MF. 2018. Voltage sensing mechanism in skeletal muscle excitation-contraction coupling: coming of age or midlife crisis? Skelet Muscle 19:22.

Hodgkin AL, Horowicz P. 1960. Potassium contractures in single muscle fibres. J Physiol 153:386-403.

Ito N, Ruegg UT, Takeda S. 2018. ATP-Induced Increase in Intracellular Calcium Levels and Subsequent Activation of mTOR as Regulators of Skeletal Muscle Hypertrophy. Int J Mol Sci 19:2804.

Jacquemond V. 1997. Indo-1 fluorescence signals elicited by membrane depolarization in enzymatically isolated mouse skeletal muscle fibers. Biophys J 73:920-928.

Jorquera G, Altamirano F, Contreras-Ferrat A, Almarza G, Buvinic S, Jacquemond V, Jaimovich E, Casas M. 2013. Cav1.1 controls frequency-dependent events regulating adult skeletal muscle plasticity.

J Cell Sci 126:1189-1198.

Kutchukian C, Lo Scrudato M, Tourneur Y, Poulard K, Vignaud A, Berthier C, Allard B, Lawlor MW, Buj-Bello A, Jacquemond V. Phosphatidylinositol 3-kinase inhibition restores Ca2+ release defects and prolongs survival in myotubularin-deficient mice. 2016. Proc Natl Acad Sci U S A113:14432-14437.

Lefebvre R, Legrand C, González-Rodríguez E, Groom L, Dirksen RT, Jacquemond V. 2011. Defects in Ca2+ release associated with local expression of pathological ryanodine receptors in mouse muscle fibres. J Physiol 589:5361-5382.

Li J, Gao Z, Kehoe V, Xing J, King N, Sinoway L. 2008. Interstitial adenosine triphosphate modulates muscle afferent nerve-mediated pressor reflex. Muscle Nerve 38:972-977.

Mackrill JJ. 2010. Ryanodine receptor calcium channels and their partners as drug targets. Biochem Pharmacol 79:1535-43.

Navis KE, Fan CY, Trang T, Thompson RJ, Derksen DJ. 2020. Pannexin 1 Channels as a Therapeutic Target: Structure, Inhibition, and Outlook. ACS Chem Neurosci 11:2163-2172.

Nyberg M, Al-Khazraji BK, Mortensen SP, Jackson DN, Ellis CG, Hellsten Y. 2013. Effect of extraluminal ATP application on vascular tone and blood flow in skeletal muscle: implications for exercise hyperemia. Am J Physiol 305:R281-R290.

Pouvreau S, Allard B, Berthier C, Jacquemond V. 2004. Control of intracellular calcium in the presence of nitric oxide donors in isolated skeletal muscle fibres from mouse. J Physiol 560:779-794.

Pouvreau S, Csernoch L, Allard B, Sabatier JM, De Waard M, Ronjat M, Jacquemond V. 2006. Transient loss of voltage control of Ca2+ release in the presence of maurocalcine in skeletal muscle.

Biophys J 91:2206-2215.

Rebbeck RT, Karunasekara Y, Board PG, Beard NA, Casarotto MG, Dulhunty AF. 2014. Skeletal muscle excitation-contraction coupling: who are the dancing partners? Int J Biochem Cell Biol 48:28-38.

Ríos E. 2018. Calcium-induced release of calcium in muscle: 50 years of work and the emerging consensus. J Gen Physiol 150:521-537.

Robbins N, Gilbert M, Kumar M, McNamara JW, Daly P, Koch SE, Conway G, Effat M, Woo JG, Sadayappan S, Rubinstein J. 2018. Probenecid Improves Cardiac Function in Patients With Heart Failure With Reduced Ejection Fraction In Vivo and Cardiomyocyte Calcium Sensitivity In Vitro. J Am Heart Assoc 7:e007148.

Roch-Ramel F, Guisan B, Diezi J. 1997. Effects of uricosuric and antiuricosuric agents on urate transport in human brush-border membrane vesicles. J Pharmacol Exp Ther 280:839-845.

Ruan Z, Orozco IJ, Du J, Lü W. 2020. Structures of human pannexin 1 reveal ion pathways and mechanism of gating. Nature 584:646-651.

Rubinstein J, Lasko VM, Koch SE, Singh VP, Carreira V, Robbins N, Patel AR, Jiang M, Bidwell P, Kranias EG, Jones WK, Lorenz JN. 2014. Novel role of transient receptor potential vanilloid 2 in the regulation of cardiac performance. Am J Physiol 306:H574-H584.

Sanchez C, Berthier C, Tourneur Y, Monteiro L, Allard B, Csernoch L, Jacquemond V. 2021. Detection of Ca2+ transients near ryanodine receptors by targeting fluorescent Ca2+ sensors to the triad.

J Gen Physiol 153:e202012592.

Selen A, Amidon GL, Welling PG. Pharmacokinetics of probenecid following oral doses to human volunteers. 1982. J Pharm Sci 71:1238-1242.

Vultaggio-Poma V, Sarti AC, Di Virgilio F. 2020. Extracellular ATP: A Feasible Target for Cancer Therapy. Cells 9:2496.

Wang N, De Bock M, Decrock E, Bol M, Gadicherla A, Vinken M, Rogiers V, Bukauskas FF, Bultynck G, Leybaert L. 2013. Paracrine signaling through plasma membrane hemichannels. Biochim Biophys Acta 1828:35-50.

Whyte-Fagundes P, Zoidl G. 2018. Mechanisms of pannexin1 channel gating and regulation. Biochim Biophys Acta Biomembr 1860:65-71.

Zanou N, Mondin L, Fuster C, Seghers F, Dufour I, de Clippele M, Schakman O, Tajeddine N, Iwata Y, Wakabayashi S, Voets T, Allard B, Gailly P. 2015. Osmosensation in TRPV2 dominant negative expressing skeletal muscle fibres. J Physiol 593:3849-3863.

Section 1.3.

IN VIVO OVEREXPRESSION OF PANNEXIN 1 AND ITS EFFECT ON CAV1.1 FUNCTION AND EXCITATION-CONTRACTION COUPLING

Since Panx1 knock-down affects voltage-activated $Ca_V1.1$-dependent Ca^{2+} current and RyR1-dependent SR Ca^{2+} release we hypothesized that the amount of Panx1 in the plasma/T-tubule membrane may be regulating the function of ECC. In that context it was thus of interest to test whether overexpression of Panx1 could affect the normal function of the ECC machinery. To this aim, we used in vivo transfection of Panx1-encoding plasmids in mouse FDB muscles.

In order to make the investigation comprehensive and limit any uncertainty or bias with respect to the expression of Panx1 or to the presence of a fused tag (which can potentially affect proper localization and function of the protein), we worked with three different constructs. We first transfected a plasmid encoding Panx1-tGFP, corresponding to Panx1 fused in frame at its C-terminal end with the turbo GFP (tGFP) green fluorescent protein. Second, we cloned an expression plasmid encoding an untagged version of Panx1 and the plasmid was co-transfected with a plasmid encoding the mEGFP green fluorescent protein. Third, we designed a bicistronic Panx1-tPT2A-mGFP plasmid construct that leads to co-expression of tag-free-Panx1 and of mGFP green fluorescence protein, thanks to the so called "self-cleaving" tPT2A peptide linking the two protein sequences (Liu et al., 2017). After either 7 or 14 days of expression, we enzymatically isolated the FDB muscle fibers, identified the transfected fibers, and used simultaneous confocal imaging of the fluorescence of the intracellularly-dialyzed Ca^{2+}-sensitive dye rhod-2 together with silicone voltage-clamp conditions. The functions of $Ca_V1.1$ Ca^{2+} current and RyR1-mediated SR Ca^{2+} release were assessed in response to 0.5 s-long depolarizing pulses of increasing amplitude from -80 mV.

Voltage-activated SR Ca^{+2} release and ICa^{2+} in FDB fibers expressing Panx1-tGFP

FDB muscle fibers were isolated after 7 days of expression of Panx1-tGFP. Control fibers for these experiments were isolated from the contralateral FDB of each mouse that had been simultaneously transfected with pEGFP-Dr-VSP. The encoded EGFP-DrVSP was used as control because, as Panx1, it is a plasma membrane protein that localizes in the T-tubules membrane (Berthier et al. 2015). We took records from 9 control fibers (from 4 mice) versus 14 Panx1-tGFP-expressing fibers (from 5 mice). We compared the voltage-dependence of the peak rate of SR Ca^{2+} release between the two groups (Results 1 (Section1.3.)) and quantified the results by fitting the voltage-dependencies using a Boltzmann function

(see Methods and materials). We obtained mean (± SE) values for the control fibers of: Maximum release rate (Max)= 51 ± 7.5 µmol $l^{-1}ms^{-1}$, half-activation potential ($V_{0.5}$)= 7.03 ± 1.04 mV and steepness factor (k)= 7.8 mV ± 0.56 mV, *versus* corresponding values for Panx1-tGFP-expressing fibers of: Max= 46 ± 8.7 µmol $l^{-1}ms^{-1}$, V05= -7.8 ± 1.74 mV, and k= 7.2 ± 0.64 mV. There was no statistically significant difference between the two groups in any parameter. Analysis of the voltage-dependence of the peak Ca^{2+} current measured simultaneously was achieved by fitting the peak current *versus* voltage (I/V) curves with the appropriate function (see Methods and materials): the only statistically significant difference was a 6 mV right-shift in half-activation voltage ($V_{0.5}$) with mean values of -3.5 ± 2.4 mV for the control group *versus* 3.07 ± 1.85 mV for the Panx1-tGFP group (p-value= 0.039). Because the t-GFP tag may affect proper trafficking and localization of Panx1, so as to potentially preclude its effectiveness to alter ECC, we checked that particular issue by analyzing the localization in muscle fibers and also in the COS-7 cell line.

Panx1-tGFP: localization in COS-7 cells and in differentiated FDB muscle fibers

Panx1-tGFP was expressed in COS-7 cells and its localization was compared after 2-3 days of expression (Results2 (Section1.3.)). The pattern of distribution of Panx1-tGFP only corresponded to a peri-nuclear and reticular localization, consistent with its accumulation in the endoplasmic reticulum. Accordingly, localization of the two fluorescent proteins after 7 days of expression in FDB muscle fibers clearly differed. EGFP-DrVSP presented with a T-tubule consistent profile, that is transverse double-bands separated by ≈ 2 µm, as previously described (Berthier et al. 2015) (Results2 (Section1.3.)). In contrast, Panx1-tGFP presented with single transverse bands also separated by ≈ 2 µm, inconsistent with T-tubule localization. Interestingly, the C-terminal tail of Panx1 was reported in the literature to present a putative leucine-rich repeat (LRR) needed for Panx1 cell surface localization and for oligomerization of Panx1 proteins to form Panx1 channels (Epp et al., 2019). Thus, a possible explanation could be that the tGFP fused at the C-terminal end precludes LRR function, preventing proper Panx1 T-tubule localization.

Because of these results, we then designed and cloned a plasmid encoding for a tag-free Panx1 (see Methods and materials).

Voltage-activated SR Ca^{+2} release and $Ca_V1.1$ Ca^{2+} current in FDB muscle fibers co-expressing untagged Panx1 and pmEGFP

FDB muscles were co-transfected with a plasmid encoding the untagged Panx1 (pCMV-PANX1) (70%) and a plasmid encoding mEGFP (pmEGFP-C1) (30%). As a control, we transfected the contralateral FDB muscle of each mouse with the equivalent amount of pmEGFP-C1. Isolated muscle fibers were tested

either 7 days or 14 days post-transfection. Using our standard simultaneous measurements of membrane current and intracellular Ca^{2+} transients with rhod-2, we assessed the voltage-dependence of $Ca_V1.1$ Ca^{2+} current and of RyR1-dependent SR Ca^{2+} release.

Results from 7 days of expression were from 10 mEGFP-expressing control fibers (from 3 mice) and 10 untagged Panx1 + mEGFP expressing fibers (from 3 mice). Analysis gave no indication for any statistical difference in the parameters of SR Ca^{2+} release (see Results3). When comparing the fit parameters for the peak $Ca_V1.1$ current voltage-dependence, there was a barely significant 18% decrease in the maximum conductance (Gmax (p-value = 0.0496)).

After 14 days of expression, we took records from 8 control fibers (from 3 mice), and 7 untagged Panx1 + mEGFP expressing fibers (from 3 mice). Results so far showed that none of the fitted parameters for both peak SR Ca^{2+} release and $Ca_V1.1$ Ca^{2+} current statistically differed between the two groups.

Voltage-activated SR Ca^{+2} release and $Ca_V1.1$ Ca^{2+} current in FDB muscle fibers expressing Panx1-tPT2A-mGFP

Because co-transfection with a Panx1 encoding plasmid (pCMV-PANX1) and a separate mEGFP encoding plasmid (pmEGFP-C1) did not ensure that green fibers were positive for exogenous Panx1 expression, we finally tested a bicistronic plasmid encoding Panx1 fused with mEGFP with the autocleavable domain tP2TA (pPanx1-tPT2A-mEGFP). As a control we transfected the contralateral FDB muscle with a mEGFP. After 14 days of expression measurements were taken in the two groups of green fibers. Again, none of the fitted parameters for both peak SR Ca^{2+} release and $Ca_V1.1$ Ca^{2+} current statistically differed between the two groups (see Results 4 (section1.3.)).

Conclusions

Exogenous expression of Panx1 in FDB muscle fibers provided no indication for a consequent alteration of ECC or $Ca_V1.1$ channel function. This could mean that there is no Panx1 over-expression in our system and we may be simply replacing native Panx1 by the exogenous one, as previously suggested when expressing exogenous RyR1 (Lefebvre et al., 2011). This will need to be checked and if true, it may be of interest in the future to express altered/truncated forms of Panx1 that may not fulfill their proper role *versus* ECC function. Alternatively, it could also simply be that Panx1 channel accumulation in the membrane, beyond the native level, does not alter ECC.

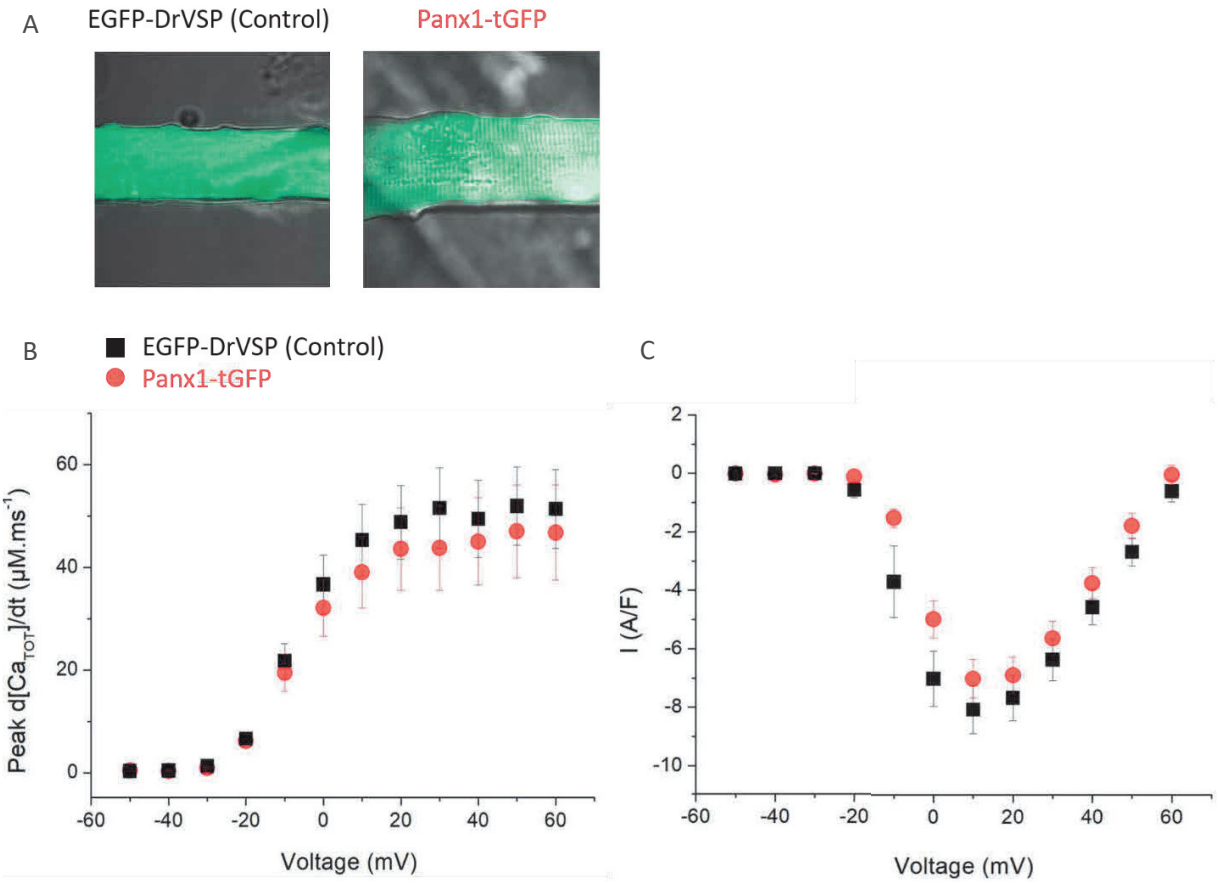

RESULTS 1 (Section1.3.). Voltage-activated SR Ca^{+2} release and $Ca_V1.1$ Ca^{2+} current in FDB muscle fibers expressing Panx1-tGFP tagged in C-terminal. *A) tGFP green fluorescence from a muscle fiber transfected with Panx1 plasmid and EGFP green fluorescence from a fiber transfected with EGFP-DrVSP, used as control (see Berthier et al., 2015). B) Voltage-dependence of the mean peak rate of SR Ca^{2+} release in control fibers (Maximum SR release flux = 51 ± 7.5 µmol^{-1}ms^{-1}, 9 fibers from 4 mice)* and in *Panx1-tGFP expressing fibers (Maximum = 46 ± 8.7 µmol^{-1}ms^{-1}, 14 fibers from 5 mice). There was no significant difference in any of the Boltzmann parameter between the two groups. C) Voltage-dependence of the peak Ca^{2+} current from the same groups of muscle fibers. There was no significant difference in the fitted I/V parameters except for a 6 mV positive shift in the half-activation voltage in the Panx1-expressing groups.*

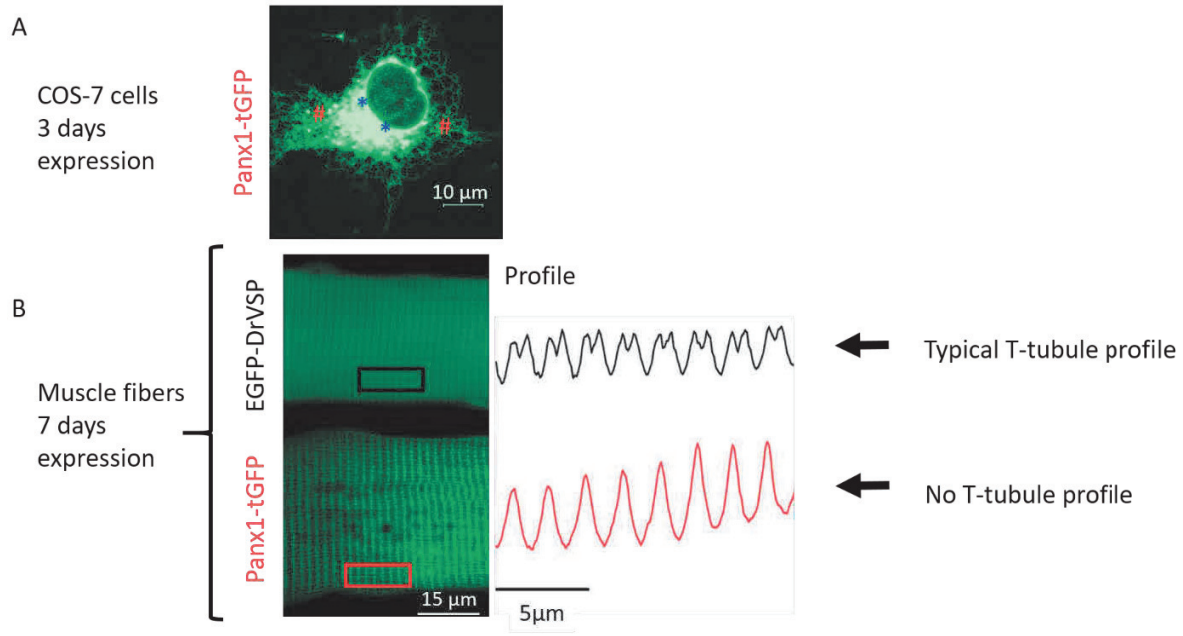

RESULTS 2 (Section1.3.). Pattern of expression of Panx1-tGFP in COS-7 culture cells and in FDB muscle fibers. *A) Distribution pattern of Panx1-tGFP after 2-days expression in the COS-7 cell line showing a perinuclear (* in blue) and a reticular (# in red) localization. B) Representative example of the pattern of localization for EGFP-DrVSP and for Panx1-tGFP after 7 days of expression in FDB muscle fibers. A T-tubule consistent pattern is clearly identified for EGFP-DrVSP but not for Panx1-tGFP C-terminal. We conclude that the C-ter tagged Panx1 does not reach the sarcolemma and T-tubule membrane.*

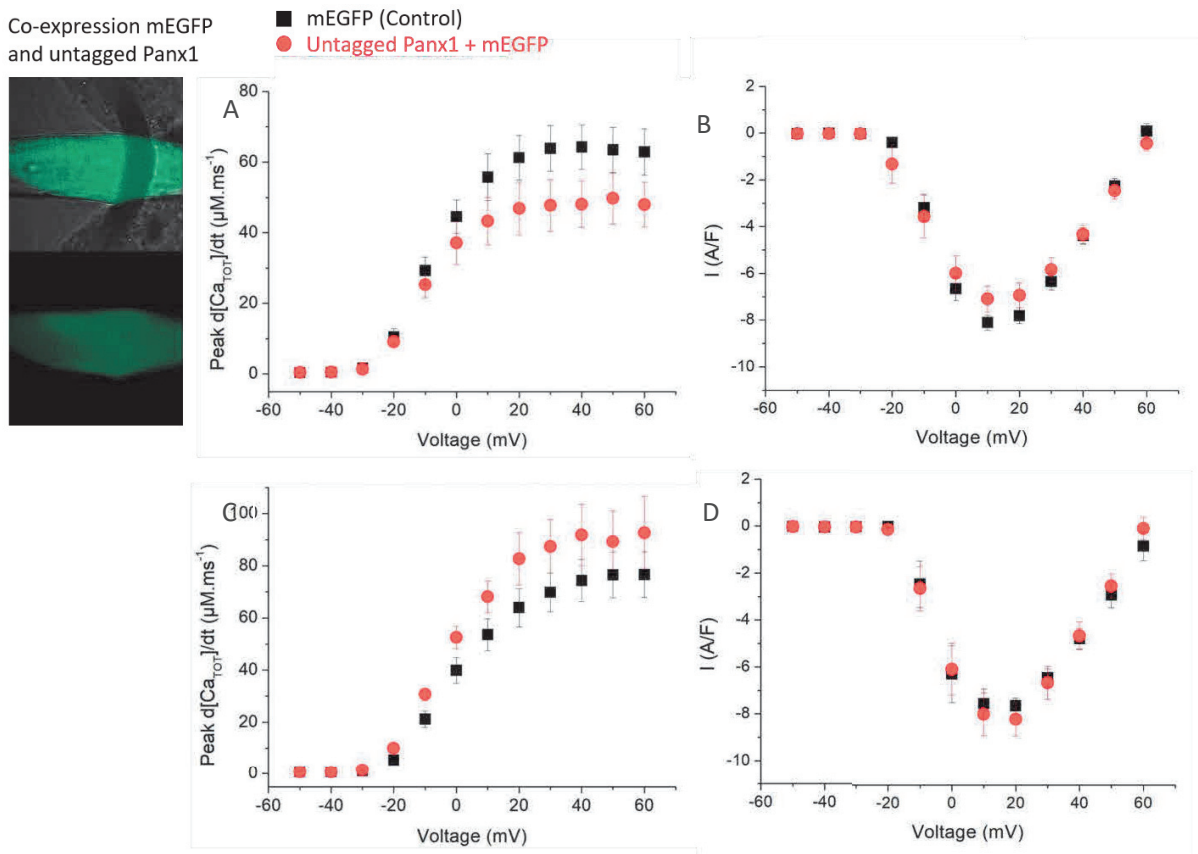

RESULTS 3 (Section1.3.). Voltage-activated SR Ca^{+2} release and $Ca_V1.1$ Ca^{2+} current in FDB muscle fibers co-expressing untagged Panx1 and mEGFP. *A) Voltage-dependence of the mean peak rate of SR Ca^{2+} release in mEGFP (control) fibers after 7 days of expression (Maximum rate of Ca^{2+} release = 63.6 ± 6.35 $\mu M^{-1}ms^{-1}$, 10 fibers from 3 mice) and in untagged Panx1 expressing fibers (Maximum = 48.6 ± 6.68 $\mu M^{-1}ms^{-1}$, 10 fibers from 3 mice). There was no significant difference in any of the Boltzmann parameters between the two groups. B) Voltage dependence of the mean peak Ca^{2+} current from the same groups of fibers. Fitting each dataset with the appropriate equation indicated a 18% decrease in maximum conductance in fibers expressing the untagged Panx1 (p-value = 0.0496). C) and D) Corresponding results from fibers tested 14 days post-transfection (mEGFP: 8 fibers from 3 mice; untagged Panx1:7 fibers from 3 mice). Fitting the respective sets of data with the appropriate equations gave no statistically significant difference for any parameter.*

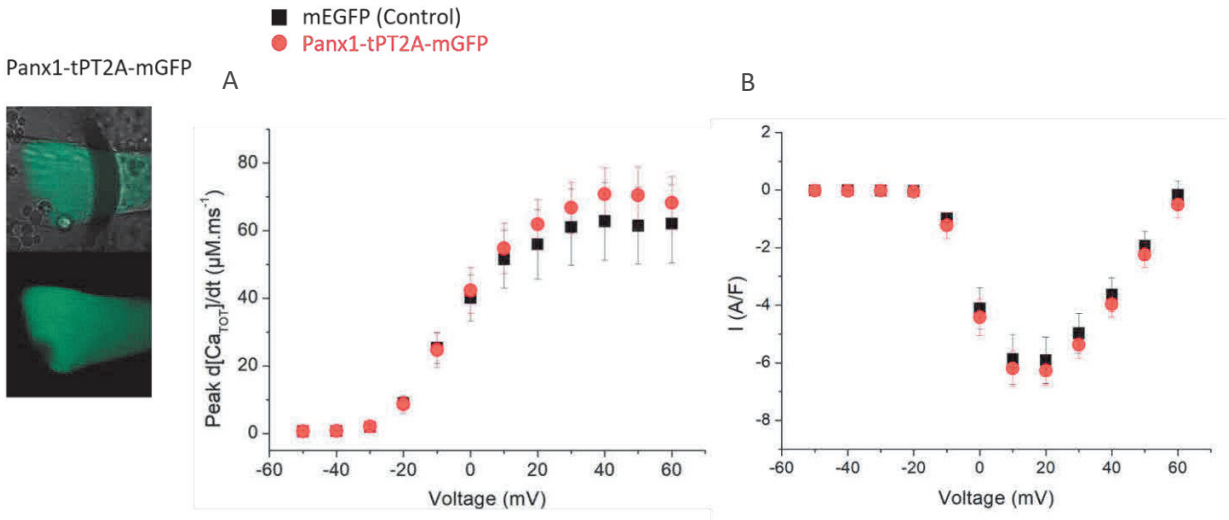

RESULTS 4 (Section1.3.). Voltage-activated SR Ca^{+2} release and $Ca_V1.1$ Ca^{2+} current in FDB muscle fibers expressing Panx1 fused with mGFP with the autocleavable site tP2TA. *A) Voltage-dependence of the mean peak rate of SR Ca^{2+} release in mEGFP (control) fibers (8 fibers from 3 mice) and in Panx1-expressing fibers (9 fibers from 3 mice) after 14 days of expression. There was no difference in any of the fitted parameters. B) Voltage-dependence of the peak Ca^{2+} current for the same groups of fibers. There was no difference either in any of the fit parameters.*

II. Results - 2nd objective

Section 2.1.

DEVELOPMENT OF A METHOD TO MEASURE ATP RELEASE FROM ADULT MUSCLE FIBERS USING ATP-SENSITIVE K^+ CHANNELS (K_{ATP}) IN INSIDE-OUT MEMBRANE PATCHES

We developed a method to measure extracellular ATP using skeletal muscle ATP-sensitive K^+ channels (K_{ATP}) (Allard et al., 1995). Opening of K_{ATP} channels is indeed inhibited by intracellular ATP in a dose-dependent manner. Monitoring of the activity of K_{ATP} channels in inside-out membrane patches excised from muscle sarcolemma thus allows to assess the concentration of ATP in the solution to which the cytoplasmic face of the patch is exposed. By positioning the inside-out membrane patch in the vicinity of a voltage-clamped skeletal muscle fiber, we expected to detect ATP released by the fiber upon stimulation. An extensive phase of testing has been required to find the appropriate bath solution to be used in order to, on one hand, preserve excitability of the stimulated muscle fiber and, on the other hand, allow opening of K_{ATP} channels. Obviously, an external Tyrode –like bath solution containing 5 mM K^+ was needed to preserve excitability and contractility of the voltage-clamped fibers. In order to maximize the release of ATP by stimulated fibers, the silicone voltage-clamped fiber was also dialyzed with an internal solution containing 15 mM ATP (diNa^+-ATP) through the pipette used for silicone-clamp. A mixture of 5 mM EGTA and 2 mM Ca^{2+} were also added to improve viability of the voltage-clamped fiber and minimize Ca^{2+}-induced K_{ATP} channel inactivation. In parallel, in order to keep a K^+ gradient on both sides of the inside-out membrane patch, a solution containing 140 mM K^+ was added in the pipette. Under these conditions, the K^+ equilibrium potential was then opposite to the physiological K^+ equilibrium potential. Finally, despite the reduced sensitivity produced by the presence of Mg^{2+} at the cytoplasmic face of K_{ATP} channels, addition of 6 mM Mg^{2+} was also found to considerably improve patch stability throughout the course of the experiment.

The voltage at which the inside-out membrane patch was clamped was chosen in order to maximize the amplitude of the unitary currents flowing through K_{ATP} channels. Since the K^+ equilibrium potential has a value of +85 mV in the presence of 140 mM and 5 mM K^+ at the external and the cytoplasmic face respectively, membrane potentials of 0, -30 and -60 mV were tested to produce inward currents. However, as observed by others, we noticed that applying voltages in the patch pipette compromised the stability of the membrane patch in the long run. The patch membrane was thus chosen

to be held at 0 mV and negative unitary currents of around 1 pA were measured as expected for K_{ATP} channels in the presence of a -85 mV electrochemical gradient (Figure 2A).

For each experiment, a systematic prerequisite was to apply 100 µM ATP at the cytoplasmic face of the inside-out membrane patch to probe the presence of K_{ATP} channels. Shortly after patch excision, the cytoplasmic face of the inside-out membrane patch being exposed to the bath solution devoid of ATP, opening of K_{ATP} channels carrying inward currents was expected to occur. ATP sensitivity was then attested by complete and reversible inhibition of channel activity produced by superfusion of the cytoplasmic face of the patch with a solution containing 1 mM ATP. As observed by others for cardiac and skeletal muscle K_{ATP} channels, a refreshment phenomenon was regularly observed, *i.e.* channel activity was potentiated upon washout of ATP as compared to activity measured before ATP addition (Figure 2B). Likely because of the presence of Ca^{2+} at micromolar concentrations in the bath solution, we frequently observed a contaminating activity of channels carrying inward currents of much larger amplitude and with clearly different opening pattern, that could be unambiguously identified as high conductance Ca^{2+}-activated K^+ channels. In this case, the proportion of K_{ATP} channel activity could be estimated by measuring the fraction of activity inhibited by ATP. However, when the proportion of Ca^{2+}-activated K^+ channel activity was too high, the membrane patch was not used to detect ATP release.

One major limitation in the study was the formation of vesicles upon patch excision. Vesicles are formed by the re-sealing of the membrane edges preventing the cytoplasmic face to be exposed to the bath solution. Formation of vesicles also generates high series resistances that contribute to produce aberrant amplitudes of single channel currents and activity. K_{ATP} channels are known to be present in the muscle sarcolemma at such high density that every membrane patch is expected to contain K_{ATP} channels (B. Allard, personal communication). Vesicles formation can thus be unambiguously detected when superfusion of the membrane patch with an ATP-containing solution had no effect on channel activity. With variable rates of success, the outer face of the vesicle could be broken to obtain the inside-out configuration by repeatedly moving the pipette out of the bath. In the whole, we were able to excise 41 membrane patches during 4 weeks of measurements. Because of either formation of vesicles that could not be ruptured, loss of patch membrane sealing during the course of the experiment, or a too high proportion of Ca^{2+}-activated K^+ channels activity in the membrane patch, we only succeeded to use 10 inside-out patches to detect ATP release by voltage-clamped muscle fibers.

Once the inside-out patch membrane was obtained and the presence of K_{ATP} channels ascertained by reversible inhibition of channel activity in the presence of ATP, the membrane patch was gently moved

closer to the portion of the silicone voltage-clamped fiber free of grease to detect release of ATP. Channel activity was recorded during 30-45 seconds before stimulation. Voltage clamp train pulses of 10 ms duration bringing the internal potential from -80 mV to +80 mV were then applied during 30-45 seconds at a frequency of 20 Hz. Channel activity was simultaneously measured during the train of stimulation and during 4-5 minutes after the train. Figure 2C shows channel activity in an inside-out patch membrane before, during and after a 30 seconds duration train of depolarizing pulses delivered at 20 Hz. In this patch, there is an apparent decrease of channel activity observed during the pulse train. This decrease in channel activity persisted several minutes after stimulation has stopped and there was a tendency to a re-increase in channel activity minutes later. Figure D shows that, in ten inside-out membrane patches containing K_{ATP} channels placed at proximity of a stimulated fiber, a 54 ± 22 % decrease of channel activity was measured after the train as compared to before the train. A mean peak of 79 ± 91 % re-increase in channel activity was also observed 380 seconds after the end of the stimulation train. However, a paired t-test indicated that this decrease induced by fiber simulation was not statistically significant ($p = 0.0852$). Facing the extremely high difficulty to implement these experimental conditions, patterns of 90 Hz-train pulses stimulation and pharmacological inhibition of Panx1 were not tested.

Conclusions

Although a tendency to a decrease in K_{ATP} channel activity was observed in response to repetitive stimulation of fibers, at this stage, we cannot conclude that, in our experimental conditions, muscle fibers stimulated at 20 Hz release ATP. Several hypotheses can be put forward to explain this absence of significant changes in K_{ATP} channel activity in response to fiber stimulation. A first hypothesis is that fibers stimulated at 20 Hz do release ATP but the concentration of ATP that reaches the cytoplasmic face of the membrane patch is too low to produce a significant inhibition of K_{ATP} channel activity. A second hypothesis is that muscle fibers do not release ATP in our experimental conditions, possibly because critical compounds in the cytosol required for the release of ATP are lost upon intracellular dialysis with the intrapipette solution used for silicone clamp. In this context, further experiments would consist in stimulating fibers with field electrodes in order to preserve the intracellular milieu. However, whatever the experimental conditions to be used, the extreme difficulty to keep K_{ATP} channel activity in inside-out membrane patches for the entire duration of the experiments remains an important limitation for the use of K_{ATP} channels as ATP biosensors.

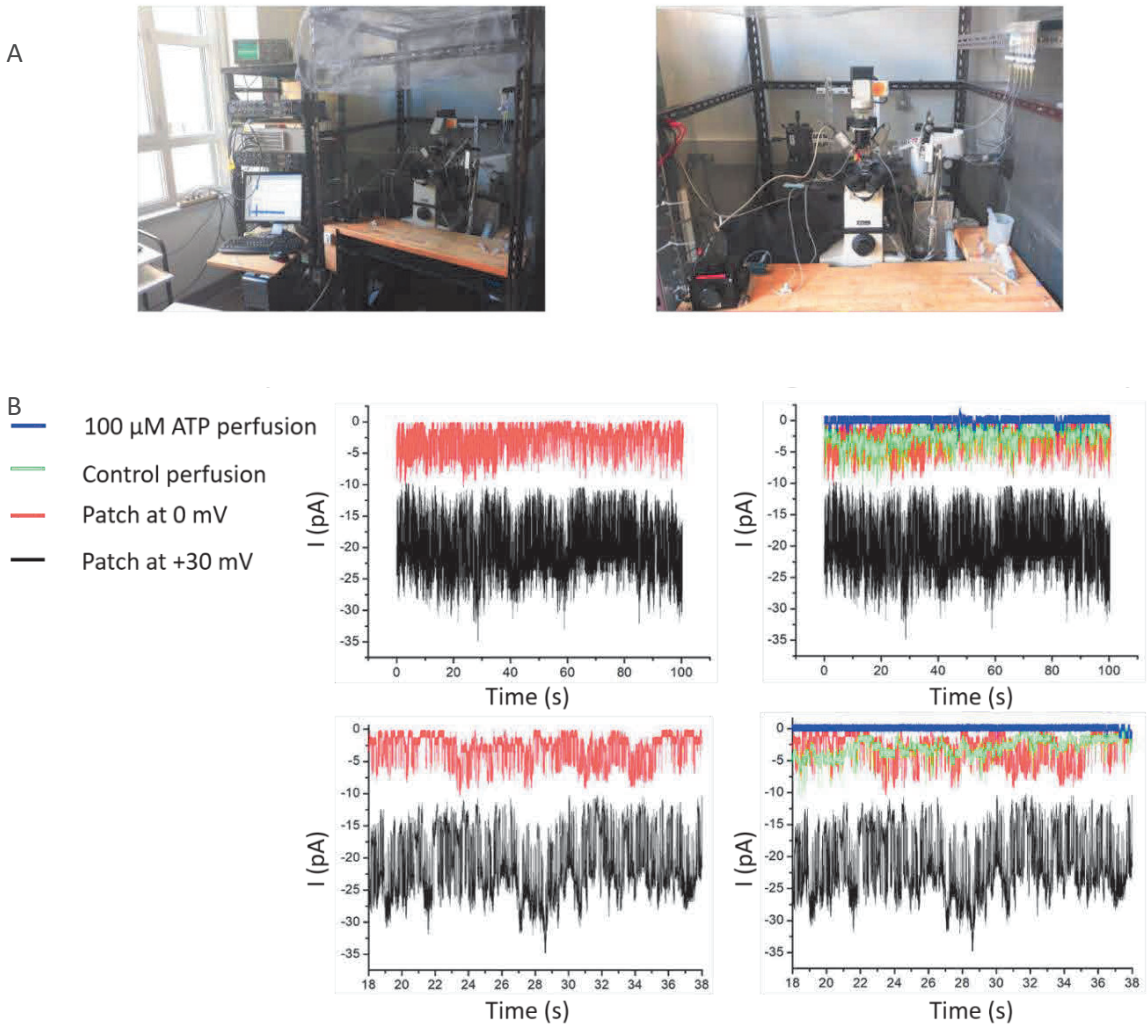

RESULTS 1. Experimental setup, and patch-clamp inside-out: K_{ATP} current voltage- and ATP-sensitivity. *A) We observe in the top some images of the electrophysiological setup with the two amplifiers, micromanipulators, pipettes and electrodes, the screen of the computer, and the oscilloscope to observed and record K^+current in the patch, and simultaneously control the fiber voltage in silicone voltage-clamp conditions. B) We observed 4 graphics. The two at the left shown exclusively the activity of the path at +30 mV (in black) vs 0 mV (in red) during 100 seconds (top) and during 20 seconds (bottom). We observe a mix between Ca^{2+} activated K^+ channels (maxi K channels) and the K_{ATP}. At the right we observe the same activity plus traces of the activity for the same patch when adding the control (green) and 100 µM of ATP perfusion (blue). We can observe a strong decrease in the patch activity under ATP perfusion.*

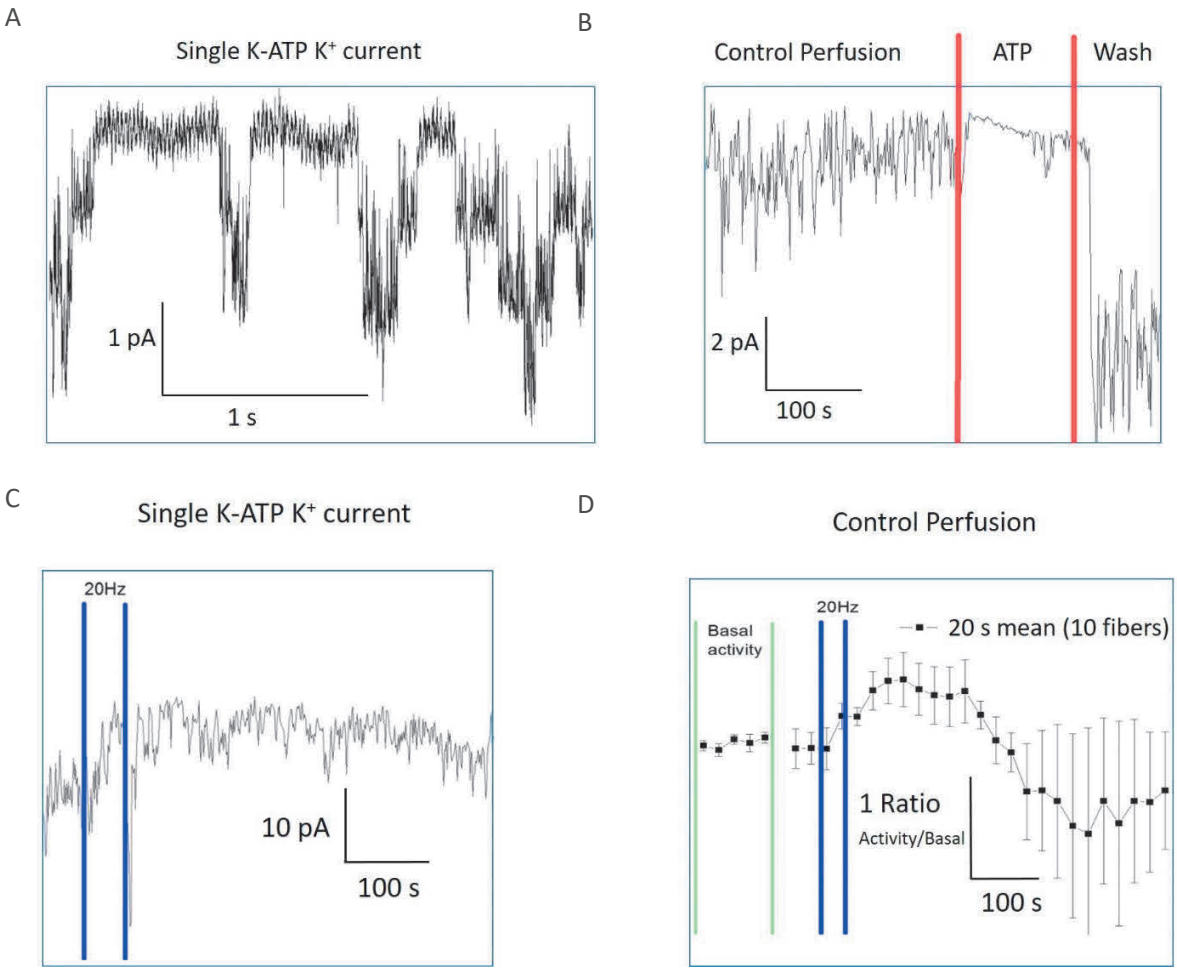

RESULTS 2. Patch-clamp inside-out: K_{ATP} current measurements under perfusion and experimental conditions. *A) Recording of K_{ATP} channel activity of an inside-out membrane patch held at 0 mV in the presence of 140 mM and 5 mM K^+ at the external and internal side of the patch respectively. B) Reversible inhibitory effect of ATP applied at the cytoplasmic face of an inside-out membrane patch held at 0 mV attesting for the presence of K_{ATP} channels. C) Changes in K_{ATP} channel activity in an inside-out membrane patch held at 0 mV and placed at proximity of a voltage-clamped muscle fiber stimulated by depolarizing pulses delivered to +80 mV at a frequency of 20 Hz. The two vertical blue bars indicate the period during which the fiber was stimulated. D) Mean changes in K_{ATP} channel activity recorded in ten inside-out membrane patches held at 0 mV before, during and after fiber stimulation. Each data point corresponds to a 20 s duration recording of the mean current normalized to the basal mean current at the beginning of the experiment. The two vertical green and blue bars indicate the period during which the basal activity was measured and the period during which the fiber was stimulated respectively.*

Section 2.2.

DEVELOPMENT OF A METHOD TO MEASURE ATP RELEASE FROM ADULT MUSCLE FIBERS USING THE EXPRESSION OF ATP-SENSITIVE PURINERGIC IONOTROPIC RECEPTORS (P2XR)

Following the conclusion of our K_{ATP} biosensor, we looked for an easier to implement and potentially more sensitive method. For this, we tested expression of an ATP-sensitive purinergic ionotropic receptor (P2XR) in the sarcolemma of the fibers, and measurement of ATP-sensitive cationic current through these channels as an estimate of changes in extracellular ATP concentration, as previously shown in HEK293T cells (Hayashi et al. 2004). The working hypothesis was that, following Casas et al. (2010) and Jorquera et al. (2013), stimulation with 20 Hz trains of short voltage-clamp depolarizing pulses should produce ATP release and thus activate the P2XR artificially expressed in the surface membrane of the same fiber. Accordingly, we anticipated being able to measure the P2XR channel activity due to the increment of extracellular ATP. We first transfected the P2XR-GCaMP plasmid in COS-7 cells and confirmed the plasma membrane localization of the protein after 2 days of expression (Data not shown). We then used in vivo transfection in FDB and IO muscles of adult mice. Isolated transfected fibers were selected from the GCaMP green fluorescence, and were handled with the silicone voltage-clamp conditions, making sure that the P2XR-GCaMP expressed portion of the fibers remains outside the silicone. Whole-cell membrane current was followed before, during and after 4 different stimuli: A) extracellular application of 100 µM ATP, B) 20 Hz stimulation and C) 90 Hz stimulation.

Pattern of expression in differentiated muscle fibers.

The efficiency of transfection with the P2XR-GCaMP plasmids was low, with <10% of the available muscle fibers presenting green fluorescence. There was also some heterogeneity in the expression pattern of the channel receptor with some fibers or some fiber's areas exhibiting a clear T-tubule profile distribution as presented in Results 3, whereas this pattern was not always so obvious in other fibers or in other regions of the same fiber. When establishing the silicone-clamp conditions, we made sure that the portion of fiber outside the silicone exhibited green fluorescence.

P2XR-GCaMP inward current as an ATP sensitive probe.

We systematically tested the efficiency of 100 µM of extracellular ATP perfusion to trigger an inward change in membrane current at the holding voltage. This worked, but there was variability in the amplitude of the response: considering voltage-clamped fiber portions of similar size and exhibiting a similar level of baseline holding current the ATP-induced maximum change corresponded to a 20-fold

increase in the holding current. On average, ATP perfusion-induced P2X response corresponded to a peak current of 43.8 ± 32 nA (mean ± SD), reached ≈1-2 seconds after the onset of the ATP perfusion. This fiber-to-fiber variability was likely related to differing levels of expression of P2XR-GCaMP.

P2XR-GCaMP Ca^2 fluorescence for measuring Ca^{2+} entry as indirect indicator of ATP release

Besides the possibility to detect ATP release from P2X channels current in voltage-clamp conditions, the plasmids provided by F. Rassendren also offered the option to track the changes in Ca^{2+} near the mouth of the channels, taking advantage of the fused GCaMP Ca^{2+} sensitive biosensor fluorescence. This was an alternative indirect indicator of ATP release after trains of stimulation at 20 Hz and 90 Hz in silicone voltage-clamped fibers, using simultaneous confocal microscopy. We were able to detect an increase in Ca^{2+} corresponding to an ~4 times increase in baseline GCaMP fluorescence upon ECC produced by the protocols of train stimulation. However, we did not observe any change in fluorescence after the stimulation at 20 or 90 Hz that could reliably be interpreted to correspond to a Ca^{2+} entry through P2X channels. One specific difficulty was related to the need for long exposure to the scanning laser (taking images every 2 seconds over a periods of 5-10 minutes) that tended to damage the fiber. Overall, although we could have attempted to further optimize the conditions of fluorescence detection, we decided to continue on by relying solely on the changes in membrane current which, in any case, provide a more direct estimate of the P2X channel activity.

P2XR current as an indicator of ATP release in differentiated muscle fibers

Following the concepts developed by Casas et al. (2010) and Jorquera et al. (2013) from measurements of ATP release from populations of differentiated muscle fibers electric-field-stimulated at various frequencies, we tested whether the ATP-sensitive inward current through P2XR at the -80 mV holding voltage, could be used as an indicator of the anticipated 20 Hz stimulation-activated ATP release. In order to enhance the ATP gradient, we dialyzed during 20 minutes each fiber with 15 mM of ATP present in the internal solution in the voltage-clamp pipette. Then, we applied in each fiber two protocols of pulses stimulation: 1) a 30 s-long train of 5 ms duration pulses from -80 to to +60 mV at 20 Hz and 2) an equivalent train of pulses at 90 Hz. The holding membrane current was followed over a 30 seconds period before each train, and over 4-5 minutes following the train.

For each fiber, we decided to present the individual results using what we called Delta (Δ) current. The Δ current corresponds to the difference between the average holding current before the pulse train

(30 s-long baseline) and the peak of "ATP-induced" increase in holding current within 5 minutes following the train.

We also tested the effect of alternating the order of frequency stimulation: either 20 Hz first and 90 Hz 2nd, or the opposite, but did not find any related difference in the outcome. We worked on two groups of transfected mice: one group with 1-week of expression and the other with 2-weeks of expression. We observed a larger percentage of P2XR-GCaMP-expressing fibers when using 2-weeks of expression (≈20%). We also used two different protocols for the ATP perfusion test: either we applied ATP perfusion before the trains of pulses or after the trains (see Results 4B).

Following either of the trains we could not detect a change in holding current that would exhibit a reproducible time-course from fiber to fiber so that we could irrefutably point it out as ATP release-induced P2XR activation. Illustrative records of corresponding membrane current traces are shown in Results 4A. Assuming that there could be a large intrinsic variability in the ATP release-induced current, we measured, for each fiber and protocol (20 Hz and 90 Hz), what we refer to as the Δ current which corresponds to the maximum inward change in holding current level throughout the 5 minutes post-stimulation, from the pre-train baseline level. We used this value as an index of the putative extent of ATP release for each fiber and protocol.

We considered, for each independent fiber, the ATP perfusion-induced maximum inward current as a reference, assuming that the size of that response was proportional to the amount of P2XRs in the sarcolemma. Values for the maximal change in current following 20 Hz and 90 Hz stimulations could then be compared to that reference value in each fiber. Using this method, we measured from all tested fibers (n= 13) a 11.9 ± 15.3 % (mean ± SD) increase in holding current after the 20 Hz stimulation and a 10.3 ± 7 % (mean ± SD) increase after 90 Hz stimulation. When comparing the absolute values of Δ current after 20Hz and 90Hz stimulation, they were not statistically different, with a p-value = 0.7161 (paired t test). This indicates that in our conditions, either there is no ATP release, or ATP release exhibits no stimulation-frequency dependence. Still, there was big dispersion of the data for both the 20 Hz and 90 Hz protocols. Within a more detailed analysis, we examined whether two different groups of fibers could be identified in terms of relative response to the 20 Hz and 90 Hz protocols: In one groups the 20 Hz stimulation produced larger Δ currents than the 90 Hz stimulation (Results 4B, red), while in the other group we observed the opposite (Results 4B, black). There was a tendency for these two types of response to be related, somehow, to whether ATP perfusion was applied before or after the trains. Rationale for an influence of this parameter could be due to ATP perfusion-induced desensitization of the P2XRs, over the

following course of the experiment, which would preclude proper detection of the following trains-induced ATP release and consequent P2XRs activation. Accordingly, only fibers tested with ATP perfusion applied after the frequency protocols would be reliable. At this point, more experiments would be needed to assess the definite influence of this parameter.

We initially anticipated the use of pharmacological blockers for either P2XR or Panx1 to achieve a convincing characterization of the role of these two proteins in ATP release following the trains of stimulations. However, the lack of reproducible responses with a well defined time-course, to the trains of stimulations, has precluded these investigations.

Conclusions

Adult differentiated muscle fibers do not exhibit functional P2XRs in the plasma membrane (Collet et al., 2002). We report here that expression of a P2XR in this tissue makes a very efficient approach for sensing extracellular ATP at the level of a single isolated muscle fiber, with 100 µM ATP generating an increase in holding current in the 10s of nA range. This should allow detection of much smaller changes in extracellular ATP possibly down to the µM range. Considering also that Panx1 is present in the T-tubule membrane (Jorquera et al., 2013; Riquelme et al., 2013), any ATP release within the associated nanovolume may elevate local ATP concentrations to larger than µM levels. The present approach is thus likely more sensitive than the use of excised K_{ATP} channels. In addition, this method is much easier to implement, and allowed us to achieve more fiber's measurements in less time and to systematically test the two different protocols at 20 Hz and 90 Hz in each fiber. Nevertheless, results related to the frequency-dependent Panx1-mediated ATP release have remained so far inconclusive. Mainly, we have been unable to detect a clear change in membrane current with a consistent time-course following any of the two protocols. Furthermore, an analysis of the data based on the best criterion we could use (the peak change in current over a time-period consistent with that described by Jorquera et al., 2013) did not provide yet convincing enough evidence for 20 Hz being a permissive stimulation frequency for ATP release.

We propose two possible explanations: either there is no Panx1-dependent ATP release after voltage-clamp stimulations in our particular conditions, or this method is again not sensitive enough to detect ATP release.

Regarding the first possibility, recent results suggest that Panx1 can be open only by two conditions: caspase cleavage and phosphorylation (Jin et al. 2020, Ruan et al. 2020). A possible explanation for why we could not confirm Jorquera et al. (2013) data may be related to the intracellular

dialysis applied before starting the experiments. It may be that this produces dilution of an important factor such as a caspase or a kinase required to open the Panx1 main pore and to allows stimulation frequency-dependent ATP release.

Future attempts will thus include P2XR current measurements in non-dialyzed fibers challenged with trains of stimulations. Conversely, intracellular dialysis of P2XR-expressing muscle fibers with enzymatic inducers of Panx1 activation may also prove useful to further decipher the mechanism of Panx1-dependent ATP release in muscle fibers. Alternatively, assuming the lack of success is due to poor sensitivity of the sensor, future approaches may also include expression of a P2XR with enhanced affinity for ATP.

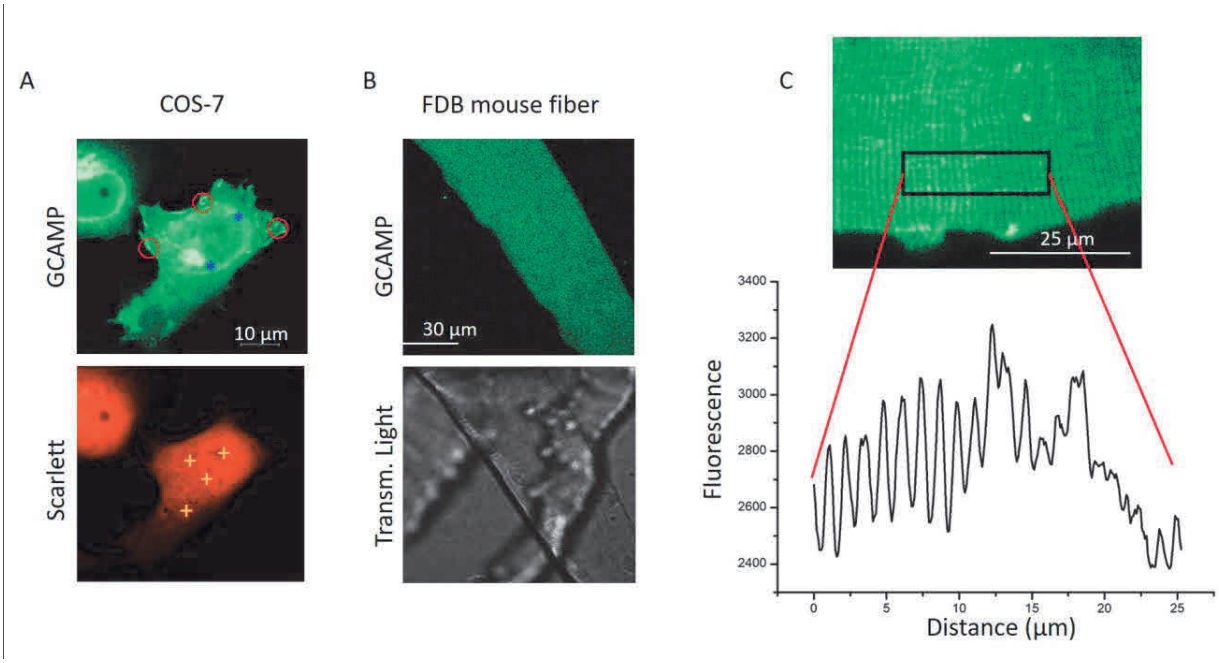

RESULTS 3. Expression of P2XR-GCaMP plasmid in COS-7 and FDB from adult mice and T-tubule profile analysis. *A) P2XR-GCaMP (left) distribution in COS-7 corresponds a plasma membrane (red circles) and perinuclear localization (* in blue) whereas the red fluorescent protein Scarlett (right) shows a diffuse cytosolic (+ in yellow) distribution. B) At the right we observe a representative example of a fiber expressing P2XR-GCaMP. We systematically selected the fibers based on their level of green GCaMP fluorescence and a good shape under visible light. C) At the right we observe the analysis of the T-tubule profile. The transverse profile of fluorescence showed in some portion the T-tubule characteristic double peak with ≈2 µm between two consecutives peaks of fluorescence. We observe that a portion of the fiber present T-tubule profile, while other portions do not.*

A

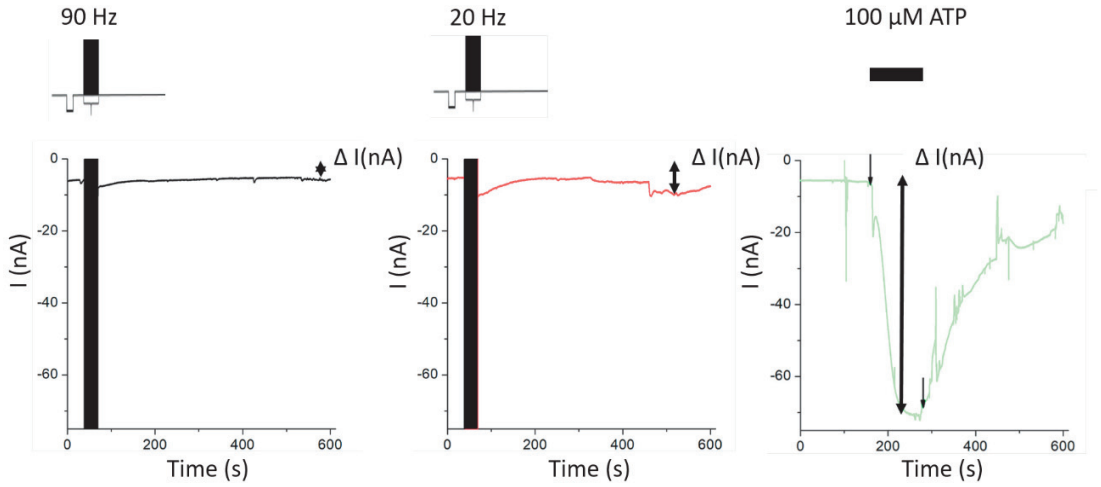

B

ATP responsive fibers

		Δ ATP-Perfusion [ηA]	Δ 20Hz [ηA]	Δ 90Hz [ηA]
1 week of expression - ATP perfusion at the end of experiment	**Fiber 1**	57	0.3	1.1
	Fiber 2	30	5.2	1
	Fiber 3	95	4.7	1.2
	Fiber 4	6	3.5	0.9
2 weeks of expression - ATP perfusion at the beginning	**Fiber 5**	22	2.9	1.8
	Fiber 6	60	0.6	12.3
	Fiber 7	64	4.6	14.7
	Fiber 8	10	0.9	1.1
	Fiber 9	32	0.3	2.2
	Fiber 10	76	1.8	4.1
	Fiber 11	93	6.9	16
	Fiber 12	10	1.2	1.3
	Fiber 13	15	3.1	1

Delta current

$\Delta I_{20Hz} > \Delta I_{90Hz}$

$\Delta I_{90Hz} > \Delta I_{20Hz}$

RESULTS 4. P2XR Ca^{2+} channel as an ATP sensitive probe. *A) A representative example of an ATP responsive fiber under silicone voltage-clamp conditions, with the Ca^{2+} current response recorded before, and during 5 minutes' post: a 90 Hz stimulation (black), a 20 Hz stimulation (red) and 100 µM ATP-perfusion (green). We measured the Delta (Δ) current obtained from the difference between the mean resting current before the pulse and the maximal Ca^{2+} current (negative values) after the stimulus. B) Table showing the Δ currents for all ATP-responsive fibers after: ATP-perfusion, 20 Hz and 90 Hz of stimulation. We observed two conditions, a) P2XR-GCAMP 1-week expression with ATP perfusion at the end of the experiment, and b) 2-weeks expression with ATP perfusion at the beginning. In this two condition we also observed two groups of response. Fibers that shown a bigger Δ current after 20 Hz (red), which represents more ATP release at this frequency (like observed by Jorquera et al., 2013) and fibers that shown bigger Δ currents after 90 Hz of stimulation, which is against Jorquera et al. (2013) results.*

III. Results - 3rd objective

Section 3

EXCITATION-CONTRACTION COUPLING IN ADULT SKELETAL MUSCLE FIBERS FROM A MOUSE MODEL OF DIABETES AND OBESITY GENERATED BY A HIGH-SUCROSE HIGH-FAT DIET (HSHFD)

Article 3: Francisco Jaque-Fernandez, Agathe Beaulant, Christine Berthier, Laloe Monteiro, Bruno Allard, Mariana Casas, Jennifer Rieusset, Vincent Jacquemond (2020). Preserved Ca^{2+} handling and excitation-contraction coupling in muscle fibres from diet-induced obese mice. Diabetologia. 63 (11): 2471-2481.

The initial hypothesis behind this work was that the described muscle function impairment in Diabetes/Obese mouse models could be explained by an alteration in the excitation-contraction coupling (ECC). Because of preliminary data in Casas' laboratory in Chile, in which they observed an alteration in ATP release regulation in differentiated muscle fibers from a High Fat Diet (HFD) mouse model, and in association with our previous results showing Panx1 as a regulator of ECC, we were also interested in the possibility that Panx1 play a role in the hypothetical ECC alteration and in muscle weakness in Diabetes/Obese model.

The literature used to study muscle dysfunctions in these diseases is enormous and inconclusive, probably because of the use of different animal models and experimental conditions (Tallis et al., 2018). However, there are several evidence showing that a long period of high-fat diet (HFD) produce a decrease in specific force production evaluated ex vivo from mouse muscles (Eshima et al., 2017; Tallis et al., 2018), and other important works shown that an alteration in the intracellular Ca^{2+} handling induce cardiac dysfunction (Carvajal et al., 2014). It has been proposed that an alteration in Ca^{2+} handling and ECC could be behind the skeletal muscle dysfunction observed in type 2 diabetes mellitus and obese models. In this work, in a collaboration with Jennifer Rieussiet' team at CarMeN laboratory, we used a diet-induced type 2 diabetes mellitus – obese mice model to study the Ca^{2+} handling and ECC in differentiated FDB muscle fibers. For this we enzymatically isolated the muscle fibers as previously described (Jacquemond, 1997) and use simultaneously electrophysiology in silicone voltage-clamped cells, Ca^{2+}-sensitives indicators and confocal microscopy.

High Fat High Sucrose Diet (HFHSD) induce a mice model with obesity, insulin resistance and glucose intolerance

This model was produced and characterized at CarMeN. After 16 weeks of HFHSD diet, the mice presented 1.7 times increase in the weight compared with their littermates under standard chow diet (SCD) conditions (Control). The mean values for body weight at the end were 28.6 ± 0.5 g (9 mice) and 50.1 ± 0.9 g (9 mice). There was no change in the weight for the gastrocnemius and the heart, while the weight for the liver and adipose tissue importantly increased in HFHSD mice. The epididymal adipose tissue was 0.51 ± 0.04 g (9 mice), and 2.06 ± 0.17 g (9 mice) with a p-value <0.0001. The mice shown glucose intolerance and insulin resistance observed in the glucose tolerance test (GTT) and insulin tolerance test (ITT) at 4, 8, 14 and 16 weeks of HFHSD (see attached article).

T-tubule network and passive electrical properties in SCD and HFHSD muscle fibers

Considering the role of the T-tubule and triad structure in the Ca^{2+} handling and ECC machinery proper function, we studied the T-tubule network and the passive electrical properties of the plasmatic membrane. We dissociated the fibers in Tyrode and load them during 30 minutes with 10 µmol/l of the plasma membrane marker Di-8-ANNEPPS. We compare 20 muscle fibers from 2 SCD mice versus 30 muscle fibers from 3 HFHSD mice. The corresponding x,y confocal images showed no alteration of the T-tubule network and the transversal profile of fluorescence showed the T-tubule characteristic double peak in mammalian muscles. Surprisingly, the mean value for the sarcomere length presented and small but statistically significant reduction with 2.11 ± 0.02 for the SCD group versus 2.04 ± 0.01 for the HFHSD group ($p<0.001$). Diameter and passive electrical properties like capacitance and input resistance shown no difference between groups. We concluded that the T-tubule network was preserved in obesity conditions.

$Ca_V1.1$ Ca^{2+} current and voltage-sensing properties in SCD and HFHSD muscle fibers

$Ca_V1.1$ regulate and interacts with RyR1 during the ECC coupling, and an alteration in his function can produce ECC coupling alteration and muscle dysfunction. Thus, we recorded $Ca_V1.1$ Ca^{2+} currents under silicone voltage-clamp conditions during increasing 0.5 s-long voltage pulses from -50 mV to +60 mV and calculate the peak Ca^{2+} current to generate our IV curve. When fitting each individual IV curve and averaging the different parameter we obtained a maximum conductance of 196 ± 13 S/F for the SCD group (n= 20 fibers from 4 mice) versus 234 ± 12 S/F for the HFHSD group (n= 29 fibers from 5 mice), showing not difference between groups.

We also studied the intra-membrane charge movement holding the fibers at -100 mV, and applying increasing 20 ms-long pulses from -80 mV to + 20 mV in extracellular solution with low levels of free Ca^{2+} (µM range). We observed no difference in the maximum amount of charge with 32.9 ± 2.0 nC/µF for the SCD group (n= 22 fibers from 3 mice) versus 30.7 ± 1.6 nC/µF for the HFHSD group (n= 21 fibers from 3 mice). We conclude that the amount of $Ca_V1.1$ in the T-tubules and its voltage-sensing properties were preserved under this conditions.

Voltage-activated SR Ca^{2+} release

The study of the voltage-activated SR Ca^{+2} release allows us to indirectly study RyR1 function and ECC, which are critical for the proper muscle function. In the FDB muscle fibers under silicone voltage-clamp condition we recorded the voltage-activated rhod-2 fluorescence transients upon a protocol of stimulation of increasing 0.5 s-long pulses from -50 mV to +60 mV as previously described (Pouvreau et al., 2006; Lefebvre et al., 2011). We used F/F0 rhod-2 fluorescence transients to calculate the rate of SR Ca^{2+} release as previously described (methods) and we studied the voltage-dependence of the maximum rate of SR Ca^{2+} release (peak $d[Ca_{Tot}]/dt$) and fitted the individual traces to obtain the Max, V05 and k parameters. We observed no difference in any of these parameters between group with mean values of 76 ± 6.5 µmol l^{-1} ms^{-1} for the SCD group (n= 21 fibers from 4 mice) versus 78 ± 4.4 µmol l^{-1} ms^{-1} for the HFHSD group (n= 30 fibers from 5 mice). Therefore, the RyR1 channel activity and SR Ca^{2+} content are preserved in HFHSD differentiated muscle fibers.

Cytosolic Ca^{2+} removal capabilities and response to a fatiguing stimulation protocol

The SERCA pump participate in relaxation during muscle contraction and is in charge of the SR Ca^{2+} re-uptake, which plays a critical role for consecutives solicitations. It has been proposed that HFD-induced obesity may alter SERCA because of and altered SR phospholipid composition (Funai et al., 2016) and/ or and alteration in the SERCA regulator sarcolipin (Paran et al., 2015). Because the critical role of SERCA in the cytosolic Ca^{2+} clearance we evaluated the cytosolic Ca^{2+} removal capabilities as an indicator of SERCA function. We load the muscle fibers with the intermediate affinity Ca^{2+}-sensitive fluorescence dye Fluo-4FF dialyzed through the pipette, and we measured the time constant of the Ca^{2+} signal decay following repolarization-induced Ca^{2+} release termination. When analyzing the mean for the time constant of decay obtained after +60 mV pulses with different long durations (2 ms, 5 ms, 10 ms, 20 ms, 50 ms and 100 ms) we observed no differences between HFHSD group (n= 8 fibers from 4 mice) versus SCD (n= 13 fibers from 5 mice). Under the same condition we studied the response of ECC machinery under an

exhausting stimulation protocol of consecutive trains of 30 pulses with 5-ms-long, from -80 mV to +60 mV, at 100 Hz. We applied 30 consecutives trains with an interval of 0.7 s. This protocol produced a rapid reduction of SR Ca^{2+} release for both SCD group (8 fibers from 4 mice) and HFHSD (12 fibers from 5 mice). The time course for each fiber was fitted by a single exponential plus constant function. The mean value of the time constant and final level did not shown difference between groups. We conclude that the SERCA function was conserved in HFHSD differentiated muscle fibers.

Spontaneous Ca^{2+} release activity at rest

The spontaneous Ca^{2+} activity at rest, called Ca^{2+} sparks have been a hallmarked of several muscle diseases (Kutchukian et al., 2017; Kutchukian et al., 2019) and has been associated with an alteration in normal RyR1 channel regulation by $Ca_V1.1$. We studied this possibility using confocal imaging of the Ca^{2+} sensitive dye fluo-4. We load the fibers in Tyrode with fluo-4 AM during 30 minutes, and taken 30 consecutive x,y confocal images (every second during ≈30 seconds). Ca^{2+} sparks activity was calculated for SCD (n= 28 fibers from 3 mice) and for HFHSD (46 fibers from 5 mice). The mean fiber area exhibiting Ca^{2+} sparks activity was significantly increased in HFHSD group (p= 0.043) in a quantitatively modest manner with 0.6% for HFHSD group vs 0.4% in the SCD group. We observed that this difference was produce by 4 muscle fibers obtained from the same HFHSD mouse, which exhibited an area exhibiting Ca^{2+} sparks of 1.5 %. Altogether we conclude that there were not significant and relevant differences between groups.

Conclusions

We demonstrated that the Ca^{2+} handling and ECC coupling in the FDB muscle fibers from a high fat high sucrose diet (HFHSD)-induced type 2 diabetes-obese mouse model is strongly preserved. Therefore, the muscle impairment observed in similar models (HFD) (Eshima et al., 2017) cannot be explained by an alteration in the force production at ECC level. Because we did not observe difference in ECC, we decide not to go further with the Panx1 study in this model. To our concern, the alteration of Panx1 observed as an alteration in ATP release, do not play a role in the regulation of ECC in this model.

Article

Preserved Ca^{2+} handling and excitation–contraction coupling in muscle fibres from diet-induced obese mice

[1]Francisco Jaque-Fernandez, [2]Agathe Beaulant, [1]Christine Berthier, [1]Laloé Monteiro, [1]Bruno Allard, [3]Mariana Casas, [2]Jennifer Rieusset, [1]Vincent Jacquemond

[1] Institut NeuroMyoGène, UMR CNRS 5310 – Inserm U1217 – Université Claude Bernard Lyon 1 – Univ Lyon, Faculté de Médecine et de Pharmacie, Lyon, France.

[2] CarMeN Laboratory, Inserm, INRA, INSA Lyon, Université Claude Bernard Lyon 1 – Univ Lyon Pierre-Bénite, France.

[3] Programa de Fisiología y Biofísica, Instituto de Ciencias Biomédicas, Facultad de Medicina, Universidad de Chile, Santiago, Chile.

Corresponding author:
Vincent Jacquemond
E-mail : vincent.jacquemond@univ-lyon1.fr
ORCID iD : 0000-0003-4944-270X

Received: 4 May 2020 / Accepted: 6 July 2020

Abstract

Aims/hypothesis Disrupted intracellular Ca^{2+} handling is known to play a role in diabetic cardiomyopathy but it has also been postulated to contribute to obesity- and type 2 diabetes-associated skeletal muscle dysfunction. Still, there is so far very limited functional insight into whether, and if so to what extent, muscular Ca^{2+} homeostasis is affected in this situation, so as to potentially determine or contribute to muscle weakness. In differentiated muscle, force production is under the control of the excitation–contraction coupling process: upon plasma membrane electrical activity, the $Ca_V1.1$ voltage sensor/Ca^{2+} channel in the plasma membrane triggers opening of the ryanodine receptor Ca^{2+} release channel in the sarcoplasmic reticulum (SR) membrane. Opening of the ryanodine receptor triggers the rise in cytosolic Ca^{2+}, which activates contraction while Ca^{2+} uptake by the SR ATPase Ca^{2+}-pump promotes relaxation. These are the core mechanisms underlying the tight control of muscle force by neuronal electrical activity. This study aimed at characterising their inherent physiological function in a diet-induced mouse model of obesity and type 2 diabetes.

Methods Intact muscle fibres were isolated from mice fed either with a standard chow diet or with a high-fat, high-sucrose diet generating obesity, insulin resistance and glucose intolerance. Properties of muscle fibres were investigated with a combination of whole-cell voltage-clamp electrophysiology and confocal fluorescence imaging. The integrity and density of the plasma membrane network (transverse tubules) that carries the membrane excitation throughout the muscle fibres was assessed with the dye Di-8-ANEPPS. $Ca_V1.1$ Ca^{2+} channel activity was studied by measuring the changes in current across the plasma membrane elicited by voltage-clamp depolarising pulses of increasing amplitude. SR Ca^{2+} release through ryanodine receptors was

simultaneously detected with the Ca^{2+}-sensitive dye Rhod-2 in the cytosol. $Ca_V1.1$ voltage-sensing activity was separately characterised from the properties of intra-plasma-membrane charge movement produced by short voltage-clamp depolarising pulses. Spontaneous Ca^{2+} release at rest was assessed with the Ca^{2+}-sensitive dye Fluo-4. The rate of SR Ca^{2+} uptake was assessed from the time course of cytosolic Ca^{2+} recovery after the end of voltage excitation using the Ca^{2+}-sensitive dye Fluo-4FF. The response to a fatigue-stimulation protocol was determined from the time course of decline of the peak Fluo-4FF Ca^{2+} transients elicited by 30 trains of 5-ms-long depolarising pulses delivered at 100 Hz.

Results The transverse tubule network architecture and density were well preserved in the fibres from the obese mice. The $Ca_V1.1$ Ca^{2+} current and voltage-sensing properties were also largely unaffected with mean values for maximum conductance and maximum amount of charge of 234±12 S/F and 30.7±1.6 nC/µF compared with 196±13 S/F and 32.9±2 nC/µF in fibres from mice fed with the standard diet, respectively. Voltage-activated SR Ca^{2+} release through ryanodine receptors also exhibited very similar properties in the two groups with mean values for maximum rate of Ca^{2+} release of 76.0±6.5 and 78.1±4.4 µmol l^{-1} ms^{-1}, in fibres from control and obese mice, respectively. The response to a fatigue protocol was also largely unaffected in fibres from the obese mice, and so were the rate of cytosolic Ca^{2+} removal and the spontaneous Ca^{2+} release activity at rest.

Conclusions/interpretation The functional properties of the main mechanisms involved in the control of muscle Ca^{2+} homeostasis are well preserved in muscle fibres from obese mice, at the

level of both the plasma membrane and of the SR. We conclude that intracellular Ca^{2+} handling and excitation–contraction coupling in skeletal muscle fibres are not primary targets of obesity and type 2 diabetes.

Keywords

Ca^{2+} homeostasis, Cytosolic Ca^{2+} clearance, Excitation–contraction coupling, Obesity, Ryanodine receptor, Sarcoplasmic reticulum Ca^{2+} release, Skeletal muscle, Type 2 diabetes

Abbreviations

BTS	*N*-benzyl-*p*-toluene sulphonamide
$[Ca_{Tot}]$	total amount of released Ca^{2+} referred to the myoplasmic water volume
$d[Ca_{Tot}]/dt$	rate of SR Ca^{2+} release
ECC	Excitation–contraction coupling
F_0	Baseline fluorescence
FDB	Flexor digitorum brevis
G_{max}	maximum conductance
HFHSD	High-fat, high-sucrose diet
k	steepness factor
Q_{max}	maximum charge
RYR1	Type 1 ryanodine receptor
SCD	Standard chow diet
SERCA	Sarco/endoplasmic reticulum Ca-ATPase
SR	Sarcoplasmic reticulum
T-tubule	Transverse tubule
$V_{0.5}$	half-activation potential
V_{rev}	apparent reversal potential

Research in context

What is already known about this subject?

- Obesity and type 2 diabetes are associated with skeletal muscle dysfunction
- A high-fat diet induces a decrease in specific muscle force production

What is the key question?

- Does impaired Ca^{2+} homeostasis contribute to skeletal muscle dysfunction and weakness in a mouse model of obesity and type 2 diabetes?

What are the new findings?

- Ca^{2+} entry and voltage-sensing steps of excitation–contraction coupling at the plasma membrane level are unaffected in muscle fibres from obese mice
- Properties of intracellular Ca^{2+} handling by the sarcoplasmic reticulum are also completely preserved in muscle fibres from obese mice

How might this impact on clinical practice in the foreseeable future?

- The Ca^{2+} handling capacities of skeletal muscle that allow control of force production are intact in a mouse model of obesity and type 2 diabetes. These findings are important for our understanding of muscle function/dysfunction and may impact on clinical practice in relation to physical exercise in individuals with obesity or diabetes

Introduction

Obesity and its deleterious complications, insulin resistance and type 2 diabetes mellitus, are associated with skeletal muscle dysfunction [1,2]. Long-term systemic impairments related to the disease status such as cardiomyopathy, peripheral neuropathy and vascular disease eventually contribute but there is also evidence that the muscle tissue itself suffers from inherently reduced performance. Still, underlying mechanisms remain unclear and the situation is also complicated by concomitant processes operating to adapt muscle function to overweight-induced increased force demand. The literature related to altered muscle function in obesity and diabetes is intricate because of the diversity of experimental conditions and animal models used to tackle this issue, including a variety of genetically-modified murine models, selected murine strains, and pharmacological- or dietary-induction protocols [3,4]. If one focuses on the most common reason for obesity and type 2 diabetes in humans, diet-induced obesity in animal models may be considered of somewhat more specific interest. Accordingly, there is reproducible evidence that a sufficiently long period (≥ 10 weeks) of high-fat diet induces a decrease in specific force production, as assessed ex vivo from mouse muscle [5-7].

Altered intracellular Ca^{2+} handling contributes to obesity-induced cardiac dysfunction [8,9] (see for review [10,11]). Skeletal muscle function critically depends upon stringent control of intracellular Ca^{2+} with three proteins playing a key role in this process: $Ca_V1.1$ (a voltage sensor and Ca^{2+} channel in the transverse tubule [T-tubule] membrane), type 1 ryanodine receptor (RYR1; the Ca^{2+} release channel in the sarcoplasmic reticulum [SR] membrane), and sarco/endoplasmic reticulum Ca-ATPase (SERCA; the SR Ca^{2+} ATPase), ensuring Ca^{2+} uptake and consequent cytosolic Ca^{2+} clearance. Muscle force is triggered by cytosolic Ca^{2+} increase, promoting Ca^{2+} binding to troponin C. This occurs when T-tubule depolarisation sensed by $Ca_V1.1$ is transduced into opening of RYR1 channels and consequent SR Ca^{2+} release: the excitation–contraction coupling (ECC) process [12-15]. Besides activation of force, intracellular Ca^{2+} also plays a key role in other aspects of muscle function including metabolism and signalling cascades involved

in gene expression [16,17], processes that may also be modified because of altered Ca^{2+} homeostasis. Altogether, there is thus strong interest in determining whether functional aspects of Ca^{2+} homeostasis are affected in diet-induced obesity. Surprisingly, this has been largely experimentally overlooked so far, at least at the level of intact muscle fibres under membrane voltage control, a condition made essential by the stringent command exerted by plasma membrane voltage on intracellular Ca^{2+} homeostasis. In other words, no quantitative characterisation of the functional features of Ca^{2+} handling at the physiological millisecond time range of activation of ECC is available in this disease situation. This is at odds with the fact that potential mechanisms involved in Ca^{2+} dysregulation and target mechanisms have been largely highlighted in the literature [2,18].

We have used single muscle fibres isolated from mice fed with a high-fat, high-sucrose diet (HFHSD) generating obesity, hyperinsulinaemia, insulin resistance and glucose intolerance [19] to perform an extensive functional characterisation of intracellular Ca^{2+} signalling and ECC in that situation.

Methods

All experiments and procedures were performed according to the ethics principles of the French Department of Veterinary Services and the French Ministry for Higher Education, Research and Innovation, in accordance with the guidelines of the local animal ethics committee of the University Claude Bernard Lyon 1, the French Ministry of Agriculture (decree 87/848), and the revised European Directive 2010/63/EU. Experiments were performed at room temperature (20–22°C).

The experimental protocol of diet-induced obesity was approved by the Animal Experimentation Committee no. C2EA-15 of the Rhône-Alpes Region.

HFHSD-induced diabetic mice Four-week-old C57BL/6JOlaHsd male mice were purchased from ENVIGO (Gannat, France) and housed at 22°C with a 12 h light/ dark cycle. Following delivery, mice were distributed within cages and left for 1 week to adapt to the new environment. Cages were then allocated to 2 groups: one with free access to a standard chow diet (SCD) (Rod16-A, Genobios: 16.9% protein, 4.3% lipids, 55.5 % carbohydrate essentially from starch with no sucrose added) and the other with free access to a pelleted HFHSD diet (260HF U8978 version 19; SAFE; 20% protein, 36% lipids, 37% carbohydrate including 14.5 % starch and 17.9 % sucrose) for 16 weeks as described previously [19]. For simplicity, mice, and fibres isolated from the mice in the two groups, are referred to as SCD and HFHSD. Two sets of five mice of each group were used in this study. The first set was dedicated to characterisation of T-tubule membrane architecture, voltage-activated Ca^{2+} current and intracellular Ca^{2+} transients, and spontaneous Ca^{2+} release events at rest. In the second set we measured intramembrane charge movement and spontaneous Ca^{2+} release events. In the first group, body mass and blood glucose were assessed twice a week and a GTT and ITT were performed during weeks 4, 8, 12 and 16 after the beginning of the diet, as previously described [19]. In the second group an ITT and GTT were performed during week 15. In all mice, body weight and blood glucose were assessed before euthanasia. Immediately following euthanasia, prior to the preparation of isolated muscle fibres (see next section), the gastrocnemius muscles, the heart, the liver and the white adipose tissue were removed and weighted.

Preparation of isolated muscle fibres Single fibres from the flexor digitorum brevis (FDB) and interosseus muscles were isolated as previously described [20]: mice were anaesthetised with isoflurane and killed by cervical dislocation before removal of the muscles. Muscles were incubated in Tyrode's solution containing 2 mg/ml collagenase (Sigma, type 1) for 60 min at 37°C. Single fibres were obtained by mechanical trituration within a culture µ-dish (Ibidi, Planegg/Martinsried, Germany) filled with culture medium containing 10% FBS (MI199; Eurobio, France), the bottom of which had been first coated with a

thin layer of silicone. Isolated fibres settled on the silicone surface and were then embedded with additional silicone so that only a portion of the fibre extremity remained in contact with the extracellular medium. The initial silicone coating of the chamber bottom was necessary because of the hydrophobic nature of the silicone grease, which makes it very hard to adhere to a solid substrate in a liquid environment. The silicone grease we used was SILBIONE Paste 70428 (Elkem Silicones, Saint-Fons, France).

Electrophysiology Voltage-clamp experiments were performed on FDB muscle fibres using a micropipette filled with an intracellular-like medium (see Buffers and incubation media). The pipette tip was inserted into the silicone-insulated part of the fibre and was gently crushed against the chamber bottom to ease dialysis and reduce series resistance. Composition of the extracellular solution and of the pipette solution were adapted to the experiment type (see Solutions). The fibre interior was dialysed for 30 min to allow for intracellular equilibration of the solution before starting measurements. The chlorided silver wire inside the pipette was connected to an RK-400 patch-clamp amplifier (Bio-Logic, Claix, France) in whole-cell configuration, in combination with an analogue–digital converter (Digidata 1440A, Axon Instruments, Foster City, CA, USA) controlled by pClamp 9 software (Axon Instruments). The effective series resistance was further decreased by analogue compensation. Unless otherwise specified, the holding voltage was set to -80 mV.

$Ca_V1.1$ Ca^{2+} current was measured in response to 0.5-s-long depolarising steps. The linear leak component of the current was removed by subtracting the adequately scaled value of the current measured during a -20 mV step. This subtraction did not fully eliminate the outward current measured during pulses to values between -50 and -30 mV, below the threshold of activation of the Ca^{2+} current. In order to correct for this, the voltage-dependence of the values for the residual current was fitted by a linear function from -50 to

-30 mV; the fit was extrapolated to the entire range of voltage values and fitted values were subtracted from the measured values for peak $Ca_V1.1$ current. The voltage-dependence of peak current values (normalised to the capacitance), was fitted with the following equation:

$$I(V) = G_{max}(V-V_{rev})/(1+\exp(V_{0.5}-V)/k])$$

with *I(V)* the peak current density at the command voltage *V*, G_{max} the maximum conductance, V_{rev} the apparent reversal potential, $V_{0.5}$ the half-activation potential and k the steepness factor. As for the values of peak Ca^{2+} current, values for G_{max} were also expressed normalized to the capacitance (S/F).

$Ca_V1.1$ charge movement currents were measured from a holding voltage of -100 mV and analysed as previously described [21,22]. In brief, adequately scaled control records elicited by 25-ms-long pulses of -20 mV were subtracted from the current elicited by test depolarising pulses of the same duration to various levels [23]. The amount of charge moved during a test pulse was measured by integrating the on and off portions of the corrected test current records. The steady-state distribution of charge (normalised to fibre capacitance) was fitted with a two-state Boltzmann function:

$$Q(V)=Q_{max}/(1+\exp[(V_{0.5}-V)/k])$$

with Q_{max} the maximal available charge, $V_{0.5}$ the voltage of equal charge distribution and k the steepness factor.

Confocal imaging Confocal imaging was conducted with a Zeiss LSM 5 Exciter equipped with a ×63 oil immersion objective (numerical aperture 1.4). For detection of Rhod-2 and Fluo-4FF fluorescence, excitation was from the 543 nm line of a HeNe laser and from the 488 nm line of an Argon laser, respectively, and fluorescence was collected above 560 nm and above 505 nm, respectively. Rhod-2 and Fluo-4FF fluorescence changes were imaged using the line-scan mode (*x,t*) of the system and expressed as F/F_0 where F_0 is the baseline fluorescence. Quantification of the Ca^{2+} release flux underlying the Rhod-

2 Ca^{2+} transients was performed as previously described [24]. In each fibre, the voltage-dependence of the peak rate of Ca^{2+} release was fitted with a Boltzmann function.

Di-8-ANEPPS and Fluo-4 fluorescence were collected above 505 nm with 488 nm excitation. For imaging the T-tubule network, interosseus muscle fibres were incubated for 30 min in the presence of 10 µmol/l Di-8-ANEPPS. The T-tubule density was estimated as described previously [24].

For Ca^{2+} sparks measurements, interosseus muscle fibres were incubated for 30 min in the presence of 10 µmol/l Fluo-4 acetoxymethyl ester (AM). Thirty consecutive confocal frames of Fluo-4 fluorescence (102.4 × 102.4 µm, 989 ms per frame) were acquired in each fibre. To quantify the Ca^{2+} sparks activity, images in the stack were smoothed and the standard deviation of fluorescence intensity at each pixel position, along the stack, was calculated. The 20% largest values in the standard deviation image were removed to calculate the mean standard deviation of silent areas. The active area was then defined as pixel positions exhibiting at least 1.5 × larger values of standard deviation than the mean standard deviation value from silent areas.

Buffers and incubation media Tyrode solution contained (in mmol/l): 140 NaCl, 5 KCl, 2.5 $CaCl_2$, 2 $MgCl_2$, 10 HEPES. The extracellular solution for measurements of $Ca_V1.1$ Ca^{2+} current and Ca^{2+} transients contained (in mmol/l) 140 tetraethylammonium-methanesulfonate, 2.5 $CaCl_2$, 2 $MgCl_2$, 1 4-aminopyridine, 10 HEPES and 0.002 tetrodotoxin. For measurements of Fluo-4FF Ca^{2+} transients, it also contained 0.05 *N*-benzyl-*p*-toluene sulphonamide (BTS) to block contraction. The pipette solution contained (in mmol/l) 120 K-glutamate, 5 Na_2-ATP, 5 Na_2-phosphocreatine, 5.5 $MgCl_2$, 5 glucose, 5 HEPES. For measurements of Rhod-2 and Fluo-4FF Ca^{2+} transients it also contained 15 EGTA, 6 $CaCl_2$, 0.1 Rhod-2, and 0.1 Fluo-4FF, respectively.

For measurements of $Ca_V1.1$ charge movement the extracellular solution contained (in mmol/l) 140 TEA-methane-sulfonate, 0.1 $CaCl_2$, 3 $MgCl_2$, 1 $CdCl_2$, 0.5 $MnCl_2$, 1 4-aminopyridine, 0.5 9-anthracene-carboxylic acid, 10 HEPES and 0.002 tetrodotoxin and fibres were dialysed through the pipette with a solution containing (in mmol/l) 140 TEA-methanesulfonate, 5 Na_2-ATP, 5 Na_2-phosphocreatine, 5.5 $MgCl_2$, 5 glucose, 5 HEPES. BTS was purchased from Tocris Bioscience (Bio-Techne, Lille, France). All fluorescent indicators were purchased from Thermo Fisher Scientific (Illkirch, France). All solutions were adjusted to pH 7.20.

Statistics No randomisation procedure was carried out. Experimenters were not blind to group assignment and outcome assessment. Statistical analysis was performed with Origin 8.0. Data values are presented as means ± SEM for *n* fibres. Statistical significance was determined using two-tailed Student's t tests comparing the means (*$p \leq 0.05$).

With respect to results shown in Fig. 3, data from one muscle fibre in the SCD group and from one muscle fibre in the HFHSD group were excluded because in both cases the fit to the peak Ca^{2+} current versus voltage data gave non-rational values for maximal conductance (~10 times less than the mean value) and apparent reversal potential (more than 80 mV more positive than the mean value). Muscle fibres from one mouse initially scheduled in the SCD group could not be used because of an experimental mistake during the protocol of incubation at 37 °C in the presence of collagenase.

Results

Obesity, insulin resistance and glucose intolerance in the HFHSD mice The status of our animals over the course of the diet protocol is shown in Fig. 1, as assessed from the first group of mice (see Methods: HFHSD-induced diabetic mice). At the end, the body weight of the HFHSD animals was ~1.7 times that of SCD ones (Fig. 1a); mean values for body weight at the end of the diet protocol for SCD and HFHSD animals

were 28.6 ± 0.5 g (n=9) and 50.1 ± 0.9 g (n=9) ($p<0.0001$), respectively. There was no associated change in the weight of the gastrocnemius (0.17 ± 0.01 g, n=9 and 0.21 ± 0.02 g, n=9; $p=0.14$) nor of the heart (0.17 ± 0.01 g, n=9 and 0.21 ± 0.02 g, n=9; $p=0.09$), whereas the weight of the liver (1.30 ± 0.04 g, n=9 and 3.11 ± 0.34 g, n=9; $p<0.0001$) and of the white adipose tissue (measured as the epididymal adipose tissue: 0.51 ± 0.04 g, n=9 and 2.06 ± 0.17 g, n=9; $p<0.0001$) were substantially increased in HFHSD vs SCD animals, respectively. Results from GTT and ITT performed at weeks 4, 8, 12 and 16 are shown in Fig. 1b and c, respectively: HFHSD mice maintained an elevated blood glucose level following injection of either glucose or insulin: from the 10 min time point following either glucose or insulin injection, the mean glucose level in HFHSD mice ranged between approximately 1.5 and 2.3 times the level in SCD mice (the difference being statistically significant between the two groups at any time point of the four sets of measurements), establishing the glucose intolerance and the systemic insulin resistance, and thus the diabetic status generated by the protocol.

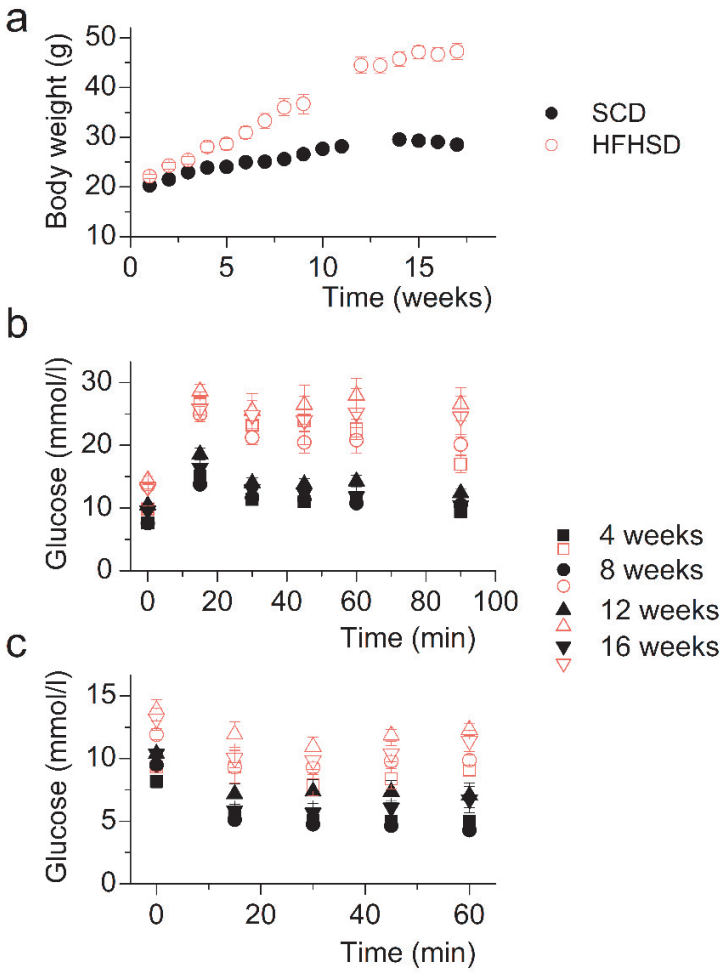

Fig. 1 Body mass, GTT and ITT in SCD and HFHSD mice. (**a**) Mean values for body weight of SCD (*n*=9) and HFHSD mice (*n*=9), over the course of the diet protocol. The gap in the SCD data and in the HFHSD data is due to a short break in data collection. (**b**, **c**), Mean values for blood glucose concentration before (*t*=0) and after intraperitoneal injection of either 2 mg/g glucose (**b**) or 0.75 U/kg insulin (**c**). Measurements were performed at weeks 4, 8, 12 and 16 after the beginning of the diet When comparing the mean glucose level between the SCD group and the HFHSD group at any given time point of the GTT protocol (**b**) using a t-test, comparisons all had $p<0.01$ (at 4, 8 and 12 weeks) and $p<0.02$ (at 16 weeks). When comparing the mean glucose level between the SCD group and the HFHSD group at any given time point of the ITT protocol (**c**) using a t-test, comparisons all had $p<0.02$ (at 4, 12 and 16 weeks) and $p<0.001$ (at 8 weeks). Data are mean ± SEM.

T-tubule network and passive electrical properties in SCD and HFHSD muscle fibres The T-tubule membrane system plays a critical role in ECC and in glucose transport and high-fat diet may enhance its cholesterol content [25] with potential adverse consequences for T-tubule integrity and function [26,27]. We labelled the plasma membrane of fibres with Di-8-ANEPPS. Corresponding *x,y* confocal images from SCD (Fig. 2a, c) and HFHSD muscle fibres (Fig. 2b, d) showed no sign of alteration of the network in the HFHSD group and the transverse profile of fluorescence showed the expected double-peak pattern characteristic of T-tubule organisation in mammalian muscle (graphs in Fig. 2c, d). Analysis of Di-8-ANEPPS images collected from 20 muscle fibres from two SCD mice and from 30 fibres from three HFHDS mice, showed no change in T-tubule density (Fig. 2e), but, incidentally, the mean value for

sarcomere length was slightly but significantly reduced in the HFHSD compared with the SCD group (2.04 ± 0.01 vs 2.11 ± 0.02; p=0.001; Fig. 2f). Preservation of the T-system in the HFHSD fibres was confirmed by the passive electrical properties of the fibres: membrane current records from fibres used to measure $Ca_V1.1$ Ca^{2+} current gave mean values for capacitance and input resistance of 949 ± 68 and 930.6 ± 61 pF, and 11.9 ± 1 and 12.5 ± 0.8 MΩ, in the SCD group (n=21 fibres from four mice) and in the HFHSD group (n=30 fibres from five mice), respectively. Because mean values for fibre diameter did not differ between the SCD (44.8 ± 1.4 µm) and HFHSD group (43.4 ± 1.4 µm) and assuming that a fibre portion of similar length was always under voltage-clamp, results establish that the T-tubule network is preserved in the obesity situation.

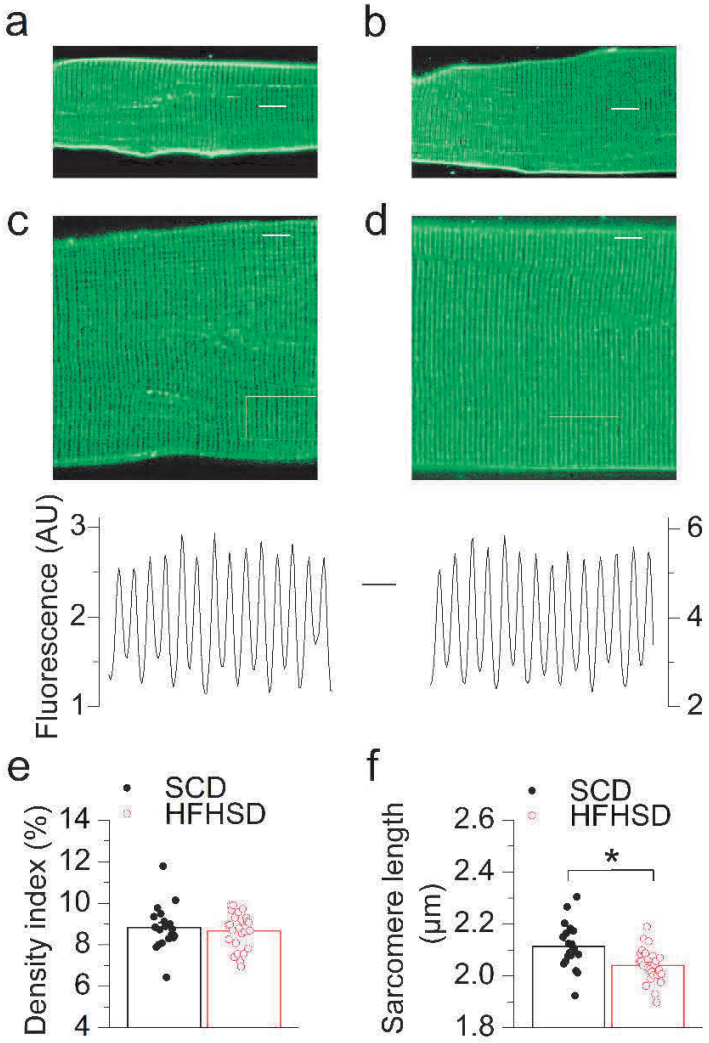

Fig. 2 T-tubule system network. (**a**–**d**) *x,y* confocal images of Di-8-ANNEPS fluorescence from separate SCD (**a**, **c**) and HFHSD muscle fibres (**b**, **d**) at two different magnifications (**a**, **b**: horizontal scale bar, 10 µm; **c**, **d**: horizontal scale bar 5, µm). (**c**, **d**) Graphs show the transverse pattern of Di-8-ANNEPS fluorescence (scale bar, 2 µm) over the highlighted region in the corresponding *x,y* images above. (**e**, **f**) Mean values for T-tubule density index and for sarcomere length in the SCD (*n*=20 fibres from 2 mice) and HFHSD (*n*=30 fibres from 3 mice) groups. Data are mean ± SEM *$p<0.05$

$Ca_V1.1$ Ca^{2+} current and voltage-sensing properties in SCD and HFHSD muscle fibres $Ca_V1.1$ is the most well-identified and characterised Ca^{2+} entry pathway across the plasma/T-tubule membrane of muscle fibres. Example $Ca_V1.1$ Ca^{2+} current records from an SCD and from an HFHSD muscle fibre are shown in Fig. 3a and b, respectively; mean values for peak Ca^{2+} current vs voltage in the two groups are shown in Fig. 3c whereas mean values for the parameters obtained from fitting each individual peak current vs voltage relationship are shown in Fig. 3d-g. There was no significant change in any parameter in the HFHSD group. Mean values for maximum conductance were 196±13 S/F and 234±12 S/F in fibres from the SCD and from the HFHSD group, respectively.

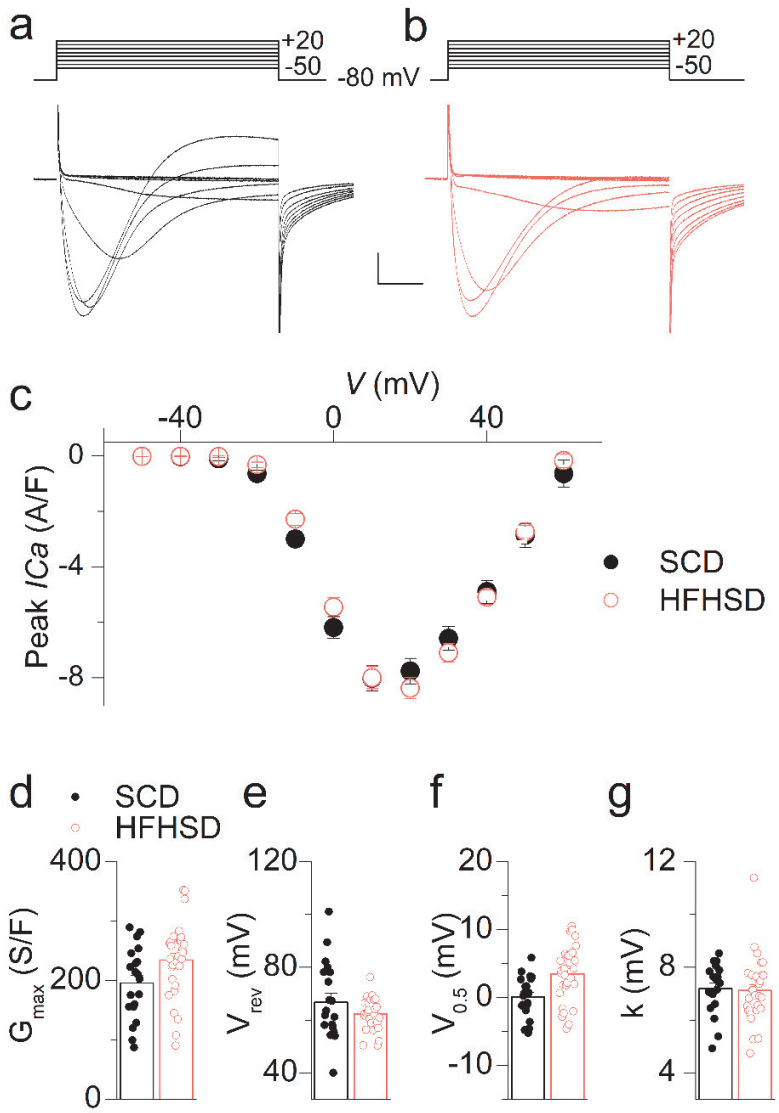

Fig. 3 $Ca_V1.1$ Ca^{2+} current. (**a**, **b**) example traces of Ca^{2+} current in an SCD (**a**) and in an HFHSD muscle fibre (**b**) in response to the voltage-clamp pulse protocol shown at the top. Horizontal axis, time (scale bar 100 ms), vertical axis, current (scale bar 2 A/F). (**c**) Mean values for the peak Ca^{2+} current density vs voltage in the SCD (*n*=20 fibres from 4 mice) and HFHSD (*n*=29 fibres from 5 mice) groups. (**d–g**) Corresponding mean values for the parameters obtained from fitting each individual peak current vs voltage relationship with the appropriate function (see Methods / Electrophysiology) Data are mean ± SEM.

$Ca_V1.1$ also exerts the critical function of coupling the T-tubule depolarisation to RYR1 Ca^{2+} channel activation in the SR membrane. $Ca_V1.1$ voltage-sensing function was assessed from intramembrane charge movement. Example traces of charge current from an SCD and from an HFHSD muscle fibre are shown in Fig. 4a whereas mean values for the amount of charge vs voltage are shown in Fig. 4b (data from 22 SCD fibres and 21 HFHSD fibres, each from three mice in each group). Properties of charge movement were

similar in SCD and HFHSD muscle fibres (Fig. 4c–e), with mean values for maximum amount of charge of 32.9±2 and 30.7±1.6 nC/µF, respectively. This demonstrates that the amount of $Ca_V1.1$ in the plasma/T-tubule membrane and its voltage-sensing properties are preserved in this situation.

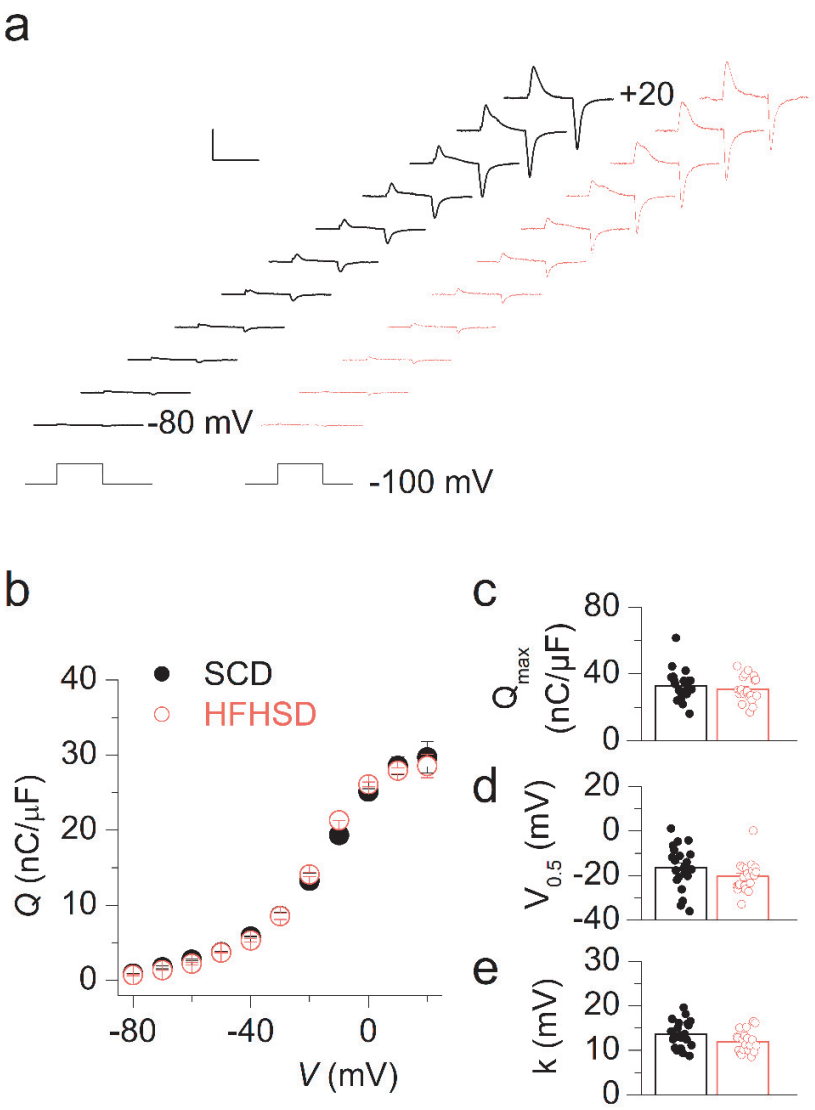

Fig. 4 $Ca_V1.1$ charge movement. (**a**) example traces of $Ca_V1.1$ charge movement currents in an SCD (left) and in an HFHSD muscle fibre (right) in response to voltage-clamp depolarising pulses from -100 mV to values ranging between -80 and +20 mV. Horizontal axis, time (scale bar 25 ms), vertical axis, current (scale bar 5 A/F). (**b**) Mean values for the amount of $Ca_V1.1$ charge density vs voltage in the SCD (*n*=22 fibres from 3 mice) and HFHSD (*n*=21 fibres from 3 mice) groups. (**c**–**e**), Mean values for the parameters obtained from fitting each individual charge vs voltage relationship with the appropriate function (see Methods/Electrophysiology) Data are mean ± SEM.

Voltage-activated SR Ca^{2+} release Properties of RYR1 channels activity upon fibre activation were assessed from voltage-clamp-activated cytosolic Ca^{2+} transients. A family of such F/F_0 Rhod-2 transients

from an SCD and an HFHSD muscle fibre are shown in Fig. 5a and b, respectively, while traces for the corresponding calculated rate of SR Ca^{2+} release are shown in Fig. 5c and d, respectively. As classically reported in this preparation, the time course of SR Ca^{2+} release exhibits an early peak followed by a decay towards a much lower level. There was no obvious qualitative feature of the Rhod-2 transients and of the rate of Ca^{2+} release that differed between SCD and HFHSD fibres. This was confirmed by the analysis showing that neither mean values for peak rate of SR Ca^{2+} release (peak $d[Ca_{Tot}]/dt$, Fig. 5e), nor for its time to peak (t_{peak}, Fig. 5f) nor for total amount of released Ca^{2+} ($[Ca_{Tot}]$ calculated from the time integral of the Ca^{2+} release trace, Fig. 5g) statistically differed between the two groups. Mean values for maximum $d[Ca_{Tot}]/dt$ assessed from fitting a Boltzmann function to the voltage dependence of the peak $d[Ca_{Tot}]/dt$ in each fibre were 76.0±6.5 and 78.1±4.4 µmol l^{-1} ms^{-1} in the SCD and HFHSD groups, respectively. Thus, the physiological RYR1 channel activity and the SR Ca^{2+} content are preserved in HFHSD fibres.

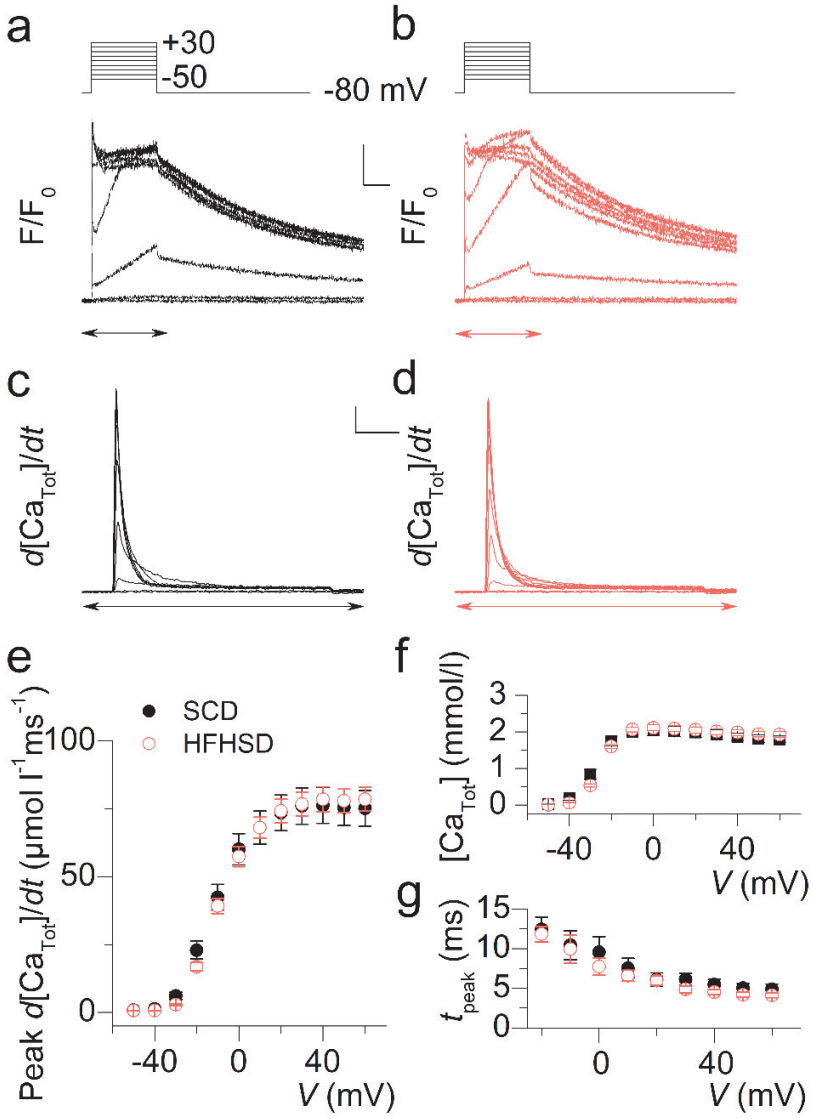

Fig. 5 Voltage-activated SR Ca^{2+} release. (**a**, **b**) Example traces of Rhod-2 F/F_0 Ca^{2+} transients in an SCD (**a**) and in an HFHSD muscle fibre (**b**) in response to the voltage-clamp pulse protocol shown at the top. Horizontal axis, time (scale bar 200 ms), vertical axis, fluorescence (scale bar 1×F_0). (**c**, **d**) Rate of SR Ca^{2+} release ($d[Ca_{Tot}]/dt$) calculated from the Rhod-2 transients shown in (**a**, **b**), respectively. Horizontal axis, time (scale bar 100 ms), vertical axis, rate of SR Ca^{2+} release (scale bar 10 µmol l^{-1} ms^{-1}). For the sake of clarity, the rate traces are only shown throughout the portion of Rhod-2 F/F_0 traces highlighted by an arrow in (**a**, **b**). (**e**) Mean values for the peak rate of SR Ca^{2+} release (peak $d[Ca_{Tot}]/dt$) vs voltage in the SCD (n=21 fibres from 4 mice) and HFHSD (n=30 fibres from 5 mice) groups. (**f**) Corresponding mean values for the total amount of released Ca^{2+} ($[Ca_{Tot}]$, calculated from the time integral of the rate). (**g**) Corresponding mean values for the time to peak SR Ca^{2+} release (t_{peak}) Data are mean ± SEM.

Cytosolic Ca^{2+}removal capabilities and response to a fatiguing stimulation protocol Functional impact of HFD-induced obesity on SERCA activity may occur because of altered SR phospholipid composition [28,29] and/or changes in expression or efficiency of the SERCA regulator sarcolipin [30]. SERCA is the major actor of cytosolic Ca^{2+} clearance. We assessed the cytosolic removal capabilities of fibres by measuring the time constant of the Ca^{2+} signal decay following repolarisation-induced Ca^{2+} release termination. For this we

used the intermediate affinity Ca^{2+}-sensitive dye Fluo-4FF under non-EGTA-buffering conditions of the intracellular medium (see Methods: Buffers and incubation media). Illustrative Fluo-4FF Ca^{2+} transients elicited by maximum activation of SR Ca^{2+} under these conditions are presented in Fig. 6a. In each fibre tested, a single exponential function was fitted to the declining phase of the transients. Corresponding mean values for the time constant of decay showed no sign of any trend of difference between the two groups (Fig. 6b, data from eight fibres from four SCD mice and from 13 fibres from five HFHSD mice).

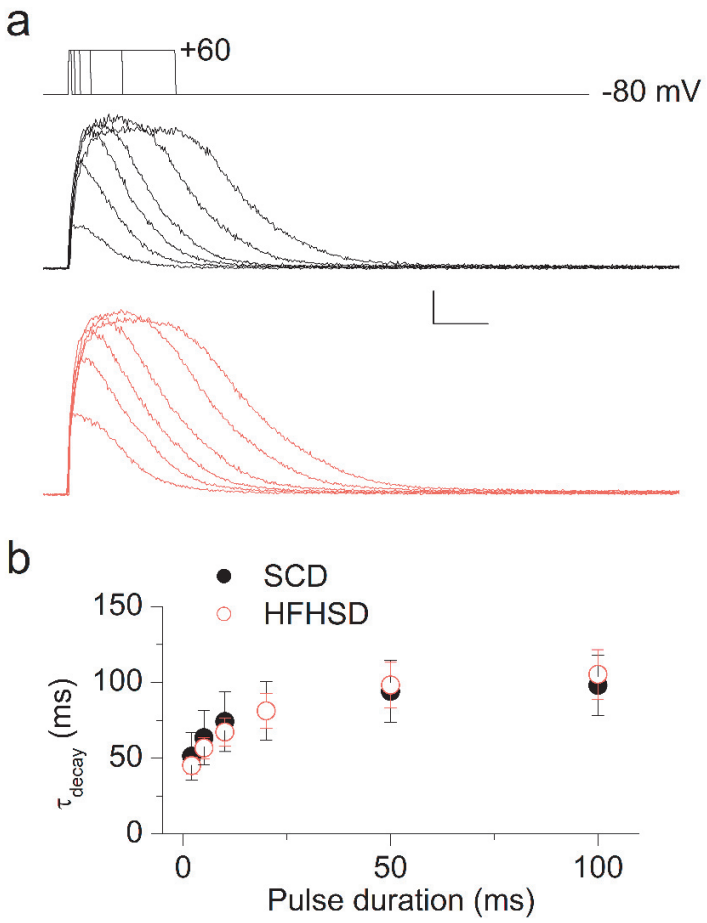

Fig. 6 Cytosolic Ca^{2+} removal. (**a**) Fluo-4FF F/F_0 Ca^{2+} transients elicited by the voltage-clamp pulse protocol shown on top in an SCD muscle fibre (top) and in an HFHSD muscle fibre (bottom). Horizontal axis, time (scale bar 50 ms), vertical axis, fluorescence (scale bar $5\times F_0$). (**b**) Mean values for the time constant of Fluo-4FF fluorescence decay (τ_{decay}) vs pulse duration in the SCD (*n*=8 fibres from 4 mice) and HFHSD (*n*=13 fibres from 5 mice) groups Data are mean ± SEM.

Under the same conditions, we explored the response of the fibres to an exhausting stimulation protocol consisting in consecutive trains of 30, 5-ms-long, pulses from -80 mV to +60 mV delivered at 100 Hz. Thirty trains were applied, separated by a 0.7 s interval. This protocol produces a rapid reduction of SR Ca^{2+} release as illustrated in Fig. 7a and b, which show examples of the first and last Fluo-4FF transients

recorded from an SCD and from an HFHSD muscle fibre, respectively, in response to a full protocol. Figure 7c and d show the entire sequence of Fluo-4FF transients from the same two fibres over time. Such records were collected from eight fibres from four SCD mice and from 12 fibres from five HFHSD mice, respectively. Mean values for the normalised time course of decline of the peak F/F_0 transients in the two groups are presented in Fig. 7e. In each fibre, the time course was fitted by a single exponential plus constant function: corresponding mean values for the time constant and final level (Fig. 7f, g) establish that there was no stringent alteration in HFHSD fibres. The time constant of decay was increased by a factor of ~1.25 in the HFHSD group, but the difference did not reach statistical significance (p=0.057).

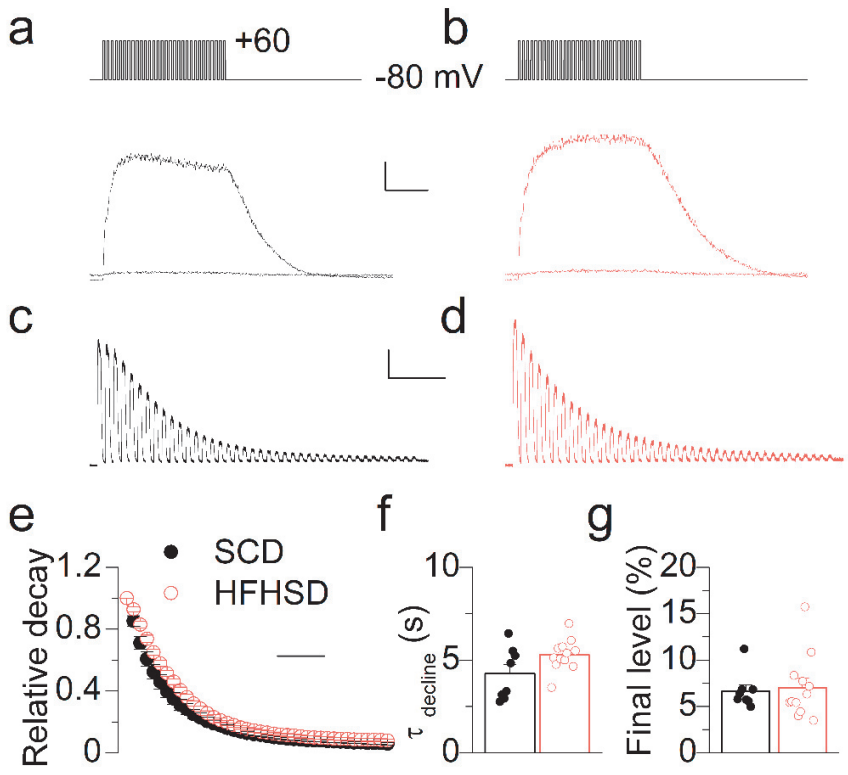

Fig. 7 Response to a fatigue protocol. (**a**, **b**) Representative Fluo-4FF fluorescence traces from an SCD (**a**) and from an HFHSD muscle fibre (**b**) challenged by the voltage-clamp depolarisation protocol shown at the top, consisting of 5-ms-long pulses from -80 mV to +60 mV delivered at 100 Hz. Horizontal axis, time (scale bar 100 ms), vertical axis, fluorescence (scale bar $5\times F_0$). This protocol was repeated 30 times: the two superimposed Fluo-4FF traces correspond to the responses to the first (largest) and to the last response of each fibre. (**c**, **d**) Full time course of the Fluo-4FF fluorescence transients over the course of the entire protocol (same muscle fibres as in **a** and **b**, respectively). Horizontal axis, time (scale bar 5 s), vertical axis, fluorescence (scale bar $5\times F_0$). (**e**) Mean time course of the decay of the relative peak Fluo-4FF Ca^{2+} transients over the full protocol. Horizontal axis, time (scale bar 5 s). (**f**, **g**) Mean values for the time constant of decay of the peak Fluo-4FF transients and corresponding final level, respectively, obtained from a single exponential plus constant fit to the data in each fibre (*n*=8 fibres from 4 SCD mice and *n*=12 fibres from 5 HFHSD mice) Data are mean ± SEM.

Spontaneous Ca^{2+} release activity at rest Spontaneous activity of RYR1 channels at rest under the form of local SR Ca^{2+} release events called Ca^{2+} sparks, is a hallmark of several muscle disease situations [24,31,32]. We tested whether this was the case in HFHSD fibres using confocal imaging of the Ca^{2+}-sensitive dye Fluo-4: *x,y* images of the standard deviation of Fluo-4 fluorescence intensity along 30 consecutive confocal frames (total time of ~30 s) from an SCD fibre and from an HFHSD fibre are shown in Fig. 8a and b, respectively: SCD fibres were basically devoid of Ca^{2+} spark activity whereas some HFHSD fibres did exhibit a few sparks. Ca^{2+} spark activity was quantified in 28 muscle fibres from three SCD mice and from 46 fibres from five HFHSD mice, respectively. Figure 8c shows the mean value for relative fibre area exhibiting Ca^{2+} spark activity over a period of ~30 s (see Methods: Confocal imaging) in the two groups. Figure 8d shows the corresponding distribution of the number of fibres according to this parameter. The mean fibre area exhibiting Ca^{2+} spark activity was significantly (p=0.043) increased in the HFHSD group but in a quantitatively very modest manner (0.6 % of the fibre area compared with 0.4 % in the SCD group), this being essentially due to four muscle fibres issued from one HFHSD mouse, exhibiting an active relative fibre area larger than 1.5%.

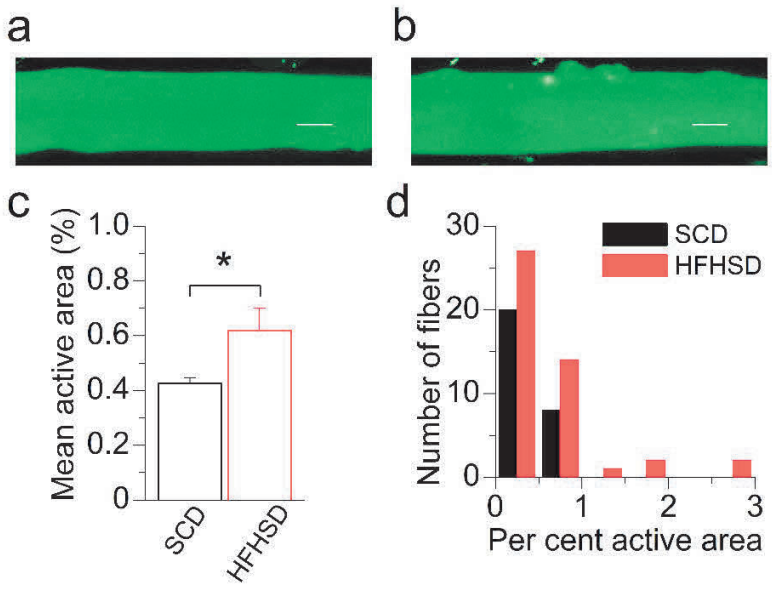

Fig. 8 Spontaneous Ca^{2+} spark activity at rest. (**a**, **b**) Images of the standard deviation of Fluo-4 fluorescence intensity in an SCD (**a**) and in an HFHSD muscle fibre (**b**) over the course of a series of 30 *x,y* confocal scans. Horizontal scale bar 10 µm. (**c**) Mean values for the relative fibre area exhibiting spontaneous Ca^{2+} release in SCD and HFHSD muscle fibres. (**d**) Corresponding distribution of the number of muscle fibres according to the relative active area.
Ca^{2+} spark activity was quantified in 28 muscle fibres from three SCD mice and from 46 fibres from five HFHSD mice, respectively. Data are mean ± SEM *p<0.05

Discussion

Altered skeletal muscle function associated with obesity and type 2 diabetes is a major burden for patient's mobility and locomotion (e.g. [33]). In the long run, muscle-extrinsic mechanisms related to cardiac and vascular complications obviously play a role and so does muscle atrophy. However, there is also evidence that muscle-intrinsic impaired force production is involved [2] but the underlying mechanisms remain obscure. HFD-induced obesity in mice is associated with reduced specific muscle force, prompting the interest of this model to decipher the muscle-intrinsic mechanisms. Intracellular Ca^{2+} plays a key role in numerous aspects of muscle function including triggering contraction. In order to ensure this particular function, intracellular Ca^{2+} concentration has to remain under tight control and, accordingly, there are numerous examples of muscle dysfunction due to altered Ca^{2+} handling and ECC (see [34-37]). Defective Ca^{2+} regulation was early suggested to occur in a pharmacologically induced diabetes model and in a genetically obese mouse model: specifically, accumulation of Ca^{2+} together with increased amount of $Ca_V1.1$ was shown in skeletal muscle from a rat model of streptozotocin-induced diabetes [38] and Ca^{2+} regulation was reported to be abnormal in the *ob/ob* mouse model of obesity, contributing to premature fatigue [39]. If referring specifically to HFD models, altered Ca^{2+} handling is suggested to play a role in obesity-induced muscle dysfunction through HFD-induced increased production of reactive oxygen species (ROS), which would promote SR Ca^{2+} leak through enhanced *S*-nitrosylation of RYR1 channels [40] and, possibly, also impair SERCA function [41,42]. In addition, altered expression and/or efficiency of sarcolipin [30] could also contribute to impair cytosolic Ca^{2+} clearance, potentially with consequences for muscle metabolism and energy expenditure through activation of Ca^{2+} signalling pathways [43,44]. Still, altogether, functional correlates for these alterations in terms of Ca^{2+} handling within the course of physiological ECC are poorly documented.

The strength of the present study is to achieve the first detailed quantitative investigation of the functional properties of intracellular Ca^{2+} handling and ECC in a diet-induced mouse model of obesity, using single isolated muscle fibres under voltage control. Our results demonstrate remarkably well preserved Ca^{2+} handling capabilities in terms of voltage-dependent Ca^{2+} entry across the plasma membrane through $Ca_V1.1$, $Ca_V1.1$ properties as ECC voltage-sensors, voltage-activated SR Ca^{2+} release through RYR1 channels, SERCA-mediated cytosolic Ca^{2+} removal and resistance to a fatiguing stimulation protocol. Results concur with data from Eshima et al [6] suggesting that HFD elicits no change in the expression levels of calcium handling-related proteins, but they further show that the physiological operating function of these proteins during ECC is largely unaffected in that situation. They also concur with results from Bruton et al [39] showing that resting and tetanic Ca^{2+} under unfatigued conditions are similar in *ob/ob* and wild-type muscle fibres. Overall, our results do not exclude the possibility that the previously suggested, above-mentioned, alterations of Ca^{2+} handling do occur, but show that they remain very minor in terms of functional impact on the basic function of ECC and are thus not likely to be directly involved in chronic reduced muscle performance. For instance, the fact that some muscle fibres from HFHSD mice exhibit an enhanced propensity for spontaneous Ca^{2+} release at rest may be related to the presence of *S*-nitrosylated leaky RYR1 channels, but overall, this clearly does not compromise the SR Ca^{2+} content and proper function of the Ca^{2+} release machinery. It may then be that the reported alterations of Ca^{2+} homeostasis remain silent with regard to ECC function but relevant with regard to activation of specific Ca^{2+}-dependent signalling pathways. Also of importance, the preserved Ca^{2+} handling capabilities in isolated fibres maintained under our controlled experimental conditions does not eliminate the possibility that the situation differs in vivo, owing to the specific environment experienced by the fibres in the diseased organism. It will thus be of high interest in the future to investigate the function of ECC and Ca^{2+} handling in isolated fibres challenged by conditions mimicking this environment, including incubation of

the fibres in the presence of insulin and glucose. In line with this, for instance, it is interesting that elevated glucose was recently reported to alter T-tubule morphology of isolated muscle fibres [26].

In summary, our results demonstrate that the intrinsic function of intracellular Ca^{2+} signalling and ECC is amazingly well preserved in muscle fibres from a mouse model of obesity and type 2 diabetes.

Data availability Original datasets and datasets generated by the described analysis procedures are available from the corresponding author upon reasonable request. Critical resources supporting the results are also available upon reasonable request.

Funding FJF was the recipient of a PhD fellowship from the Chilean Comisión Nacional de Investigación Científica y Tecnológica (CONYCIT). AB was supported by a research fellowship from the French Ministry of Higher Education and Research. This work was also supported by grants from CNRS, Inserm, the Université Claude Bernard - Lyon 1 to the Institut NeuroMyoGène and by the Chilean–French cooperation programme ECOS-CONICYT (#C13B01).

Authors' relationships and activities The authors declare that there are no relationships or activities that might bias, or be perceived to bias, their work.

Contribution statement VJ, JR and FJF conceived and coordinated the study. JR and AB generated the mouse model and collected metabolic data. FJF conducted the electrophysiological and fluorescence experiments. FJF, LM and VJ performed the main electrophysiological and fluorescence data analysis. All authors made critical contributions to data analysis, interpretation and discussion and to manuscript preparation, and approved the final version. VJ and JR wrote the manuscript.

VJ is the guarantor of this work and, as such, accepts full responsibility for the work and/or the conduct of the study, had access to the data, and controlled the decision to publish.

References

1. Allen MD, Doherty TJ, Rice CL, Kimpinski K (2016) Physiology in medicine: neuromuscular consequences of diabetic neuropathy. J Appl Physiol 121(1):1-6. https://doi.org/10.1152/japplphysiol.00733.2015
2. Tallis J, James RS, Seebacher F (2018) The effects of obesity on skeletal muscle contractile function. J Exp Biol 221:jeb163840. https://doi.org/10.1242/jeb.163840
3. King AJ (2012) The use of animal models in diabetes research. Br J Pharmacol 166(3):877-894. https://doi.org/10.1111/j.1476-5381.2012.01911.x
4. King A, Bowe J (2016) Animal models for diabetes: understanding the pathogenesis and finding new treatments. Biochem Pharmacol 99:1-10. https://doi.org/10.1016/j.bcp.2015.08.108
5. Matsakas A, Prosdocimo DA, Mitchell R et al (2015) Investigating mechanisms underpinning the detrimental impact of a high-fat diet in the developing and adult hypermuscular myostatin null mouse. Skelet Muscle 5:38. https://doi.org/10.1186/s13395-015-0063-5
6. Eshima H, Tamura Y, Kakehi S et al (2017) Long-term, but not short-term high-fat diet induces fiber composition changes and impaired contractile force in mouse fast-twitch skeletal muscle. Physiol Rep 5(7):e13250. https://doi.org/10.14814/phy2.13250
7. Tallis J, Hill C, James RS, Cox VM, Seebacher F (2017) The effect of obesity on the contractile performance of isolated mouse soleus, EDL, and diaphragm muscles. J Appl Physiol 122(1):170-181. https://doi.org/10.1152/japplphysiol.00836.2016
8. Leopoldo AS, Lima-Leopoldo AP, Sugizaki MM et al (2011) Involvement of L-type calcium channel and SERCA2a in myocardial dysfunction induced by obesity. J Cell Physiol 226(11):2934-2942. https://doi.org/10.1002/jcp.22643
9. Sánchez G, Araneda F, Peña JP et al (2018) High-fat-diet-induced obesity produces spontaneous ventricular arrhythmias and increases the activity of ryanodine receptors in mice. Int J Mol Sci 19(2):533. https://doi.org/10.3390/ijms19020533
10. Carvajal K, Balderas-Villalobos J, Bello-Sanchez MD et al (2014) Ca^{2+} mishandling and cardiac dysfunction in obesity and insulin resistance: role of oxidative stress. Cell Calcium 56(5):408-415. https://doi.org/10.1016/j.ceca.2014.08.003
11. Jia G, DeMarco VG, Sowers JR (2016) Insulin resistance and hyperinsulinaemia in diabetic cardiomyopathy. Nat Rev Endocrinol 12(3):144-153. https://doi.org/10.1038/nrendo.2015.216
12. Melzer W, Herrmann-Frank A, Lüttgau HC (1995) The role of Ca^{2+} ions in excitation–contraction coupling of skeletal muscle fibres. Biochim Biophys Acta 1241(1):59-116. https://doi.org/10.1016/0304-4157(94)00014-5
13. Rebbeck RT, Karunasekara Y, Board PG, Beard NA, Casarotto MG, Dulhunty AF (2014) Skeletal muscle excitation–contraction coupling: who are the dancing partners? Int J Biochem Cell Biol 48:28-38. https://doi.org/10.1016/j.biocel.2013.12.001
14. Hernández-Ochoa EO, Schneider MF (2018) Voltage sensing mechanism in skeletal muscle excitation–contraction coupling: coming of age or midlife crisis? Skeletal Muscle 8(1):22. https://doi.org/10.1186/s13395-018-0167-9
15. Ríos E (2018) Calcium-induced release of calcium in muscle: 50 years of work and the emerging consensus. J Gen Physiol 150(4):521-537. https://doi.org/10.1085/jgp.201711959
16. Bassel-Duby R, Olson EN (2006) Signaling pathways in skeletal muscle remodeling. Annu Rev Biochem 75:19-37. https://doi.org/10.1146/annurev.biochem.75.103004.142622
17. Gehlert S, Bloch W, Suhr F (2015) Ca^{2+}-dependent regulations and signaling in skeletal muscle: from electro-mechanical coupling to adaptation. Int J Mol Sci 16(1):1066-1095. https://doi.org/10.3390/ijms16011066
18. Eshima H, Poole DC, Kano Y (2014) In vivo calcium regulation in diabetic skeletal muscle. Cell Calcium 56(5):381-389. https://doi.org/10.1016/j.ceca.2014.08.008

19. Vial G, Chauvin MA, Bendridi N et al (2015) Imeglimin normalizes glucose tolerance and insulin sensitivity and improves mitochondrial function in liver of a high-fat, high-sucrose diet mice model. Diabetes 64(6):2254-2264. https://doi.org/10.2337/db14-1220
20. Jacquemond V (1997) Indo-1 fluorescence signals elicited by membrane depolarization in enzymatically isolated mouse skeletal muscle fibers. Biophys J 73(2):920-928. https://doi.org/10.1016/S0006-3495(97)78124-4
21. Collet C, Csernoch L, Jacquemond V (2003) Intramembrane charge movement and L-type calcium current in skeletal muscle fibers isolated from control and mdx mice. Biophys J 84(1):251-265. https://doi.org/10.1016/S0006-3495(03)74846-2
22. Pouvreau S, Allard B, Berthier C, Jacquemond V (2004) Control of intracellular calcium in the presence of nitric oxide donors in isolated skeletal muscle fibres from mouse. J Physiol 560(3):779-794. https://doi.org/10.1113/jphysiol.2004.072397
23. Horowicz P, Schneider MF (1981) Membrane charge movement in contracting and non-contracting skeletal muscle fibres. J Physiol 314:565-593. https://doi.org/10.1113/jphysiol.1981.sp013725
24. Kutchukian C, Szentesi P, Allard B et al (2017) Impaired excitation–contraction coupling in muscle fibres from the dynamin2R465W mouse model of centronuclear myopathy. J Physiol 595(24):7369-7382. https://doi.org/10.1113/JP274990
25. Grice BA, Barton KJ, Covert JD et al (2019) Excess membrane cholesterol is an early contributing reversible aspect of skeletal muscle insulin resistance in C57BL/6NJ mice fed a Western-style high-fat diet. Am J Physiol 317(2):E362-E373. https://doi.org/10.1152/ajpendo.00396.2018
26. Hernández-Ochoa EO, Robison P, Contreras M, Shen T, Zhao Z, Schneider MF (2012) Elevated extracellular glucose and uncontrolled type 1 diabetes enhance NFAT5 signaling and disrupt the transverse tubular network in mouse skeletal muscle. Exp Biol Med 237(9):1068-1083. https://doi.org/10.1258/ebm.2012.012052
27. Llanos P, Contreras-Ferrat A, Georgiev T et al (2015) The cholesterol-lowering agent methyl-β-cyclodextrin promotes glucose uptake via GLUT4 in adult muscle fibers and reduces insulin resistance in obese mice. Am J Physiol 308(4):E294-E305. https://doi.org/10.1152/ajpendo.00189.2014
28. Funai K, Song H, Yin L et al (2013) Muscle lipogenesis balances insulin sensitivity and strength through calcium signaling. J Clin Invest 123(3):1229-1240. https://doi.org/10.1172/JCI65726
29. Funai K, Lodhi IJ, Spears LD et al (2016) Skeletal muscle phospholipid metabolism regulates insulin sensitivity and contractile function. Diabetes 65(2):358-370. https://doi.org/10.2337/db15-0659
30. Paran CW, Verkerke AR, Heden TD et al (2015) Reduced efficiency of sarcolipin-dependent respiration in myocytes from humans with severe obesity. Obesity 23(7):1440-1449. https://doi.org/10.1002/oby.21123
31. Kutchukian C, Szentesi P, Allard B, Buj-Bello A, Csernoch L, Jacquemond V (2019) Ca^{2+}-induced sarcoplasmic reticulum Ca^{2+} release in myotubularin-deficient muscle fibers. Cell Calcium 80:91-100. https://doi.org/10.1016/j.ceca.2019.04.004
32. Lotteau S, Ivarsson N, Yang Z et al (2019) A mechanism for statin-induced susceptibility to myopathy. JACC Basic Transl Sci 4(4):509-523. https://doi.org/10.1016/j.jacbts.2019.03.012
33. Bianchi L, Volpato S (2016) Muscle dysfunction in type 2 diabetes: a major threat to patient's mobility and independence. Acta Diabetol 53(6):879-889. https://doi.org/10.1007/s00592-016-0880-y
34. Ríos E, Figueroa L, Manno C, Kraeva N, Riazi S (2015) The couplonopathies: A comparative approach to a class of diseases of skeletal and cardiac muscle. J Gen Physiol 145(6):459-474. https://doi.org/10.1085/jgp.201411321
35. Allard B (2018) From excitation to intracellular Ca^{2+} movements in skeletal muscle: Basic aspects and related clinical disorders. Neuromuscul Disord 28(5):394-401. https://doi.org/10.1016/j.nmd.2018.03.004

36. Avila G (2018) Disturbed Ca^{2+} homeostasis in muscle-wasting disorders. Adv Exp Med Biol 1088:307-326. https://doi.org/10.1007/978-981-13-1435-3_14
37. Denniss A, Dulhunty AF, Beard NA (2018) Ryanodine receptor Ca^{2+} release channel post-translational modification: central player in cardiac and skeletal muscle disease. Int J Biochem Cell Biol 101:49-53. https://doi.org/10.1016/j.biocel.2018.05.004
38. Ogawa T, Kashiwagi A, Kikkawa R, Shigeta Y (1995) Increase of voltage-sensitive calcium channels and calcium accumulation in skeletal muscles of streptozocin-induced diabetic rats. Metabolism 44(11):1455-1461. https://doi.org/10.1016/0026-0495(95)90146-9
39. Bruton JD, Katz A, Lännergren J, Abbate F, Westerblad H (2002) Regulation of myoplasmic Ca^{2+} in genetically obese (*ob/ob*) mouse single skeletal muscle fibres. Pflugers Arch 444(6):692-699. https://doi.org/10.1007/s00424-002-0882-1
40. Jain SS, Paglialunga S, Vigna C et al (2014) High-fat diet-induced mitochondrial biogenesis is regulated by mitochondrial-derived reactive oxygen species activation of CaMKII. Diabetes 63(6):1907-1913. https://doi.org/10.2337/db13-0816
41. Matsunaga S, Inashima S, Yamada T, Watanabe H, Hazama T, Wada M (2003) Oxidation of sarcoplasmic reticulum Ca^{2+}-ATPase induced by high-intensity exercise. Pflugers Arch 446(3):394-399. https://doi.org/10.1007/s00424-003-1040-0
42. Vázquez P, Tirado-Cortés A, Álvarez R, Ronjat M, Amaya A, Ortega A (2016) Reversible oxidation of vicinal-thiols motif in sarcoplasmic reticulum calcium regulatory proteins is involved in muscle fatigue mechanism. Cell Calcium 60(4):245-255. https://doi.org/10.1016/j.ceca.2016.06.001
43. Maurya SK, Bal NC, Sopariwala DH, Pant M, Rowland LA, Shaikh SA, Periasamy M (2015) Sarcolipin is a key determinant of the basal metabolic rate, and its overexpression enhances energy expenditure and resistance against diet-induced obesity. J Biol Chem 290(17):10840-10949. https://doi.org/10.1074/jbc.M115.636878
44. Maurya SK, Herrera JL, Sahoo SK et al (2018) Sarcolipin signaling promotes mitochondrial biogenesis and oxidative metabolism in skeletal muscle. Cell Rep 24(11):2919-2931. https://doi.org/10.1016/j.celrep.2018.08.036

DISCUSSION AND PERSPECTIVES

DISCUSSION AND PERSPECTIVES

Pannexins were discovered in 2003 (Bruzzone et al., 2003) and first proposed to act as plasma membrane ATP channels in 2004 (Bao et al., 2004). This is thus a very young domain of knowledge (as compared to ECC, Sandow, 1952) generating a growing interest within a number of signaling processes in distinct tissues, and in potential relation with a variety of pathological situations.

The present project aimed at further understanding the function of Panx1 in muscle and its interactions with ECC, with a large part of the work relying on single-muscle-fiber physiology techniques including fluorescence imaging and several configurations of electrophysiology. In this respect, it is of strong relevance that, our whole-cell experimental conditions on intact muscle fibers, leave the T-tubules, the triadic organization, the ECC molecular machinery and the entire cellular physiological context quite untouched, while allowing full quantitative control of membrane excitation and quantitative assessment of the function of the mechanisms under study. This gives to our conclusions a unique physiological relevance.

Altogether, the present work provides the first evidence favoring a role for Panx1 as a functional partner for the regulation of the excitation-contraction coupling (ECC) machinery in differentiated muscle. Both the decrease in Panx1 expression and Panx1 pharmacological block depress SR Ca^{2+} release during ECC, which we like to speculate that it could be involved in muscle dysfunction associated with certain physiopathological situations. Within this overall context we also attempted to better characterize Panx1 function at the cellular level and developed, to this aim, two different methods to measure Panx1-dependent ATP release from single isolated muscle fibers. Both methods qualitatively work but both failed to reveal a clear and reproducible ATP release following permissive stimulation conditions (20 Hz trains of voltage excitation). Nevertheless, the energy and time spent were not wasted because of everything we learned during the process, because proof of concept is made for feasibility for both methods, and because we believe there is still the perspective that minor changes/adjustments in the experimental conditions may make these measurements successful and allow breakthrough understanding regarding Panx1 function in muscle.

Finally, we took, within this project, the opportunity to work with a diet-induced mouse model of diabetes and obesity and proved, for the first time, that the previously described associated muscle function impairments are not related to ECC and Ca^{2+} handling dysfunction. These “negative results”

represent, we believe, particularly important information for general understanding of diabetes-associated muscle function disorders.

Panx1 and Excitation-Contraction Coupling

In this project, the first objective was to determine if Panx1, a heptameric, triadic-located ATP-channel, plays a role in ECC in adult skeletal muscle fibers and if, therefore, $Ca_V1.1$ and Panx1 present a bidirectional relationship. As already mentioned, Panx1 has been already related to 3 different important processes in skeletal muscle physiology: 1) differentiation, in which there are associations between Panx1 and Panx3 expression, glycosylated and non-glycosylated isoforms and muscle fibers developmental stage (Pham et al., 2018), 2) contractile potentiation, related with ATP release and preservation of tetanic force (Riquelme et al., 2013), and 3) ETC, in which $Ca_V1.1$ activates Panx1 upon 20 Hz electrical stimulation, producing ATP release and purinergic activation, which triggers an intracellular pathway of gene expression regulation (Jorquera et al., 2013). Previous work on this ETC pathway was of critical relevance for initiation of the present project, and prompted us to focus on the $Ca_V1.1$-Panx1 relationship. More specifically, Jorquera et al. (2013) showed that $Ca_V1.1$ is able to regulate Panx1 channel activity, and together with other groups showed that Panx1 and $Ca_V1.1$ co-localize at the triads of differentiated skeletal muscle fibers (Jorquera et al., 2013; Riquelme et al., 2013; Valladares et al., 2013). In the first manuscript presented in the present document, we describe that transitory knockdown of Panx1 produces an alteration in $Ca_V1.1$-dependent Ca^{2+} current and more importantly, a severe decrease in RyR1-dependent SR Ca^{2+} release. We showed that the decreased SR Ca^{2+} release was not due to a change in the SR Ca^{2+} content, nor to altered density or voltage-sensing function of $Ca_V1.1$. There are several possible explanations: 1) Panx1 interacts directly or indirectly with $Ca_V1.1$, and removal of this interaction affects $Ca_V1.1$ channel properties and precludes proper orthograde control of RyR1 function; 2) Panx1 interacts indirectly with RyR1 and removal of this interaction affects RyR1 function and also feeds back on $Ca_V1.1$ channel function; and 3) somewhat similar, Panx1 interacts directly or indirectly with the $Ca_V1.1$-RyR1 coupling process, for instance through another partner protein of ECC. It is important to note that "interaction" may not solely be thought in terms of a required local molecular static or dynamic phenomenon between Panx1 and a protein partner; for instance, it may also be that Panx1 removal physically disturbs proper triadic organization and/or arrangement of $Ca_V1.1$-RyR1 clusters.

There are several proteins with triadic localization that were already shown to have the capacity to alter ECC through such mechanisms, as described in the Introductory section (Introduction: chapter II). Our primary working hypothesis was the existence of a $Ca_V1.1$-Panx1 relationship. If we compare our

results with those from Nakai et al. (1996) which established the $Ca_V1.1$-RyR1 bidirectional relationship, they found that RyR1 deficiency in myotubes generates an important decrease of SR Ca^{2+} release and $Ca_V1.1$ Ca^{2+} current, with no change in $Ca_V1.1$ density. In our case: Panx1 deficiency in adult muscle fibers also generated an important decrease (≈60%) in SR Ca^{2+} release, $Ca_V1.1$ Ca^{2+} current (≈30%) with no change in $Ca_V1.1$ density. The similarity between the two sets of results encourages us to believe that an analogous bi-directional relationship takes place in both cases. Nevertheless, complete elucidation of this issue will require further efforts and there are still questions that remain unanswered. For instance, we cannot completely exclude that the Panx1 deficiency-associated ECC alterations results from removal of a Panx1-mediated signaling cascade that feeds back onto ECC and is necessary for its proper maintenance/function. This issue is further discussed later in this section. Also, the fact that Panx1-KO mice do not suffer from major muscle function defects will need further investigations as there has to be some compensation mechanisms taking place.

Panx1 presents several pharmacological inhibitors. Two relevant drugs with clinical use are described as, not entirely selective but at least efficient blockers of Panx1 channels and ATP release. These are carbenoxolone and probenecid. Carbenoxolone was used in Europe in the past century for the treatment of digestive tract ulcers, especially the stomach, and is described with low toxicity (Pinder et al., 1976). Probenecid has been and is currently used for the treatment of gout disease and to increase the renal reabsorption of antibiotics, chemotherapeutics, and other drugs (Willebrords et al., 2017). Both drugs have been shown to inhibit ATP release from Panx1 in several models and conditions (Patel et al., 2014). Because of the clinical use of these inhibitors and the role of Panx1 in ECC that is highlighted in the present work, we studied, during my PhD thesis, the effect of these Panx1 inhibitors on RyR1-dependent SR Ca^{2+} release.

Both probenecid and carbenoxolone depress voltage-activated SR Ca^{2+} release. Investigations were pushed further with probenecid, showing that it also rapidly affects resting Ca^{2+} homeostasis and that it decreases the maximal tetanic force measured from isolated mouse muscle.

Both probenecid and carbenoxolone were originally described as interacting with the first extracellular loop of Panx1, triggering an allosteric inhibition (Michalski et al., 2016). However, recently, the carbenoxolone interaction with Panx1 has been characterized by Cryo-EM by two independent groups (Jin et al., 2020; Ruan et al., 2020). They showed that carbenoxolone interaction does not produce a detectable Panx1 conformational change: when interacting with Panx1, carbenoxolone locates in the selectivity filter of the main pore, acting as a channel blocker. These results are of relevance to our

interpretation of the drug effects and to the perspectives of the present work. Indeed, excluding a carbenoxolone-induced change in Panx1 conformation makes it complicated to foresee that this could, in return, affect an interaction of Panx1 with an ECC protein. At this point, this remains an unclear issue. One thing is that carbenoxolone and probenecid may not share entirely identical mechanisms of molecular action on Panx1 conformation. Accordingly, in our hands, probenecid induced a rapid SR Ca^{2+} leak which we think is contributing to the eventual depression of voltage-activated Ca^{2+} release. Somewhat different, carbenoxolone also did generate an increase in resting Ca^{2+}, but it seemed, on a longer time-scale. Thus, there may be subtle differences in the molecular mechanisms of action of the two on Ca^{2+} homeostasis, through their interaction with Panx1, with the outcome being that probenecid and carbenoxolone produce a rapid and slow SR Ca^{2+} leak, respectively. Finally, as discussed in the corresponding manuscript included in the present Thesis, we also cannot exclude that other molecular targets of the two drugs are involved in, or contribute to, the effects we describe.

Independent of the molecular mechanisms underlying the effects of carbenoxolone and probenecid on Ca^{2+} homeostasis and ECC, one important point is the potential clinical relevance of our results. Because Panx1 block, specifically with probenecid, is still being considered of therapeutical benefit, or of potential therapeutical benefit for a number of disease situations (Ahmed et al., 2015), we believe that consequent alterations of Ca^{2+} homeostasis in muscle, and maybe also in other tissues, should be taken into consideration. Until now, there is no indication that skeletal muscle weakness occurs as a secondary effect of probenecid treatment. However, the skeletal muscle condition of the patients with gout could mask the muscle effect of the drug, because evolution of that disease normally presents with a decrease in muscle function (Stewart et al., 2016). It is also possible that the drug never reaches the levels used in our work in the interstitial tissue.

A third workpackage within my first objective was to assess the consequences of Panx1 overexpression on ECC. We so far found no effect, suggesting that either we do not over-express Panx1 in the muscle fibers, and instead that we only replace the native one by the exogenous one. This will need to be checked. Alternatively, the inherent Panx1 level may be optimized with respect to its function versus ECC so that adding more Panx1 into the membrane neither affects nor promotes the function of ECC.

Altogether, it seems that in the physiology of adult skeletal muscle fibers requires Panx1 and/or Panx1 function for normal Ca^{2+} handling, ECC, and force production, whereas Panx1 overexpression appears to produce no change in ECC. while overexpression may not produce any change in ECC.

Throughout this work we have essentially reasoned with Panx1 acting either as a molecular partner of the ECC machinery and/or as an ATP channel involved in purinergic signaling. However, because Panx1 also conducts Cl^- ions, Panx1 contribution to the muscle fiber plasma membrane Cl^--conductance may be raised. To test for this, we made preliminary measurements, taking advantage of the fact that Cl^- permeation through Panx1 is known to be blocked by carbenoxolone (Ruan et al. 2020). We used a voltage-clamp protocol of ramps to study the effect of carbenoxolone on the whole-cell membrane conductance. With this, we found no clear indication for a carbenoxolone-induced change in membrane conductance (data not shown). Although we cannot exclude that our experimental conditions were not appropriate to detect blockade of the Panx1 Cl^- current, it may as well be that the huge resting conductance for Cl^- in adult muscle made the influence of Panx1 undetectable.

An issue that needs to be considered is the potential role of the Panx1-dependent signaling cascade. Panx1-mediated ATP release was reported to be needed for the process of contractile potentiation (Riquelme et al., 2013; Cea et al., 2014; Ziganshin et al., 2019). Still, it is hard to foresee that the same signaling cascade triggered by ATP release through purinergic receptors activation, is also involved in the effects that we report of Panx1 down-expression and of Panx1 blockers. Indeed, this would mean that there is a constant need for this feedback through activation of purinergic receptors for proper ECC function, making this process a critical partner of basic ECC function. We do not believe that this is plausible.

In terms of future experimental work that could help clarify the role of Panx1 and ATP release in ECC, there are relevant options: 1) test whether Panx1 blockers still affect ECC in the presence of high extracellular ATP. If still effective, this would definitely exclude the role of ATP release in the ECC depression. 2) Test whether Panx1 blockers still generate a rise in resting Ca^{2+} in the absence of RyR1. This would assess or exclude the contribution of RyR1 to this effect. We already made attempts using a combination of RyR1 blockers, but this proved to be more complicated than we expected. For this, the use of dyspedic myotubes would likely be a preferred alternative. 3) Study the effect of the drugs in a Panx1 knockout model. This could help us to prove unequivocally that Panx1 is the main target behind probenecid and carbenoxolone effects on ECC. 4) Study the molecular interaction between Panx1 and the ECC machinery using intracellular dialysis of synthetic peptides that reproduce Panx1 intracellular loops, C-terminal or N-terminal portions, associated with voltage-activated SR Ca^{2+} release measurements. This may also help to elucidate the details of Panx1 interaction with the ECC molecular machinery.

Detection of ATP release from a single muscle fiber

Results of the two approaches that we developed were not conclusive with respect to detection of ATP release in response to a 20 Hz train of stimulations. Still, we provide the proof of concept that these methods are efficient to measure extracellular ATP down to the µM range.

The K_{ATP} biosensor, under the inside-out configuration of patch-clamp, nicely responds to application of ATP. ATP rapidly inhibits the K^+ current with a maximum decrease of ≈90% with 100 µM ATP, as described in the literature (Tinker et al., 2018). Temporal resolution of the technique is definitely better than the one of the Luciferin/luciferase assay used for measuring ATP release from a population of muscle fibers (Jorquera et al., 2013). We estimated that under optimal conditions, the sensitivity of the method should be sufficient to detect an increase in extracellular ATP within the µM range. However, even if, on average, measurements from 10 fibers generated a 55% decrease in the K_{ATP} biosensor activity following 20 Hz stimulation of the tested fibers, the variability between fibers was too big to assess a significant difference between the K^+ current post-20 Hz stimulation and the baseline activity before. We initially planned duplicating these experiments in the presence of Panx1 inhibitors. However, considering the difficulty to detect a reliable response to 20 Hz stimulation, added to the complexity of the configuration and combination of 2 micropipettes recording, clearly made this approach too challenging to also consider implementing the use of Panx1 blockers. One issue that may have contributed to reliably preclude ATP release detection is the distance between the ATP-biosensing membrane patch and the plasma membrane of the fiber challenged by the trains of stimulation. Although we tried our best, there had to be a distance of approximately 5-10 µM where the change in released ATP may have been already dampened by diffusion.

The expression of a P2XR provided a much easier working configuration, with the ATP biosensor being readily expressed within the plasma membrane of the fibers to be tested. One also clear advantage was that the P2XR, as Panx1, was present in the T-tubule membrane. This proximity within the restricted volume available in the T-tubules should favor large changes in ATP concentration and provide an optimized detection configuration. The sensitivity of the technique to application of extracellular ATP was amazing, with 100 µM ATP producing inward currents in the tens of nA range, within a second. This method was more stable, easier and faster to implement than the use of the K_{ATP} biosensor. It allowed us study the effect of different frequencies of stimulation in each fiber. We were able to take measurements from 13 fibers (within two months including Christmas break). In each case, membrane current was recorded during 5 minutes after 20-Hz-stimulation and 5 minutes after 90-Hz-stimulation. Still, we did not

observe reproducible differences in the membrane current after 20 Hz and 90 Hz stimuli and there was also no reproducible current change with well-defined kinetics that would allow clear-cut identification of ATP release.

These negative results may have two possible explanations: 1) either these sensors are still not sensitive enough, which means that the changes in ATP concentration close to a single fiber or within the T-tubules of a single fiber are in the pM to nM range, 2) or the 20 Hz stimulation does not produce ATP release in muscle fibers under silicone voltage-clamp conditions.

For the first alternative, because we dialyzed the fibers with 15 mM ATP during 10-20 minutes to enhance the ATP gradient and, when using the P2XRs, these were expressed in the T-tubules, it is hard to believe that upon Panx1 channels opening, ATP release could not be detected. Future attempts will make use of P2XRs with enhanced ATP sensitivity to try resolve this issue. Another explanation could be that, in our condition, there is no such thing as 20 Hz-activated Panx1-dependent ATP release. The arguments behind this hypothesis become stronger when considering recent works that proved that Panx1-dependent ATP release can only be activated after irreversible caspases-dependent cleavage or reversible Src tyrosine kinases family (SKF)-dependent phosphorylation (Jin et al., 2020; Ruan et al., 2020). Considering these new finding, the Panx1 opening stimulated by $Ca_V1.1$ activation at different frequencies (Jorquera et al., 2013) may need an intermediate signal, which could somehow activate either the caspases or the SKF, and in a second step activate Panx1-dependent ATP release by cleavages or phosphorylation. The SFK activation has been shown to be regulated by cytosolic Ca^{2+} changes: an increase in Ca^{2+} decreases c-Src activity through calmodulin activation (Anguita & Villalobo, 2018). If we consider this knowledge, it could be possible, for example, that with the different frequencies of stimulation we produce different Ca^{2+} signals through $Ca_V1.1$, or through $Ca_V1.1$-RyR1 interaction as previously suggested (Chin et al., 2003). In muscle, different levels of intracellular [Ca^{2+}] rise have been associated with the different frequencies of stimulation, with larger [Ca^{2+}] levels upon 90 Hz of stimulation (which supposedly could decrease the s-Src activity) and lower [Ca^{2+}] levels upon 20 Hz stimulation (Hughes et al., 1998; Spangenburg et al., 2003). During ECC, these different [Ca^{2+}] levels have been associated with the activation of distinct, independent signaling pathways and it has been shown that Panx1 is activated by SFK-dependent phosphorylation independently of cytosolic [Ca^{2+}] changes (Delalio et al., 2019). Considering these works, activation of Src tyrosine kinase family associated, or not, to a rise in intracellular Ca^{2+} could be a possibility to explain the transient activation of Panx1, through phosphorylation. According to this, one explanation to our negative results could be the intracellular dialysis of the muscle fibers with

the intracellular solution through the voltage-clamp pipette. This may wash out either of the needed mediators (caspase or SFK) and prevent ATP release.

The above considerations open several experimental possibilities to improve our knowledge about Panx1-dependent ATP release at the single muscle fiber level. If Panx1 needs an intracellular mediator to open and produce ATP release, then use of another way of Panx1 opening is of strong interest. First, we should use a condition that we know will open the main pore of Panx1 channel, which means stimulate the activation of Src kinases family or caspases in P2XR expressing muscle fibers (Delalio et al., 2019). These experiments could help clarify if it is the sensitivity of the sensor or the dialysis in voltage-clamp conditions, which is limiting. However, the development of such conditions will be not straightforward because tools to activate these enzymes in a fast and specific way are, to our knowledge, not readily available (Delalio et al., 2018; Delalio et al., 2019).

Another easily implementable perspective would be to perform experiments in the P2XR expressing fibers without dialysis, and study 20 Hz stimulation in standard condition versus another group of cells stimulated at 20 Hz in the presence of extracellular Panx1 blockers. This could help determine if dialysis plays a role in the absence of response after 20 Hz stimulation.

ECC in obesity and diabetes

We prove that intracellular Ca^{2+} signaling and the function of the ECC machinery remain well preserved in the obesity/diabetic condition so that depressed muscle force production has to be a consequence of an alteration at another level of muscle function. This is in striking contrast with the situation in cardiac and vascular muscles for which there is clear evidence that altered Ca^{2+} signaling contributes to dysfunction in the diabetic environment (e.g. Fernández-Velasco et al., 2014; Pereira et al., 2014). The preserved skeletal muscle ECC function in our conditions does not exclude the possibility that the specific in vivo diabetic environment, including elevated circulating levels of insulin and glucose, may differentially affect muscle Ca^{2+} signaling and ECC. Future experiments should help resolve this issue.

As a final point, our data pointing out a role for Panx1 in the regulation of ECC open the possibility that Panx1 is involved in ECC-related muscle disease situations. There is no identified example yet but this is something that may be important to keep in mind for the future.

REFERENCES

References

Adams, B. A., Tanabe, T., Mikami, A., Numa, S., & Beam, K. G. (1990). Intramembrane charge movement restored in dysgenic skeletal muscle by injection of dihydropyridine receptor cDNAs. *Nature, 346*(6284), 569-572. doi:10.1038/346569a0

Adrian, R. H., Chandler, W. K., & Hodgkin, A. L. (1970). Voltage clamp experiments in striated muscle fibres. *J Physiol, 208*(3), 607-644. doi:10.1113/jphysiol.1970.sp009139

Adrian, R. H., Costantin, L. L., & Peachey, L. D. (1969). Radial spread of contraction in frog muscle fibres. *J Physiol, 204*(1), 231-257. doi:10.1113/jphysiol.1969.sp008910

Adrian, R. H., & Marshall, M. W. (1977). Sodium currents in mammalian muscle. *J Physiol, 268*(1), 223-250. doi:10.1113/jphysiol.1977.sp011855

Ahern, G. P., Junankar, P. R., & Dulhunty, A. F. (1997). Subconductance states in single-channel activity of skeletal muscle ryanodine receptors after removal of FKBP12. *Biophys J, 72*(1), 146-162. doi:10.1016/s0006-3495(97)78654-5

Akopova, I., Tatur, S., Grygorczyk, M., Luchowski, R., Gryczynski, I., Gryczynski, Z., . . . Grygorczyk, R. (2012). Imaging exocytosis of ATP-containing vesicles with TIRF microscopy in lung epithelial A549 cells. *Purinergic Signal, 8*(1), 59-70. doi:10.1007/s11302-011-9259-2

Al-Qusairi, L., Weiss, N., Toussaint, A., Berbey, C., Messaddeq, N., Kretz, C., . . . Buj-Bello, A. (2009). T-tubule disorganization and defective excitation-contraction coupling in muscle fibers lacking myotubularin lipid phosphatase. *Proc Natl Acad Sci U S A, 106*(44), 18763-18768. doi:10.1073/pnas.0900705106

Allard, B., Couchoux, H., Pouvreau, S., & Jacquemond, V. (2006). Sarcoplasmic reticulum Ca2+ release and depletion fail to affect sarcolemmal ion channel activity in mouse skeletal muscle. *J Physiol, 575*(Pt 1), 69-81. doi:10.1113/jphysiol.2006.112367

Allard, B., & Lazdunski, M. (1993). Pharmacological properties of ATP-sensitive K+ channels in mammalian skeletal muscle cells. *Eur J Pharmacol, 236*(3), 419-426. doi:10.1016/0014-2999(93)90480-6

Allard, B., Lazdunski, M., & Rougier, O. (1995). Activation of ATP-dependent K+ channels by metabolic poisoning in adult mouse skeletal muscle: role of intracellular Mg(2+) and pH. *J Physiol, 485 (Pt 2)*(Pt 2), 283-296. doi:10.1113/jphysiol.1995.sp020730

Allard, B., & Rougier, O. (1997). Similarity of ATP-dependent K+ channels in skeletal muscle fibres from normal and mutant mdx mice. *J Physiol, 498 (Pt 2)*(Pt 2), 319-325. doi:10.1113/jphysiol.1997.sp021860

Allen, D. G., Whitehead, N. P., & Froehner, S. C. (2016). Absence of Dystrophin Disrupts Skeletal Muscle Signaling: Roles of Ca2+, Reactive Oxygen Species, and Nitric Oxide in the Development of Muscular Dystrophy. *Physiol Rev, 96*(1), 253-305. doi:10.1152/physrev.00007.2015

Allen, D. L., Harrison, B. C., Maass, A., Bell, M. L., Byrnes, W. C., & Leinwand, L. A. (2001). Cardiac and skeletal muscle adaptations to voluntary wheel running in the mouse. *J Appl Physiol (1985), 90*(5), 1900-1908. doi:10.1152/jappl.2001.90.5.1900

Allen, D. L., & Leinwand, L. A. (2002). Intracellular calcium and myosin isoform transitions. Calcineurin and calcium-calmodulin kinase pathways regulate preferential activation of the IIa myosin heavy chain promoter. *J Biol Chem, 277*(47), 45323-45330. doi:10.1074/jbc.M208302200

Altamirano, F., Valladares, D., Henriquez-Olguin, C., Casas, M., Lopez, J. R., Allen, P. D., & Jaimovich, E. (2013). Nifedipine treatment reduces resting calcium concentration, oxidative and apoptotic gene expression, and improves muscle function in dystrophic mdx mice. *PLoS One, 8*(12), e81222. doi:10.1371/journal.pone.0081222

Anderson, A. A., Altafaj, X., Zheng, Z., Wang, Z. M., Delbono, O., Ronjat, M., . . . Zorzato, F. (2006). The junctional SR protein JP-45 affects the functional expression of the voltage-dependent Ca2+ channel Cav1.1. *J Cell Sci, 119*(Pt 10), 2145-2155. doi:10.1242/jcs.02935

Anderson, D. M., Anderson, K. M., Chang, C. L., Makarewich, C. A., Nelson, B. R., McAnally, J. R., . . . Olson, E. N. (2015). A micropeptide encoded by a putative long noncoding RNA regulates muscle performance. *Cell, 160*(4), 595-606. doi:10.1016/j.cell.2015.01.009

Andersson, D. C., Betzenhauser, M. J., Reiken, S., Meli, A. C., Umanskaya, A., Xie, W., . . . Marks, A. R. (2011). Ryanodine receptor oxidation causes intracellular calcium leak and muscle weakness in aging. *Cell Metab, 14*(2), 196-207. doi:10.1016/j.cmet.2011.05.014

Andersson, D. C., Betzenhauser, M. J., Reiken, S., Umanskaya, A., Shiomi, T., & Marks, A. R. (2012). Stress-induced increase in skeletal muscle force requires protein kinase A phosphorylation of the ryanodine receptor. *J Physiol, 590*(24), 6381-6387. doi:10.1113/jphysiol.2012.237925

Andronache, Z., Hamilton, S. L., Dirksen, R. T., & Melzer, W. (2009). A retrograde signal from RyR1 alters DHP receptor inactivation and limits window Ca2+ release in muscle fibers of Y522S RyR1 knock-in mice. *Proc Natl Acad Sci U S A, 106*(11), 4531-4536. doi:10.1073/pnas.0812661106

Andronache, Z., Ursu, D., Lehnert, S., Freichel, M., Flockerzi, V., & Melzer, W. (2007). The auxiliary subunit gamma 1 of the skeletal muscle L-type Ca2+ channel is an endogenous Ca2+ antagonist. *Proc Natl Acad Sci U S A, 104*(45), 17885-17890. doi:10.1073/pnas.0704340104

Anguita, E., & Villalobo, A. (2018). Ca(2+) signaling and Src-kinases-controlled cellular functions. *Arch Biochem Biophys, 650*, 59-74. doi:10.1016/j.abb.2018.05.005

Anselmi, F., Hernandez, V. H., Crispino, G., Seydel, A., Ortolano, S., Roper, S. D., . . . Mammano, F. (2008). ATP release through connexin hemichannels and gap junction transfer of second messengers propagate Ca2+ signals across the inner ear. *Proc Natl Acad Sci U S A, 105*(48), 18770-18775. doi:10.1073/pnas.0800793105

Aracena, P., Sánchez, G., Donoso, P., Hamilton, S. L., & Hidalgo, C. (2003). S-glutathionylation decreases Mg2+ inhibition and S-nitrosylation enhances Ca2+ activation of RyR1 channels. *J Biol Chem, 278*(44), 42927-42935. doi:10.1074/jbc.M306969200

Aracena-Parks, P., Goonasekera, S. A., Gilman, C. P., Dirksen, R. T., Hidalgo, C., & Hamilton, S. L. (2006). Identification of cysteines involved in S-nitrosylation, S-glutathionylation, and oxidation to disulfides in ryanodine receptor type 1. *J Biol Chem, 281*(52), 40354-40368. doi:10.1074/jbc.M600876200

Araya, R., Liberona, J. L., Cárdenas, J. C., Riveros, N., Estrada, M., Powell, J. A., . . . Jaimovich, E. (2003). Dihydropyridine receptors as voltage sensors for a depolarization-evoked, IP3R-mediated, slow calcium signal in skeletal muscle cells. *J Gen Physiol, 121*(1), 3-16. doi:10.1085/jgp.20028671

Arias-Calderon, M., Almarza, G., Diaz-Vegas, A., Contreras-Ferrat, A., Valladares, D., Casas, M., . . . Buvinic, S. (2016). Characterization of a multiprotein complex involved in excitation-transcription coupling of skeletal muscle. *Skelet Muscle, 6*, 15. doi:10.1186/s13395-016-0087-5

Asahi, M., Sugita, Y., Kurzydlowski, K., De Leon, S., Tada, M., Toyoshima, C., & MacLennan, D. H. (2003). Sarcolipin regulates sarco(endo)plasmic reticulum Ca2+-ATPase (SERCA) by binding to transmembrane helices alone or in association with phospholamban. *Proc Natl Acad Sci U S A, 100*(9), 5040-5045. doi:10.1073/pnas.0330962100

Ausoni, S., Gorza, L., Schiaffino, S., Gundersen, K., & Lømo, T. (1990). Expression of myosin heavy chain isoforms in stimulated fast and slow rat muscles. *J Neurosci, 10*(1), 153-160. doi:10.1523/jneurosci.10-01-00153.1990

Avila, G., & Dirksen, R. T. (2000). Functional impact of the ryanodine receptor on the skeletal muscle L-type Ca(2+) channel. *J Gen Physiol, 115*(4), 467-480. doi:10.1085/jgp.115.4.467

Avila, G., & Dirksen, R. T. (2001). Functional effects of central core disease mutations in the cytoplasmic region of the skeletal muscle ryanodine receptor. *J Gen Physiol, 118*(3), 277-290. doi:10.1085/jgp.118.3.277

Avila, G., Lee, E. H., Perez, C. F., Allen, P. D., & Dirksen, R. T. (2003). FKBP12 binding to RyR1 modulates excitation-contraction coupling in mouse skeletal myotubes. *J Biol Chem, 278*(25), 22600-22608. doi:10.1074/jbc.M205866200

Aydin, J., Shabalina, I. G., Place, N., Reiken, S., Zhang, S. J., Bellinger, A. M., . . . Westerblad, H. (2008). Nonshivering thermogenesis protects against defective calcium handling in muscle. *Faseb j, 22*(11), 3919-3924. doi:10.1096/fj.08-113712

Babu, G. J., Bhupathy, P., Carnes, C. A., Billman, G. E., & Periasamy, M. (2007). Differential expression of sarcolipin protein during muscle development and cardiac pathophysiology. *J Mol Cell Cardiol, 43*(2), 215-222. doi:10.1016/j.yjmcc.2007.05.009

Babu, G. J., Bhupathy, P., Timofeyev, V., Petrashevskaya, N. N., Reiser, P. J., Chiamvimonvat, N., & Periasamy, M. (2007). Ablation of sarcolipin enhances sarcoplasmic reticulum calcium transport and atrial contractility. *Proc Natl Acad Sci U S A, 104*(45), 17867-17872. doi:10.1073/pnas.0707722104

Bai, X. C., Yan, Z., Wu, J., Li, Z., & Yan, N. (2016). The Central domain of RyR1 is the transducer for long-range allosteric gating of channel opening. *Cell Res, 26*(9), 995-1006. doi:10.1038/cr.2016.89

Bal, N. C., Maurya, S. K., Sopariwala, D. H., Sahoo, S. K., Gupta, S. C., Shaikh, S. A., . . . Periasamy, M. (2012). Sarcolipin is a newly identified regulator of muscle-based thermogenesis in mammals. *Nat Med, 18*(10), 1575-1579. doi:10.1038/nm.2897

Bang, S., Kim, K. Y., Yoo, S., Lee, S. H., & Hwang, S. W. (2007). Transient receptor potential V2 expressed in sensory neurons is activated by probenecid. *Neurosci Lett, 425*(2), 120-125. doi:10.1016/j.neulet.2007.08.035

Bannister, R. A. (2007). Bridging the myoplasmic gap: recent developments in skeletal muscle excitation-contraction coupling. *J Muscle Res Cell Motil, 28*(4-5), 275-283. doi:10.1007/s10974-007-9118-5

Bannister, R. A., & Beam, K. G. (2005). The alpha1S N-terminus is not essential for bi-directional coupling with RyR1. *Biochem Biophys Res Commun, 336*(1), 134-141. doi:10.1016/j.bbrc.2005.08.047

Bannister, R. A., & Beam, K. G. (2009). Ryanodine modification of RyR1 retrogradely affects L-type Ca(2+) channel gating in skeletal muscle. *J Muscle Res Cell Motil, 30*(5-6), 217-223. doi:10.1007/s10974-009-9190-0

Bannister, R. A., & Beam, K. G. (2013). Ca(V)1.1: The atypical prototypical voltage-gated Ca(2)(+) channel. *Biochim Biophys Acta, 1828*(7), 1587-1597. doi:10.1016/j.bbamem.2012.09.007

Bannister, R. A., Estève, E., Eltit, J. M., Pessah, I. N., Allen, P. D., López, J. R., & Beam, K. G. (2010). A malignant hyperthermia-inducing mutation in RYR1 (R163C): consequent alterations in the functional properties of DHPR channels. *J Gen Physiol, 135*(6), 629-640. doi:10.1085/jgp.200910329

Bannister, R. A., Grabner, M., & Beam, K. G. (2008). The alpha(1S) III-IV loop influences 1,4-dihydropyridine receptor gating but is not directly involved in excitation-contraction coupling interactions with the type 1 ryanodine receptor. *J Biol Chem, 283*(34), 23217-23223. doi:10.1074/jbc.M804312200

Bannister, R. A., Pessah, I. N., & Beam, K. G. (2009). The skeletal L-type Ca(2+) current is a major contributor to excitation-coupled Ca(2+) entry. *J Gen Physiol, 133*(1), 79-91. doi:10.1085/jgp.200810105

Bannister, R. A., Sheridan, D. C., & Beam, K. G. (2016). Distinct Components of Retrograde Ca(V)1.1-RyR1 Coupling Revealed by a Lethal Mutation in RyR1. *Biophys J, 110*(4), 912-921. doi:10.1016/j.bpj.2015.12.031

Bao, B. A., Lai, C. P., Naus, C. C., & Morgan, J. R. (2012). Pannexin1 drives multicellular aggregate compaction via a signaling cascade that remodels the actin cytoskeleton. *J Biol Chem, 287*(11), 8407-8416. doi:10.1074/jbc.M111.306522

Bao, L., Locovei, S., & Dahl, G. (2004). Pannexin membrane channels are mechanosensitive conduits for ATP. *FEBS Lett, 572*(1-3), 65-68. doi:10.1016/j.febslet.2004.07.009

S001457930400866X [pii]

Baranova, A., Ivanov, D., Petrash, N., Pestova, A., Skoblov, M., Kelmanson, I., . . . Panchin, Y. (2004). The mammalian pannexin family is homologous to the invertebrate innexin gap junction proteins. *Genomics, 83*(4), 706-716. doi:10.1016/j.ygeno.2003.09.025

Bargiotas, P., Krenz, A., Hormuzdi, S. G., Ridder, D. A., Herb, A., Barakat, W., . . . Schwaninger, M. (2011). Pannexins in ischemia-induced neurodegeneration. *Proc Natl Acad Sci U S A, 108*(51), 20772-20777. doi:10.1073/pnas.1018262108

Bargiotas, P., Krenz, A., Monyer, H., & Schwaninger, M. (2012). Functional outcome of pannexin-deficient mice after cerebral ischemia. *Channels (Austin), 6*(6), 453-456. doi:10.4161/chan.22315

Bassel-Duby, R., & Olson, E. N. (2006). Signaling pathways in skeletal muscle remodeling. *Annu Rev Biochem, 75*, 19-37. doi:10.1146/annurev.biochem.75.103004.142622

Bauerová-Hlinková, V., Hajdúchová, D., & Bauer, J. A. (2020). Structure and Function of the Human Ryanodine Receptors and Their Association with Myopathies-Present State, Challenges, and Perspectives. *Molecules, 25*(18). doi:10.3390/molecules25184040

Baylor, S. M., Chandler, W. K., & Marshall, M. W. (1982). Use of metallochromic dyes to measure changes in myoplasmic calcium during activity in frog skeletal muscle fibres. *J Physiol, 331*, 139-177. doi:10.1113/jphysiol.1982.sp014368

Baylor, S. M., & Hollingworth, S. (2003). Sarcoplasmic reticulum calcium release compared in slow-twitch and fast-twitch fibres of mouse muscle. *J Physiol, 551*(Pt 1), 125-138. doi:10.1113/jphysiol.2003.041608

Baylor, S. M., & Hollingworth, S. (2012). Intracellular calcium movements during excitation-contraction coupling in mammalian slow-twitch and fast-twitch muscle fibers. *J Gen Physiol, 139*(4), 261-272. doi:10.1085/jgp.201210773

Beam, K. G., & Bannister, R. A. (2010). Looking for answers to EC coupling's persistent questions. *J Gen Physiol, 136*(1), 7-12. doi:10.1085/jgp.201010461

Beam, K. G., Knudson, C. M., & Powell, J. A. (1986). A lethal mutation in mice eliminates the slow calcium current in skeletal muscle cells. *Nature, 320*(6058), 168-170. doi:10.1038/320168a0

Beard, N. A., Wei, L., & Dulhunty, A. F. (2009). Ca(2+) signaling in striated muscle: the elusive roles of triadin, junctin, and calsequestrin. *Eur Biophys J, 39*(1), 27-36. doi:10.1007/s00249-009-0449-6

Beckel, J. M., Daugherty, S. L., Tyagi, P., Wolf-Johnston, A. S., Birder, L. A., Mitchell, C. H., & de Groat, W. C. (2015). Pannexin 1 channels mediate the release of ATP into the lumen of the rat urinary bladder. *J Physiol, 593*(8), 1857-1871. doi:10.1113/jphysiol.2014.283119

Befroy, D. E., Rothman, D. L., Petersen, K. F., & Shulman, G. I. (2012). ^{31}P-magnetization transfer magnetic resonance spectroscopy measurements of in vivo metabolism. *Diabetes, 61*(11), 2669-2678. doi:10.2337/db12-0558

Bellinger, A. M., Mongillo, M., & Marks, A. R. (2008). Stressed out: the skeletal muscle ryanodine receptor as a target of stress. *J Clin Invest, 118*(2), 445-453. doi:10.1172/jci34006

Bellinger, A. M., Reiken, S., Carlson, C., Mongillo, M., Liu, X., Rothman, L., . . . Marks, A. R. (2009). Hypernitrosylated ryanodine receptor calcium release channels are leaky in dystrophic muscle. *Nat Med, 15*(3), 325-330. doi:10.1038/nm.1916

Berg, J., Hung, Y. P., & Yellen, G. (2009). A genetically encoded fluorescent reporter of ATP:ADP ratio. *Nat Methods, 6*(2), 161-166. doi:10.1038/nmeth.1288

Bezanilla, F. (2000). The voltage sensor in voltage-dependent ion channels. *Physiol Rev, 80*(2), 555-592. doi:10.1152/physrev.2000.80.2.555

Bezanilla, F. (2008). How membrane proteins sense voltage. *Nat Rev Mol Cell Biol, 9*(4), 323-332. doi:10.1038/nrm2376

Bezanilla, F., Caputo, C., Gonzalez-Serratos, H., & Venosa, R. A. (1972). Sodium dependence of the inward spread of activation in isolated twitch muscle fibres of the frog. *J Physiol, 223*(2), 507-523. doi:10.1113/jphysiol.1972.sp009860

Bhalla-Gehi, R., Penuela, S., Churko, J. M., Shao, Q., & Laird, D. W. (2010). Pannexin1 and pannexin3 delivery, cell surface dynamics, and cytoskeletal interactions. *J Biol Chem, 285*(12), 9147-9160. doi:10.1074/jbc.M109.082008

Bhupathy, P., Babu, G. J., Ito, M., & Periasamy, M. (2009). Threonine-5 at the N-terminus can modulate sarcolipin function in cardiac myocytes. *J Mol Cell Cardiol, 47*(5), 723-729. doi:10.1016/j.yjmcc.2009.07.014

Billaud, M., Chiu, Y. H., Lohman, A. W., Parpaite, T., Butcher, J. T., Mutchler, S. M., . . . Isakson, B. E. (2015). A molecular signature in the pannexin1 intracellular loop confers channel activation by the α1 adrenoreceptor in smooth muscle cells. *Sci Signal, 8*(364), ra17. doi:10.1126/scisignal.2005824

Billaud, M., Lohman, A. W., Straub, A. C., Looft-Wilson, R., Johnstone, S. R., Araj, C. A., . . . Isakson, B. E. (2011). Pannexin1 regulates α1-adrenergic receptor- mediated vasoconstriction. *Circ Res, 109*(1), 80-85. doi:10.1161/circresaha.110.237594

Black, B. L., & Olson, E. N. (1998). Transcriptional control of muscle development by myocyte enhancer factor-2 (MEF2) proteins. *Annu Rev Cell Dev Biol, 14*, 167-196. doi:10.1146/annurev.cellbio.14.1.167

Block, B. A., Imagawa, T., Campbell, K. P., & Franzini-Armstrong, C. (1988). Structural evidence for direct interaction between the molecular components of the transverse tubule/sarcoplasmic reticulum junction in skeletal muscle. *J Cell Biol, 107*(6 Pt 2), 2587-2600. doi:10.1083/jcb.107.6.2587

Bombardier, E., Smith, I. C., Vigna, C., Fajardo, V. A., & Tupling, A. R. (2013). Ablation of sarcolipin decreases the energy requirements for Ca2+ transport by sarco(endo)plasmic reticulum Ca2+-ATPases in resting skeletal muscle. *FEBS Lett, 587*(11), 1687-1692. doi:10.1016/j.febslet.2013.04.019

Boncompagni, S., Thomas, M., Lopez, J. R., Allen, P. D., Yuan, Q., Kranias, E. G., . . . Perez, C. F. (2012). Triadin/Junctin double null mouse reveals a differential role for Triadin and Junctin in anchoring CASQ to the jSR and regulating Ca(2+) homeostasis. *PLoS One, 7*(7), e39962. doi:10.1371/journal.pone.0039962

Bottinelli, R., Betto, R., Schiaffino, S., & Reggiani, C. (1994). Maximum shortening velocity and coexistence of myosin heavy chain isoforms in single skinned fast fibres of rat skeletal muscle. *J Muscle Res Cell Motil, 15*(4), 413-419. doi:10.1007/bf00122115

Branchini, B. R., Ablamsky, D. M., Davis, A. L., Southworth, T. L., Butler, B., Fan, F., . . . Pule, M. A. (2010). Red-emitting luciferases for bioluminescence reporter and imaging applications. *Anal Biochem, 396*(2), 290-297. doi:10.1016/j.ab.2009.09.009

Branchini, B. R., Southworth, T. L., Fontaine, D. M., Kohrt, D., Talukder, M., Michelini, E., . . . Grossel, M. J. (2015). An enhanced chimeric firefly luciferase-inspired enzyme for ATP detection and bioluminescence reporter and imaging applications. *Anal Biochem, 484*, 148-153. doi:10.1016/j.ab.2015.05.020

Bravo, D., Ibarra, P., Retamal, J., Pelissier, T., Laurido, C., Hernandez, A., & Constandil, L. (2014). Pannexin 1: a novel participant in neuropathic pain signaling in the rat spinal cord. *Pain, 155*(10), 2108-2115. doi:10.1016/j.pain.2014.07.024

Brennan, S., Garcia-Castañeda, M., Michelucci, A., Sabha, N., Malik, S., Groom, L., . . . Dirksen, R. T. (2019). Mouse model of severe recessive RYR1-related myopathy. *Hum Mol Genet, 28*(18), 3024-3036. doi:10.1093/hmg/ddz105

Briggs, F. N., Lee, K. F., Wechsler, A. W., & Jones, L. R. (1992). Phospholamban expressed in slow-twitch and chronically stimulated fast-twitch muscles minimally affects calcium affinity of sarcoplasmic reticulum Ca(2+)-ATPase. *J Biol Chem, 267*(36), 26056-26061.

Brillantes, A. B., Ondrias, K., Scott, A., Kobrinsky, E., Ondriasová, E., Moschella, M. C., . . . Marks, A. R. (1994). Stabilization of calcium release channel (ryanodine receptor) function by FK506-binding protein. *Cell, 77*(4), 513-523. doi:10.1016/0092-8674(94)90214-3

Brum, G., Ríos, E., & Stéfani, E. (1988). Effects of extracellular calcium on calcium movements of excitation-contraction coupling in frog skeletal muscle fibres. *J Physiol, 398*, 441-473. doi:10.1113/jphysiol.1988.sp017052

Bruusgaard, J. C., Liestøl, K., Ekmark, M., Kollstad, K., & Gundersen, K. (2003). Number and spatial distribution of nuclei in the muscle fibres of normal mice studied in vivo. *J Physiol, 551*(Pt 2), 467-478. doi:10.1113/jphysiol.2003.045328

Bruzzone, R., Barbe, M. T., Jakob, N. J., & Monyer, H. (2005). Pharmacological properties of homomeric and heteromeric pannexin hemichannels expressed in Xenopus oocytes. *J Neurochem, 92*(5), 1033-1043. doi:10.1111/j.1471-4159.2004.02947.x

Bruzzone, R., Hormuzdi, S. G., Barbe, M. T., Herb, A., & Monyer, H. (2003). Pannexins, a family of gap junction proteins expressed in brain. *Proc Natl Acad Sci U S A, 100*(23), 13644-13649. doi:10.1073/pnas.2233464100

Buller, A. J., Eccles, J. C., & Eccles, R. M. (1960). Interactions between motoneurones and muscles in respect of the characteristic speeds of their responses. *J Physiol, 150*(2), 417-439. doi:10.1113/jphysiol.1960.sp006395

Burke, R. E., Levine, D. N., & Zajac, F. E., 3rd. (1971). Mammalian motor units: physiological-histochemical correlation in three types in cat gastrocnemius. *Science, 174*(4010), 709-712. doi:10.1126/science.174.4010.709

Burnstock, G. (2010). Control of vascular tone by purines and pyrimidines. *Br J Pharmacol, 161*(3), 527-529. doi:10.1111/j.1476-5381.2010.00937.x

Burnstock, G. (2017). Purinergic Signaling in the Cardiovascular System. *Circ Res, 120*(1), 207-228. doi:10.1161/circresaha.116.309726

Butler-Browne, G. S., & Whalen, R. G. (1984). Myosin isozyme transitions occurring during the postnatal development of the rat soleus muscle. *Dev Biol, 102*(2), 324-334. doi:10.1016/0012-1606(84)90197-0

Buvinic, S., Almarza, G., Bustamante, M., Casas, M., Lopez, J., Riquelme, M., . . . Jaimovich, E. (2009). ATP released by electrical stimuli elicits calcium transients and gene expression in skeletal muscle. *J Biol Chem, 284*(50), 34490-34505. doi:10.1074/jbc.M109.057315

Bárány, M. (1967). ATPase activity of myosin correlated with speed of muscle shortening. *J Gen Physiol, 50*(6), Suppl:197-218. doi:10.1085/jgp.50.6.197

Bär, A., & Pette, D. (1988). Three fast myosin heavy chains in adult rat skeletal muscle. *FEBS Lett, 235*(1-2), 153-155. doi:10.1016/0014-5793(88)81253-5

C Franzini-Armstrong, a., & Jorgensen, A. O. (1994). Structure and Development of E-C Coupling Units in Skeletal Muscle. *Annual Review of Physiology, 56*(1), 509-534. doi:10.1146/annurev.ph.56.030194.002453

Caiozzo, V. J., Baker, M. J., & Baldwin, K. M. (1998). Novel transitions in MHC isoforms: separate and combined effects of thyroid hormone and mechanical unloading. *J Appl Physiol (1985), 85*(6), 2237-2248. doi:10.1152/jappl.1998.85.6.2237

Caiozzo, V. J., Baker, M. J., Huang, K., Chou, H., Wu, Y. Z., & Baldwin, K. M. (2003). Single-fiber myosin heavy chain polymorphism: how many patterns and what proportions? *Am J Physiol Regul Integr Comp Physiol, 285*(3), R570-580. doi:10.1152/ajpregu.00646.2002

Caiozzo, V. J., Haddad, F., Baker, M., McCue, S., & Baldwin, K. M. (2000). MHC polymorphism in rodent plantaris muscle: effects of mechanical overload and hypothyroidism. *Am J Physiol Cell Physiol, 278*(4), C709-717. doi:10.1152/ajpcell.2000.278.4.C709

Calderón, J. C., Bolaños, P., & Caputo, C. (2010). Myosin heavy chain isoform composition and Ca(2+) transients in fibres from enzymatically dissociated murine soleus and extensor digitorum longus muscles. *J Physiol, 588*(Pt 1), 267-279. doi:10.1113/jphysiol.2009.180893

Campbell, W. G., Gordon, S. E., Carlson, C. J., Pattison, J. S., Hamilton, M. T., & Booth, F. W. (2001). Differential global gene expression in red and white skeletal muscle. *Am J Physiol Cell Physiol, 280*(4), C763-768. doi:10.1152/ajpcell.2001.280.4.C763

Canato, M., Scorzeto, M., Giacomello, M., Protasi, F., Reggiani, C., & Stienen, G. J. (2010). Massive alterations of sarcoplasmic reticulum free calcium in skeletal muscle fibers lacking calsequestrin revealed by a genetically encoded probe. *Proc Natl Acad Sci U S A, 107*(51), 22326-22331. doi:10.1073/pnas.1009168108

Cannell, M. B., Cheng, H., & Lederer, W. J. (1995). The control of calcium release in heart muscle. *Science, 268*(5213), 1045. doi:10.1126/science.7754384

Cannon, S. C. (2015). Channelopathies of skeletal muscle excitability. *Compr Physiol, 5*(2), 761-790. doi:10.1002/cphy.c140062

Capes, E. M., Loaiza, R., & Valdivia, H. H. (2011). Ryanodine receptors. *Skelet Muscle, 1*(1), 18. doi:10.1186/2044-5040-1-18

Carroll, S., Nicotera, P., & Pette, D. (1999). Calcium transients in single fibers of low-frequency stimulated fast-twitch muscle of rat. *Am J Physiol, 277*(6), C1122-1129. doi:10.1152/ajpcell.1999.277.6.C1122

Carroll, S. L., Klein, M. G., & Schneider, M. F. (1997). Decay of calcium transients after electrical stimulation in rat fast- and slow-twitch skeletal muscle fibres. *J Physiol, 501 (Pt 3)*(Pt 3), 573-588. doi:10.1111/j.1469-7793.1997.573bm.x

Carvajal, K., Balderas-Villalobos, J., Bello-Sanchez, M. D., Phillips-Farfán, B., Molina-Muñoz, T., Aldana-Quintero, H., & Gómez-Viquez, N. L. (2014). Ca(2+) mishandling and cardiac dysfunction in obesity and insulin resistance: role of oxidative stress. *Cell Calcium, 56*(5), 408-415. doi:10.1016/j.ceca.2014.08.003

Casas, M., Buvinic, S., & Jaimovich, E. (2014). ATP signaling in skeletal muscle: from fiber plasticity to regulation of metabolism. *Exerc Sport Sci Rev, 42*(3), 110-116. doi:10.1249/jes.0000000000000017

Casas, M., Figueroa, R., Jorquera, G., Escobar, M., Molgo, J., & Jaimovich, E. (2010). IP(3)-dependent, post-tetanic calcium transients induced by electrostimulation of adult skeletal muscle fibers. *J Gen Physiol, 136*(4), 455-467. doi:10.1085/jgp.200910397

Catterall, W. A. (2000). Structure and regulation of voltage-gated Ca2+ channels. *Annu Rev Cell Dev Biol, 16*, 521-555. doi:10.1146/annurev.cellbio.16.1.521

Catterall, W. A. (2011). Voltage-gated calcium channels. *Cold Spring Harb Perspect Biol, 3*(8), a003947. doi:10.1101/cshperspect.a003947

Catterall, W. A., Lenaeus, M. J., & Gamal El-Din, T. M. (2020). Structure and Pharmacology of Voltage-Gated Sodium and Calcium Channels. *Annu Rev Pharmacol Toxicol, 60*, 133-154. doi:10.1146/annurev-pharmtox-010818-021757

Cea, L. A., Riquelme, M. A., Vargas, A. A., Urrutia, C., & Sáez, J. C. (2014). Pannexin 1 channels in skeletal muscles. *Front Physiol, 5*, 139. doi:10.3389/fphys.2014.00139

Chakkalakal, J. V., Harrison, M. A., Carbonetto, S., Chin, E., Michel, R. N., & Jasmin, B. J. (2004). Stimulation of calcineurin signaling attenuates the dystrophic pathology in mdx mice. *Hum Mol Genet, 13*(4), 379-388. doi:10.1093/hmg/ddh037

Chanda, B., & Bezanilla, F. (2008). A common pathway for charge transport through voltage-sensing domains. *Neuron, 57*(3), 345-351. doi:10.1016/j.neuron.2008.01.015

Chang, K. C., Figueredo, V. M., Schreur, J. H., Kariya, K., Weiner, M. W., Simpson, P. C., & Camacho, S. A. (1997). Thyroid hormone improves function and Ca2+ handling in pressure overload hypertrophy. Association with increased sarcoplasmic reticulum Ca2+-ATPase and alpha-myosin heavy chain in rat hearts. *J Clin Invest, 100*(7), 1742-1749. doi:10.1172/jci119699

Chekeni, F. B., Elliott, M. R., Sandilos, J. K., Walk, S. F., Kinchen, J. M., Lazarowski, E. R., . . . Ravichandran, K. S. (2010). Pannexin 1 channels mediate 'find-me' signal release and membrane permeability during apoptosis. *Nature, 467*(7317), 863-867. doi:10.1038/nature09413

Chelu, M. G., Goonasekera, S. A., Durham, W. J., Tang, W., Lueck, J. D., Riehl, J., . . . Hamilton, S. L. (2006). Heat- and anesthesia-induced malignant hyperthermia in an RyR1 knock-in mouse. *Faseb j, 20*(2), 329-330. doi:10.1096/fj.05-4497fje

Chen, T. W., Wardill, T. J., Sun, Y., Pulver, S. R., Renninger, S. L., Baohan, A., . . . Kim, D. S. (2013). Ultrasensitive fluorescent proteins for imaging neuronal activity. *Nature, 499*(7458), 295-300. doi:10.1038/nature12354

Cheng, H., Lederer, W. J., & Cannell, M. B. (1993). Calcium sparks: elementary events underlying excitation-contraction coupling in heart muscle. *Science, 262*(5134), 740-744. doi:10.1126/science.8235594

Cheng, W., Altafaj, X., Ronjat, M., & Coronado, R. (2005). Interaction between the dihydropyridine receptor Ca2+ channel beta-subunit and ryanodine receptor type 1 strengthens excitation-contraction coupling. *Proc Natl Acad Sci U S A, 102*(52), 19225-19230. doi:10.1073/pnas.0504334102

Cherednichenko, G., Hurne, A. M., Fessenden, J. D., Lee, E. H., Allen, P. D., Beam, K. G., & Pessah, I. N. (2004). Conformational activation of Ca²⁺ entry by depolarization of skeletal myotubes. *Proceedings of the National Academy of Sciences of the United States of America, 101*(44), 15793-15798. doi:10.1073/pnas.0403485101

Chiarandini, D. J., Sanchez, J. A., & Stefani, E. (1980). Effect of calcium withdrawal on mechanical threshold in skeletal muscle fibres of the frog. *J Physiol, 303*, 153-163. doi:10.1113/jphysiol.1980.sp013277

Chin, E. R., & Allen, D. G. (1996). The role of elevations in intracellular [Ca2+] in the development of low frequency fatigue in mouse single muscle fibres. *J Physiol, 491 (Pt 3)*(Pt 3), 813-824. doi:10.1113/jphysiol.1996.sp021259

Chin, E. R., Grange, R. W., Viau, F., Simard, A. R., Humphries, C., Shelton, J., . . . Michel, R. N. (2003). Alterations in slow-twitch muscle phenotype in transgenic mice overexpressing the Ca2+ buffering protein parvalbumin. *J Physiol, 547*(Pt 2), 649-663. doi:10.1113/jphysiol.2002.024760

Chin, E. R., Olson, E. N., Richardson, J. A., Yang, Q., Humphries, C., Shelton, J. M., . . . Williams, R. S. (1998). A calcineurin-dependent transcriptional pathway controls skeletal muscle fiber type. *Genes Dev, 12*(16), 2499-2509. doi:10.1101/gad.12.16.2499

Chiu, Y. H., Jin, X., Medina, C. B., Leonhardt, S. A., Kiessling, V., Bennett, B. C., . . . Bayliss, D. A. (2017). A quantized mechanism for activation of pannexin channels. *Nat Commun, 8*, 14324. doi:10.1038/ncomms14324

Chiu, Y. H., Schappe, M. S., Desai, B. N., & Bayliss, D. A. (2018). Revisiting multimodal activation and channel properties of Pannexin 1. *J Gen Physiol, 150*(1), 19-39. doi:10.1085/jgp.201711888

Chopra, N., & Knollmann, B. C. (2009). Cardiac calsequestrin: the new kid on the block in arrhythmias. *J Cardiovasc Electrophysiol, 20*(10), 1179-1185. doi:10.1111/j.1540-8167.2009.01531.x

Chu, J., Oh, Y., Sens, A., Ataie, N., Dana, H., Macklin, J. J., . . . Lin, M. Z. (2016). A bright cyan-excitable orange fluorescent protein facilitates dual-emission microscopy and enhances bioluminescence imaging in vivo. *Nat Biotechnol, 34*(7), 760-767. doi:10.1038/nbt.3550

Clarke, D. M., Loo, T. W., Inesi, G., & MacLennan, D. H. (1989). Location of high affinity Ca2+-binding sites within the predicted transmembrane domain of the sarcoplasmic reticulum Ca2+-ATPase. *Nature, 339*(6224), 476-478. doi:10.1038/339476a0

Close, R. (1967). Properties of motor units in fast and slow skeletal muscles of the rat. *J Physiol, 193*(1), 45-55. doi:10.1113/jphysiol.1967.sp008342

Cohen, A. W., Hnasko, R., Schubert, W., & Lisanti, M. P. (2004). Role of caveolae and caveolins in health and disease. *Physiol Rev, 84*(4), 1341-1379. doi:10.1152/physrev.00046.2003

Collet, C., Allard, B., Tourneur, Y., & Jacquemond, V. (1999). Intracellular calcium signals measured with indo-1 in isolated skeletal muscle fibres from control and mdx mice. *J Physiol, 520 Pt 2*(Pt 2), 417-429. doi:10.1111/j.1469-7793.1999.00417.x

Collet, C., Csernoch, L., & Jacquemond, V. (2003). Intramembrane charge movement and L-type calcium current in skeletal muscle fibers isolated from control and mdx mice. *Biophys J, 84*(1), 251-265. doi:10.1016/s0006-3495(03)74846-2

Collet, C., & Jacquemond, V. (2002). Sustained release of calcium elicited by membrane depolarization in ryanodine-injected mouse skeletal muscle fibers. *Biophys J, 82*(3), 1509-1523. doi:10.1016/s0006-3495(02)75504-5

Collet, C., Pouvreau, S., Csernoch, L., Allard, B., & Jacquemond, V. (2004). Calcium signaling in isolated skeletal muscle fibers investigated under "Silicone Voltage-Clamp" conditions. *Cell Biochem Biophys, 40*(2), 225-236. doi:10.1385/cbb:40:2:225

Collins, J. H. (1991). Sequence analysis of the ryanodine receptor: possible association with a 12K, FK506-binding immunophilin/protein kinase C inhibitor. *Biochem Biophys Res Commun, 178*(3), 1288-1290. doi:10.1016/0006-291x(91)91033-9

Corriden, R., & Insel, P. A. (2010). Basal release of ATP: an autocrine-paracrine mechanism for cell regulation. *Sci Signal, 3*(104), re1. doi:10.1126/scisignal.3104re1

Costantin, L. L., & Podolsky, R. J. (1967). Depolarization of the internal membrane system in the activation of frog skeletal muscle. *J Gen Physiol, 50*(5), 1101-1124. doi:10.1085/jgp.50.5.1101

Couchoux, H., Allard, B., Legrand, C., Jacquemond, V., & Berthier, C. (2007). Loss of caveolin-3 induced by the dystrophy-associated P104L mutation impairs L-type calcium channel function in mouse skeletal muscle cells. *J Physiol, 580*(Pt.3), 745-754. doi:10.1113/jphysiol.2006.124198

Couchoux, H., Bichraoui, H., Chouabe, C., Altafaj, X., Bonvallet, R., Allard, B., . . . Berthier, C. (2011). Caveolin-3 is a direct molecular partner of the Cav1.1 subunit of the skeletal muscle L-type calcium channel. *Int J Biochem Cell Biol, 43*(5), 713-720. doi:10.1016/j.biocel.2011.01.011

Crabtree, G. R. (1999). Generic signals and specific outcomes: signaling through Ca2+, calcineurin, and NF-AT. *Cell, 96*(5), 611-614. doi:10.1016/s0092-8674(00)80571-1

Csernoch, L. (2007). Sparks and embers of skeletal muscle: the exciting events of contractile activation. *Pflugers Arch, 454*(6), 869-878. doi:10.1007/s00424-007-0244-0

Csernoch, L., Szentesi, P., Sárközi, S., Szegedi, C., Jona, I., & Kovács, L. (1999). Effects of tetracaine on sarcoplasmic calcium release in mammalian skeletal muscle fibres. *J Physiol, 515 (Pt 3)*(Pt 3), 843-857. doi:10.1111/j.1469-7793.1999.843ab.x

D'Hondt, C., Ponsaerts, R., De Smedt, H., Vinken, M., De Vuyst, E., De Bock, M., . . . Bultynck, G. (2011). Pannexin channels in ATP release and beyond: an unexpected rendezvous at the endoplasmic reticulum. *Cell Signal, 23*(2), 305-316. doi:10.1016/j.cellsig.2010.07.018

Dahl, G. (2015). ATP release through pannexon channels. *Philos Trans R Soc Lond B Biol Sci, 370*(1672). doi:10.1098/rstb.2014.0191

Dahl, G., Qiu, F., & Wang, J. (2013). The bizarre pharmacology of the ATP release channel pannexin1. *Neuropharmacology, 75*, 583-593. doi:10.1016/j.neuropharm.2013.02.019

Dahl, G. P., Conner, G. E., Qiu, F., Wang, J., Spindler, E., Campagna, J. A., & Larsson, H. P. (2016). High affinity complexes of pannexin channels and L-type calcium channel splice-variants in human lung: Possible role in clevidipine-induced dyspnea relief in acute heart failure. *EBioMedicine, 10*, 291-297. doi:10.1016/j.ebiom.2016.06.027

Dainese, M., Quarta, M., Lyfenko, A. D., Paolini, C., Canato, M., Reggiani, C., . . . Protasi, F. (2009). Anesthetic- and heat-induced sudden death in calsequestrin-1-knockout mice. *Faseb j, 23*(6), 1710-1720. doi:10.1096/fj.08-121335

Dayal, A., Schrotter, K., Pan, Y., Fohr, K., Melzer, W., & Grabner, M. (2017). The Ca(2+) influx through the mammalian skeletal muscle dihydropyridine receptor is irrelevant for muscle performance. *Nat Commun, 8*(1), 475. doi:10.1038/s41467-017-00629-x

Dayal, A., Schrötter, K., Pan, Y., Föhr, K., Melzer, W., & Grabner, M. (2017). The Ca2+ influx through the mammalian skeletal muscle dihydropyridine receptor is irrelevant for muscle performance. *Nature Communications, 8*(1), 475. doi:10.1038/s41467-017-00629-x

DeLalio, L. J., Billaud, M., Ruddiman, C. A., Johnstone, S. R., Butcher, J. T., Wolpe, A. G., . . . Isakson, B. E. (2019). Constitutive SRC-mediated phosphorylation of pannexin 1 at tyrosine 198 occurs at the plasma membrane. *J Biol Chem, 294*(17), 6940-6956. doi:10.1074/jbc.RA118.006982

Delbono, O., & Meissner, G. (1996). Sarcoplasmic reticulum Ca2+ release in rat slow- and fast-twitch muscles. *J Membr Biol, 151*(2), 123-130. doi:10.1007/s002329900063

Deneka, D., Sawicka, M., Lam, A. K. M., Paulino, C., & Dutzler, R. (2018). Structure of a volume-regulated anion channel of the LRRC8 family. *Nature, 558*(7709), 254-259. doi:10.1038/s41586-018-0134-y

Deng, Z., He, Z., Maksaev, G., Bitter, R. M., Rau, M., Fitzpatrick, J. A. J., & Yuan, P. (2020). Cryo-EM structures of the ATP release channel pannexin 1. *Nat Struct Mol Biol, 27*(4), 373-381. doi:10.1038/s41594-020-0401-0

des Georges, A., Clarke, O. B., Zalk, R., Yuan, Q., Condon, K. J., Grassucci, R. A., . . . Frank, J. (2016). Structural Basis for Gating and Activation of RyR1. *Cell, 167*(1), 145-157.e117. doi:10.1016/j.cell.2016.08.075

Dewulf, M., Köster, D. V., Sinha, B., Viaris de Lesegno, C., Chambon, V., Bigot, A., . . . Blouin, C. M. (2019). Dystrophy-associated caveolin-3 mutations reveal that caveolae couple IL6/STAT3 signaling with mechanosensing in human muscle cells. *Nat Commun, 10*(1), 1974. doi:10.1038/s41467-019-09405-5

Diaz-Sylvester, P. L., Porta, M., & Copello, J. A. (2008). Halothane modulation of skeletal muscle ryanodine receptors: dependence on Ca2+, Mg2+, and ATP. *Am J Physiol Cell Physiol, 294*(4), C1103-1112. doi:10.1152/ajpcell.90642.2007

Diezmos, E. F., Bertrand, P. P., & Liu, L. (2016). Purinergic Signaling in Gut Inflammation: The Role of Connexins and Pannexins. *Front Neurosci, 10*, 311. doi:10.3389/fnins.2016.00311

Diezmos, E. F., Sandow, S. L., Markus, I., Shevy Perera, D., Lubowski, D. Z., King, D. W., . . . Liu, L. (2013). Expression and localization of pannexin-1 hemichannels in human colon in health and disease. *Neurogastroenterol Motil, 25*(6), e395-405. doi:10.1111/nmo.12130

DiFranco, M., Capote, J., & Vergara, J. L. (2005). Optical imaging and functional characterization of the transverse tubular system of mammalian muscle fibers using the potentiometric indicator di-8-ANEPPS. *J Membr Biol, 208*(2), 141-153. doi:10.1007/s00232-005-0825-9

DiFranco, M., Woods, C. E., Capote, J., & Vergara, J. L. (2008). Dystrophic skeletal muscle fibers display alterations at the level of calcium microdomains. *Proc Natl Acad Sci U S A, 105*(38), 14698-14703. doi:10.1073/pnas.0802217105

Dirksen, R. T., & Beam, K. G. (1999). Role of calcium permeation in dihydropyridine receptor function. Insights into channel gating and excitation-contraction coupling. *J Gen Physiol, 114*(3), 393-403. doi:10.1085/jgp.114.3.393

Diszházi, G., Magyar, Z., Mótyán, J. A., Csernoch, L., Jóna, I., Nánási, P. P., & Almássy, J. (2019). Dantrolene Requires Mg(2+) and ATP To Inhibit the Ryanodine Receptor. *Mol Pharmacol, 96*(3), 401-407. doi:10.1124/mol.119.116475

Divet, A., Paesante, S., Grasso, C., Cavagna, D., Tiveron, C., Paolini, C., . . . Zorzato, F. (2007). Increased Ca2+ storage capacity of the skeletal muscle sarcoplasmic reticulum of transgenic mice over-expressing membrane bound calcium binding protein junctate. *Journal of Cellular Physiology, 213*(2), 464-474. doi:10.1002/jcp.21121

Dolmetsch, R. E., Lewis, R. S., Goodnow, C. C., & Healy, J. I. (1997). Differential activation of transcription factors induced by Ca2+ response amplitude and duration. *Nature, 386*(6627), 855-858. doi:10.1038/386855a0

Dowling, J. J., Lawlor, M. W., & Dirksen, R. T. (2014). Triadopathies: an emerging class of skeletal muscle diseases. *Neurotherapeutics, 11*(4), 773-785. doi:10.1007/s13311-014-0300-3

Duarte-Costa, S., Castro-Ferreira, R., Neves, J. S., & Leite-Moreira, A. F. (2014). S100A1: a major player in cardiovascular performance. *Physiol Res, 63*(6), 669-681. doi:10.33549/physiolres.932712

Dulhunty, A. F., Wei-LaPierre, L., Casarotto, M. G., & Beard, N. A. (2017). Core skeletal muscle ryanodine receptor calcium release complex. *Clin Exp Pharmacol Physiol, 44*(1), 3-12. doi:10.1111/1440-1681.12676

Durham, W. J., Aracena-Parks, P., Long, C., Rossi, A. E., Goonasekera, S. A., Boncompagni, S., . . . Hamilton, S. L. (2008). RyR1 S-nitrosylation underlies environmental heat stroke and sudden death in Y522S RyR1 knockin mice. *Cell, 133*(1), 53-65. doi:10.1016/j.cell.2008.02.042

Dvoriantchikova, G., Ivanov, D., Barakat, D., Grinberg, A., Wen, R., Slepak, V. Z., & Shestopalov, V. I. (2012). Genetic ablation of Pannexin1 protects retinal neurons from ischemic injury. *PLoS One, 7*(2), e31991. doi:10.1371/journal.pone.0031991

Dvoriantchikova, G., Ivanov, D., Panchin, Y., & Shestopalov, V. I. (2006). Expression of pannexin family of proteins in the retina. *FEBS Lett, 580*(9), 2178-2182. doi:10.1016/j.febslet.2006.03.026

Edström, L., & Kugelberg, E. (1968). Histochemical composition, distribution of fibres and fatiguability of single motor units. Anterior tibial muscle of the rat. *J Neurol Neurosurg Psychiatry, 31*(5), 424-433. doi:10.1136/jnnp.31.5.424

Efremov, R. G., Leitner, A., Aebersold, R., & Raunser, S. (2015). Architecture and conformational switch mechanism of the ryanodine receptor. *Nature, 517*(7532), 39-43. doi:10.1038/nature13916

Eltit, J. M., Feng, W., Lopez, J. R., Padilla, I. T., Pessah, I. N., Molinski, T. F., . . . Perez, C. F. (2010). Ablation of skeletal muscle triadin impairs FKBP12/RyR1 channel interactions essential for maintaining resting cytoplasmic Ca2+. *J Biol Chem, 285*(49), 38453-38462. doi:10.1074/jbc.M110.164525

Eltit, J. M., Franzini-Armstrong, C., & Perez, C. F. (2014). Amino acid residues 489-503 of dihydropyridine receptor (DHPR) beta1a subunit are critical for structural communication between the skeletal muscle DHPR complex and type 1 ryanodine receptor. *J Biol Chem, 289*(52), 36116-36124. doi:10.1074/jbc.M114.615526

Eltit, J. M., Szpyt, J., Li, H., Allen, P. D., & Perez, C. F. (2011). Reduced gain of excitation-contraction coupling in triadin-null myotubes is mediated by the disruption of FKBP12/RyR1 interaction. *Cell Calcium, 49*(2), 128-135. doi:10.1016/j.ceca.2011.01.005

Endo, M. (2009). Calcium-induced calcium release in skeletal muscle. *Physiol Rev, 89*(4), 1153-1176. doi:10.1152/physrev.00040.2008

Epp, A. L., Ebert, S. N., Sanchez-Arias, J. C., Wicki-Stordeur, L. E., Boyce, A. K. J., & Swayne, L. A. (2019). A novel motif in the proximal C-terminus of Pannexin 1 regulates cell surface localization. *Sci Rep, 9*(1), 9721. doi:10.1038/s41598-019-46144-5

Ertel, E. A., Campbell, K. P., Harpold, M. M., Hofmann, F., Mori, Y., Perez-Reyes, E., . . . Catterall, W. A. (2000). Nomenclature of voltage-gated calcium channels. In *Neuron* (Vol. 25, pp. 533-535). United States.

Eshima, H., Tamura, Y., Kakehi, S., Kurebayashi, N., Murayama, T., Nakamura, K., . . . Watada, H. (2017). Long-term, but not short-term high-fat diet induces fiber composition changes and impaired contractile force in mouse fast-twitch skeletal muscle. *Physiol Rep, 5*(7). doi:10.14814/phy2.13250

Esser, K., Gunning, P., & Hardeman, E. (1993). Nerve-dependent and -independent patterns of mRNA expression in regenerating skeletal muscle. *Dev Biol, 159*(1), 173-183. doi:10.1006/dbio.1993.1231

Esteve, E., Eltit, J. M., Bannister, R. A., Liu, K., Pessah, I. N., Beam, K. G., . . . Lopez, J. R. (2010). A malignant hyperthermia-inducing mutation in RYR1 (R163C): alterations in Ca2+ entry, release, and retrograde signaling to the DHPR. *J Gen Physiol, 135*(6), 619-628. doi:10.1085/jgp.200910328

Eu, J. P., Sun, J., Xu, L., Stamler, J. S., & Meissner, G. (2000). The skeletal muscle calcium release channel: coupled O2 sensor and NO signaling functions. *Cell, 102*(4), 499-509. doi:10.1016/s0092-8674(00)00054-4

Fan, C., Lehmann-Horn, F., Weber, M. A., Bednarz, M., Groome, J. R., Jonsson, M. K., & Jurkat-Rott, K. (2013). Transient compartment-like syndrome and normokalaemic periodic paralysis due to a Ca(v)1.1 mutation. *Brain, 136*(Pt 12), 3775-3786. doi:10.1093/brain/awt300

Figueroa, L., Kraeva, N., Manno, C., Toro, S., Ríos, E., & Riazi, S. (2019). Abnormal calcium signalling and the caffeine-halothane contracture test. *Br J Anaesth, 122*(1), 32-41. doi:10.1016/j.bja.2018.08.009

Fill, M., & Copello, J. A. (2002). Ryanodine receptor calcium release channels. *Physiol Rev, 82*(4), 893-922. doi:10.1152/physrev.00013.2002

Flagg, T. P., Enkvetchakul, D., Koster, J. C., & Nichols, C. G. (2010). Muscle KATP channels: recent insights to energy sensing and myoprotection. *Physiol Rev, 90*(3), 799-829. doi:10.1152/physrev.00027.2009

Fleischer, S., Ogunbunmi, E. M., Dixon, M. C., & Fleer, E. A. (1985). Localization of Ca2+ release channels with ryanodine in junctional terminal cisternae of sarcoplasmic reticulum of fast skeletal muscle. *Proc Natl Acad Sci U S A, 82*(21), 7256-7259. doi:10.1073/pnas.82.21.7256

Flucher, B. E. (1992). Structural analysis of muscle development: transverse tubules, sarcoplasmic reticulum, and the triad. *Dev Biol, 154*(2), 245-260. doi:10.1016/0012-1606(92)90065-o

Flucher, B. E. (2020). Skeletal muscle Ca(V)1.1 channelopathies. *Pflugers Arch*. doi:10.1007/s00424-020-02368-3

Flucher, B. E., & Campiglio, M. (2019). STAC proteins: The missing link in skeletal muscle EC coupling and new regulators of calcium channel function. *Biochim Biophys Acta Mol Cell Res, 1866*(7), 1101-1110. doi:10.1016/j.bbamcr.2018.12.004

Flucher, B. E., & Franzini-Armstrong, C. (1996). Formation of junctions involved in excitation-contraction coupling in skeletal and cardiac muscle. *Proc Natl Acad Sci U S A, 93*(15), 8101-8106. doi:10.1073/pnas.93.15.8101

Flucher, B. E., Kasielke, N., & Grabner, M. (2000). The triad targeting signal of the skeletal muscle calcium channel is localized in the COOH terminus of the alpha(1S) subunit. *J Cell Biol, 151*(2), 467-478. doi:10.1083/jcb.151.2.467

Fodor, J., Gönczi, M., Sztretye, M., Dienes, B., Oláh, T., Szabó, L., . . . Csernoch, L. (2008). Altered expression of triadin 95 causes parallel changes in localized Ca2+ release events and global Ca2+ signals in skeletal muscle cells in culture. *J Physiol, 586*(23), 5803-5818. doi:10.1113/jphysiol.2008.160457

Foster, M. N., & Coetzee, W. A. (2016). KATP Channels in the Cardiovascular System. *Physiol Rev, 96*(1), 177-252. doi:10.1152/physrev.00003.2015

Franzini-Armstrong, C., & Kish, J. W. (1995). Alternate disposition of tetrads in peripheral couplings of skeletal muscle. *J Muscle Res Cell Motil, 16*(3), 319-324. doi:10.1007/bf00121140

Franzini-Armstrong, C., & Protasi, F. (1997). Ryanodine receptors of striated muscles: a complex channel capable of multiple interactions. *Physiol Rev, 77*(3), 699-729. doi:10.1152/physrev.1997.77.3.699

Franzini-Armstrong, C., Protasi, F., & Ramesh, V. (1998). Comparative ultrastructure of Ca2+ release units in skeletal and cardiac muscle. *Ann N Y Acad Sci, 853*, 20-30. doi:10.1111/j.1749-6632.1998.tb08253.x

Franzini-Armstrong, C., Protasi, F., & Ramesh, V. (1999). Shape, size, and distribution of Ca(2+) release units and couplons in skeletal and cardiac muscles. *Biophys J, 77*(3), 1528-1539. doi:10.1016/s0006-3495(99)77000-1

Fraysse, B., Desaphy, J. F., Pierno, S., De Luca, A., Liantonio, A., Mitolo, C. I., & Camerino, D. C. (2003). Decrease in resting calcium and calcium entry associated with slow-to-fast transition in unloaded rat soleus muscle. *Faseb j, 17*(13), 1916-1918. doi:10.1096/fj.02-1012fje

Freise, D., Held, B., Wissenbach, U., Pfeifer, A., Trost, C., Himmerkus, N., . . . Flockerzi, V. (2000). Absence of the gamma subunit of the skeletal muscle dihydropyridine receptor increases L-type Ca2+ currents and alters channel inactivation properties. *J Biol Chem, 275*(19), 14476-14481. doi:10.1074/jbc.275.19.14476

Funai, K., Lodhi, I. J., Spears, L. D., Yin, L., Song, H., Klein, S., & Semenkovich, C. F. (2016). Skeletal Muscle Phospholipid Metabolism Regulates Insulin Sensitivity and Contractile Function. *Diabetes, 65*(2), 358-370. doi:10.2337/db15-0659

Furuya, K., Sokabe, M., & Grygorczyk, R. (2014). Real-time luminescence imaging of cellular ATP release. *Methods, 66*(2), 330-344. doi:10.1016/j.ymeth.2013.08.007

Fuster, C., Perrot, J., Berthier, C., Jacquemond, V., & Allard, B. (2017). Elevated resting H(+) current in the R1239H type 1 hypokalaemic periodic paralysis mutated Ca(2+) channel. *J Physiol, 595*(20), 6417-6428. doi:10.1113/jp274638

Gallot, Y. S., McMillan, J. D., Xiong, G., Bohnert, K. R., Straughn, A. R., Hill, B. G., & Kumar, A. (2017). Distinct roles of TRAF6 and TAK1 in the regulation of adipocyte survival, thermogenesis program, and high-fat diet-induced obesity. *Oncotarget, 8*(68), 112565-112583. doi:10.18632/oncotarget.22575

Gamu, D., Bombardier, E., Smith, I. C., Fajardo, V. A., & Tupling, A. R. (2014). Sarcolipin provides a novel muscle-based mechanism for adaptive thermogenesis. *Exerc Sport Sci Rev, 42*(3), 136-142. doi:10.1249/jes.0000000000000016

Gamu, D., Juracic, E. S., Fajardo, V. A., Rietze, B. A., Tran, K., Bombardier, E., & Tupling, A. R. (2019). Phospholamban deficiency does not alter skeletal muscle SERCA pumping efficiency or predispose mice to diet-induced obesity. *Am J Physiol Endocrinol Metab, 316*(3), E432-e442. doi:10.1152/ajpendo.00288.2018

Gazzerro, E., Sotgia, F., Bruno, C., Lisanti, M. P., & Minetti, C. (2010). Caveolinopathies: from the biology of caveolin-3 to human diseases. *Eur J Hum Genet, 18*(2), 137-145. doi:10.1038/ejhg.2009.103

Gellen, B., Fernández-Velasco, M., Briec, F., Vinet, L., LeQuang, K., Rouet-Benzineb, P., . . . Mercadier, J. J. (2008). Conditional FKBP12.6 overexpression in mouse cardiac myocytes prevents triggered

ventricular tachycardia through specific alterations in excitation-contraction coupling. *Circulation, 117*(14), 1778-1786. doi:10.1161/circulationaha.107.731893

Georgiou, D. K., Dagnino-Acosta, A., Lee, C. S., Griffin, D. M., Wang, H., Lagor, W. R., . . . Hamilton, S. L. (2015). Ca2+ Binding/Permeation via Calcium Channel, CaV1.1, Regulates the Intracellular Distribution of the Fatty Acid Transport Protein, CD36, and Fatty Acid Metabolism. *J Biol Chem, 290*(39), 23751-23765. doi:10.1074/jbc.M115.643544

Giaume, C., Leybaert, L., Naus, C. C., & Sáez, J. C. (2013). Connexin and pannexin hemichannels in brain glial cells: properties, pharmacology, and roles. *Front Pharmacol, 4*, 88. doi:10.3389/fphar.2013.00088

Girgenrath, T., Mahalingam, M., Svensson, B., Nitu, F. R., Cornea, R. L., & Fessenden, J. D. (2013). N-terminal and central segments of the type 1 ryanodine receptor mediate its interaction with FK506-binding proteins. *J Biol Chem, 288*(22), 16073-16084. doi:10.1074/jbc.M113.463299

Golini, L., Chouabe, C., Berthier, C., Cusimano, V., Fornaro, M., Bonvallet, R., . . . Sorrentino, V. (2011). Junctophilin 1 and 2 proteins interact with the L-type Ca2+ channel dihydropyridine receptors (DHPRs) in skeletal muscle. *J Biol Chem, 286*(51), 43717-43725. doi:10.1074/jbc.M111.292755

Gonzalez, L. L., Garrie, K., & Turner, M. D. (2020). Role of S100 proteins in health and disease. *Biochim Biophys Acta Mol Cell Res, 1867*(6), 118677. doi:10.1016/j.bbamcr.2020.118677

Gonzalez-Serratos, H., Valle-Aguilera, R., Lathrop, D. A., & Garcia, M. C. (1982). Slow inward calcium currents have no obvious role in muscle excitation-contraction coupling. *Nature, 298*(5871), 292-294. doi:10.1038/298292a0

Goody, R. S. (2003). The missing link in the muscle cross-bridge cycle. *Nature Structural & Molecular Biology, 10*(10), 773-775. doi:10.1038/nsb1003-773

Goonasekera, S. A., Beard, N. A., Groom, L., Kimura, T., Lyfenko, A. D., Rosenfeld, A., . . . Dirksen, R. T. (2007). Triadin binding to the C-terminal luminal loop of the ryanodine receptor is important for skeletal muscle excitation contraction coupling. *J Gen Physiol, 130*(4), 365-378. doi:10.1085/jgp.200709790

Gordon, A. M., Homsher, E., & Regnier, M. (2000). Regulation of contraction in striated muscle. *Physiol Rev, 80*(2), 853-924. doi:10.1152/physrev.2000.80.2.853

Gorza, L. (1990). Identification of a novel type 2 fiber population in mammalian skeletal muscle by combined use of histochemical myosin ATPase and anti-myosin monoclonal antibodies. *J Histochem Cytochem, 38*(2), 257-265. doi:10.1177/38.2.2137154

Gramolini, A. O., Trivieri, M. G., Oudit, G. Y., Kislinger, T., Li, W., Patel, M. M., . . . Maclennan, D. H. (2006). Cardiac-specific overexpression of sarcolipin in phospholamban null mice impairs myocyte function that is restored by phosphorylation. *Proc Natl Acad Sci U S A, 103*(7), 2446-2451. doi:10.1073/pnas.0510883103

Gregg, R. G., Messing, A., Strube, C., Beurg, M., Moss, R., Behan, M., . . . Powers, P. A. (1996). Absence of the beta subunit (cchb1) of the skeletal muscle dihydropyridine receptor alters expression of the alpha 1 subunit and eliminates excitation-contraction coupling. *Proc Natl Acad Sci U S A, 93*(24), 13961-13966. doi:10.1073/pnas.93.24.13961

Gribble, F. M., Loussouarn, G., Tucker, S. J., Zhao, C., Nichols, C. G., & Ashcroft, F. M. (2000). A novel method for measurement of submembrane ATP concentration. *J Biol Chem, 275*(39), 30046-30049. doi:10.1074/jbc.M001010200

Grimby, G., Broberg, C., Krotkiewska, I., & Krotkiewski, M. (1976). Muscle fiber composition in patients with traumatic cord lesion. *Scand J Rehabil Med, 8*(1), 37-42.

Grundy, D. (2015). Principles and standards for reporting animal experiments in The Journal of Physiology and Experimental Physiology. *J Physiol, 593*(12), 2547-2549. doi:10.1113/jp270818

Grzybowski, M., Schänzer, A., Pepler, A., Heller, C., Neubauer, B. A., & Hahn, A. (2017). Novel STAC3 Mutations in the First Non-Amerindian Patient with Native American Myopathy. *Neuropediatrics, 48*(6), 451-455. doi:10.1055/s-0037-1601868

Gulbransen, B. D., Bashashati, M., Hirota, S. A., Gui, X., Roberts, J. A., MacDonald, J. A., . . . Sharkey, K. A. (2012). Activation of neuronal P2X7 receptor-pannexin-1 mediates death of enteric neurons during colitis. *Nat Med, 18*(4), 600-604. doi:10.1038/nm.2679

Haberland, M., Montgomery, R. L., & Olson, E. N. (2009). The many roles of histone deacetylases in development and physiology: implications for disease and therapy. *Nat Rev Genet, 10*(1), 32-42. doi:10.1038/nrg2485

Haddad, F., Qin, A. X., Bodell, P. W., Jiang, W., Giger, J. M., & Baldwin, K. M. (2008). Intergenic transcription and developmental regulation of cardiac myosin heavy chain genes. *Am J Physiol Heart Circ Physiol, 294*(1), H29-40. doi:10.1152/ajpheart.01125.2007

Hagiwara, N., Ma, B., & Ly, A. (2005). Slow and fast fiber isoform gene expression is systematically altered in skeletal muscle of the Sox6 mutant, p100H. *Dev Dyn, 234*(2), 301-311. doi:10.1002/dvdy.20535

Hagiwara, N., Yeh, M., & Liu, A. (2007). Sox6 is required for normal fiber type differentiation of fetal skeletal muscle in mice. *Dev Dyn, 236*(8), 2062-2076. doi:10.1002/dvdy.21223

Hanstein, R., Negoro, H., Patel, N. K., Charollais, A., Meda, P., Spray, D. C., . . . Scemes, E. (2013). Promises and pitfalls of a Pannexin1 transgenic mouse line. *Front Pharmacol, 4*, 61. doi:10.3389/fphar.2013.00061

Harkins, A. B., Kurebayashi, N., & Baylor, S. M. (1993). Resting myoplasmic free calcium in frog skeletal muscle fibers estimated with fluo-3. *Biophys J, 65*(2), 865-881. doi:10.1016/s0006-3495(93)81112-3

Hayashi, S., Hazama, A., Dutta, A. K., Sabirov, R. Z., & Okada, Y. (2004). Detecting ATP release by a biosensor method. *Sci STKE, 2004*(258), pl14. doi:10.1126/stke.2582004pl14

He, H., Liu, D., Long, Y., Wang, X., & Yao, B. (2018). The Pannexin-1 Channel Inhibitor Probenecid Attenuates Skeletal Muscle Cellular Energy Crisis and Histopathological Injury in a Rabbit Endotoxemia Model. *Inflammation, 41*(6), 2030-2040. doi:10.1007/s10753-018-0846-z

Head, S. I. (1993). Membrane potential, resting calcium and calcium transients in isolated muscle fibres from normal and dystrophic mice. *J Physiol, 469*, 11-19. doi:10.1113/jphysiol.1993.sp019801

Hehl, S., Moser, C., Weik, R., & Neumcke, B. (1994). Internal Ca2+ ions inactivate and modify ATP-sensitive potassium channels in adult mouse skeletal muscle. *Biochim Biophys Acta, 1190*(2), 257-263. doi:10.1016/0005-2736(94)90082-5

Hemmersbach, P. (2020). The Probenecid-story - A success in the fight against doping through out-of-competition testing. *Drug Test Anal, 12*(5), 589-594. doi:10.1002/dta.2727

Hennig, R., & Lømo, T. (1985). Firing patterns of motor units in normal rats. *Nature, 314*(6007), 164-166. doi:10.1038/314164a0

Hernandez-Ochoa, E. O., & Schneider, M. F. (2018). Voltage sensing mechanism in skeletal muscle excitation-contraction coupling: coming of age or midlife crisis? *Skelet Muscle, 8*(1), 22. doi:10.1186/s13395-018-0167-9

Hernández-Ochoa, E. O., & Schneider, M. F. (2012). Voltage clamp methods for the study of membrane currents and SR Ca(2+) release in adult skeletal muscle fibres. *Prog Biophys Mol Biol, 108*(3), 98-118. doi:10.1016/j.pbiomolbio.2012.01.001

Ho, T., Jobling, A. I., Greferath, U., Chuang, T., Ramesh, A., Fletcher, E. L., & Vessey, K. A. (2015). Vesicular expression and release of ATP from dopaminergic neurons of the mouse retina and midbrain. *Front Cell Neurosci, 9*, 389. doi:10.3389/fncel.2015.00389

Hoh, J. F. (1975). Selective and non-selective reinnervation of fast-twitch and slow-twitch rat skeletal muscle. *J Physiol, 251*(3), 791-801. doi:10.1113/jphysiol.1975.sp011122

Hollingworth, S., Kim, M. M., & Baylor, S. M. (2012). Measurement and simulation of myoplasmic calcium transients in mouse slow-twitch muscle fibres. *J Physiol, 590*(3), 575-594. doi:10.1113/jphysiol.2011.220780

Hollingworth, S., Zeiger, U., & Baylor, S. M. (2008). Comparison of the myoplasmic calcium transient elicited by an action potential in intact fibres of mdx and normal mice. *J Physiol, 586*(21), 5063-5075. doi:10.1113/jphysiol.2008.160507

Hook, S. S., & Means, A. R. (2001). Ca(2+)/CaM-dependent kinases: from activation to function. *Annu Rev Pharmacol Toxicol, 41*, 471-505. doi:10.1146/annurev.pharmtox.41.1.471

Horowicz, P., & Schneider, M. F. (1981). Membrane charge moved at contraction thresholds in skeletal muscle fibres. *J Physiol, 314*, 595-633.

Horstick, E. J., Linsley, J. W., Dowling, J. J., Hauser, M. A., McDonald, K. K., Ashley-Koch, A., . . . Kuwada, J. Y. (2013). Stac3 is a component of the excitation-contraction coupling machinery and mutated in Native American myopathy. *Nat Commun, 4*, 1952. doi:10.1038/ncomms2952

Hossain, M. I., Iwasaki, H., Okochi, Y., Chahine, M., Higashijima, S., Nagayama, K., & Okamura, Y. (2008). Enzyme domain affects the movement of the voltage sensor in ascidian and zebrafish voltage-sensing phosphatases. *J Biol Chem, 283*(26), 18248-18259. doi:10.1074/jbc.M706184200

Hu, H., Wang, Z., Wei, R., Fan, G., Wang, Q., Zhang, K., & Yin, C. C. (2015). The molecular architecture of dihydropyrindine receptor/L-type Ca2+ channel complex. *Sci Rep, 5*, 8370. doi:10.1038/srep08370

Hubbard, J. I. (1973). Microphysiology of vertebrate neuromuscular transmission. *Physiol Rev, 53*(3), 674-723. doi:10.1152/physrev.1973.53.3.674

Huber, B., & Pette, D. (1996). Dynamics of parvalbumin expression in low-frequency-stimulated fast-twitch rat muscle. *Eur J Biochem, 236*(3), 814-819. doi:10.1111/j.1432-1033.1996.t01-2-00814.x

Hughes, S. M. (1998). Muscle development: electrical control of gene expression. *Curr Biol, 8*(24), R892-894. doi:10.1016/s0960-9822(07)00554-4

Huntoon, V., Widrick, J. J., Sanchez, C., Rosen, S. M., Kutchukian, C., Cao, S., . . . Agrawal, P. B. (2018). SPEG-deficient skeletal muscles exhibit abnormal triad and defective calcium handling. *Hum Mol Genet, 27*(9), 1608-1617. doi:10.1093/hmg/ddy068

Huxley, A. F., & Taylor, R. E. (1958). Local activation of striated muscle fibres. *J Physiol, 144*(3), 426-441. doi:10.1113/jphysiol.1958.sp006111

Hymel, L., Inui, M., Fleischer, S., & Schindler, H. (1988). Purified ryanodine receptor of skeletal muscle sarcoplasmic reticulum forms Ca2+-activated oligomeric Ca2+ channels in planar bilayers. *Proc Natl Acad Sci U S A, 85*(2), 441-445. doi:10.1073/pnas.85.2.441

Imamura, H., Nhat, K. P., Togawa, H., Saito, K., Iino, R., Kato-Yamada, Y., . . . Noji, H. (2009). Visualization of ATP levels inside single living cells with fluorescence resonance energy transfer-based genetically encoded indicators. *Proc Natl Acad Sci U S A, 106*(37), 15651-15656. doi:10.1073/pnas.0904764106

Isakson, B. E., & Thompson, R. J. (2014). Pannexin-1 as a potentiator of ligand-gated receptor signaling. *Channels (Austin), 8*(2), 118-123. doi:10.4161/chan.27978

Ito, K., Komazaki, S., Sasamoto, K., Yoshida, M., Nishi, M., Kitamura, K., & Takeshima, H. (2001). Deficiency of triad junction and contraction in mutant skeletal muscle lacking junctophilin type 1. *J Cell Biol, 154*(5), 1059-1067. doi:10.1083/jcb.200105040

Ivarsson, N., Mattsson, C. M., Cheng, A. J., Bruton, J. D., Ekblom, B., Lanner, J. T., & Westerblad, H. (2019). SR Ca(2+) leak in skeletal muscle fibers acts as an intracellular signal to increase fatigue resistance. *J Gen Physiol, 151*(4), 567-577. doi:10.1085/jgp.201812152

Iwasa, K., Furukawa, Y., Yoshikawa, H., & Yamada, M. (2016). Caveolin-3 is aberrantly expressed in skeletal muscle cells in myasthenia gravis. *J Neuroimmunol, 301*, 30-34. doi:10.1016/j.jneuroim.2016.10.011

Iyer, K. A., Hu, Y., Nayak, A. R., Kurebayashi, N., Murayama, T., & Samsó, M. (2020). Structural mechanism of two gain-of-function cardiac and skeletal RyR mutations at an equivalent site by cryo-EM. *Sci Adv, 6*(31), eabb2964. doi:10.1126/sciadv.abb2964

Jackson, D. G., Wang, J., Keane, R. W., Scemes, E., & Dahl, G. (2014). ATP and potassium ions: a deadly combination for astrocytes. *Sci Rep, 4*, 4576. doi:10.1038/srep04576

Jacquemond, V. (1997). Indo-1 fluorescence signals elicited by membrane depolarization in enzymatically isolated mouse skeletal muscle fibers. *Biophys J, 73*(2), 920-928. doi:10.1016/s0006-3495(97)78124-4

Jacquemond, V. (2012). Waveless mammalian muscle. In *J Physiol* (Vol. 590, pp. 1783).

Jaimovich, E., Reyes, R., Liberona, J. L., & Powell, J. A. (2000). IP(3) receptors, IP(3) transients, and nucleus-associated Ca(2+) signals in cultured skeletal muscle. *Am J Physiol Cell Physiol, 278*(5), C998-c1010. doi:10.1152/ajpcell.2000.278.5.C998

Jentsch, T. J., & Pusch, M. (2018). CLC Chloride Channels and Transporters: Structure, Function, Physiology, and Disease. *Physiol Rev, 98*(3), 1493-1590. doi:10.1152/physrev.00047.2017

Jin, Q., Zhang, B., Zheng, X., Li, N., Xu, L., Xie, Y., . . . Ye, S. (2020). Cryo-EM structures of human pannexin 1 channel. In *Cell Res* (Vol. 30, pp. 449-451).

Jones, S. W. (1998). Overview of voltage-dependent calcium channels. *J Bioenerg Biomembr, 30*(4), 299-312. doi:10.1023/a:1021977304001

Jorquera, G., Altamirano, F., Contreras-Ferrat, A., Almarza, G., Buvinic, S., Jacquemond, V., . . . Casas, M. (2013). Cav1.1 controls frequency-dependent events regulating adult skeletal muscle plasticity. *J Cell Sci, 126*(Pt 5), 1189-1198. doi:10.1242/jcs.116855

Jorquera, G., Altamirano, F., Contreras-Ferrat, A., Almarza, G., Buvinic, S., Jacquemond, V., . . . Casas, M. (2013). Cav1.1 controls frequency-dependent events regulating adult skeletal muscle plasticity. *Journal of Cell Science, 126*(5), 1189-1198. doi:10.1242/jcs.116855

Jungbluth, H., Treves, S., Zorzato, F., Sarkozy, A., Ochala, J., Sewry, C., . . . Muntoni, F. (2018). Congenital myopathies: disorders of excitation-contraction coupling and muscle contraction. *Nat Rev Neurol, 14*(3), 151-167. doi:10.1038/nrneurol.2017.191

Jurkat-Rott, K., Fauler, M., & Lehmann-Horn, F. (2006). Ion channels and ion transporters of the transverse tubular system of skeletal muscle. *J Muscle Res Cell Motil, 27*(5-7), 275-290. doi:10.1007/s10974-006-9088-z

Jurkat-Rott, K., McCarthy, T., & Lehmann-Horn, F. (2000). Genetics and pathogenesis of malignant hyperthermia. *Muscle Nerve, 23*(1), 4-17. doi:10.1002/(sici)1097-4598(200001)23:1<4::aid-mus3>3.0.co;2-d

Jurkat-Rott, K., Uetz, U., Pika-Hartlaub, U., Powell, J., Fontaine, B., Melzer, W., & Lehmann-Horn, F. (1998). Calcium currents and transients of native and heterologously expressed mutant skeletal muscle DHP receptor alpha1 subunits (R528H). *FEBS Lett, 423*(2), 198-204. doi:10.1016/s0014-5793(98)00090-8

Kahn, A. J., & Sandow, A. (1950). The potentiation of muscular contraction by the nitrate-ion. *Science, 112*(2918), 647-649. doi:10.1126/science.112.2918.647

Kakizawa, S., Moriguchi, S., Ikeda, A., Iino, M., & Takeshima, H. Functional Crosstalk Between Cell-Surface and Intracellular Channels Mediated by Junctophilins Essential for Neuronal Functions.

Katayama, S., Tomaru, Y., Kasukawa, T., Waki, K., Nakanishi, M., Nakamura, M., . . . Wahlestedt, C. (2005). Antisense transcription in the mammalian transcriptome. *Science, 309*(5740), 1564-1566. doi:10.1126/science.1112009

Katz, B. (1996). Neural transmitter release: from quantal secretion to exocytosis and beyond. The Fenn Lecture. *J Neurocytol, 25*(12), 677-686. doi:10.1007/bf02284834

Katz, B., & Miledi, R. (1967). Ionic requirements of synaptic transmitter release. *Nature, 215*(5101), 651. doi:10.1038/215651a0

Kemi, O. J., Ellingsen, O., Ceci, M., Grimaldi, S., Smith, G. L., Condorelli, G., & Wisløff, U. (2007). Aerobic interval training enhances cardiomyocyte contractility and Ca2+ cycling by phosphorylation of CaMKII and Thr-17 of phospholamban. *J Mol Cell Cardiol, 43*(3), 354-361. doi:10.1016/j.yjmcc.2007.06.013

Kim, S. K., & Kim, T. K. (2018). New Molecular Insights into the Excitation-Transcription Coupling. *Neuron, 98*(3), 453-456. doi:10.1016/j.neuron.2018.04.019

Kirschbaum, B. J., Kucher, H. B., Termin, A., Kelly, A. M., & Pette, D. (1990). Antagonistic effects of chronic low frequency stimulation and thyroid hormone on myosin expression in rat fast-twitch muscle. *J Biol Chem, 265*(23), 13974-13980.

Kiss, E., Jakab, G., Kranias, E. G., & Edes, I. (1994). Thyroid hormone-induced alterations in phospholamban protein expression. Regulatory effects on sarcoplasmic reticulum Ca2+ transport and myocardial relaxation. *Circ Res, 75*(2), 245-251. doi:10.1161/01.res.75.2.245

Klaus, M. M., Scordilis, S. P., Rapalus, J. M., Briggs, R. T., & Powell, J. A. (1983). Evidence for dysfunction in the regulation of cytosolic Ca2+ in excitation-contraction uncoupled dysgenic muscle. *Dev Biol, 99*(1), 152-165. doi:10.1016/0012-1606(83)90262-2

Klein, M. G., Cheng, H., Santana, L. F., Jiang, Y. H., Lederer, W. J., & Schneider, M. F. (1996). Two mechanisms of quantized calcium release in skeletal muscle. *Nature, 379*(6564), 455-458. doi:10.1038/379455a0

Klitgaard, H., Bergman, O., Betto, R., Salviati, G., Schiaffino, S., Clausen, T., & Saltin, B. (1990). Co-existence of myosin heavy chain I and IIa isoforms in human skeletal muscle fibres with endurance training. *Pflugers Arch, 416*(4), 470-472. doi:10.1007/bf00370757

Kobayashi, S., Bannister, M. L., Gangopadhyay, J. P., Hamada, T., Parness, J., & Ikemoto, N. (2005). Dantrolene stabilizes domain interactions within the ryanodine receptor. *J Biol Chem, 280*(8), 6580-6587. doi:10.1074/jbc.M408375200

Komazaki, S., Ito, K., Takeshima, H., & Nakamura, H. (2002). Deficiency of triad formation in developing skeletal muscle cells lacking junctophilin type 1. *FEBS letters, 524*(1-3), 225-229. doi:10.1016/s0014-5793(02)03042-9

Kovács, L., Schümperli, R. A., & Szücs, G. (1983). Comparison of birefringence signals and calcium transients in voltage-clamped cut skeletal muscle fibres of the frog. *J Physiol, 341*, 579-593. doi:10.1113/jphysiol.1983.sp014825

Kubis, H. P., Haller, E. A., Wetzel, P., & Gros, G. (1997). Adult fast myosin pattern and Ca2+-induced slow myosin pattern in primary skeletal muscle culture. *Proc Natl Acad Sci U S A, 94*(8), 4205-4210. doi:10.1073/pnas.94.8.4205

Kushnir, A., & Marks, A. R. (2012). Ryanodine receptor patents. *Recent Pat Biotechnol, 6*(3), 157-166. doi:10.2174/1872208311206030157

Kushnir, A., Wajsberg, B., & Marks, A. R. (2018). Ryanodine receptor dysfunction in human disorders. *Biochim Biophys Acta Mol Cell Res, 1865*(11 Pt B), 1687-1697. doi:10.1016/j.bbamcr.2018.07.011

Kutchukian, C., Lo Scrudato, M., Tourneur, Y., Poulard, K., Vignaud, A., Berthier, C., . . . Jacquemond, V. (2016). Phosphatidylinositol 3-kinase inhibition restores Ca2+ release defects and prolongs survival in myotubularin-deficient mice. *Proc Natl Acad Sci U S A, 113*(50), 14432-14437. doi:10.1073/pnas.1604099113

Kutchukian, C., Szentesi, P., Allard, B., Trochet, D., Beuvin, M., Berthier, C., . . . Jacquemond, V. (2017). Impaired excitation-contraction coupling in muscle fibres from the dynamin2(R465W) mouse model of centronuclear myopathy. *J Physiol, 595*(24), 7369-7382. doi:10.1113/jp274990

Lai, C. P., Bechberger, J. F., Thompson, R. J., MacVicar, B. A., Bruzzone, R., & Naus, C. C. (2007). Tumor-suppressive effects of pannexin 1 in C6 glioma cells. *Cancer Res, 67*(4), 1545-1554. doi:10.1158/0008-5472.can-06-1396

Lai, F. A., Erickson, H. P., Rousseau, E., Liu, Q. Y., & Meissner, G. (1988). Purification and reconstitution of the calcium release channel from skeletal muscle. *Nature, 331*(6154), 315-319. doi:10.1038/331315a0

Lamb, G. D. (1992). DHP receptors and excitation-contraction coupling. *J Muscle Res Cell Motil, 13*(4), 394-405. doi:10.1007/bf01738035

Landstrom, A. P., Kellen, C. A., Dixit, S. S., van Oort, R. J., Garbino, A., Weisleder, N., . . . Ackerman, M. J. (2011). Junctophilin-2 expression silencing causes cardiocyte hypertrophy and abnormal intracellular calcium-handling. *Circulation. Heart failure, 4*(2), 214-223. doi:10.1161/CIRCHEARTFAILURE.110.958694

Langlois, S., Xiang, X., Young, K., Cowan, B. J., Penuela, S., & Cowan, K. N. (2014). Pannexin 1 and pannexin 3 channels regulate skeletal muscle myoblast proliferation and differentiation. *J Biol Chem, 289*(44), 30717-30731. doi:10.1074/jbc.M114.572131

Lanner, J. T., Georgiou, D. K., Joshi, A. D., & Hamilton, S. L. (2010). Ryanodine receptors: structure, expression, molecular details, and function in calcium release. *Cold Spring Harb Perspect Biol, 2*(11), a003996. doi:10.1101/cshperspect.a003996

Lansman, J. B., Hess, P., & Tsien, R. W. (1986). Blockade of current through single calcium channels by Cd2+, Mg2+, and Ca2+. Voltage and concentration dependence of calcium entry into the pore. *J Gen Physiol, 88*(3), 321-347. doi:10.1085/jgp.88.3.321

Lapie, P., Goudet, C., Nargeot, J., Fontaine, B., & Lory, P. (1996). Electrophysiological properties of the hypokalaemic periodic paralysis mutation (R528H) of the skeletal muscle α1S subunit as expressed in mouse L cells. *FEBS Letters, 382*(3), 244-248. doi:https://doi.org/10.1016/0014-5793(96)00173-1

Larsson, L., Edström, L., Lindegren, B., Gorza, L., & Schiaffino, S. (1991). MHC composition and enzyme-histochemical and physiological properties of a novel fast-twitch motor unit type. *Am J Physiol, 261*(1 Pt 1), C93-101. doi:10.1152/ajpcell.1991.261.1.C93

Lawal, T. A., Todd, J. J., & Meilleur, K. G. (2018). Ryanodine Receptor 1-Related Myopathies: Diagnostic and Therapeutic Approaches. *Neurotherapeutics, 15*(4), 885-899. doi:10.1007/s13311-018-00677-1

Lawal, T. A., Todd, J. J., Witherspoon, J. W., Bönnemann, C. G., Dowling, J. J., Hamilton, S. L., . . . Dirksen, R. T. (2020). Ryanodine receptor 1-related disorders: an historical perspective and proposal for a unified nomenclature. *Skelet Muscle, 10*(1), 32. doi:10.1186/s13395-020-00243-4

Lawal, T. A., Wires, E. S., Terry, N. L., Dowling, J. J., & Todd, J. J. (2020). Preclinical model systems of ryanodine receptor 1-related myopathies and malignant hyperthermia: a comprehensive scoping review of works published 1990-2019. *Orphanet J Rare Dis, 15*(1), 113. doi:10.1186/s13023-020-01384-x

Lee, C. S., Dagnino-Acosta, A., Yarotskyy, V., Hanna, A., Lyfenko, A., Knoblauch, M., . . . Hamilton, S. L. (2015). Ca(2+) permeation and/or binding to CaV1.1 fine-tunes skeletal muscle Ca(2+) signaling to sustain muscle function. *Skelet Muscle, 5*, 4. doi:10.1186/s13395-014-0027-1

Lee, C. S., Dagnino-Acosta, A., Yarotskyy, V., Hanna, A., Lyfenko, A., Knoblauch, M., . . . Hamilton, S. L. (2015). Ca(2+) permeation and/or binding to CaV1.1 fine-tunes skeletal muscle Ca(2+) signaling to sustain muscle function. *Skelet Muscle, 5*, 4. doi:10.1186/s13395-014-0027-1

Lefebvre, R., Legrand, C., González-Rodríguez, E., Groom, L., Dirksen, R. T., & Jacquemond, V. (2011). Defects in Ca2+ release associated with local expression of pathological ryanodine receptors in mouse muscle fibres. *J Physiol, 589*(Pt 22), 5361-5382. doi:10.1113/jphysiol.2011.216408

Lefebvre, R., Legrand, C., Groom, L., Dirksen, R. T., & Jacquemond, V. (2013). Ca2+ release in muscle fibers expressing R4892W and G4896V type 1 ryanodine receptor disease mutants. *PLoS One, 8*(1), e54042. doi:10.1371/journal.pone.0054042

Legrand, C., Giacomello, E., Berthier, C., Allard, B., Sorrentino, V., & Jacquemond, V. (2008). Spontaneous and voltage-activated Ca2+ release in adult mouse skeletal muscle fibres expressing the type 3 ryanodine receptor. *J Physiol, 586*(2), 441-457. doi:10.1113/jphysiol.2007.145862

Leyssens, A., Nowicky, A. V., Patterson, L., Crompton, M., & Duchen, M. R. (1996). The relationship between mitochondrial state, ATP hydrolysis, [Mg2+]i and [Ca2+]i studied in isolated rat cardiomyocytes. *J Physiol, 496 (Pt 1)*(Pt 1), 111-128. doi:10.1113/jphysiol.1996.sp021669

Li, N., Chiang, D. Y., Wang, S., Wang, Q., Sun, L., Voigt, N., . . . Wehrens, X. H. T. (2014). Ryanodine receptor-mediated calcium leak drives progressive development of an atrial fibrillation substrate in a transgenic mouse model. *Circulation, 129*(12), 1276-1285. doi:10.1161/circulationaha.113.006611

Liang, Y., Walczak, P., & Bulte, J. W. (2012). Comparison of red-shifted firefly luciferase Ppy RE9 and conventional Luc2 as bioluminescence imaging reporter genes for in vivo imaging of stem cells. *J Biomed Opt, 17*(1), 016004. doi:10.1117/1.jbo.17.1.016004

Linsley, J. W., Hsu, I. U., Groom, L., Yarotskyy, V., Lavorato, M., Horstick, E. J., . . . Kuwada, J. Y. (2017). Congenital myopathy results from misregulation of a muscle Ca2+ channel by mutant Stac3. *Proc Natl Acad Sci U S A, 114*(2), E228-e236. doi:10.1073/pnas.1619238114

Liu, Y., Cseresnyés, Z., Randall, W. R., & Schneider, M. F. (2001). Activity-dependent nuclear translocation and intranuclear distribution of NFATc in adult skeletal muscle fibers. *J Cell Biol, 155*(1), 27-39. doi:10.1083/jcb.200103020

Liu, Y., Randall, W. R., & Schneider, M. F. (2005). Activity-dependent and -independent nuclear fluxes of HDAC4 mediated by different kinases in adult skeletal muscle. *J Cell Biol, 168*(6), 887-897. doi:10.1083/jcb.200408128

Liu, Z., Chen, O., Wall, J. B. J., Zheng, M., Zhou, Y., Wang, L., . . . Liu, J. (2017). Systematic comparison of 2A peptides for cloning multi-genes in a polycistronic vector. *Sci Rep, 7*(1), 2193. doi:10.1038/s41598-017-02460-2

Locovei, S., Bao, L., & Dahl, G. (2006). Pannexin 1 in erythrocytes: function without a gap. *Proc Natl Acad Sci U S A, 103*(20), 7655-7659. doi:10.1073/pnas.0601037103

Locovei, S., Scemes, E., Qiu, F., Spray, D. C., & Dahl, G. (2007). Pannexin1 is part of the pore forming unit of the P2X(7) receptor death complex. *FEBS Lett, 581*(3), 483-488. doi:10.1016/j.febslet.2006.12.056

Locovei, S., Wang, J., & Dahl, G. (2006). Activation of pannexin 1 channels by ATP through P2Y receptors and by cytoplasmic calcium. *FEBS Lett, 580*(1), 239-244. doi:10.1016/j.febslet.2005.12.004

Lohman, A. W., Leskov, I. L., Butcher, J. T., Johnstone, S. R., Stokes, T. A., Begandt, D., . . . Isakson, B. E. (2015). Pannexin 1 channels regulate leukocyte emigration through the venous endothelium during acute inflammation. *Nat Commun, 6*, 7965. doi:10.1038/ncomms8965

Long, Y. C., Glund, S., Garcia-Roves, P. M., & Zierath, J. R. (2007). Calcineurin regulates skeletal muscle metabolism via coordinated changes in gene expression. *J Biol Chem, 282*(3), 1607-1614. doi:10.1074/jbc.M609208200

Lowell, B. B., & Shulman, G. I. (2005). Mitochondrial dysfunction and type 2 diabetes. *Science, 307*(5708), 384-387. doi:10.1126/science.1104343

Loy, R. E., Orynbayev, M., Xu, L., Andronache, Z., Apostol, S., Zvaritch, E., . . . Dirksen, R. T. (2011). Muscle weakness in Ryr1I4895T/WT knock-in mice as a result of reduced ryanodine receptor Ca2+ ion permeation and release from the sarcoplasmic reticulum. *J Gen Physiol, 137*(1), 43-57. doi:10.1085/jgp.201010523

Lu, X., Xu, L., & Meissner, G. (1994). Activation of the skeletal muscle calcium release channel by a cytoplasmic loop of the dihydropyridine receptor. *J Biol Chem, 269*(9), 6511-6516.

Lueck, J. D., Mankodi, A., Swanson, M. S., Thornton, C. A., & Dirksen, R. T. (2007). Muscle chloride channel dysfunction in two mouse models of myotonic dystrophy. *J Gen Physiol, 129*(1), 79-94. doi:10.1085/jgp.200609635

Lundin, A. (2014). Optimization of the firefly luciferase reaction for analytical purposes. *Adv Biochem Eng Biotechnol, 145*, 31-62. doi:10.1007/978-3-662-43619-6_2

Luther, P. K. (2009). The vertebrate muscle Z-disc: sarcomere anchor for structure and signalling. *J Muscle Res Cell Motil, 30*(5-6), 171-185. doi:10.1007/s10974-009-9189-6

Ma, W., Hui, H., Pelegrin, P., & Surprenant, A. (2009). Pharmacological characterization of pannexin-1 currents expressed in mammalian cells. *J Pharmacol Exp Ther, 328*(2), 409-418. doi:10.1124/jpet.108.146365

MacKenzie, A. E., Korneluk, R. G., Zorzato, F., Fujii, J., Phillips, M., Iles, D., . . . et al. (1990). The human ryanodine receptor gene: its mapping to 19q13.1, placement in a chromosome 19 linkage group, and exclusion as the gene causing myotonic dystrophy. *Am J Hum Genet, 46*(6), 1082-1089.

Mankodi, A., Takahashi, M. P., Jiang, H., Beck, C. L., Bowers, W. J., Moxley, R. T., . . . Thornton, C. A. (2002). Expanded CUG repeats trigger aberrant splicing of ClC-1 chloride channel pre-mRNA and hyperexcitability of skeletal muscle in myotonic dystrophy. *Mol Cell, 10*(1), 35-44. doi:10.1016/s1097-2765(02)00563-4

Manno, C., Figueroa, L. C., Gillespie, D., Fitts, R., Kang, C., Franzini-Armstrong, C., & Rios, E. (2017). Calsequestrin depolymerizes when calcium is depleted in the sarcoplasmic reticulum of working muscle. *Proc Natl Acad Sci U S A, 114*(4), E638-e647. doi:10.1073/pnas.1620265114

Marty, I. (2004). Triadin: a multi-protein family for which purpose? *Cell Mol Life Sci, 61*(15), 1850-1853. doi:10.1007/s00018-004-4196-7

Marty, I. (2015). Triadin regulation of the ryanodine receptor complex. *J Physiol, 593*(15), 3261-3266. doi:10.1113/jphysiol.2014.281147

Marx, S. O., Reiken, S., Hisamatsu, Y., Jayaraman, T., Burkhoff, D., Rosemblit, N., & Marks, A. R. (2000). PKA phosphorylation dissociates FKBP12.6 from the calcium release channel (ryanodine receptor): defective regulation in failing hearts. *Cell, 101*(4), 365-376. doi:10.1016/s0092-8674(00)80847-8

Mayrleitner, M., Timerman, A. P., Wiederrecht, G., & Fleischer, S. (1994). The calcium release channel of sarcoplasmic reticulum is modulated by FK-506 binding protein: effect of FKBP-12 on single channel activity of the skeletal muscle ryanodine receptor. *Cell Calcium, 15*(2), 99-108. doi:10.1016/0143-4160(94)90048-5

McCullagh, K. J., Calabria, E., Pallafacchina, G., Ciciliot, S., Serrano, A. L., Argentini, C., . . . Schiaffino, S. (2004). NFAT is a nerve activity sensor in skeletal muscle and controls activity-dependent myosin switching. *Proc Natl Acad Sci U S A, 101*(29), 10590-10595. doi:10.1073/pnas.0308035101

McKinsey, T. A., Zhang, C. L., Lu, J., & Olson, E. N. (2000). Signal-dependent nuclear export of a histone deacetylase regulates muscle differentiation. *Nature, 408*(6808), 106-111. doi:10.1038/35040593

Meissner, G. (2017). The structural basis of ryanodine receptor ion channel function. *J Gen Physiol, 149*(12), 1065-1089. doi:10.1085/jgp.201711878

Meissner, G., Darling, E., & Eveleth, J. (1986). Kinetics of rapid Ca2+ release by sarcoplasmic reticulum. Effects of Ca2+, Mg2+, and adenine nucleotides. *Biochemistry, 25*(1), 236-244. doi:10.1021/bi00349a033

Meissner, G., Rios, E., Tripathy, A., & Pasek, D. A. (1997). Regulation of skeletal muscle Ca2+ release channel (ryanodine receptor) by Ca2+ and monovalent cations and anions. *J Biol Chem, 272*(3), 1628-1638. doi:10.1074/jbc.272.3.1628

Melhorn, M. I., Brodsky, A. S., Estanislau, J., Khoory, J. A., Illigens, B., Hamachi, I., . . . Ghiran, I. C. (2013). CR1-mediated ATP release by human red blood cells promotes CR1 clustering and modulates the immune transfer process. *J Biol Chem, 288*(43), 31139-31153. doi:10.1074/jbc.M113.486035

Melzer, W., & Dietze, B. (2001). Malignant hyperthermia and excitation-contraction coupling. *Acta Physiol Scand, 171*(3), 367-378. doi:10.1046/j.1365-201x.2001.00840.x

Michalski, K., & Kawate, T. (2016). Carbenoxolone inhibits Pannexin1 channels through interactions in the first extracellular loop. *J Gen Physiol, 147*(2), 165-174. doi:10.1085/jgp.201511505

Michalski, K., Syrjanen, J. L., Henze, E., Kumpf, J., Furukawa, H., & Kawate, T. (2020). The Cryo-EM structure of pannexin 1 reveals unique motifs for ion selection and inhibition. *Elife, 9*. doi:10.7554/eLife.54670

Michelucci, A., Paolini, C., Boncompagni, S., Canato, M., Reggiani, C., & Protasi, F. (2017). Strenuous exercise triggers a life-threatening response in mice susceptible to malignant hyperthermia. *Faseb j, 31*(8), 3649-3662. doi:10.1096/fj.201601292R

Miledi, R., Parker, I., & Schalow, G. (1977). Calcium transients in frog slow muscle fibres. *Nature, 268*(5622), 750-752. doi:10.1038/268750a0

Miller, J. W., Urbinati, C. R., Teng-Umnuay, P., Stenberg, M. G., Byrne, B. J., Thornton, C. A., & Swanson, M. S. (2000). Recruitment of human muscleblind proteins to (CUG)(n) expansions associated with myotonic dystrophy. *Embo j, 19*(17), 4439-4448. doi:10.1093/emboj/19.17.4439

Minta, A., Kao, J. P., & Tsien, R. Y. (1989). Fluorescent indicators for cytosolic calcium based on rhodamine and fluorescein chromophores. *J Biol Chem, 264*(14), 8171-8178.

Moore, C. P., Rodney, G., Zhang, J. Z., Santacruz-Toloza, L., Strasburg, G., & Hamilton, S. L. (1999). Apocalmodulin and Ca2+ calmodulin bind to the same region on the skeletal muscle Ca2+ release channel. *Biochemistry, 38*(26), 8532-8537. doi:10.1021/bi9907431

Moreau, A., Gosselin-Badaroudine, P., & Chahine, M. (2014). Biophysics, pathophysiology, and pharmacology of ion channel gating pores. *Front Pharmacol, 5*, 53. doi:10.3389/fphar.2014.00053

Mormeneo, E., Jimenez-Mallebrera, C., Palomer, X., De Nigris, V., Vazquez-Carrera, M., Orozco, A., . . . Gomez-Foix, A. M. (2012). PGC-1alpha induces mitochondrial and myokine transcriptional programs and lipid droplet and glycogen accumulation in cultured human skeletal muscle cells. *PLoS One, 7*(1), e29985. doi:10.1371/journal.pone.0029985

Morrill, J. A., Brown, R. H., Jr., & Cannon, S. C. (1998). Gating of the L-type Ca channel in human skeletal myotubes: an activation defect caused by the hypokalemic periodic paralysis mutation R528H. *J Neurosci, 18*(24), 10320-10334.

Morrill, J. A., & Cannon, S. C. (1999). Effects of mutations causing hypokalaemic periodic paralysis on the skeletal muscle L-type Ca2+ channel expressed in Xenopus laevis oocytes. *J Physiol, 520 Pt 2*(Pt 2), 321-336. doi:10.1111/j.1469-7793.1999.00321.x

Mosca, B., Delbono, O., Laura Messi, M., Bergamelli, L., Wang, Z. M., Vukcevic, M., . . . Zorzato, F. (2013). Enhanced dihydropyridine receptor calcium channel activity restores muscle strength in JP45/CASQ1 double knockout mice. *Nat Commun, 4*, 1541. doi:10.1038/ncomms2496

Most, P., Pleger, S. T., Völkers, M., Heidt, B., Boerries, M., Weichenhan, D., . . . Koch, W. J. (2004). Cardiac adenoviral S100A1 gene delivery rescues failing myocardium. *J Clin Invest, 114*(11), 1550-1563. doi:10.1172/jci21454

Most, P., Seifert, H., Gao, E., Funakoshi, H., Völkers, M., Heierhorst, J., . . . Koch, W. J. (2006). Cardiac S100A1 protein levels determine contractile performance and propensity toward heart failure after myocardial infarction. *Circulation, 114*(12), 1258-1268. doi:10.1161/circulationaha.106.622415

Mou, L., Ke, M., Song, M., Shan, Y., Xiao, Q., Liu, Q., . . . Deng, D. (2020). Structural basis for gating mechanism of Pannexin 1 channel. In *Cell Res* (Vol. 30, pp. 452-454).

Mukund, K., & Subramaniam, S. (2020). Skeletal muscle: A review of molecular structure and function, in health and disease. *WIREs Systems Biology and Medicine, 12*(1), e1462. doi:10.1002/wsbm.1462

Murphy, R. M., Larkins, N. T., Mollica, J. P., Beard, N. A., & Lamb, G. D. (2009). Calsequestrin content and SERCA determine normal and maximal Ca2+ storage levels in sarcoplasmic reticulum of fast- and slow-twitch fibres of rat. *J Physiol, 587*(2), 443-460. doi:10.1113/jphysiol.2008.163162

Murphy, R. M., Mollica, J. P., & Lamb, G. D. (2009). Plasma membrane removal in rat skeletal muscle fibers reveals caveolin-3 hot-spots at the necks of transverse tubules. *Exp Cell Res, 315*(6), 1015-1028. doi:10.1016/j.yexcr.2008.11.022

Nakada, T., Kashihara, T., Komatsu, M., Kojima, K., Takeshita, T., & Yamada, M. (2018a). Physical interaction of junctophilin and the Ca(V)1.1 C terminus is crucial for skeletal muscle contraction. *Proc Natl Acad Sci U S A, 115*(17), 4507-4512. doi:10.1073/pnas.1716649115

Nakada, T., Kashihara, T., Komatsu, M., Kojima, K., Takeshita, T., & Yamada, M. (2018b). Physical interaction of junctophilin and the CaV1.1 C terminus is crucial for skeletal muscle contraction. *Proc Natl Acad Sci U S A, 115*(17), 4507-4512. doi:10.1073/pnas.1716649115

Nakai, J., Dirksen, R. T., Nguyen, H. T., Pessah, I. N., Beam, K. G., & Allen, P. D. (1996). Enhanced dihydropyridine receptor channel activity in the presence of ryanodine receptor. *Nature, 380*(6569), 72-75. doi:10.1038/380072a0

Nakai, J., Imagawa, T., Hakamat, Y., Shigekawa, M., Takeshima, H., & Numa, S. (1990). Primary structure and functional expression from cDNA of the cardiac ryanodine receptor/calcium release channel. *FEBS Lett, 271*(1-2), 169-177. doi:10.1016/0014-5793(90)80399-4

Nakano, M., Imamura, H., Nagai, T., & Noji, H. (2011). Ca^{2+} regulation of mitochondrial ATP synthesis visualized at the single cell level. *ACS Chem Biol, 6*(7), 709-715. doi:10.1021/cb100313n

Nance, J. R., Dowling, J. J., Gibbs, E. M., & Bönnemann, C. G. (2012). Congenital myopathies: an update. *Curr Neurol Neurosci Rep, 12*(2), 165-174. doi:10.1007/s11910-012-0255-x

Naya, F. J., Mercer, B., Shelton, J., Richardson, J. A., Williams, R. S., & Olson, E. N. (2000). Stimulation of slow skeletal muscle fiber gene expression by calcineurin in vivo. *J Biol Chem, 275*(7), 4545-4548. doi:10.1074/jbc.275.7.4545

Needham, D. M. (1926). RED AND WHITE MUSCLE. *Physiological Reviews, 6*(1), 1-27. doi:10.1152/physrev.1926.6.1.1

Nelson, B. R., Makarewich, C. A., Anderson, D. M., Winders, B. R., Troupes, C. D., Wu, F., . . . Olson, E. N. (2016). A peptide encoded by a transcript annotated as long noncoding RNA enhances SERCA activity in muscle. *Science, 351*(6270), 271-275. doi:10.1126/science.aad4076

Nelson, B. R., Wu, F., Liu, Y., Anderson, D. M., McAnally, J., Lin, W., . . . Olson, E. N. (2013). Skeletal muscle-specific T-tubule protein STAC3 mediates voltage-induced Ca2+ release and contractility. *Proc Natl Acad Sci U S A, 110*(29), 11881-11886. doi:10.1073/pnas.1310571110

Niranjan, N., Mareedu, S., Tian, Y., Kodippili, K., Fefelova, N., Voit, A., . . . Babu, G. J. (2019). Sarcolipin overexpression impairs myogenic differentiation in Duchenne muscular dystrophy. *Am J Physiol Cell Physiol, 317*(4), C813-c824. doi:10.1152/ajpcell.00146.2019

Nishida, M., Sato, Y., Uemura, A., Narita, Y., Tozaki-Saitoh, H., Nakaya, M., . . . Kurose, H. (2008). P2Y6 receptor-Galpha12/13 signalling in cardiomyocytes triggers pressure overload-induced cardiac fibrosis. *EMBO J, 27*(23), 3104-3115. doi:emboj2008237 [pii]

10.1038/emboj.2008.237

Niu, J., Yang, W., Yue, D. T., Inoue, T., & Ben-Johny, M. (2018). Duplex signaling by CaM and Stac3 enhances Ca(V)1.1 function and provides insights into congenital myopathy. *J Gen Physiol, 150*(8), 1145-1161. doi:10.1085/jgp.201812005

Nixon, S. J., Wegner, J., Ferguson, C., Méry, P. F., Hancock, J. F., Currie, P. D., . . . Parton, R. G. (2005). Zebrafish as a model for caveolin-associated muscle disease; caveolin-3 is required for myofibril

organization and muscle cell patterning. *Hum Mol Genet, 14*(13), 1727-1743. doi:10.1093/hmg/ddi179

Noma, A. (1983). ATP-regulated K+ channels in cardiac muscle. *Nature, 305*(5930), 147-148. doi:10.1038/305147a0

Nouri-Nejad, D., O'Donnell, B. L., Patil, C. S., Sanchez-Pupo, R. E., Johnston, D., Sayedyahossein, S., . . . Penuela, S. (2021). Pannexin 1 mutation found in melanoma tumour reduces phosphorylation, glycosylation, and trafficking of the channel-forming protein. *Mol Biol Cell*, mbcE19100585. doi:10.1091/mbc.E19-10-0585

Nyberg, M., Piil, P., Kiehn, O. T., Maagaard, C., Jørgensen, T. S., Egelund, J., . . . Hellsten, Y. (2018). Probenecid Inhibits α-Adrenergic Receptor-Mediated Vasoconstriction in the Human Leg Vasculature. *Hypertension, 71*(1), 151-159. doi:10.1161/hypertensionaha.117.10251

O'Connell, K. M., Yamaguchi, N., Meissner, G., & Dirksen, R. T. (2002). Calmodulin binding to the 3614-3643 region of RyR1 is not essential for excitation-contraction coupling in skeletal myotubes. *J Gen Physiol, 120*(3), 337-347. doi:10.1085/jgp.20028617

Obermair, G. J., Kugler, G., Baumgartner, S., Tuluc, P., Grabner, M., & Flucher, B. E. (2005). The Ca2+ channel alpha2delta-1 subunit determines Ca2+ current kinetics in skeletal muscle but not targeting of alpha1S or excitation-contraction coupling. *J Biol Chem, 280*(3), 2229-2237. doi:10.1074/jbc.M411501200

Oddoux, S., Brocard, J., Schweitzer, A., Szentesi, P., Giannesini, B., Fauré, J., . . . Marty, I. (2009). Triadin deletion induces impaired skeletal muscle function. *J Biol Chem, 284*(50), 34918-34929. doi:10.1074/jbc.M109.022442

Odermatt, A., Taschner, P. E., Khanna, V. K., Busch, H. F., Karpati, G., Jablecki, C. K., . . . MacLennan, D. H. (1996). Mutations in the gene-encoding SERCA1, the fast-twitch skeletal muscle sarcoplasmic reticulum Ca2+ ATPase, are associated with Brody disease. *Nat Genet, 14*(2), 191-194. doi:10.1038/ng1096-191

Ogata, T., & Yamasaki, Y. (1997). Ultra-high-resolution scanning electron microscopy of mitochondria and sarcoplasmic reticulum arrangement in human red, white, and intermediate muscle fibers. *The Anatomical Record, 248*(2), 214-223. doi:10.1002/(sici)1097-0185(199706)248:2<214::aid-ar8>3.0.co;2-s

Ogawa, H., Kurebayashi, N., Yamazawa, T., & Murayama, T. (2020). Regulatory mechanisms of ryanodine receptor/Ca(2+) release channel revealed by recent advancements in structural studies. *J Muscle Res Cell Motil*. doi:10.1007/s10974-020-09575-6

Oh, M., Rybkin, II, Copeland, V., Czubryt, M. P., Shelton, J. M., van Rooij, E., . . . Rothermel, B. A. (2005). Calcineurin is necessary for the maintenance but not embryonic development of slow muscle fibers. *Mol Cell Biol, 25*(15), 6629-6638. doi:10.1128/mcb.25.15.6629-6638.2005

Ohrtman, J., Ritter, B., Polster, A., Beam, K. G., & Papadopoulos, S. (2008). Sequence differences in the IQ motifs of CaV1.1 and CaV1.2 strongly impact calmodulin binding and calcium-dependent inactivation. *J Biol Chem, 283*(43), 29301-29311. doi:10.1074/jbc.M805152200

Olivares, E., Arispe, N., & Rojas, E. (1993). Properties of the ryanodine receptor present in the sarcoplasmic reticulum from lobster skeletal muscle. *Membr Biochem, 10*(4), 221-235. doi:10.3109/09687689309150270

Ollivier, M., Beudez, J., Linck, N., Grutter, T., Compan, V., & Rassendren, F. (2021). P2X-GCaMPs as Versatile Tools for Imaging Extracellular ATP Signaling. *eNeuro, 8*(1). doi:10.1523/eneuro.0185-20.2020

Oo, Y. W., Gomez-Hurtado, N., Walweel, K., van Helden, D. F., Imtiaz, M. S., Knollmann, B. C., & Laver, D. R. (2015). Essential Role of Calmodulin in RyR Inhibition by Dantrolene. *Mol Pharmacol, 88*(1), 57-63. doi:10.1124/mol.115.097691

Palade, P., & Vergara, J. (1982). Arsenazo III and antipyrylazo III calcium transients in single skeletal muscle fibers. *J Gen Physiol, 79*(4), 679-707. doi:10.1085/jgp.79.4.679

Panchin, Y., Kelmanson, I., Matz, M., Lukyanov, K., Usman, N., & Lukyanov, S. (2000). A ubiquitous family of putative gap junction molecules. In *Curr Biol* (Vol. 10, pp. R473-474). England.

Pandorf, C. E., Haddad, F., Roy, R. R., Qin, A. X., Edgerton, V. R., & Baldwin, K. M. (2006). Dynamics of myosin heavy chain gene regulation in slow skeletal muscle: role of natural antisense RNA. *J Biol Chem, 281*(50), 38330-38342. doi:10.1074/jbc.M607249200

Paolini, C., Fessenden, J. D., Pessah, I. N., & Franzini-Armstrong, C. (2004a). Evidence for conformational coupling between two calcium channels. *Proc Natl Acad Sci U S A, 101*(34), 12748-12752. doi:10.1073/pnas.0404836101

Paolini, C., Fessenden, J. D., Pessah, I. N., & Franzini-Armstrong, C. (2004b). Evidence for conformational coupling between two calcium channels. *Proceedings of the National Academy of Sciences of the United States of America, 101*(34), 12748-12752. doi:10.1073/pnas.0404836101

Paran, C. W., Verkerke, A. R., Heden, T. D., Park, S., Zou, K., Lawson, H. A., . . . Funai, K. (2015). Reduced efficiency of sarcolipin-dependent respiration in myocytes from humans with severe obesity. *Obesity (Silver Spring), 23*(7), 1440-1449. doi:10.1002/oby.21123

Parsons, S. A., Wilkins, B. J., Bueno, O. F., & Molkentin, J. D. (2003). Altered skeletal muscle phenotypes in calcineurin Aalpha and Abeta gene-targeted mice. *Mol Cell Biol, 23*(12), 4331-4343. doi:10.1128/mcb.23.12.4331-4343.2003

Parton, R. G., Way, M., Zorzi, N., & Stang, E. (1997). Caveolin-3 associates with developing T-tubules during muscle differentiation. *J Cell Biol, 136*(1), 137-154. doi:10.1083/jcb.136.1.137

Paul-Pletzer, K., Yamamoto, T., Bhat, M. B., Ma, J., Ikemoto, N., Jimenez, L. S., . . . Parness, J. (2002). Identification of a dantrolene-binding sequence on the skeletal muscle ryanodine receptor. *J Biol Chem, 277*(38), 34918-34923. doi:10.1074/jbc.M205487200

Pelegrin, P., & Surprenant, A. (2006). Pannexin-1 mediates large pore formation and interleukin-1beta release by the ATP-gated P2X7 receptor. *EMBO J, 25*(21), 5071-5082. doi:7601378 [pii]

10.1038/sj.emboj.7601378

Pelletier, L., Petiot, A., Brocard, J., Giannesini, B., Giovannini, D., Sanchez, C., . . . Marty, I. (2020). In vivo RyR1 reduction in muscle triggers a core-like myopathy. *Acta Neuropathol Commun, 8*(1), 192. doi:10.1186/s40478-020-01068-4

Peng, M., Fan, H., Kirley, T. L., Caswell, A. H., & Schwartz, A. (1994). Structural diversity of triadin in skeletal muscle and evidence of its existence in heart. *FEBS Lett, 348*(1), 17-20. doi:10.1016/0014-5793(94)00556-7

Penuela, S., Gyenis, L., Ablack, A., Churko, J. M., Berger, A. C., Litchfield, D. W., . . . Laird, D. W. (2012). Loss of pannexin 1 attenuates melanoma progression by reversion to a melanocytic phenotype. *J Biol Chem, 287*(34), 29184-29193. doi:10.1074/jbc.M112.377176

Penuela, S., Harland, L., Simek, J., & Laird, D. W. (2014). Pannexin channels and their links to human disease. *Biochem J, 461*(3), 371-381. doi:10.1042/bj20140447

Periasamy, M., Bhupathy, P., & Babu, G. J. (2008). Regulation of sarcoplasmic reticulum Ca2+ ATPase pump expression and its relevance to cardiac muscle physiology and pathology. *Cardiovasc Res, 77*(2), 265-273. doi:10.1093/cvr/cvm056

Periasamy, M., & Kalyanasundaram, A. (2007). SERCA pump isoforms: Their role in calcium transport and disease. *Muscle & Nerve, 35*(4), 430-442. doi:10.1002/mus.20745

Perni, S., Lavorato, M., & Beam, K. G. (2017). De novo reconstitution reveals the proteins required for skeletal muscle voltage-induced Ca(2+) release. *Proc Natl Acad Sci U S A, 114*(52), 13822-13827. doi:10.1073/pnas.1716461115

Peter, J. B., Barnard, R. J., Edgerton, V. R., Gillespie, C. A., & Stempel, K. E. (1972). Metabolic profiles of three fiber types of skeletal muscle in guinea pigs and rabbits. *Biochemistry, 11*(14), 2627-2633. doi:10.1021/bi00764a013

Pette, D., & Staron, R. S. (1997). Mammalian skeletal muscle fiber type transitions. *Int Rev Cytol, 170*, 143-223. doi:10.1016/s0074-7696(08)61622-8

Pette, D., & Vrbová, G. (1999). What does chronic electrical stimulation teach us about muscle plasticity? *Muscle Nerve, 22*(6), 666-677. doi:10.1002/(sici)1097-4598(199906)22:6<666::aid-mus3>3.0.co;2-z

Pham, T. L., St-Pierre, M. E., Ravel-Chapuis, A., Parks, T. E. C., Langlois, S., Penuela, S., . . . Cowan, K. N. (2018). Expression of Pannexin 1 and Pannexin 3 during skeletal muscle development, regeneration, and Duchenne muscular dystrophy. *J Cell Physiol, 233*(10), 7057-7070. doi:10.1002/jcp.26629

Pietri-Rouxel, F., Gentil, C., Vassilopoulos, S., Baas, D., Mouisel, E., Ferry, A., . . . Garcia, L. (2010). DHPR alpha1S subunit controls skeletal muscle mass and morphogenesis. *EMBO J, 29*(3), 643-654. doi:10.1038/emboj.2009.366

Pirone, A., Schredelseker, J., Tuluc, P., Gravino, E., Fortunato, G., Flucher, B. E., . . . Grabner, M. (2010). Identification and functional characterization of malignant hyperthermia mutation T1354S in the outer pore of the Cavalpha1S-subunit. *Am J Physiol Cell Physiol, 299*(6), C1345-1354. doi:10.1152/ajpcell.00008.2010

Poklis, J. L., Gonek, M. M., Wolf, C. E., Akbarali, H. I., & Dewey, W. L. (2019). Analysis of carbenoxolone by ultra-high-performance liquid chromatography tandem mass spectrometry in mouse brain and blood after systemic administration. *Biomed Chromatogr, 33*(4), e4465. doi:10.1002/bmc.4465

Polster, A., Nelson, B. R., Olson, E. N., & Beam, K. G. (2016). Stac3 has a direct role in skeletal muscle-type excitation-contraction coupling that is disrupted by a myopathy-causing mutation. *Proc Natl Acad Sci U S A, 113*(39), 10986-10991. doi:10.1073/pnas.1612441113

Potthoff, M. J., Wu, H., Arnold, M. A., Shelton, J. M., Backs, J., McAnally, J., . . . Olson, E. N. (2007). Histone deacetylase degradation and MEF2 activation promote the formation of slow-twitch myofibers. *J Clin Invest, 117*(9), 2459-2467. doi:10.1172/jci31960

Pouvreau, S., Allard, B., Berthier, C., & Jacquemond, V. (2004). Control of intracellular calcium in the presence of nitric oxide donors in isolated skeletal muscle fibres from mouse. *J Physiol, 560*(Pt 3), 779-794. doi:10.1113/jphysiol.2004.072397

Pouvreau, S., Royer, L., Yi, J., Brum, G., Meissner, G., Ríos, E., & Zhou, J. (2007). Ca(2+) sparks operated by membrane depolarization require isoform 3 ryanodine receptor channels in skeletal muscle. *Proceedings of the National Academy of Sciences of the United States of America, 104*(12), 5235-5240. doi:10.1073/pnas.0700748104

Powell, J. A., Carrasco, M. A., Adams, D. S., Drouet, B., Rios, J., Müller, M., . . . Jaimovich, E. (2001). IP(3) receptor function and localization in myotubes: an unexplored Ca(2+) signaling pathway in skeletal muscle. *J Cell Sci, 114*(Pt 20), 3673-3683.

Praetorius, H. A., & Leipziger, J. (2009). ATP release from non-excitable cells. *Purinergic Signal, 5*(4), 433-446. doi:10.1007/s11302-009-9146-2

Prosser, B. L., Wright, N. T., Hernãndez-Ochoa, E. O., Varney, K. M., Liu, Y., Olojo, R. O., . . . Schneider, M. F. (2008). S100A1 binds to the calmodulin-binding site of ryanodine receptor and modulates skeletal muscle excitation-contraction coupling. *J Biol Chem, 283*(8), 5046-5057. doi:10.1074/jbc.M709231200

Protasi, F., Franzini-Armstrong, C., & Allen, P. D. (1998). Role of ryanodine receptors in the assembly of calcium release units in skeletal muscle. *J Cell Biol, 140*(4), 831-842. doi:10.1083/jcb.140.4.831

Qiang, W., Hu, H., Sun, L., Li, H., & Xu, D. (2015). Aptamer/Polydopamine Nanospheres Nanocomplex for in Situ Molecular Sensing in Living Cells. *Anal Chem, 87*(24), 12190-12196. doi:10.1021/acs.analchem.5b03075

Qiu, F., Wang, J., Spray, D. C., Scemes, E., & Dahl, G. (2011). Two non-vesicular ATP release pathways in the mouse erythrocyte membrane. *FEBS Lett, 585*(21), 3430-3435. doi:10.1016/j.febslet.2011.09.033

Qu, R., Dong, L., Zhang, J., Yu, X., Wang, L., & Zhu, S. (2020). Cryo-EM structure of human heptameric Pannexin 1 channel. In *Cell Res* (Vol. 30, pp. 446-448).

Qu, Y., Misaghi, S., Newton, K., Gilmour, L. L., Louie, S., Cupp, J. E., . . . Dixit, V. M. (2011). Pannexin-1 is required for ATP release during apoptosis but not for inflammasome activation. *J Immunol, 186*(11), 6553-6561. doi:10.4049/jimmunol.1100478

Rajendran, M., Dane, E., Conley, J., & Tantama, M. (2016). Imaging Adenosine Triphosphate (ATP). *Biol Bull, 231*(1), 73-84. doi:10.1086/689592

Rana, Z. A., Gundersen, K., & Buonanno, A. (2009). The ups and downs of gene regulation by electrical activity in skeletal muscles. *J Muscle Res Cell Motil, 30*(7-8), 255-260. doi:10.1007/s10974-010-9200-2

Rao, A., Luo, C., & Hogan, P. G. (1997). Transcription factors of the NFAT family: regulation and function. *Annu Rev Immunol, 15*, 707-747. doi:10.1146/annurev.immunol.15.1.707

Rebbeck, R. T., Karunasekara, Y., Board, P. G., Beard, N. A., Casarotto, M. G., & Dulhunty, A. F. (2014). Skeletal muscle excitation-contraction coupling: who are the dancing partners? *Int J Biochem Cell Biol, 48*, 28-38. doi:10.1016/j.biocel.2013.12.001

Reggiani, C., & te Kronnie, T. (2006). RyR isoforms and fibre type-specific expression of proteins controlling intracellular calcium concentration in skeletal muscles. *J Muscle Res Cell Motil, 27*(5-7), 327-335. doi:10.1007/s10974-006-9076-3

Ren, D., Tu, H. C., Kim, H., Wang, G. X., Bean, G. R., Takeuchi, O., . . . Cheng, E. H. (2010). BID, BIM, and PUMA are essential for activation of the BAX- and BAK-dependent cell death program. *Science, 330*(6009), 1390-1393. doi:10.1126/science.1190217

Rezgui, S. S., Vassilopoulos, S., Brocard, J., Platel, J. C., Bouron, A., Arnoult, C., . . . Marty, I. (2005). Triadin (Trisk 95) overexpression blocks excitation-contraction coupling in rat skeletal myotubes. *J Biol Chem, 280*(47), 39302-39308. doi:10.1074/jbc.M506566200

Rinaldi, C., Haddad, F., Bodell, P. W., Qin, A. X., Jiang, W., & Baldwin, K. M. (2008). Intergenic bidirectional promoter and cooperative regulation of the IIx and IIb MHC genes in fast skeletal muscle. *Am J Physiol Regul Integr Comp Physiol, 295*(1), R208-218. doi:10.1152/ajpregu.00134.2008

Rios, E., & Brum, G. (1987). Involvement of dihydropyridine receptors in excitation-contraction coupling in skeletal muscle. *Nature, 325*(6106), 717-720. doi:10.1038/325717a0

Rios, E., & Pizarro, G. (1991). Voltage sensor of excitation-contraction coupling in skeletal muscle. *Physiol Rev, 71*(3), 849-908.

Rios, E., Pizarro, G., & Stefani, E. (1992). Charge movement and the nature of signal transduction in skeletal muscle excitation-contraction coupling. *Annu Rev Physiol, 54*, 109-133. doi:10.1146/annurev.ph.54.030192.000545

Riquelme, M. A., Cea, L. A., Vega, J. L., Boric, M. P., Monyer, H., Bennett, M. V., . . . Sáez, J. C. (2013). The ATP required for potentiation of skeletal muscle contraction is released via pannexin hemichannels. *Neuropharmacology, 75*, 594-603. doi:10.1016/j.neuropharm.2013.03.022

Riquelme, M. A., Cea, L. A., Vega, J. L., Puebla, C., Vargas, A. A., Shoji, K. F., . . . Sáez, J. C. (2015). Pannexin channels mediate the acquisition of myogenic commitment in C2C12 reserve cells promoted by P2 receptor activation. *Front Cell Dev Biol, 3*, 25. doi:10.3389/fcell.2015.00025

Robbins, N., Gilbert, M., Kumar, M., McNamara, J. W., Daly, P., Koch, S. E., . . . Rubinstein, J. (2018). Probenecid Improves Cardiac Function in Patients With Heart Failure With Reduced Ejection Fraction In Vivo and Cardiomyocyte Calcium Sensitivity In Vitro. *J Am Heart Assoc, 7*(2). doi:10.1161/jaha.117.007148

Robin, G., & Allard, B. (2015). Voltage-gated Ca(2+) influx through L-type channels contributes to sarcoplasmic reticulum Ca(2+) loading in skeletal muscle. *J Physiol, 593*(21), 4781-4797. doi:10.1113/jp270252

Romanov, R. A., Bystrova, M. F., Rogachevskaya, O. A., Sadovnikov, V. B., Shestopalov, V. I., & Kolesnikov, S. S. (2012). The ATP permeability of pannexin 1 channels in a heterologous system and in mammalian taste cells is dispensable. *J Cell Sci, 125*(Pt 22), 5514-5523. doi:10.1242/jcs.111062

Romanov, R. A., Rogachevskaja, O. A., Bystrova, M. F., Jiang, P., Margolskee, R. F., & Kolesnikov, S. S. (2007). Afferent neurotransmission mediated by hemichannels in mammalian taste cells. *EMBO J, 26*(3), 657-667. doi:10.1038/sj.emboj.7601526

Rose, A. J., Frøsig, C., Kiens, B., Wojtaszewski, J. F., & Richter, E. A. (2007). Effect of endurance exercise training on Ca2+ calmodulin-dependent protein kinase II expression and signalling in skeletal muscle of humans. *J Physiol, 583*(Pt 2), 785-795. doi:10.1113/jphysiol.2007.138529

Rosenberg, H., Davis, M., James, D., Pollock, N., & Stowell, K. (2007). Malignant hyperthermia. *Orphanet J Rare Dis, 2*, 21. doi:10.1186/1750-1172-2-21

Rothermel, B., Vega, R. B., Yang, J., Wu, H., Bassel-Duby, R., & Williams, R. S. (2000). A protein encoded within the Down syndrome critical region is enriched in striated muscles and inhibits calcineurin signaling. *J Biol Chem, 275*(12), 8719-8725. doi:10.1074/jbc.275.12.8719

Roux-Buisson, N., Rendu, J., Denjoy, I., Guicheney, P., Goldenberg, A., David, N., . . . Fauré, J. (2011). Functional analysis reveals splicing mutations of the CASQ2 gene in patients with CPVT: implication for genetic counselling and clinical management. *Hum Mutat, 32*(9), 995-999. doi:10.1002/humu.21537

Ruan, Z., Orozco, I. J., Du, J., & Lü, W. (2020). Structures of human pannexin 1 reveal ion pathways and mechanism of gating. *Nature, 584*(7822), 646-651. doi:10.1038/s41586-020-2357-y

Rueda, C. B., Traba, J., Amigo, I., Llorente-Folch, I., González-Sánchez, P., Pardo, B., . . . Satrústegui, J. (2015). Mitochondrial ATP-Mg/Pi carrier SCaMC-3/Slc25a23 counteracts PARP-1-dependent fall in mitochondrial ATP caused by excitotoxic insults in neurons. *J Neurosci, 35*(8), 3566-3581. doi:10.1523/jneurosci.2702-14.2015

Ryder, J. W., Bassel-Duby, R., Olson, E. N., & Zierath, J. R. (2003). Skeletal muscle reprogramming by activation of calcineurin improves insulin action on metabolic pathways. *J Biol Chem, 278*(45), 44298-44304. doi:10.1074/jbc.M304510200

Róg, J., Oksiejuk, A., Gosselin, M. R. F., Brutkowski, W., Dymkowska, D., Nowak, N., . . . Zabłocki, K. (2019). Dystrophic mdx mouse myoblasts exhibit elevated ATP/UTP-evoked metabotropic purinergic responses and alterations in calcium signalling. *Biochim Biophys Acta Mol Basis Dis, 1865*(6), 1138-1151. doi:10.1016/j.bbadis.2019.01.002

Samso, M. (2015). 3D Structure of the Dihydropyridine Receptor of Skeletal Muscle. *Eur J Transl Myol, 25*(1), 4840. doi:10.4081/ejtm.2015.4840

Samsó, M. (2015). 3D Structure of the Dihydropyridine Receptor of Skeletal Muscle. *Eur J Transl Myol, 25*(1), 4840. doi:10.4081/ejtm.2015.4840

Samsó, M. (2017). A guide to the 3D structure of the ryanodine receptor type 1 by cryoEM. *Protein Sci, 26*(1), 52-68. doi:10.1002/pro.3052

Samsó, M., Shen, X., & Allen, P. D. (2006). Structural characterization of the RyR1-FKBP12 interaction. *J Mol Biol, 356*(4), 917-927. doi:10.1016/j.jmb.2005.12.023

Sandilos, J. K., Chiu, Y. H., Chekeni, F. B., Armstrong, A. J., Walk, S. F., Ravichandran, K. S., & Bayliss, D. A. (2012). Pannexin 1, an ATP release channel, is activated by caspase cleavage of its pore-associated C-terminal autoinhibitory region. *J Biol Chem, 287*(14), 11303-11311. doi:10.1074/jbc.M111.323378

Sandonà, D., Danieli-Betto, D., Germinario, E., Biral, D., Martinello, T., Lioy, A., . . . Betto, R. (2005). The T-tubule membrane ATP-operated P2X4 receptor influences contractility of skeletal muscle. *Faseb j, 19*(9), 1184-1186. doi:10.1096/fj.04-3333fje

Sandow, A. (1952). Excitation-contraction coupling in muscular response. *Yale J Biol Med, 25*(3), 176-201.

Sang, Q., Zhang, Z., Shi, J., Sun, X., Li, B., Yan, Z., . . . Wang, L. (2019). A pannexin 1 channelopathy causes human oocyte death. *Sci Transl Med, 11*(485). doi:10.1126/scitranslmed.aav8731

Sayen, M. R., Rohrer, D. K., & Dillmann, W. H. (1992). Thyroid hormone response of slow and fast sarcoplasmic reticulum Ca2+ ATPase mRNA in striated muscle. *Mol Cell Endocrinol, 87*(1-3), 87-93. doi:10.1016/0303-7207(92)90236-y

Scemes, E., & Velíšková, J. (2019). Exciting and not so exciting roles of pannexins. *Neurosci Lett, 695*, 25-31. doi:10.1016/j.neulet.2017.03.010

Schartner, V., Romero, N. B., Donkervoort, S., Treves, S., Munot, P., Pierson, T. M., . . . Laporte, J. (2017). Dihydropyridine receptor (DHPR, CACNA1S) congenital myopathy. *Acta Neuropathol, 133*(4), 517-533. doi:10.1007/s00401-016-1656-8

Schiaffino, S., Gorza, L., Sartore, S., Saggin, L., Ausoni, S., Vianello, M., . . . Lømo, T. (1989). Three myosin heavy chain isoforms in type 2 skeletal muscle fibres. *J Muscle Res Cell Motil, 10*(3), 197-205. doi:10.1007/bf01739810

Schiaffino, S., Hanzlíková, V., & Pierobon, S. (1970). Relations between structure and function in rat skeletal muscle fibers. *J Cell Biol, 47*(1), 107-119. doi:10.1083/jcb.47.1.107

Schiaffino, S., Murgia, M., Serrano, A. L., Calabria, E., & Pallafacchina, G. (1999). How is muscle phenotype controlled by nerve activity? *Ital J Neurol Sci, 20*(6), 409-412. doi:10.1007/s100720050060

Schiaffino, S., & Reggiani, C. (2011). Fiber types in mammalian skeletal muscles. *Physiol Rev, 91*(4), 1447-1531. doi:10.1152/physrev.00031.2010

Schneider, J. S., Shanmugam, M., Gonzalez, J. P., Lopez, H., Gordan, R., Fraidenraich, D., & Babu, G. J. (2013). Increased sarcolipin expression and decreased sarco(endo)plasmic reticulum Ca2+ uptake in skeletal muscles of mouse models of Duchenne muscular dystrophy. *J Muscle Res Cell Motil, 34*(5-6), 349-356. doi:10.1007/s10974-013-9350-0

Schneider, M. F. (1994). Control of calcium release in functioning skeletal muscle fibers. *Annu Rev Physiol, 56*, 463-484. doi:10.1146/annurev.ph.56.030194.002335

Schneider, M. F., & Chandler, W. K. (1973). Voltage Dependent Charge Movement in Skeletal Muscle: a Possible Step in Excitation–Contraction Coupling. *Nature, 242*(5395), 244-246. doi:10.1038/242244a0

Schredelseker, J., Dayal, A., Schwerte, T., Franzini-Armstrong, C., & Grabner, M. (2009). Proper restoration of excitation-contraction coupling in the dihydropyridine receptor beta1-null zebrafish relaxed is an exclusive function of the beta1a subunit. *J Biol Chem, 284*(2), 1242-1251. doi:10.1074/jbc.M807767200

Schredelseker, J., Di Biase, V., Obermair, G. J., Felder, E. T., Flucher, B. E., Franzini-Armstrong, C., & Grabner, M. (2005). The beta 1a subunit is essential for the assembly of dihydropyridine-receptor arrays in skeletal muscle. *Proc Natl Acad Sci U S A, 102*(47), 17219-17224. doi:10.1073/pnas.0508710102

Schredelseker, J., Shrivastav, M., Dayal, A., & Grabner, M. (2010). Non-Ca2+-conducting Ca2+ channels in fish skeletal muscle excitation-contraction coupling. *Proc Natl Acad Sci U S A, 107*(12), 5658-5663. doi:10.1073/pnas.0912153107

Schwaller, B., Dick, J., Dhoot, G., Carroll, S., Vrbova, G., Nicotera, P., . . . Celio, M. R. (1999). Prolonged contraction-relaxation cycle of fast-twitch muscles in parvalbumin knockout mice. *Am J Physiol, 276*(2), C395-403. doi:10.1152/ajpcell.1999.276.2.C395

Seminario-Vidal, L., Kreda, S., Jones, L., O'Neal, W., Trejo, J., Boucher, R. C., & Lazarowski, E. R. (2009). Thrombin promotes release of ATP from lung epithelial cells through coordinated activation of rho- and Ca2+-dependent signaling pathways. *J Biol Chem, 284*(31), 20638-20648. doi:10.1074/jbc.M109.004762

Serrano, A. L., Murgia, M., Pallafacchina, G., Calabria, E., Coniglio, P., Lømo, T., & Schiaffino, S. (2001). Calcineurin controls nerve activity-dependent specification of slow skeletal muscle fibers but not muscle growth. *Proc Natl Acad Sci U S A, 98*(23), 13108-13113. doi:10.1073/pnas.231148598

Seto, E., & Yoshida, M. (2014). Erasers of histone acetylation: the histone deacetylase enzymes. *Cold Spring Harb Perspect Biol, 6*(4), a018713. doi:10.1101/cshperspect.a018713

Shagin, D. A., Barsova, E. V., Yanushevich, Y. G., Fradkov, A. F., Lukyanov, K. A., Labas, Y. A., . . . Matz, M. V. (2004). GFP-like proteins as ubiquitous metazoan superfamily: evolution of functional features and structural complexity. *Mol Biol Evol, 21*(5), 841-850. doi:10.1093/molbev/msh079

Shah, D. S., Nisr, R. B., Stretton, C., Krasteva-Christ, G., & Hundal, H. S. (2020). Caveolin-3 deficiency associated with the dystrophy P104L mutation impairs skeletal muscle mitochondrial form and function. *J Cachexia Sarcopenia Muscle, 11*(3), 838-858. doi:10.1002/jcsm.12541

Shan, J., Kushnir, A., Betzenhauser, M. J., Reiken, S., Li, J., Lehnart, S. E., . . . Marks, A. R. (2010). Phosphorylation of the ryanodine receptor mediates the cardiac fight or flight response in mice. *J Clin Invest, 120*(12), 4388-4398. doi:10.1172/jci32726

Shen, X., Franzini-Armstrong, C., Lopez, J. R., Jones, L. R., Kobayashi, Y. M., Wang, Y., . . . Perez, C. F. (2007). Triadins modulate intracellular Ca(2+) homeostasis but are not essential for excitation-contraction coupling in skeletal muscle. *J Biol Chem, 282*(52), 37864-37874. doi:10.1074/jbc.M705702200

Sheridan, D. C., Cheng, W., Carbonneau, L., Ahern, C. A., & Coronado, R. (2004). Involvement of a heptad repeat in the carboxyl terminus of the dihydropyridine receptor beta1a subunit in the mechanism of excitation-contraction coupling in skeletal muscle. *Biophys J, 87*(2), 929-942. doi:10.1529/biophysj.104.043810

Sheridan, D. C., Takekura, H., Franzini-Armstrong, C., Beam, K. G., Allen, P. D., & Perez, C. F. (2006). Bidirectional signaling between calcium channels of skeletal muscle requires multiple direct and indirect interactions. *Proc Natl Acad Sci U S A, 103*(52), 19760-19765. doi:10.1073/pnas.0609473103

Shin, D. W., Pan, Z., Kim, E. K., Lee, J. M., Bhat, M. B., Parness, J., . . . Ma, J. (2003). A retrograde signal from calsequestrin for the regulation of store-operated Ca2+ entry in skeletal muscle. *J Biol Chem, 278*(5), 3286-3292. doi:10.1074/jbc.M209045200

Shull, G. E., Okunade, G., Liu, L. H., Kozel, P., Periasamy, M., Lorenz, J. N., & Prasad, V. (2003). Physiological functions of plasma membrane and intracellular Ca2+ pumps revealed by analysis of null mutants. *Ann N Y Acad Sci, 986*, 453-460. doi:10.1111/j.1749-6632.2003.tb07229.x

Silverman, W., Locovei, S., & Dahl, G. (2008). Probenecid, a gout remedy, inhibits pannexin 1 channels. *Am J Physiol Cell Physiol, 295*(3), C761-767. doi:10.1152/ajpcell.00227.2008

Silverman, W. R., de Rivero Vaccari, J. P., Locovei, S., Qiu, F., Carlsson, S. K., Scemes, E., . . . Dahl, G. (2009). The pannexin 1 channel activates the inflammasome in neurons and astrocytes. *J Biol Chem, 284*(27), 18143-18151. doi:10.1074/jbc.M109.004804

Simmerman, H. K., & Jones, L. R. (1998). Phospholamban: protein structure, mechanism of action, and role in cardiac function. *Physiol Rev, 78*(4), 921-947. doi:10.1152/physrev.1998.78.4.921

Simon, B. J., & Hill, D. A. (1992). Charge movement and SR calcium release in frog skeletal muscle can be related by a Hodgkin-Huxley model with four gating particles. *Biophys J, 61*(5), 1109-1116. doi:10.1016/s0006-3495(92)81920-3

Sitsapesan, R., & Williams, A. J. (1995). The gating of the sheep skeletal sarcoplasmic reticulum Ca(2+)-release channel is regulated by luminal Ca2+. *J Membr Biol, 146*(2), 133-144. doi:10.1007/bf00238004

Smerdu, V., Karsch-Mizrachi, I., Campione, M., Leinwand, L., & Schiaffino, S. (1994). Type IIx myosin heavy chain transcripts are expressed in type IIb fibers of human skeletal muscle. *Am J Physiol, 267*(6 Pt 1), C1723-1728. doi:10.1152/ajpcell.1994.267.6.C1723

Smith, I. C., Bombardier, E., Vigna, C., & Tupling, A. R. (2013). ATP consumption by sarcoplasmic reticulum Ca^{2+} pumps accounts for 40-50% of resting metabolic rate in mouse fast and slow twitch skeletal muscle. *PLoS One, 8*(7), e68924. doi:10.1371/journal.pone.0068924

Smith, J. S., Imagawa, T., Ma, J., Fill, M., Campbell, K. P., & Coronado, R. (1988). Purified ryanodine receptor from rabbit skeletal muscle is the calcium-release channel of sarcoplasmic reticulum. *J Gen Physiol, 92*(1), 1-26. doi:10.1085/jgp.92.1.1

Spangenburg, E. E., & Booth, F. W. (2003). Molecular regulation of individual skeletal muscle fibre types. *Acta Physiol Scand, 178*(4), 413-424. doi:10.1046/j.1365-201X.2003.01158.x

Spruce, A. E., Standen, N. B., & Stanfield, P. R. (1985). Voltage-dependent ATP-sensitive potassium channels of skeletal muscle membrane. *Nature, 316*(6030), 736-738. doi:10.1038/316736a0

Sreter, F. A., Lopez, J. R., Alamo, L., Mabuchi, K., & Gergely, J. (1987). Changes in intracellular ionized Ca concentration associated with muscle fiber type transformation. *Am J Physiol, 253*(2 Pt 1), C296-300. doi:10.1152/ajpcell.1987.253.2.C296

Sridharan, M., Adderley, S. P., Bowles, E. A., Egan, T. M., Stephenson, A. H., Ellsworth, M. L., & Sprague, R. S. (2010). Pannexin 1 is the conduit for low oxygen tension-induced ATP release from human erythrocytes. *Am J Physiol Heart Circ Physiol, 299*(4), H1146-1152. doi:ajpheart.00301.2010 [pii]

10.1152/ajpheart.00301.2010

Stammers, A. N., Susser, S. E., Hamm, N. C., Hlynsky, M. W., Kimber, D. E., Kehler, D. S., & Duhamel, T. A. (2015). The regulation of sarco(endo)plasmic reticulum calcium-ATPases (SERCA). *Can J Physiol Pharmacol, 93*(10), 843-854. doi:10.1139/cjpp-2014-0463

Starace, D. M., & Bezanilla, F. (2004). A proton pore in a potassium channel voltage sensor reveals a focused electric field. *Nature, 427*(6974), 548-553. doi:10.1038/nature02270

Stern, M. D., Pizarro, G., & Ríos, E. (1997). Local control model of excitation-contraction coupling in skeletal muscle. *J Gen Physiol, 110*(4), 415-440. doi:10.1085/jgp.110.4.415

Stewart, S., Mawston, G., Davidtz, L., Dalbeth, N., Vandal, A. C., Carroll, M., . . . Rome, K. (2016). Foot and ankle muscle strength in people with gout: A two-arm cross-sectional study. *Clin Biomech (Bristol, Avon), 32*, 207-211. doi:10.1016/j.clinbiomech.2015.11.009

Striessnig, J., Grabner, M., Mitterdorfer, J., Hering, S., Sinnegger, M. J., & Glossmann, H. (1998). Structural basis of drug binding to L Ca2+ channels. *Trends Pharmacol Sci, 19*(3), 108-115. doi:10.1016/s0165-6147(98)01171-7

Striessnig, J., Ortner, N. J., & Pinggera, A. (2015). Pharmacology of L-type Calcium Channels: Novel Drugs for Old Targets? *Curr Mol Pharmacol, 8*(2), 110-122. doi:10.2174/1874467208666150507105845

Stroffekova, K. (2008). Ca2+/CaM-dependent inactivation of the skeletal muscle L-type Ca2+ channel (Cav1.1). *Pflugers Arch, 455*(5), 873-884. doi:10.1007/s00424-007-0344-x

Sultana, N., Dienes, B., Benedetti, A., Tuluc, P., Szentesi, P., Sztretye, M., . . . Flucher, B. E. (2016). Restricting calcium currents is required for correct fiber type specification in skeletal muscle. *Development, 143*(9), 1547-1559. doi:10.1242/dev.129676

Sumbilla, C., Cavagna, M., Zhong, L., Ma, H., Lewis, D., Farrance, I., & Inesi, G. (1999). Comparison of SERCA1 and SERCA2a expressed in COS-1 cells and cardiac myocytes. *Am J Physiol, 277*(6), H2381-2391. doi:10.1152/ajpheart.1999.277.6.H2381

Sutko, J. L., Airey, J. A., Welch, W., & Ruest, L. (1997). The pharmacology of ryanodine and related compounds. *Pharmacol Rev, 49*(1), 53-98.

Sweadner, K. J., & Donnet, C. (2001). Structural similarities of Na,K-ATPase and SERCA, the Ca(2+)-ATPase of the sarcoplasmic reticulum. *Biochem J, 356*(Pt 3), 685-704. doi:10.1042/0264-6021:3560685

Szentesi, P., Collet, C., Sárközi, S., Szegedi, C., Jona, I., Jacquemond, V., . . . Csernoch, L. (2001). Effects of dantrolene on steps of excitation-contraction coupling in mammalian skeletal muscle fibers. *J Gen Physiol, 118*(4), 355-375. doi:10.1085/jgp.118.4.355

Szentesi, P., Kovács, L., & Csernoch, L. (2000). Deterministic inactivation of calcium release channels in mammalian skeletal muscle. *J Physiol, 528*(Pt 3), 447-456. doi:10.1111/j.1469-7793.2000.00447.x

Sztretye, M., Yi, J., Figueroa, L., Zhou, J., Royer, L., Allen, P., . . . Ríos, E. (2011). Measurement of RyR permeability reveals a role of calsequestrin in termination of SR Ca(2+) release in skeletal muscle. *J Gen Physiol, 138*(2), 231-247. doi:10.1085/jgp.201010592

Takeshima, H., Iino, M., Takekura, H., Nishi, M., Kuno, J., Minowa, O., . . . Noda, T. (1994). Excitation-contraction uncoupling and muscular degeneration in mice lacking functional skeletal muscle ryanodine-receptor gene. *Nature, 369*(6481), 556-559. doi:10.1038/369556a0

Takeshima, H., Komazaki, S., Nishi, M., Iino, M., & Kangawa, K. (2000). Junctophilins: a novel family of junctional membrane complex proteins. *Mol Cell, 6*(1), 11-22. doi:10.1016/s1097-2765(00)00003-4

Takeshima, H., Nishimura, S., Matsumoto, T., Ishida, H., Kangawa, K., Minamino, N., . . . et al. (1989). Primary structure and expression from complementary DNA of skeletal muscle ryanodine receptor. *Nature, 339*(6224), 439-445. doi:10.1038/339439a0

Tallis, J., James, R. S., & Seebacher, F. (2018). The effects of obesity on skeletal muscle contractile function. *J Exp Biol, 221*(Pt 13). doi:10.1242/jeb.163840

Tanabe, T., Beam, K. G., Adams, B. A., Niidome, T., & Numa, S. (1990). Regions of the skeletal muscle dihydropyridine receptor critical for excitation-contraction coupling. *Nature, 346*(6284), 567-569. doi:10.1038/346567a0

Tanabe, T., Beam, K. G., Powell, J. A., & Numa, S. (1988). Restoration of excitation-contraction coupling and slow calcium current in dysgenic muscle by dihydropyridine receptor complementary DNA. *Nature, 336*(6195), 134-139. doi:10.1038/336134a0

Tanabe, T., Takeshima, H., Mikami, A., Flockerzi, V., Takahashi, H., Kangawa, K., . . . Numa, S. (1987). Primary structure of the receptor for calcium channel blockers from skeletal muscle. *Nature, 328*(6128), 313-318. doi:10.1038/328313a0

Tang, W., Sencer, S., & Hamilton, S. L. (2002). Calmodulin modulation of proteins involved in excitation-contraction coupling. *Front Biosci, 7*, d1583-1589. doi:10.2741/tang

Tang, Z. Z., Yarotskyy, V., Wei, L., Sobczak, K., Nakamori, M., Eichinger, K., . . . Thornton, C. A. (2012). Muscle weakness in myotonic dystrophy associated with misregulated splicing and altered gating of Ca(V)1.1 calcium channel. *Hum Mol Genet, 21*(6), 1312-1324. doi:10.1093/hmg/ddr568

Tantama, M., Martínez-François, J. R., Mongeon, R., & Yellen, G. (2013). Imaging energy status in live cells with a fluorescent biosensor of the intracellular ATP-to-ADP ratio. *Nat Commun, 4*, 2550. doi:10.1038/ncomms3550

Telegrafi, A., Webb, B. D., Robbins, S. M., Speck-Martins, C. E., FitzPatrick, D., Fleming, L., . . . Sobreira, N. L. M. (2017). Identification of STAC3 variants in non-Native American families with overlapping features of Carey-Fineman-Ziter syndrome and Moebius syndrome. *Am J Med Genet A, 173*(10), 2763-2771. doi:10.1002/ajmg.a.38375

Thomas, N. L., & Williams, A. J. (2012). Pharmacology of ryanodine receptors and Ca2+-induced Ca2+ release. *Wiley Interdisciplinary Reviews: Membrane Transport and Signaling, 1*(4), 383-397. doi:https://doi.org/10.1002/wmts.34

Thompson, R. J., Jackson, M. F., Olah, M. E., Rungta, R. L., Hines, D. J., Beazely, M. A., . . . MacVicar, B. A. (2008). Activation of pannexin-1 hemichannels augments aberrant bursting in the hippocampus. *Science, 322*(5907), 1555-1559. doi:322/5907/1555 [pii]

10.1126/science.1165209

Thompson, R. J., Zhou, N., & MacVicar, B. A. (2006). Ischemia opens neuronal gap junction hemichannels. *Science, 312*(5775), 924-927. doi:10.1126/science.1126241

Tinker, A., Aziz, Q., Li, Y., & Specterman, M. (2018). ATP-Sensitive Potassium Channels and Their Physiological and Pathophysiological Roles. *Compr Physiol, 8*(4), 1463-1511. doi:10.1002/cphy.c170048

Toloe, J., Mollajew, R., Kügler, S., & Mironov, S. L. (2014). Metabolic differences in hippocampal 'Rett' neurons revealed by ATP imaging. *Mol Cell Neurosci, 59*, 47-56. doi:10.1016/j.mcn.2013.12.008

Torabi, S. F., & Lu, Y. (2014). Functional DNA nanomaterials for sensing and imaging in living cells. *Curr Opin Biotechnol, 28*, 88-95. doi:10.1016/j.copbio.2013.12.011

Toyoshima, C. (2009). How Ca2+-ATPase pumps ions across the sarcoplasmic reticulum membrane. *Biochim Biophys Acta, 1793*(6), 941-946. doi:10.1016/j.bbamcr.2008.10.008

Toyoshima, C., Asahi, M., Sugita, Y., Khanna, R., Tsuda, T., & MacLennan, D. H. (2003). Modeling of the inhibitory interaction of phospholamban with the Ca2+ ATPase. *Proc Natl Acad Sci U S A, 100*(2), 467-472. doi:10.1073/pnas.0237326100

Tripathy, A., & Meissner, G. (1996). Sarcoplasmic reticulum lumenal Ca2+ has access to cytosolic activation and inactivation sites of skeletal muscle Ca2+ release channel. *Biophys J, 70*(6), 2600-2615. doi:10.1016/s0006-3495(96)79831-4

Tripathy, A., Xu, L., Mann, G., & Meissner, G. (1995). Calmodulin activation and inhibition of skeletal muscle Ca2+ release channel (ryanodine receptor). *Biophys J, 69*(1), 106-119. doi:10.1016/s0006-3495(95)79880-0

Tsuboi, T., Lippiat, J. D., Ashcroft, F. M., & Rutter, G. A. (2004). ATP-dependent interaction of the cytosolic domains of the inwardly rectifying K+ channel Kir6.2 revealed by fluorescence resonance energy transfer. *Proc Natl Acad Sci U S A, 101*(1), 76-81. doi:10.1073/pnas.0306347101

Tsugorka, A., Ríos, E., & Blatter, L. A. (1995). Imaging elementary events of calcium release in skeletal muscle cells. *Science, 269*(5231), 1723-1726. doi:10.1126/science.7569901

Tuluc, P., Molenda, N., Schlick, B., Obermair, G. J., Flucher, B. E., & Jurkat-Rott, K. (2009). A CaV1.1 Ca2+ channel splice variant with high conductance and voltage-sensitivity alters EC coupling in developing skeletal muscle. *Biophys J, 96*(1), 35-44. doi:10.1016/j.bpj.2008.09.027

Tyssowski, K. M., DeStefino, N. R., Cho, J. H., Dunn, C. J., Poston, R. G., Carty, C. E., . . . Gray, J. M. (2018). Different Neuronal Activity Patterns Induce Different Gene Expression Programs. *Neuron, 98*(3), 530-546.e511. doi:10.1016/j.neuron.2018.04.001

Ursu, D., Schuhmeier, R. P., Freichel, M., Flockerzi, V., & Melzer, W. (2004). Altered inactivation of Ca2+ current and Ca2+ release in mouse muscle fibers deficient in the DHP receptor gamma1 subunit. *J Gen Physiol, 124*(5), 605-618. doi:10.1085/jgp.200409168

Ursu, D., Sebille, S., Dietze, B., Freise, D., Flockerzi, V., & Melzer, W. (2001). Excitation-contraction coupling in skeletal muscle of a mouse lacking the dihydropyridine receptor subunit gamma1. *J Physiol, 533*(Pt 2), 367-377. doi:10.1111/j.1469-7793.2001.0367a.x

Valdivia, H. H., Hogan, K., & Coronado, R. (1991). Altered binding site for Ca2+ in the ryanodine receptor of human malignant hyperthermia. *Am J Physiol, 261*(2 Pt 1), C237-245. doi:10.1152/ajpcell.1991.261.2.C237

Valladares, D., Almarza, G., Contreras, A., Pavez, M., Buvinic, S., Jaimovich, E., & Casas, M. (2013). Electrical stimuli are anti-apoptotic in skeletal muscle via extracellular ATP. Alteration of this signal in Mdx mice is a likely cause of dystrophy. *PLoS One, 8*(11), e75340. doi:10.1371/journal.pone.0075340

van Rooij, E., Liu, N., & Olson, E. N. (2008). MicroRNAs flex their muscles. *Trends Genet, 24*(4), 159-166. doi:10.1016/j.tig.2008.01.007

van Rooij, E., Quiat, D., Johnson, B. A., Sutherland, L. B., Qi, X., Richardson, J. A., . . . Olson, E. N. (2009). A family of microRNAs encoded by myosin genes governs myosin expression and muscle performance. *Dev Cell, 17*(5), 662-673. doi:10.1016/j.devcel.2009.10.013

Vancraenenbroeck, R., & Webb, M. R. (2015). A Fluorescent, Reagentless Biosensor for ATP, Based on Malonyl-Coenzyme A Synthetase. *ACS Chem Biol, 10*(11), 2650-2657. doi:10.1021/acschembio.5b00346

Vettel, C., Wittig, K., Vogt, A., Wuertz, C. M., El-Armouche, A., Lutz, S., & Wieland, T. (2012). A novel player in cellular hypertrophy: Giβγ/PI3K-dependent activation of the RacGEF TIAM-1 is required for α_1-adrenoceptor induced hypertrophy in neonatal rat cardiomyocytes. *J Mol Cell Cardiol, 53*(2), 165-175. doi:10.1016/j.yjmcc.2012.04.015

Voit, A., Patel, V., Pachon, R., Shah, V., Bakhutma, M., Kohlbrenner, E., . . . Babu, G. J. (2017). Reducing sarcolipin expression mitigates Duchenne muscular dystrophy and associated cardiomyopathy in mice. *Nat Commun, 8*(1), 1068. doi:10.1038/s41467-017-01146-7

von Breunig, F., Wappler, F., Hagel, C., von Richthofen, V., Fiege, M., Weisshorn, R., . . . Schulte am Esch, J. (2004). Histomorphologic examination of skeletal muscle preparations does not differentiate between malignant hyperthermia-susceptible and -normal patients. *Anesthesiology, 100*(4), 789-794. doi:10.1097/00000542-200404000-00007

Vultaggio-Poma, V., Sarti, A. C., & Di Virgilio, F. (2020). Extracellular ATP: A Feasible Target for Cancer Therapy. *Cells, 9*(11). doi:10.3390/cells9112496

Wagner, L. E., 2nd, Groom, L. A., Dirksen, R. T., & Yule, D. I. (2014). Characterization of ryanodine receptor type 1 single channel activity using "on-nucleus" patch clamp. *Cell Calcium, 56*(2), 96-107. doi:10.1016/j.ceca.2014.05.004

Wang, C., Huang, C. Y., & Lin, W. C. (2013). Optical ATP biosensor for extracellular ATP measurement. *Biosens Bioelectron, 43*, 355-361. doi:10.1016/j.bios.2012.12.027

Wang, J., Ambrosi, C., Qiu, F., Jackson, D. G., Sosinsky, G., & Dahl, G. (2014). The membrane protein Pannexin1 forms two open-channel conformations depending on the mode of activation. *Sci Signal, 7*(335), ra69. doi:10.1126/scisignal.2005431

Wang, Y., Li, X., Duan, H., Fulton, T. R., Eu, J. P., & Meissner, G. (2009). Altered stored calcium release in skeletal myotubes deficient of triadin and junctin. *Cell Calcium, 45*(1), 29-37. doi:10.1016/j.ceca.2008.05.006

Waning, D. L., Mohammad, K. S., Reiken, S., Xie, W., Andersson, D. C., John, S., . . . Guise, T. A. (2015). Excess TGF-β mediates muscle weakness associated with bone metastases in mice. *Nat Med, 21*(11), 1262-1271. doi:10.1038/nm.3961

Way, M., & Parton, R. G. (1995). M-caveolin, a muscle-specific caveolin-related protein. *FEBS Lett, 376*(1-2), 108-112. doi:10.1016/0014-5793(95)01256-7

Weaver, J. L., Arandjelovic, S., Brown, G., S, K. M., M, S. S., Buckley, M. W., . . . Bayliss, D. A. (2017). Hematopoietic pannexin 1 function is critical for neuropathic pain. *Sci Rep, 7*, 42550. doi:10.1038/srep42550

Wei, R., Bao, W., He, F., Meng, F., Liang, H., & Luo, B. (2020). Pannexin1 Channel Inhibitor ((10)panx) Protects Against Transient Focal Cerebral Ischemic Injury by Inhibiting RIP3 Expression and Inflammatory Response in Rats. *Neuroscience, 437*, 23-33. doi:10.1016/j.neuroscience.2020.02.042

Wei, R., Wang, X., Zhang, Y., Mukherjee, S., Zhang, L., Chen, Q., . . . Yin, C. C. (2016). Structural insights into Ca(2+)-activated long-range allosteric channel gating of RyR1. *Cell Res, 26*(9), 977-994. doi:10.1038/cr.2016.99

Weilinger, N. L., Lohman, A. W., Rakai, B. D., Ma, E. M., Bialecki, J., Maslieieva, V., . . . Thompson, R. J. (2016). Metabotropic NMDA receptor signaling couples Src family kinases to pannexin-1 during excitotoxicity. *Nat Neurosci, 19*(3), 432-442. doi:10.1038/nn.4236

Weilinger, N. L., Tang, P. L., & Thompson, R. J. (2012). Anoxia-induced NMDA receptor activation opens pannexin channels via Src family kinases. *J Neurosci, 32*(36), 12579-12588. doi:10.1523/jneurosci.1267-12.2012

Weisleder, N., & Ma, J. (2008). Altered Ca2+ sparks in aging skeletal and cardiac muscle. *Ageing Res Rev, 7*(3), 177-188. doi:10.1016/j.arr.2007.12.003

Weiss, N., Couchoux, H., Legrand, C., Berthier, C., Allard, B., & Jacquemond, V. (2008). Expression of the muscular dystrophy-associated caveolin-3(P104L) mutant in adult mouse skeletal muscle specifically alters the Ca(2+) channel function of the dihydropyridine receptor. *Pflugers Arch, 457*(2), 361-375. doi:10.1007/s00424-008-0528-z

Weiss, N., Legrand, C., Pouvreau, S., Bichraoui, H., Allard, B., Zamponi, G. W., . . . Jacquemond, V. (2010). In vivo expression of G-protein beta1gamma2 dimer in adult mouse skeletal muscle alters L-type calcium current and excitation-contraction coupling. *J Physiol, 588*(Pt 15), 2945-2960. doi:10.1113/jphysiol.2010.191593

Weiss, R. G., O'Connell, K. M., Flucher, B. E., Allen, P. D., Grabner, M., & Dirksen, R. T. (2004). Functional analysis of the R1086H malignant hyperthermia mutation in the DHPR reveals an unexpected influence of the III-IV loop on skeletal muscle EC coupling. *Am J Physiol Cell Physiol, 287*(4), C1094-1102. doi:10.1152/ajpcell.00173.2004

Westerblad, H., & Allen, D. G. (1991). Changes of myoplasmic calcium concentration during fatigue in single mouse muscle fibers. *J Gen Physiol, 98*(3), 615-635. doi:10.1085/jgp.98.3.615

Willebrords, J., Maes, M., Crespo Yanguas, S., & Vinken, M. (2017). Inhibitors of connexin and pannexin channels as potential therapeutics. *Pharmacol Ther, 180*, 144-160. doi:10.1016/j.pharmthera.2017.07.001

Wilmshurst, J. M., Lillis, S., Zhou, H., Pillay, K., Henderson, H., Kress, W., . . . Jungbluth, H. (2010). RYR1 mutations are a common cause of congenital myopathies with central nuclei. *Ann Neurol, 68*(5), 717-726. doi:10.1002/ana.22119

Wisløff, U., Loennechen, J. P., Currie, S., Smith, G. L., & Ellingsen, Ø. (2002). Aerobic exercise reduces cardiomyocyte hypertrophy and increases contractility, Ca2+ sensitivity and SERCA-2 in rat after myocardial infarction. *Cardiovasc Res, 54*(1), 162-174. doi:10.1016/s0008-6363(01)00565-x

Woods, C. E., Novo, D., DiFranco, M., & Vergara, J. L. (2004). The action potential-evoked sarcoplasmic reticulum calcium release is impaired in mdx mouse muscle fibres. *J Physiol, 557*(Pt 1), 59-75. doi:10.1113/jphysiol.2004.061291

Wright, N. T., Prosser, B. L., Varney, K. M., Zimmer, D. B., Schneider, M. F., & Weber, D. J. (2008). S100A1 and calmodulin compete for the same binding site on ryanodine receptor. *J Biol Chem, 283*(39), 26676-26683. doi:10.1074/jbc.M804432200

Wu, G. Y., Deisseroth, K., & Tsien, R. W. (2001). Activity-dependent CREB phosphorylation: convergence of a fast, sensitive calmodulin kinase pathway and a slow, less sensitive mitogen-activated protein kinase pathway. *Proc Natl Acad Sci U S A, 98*(5), 2808-2813. doi:10.1073/pnas.051634198

Wu, H., Naya, F. J., McKinsey, T. A., Mercer, B., Shelton, J. M., Chin, E. R., . . . Williams, R. S. (2000). MEF2 responds to multiple calcium-regulated signals in the control of skeletal muscle fiber type. *Embo j, 19*(9), 1963-1973. doi:10.1093/emboj/19.9.1963

Wu, H., Rothermel, B., Kanatous, S., Rosenberg, P., Naya, F. J., Shelton, J. M., . . . Williams, R. S. (2001). Activation of MEF2 by muscle activity is mediated through a calcineurin-dependent pathway. *Embo j, 20*(22), 6414-6423. doi:10.1093/emboj/20.22.6414

Xia, R., Stangler, T., & Abramson, J. J. (2000). Skeletal muscle ryanodine receptor is a redox sensor with a well defined redox potential that is sensitive to channel modulators. *J Biol Chem, 275*(47), 36556-36561. doi:10.1074/jbc.M007613200

Xiong, X. X., Gu, L. J., Shen, J., Kang, X. H., Zheng, Y. Y., Yue, S. B., & Zhu, S. M. (2014). Probenecid protects against transient focal cerebral ischemic injury by inhibiting HMGB1 release and attenuating AQP4 expression in mice. *Neurochem Res, 39*(1), 216-224. doi:10.1007/s11064-013-1212-z

Yaginuma, H., Kawai, S., Tabata, K. V., Tomiyama, K., Kakizuka, A., Komatsuzaki, T., . . . Imamura, H. (2014). Diversity in ATP concentrations in a single bacterial cell population revealed by quantitative single-cell imaging. *Sci Rep, 4*, 6522. doi:10.1038/srep06522

Yan, Z., Bai, X., Yan, C., Wu, J., Li, Z., Xie, T., . . . Yan, N. (2015). Structure of the rabbit ryanodine receptor RyR1 at near-atomic resolution. *Nature, 517*(7532), 50-55. doi:10.1038/nature14063

Yang, J., Ellinor, P. T., Sather, W. A., Zhang, J. F., & Tsien, R. W. (1993). Molecular determinants of Ca2+ selectivity and ion permeation in L-type Ca2+ channels. *Nature, 366*(6451), 158-161. doi:10.1038/366158a0

Yasuda, T., Delbono, O., Wang, Z. M., Messi, M. L., Girard, T., Urwyler, A., . . . Zorzato, F. (2013). JP-45/JSRP1 variants affect skeletal muscle excitation-contraction coupling by decreasing the sensitivity of the dihydropyridine receptor. *Hum Mutat, 34*(1), 184-190. doi:10.1002/humu.22209

Yen, M. R., & Saier, M. H., Jr. (2007). Gap junctional proteins of animals: the innexin/pannexin superfamily. *Prog Biophys Mol Biol, 94*(1-2), 5-14. doi:10.1016/j.pbiomolbio.2007.03.006

Zacharias, D. A., Violin, J. D., Newton, A. C., & Tsien, R. Y. (2002). Partitioning of lipid-modified monomeric GFPs into membrane microdomains of live cells. *Science, 296*(5569), 913-916. doi:10.1126/science.1068539

Zaharieva, I. T., Sarkozy, A., Munot, P., Manzur, A., O'Grady, G., Rendu, J., . . . Muntoni, F. (2018). STAC3 variants cause a congenital myopathy with distinctive dysmorphic features and malignant hyperthermia susceptibility. *Hum Mutat, 39*(12), 1980-1994. doi:10.1002/humu.23635

Zalk, R., Clarke, O. B., des Georges, A., Grassucci, R. A., Reiken, S., Mancia, F., . . . Marks, A. R. (2015). Structure of a mammalian ryanodine receptor. *Nature, 517*(7532), 44-49. doi:10.1038/nature13950

Zamponi, G. W., Striessnig, J., Koschak, A., & Dolphin, A. C. (2015). The Physiology, Pathology, and Pharmacology of Voltage-Gated Calcium Channels and Their Future Therapeutic Potential. *Pharmacol Rev, 67*(4), 821-870. doi:10.1124/pr.114.009654

Zheng, J., Yancey, D. M., Ahmed, M. I., Wei, C. C., Powell, P. C., Shanmugam, M., . . . Dell'Italia, L. J. (2014). Increased sarcolipin expression and adrenergic drive in humans with preserved left ventricular ejection fraction and chronic isolated mitral regurgitation. *Circ Heart Fail, 7*(1), 194-202. doi:10.1161/circheartfailure.113.000519

Ziganshin, A. U., Khairullin, A. E., Teplov, A. Y., Gabdrakhmanov, A. I., Ziganshina, L. E., Hoyle, C. H. V., . . . Grishin, S. N. (2019). The effects of ATP on the contractions of rat and mouse fast skeletal muscle. *Muscle Nerve, 59*(4), 509-516. doi:10.1002/mus.26423

Zucchi, R., & Ronca-Testoni, S. (1997). The sarcoplasmic reticulum Ca2+ channel/ryanodine receptor: modulation by endogenous effectors, drugs and disease states. *Pharmacol Rev, 49*(1), 1-51.